EXPERIMENTAL AND THEORETICAL STUDY OF SHALLOW DOUBLY CURVED SHELLS

A thesis presented for the
degree of Ph.D. in Civil Engineering
in the University of Canterbury,
Christchurch, New Zealand.

by

J. G. A. CROLL

1967

ABSTRACT

This investigation is concerned with the application of finite difference methods to the solution of thin elastic shallow shells. In particular, the ruled surface hyperbolic paraboloid is systematically studied to determine the influences of boundary conditions, geometric shape and material properties.

The method developed for representing and solving the discretised system is suitable for use on digital computers of limited storage capacity and arithmetic speed. For all boundary types considered, solutions upon successively finer difference grids have demonstrated convergence to the analytic solution. A number of methods for accelerating this convergence were found to result in an increase of total computational labour for a given numerical accuracy.

The considerable differences in the behaviour of the degenerate clamped and free edged shells demonstrate the necessity of theoretical solutions embodying the influence of edge members. A number of numerical-physical analogues for the shell-edge member interaction are studied to ensure compatibility with the degenerate boundary conditions upon choice of suitable beam dimensions.

The construction and testing of a "perspex" model with varied boundary and corner support conditions is described.

Results from these tests are used as a basis for comparison with theoretical solutions and to provide additional information concerning the critical influence of the corner diagonal thrust. Conclusions from the theoretical and experimental investigations are in close agreement, and also verify solutions obtained in past research.

ACKNOWLEDGEMENTS

The author wishes to acknowledge and thank the following:

Professor H. J. Hopkins, Head of the Department of Civil Engineering, under whose overall guidance this research was made.

Dr. J. C. Scrivener and latterly Dr. P. J. Moss for their interest, encouragement and detailed supervision.

Dr. A. H. Bryant for his assistance and generous advice on the experimental programme, and for valuable suggestions concerning the script.

The Technical Staff of the Department of Civil Engineering for their assistance in the experimental work.

The Staff of the Mobil Computer Laboratory for punching cards and processing programmes.

Mrs. D. E. Ball for typing the manuscript.

The University Grants Committee for financial aid.

My wife, for her continued encouragement and patience.

C O N T E N T S

L I S T O F F I G U R E S

LIST OF PLATES

L I S T O F T A B L E S

INDEX OF NOTATION

The symbols used are defined in the text where they first appear. For convenience of reference the more important symbols are summarised in alphabetic order.

a,b	:	half span of the ruled surface hyperbolic paraboloid in the z_1 and z_2 coordinate directions
A	:	area of edge beam
$\mathbf{A}$	:	matrix of difference coefficients
a_{rs}	:	element of matrix $\mathbf{A}$ at the r th row and s th column
b_b	:	width of edge beam
D	:	$\frac{Et_s^3}{12(1-\nu^2)}$ = flexural rigidity
$e_k,(k=2,3)$	:	eccentricity of shell edge intersection with respect to edge member centroidal axis
$e_k',(k=2,3)$	:	eccentricity of grid line i = 3 with respect to line i = b
E_s	:	Young's modulus of elasticity for the shell
E_b	:	Young's modulus for elasticity for the edge beam
f	:	maximum rise of the ruled surface hyperbolic paraboloid
G_k	:	edge member line loading in the z_k coordinate direction
h	:	maximum of the difference grid spacings h_k
$\mathbf{H}$	:	successive over-relaxation iteration matrix

$h_k, (k = 1,2)$: difference grid spacing in the z_k coordinate directions

H_k : shell-edge member interaction load components in z_k coordinate directions

H_j^k : the discrete value of H_k at the grid position (b,j)

$H_{k_r}, (k = 0,4)$: sums of horizontal components of actions

i,j : difference grid row and column subscripts

i',j' : difference grid row and column subscripts used fc modified difference technique

I_k : second moments of inertia of edge beam about z_k axes

K : $\frac{E_s t_s}{1-\nu^2}$ = extensional rigidity

K_k : Shell-edge member interaction moment components about the z_k axes

K_j^k : the discrete value of K_k at the grid position (b,j)

$k_{H_{k_r}}, (k = 0,4)$: dimensionless coefficients describing H_{k_r}

$k_{m_{kl}}$, $k_{n_{kl}}$: dimensionless coefficients for m_{kl} and n_{kl}

$k_{m_{ij}}^{kl}$, $k_{n_{ij}}^{kl}$: discrete values of dimensionless coeeficients $k_{m_{kl}}$ and $k_{n_{kl}}$ at (i,j)

k_{M_k}, k_{N_1} : dimensionless coefficients for M_k and N_1

$k_{M_j}^k$, $k_{N_j}^1$: discrete value of dimensionless coefficients k_{M_k} and k_{N_1} at (b,j)

$k_{P_{ij}}^3$: dimensionless coefficient describing normal load distribution

$k_{V_{k_r}}$: dimensionless coefficients describing V_{k_r}

k_{w_k} : dimensionless coefficient for w_k

$k^k_{w_{ij}}$: discrete value of k_{w_k} at grid position (i,j)

L : span of shell

m : number of difference grid spaces over half the shell

m_{kl} : shell stress couples (moments per unit length)

M_k : edge beam moments

m^{kl}_{ij} : discrete value of m_{kl} at (i,j)

M^k_j : discrete value of M_k at (b,j)

n : order of predominant truncation error

N : order of matrix $\mathbb{A}$

n_{kl} : shell stress resultants (force per unit length)

N_l : edge beam axial force

n^{kl}_{ij} : discrete value of n_{kl} at (i,j)

N^l_j : discrete value of N_l at (b,j)

O_k, P_k, Q_k : coefficients used in edge member difference molecules

$\mathbb{P}$: vector of load components

P_k : shell unit load per unit area in z_k coordinate direction

q : magnitude of normal loading

q_{kk} : shell transverse shears (force per unit length)

Q_k : edge beam transverse shears

R_k : radii of curvature of the edge member before deformation

R'_k : radii of curvature of the edge member after deformation

R_{kl} : radii of curvature of the shell before deformation

R'_{kl} : radii of curvature of the shell after deformation

R_k, S_k, T_k : coefficients used in the conventional shell difference molecules

R'_k, S'_k, T'_k : coefficients used in the modified shell difference molecules

t_s : shell thickness

t_b : edge member thickness

T_1 : corner diagonal thrust

u_k : displacement components of middle surface in x_k coordinate directions

v_k : displacement components of middle surface in y_k coordinate directions

V_{k_r}, $(k = 0,4)$: sums of vertical components of actions

W : vector of displacement components

w_k : displacement components of middle surface in z_k coordinate directions

$w_{k_{ij}}$: values of w_k at (i,j)

w^k : discrete values of w_k

w^k_{ij} : values of w^k at (i,j)

$W^{(k)}$: value of W after the kth iteration

$w_r^{(k)}$: value of the rth element of $W^{(k)}$

x_k : orthogonal shell coordinates

y_y : orthogonal edge member coordinates

z_k : orthogonal spatial coordinates

α_1, α_2 : metric coefficients

β : ratio $\frac{h_1}{h_2}$

β : over-relaxation factor

β_o : optimum over-relaxation factor

δ_k, $(k = 1,4)$: corner diagonal displacements

$\delta^{(k)}$: vector of iteration displacements

ϵ_{kl} : midsurface strains

ϵ^t_{kl} : top surface strains

ϵ^b_{kl} : bottom surface strains

ϕ, θ : slopes of shell about z_1 and z_2 axes

ϕ_j, θ_i : slopes ϕ and θ at constant j and i

γ : torsion stiffness constant

λ_k, $(k = 1,6)$: dimensionless shell-edge beam parameter

ν : Poisson's ratio

σ_{kl} : midsurface stresses

$\left(\frac{\partial^n w_k}{\partial z_1^r \ \partial z_2^s}\right)_{ij}$: nth mixed derivative of w_k, employing discrete values of w^k, and computed at the position (i,j)

The terms "pivotal" and "grid position" are used to denote members of the set of points defined by the intersection of the difference grid lines i and columns j , and are written as (i,j).

For convenience the comma separating subscripts is omitted, so that $w^k_{i,j}$ is written w^k_{ij} . To avoid confusion products are never used in sub- or super- scripts.

"Truncation errors" refer to individual errors involved in each difference expression due to termination of the Taylor series expansion. The total error caused by the individual truncation errors is termed the "discretisation error".

CHAPTER ONE

INTRODUCTION

1.1 INTRODUCTION

Architectural freedom for the conception of shell forms is at present restricted by the limited scope of existing mathematical solution techniques. Although the behaviour of general shells may be obtained from empirical studies, a theoretical method capable of providing solutions for general shell shapes and boundary constraints would be invaluable.

Extensive historical reviews of the development of shell theory and its associated solutions have been presented by a number of authors (see for example [56,7]). In all, the gulf between existing solutions and the requirements of industry, if not specifically mentioned are at least indicated. The theory of thin shallow shells, initiated in 1944 by Vlasov [57], is an attempt to reduce the general theory to a workable model. Even with the assumptions of shallow shell theory, analytic solutions obtained are few and extremely restrictive in both shell class and boundary support conditions.

One class of shells which are amenable to analytic treatment, and which have been extensively considered over the last decade, are those belonging to the doubly curved second order translational surfaces. As a consequence, these shells have become popular

constructional forms - especially the cylindrical shell. Apeland and Popov [4] however, attribute this theoretical popularity to the frequent use of these shells in recent years. In fact, it is probable that each has influenced the consideration of the other. Even for this restrictive class of shells, the freedom in the choice of boundary and corner conditions is limited. Alternative methods are therefore required.

Further attempts at simplification of the mathematical models generally yield either unsatisfactory solutions or badly posed physical problems. In order that solutions be obtained, it is necessary to either circumvent the need for differential representation or to develop a solution technique of these equations which is simple, adaptable and yet mathematically rigorous.

Within the first of these techniques a number of methods have been developed to replace the continuous problem with a finite number of approximately equivalent discrete and predictable elements. While the method can be effectively applied in certain circumstances, it is likely that difficulties in the representation of shell-edge member interaction and corner support conditions detract from their general use. For cases of structures constructed from physically discrete elements, such as those used in a number of precast structural forms, the method may provide a realistic model. The ease with which the behaviour of these analogues can be physically visualised has been an important contributing factor in their development.

A method which stands alone in the second of the techniques given above, if from simplicity considerations alone, is the finite difference method. The adaptability and the relationship with a discrete element method have been demonstrated by Utku [56], who employs a lattice analogy to provide this method with a physical meaning. The expected accuracy and therefore mathematical rigour of the method has been demonstrated for simplified forms of the second order translational shells with restrictive boundary constraints by Chuang, Noor and Veletsos [16, 43].

An extension of this work to include other shell forms not amenable to analytic treatment, as well as the systematic study of the influence of shell-edge member interaction, is therefore a further step toward narrowing this gap between existing solutions and the requirements of industry.

1.2 OBJECT AND SCOPE

The general object of the present investigation is to determine the practicability and adaptability of the finite difference method as used for the analysis of thin shallow elastic shell structures. By way of illustrative example on the application of the method, detailed consideration is given to the ruled surface hyperbolic paraboloid on rectangular planform. This particular shell form is chosen because of its ever increasing architectural popularity and because existing solutions are few. From a detailed and systematic study of this shell class, the following particular objectives are considered:

1. To determine the applicability of small digital computers, and to estimate the resulting accuracy for the finite difference solutions of thin shallow shell problems.

2. To assess the merits of a number of techniques suggested for the improvement of numerical accuracy.

3. To demonstrate the important influence of the boundary and corner support conditions and to measure quantitatively the relative contributions of each of the constraint modes for a number of typical cases.

4. To make comparative studies of the effect of shell geometric and material properties.

5. To compare the results for each of the boundary conditions considered with both independent solutions and those obtained from other investigations.

6. To construct and test elastic ruled surface hyperbolic paraboloid shell models for the purposes of comparison where the methods of 5. are not possible. It is also intended that these empirical studies should provide further information not easily obtained from theoretical treatment.

This thesis is divided into three parts. In Part I the development of the general thin shell and edge member equations, in terms of displacement components in the directions of a curvilinear set of coordinates, is briefly reviewed. After

making the necessary assumptions, these equations are reduced to those of thin shallow shell and edge member theory. The general conventional finite difference analogues of both thin shallow shell and edge member theory are developed, simplified and given with the modified finite difference analogues for the case of the ruled surface hyperbolic paraboloid.

As an introduction to Part II, chapter 6 considers a number of techniques for the formulation and solution of the difference systems resulting from the discretisation process described in Part I. A suitable method of solution and the necessary programming techniques are then developed. The conventional finite difference technique is applied to determine the rates of convergence (as the difference grid is refined) for each of the simple, clamped, free and beam edged ruled surface hyperbolic paraboloid shells. In addition, a number of methods suggested for the reduction of truncation errors involved in the discretisation process are considered. Where applicable, these methods are first applied to the encastré beam and single panel flat plate and are then extended to the clamped and simply supported ruled surface hyperbolic paraboloid shells. The efficiency of the various methods are assessed from considerations of total computational labour required for a given numerical accuracy. The most efficient model is then used in the remaining chapters of Part II.

Overall influences of boundary conditions are demonstrated by the three degenerate boundary types. Analogues for the edge beam representation are then developed, with special emphasis placed upon consistency with each of the degenerate boundary conditions upon suitable choice of edge beam parameters. The influence of a number of second order edge member-shell interaction terms are then considered, so that a simplified boundary model embodying all those terms which are likely to effect the solution to an extent equal to, or greater than the expected numerical accuracy, may be developed. The influences of corner conditions are then assessed from the results of four diagonally and axi-symmetric examples.

With the programmes for each of the above boundary types, the influences of a number of shell geometric and material properties are investigated. It is hoped that sufficient cases have been considered for the trends to be of some assistance in design. For each of the four boundary types - the clamped, simple, free and edge beam - vertical and horizontal equilibrium checks are carried out, while for the first two of these boundary types, comparisons are made with existing solutions.

Part III describes in detail the construction, instrumentation, testing and results of free and beam edged perspex models. Corner support conditions and loading are varied in such a way that a number of independent checks upon model behaviour can be made. Results of these tests are then used for purposes of

comparison with the theoretical solutions not compared to other theoretical solutions.

Finally, a number of conclusions and suggestions for future consideration are presented.

PART I

THEORETICAL REVIEW

CHAPTER TWO

SHELL DIFFERENTIAL SYSTEM

After a summary of basic assumptions and the development of the theory of thin elastic shells, the shallow shell equations in terms of displacement components are given. This review is given so that in chapter three an edge member model consistent with the assumptions of shallow shell theory, may be developed. Displacement components are used as dependent variables in preference to any of the other possible combinations of variables, as it is felt they display superior boundary representation properties - especially where a general edge member is considered. The material which is based upon the work of Love[41] and Vlasov[57], is adequately reviewed by a number of authors[14,58].

2.1 ASSUMPTIONS

With reference to the right handed system x_k* of figure 2.1(a), the curvilinear coordinates x_k, ($k = 1,2$) are defined to describe a smooth spatial surface, and together with x_3 form a moving trihedron which is orthogonal if the x_k, ($k = 1,2$) axes are coincident with the lines of principal curvature.

---

* Unless otherwise stated the use of the group subscripts k and l will imply the summation of ($k,l = 1,2,3$).

Orthogonality for practical reasons, is assumed throughout this thesis, and although this implies that strains and displacements are small, this assumption is not made concerning the computation of the curvatures. In order that the model be further simplified the following generally accepted assumptions are made:

1. That the extension of Kirchoff's assumptions for flat plates - "Normals to the middle surface before deformation remain normal to it after deformation, and do not undergo any change in length" - to the case of thin shells, is valid.

2. The material is isotropic, and obeys linear stress strain laws.

3. That Love's first assumption holds true, that is, the shell is sufficiently thin for

$$\frac{x_3}{R_{kk}}, \quad (k = 1,2) \ll 1,$$

where $|x_3| \leq \frac{t_s}{2}$ and t_s denotes the shell thickness.

The implications and inconsistencies resulting from these assumptions are discussed in reference [21]. The usual assumption of homogeneity, which implies that the shell elastic constants E_s and μ are functions of the coordinates x_k, $(k = 1,2)$, is not made.

2.2 EQUILIBRIUM

Force and moment equilibrium along and about the x_k axes, result in the following equations [58, 21]:

$$\frac{\partial}{\partial x_1}(\alpha_2 n_{11}) + \frac{\partial}{\partial x_2}(\alpha_1 n_{21}) + n_{12}\cdot\frac{\partial \alpha_1}{\partial x_2} - n_{22}\cdot\frac{\partial \alpha_2}{\partial x_1} - \frac{q_{11}\cdot\alpha_1\cdot\alpha_2}{R'_{11}} - \frac{q_{22}\cdot\alpha_1\cdot\alpha_2}{R'_{12}} + \alpha_1\alpha_2 p_1 = 0, \quad (2.1)$$

$$\frac{\partial}{\partial x_2}(\alpha_1 n_{22}) + \frac{\partial}{\partial x_1}(\alpha_2 n_{12}) + n_{21}\cdot\frac{\partial \alpha_2}{\partial x_1} - n_{11}\cdot\frac{\partial \alpha_1}{\partial x_2} - \frac{q_{22}\cdot\alpha_1\cdot\alpha_2}{R'_{22}} - \frac{q_{11}\cdot\alpha_1\cdot\alpha_2}{R'_{12}} + \alpha_1\cdot\alpha_2\cdot p_2 = 0, \quad (2.2)$$

$$\frac{\partial}{\partial x_1}(\alpha_2 q_{11}) + \frac{\partial}{\partial x_2}(\alpha_1 q_{22}) + \alpha_1\cdot\alpha_2\cdot\left(\frac{n_{11}}{R'_{11}} + \frac{n_{12}}{R'_{12}} + \frac{n_{21}}{R'_{12}} + \frac{n_{22}}{R'_{22}}\right) + \alpha_1\cdot\alpha_2\cdot p_3 = 0, \quad (2.3)$$

$$-\frac{\partial}{\partial x_1}(\alpha_2 m_{11}) - \frac{\partial}{\partial x_2}(\alpha_1 m_{21}) + m_{12}\cdot\frac{\partial \alpha_1}{\partial x_2} - m_{22}\cdot\frac{\partial \alpha_2}{\partial x_1} + \alpha_1\cdot\alpha_2\cdot q_{11} = 0, \quad (2.4)$$

$$\frac{\partial}{\partial x_2}(\alpha_1 m_{22}) + \frac{\partial}{\partial x_1}(\alpha_2 m_{12}) - m_{21}\cdot\frac{\partial \alpha_2}{\partial x_1} + m_{11}\cdot\frac{\partial \alpha_1}{\partial x_2} + \alpha_1\cdot\alpha_2\cdot q_{22} = 0, \quad (2.5)$$

$$\frac{m_{11}}{R'_{12}} + \frac{m_{12}}{R'_{11}} + \frac{m_{21}}{R'_{22}} + \frac{m_{22}}{R'_{12}} + n_{12} - n_{21} = 0, \quad (2.6)$$

where (n_{kl}, m_{kl}), $(k,l = 1,2)$ are respectively stress resultants and stress couples per unit length, and p_k the loading components per unit area in the coordinates directions x_k. The quantities q_{kk}, $(k = 1,2)$ are the normal stress resultants, which under the first of the above assumptions

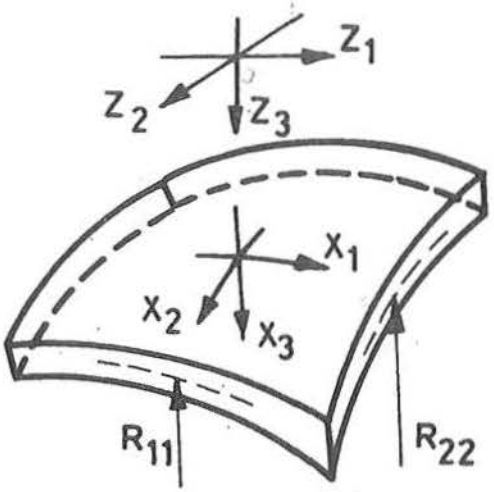

(a) Positive directions of shell axes.

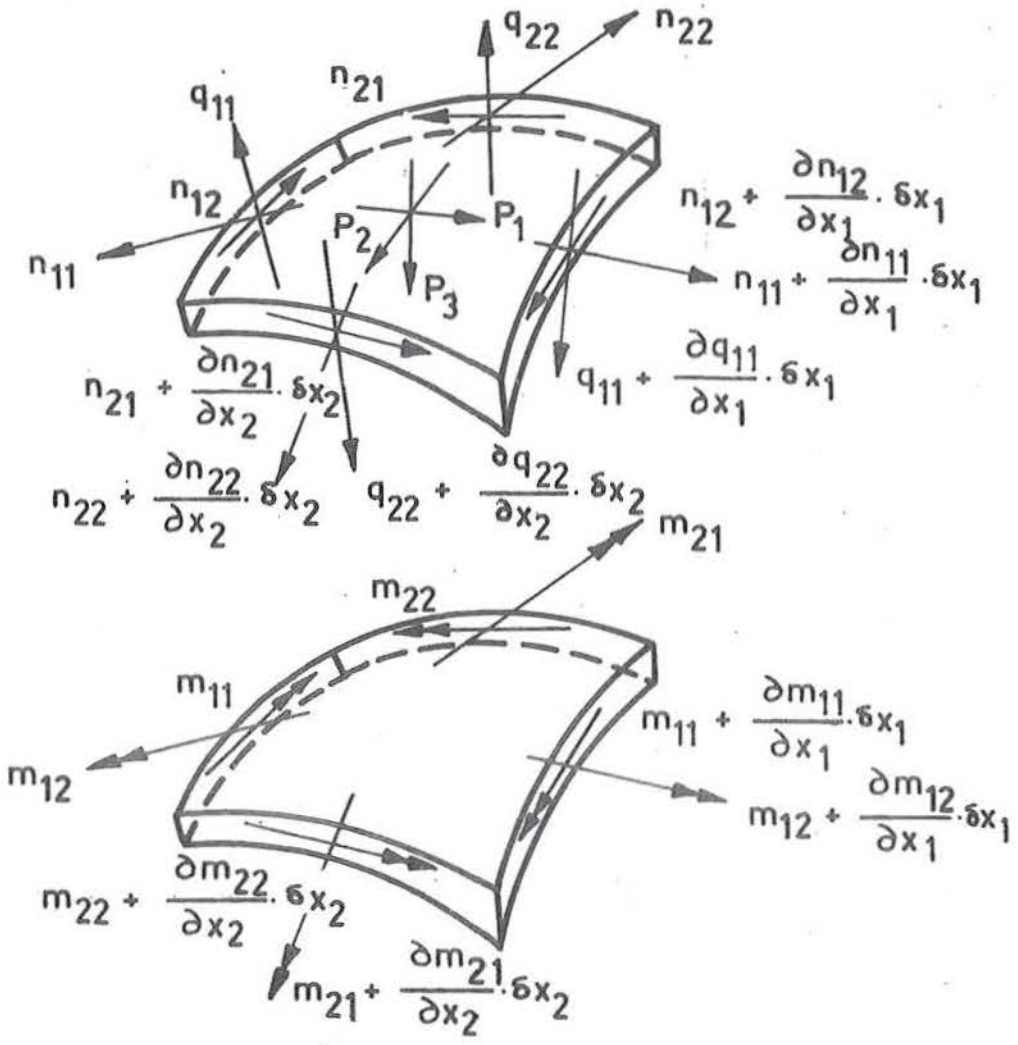

Fig.2.1 (b) Positive directions of shell internal actions.

are not associated with shear strain. The convention used for the directions of positive stress and moment resultants are shown in figure 2.1(b). The $\frac{1}{R'_{kl}}$, (k,l = 1,2) refer to the deformed curvatures of the shell, while the metric coefficients α_k , (k = 1,2), which are functions of the position in space for orthoginal coordinates x_k , have been known in the present context as the Lamé coefficients[2].

2.3 STRESS AND MOMENT RESULTANTS IN TERMS OF DISPLACEMENT COMPONENTS:

Stress resultants (n_{kl}, q_{kk}), (k,l = 1,2) and the stress couples m_{kl} , (k,l = 1,2) above, are written in terms of the displacement components u_k , where the displacements u_k refer to the mid-surface displacements in the coordinate directions x_k . These equations are given by Vlasov[57] and Wang[58] in the following form:

$$n_{11} = +K\left[\frac{1}{\alpha_1}\cdot\frac{\partial u_1}{\partial x_1} + \frac{u_2}{\alpha_1\cdot\alpha_2}\cdot\frac{\partial \alpha_1}{\partial x_2} + \mu\cdot\frac{1}{\alpha_2}\cdot\frac{\partial u_2}{\partial x_2} + \mu\cdot\frac{u_1}{\alpha_1\cdot\alpha_2}\cdot\frac{\partial \alpha_2}{\partial x_1} - \frac{u_3}{R'_{11}} - \mu\cdot\frac{u_3}{R'_{22}}\right], \tag{2.7}$$

$$n_{22} = +K\left[\frac{1}{\alpha_2}\frac{\partial u_2}{\partial x_2} + \frac{u_1}{\alpha_1\cdot\alpha_2}\cdot\frac{\partial \alpha_2}{\partial x_1} + \mu\cdot\frac{1}{\alpha_1}\cdot\frac{\partial u_1}{\partial x_1} + \mu\cdot\frac{u_2}{\alpha_1\cdot\alpha_2}\frac{\partial \alpha_1}{\partial x_2} - \frac{u_3}{R'_{22}} - \mu\cdot\frac{u_3}{R'_{11}}\right], \tag{2.8}$$

$$n_{12} = +K\cdot\left(\frac{1-\mu}{2}\right)\cdot\left[\frac{\alpha_2}{\alpha_1}\cdot\frac{\partial}{\partial x_1}\left(\frac{u_2}{\alpha_2}\right) + \frac{\alpha_1}{\alpha_2}\cdot\frac{\partial}{\partial x_2}\left(\frac{u_1}{\alpha_1}\right) - 2\cdot\frac{u_3}{R'_{12}}\right], \tag{2.9}$$

$$m_{11} = -D\cdot\left[\frac{1}{\alpha_1}\cdot\frac{\partial}{\partial x_1}\left(\frac{u_1}{R'_{11}}+\frac{1}{\alpha_1}\cdot\frac{\partial u_3}{\partial x_1}\right)+\nu\cdot\frac{1}{\alpha_2}\cdot\frac{\partial}{\partial x_2}\left(\frac{u_2}{R'_{22}}+\frac{1}{\alpha_2}\cdot\frac{\partial u_3}{\partial x_2}\right)\right.$$
$$+\frac{1}{\alpha_1\cdot\alpha_2}\cdot\left(\frac{u_2}{R'_{22}}+\frac{1}{\alpha_2}\cdot\frac{\partial u_3}{\partial x_2}\right)\cdot\frac{\partial\alpha_1}{\partial x_2}$$
$$\left.+\nu\cdot\frac{1}{\alpha_1\cdot\alpha_2}\cdot\left(\frac{u_1}{R'_{11}}+\frac{1}{\alpha_1}\cdot\frac{\partial u_3}{\partial x_1}\right)\cdot\frac{\partial\alpha_2}{\partial x_1}\right], \quad (2.10)$$

$$m_{22} = +D\cdot\left[\frac{1}{\alpha_2}\cdot\frac{\partial}{\partial x_2}\left(\frac{u_2}{R'_{22}}+\frac{1}{\alpha_2}\cdot\frac{\partial u_3}{\partial x_2}\right)+\nu\cdot\frac{1}{\alpha_1}\cdot\frac{\partial}{\partial x_1}\left(\frac{u_1}{R'_{11}}+\frac{1}{\alpha_1}\cdot\frac{\partial u_3}{\partial x_1}\right)\right.$$
$$+\frac{1}{\alpha_1\cdot\alpha_2}\cdot\left(\frac{u_1}{R'_{11}}+\frac{1}{\alpha_1}\cdot\frac{\partial u_3}{\partial x_1}\right)\cdot\frac{\partial\alpha_2}{\partial x_1}$$
$$\left.+\nu\cdot\frac{1}{\alpha_1\cdot\alpha_2}\cdot\left(\frac{u_2}{R'_{22}}+\frac{1}{\alpha_2}\cdot\frac{\partial u_3}{\partial x_2}\right)\cdot\frac{\partial\alpha_1}{\partial x_2}\right], \quad (2.11)$$

$$m_{12} = +D\cdot\left(\frac{1-\nu}{2}\right)\cdot\left[\frac{\alpha_2}{\alpha_1}\cdot\frac{\partial}{\partial x_2}\left(\frac{u_2}{\alpha_2 R'_{22}}+\frac{1}{\alpha_2^2}\cdot\frac{\partial u_3}{\partial x_2}\right)\right.$$
$$\left.+\frac{\alpha_1}{\alpha_2}\cdot\frac{\partial}{\partial x_1}\left(\frac{u_1}{\alpha_1 R'_{11}}+\frac{1}{\alpha_1^2}\cdot\frac{\partial u_3}{\partial x_1}\right)\right], \quad (2.12)$$

where $K = \dfrac{E_s\cdot t_s}{(1-\nu^2)}$, $D = \dfrac{E_s\cdot t_s^3}{12\cdot(1-\nu^2)}$ and may be functions of x_k, (k = 1,2). The expressions for q_{kk}, (k = 1,2) may be obtained by replacing m_{kl}, (k,1 = 1,2) in (2.4) and (2.5) with the values given by equations (2.10), (2.11) and (2.12). For the representation of mid-surface strains ϵ_{kl} (k,1 = 1,2) in terms of mid-surface displacements u_k, the assumption of small displacements is again required. It is asserted however, that the consequences of these simplifications are likely to be considerably less than the effects of this same assumption upon the curvature $\dfrac{1}{R'_{kl}}$, (k,1 = 1.2).

2.4 THE THIN ELASTIC SHELL DIFFERENTIAL EQUATIONS

Although it is possible to substitute equations (2.7) to (2.12) into the equilibrium equations (2.1) to (2.3), after the elimination of q_{kk} , (k = 1,2) using (2.4) and (2.5) and obtain three independent equations for the dependent variables u_k , this is not attempted. The algebraic manipulations are tedious, and the benefits to be derived are doubtful. The resulting system of three quasi-linear partial differential equations is generally insoluble and requires additional simplifications to become a practical working model.

2.5 THE THIN SHALLOW ELASTIC SHELL DIFFERENTIAL EQUATIONS

Projections from the rectangular cartesian coordinate system z_k on to the shell mid-surface form the x_k system shown in figure 2.1(a). Displacement components w_k represent the shell mid-surface displacements in the coordinate directions z_k , and in addition to the general assumptions of section 2.1, it is further assumed that:

1. The first derivatives $\frac{\partial z_3}{\partial z_k}$, (k = 1,2) of the shell surface are small.

2. The rates of change of the first derivatives are small.

3. The in-plane stress resultants n_{kl} are predominant in carrying surface loads, while because of the shallowness and vertical flexibility, the normal deflections w_3 will be greater than the in-plane deflections w_1 and w_2 .

4. The rates of change of curvatures are everywhere small.

It can be shown from assumption 1 that not only are Lamé coefficients given by[2]

$$\alpha_1 \doteq \alpha_2 \doteq 1 \quad ,$$

but the derivatives $\frac{\partial u_k}{\partial x_1}$, ($k,1 = 1,2$) may be replaced with the corresponding derivatives $\frac{\partial w_k}{\partial z_1}$, ($k,1 = 1,2$). Assumptions 2 and 3 imply that the terms such as $\frac{q_{kk}}{R'_{kk}}$, ($k = 1,2$) in the equilibrium equations (2.1) and (2.2), $\frac{m_{11}}{R'_{12}}$ and $\frac{m_{12}}{R'_{11}}$ in equation (2.6) and $\frac{1}{R_{kk}} \cdot \frac{\partial u_k}{\partial z_k}$, ($k = 1,2$) in equations (2.10) to (2.12) are negligible, while according to 4, derivatives of the curvatures $\frac{\partial}{\partial z_k}\left(\frac{1}{R'_{k1}}\right)$, ($k,1 = 1,2$) in equations (2.10) to (2.12) are small at all points.

The equilibrium equations then become

$$\frac{\partial n_{11}}{\partial z_1} + \frac{\partial n_{21}}{\partial z_2} + p_1 = 0, \quad (2.13)$$

$$\frac{\partial n_{12}}{\partial z_1} + \frac{\partial n_{22}}{\partial z_2} + p_2 = 0, \quad (2.14)$$

$$\frac{\partial q_{11}}{\partial z_1} + \frac{\partial q_{22}}{\partial z_2} + \left(\frac{n_{11}}{R'_{11}} + 2 \cdot \frac{n_{12}}{R'_{12}} + \frac{n_{22}}{R'_{22}} \right) + p_3 = 0, \quad (2.15)$$

$$-\frac{\partial m_{11}}{\partial z_1} - \frac{\partial m_{12}}{\partial z_2} + q_{11} = 0, \quad (2.16)$$

$$\frac{\partial m_{12}}{\partial z_1} + \frac{\partial m_{22}}{\partial z_2} + q_{22} = 0, \quad (2.17)$$

$$n_{12} - n_{21} = 0, \qquad (2.18)$$

and the associated action-displacement equations

$$n_{11} = + K \cdot \left(\frac{\partial w_1}{\partial z_1} + \nu \cdot \frac{\partial w_2}{\partial z_2} - \frac{w_3}{R'_{11}} - \nu \cdot \frac{w_3}{R'_{22}} \right), \qquad (2.19)$$

$$n_{22} = + K \cdot \left(\frac{\partial w_2}{\partial z_2} + \nu \cdot \frac{\partial w_1}{\partial z_1} - \frac{w_3}{R'_{22}} - \nu \cdot \frac{w_3}{R'_{11}} \right), \qquad (2.20)$$

$$n_{12} = + K \cdot \left(\frac{1-\nu}{2} \right) \cdot \left(\frac{\partial w_1}{\partial z_2} + \frac{\partial w_2}{\partial z_1} - 2 \cdot \frac{w_3}{R'_{12}} \right) = n_{21}, \qquad (2.21)$$

$$m_{11} = - D \cdot \left(\frac{\partial^2 w_3}{\partial z_1^2} + \nu \cdot \frac{\partial^2 w_3}{\partial z_2^2} \right), \qquad (2.22)$$

$$m_{22} = + D \cdot \left(\frac{\partial^2 w_3}{\partial z_2^2} + \nu \cdot \frac{\partial^2 w_3}{\partial z_1^2} \right), \qquad (2.23)$$

$$m_{12} = + D \cdot \left(\frac{1-\nu}{2} \right) \cdot \left(\frac{\partial^2 w_3}{\partial z_1 \partial z_2} \right) = - m_{21} \qquad (2.24)$$

It is noted that to this point it was not necessary to assume material homogeneity. If it is further assumed that the material properties E_s and ν are sufficiently smooth, slowly varying functions of (z_1, z_2), for the derivatives $\left(\frac{\partial E_s}{\partial z_k}, \frac{\partial \nu}{\partial z_k}\right)$, $(k = 1, 2)$ to be negligible, equations (2.19) to (2.24) may be substituted into (2.13) to (2.15) to produce the following thin shallow elastic shell equations:

$$\frac{\partial^2 w_1}{\partial z_1^2} + \left(\frac{1-\nu}{2} \right) \cdot \frac{\partial^2 w_1}{\partial z_2^2} + \left(\frac{1+\nu}{2} \right) \cdot \frac{\partial^2 w_2}{\partial z_1 \partial z_2} -$$

$$-\left(\frac{1}{R_{11}'}+\nu\cdot\frac{1}{R_{22}'}\right)\cdot\frac{\partial w_3}{\partial z_1}-(1-\nu)\cdot\frac{1}{R_{12}'}\cdot\frac{\partial w_3}{\partial z_2}+\frac{P_1}{K}=0, \quad (2.25)$$

$$\frac{\partial^2 w_2}{\partial z_2^2}+\left(\frac{1-\nu}{2}\right)\cdot\frac{\partial^2 w_2}{\partial z_1^2}+\left(\frac{1+\nu}{2}\right)\cdot\frac{\partial^2 w_1}{\partial z_1\partial z_2}$$
$$-\left(\frac{1}{R_{22}'}+\nu\cdot\frac{1}{R_{11}'}\right)\cdot\frac{\partial w_3}{\partial z_2}-(1-\nu)\cdot\frac{1}{R_{12}'}\cdot\frac{\partial w_3}{\partial z_1}+\frac{P_2}{K}=0, \quad (2.26)$$

$$\nabla^2\cdot\nabla w_3-\frac{K}{D}\cdot\left[\left(\frac{1}{R_{11}'}+\nu\cdot\frac{1}{R_{22}'}\right)\cdot\frac{\partial w_1}{\partial z_1}\right.$$
$$-\left(\frac{1}{R_{22}'}+\nu\cdot\frac{1}{R_{11}'}\right)\cdot\frac{\partial w_2}{\partial z_2}-(1-\nu)\cdot\frac{1}{R_{12}'}\cdot\left(\frac{\partial w_1}{\partial z_2}+\frac{\partial w_2}{\partial z_1}\right)\cdot$$
$$\left.+\left(\frac{1}{R_{11}'^2}+2\cdot\nu\cdot\frac{1}{R_{11}'\cdot R_{22}'}+\frac{1}{R_{22}'^2}+2\cdot(1-\nu)\cdot\frac{1}{R_{12}'^2}\right)\cdot w_3\right]-\frac{P_3}{D}=0, \quad (2.27)$$

where $\nabla^2=\frac{\partial^2}{\partial z_1^2}+\frac{\partial^2}{\partial z_2^2}$. The remainder of this thesis is concerned with the solution of these equations.

CHAPTER THREE

BOUNDARY DIFFERENTIAL SYSTEM

The general bending extension of a curved rod with rectangular cross-section under the action of applied loading and moments is developed. The procedure used in this chapter is similar to that employed in chapter 2 for the bending of thin shells.

3.1 ASSUMPTIONS

With reference to the right handed system y_k of figure 3.1(a), the coordinate curve y_1 is defined to generate a smooth spatial line, which together with y_2 and y_3 form a mutually orthogonal moving trihedron. A rectangular plane, not necessarily uniform, is then moved such that its centre of gravity is everywhere colinear with the y_1 axis, and the plane lies in such a way that the principal axes of inertia are at all points coincident with the y_k , ($k = 2,3$) axes. The assumptions of section 2.1, modified, are that:

1. Kirchoff's assumptions hold true for bending about both y_k , ($k = 2,3$) axes.

2. The material is isotropic and obeys linear stress-strain laws.

Also, it is further assumed:

3. That torsional distortions in no way effect the assumptions made in 1 above.

3.2 EQUILIBRIUM

Using the notation of figure 3.1 and denoting the edge member cross-sectional area by A, the following force and moment equilibrium equations along and about the y_k axes can be derived:

$$\frac{dN_1}{dy_1} + \frac{N_1}{A}\frac{dA}{dy_1} - \frac{Q_3}{R_3'} - \frac{Q_2}{R_2'} + H_1 = 0, \qquad (3.1)$$

$$\frac{dQ_2}{dy_1} + \frac{Q_2}{A}\frac{dA}{dy_1} + \frac{N_1}{R_2'} - \frac{Q_3}{R_1'} + H_2 = 0, \qquad (3.2)$$

$$\frac{dQ_3}{dy_1} + \frac{Q_3}{A}\frac{dA}{dy_1} + \frac{Q_2}{R_1'} + \frac{N_1}{R_3'} + H_3 = 0, \qquad (3.3)$$

$$\frac{dM_1}{dy_1} + \frac{M_1}{A}\frac{dA}{dy_1} - \frac{M_3}{R_3'} - \frac{M_2}{R_2'} + K_1 = 0, \qquad (3.4)$$

$$\frac{dM_2}{dy_1} + \frac{M_2}{A}\frac{dA}{dy_1} + \frac{M_1}{R_2'} - \frac{M_3}{R_1'} - Q_3 + K_2 = 0, \qquad (3.5)$$

$$\frac{dM_3}{dy_1} + \frac{M_3}{A}\frac{dA}{dy_1} + \frac{M_1}{R_3'} + \frac{M_2}{R_1'} + Q_2 + K_3 = 0, \qquad (3.6)$$

where H_k and K_k are applied forces and moments per unit length along and about the y_k axes. Positive directions of the edge member moments M_k, direct force N_1 and shear forces Q_k, ($k = 2,3$), are shown in figure 3.1(b). The $\frac{1}{R_3'}$ and

and $\frac{1}{R_2'}$ refer to the deformed curvatures of the member in the (y_1, y_3) plane and (y_1, y_2) plane respectively, while $\frac{1}{R_1'}$ represents the twist of the deformed member along the y_1 axis.

3.3 FORCE AND MOMENT RESULTANTS IN TERMS OF DISPLACEMENT COMPONENTS

Where the displacement components v_k represent the displacements of the member centroidal axis in the component direction y_k, the force resultant N_1, and the moment resultants M_k, are expressed in terms of the displacement components v_k as follows:

$$N_1 = + E_b A \left(\frac{dv_1}{dy_1} - \frac{v_2}{R_2'} - \frac{v_3}{R_3'} \right), \tag{3.7}$$

$$M_1 = + E_b I_1 \left(\frac{d^2 v_3}{dy_1 dy_2} \right), \tag{3.8}$$

$$M_2 = - E_b I_2 \left(\frac{d^2 v_3}{dy_1^2} + \frac{d}{dy_1} \left(\frac{v_1}{R_3'} \right) \right), \tag{3.9}$$

$$M_3 = + E_b I_3 \left(\frac{d^2 v_2}{dy_1^2} + \frac{d}{dy_1} \left(\frac{v_1}{R_2'} \right) \right). \tag{3.10}$$

By substitution of equations (3.8) to (3.10) into (3.5) and (3.6) above, expressions for Q_2 and Q_3 may be obtained. In the above, the I_k refer to the moments of inertia of the section about each of the y_k axes.

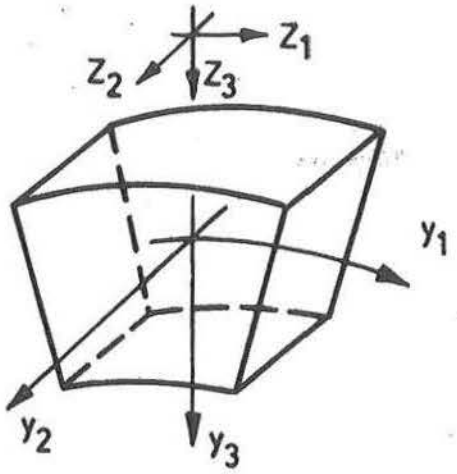

(a) Positive directions of beam axes.

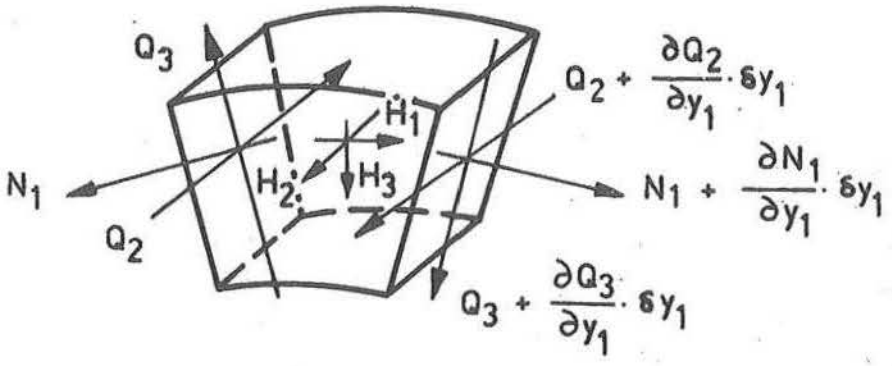

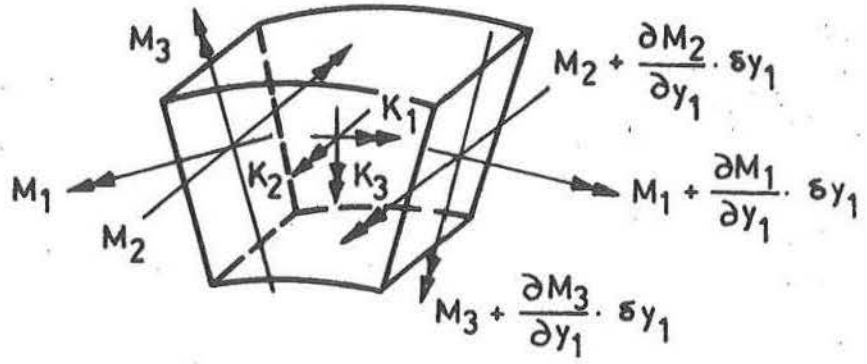

Fig. 3.1 (b) Positive directions of beam internal actions.

3.4 THIN ELASTIC EDGE MEMBER DIFFERENTIAL EQUATIONS

By substitution of equations (3.7) to (3.10) into the equilibrium equations (3.1) to (3.4) it is possible to develop the general edge member shell interaction equations. Four equations with dependent variables v_k and $\frac{dv_3}{dy_2}$ will result in terms of applied internal shell stress and moment resultants as the loading. For reasons similar to those of section 2.4 this substitution is not attempted, but instead, a number of further simplifications are carried out in order that the resulting boundary conditions be consistent with the equations (2.25) to (2.27).

3.5 THIN SHALLOW ELASTIC EDGE MEMBER DIFFERENTIAL EQUATIONS

Before considering the simplifications made due to the concept of shallowness, the restrictive class of boundary geometry considered is given. The work described is limited to shells of rectangular plan-form. Thus, by suitable choice of the z_k ($k = 1,2$) axes, described in section 2.5, the projections of constant z_1 or z_2 are made colinear or parallel to the y_1 or y_2 axes (see figure 3.1(a)). The assumption of rectangular plan-form also implies that $\frac{1}{R_2} = 0$.

Assumptions 1, 2 and 4 of section 2.5 are assumed to apply to the line geometry of the edge member centre line. However, in this case the third assumption, concerning the predominance of membrane force over bending force, is not made.

As a further simplifying assumption, the edge member cross-sectional area A is assumed to vary sufficiently gradually for its first derivative with respect to y_1 to be negligible. The derivatives of v_k with respect to y_1 are replaced by derivations of w_k with respect to z_1 - implying that the edge member is positioned at z_2 constant with the shell lying on side with z_2 increasing. In this case equations (3.1) to (3.6) reduce to:

$$\frac{dN_1}{dz_1} - \frac{Q_3}{R_3} + H_1 = 0 , \qquad (3.11)$$

$$\frac{dQ_2}{dz_1} - \frac{Q_3}{R_1} + H_2 = 0 , \qquad (3.12)$$

$$\frac{dQ_3}{dz_1} + \frac{N_1}{R_3} + \frac{Q_2}{R_1} + H_3 = 0 , \qquad (3.13)$$

$$\frac{dM_1}{dz_1} - \frac{M_3}{R_3} + K_1 = 0 , \qquad (3.14)$$

$$\frac{dM_2}{dz_1} - \frac{M_3}{R_1} - Q_3 + K_2 = 0 , \qquad (3.15)$$

$$\frac{dM_3}{dz_1} + \frac{M_1}{R_3} + \frac{M_2}{R_1} + Q_2 + K_3 = 0 , \qquad (3.16)$$

while equations (3.7) to (3.10) become:

$$N_1 = + E_b A \left(\frac{dw_1}{dz_1} - \frac{w_3}{R_3} \right)_b , \qquad (3.17)$$

$$M_1 = + E_b I_1 \left(\frac{d^2 w_3}{dz_1 dz_2} \right)_b , \qquad (3.18)$$

$$M_2 = -E_b \cdot I_2 \cdot \left(\frac{d^2 w_3}{dz_1^2} + \frac{1}{R_3} \cdot \frac{dw_1}{dz_1} \right)_b , \qquad (3.19)$$

$$M_3 = +E_b \cdot I_3 \cdot \left(\frac{d^2 w_2}{dz_1^2} \right)_b . \qquad (3.20)$$

The subscript b is used to denote the actions and displacements computed at the edge member centroidal axis, in order that they be distinguished from the actions and displacements computed at the shell mid-surface.

The elimination of Q_2 and Q_3 in equations (3.11) to (3.13) using equations (3.15) and (3.16), substitution of (3.17) to (3.20) and neglect of second order terms, reduce the general edge member equations (3.11) to (3.14) to

$$+ E_b \cdot A \cdot \left(\frac{d^2 w_1}{dz_1^2} - \frac{1}{R_3} \cdot \frac{dw_3}{dz_1} \right)_b + \frac{1}{R_3} \cdot E_b I_2 \cdot \left(\frac{d^3 w_3}{dz_1^3} \right)_b + H_1 - \frac{1}{R_3} \cdot K_2 = 0 , \qquad (3.21)$$

$$- E_b \cdot I_3 \cdot \left(\frac{d^4 w_2}{dz_1^4} \right)_b - \frac{1}{R_3} \cdot E_b I_1 \cdot \left(\frac{d^3 w_3}{dz_1^2 dz_2} \right)_b + 2 \cdot \frac{1}{R_1} \cdot E_b I_2 \left(\frac{d^3 w_3}{dz_1^3} \right)_b + H_2 - \frac{dK_3}{dz_1} - \frac{1}{R_1} \cdot K_2 = 0 , \qquad (3.22)$$

$$- E_b \cdot I_2 \cdot \left(\frac{d^4 w_3}{dz_1^4} + \frac{1}{R_3} \cdot \frac{d^3 w_1}{dz_1^3} \right)_b + \frac{1}{R_3} \cdot E_b A \cdot \left(\frac{dw_1}{dz_1} \right)_b - 2 \cdot \frac{1}{R_1} \cdot E_b I_3 \cdot \left(\frac{d^3 w_2}{dz_1^3} \right)_b + H_3 + \frac{dK_2}{dz_1} - \frac{1}{R_1} \cdot K_3 = 0 , \qquad (3.23)$$

$$+ E_b I_1 \left(\frac{d^3 w_3}{dz_1^2 dz_2}\right)_b - \frac{1}{R_3} E_b I_3 \left(\frac{d^2 w_2}{dz_1^2}\right) + K_1 = 0 , \quad (3.24)$$

It is noted that the $\frac{1}{R_3}$ and $\frac{1}{R_1}$ refer to the original edge member curvature and twist respectively. It is assumed that the edge member, which is normally considerably stiffer than the shell, is less likely to behave in a non linear manner. Further simplifications of these equations are made in subsequent chapters.

3.6 EDGE MEMBER LOADING

In sections 3.1 to 3.5 the general edge member behaviour in terms of applied loading H_k and moments K_k per unit length, were developed. It remains to estimate H_k and K_k in terms of applied internal shell actions. Figure 3.2 shows these actions and the positive convention for eccentricity of shell-edge member intersection and the angle ϕ. More general loading could be developed if it were considered that the edge beam lay at the intersection of two shells, and that loading components were from both faces. Extension to multishells would therefore follow a similar pattern. With the orientation of y_k and z_k axes shown, the following equilibrium equations can be developed.

$$H_1 = G_1 + n_{21} , \quad (3.25)$$

$$H_2 = G_2 + n_{22} \cdot \cos\phi - q_{22} \cdot \sin\phi , \quad (3.26)$$

$$H_3 = G_3 + q_{22} \cdot \cos\phi + n_{22} \cdot \sin\phi , \quad (3.27)$$

$$K_1 = m_{22} + q_{22}\cdot(e_2\cdot\cos\phi + e_3\cdot\sin\phi) + n_{22}\cdot(e_2\cdot\sin\phi - e_3\cdot\cos\phi), \tag{3.28}$$

$$K_2 = m_{21}\cdot\cos\phi - e_3\cdot n_{21}, \tag{3.29}$$

$$K_3 = m_{21}\cdot\sin\phi - e_2\cdot n_{21}, \tag{3.30}$$

which, on neglect of second orders and substitution of equations (2.19) to (2.24), become:

$$H_1 = G_1 + K\cdot\left(\frac{1-N}{2}\right)\cdot\left(\frac{\partial w_1}{\partial z_2} + \frac{\partial w_2}{\partial z_1} - 2\cdot\frac{w_3}{R'_{12}}\right)_S, \tag{3.31}$$

$$H_2 = G_2 + K\cdot\left(\frac{\partial w_2}{\partial z_2} + \mu\cdot\frac{\partial w_1}{\partial z_1} - \frac{w_3}{R'_{11}} - \mu\cdot\frac{w_3}{R'_{22}}\right)_S\cdot\cos\phi + D\cdot\left(\frac{\partial^3 w_3}{\partial z_2^3} + \frac{\partial^3 w_3}{\partial z_2\,\partial z_1^2}\right)_S\cdot\sin\phi, \tag{3.32}$$

$$H_3 = G_3 + K\cdot\left(\frac{\partial w_2}{\partial z_2} + \mu\cdot\frac{\partial w_1}{\partial z_1} - \frac{w_3}{R'_{22}} - \mu\,\frac{w_3}{R'_{11}}\right)_S\cdot\sin\phi - D\cdot\left(\frac{\partial^3 w_3}{\partial z_2^3} + \frac{\partial^3 w_3}{\partial z_2\,\partial z_1^2}\right)_S\cdot\cos\phi, \tag{3.33}$$

$$K_1 = +D\cdot\left(\frac{\partial^2 w_3}{\partial z_2^2} + \mu\cdot\frac{\partial^2 w_3}{\partial z_1^2}\right)_S - D\cdot\left(\frac{\partial^3 w_3}{\partial z_2^3} + \frac{\partial^3 w_3}{\partial z_2\,\partial z_1^2}\right)_S\cdot(e_2\cdot\cos\phi + e_3\cdot\sin\phi) - K\cdot\left(\frac{\partial w_2}{\partial z_2} + \mu\cdot\frac{\partial w_1}{\partial z_1} - \frac{w_3}{R'_{22}} - \mu\cdot\frac{w_3}{R'_{11}}\right)_S\cdot(e_2\cdot\sin\phi - e_3\cdot\cos\phi), \tag{3.34}$$

$$K_2 = -D\cdot(1-\nu)\cdot\left(\frac{\partial^2 w_3}{\partial z_1 \partial z_2}\right)_s \cdot \cos\phi + K\cdot\left(\frac{1-\nu}{2}\right)\cdot\left(\frac{\partial w_1}{\partial z_2} + \frac{\partial w_2}{\partial z_1} - 2\cdot\frac{w_3}{R'_{12}}\right)_s \cdot a_3 , \qquad (3.35)$$

$$K_3 = -D\cdot(1-\nu)\cdot\left(\frac{\partial^2 w_3}{\partial z_1 \partial z_2}\right)_s \cdot \sin\phi - K\cdot\left(\frac{1-\nu}{2}\right)\cdot\left(\frac{\partial w_1}{\partial z_2} + \frac{\partial w_2}{\partial z_1} - 2\cdot\frac{w_3}{R'_{12}}\right)_s \cdot a_2 . \qquad (3.36)$$

The subscript s refers to shell actions and displacements computed at the shell-edge member intersection, while G_k refer to the components of edge member line load in the coordinate directions z_k .

These expressions when used in conjunction with the equations (3.21) to (3.24) represent the general shallow edge member - shell interaction equations. In section 8.4, the significance of a number of these terms is assessed, and terms are retained whose significance are of the same order as the expected numerical accuracy of the discretised problem.

In the above, the edge beam was considered loaded with the resultants of internal shell actions at the edge member-shell intersection. If the equations (3.21) to (3.24) are viewed as expressing the resultant loads H_k and moments K_k

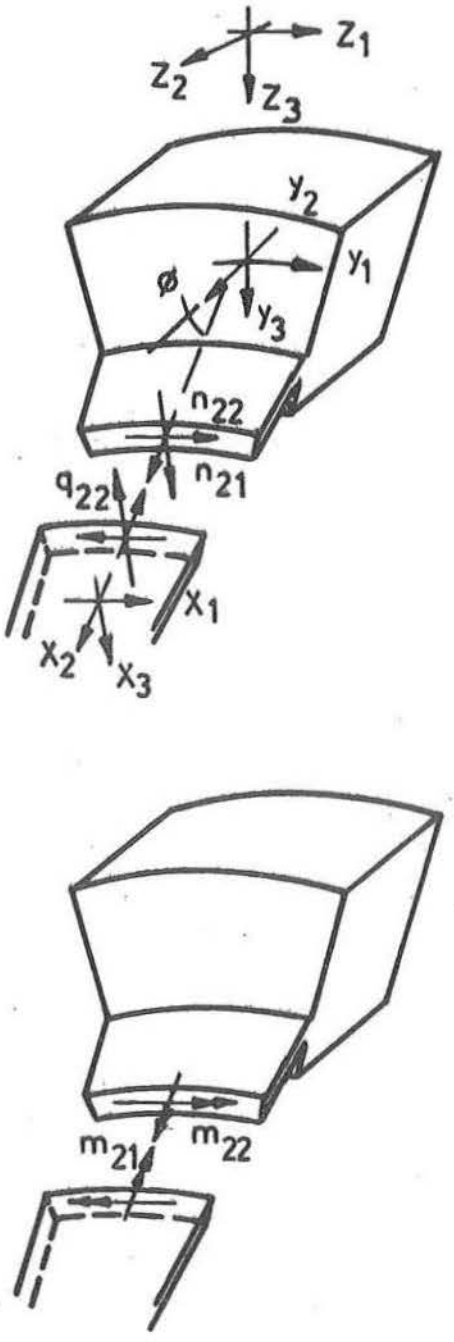

Fig. 3.2 Positive directions of shell internal actions at edge support, and edge beam orientation.

resulting from the beam internal actions, then the equations (3.21) to (3.24) represent the shell edge loaded with the resultants of internal beam actions. It is shown in section 8.2 that this difference in approach corresponds in the first instance to the displacement boundary, while the second refers to the traction boundary condition.

3.7 CORNER CONDITIONS

In the case of the edge member described in the above, the shell corner conditions may be reduced to the boundary conditions of the edge member, and therefore require at all corners the satisfaction of four conditions in each of the coordinate directions z_k , (k = 1,2). Although it is possible to formulate corner conditions assuming a column of finite flexibility in all modes, this is not examined in the present text. Instead, the degenerate cases of clamped, simple and free corners in each of the support modes are developed. These conditions are considered as required in the proceeding chapters. The boundary, corner conditions, loading and shell are considered symmetric about the diagonals joining opposite corners.

CHAPTER FOUR

SHELL DIFFERENCE SYSTEM

After a brief review of pertinent difference equations, the thin shallow shell equations (2.25) to (2.27) and their corresponding stress and moment resultants (2.19) to (2.24), are expressed in conventional finite difference form, and the equations for the ruled surface hyperbolic paraboloid are given as a special case. For this class of shell, the modified finite difference presentation with associated stress resultants is also given.

4.1 BASIC DIFFERENCE FORMULAE

In this section the difference patterns for the derivatives up to order 4, of the dependent variables w_k, are given with truncation errors of the order (h^2), where h is the largest of h_1 and h_2, which are the grid spacings in the z_1 and z_2 coordinate directions.

The subscript i refers to the i th row of the difference grid parallel to the z_1 axis, the subscript j refers to the j th column of the difference grid parallel to the z_2 axis, while the set of points defined by the intersection of the i th row and j th column termed pivotal or nodal positions, is denoted (i,j). In what follows the group subscript k is replaced by

a similar superscript. This notation change is carried out for convenience of presentation, as well as implying that w_{ij}^{k} denotes the discretised value of the analytic function w_k at the pivotal position (i,j). In this case

$$w_{ij}^{k} \doteq w_{k_{ij}},$$

and where the meaning is obvious, the grid subscripts are dropped and the above becomes

$$w^{k} \doteq w_k .$$

The difference between w_k and w^k, known as the truncation error, is further considered in chapter 7. Derivatives are given at the nodal positions (i,j). These formulae may be found in any text on numerical analysis [49,53]. One dimensional derivatives with respect to z_1 are given

$$\left(\frac{\partial w_k}{\partial z_1}\right)_{ij} = \frac{1}{2h_1}\cdot\left(w_{ij+1}^{k} - w_{ij-1}^{k}\right) + O(h_1^2), \tag{4.1}$$

$$\left(\frac{\partial^2 w_k}{\partial z_1^2}\right)_{ij} = \frac{1}{h_1^2}\cdot\left(w_{ij+1}^{k} - 2\cdot w_{ij}^{k} + w_{ij-1}^{k}\right) + O(h_1^2), \tag{4.2}$$

$$\left(\frac{\partial^3 w_k}{\partial z_1^3}\right)_{ij} = \frac{1}{2h_1^3}\cdot\left(w_{ij+2}^{k} - 2\cdot\left(w_{ij+1}^{k} - w_{ij-1}^{k}\right) - w_{ij-2}^{k}\right) + O(h_1^2), \tag{4.3}$$

$$\left(\frac{\partial^4 w_k}{\partial z_1^4}\right)_{ij} = \frac{1}{h_1^4}\cdot\left(w_{ij+2}^{k} - 4\cdot w_{ij+1}^{k} + 6w_{ij}^{k} - 4\cdot w_{ij-1}^{k} + w_{ij-2}^{k}\right) + O(h_1^2), \tag{4.4}$$

with similar expressions given for derivatives with respect to z_2. Two dimensional derivatives with respect to (z_1,z_2) are given by

$$\left(\frac{\partial^2 w_k}{\partial z_1 \partial z_2}\right)_{ij} = \frac{1}{4 \cdot h_1 \cdot h_2} \left(w^k_{i+1j+1} + w^k_{i+1j-1} - w^k_{i-1j+1} + w^k_{i-1j-1} \right) + O(h^2) , \qquad (4.5)$$

$$\left(\frac{\partial^3 w_k}{\partial z_1 \partial z_2^2}\right)_{ij} = \frac{1}{2 \cdot h_1 \cdot h_2^2} \left(w^k_{i+1j+1} - 2 \cdot w^k_{ij+1} + w^k_{i-1j+1} - w^k_{i+1j-1} + 2 \cdot w^k_{ij-1} - w^k_{i-1j-1} \right) + O(h^2) , \qquad (4.6)$$

$$\left(\frac{\partial^3 w_k}{\partial z_1^2 \partial z_2}\right)_{ij} = \frac{1}{2 \cdot h_1^2 h_2} \left(w^k_{i+1j+1} - 2 \cdot w^k_{i+1j} + w^k_{i+1j-1} - w^k_{i-1j+1} + 2 \cdot w^k_{i-1j} - w^k_{i-1j-1} \right) + O(h^2) , \qquad (4.7)$$

$$\left(\frac{\partial^4 w_k}{\partial z_1^2 \partial z_2^2}\right)_{ij} = \frac{1}{h_1^2 \cdot h_2^2} \left(w^k_{i+1j+1} - 2 \cdot w^k_{i+1j} + w^k_{i+1j-1} - 2 \cdot \left(w^k_{ij+1} - 2 \cdot w^k_{ij} + w^k_{ij-1} \right) + w^k_{i-1j+1} - 2 \cdot w^k_{i-1j} + w^k_{i-1j-1} \right) + O(h^2) . \qquad (4.8)$$

4.2 THE THIN ELASTIC SHALLOW SHELL DIFFERENCE SYSTEM

Difference patterns are presented schematically in the form of computation molecules, with the nodal position (i,j) defined by ⊗. The z_2 axis is considered increasing from the top to the bottom of the page, while z_1 from left to right. Substitution of the difference quotients forms above, into the shallow shell equations given by (2.25) to (2.27), result in

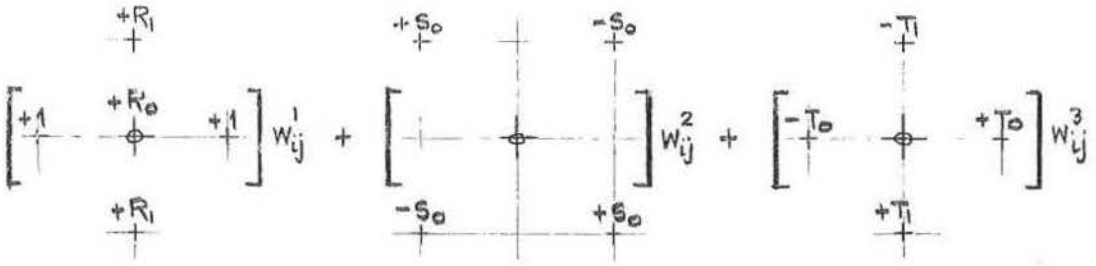

$$+ P^1_{ij} \cdot \frac{h_1^2}{K} = 0, \quad (4.9)$$

Equilibrium in z_1 direction.

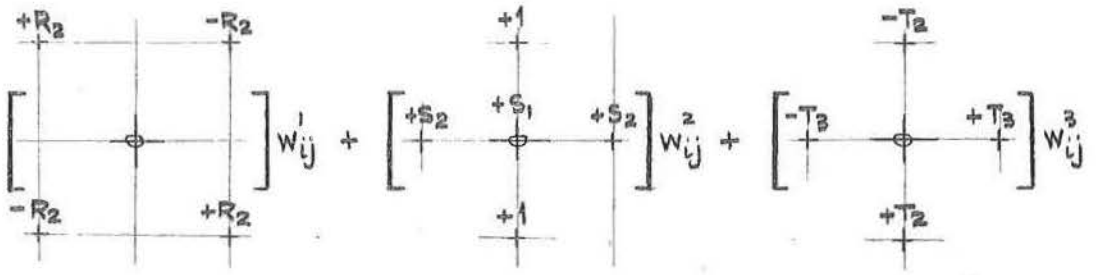

$$+ P^2_{ij} \cdot \frac{h_2^2}{K} = 0, \quad (4.10)$$

Equilibrium in z_2 direction.

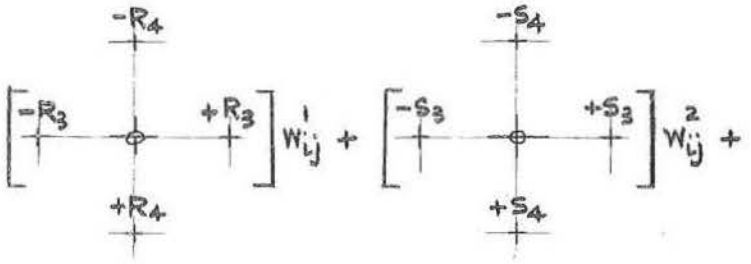

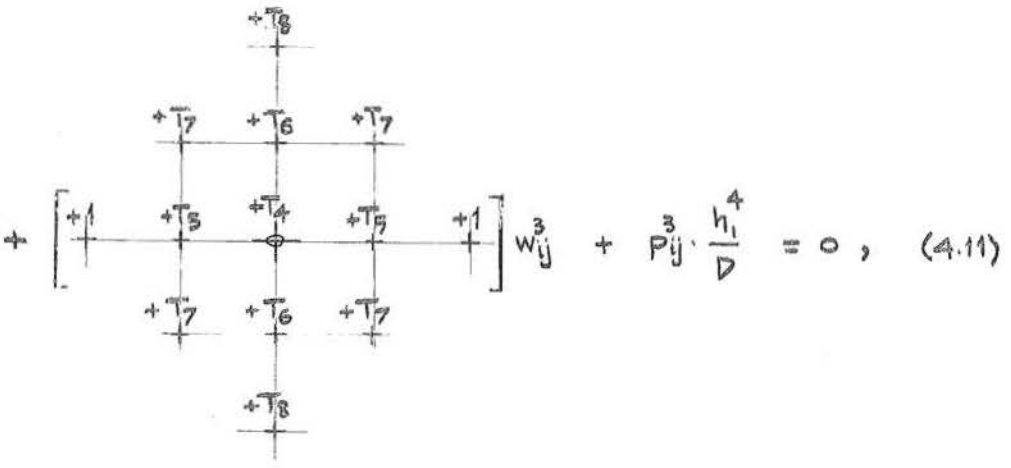

$$w_{ij}^3 + P_{ij}^3 \cdot \frac{h_1^4}{D} = 0 , \qquad (4.11)$$

Equilibrium in z_3 direction.

while the corresponding stress resultants and couples (2.19) to (2.24) are given as

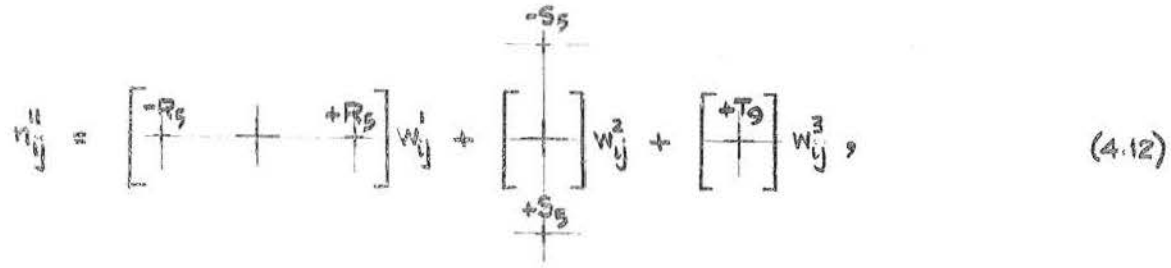

(4.12)

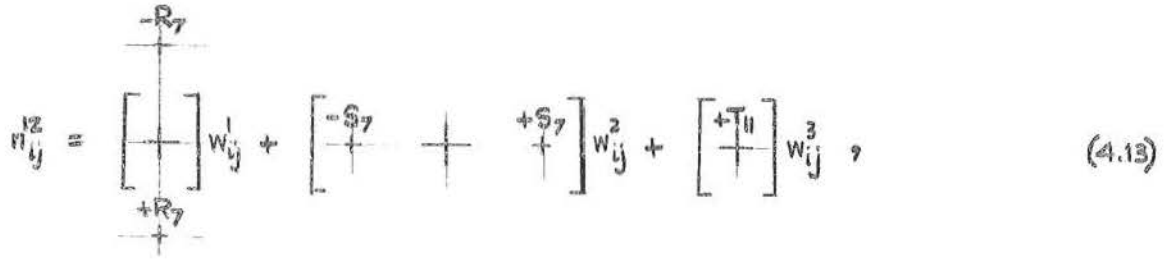

(4.13)

$$m_{ij}^{22} = \left[-R_6 \quad +R_6 \right] W_{ij}^{1} + \left[\begin{matrix} -S_6 \\ \\ +S_6 \end{matrix} \right] W_{ij}^{2} + \left[+T_{10} \right] W_{ij}^{3}, \qquad (4.14)$$

$$m_{ij}^{11} = \left[\begin{matrix} & +T_{14} & \\ +T_{13} & +T_{12} & +T_{13} \\ & +T_{14} & \end{matrix} \right] W_{ij}^{3}, \qquad (4.15)$$

$$m_{ij}^{22} = \left[\begin{matrix} & +T_{17} & \\ +T_{16} & +T_{15} & +T_{16} \\ & +T_{17} & \end{matrix} \right] W_{ij}^{3}, \qquad (4.16)$$

$$m_{ij}^{12} = \left[\begin{matrix} +T_{18} & & -T_{18} \\ & & \\ -T_{18} & & +T_{18} \end{matrix} \right] W_{ij}^{3}. \qquad (4.17)$$

The coefficients (R_k, S_k), (k = 0,7) and T_k , (k = 0,18) used in the equations (4.9) to (4.17) are given in table 4.1.

R_0	$-2.(1.+R_1)$	T_2	$-(\frac{1.}{R'_{22}}+\mu.\frac{1.}{R'_{11}}).\frac{h_2}{2.}$
R_1	$+\rho^2.\frac{(1.-\mu)}{2.}$	T_3	$-\frac{1.}{\rho}.(1.-\mu).\frac{1.}{R'_{12}}.\frac{h_2}{2.}$
R_2	$+\frac{1.}{\rho}.\frac{(1.+\mu)}{8.}$	T_4	$+\frac{12.}{t_s^3}.h_1^4.(\frac{1.}{R'^2_{11}}+2.\mu.\frac{1.}{R_{11}R_{22}}+\frac{1.}{R'^2_{22}}$
R_3	$-\frac{6}{t_s^2}.h_1^3.(\frac{1}{R'_{11}}+\mu.\frac{1}{R'_{22}})$		$+2.(1.-\mu)\frac{1.}{R'^2_{12}})+6.\rho^4+8.\rho^2+6.$
R_4	$-\rho.\frac{6}{t_s^2}.h_1^3.(1.-\mu).\frac{1}{R'_{12}}$	T_5	$-4.(1.+\rho^2)$
R_5	$+K.\frac{1}{2.h_1}$	T_6	$+\rho^2.T_5$
R_6	$+\mu.R_5$	T_7	$+2.\rho^2$
R_7	$+K.\frac{1}{2.h_2}.\frac{(1.-\mu)}{2.}$	T_8	$+\rho^4$
S_0	$+\rho.\frac{(1.+\mu)}{8.}$	T_9	$-(\frac{1.}{R'_{11}}+\mu.\frac{1.}{R'_{22}})$
S_1	$-2.(1.+S_2)$	T_{10}	$-(\frac{1.}{R'_{22}}+\mu.\frac{1.}{R'_{11}})$
S_2	$+\frac{1.}{\rho^2}.\frac{(1.-\mu)}{2.}$	T_{11}	$-K.(1.-\mu).\frac{1.}{R'_{12}}$
S_3	$-\frac{6}{t_s^2}.h_1^3.(1.-\mu).\frac{1.}{R'_{12}}$	T_{12}	$-2.(T_{13}+T_{14})$
S_4	$-\rho.\frac{6}{t_s^2}.h_1^3.(\frac{1}{R'_{22}}+\mu.\frac{1}{R'_{11}})$	T_{13}	$-D.\frac{1.}{h_1^2}$
S_5	$+\mu.K.\frac{1.}{2.h_2}$	T_{14}	$-\mu.D.\frac{1.}{h_2^2}$
S_6	$+\frac{1}{\mu}.S_5$	T_{15}	$-2.(T_{16}+T_{17})$
S_7	$+K.\frac{1.}{2.h_1}.\frac{(1.-\mu)}{2.}$	T_{16}	$+\mu.T_{13}$
T_0	$-(\frac{1.}{R'_{11}}+\mu.\frac{1.}{R'_{22}}).\frac{h_1}{2}$	T_{17}	$+\frac{1.}{\mu}.T_{14}$
T_1	$-\rho.(1.-\mu).\frac{1.}{R'_{12}}.\frac{h_1}{2.}$	T_{18}	$+D.(1.-\mu).\frac{1.}{4.h_1h_2}$

TABLE 4.1 Coefficients R_k, S_k and T_k required for the shallow shell difference analogue of section 4.2, $\rho = \frac{h_1}{h_2}$.

Equations (4.9) to (4.11) represent the conventional difference analogues of the general thin shallow shell equations, while (4.12) to (4.17) define the associated stress resultants and stress couples. A number of specialised forms of these equations have been given previously (see for example [2,43]).

4.3 THE RULED SURFACE HYPERBOLIC PARABOLOID

As the remainder of this thesis is concerned primarily with the analysis of ruled surface hyperbolic parabolid shells, the specialised difference equations for this particular shell class are given.

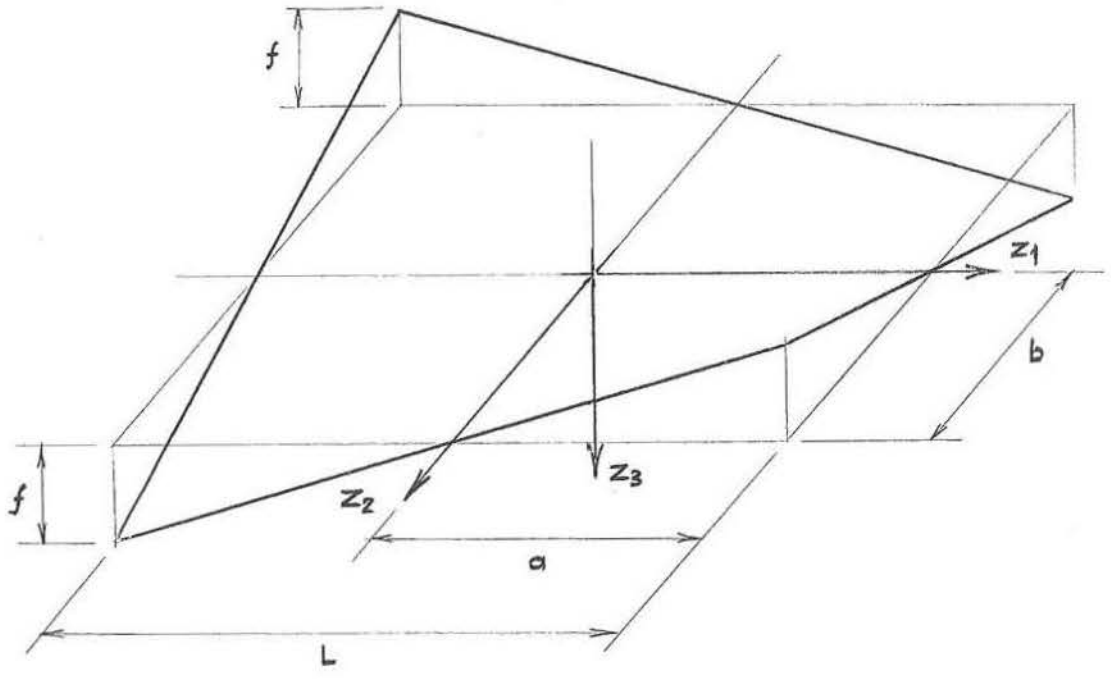

Fig. 4.1 Orientation of z_k axes and notation used for the ruled surface hyperbolic paraboloid.

If the z_1 and z_2 axes are orientated as in figure 4.1, the mid-surface of this shell is represented by

$$z_3 = -\frac{f}{ab} \cdot z_1 z_2 . \qquad (4.18)$$

Using assumption 1 of section 2.5, and considering the shell to behave in a linear manner (that is linear in the sense that the curvatures remain constant and equal to those of the undeformed shell), the R'_{kl}, (k,l = 1,2) terms may be replaced by R_{kl} , (k,l = 1,2) values, which for the ruled surface hyperbolic paraboloid become

$$\frac{1.}{R_{11}} = \frac{1.}{R_{22}} = 0. \quad , \quad \frac{1.}{R_{12}} = -\frac{f}{a.b} .$$

It is further assumed that

$$\frac{a}{b} = 1. \quad , \quad \beta = 1. \quad ,$$

which, although restricting the generality of the programmes developed, in no way effects the objectives of section 1.2.

4.3.1 Conventional Finite Differene Analogue

The general shell equilibrium difference equations (4.9) to (4.11), where m is given by

$$m = \frac{a}{h} ,$$

reduce to

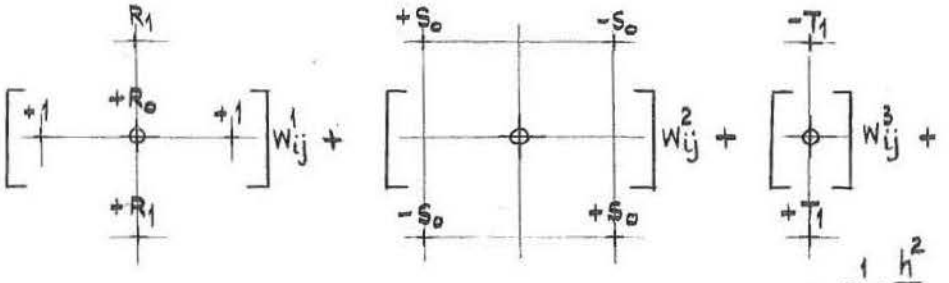

$$+ P^1_{ij} \cdot \frac{h^2}{K} = 0. , \qquad (4.19)$$

Equilibrium in z_1 direction.

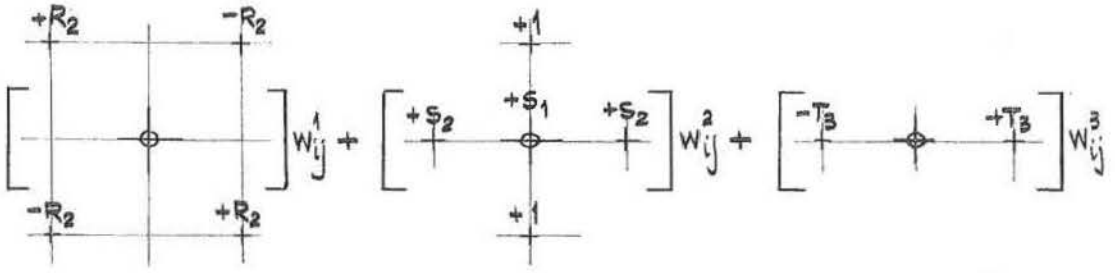

$$+ P^2_{ij} \cdot \frac{h^2}{K} = 0., \quad (4.20)$$

Equilibrium in z_2 direction.

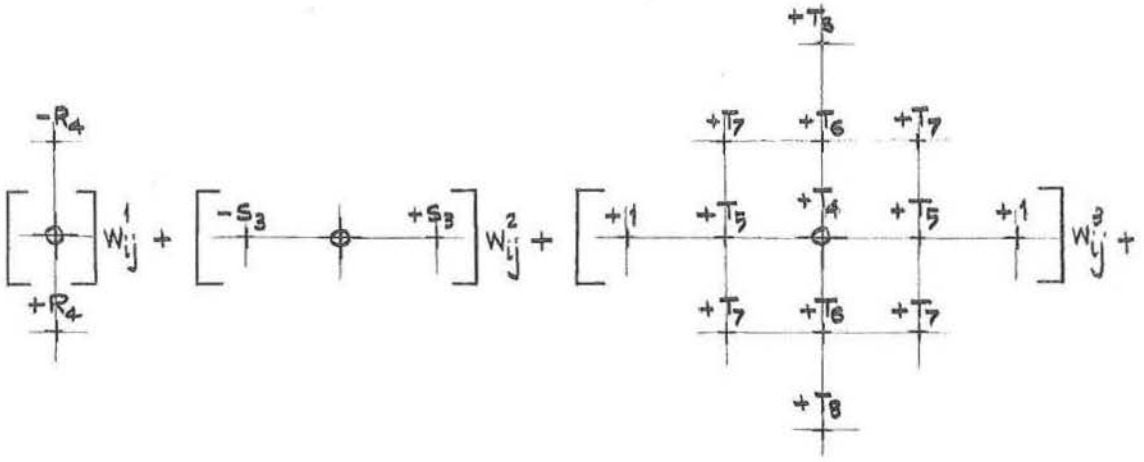

$$+ P^3_{ij} \cdot \frac{h^4}{D} = 0.. \quad (4.21)$$

Equilibrium in z_3 direction.

Associated resultant stresses and couples (4.12) to (4.17) are given as

$$n_{ij}^{11} = \left[\begin{array}{ccc} & & \\ -R_5 & \oplus & +R_5 \\ & & \end{array} \right] w_{ij}^{1} + \left[\begin{array}{c} -S_5 \\ \oplus \\ +S_5 \end{array} \right] w_{ij}^{2} , \qquad (4.22)$$

$$n_{ij}^{12} = \left[\begin{array}{c} -R_7 \\ \oplus \\ +R_7 \end{array} \right] w_{ij}^{1} + \left[\begin{array}{ccc} & & \\ -S_7 & \oplus & +S_7 \\ & & \end{array} \right] w_{ij}^{2} + \left[\begin{array}{c} +T_{11} \\ \oplus \end{array} \right] w_{ij}^{3} , \qquad (4.23)$$

$$n_{ij}^{22} = \left[\begin{array}{ccc} & & \\ -R_6 & \oplus & +R_6 \\ & & \end{array} \right] w_{ij}^{1} + \left[\begin{array}{c} -S_6 \\ \oplus \\ +S_6 \end{array} \right] w_{ij}^{2} , \qquad (4.24)$$

$$m_{ij}^{11} = \left[\begin{array}{ccc} & +T_{14} & \\ +T_{13} & +T_{12} \oplus & +T_{13} \\ & +T_{14} & \end{array} \right] w_{ij}^{3} , \qquad (4.25)$$

$$m_{ij}^{22} = \left[\begin{array}{ccc} & +T_{17} & \\ +T_{16} & T_{15} \oplus & +T_{16} \\ & +T_{17} & \end{array} \right] w_{ij}^{3} , \qquad (4.26)$$

$$m_{ij}^{12} = \left[\begin{array}{ccc} +T_{18} & & -T_{18} \\ & \oplus & \\ -T_{18} & & +T_{18} \end{array} \right] w_{ij}^{3} , \qquad (4.27)$$

with the respective coefficients R_k, S_k and T_k given in table 4.2.

4.3.2 Modified Finite Difference Analogue

The inconsistancy between the conventional finite difference analogues (given in section 4.2), and a similar expression resulting from a variational approach, for the case of the cylindrical shell was first noted by Chuang and Veletsos[16]. A modified analogue was developed in order that this discrepancy be eliminated, and was later extended to the case of the second order translational surface by Noor and Veletsos[43]. In this latter study the advantages of the modified technique over the conventional technique for the case of second order translational shells were conclusively demonstrated, and an extension of the method to ruled surface hyperbolic paraboloids was indicated, although numerical studies were not attempted. Similar comparisons are made in section 7.5 for the ruled surface hyperbolic paraboloid, so that for ease of reference, the modified equations are briefly reviewed.

R_0, S_1	$-2.(1.+R_1)$	T_5, T_6	$-8.$
R_1, S_2	$+\frac{(1.-\mu)}{2.}$	T_7	$+2.$
R_2, S_0	$+\frac{(1.+\mu)}{8.}$	T_8	$+1.$
R_4, S_3	$+\frac{6.(1.-\mu)}{m^3}\cdot\frac{a.f}{t_s^2}$	T_{11}	$+E_s\cdot\frac{1.}{(1.+\mu)}\cdot\frac{f.t_s}{a^2}$
R_5, S_6	$+E_s\cdot\frac{m}{2.(1.-\mu^2)}\cdot\frac{t_s}{a}$	T_{12}, T_{15}	$-2.(T_{13}+T_{14})$
R_6, S_5	$+\mu.R_5$	T_{13}, T_{17}	$-E_s\cdot\frac{m^2}{12.(1.-\mu^2)}\cdot\frac{t_s^3}{a^2}$
R_7, S_7	$+E_s\cdot\frac{m}{4.(1.+\mu)}\cdot\frac{t_s}{a}$	T_{14}, T_{16}	$+\mu.T_{13}$
T_1, T_3	$+\frac{(1.-\mu)}{2.m}\cdot\frac{f}{a}$	T_{18}	$+E_s\cdot\frac{m^2}{48.(1.+\mu)}\cdot\frac{t_s^3}{a^2}$
T_4	$+20.+\frac{24.(1.-\mu)}{m^4}\cdot\frac{f^2}{a^2}$		

TABLE 4.2 Coefficients R_k, S_k and T_k required for the conventional difference analogue of the ruled surface hyperbolic paraboloid, given in section 4.3.1.

R'_0, S'_1	$-2.(1.+R'_1)$	T'_1, T'_3	$+\frac{(1.-\mu)}{m}\cdot\frac{f}{a}$
R'_1, S'_2	$+\frac{(1.-\mu)}{2.}$	T'_4	$+20.+\frac{24.(1.-\mu)}{m^4}\cdot\frac{f^2}{a^2}$
R'_2, S'_0	$+\frac{(1.+\mu)}{2.}$	T'_5, T'_6	$-8.$
R'_4, S'_3	$+\frac{12.(1.-\mu)}{m^3}\frac{a.f}{t_s^2}$	T'_7	$+2.$
R'_5, S'_6	$+E_s\cdot\frac{m}{(1.-\mu^2)}\cdot\frac{t_s}{a}$	T'_8	$+1.$
R'_6, S'_5	$+\mu.R'_5$	T'_{11}	$+E_s\cdot\frac{1.}{(1.+\mu)}\cdot\frac{f.t_s}{a^2}$
R'_7, S'_7	$+E_s\cdot\frac{m}{2.(1.+\mu)}\cdot\frac{t_s}{a}$		

TABLE 4.3 Coefficients R'_k, S'_k and T'_k required for the modified difference analogue of the ruled surface hyperbolic paraboloid, given in section 4.3.2.

A rectangular grid, with i once again denoting the i th grid line parallel to the z_1 axis, and j denoting the j th grid line parallel to the z_2 axis, is superimposed upon the domain of differential dependence. A diagrid (i',j') is also placed upon this domain, in such a way that the i' th row and j' th column are $+ 0.5h$ out of phase with the corresponding i th row and j th column.

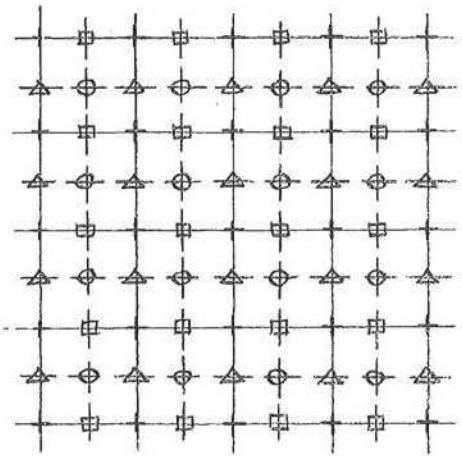

○ Position for the definition of $(n_{ij}^{kk}, m_{ij}^{kl})$, $(k,l = 1,2)$

\+ Position for the definition of n_{ij}^{12}

△ Position for the definition of w_{ij}^{1}

□ Position for the definition of w_{ij}^{2}

\+ Position for the definition of w_{ij}^{3}

Fig. 4.2 Positions for the definition of displacement components and stress and moment resultants.

Discrete values of the dependent variables w_k are now chosen (see figure 4.2), such that w_1 is defined at the intersection of the i' th row and j th column, w_2 at the intersection of the i th row and the j' th column, while w_3 is defined as previously at the intersection of the i th row and the j th column. Employing this pattern of discrete variables it is now possible to write the special forms of each of the z_k equilibrium equations for a molecule centred upon the position of definition of the particular w_k, but with all odd differentials computed with a halved grid size - and therefore corresponding decrease in discretisation error. Similar advantages are seen to hold for the computation of stress resultants.

Assumptions of 4.3.1 are once again made, and for recording if not reading convenience the diagrid inflexion for subscripts is omitted. So that

$$w^1_{i'j} \equiv w^1_{ij},$$

it being tacitly assumed that the discrete variables are defined at positions as indicated above. Equations (2.25) to (2.27) then become schematically:

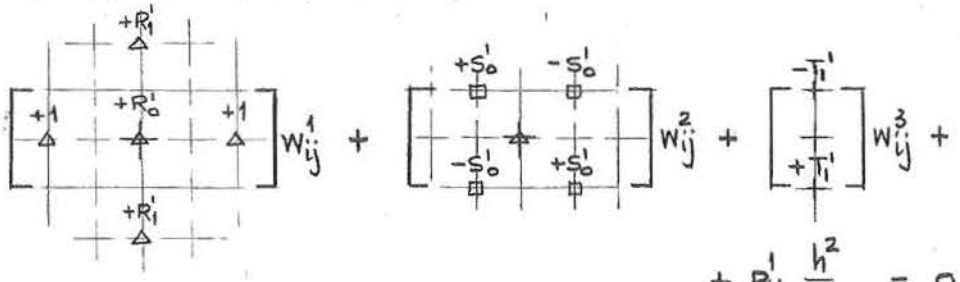

$$+ P^1_{ij} \frac{h^2}{K} = 0., \qquad (4.28)$$

Equilibrium in the z_1 direction.

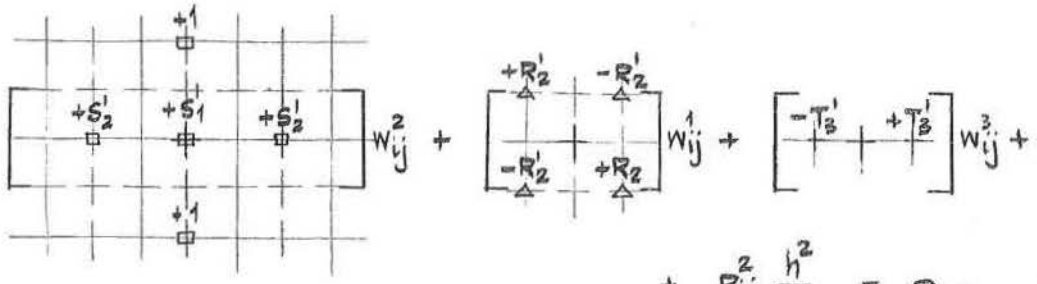

$$+ P^2_{ij}\,\frac{h^2}{K} = 0., \qquad (4.29)$$

Equilibrium in z_2 direction.

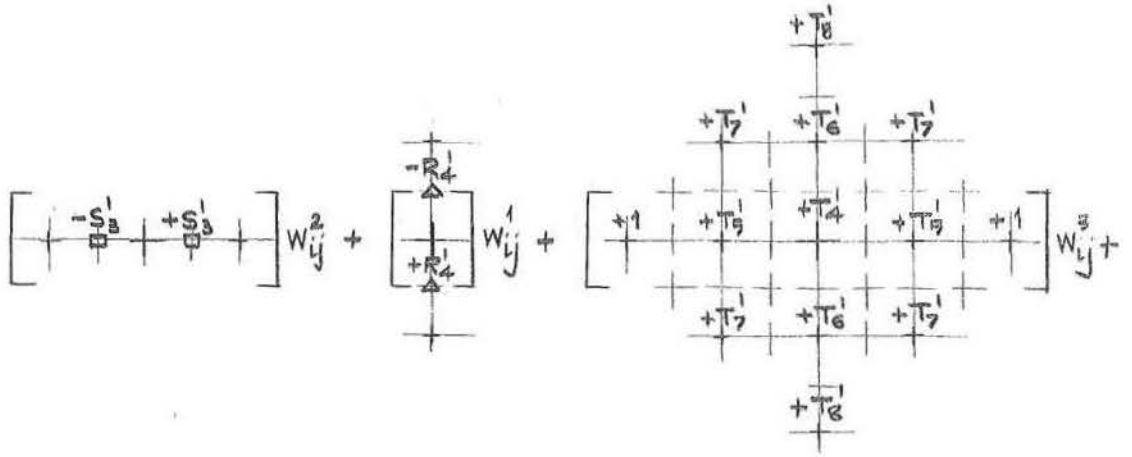

$$+ P^3_{ij}\,\frac{h^4}{D} = 0. . \qquad (4.30)$$

Equilibrium in z_3 direction.

The resultant couples m_{kl}, (k,l = 1,2) are once again given by equation (4.23), while the stress resultants (2.19) to (2.21) become:

$$n_{ij}^{11} = \left[-R_5' \quad +R_5' \right] W_{ij}^{1} + \left[\begin{matrix} -S_5' \\ +S_5' \end{matrix} \right] W_{ij}^{2} , \qquad (4.31)$$

$$n_{ij}^{22} = \left[-R_6' \quad +R_6' \right] W_{ij}^{1} + \left[\begin{matrix} -S_6' \\ +S_6' \end{matrix} \right] W_{ij}^{2} , \qquad (4.32)$$

$$n_{ij}^{12} = \left[\begin{matrix} -R_7' \\ +R_7' \end{matrix} \right] W_{ij}^{1} + \left[-S_7' \quad +S_7' \right] W_{ij}^{2} + \left[+T_{11}' \right] W_{ij}^{3} , \qquad (4.33)$$

with appropriate coefficients R_k' , S_k' and T_k' given in table 4.3. In the above molecules the grid (i,j) is represented with the full line, and the grid (i',j') with the broken lines.

CHAPTER FIVE

BOUNDARY DIFFERENCE SYSTEM

The difference quotients of section 4.1, are used to express the thin shallow elastic edge member equations (3.21) to (3.24), and the edge member loading terms (3.31) to (3.36) in their equivalent discrete form. The transformation between the beam displacements $(w_k)_b$ and the shell displacements $(w_k)_s$ are then given so that in sections 8.3 and 8.4 a number of possible practical combinations of the sets of equations can be considered in detail for the special case of the ruled surface hyperbolic paraboloid.

5.1 THIN SHALLOW ELASTIC EDGE MEMBER DIFFERENCE SYSTEM

In the following the centres of computation molecules (the (b,j) pivotal position) are denoted ⊕ while H_j^k, G_j^k and K_j^k represent the discretised values of H_k, G_k and K_k at the grid positions (b,j). The b and s subscripts are used to represent actions and displacements at the edge member centroidal axis and the edge member shell intersection. Equations (3.21) to (3.24) become

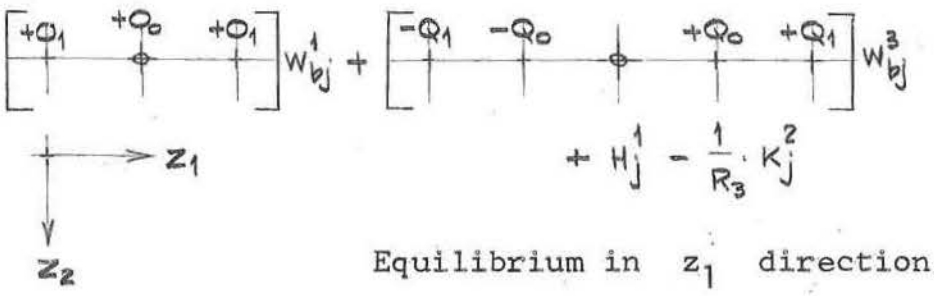

$$+ H_j^1 - \frac{1}{R_3} \cdot K_j^2 = 0., \quad (5.1)$$

Equilibrium in z_1 direction.

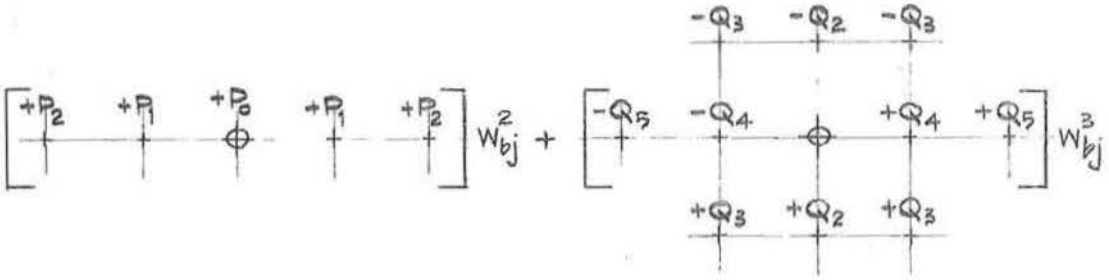

$$+ H_j^2 - \frac{1}{R_1} K_j^2 - \left(\frac{dK_3}{dz_1}\right)_j = 0., \quad (5.2)$$

Equilibrium in z_2 direction.

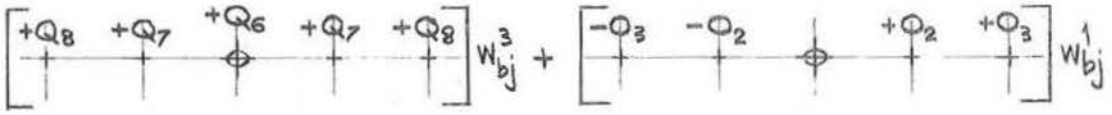

$$W_{bj}^2 + H_j^3 - \frac{1}{R_1} K_j^3 + \left(\frac{dK^2}{dz_1}\right)_j = 0., \quad (5.3)$$

Equilibrium in z_3 direction.

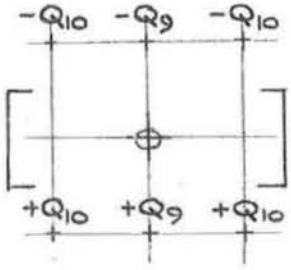

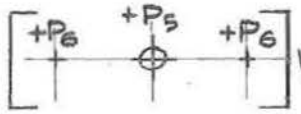

$$W_{bj}^2 + K_j^1 = 0., \quad (5.4)$$

Equilibrium about z_1 axis.

while the beam internal forces and moments (3.17) to (3.20) are written

$$N_j^1 \equiv \left[-Q_4 \quad +Q_4 \right] W_{bj}^1 + \left[Q_{11} \right] W_{bj}^3 , \qquad (5.5)$$

$$M_j^1 \equiv \begin{matrix} +Q_{12} & & -Q_{12} \\ & \left[\quad \right] W_{bj}^3 , & \\ -Q_{12} & & +Q_{12} \end{matrix} \qquad (5.6)$$

$$M_j^2 \equiv \left[+Q_{14} \quad +Q_{13} \quad +Q_{14} \right] W_{bj}^3 + \left[-Q_5 \quad +Q_5 \right] W_{bj}^1 , \qquad (5.7)$$

$$M_j^3 \equiv \left[+P_8 \quad +P_7 \quad +P_8 \right] W_{bj}^2 , \qquad (5.8)$$

with the appropriate coefficients O_k , P_k and Q_k given in table 5.1.

It is noted that the grid line b used in the above presentation, although parallel, is not in general colinear with a mesh line of the set (i,j). This also implies that the $(b \pm 1, j)$ grid positions, required in (5.2), (5.4) and (5.6), necessarily require some form of approximation. Techniques for minimising the effects of these approximations are presented in section 8.3.

O_0	$-2.O_1$	Q_0	$-2.Q_1-\frac{E_b.A}{2.R_3.h_1^3}$
O_1	$+\frac{E_b.A}{h_1^2}$	Q_1	$+\frac{E_b.I_2}{2.R_3.h_1^3}$
O_2	$-2.O_3+\frac{E_b.A}{2.R_3.h_1^3}$	Q_2	$-2.Q_3$
O_3	$-\frac{E_b.I_2}{2.R_3.h_1^3}$	Q_3	$-\frac{E_b.I_1}{2.R_3.h_1^2.h_2}$
O_4	$+\frac{E_b.A}{2.h_1}$	Q_4	$-2.Q_5$
O_5	$-\frac{E_b.I_2}{2.R_3.h_1}$	Q_5	$+\frac{E_b.I_2}{R_1.h_1^3}$
P_0	$+6.P_2$	Q_6	$+6.Q_8$
P_1	$-4.P_2$	Q_7	$-4.Q_8$
P_2	$-\frac{E_b.I_3}{h_1^4}$	Q_8	$-\frac{E_b.I_2}{h_1^4}$
P_3	$-2.P_4$	Q_9	$-2.Q_{10}$
P_4	$-\frac{E_b.I_3}{R_1 h_1^3}$	Q_{10}	$+\frac{E_b.I_1}{2.h_1^2.h_2}$
P_5	$-2.P_6$	Q_{11}	$-\frac{E_b.A}{R_3}$
P_6	$-\frac{E_b.I_3}{R_3.h_1^2}$	Q_{12}	$+\frac{E_b.I_1}{4.h_1.h_2}$
P_7	$-2.P_8$	Q_{13}	$-2.Q_{14}$
P_8	$+\frac{E_b.I_3}{h_1^2}$	Q_{14}	$-\frac{E_b.I_2}{h_1^2}$

TABLE 5.1 Coefficients O_k, P_k and Q_k required for the difference analogue of the thin edge member equations. (section 5.1)

5.2 EDGE MEMBER LOADING

The combinations of load resultants H_k and the moment resultants K_k, developed in section 3.5, when expressed in difference form become:

$$H_j^1 - \frac{1}{R_3} K_j^2 = G_{bj}^1 + \begin{bmatrix} -Q_6 \\ \\ +Q_6 \end{bmatrix} W_{sj}^1 + \begin{bmatrix} -P_9 & & +P_9 \\ +Q_{16} & & -Q_{16} \\ & + & \\ -Q_{16} & & +Q_{16} \end{bmatrix} W_{sj}^2 + W_{sj}^3, \quad (5.9)$$

Equilibrium in z_1 direction.

$$H_j^2 - \frac{1}{R_1} K_j^2 - \left(\frac{dK_3}{dz_1}\right)_j = G_{bj}^2 + \begin{bmatrix} +Q_8 & & -Q_8 \\ -Q_7 & & +Q_7 \\ -Q_8 & & +Q_8 \end{bmatrix} W_{sj}^1 + \begin{bmatrix} & -P_{12} & \\ P_{11} & +P_{10} & +P_{11} \\ & +P_{12} & \end{bmatrix} W_{sj}^2 +$$

$$+ \begin{bmatrix} & -Q_{22} & \\ -Q_{21} & -Q_{20} & -Q_{19} \\ -Q_{18} & +Q_{17} & +Q_{18} \\ +Q_{21} & +Q_{20} & +Q_{19} \\ & +Q_{22} & \end{bmatrix} W_{sj}^3, \quad (5.10)$$

Equilibrium in z_2 direction.

$$H_j^3 - \frac{1}{R_1} K_j^3 + \left(\frac{dK_2}{dz_1}\right)_j = G_{bj}^3 +$$

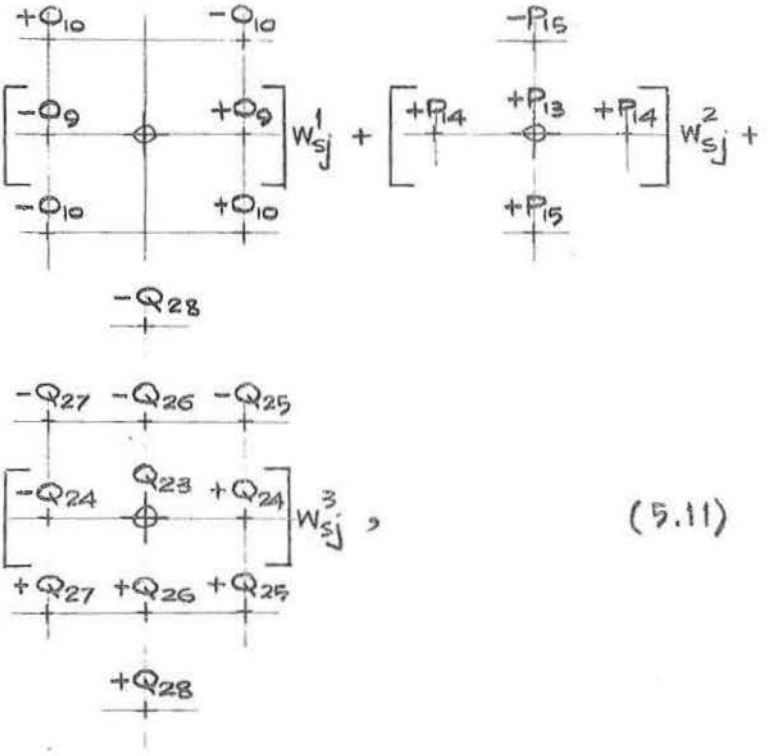

(5.11)

Equilibrium in z_3 direction.

$$K_j^1 =$$

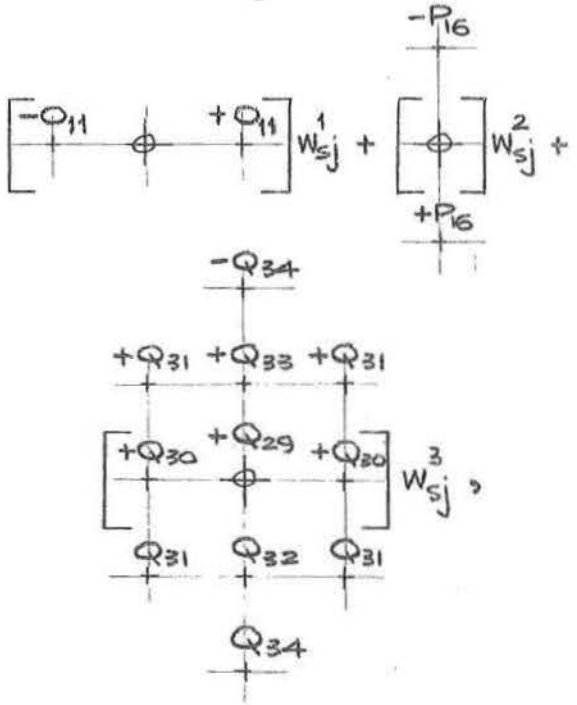

(5.12)

Equilibrium about z_1 axis.

with the coefficients O_k , P_k and Q_k given in table 5.2.

Third order terms, such as those having coefficients of form $\frac{e_2}{R_1}$ or $\frac{e_3}{R_1}$, have been neglected (this is justified by assumption 1 in section 3.1). The row subscript b in each of G^k_{bj} refers to loads applied at the edge member centroidal axis in the directions z_k . In the above, molecule centres are positioned at, or as near as possible to, the shell edge member intersection, while ϕ_j represents the angle ϕ at the grid positions (s,j). This approximation is considered further in section 8.3.

5.3 COMPATIBILITY OF BEAM AND BEAM-SHELL INTERSECTION DISPLACEMENT COMPONENTS

The replacement of the i subscript with b in equations (5.1) to (5.8) implies that member actions and displacements are computed at the edge member centroidal axis (which for the purpose of this discussion is assumed colinear with the neutral axis of the section), while the replacement of the i subscript with s in equations (5.9) to (5.12) assumes this grid line lies as close as possible to the shell-edge member intersection. In order that compatibility of edge member and shell be produced, it is now necessary to determine the relationship between w^k_{bj} and w^k_{sj} . This problem has also been considered by Powell [45], who used expressions similar to the following:

O_6	$+K.(1.-\mu).\frac{1.}{4.h_2}$
O_7	$+K.\mu.\frac{1.}{2.h_1}.\cos\phi_j$
O_8	$+K.(1.-\mu)\frac{e_2}{8.h_1.h_2}$
O_9	$+K.\mu.\frac{1.}{2.h_1}.\sin\phi_j$
O_{10}	$-K.(1.-\mu).\frac{e_3}{8.h_1.h_2}$
O_{11}	$-K.\mu.\frac{1.}{2.h_1}.(e_2.\cos\phi_j - e_3.\sin\phi_j)$
P_9	$+K.(1.-\mu).\frac{1.}{4.h_1}$
P_{10}	$-2.P_{11}$
P_{11}	$+K.(1.-\mu)\frac{e_2}{2.h_1^2}$
P_{12}	$+K.\frac{1.}{2.h_2}.\cos\phi_j$
P_{13}	$-2.P_{14}$
P_{14}	$-K.(1.-\mu)\frac{e_3}{2.h_1^2}$
P_{15}	$+K.\frac{1.}{2.h_2}.\sin\phi_j$
P_{16}	$-K.\frac{1.}{2.h_2}.(e_2.\cos\phi_j - e_3.\sin\phi_j)$
Q_{15}	$-K\frac{1.}{R'_{12}}.(1.-\mu)$
Q_{16}	$+D.(1.-\mu)\frac{1.}{4.R_3.h_1.h_2}.\cos\phi_j$
Q_{17}	$-K.(\frac{1.}{R'_{22}}+\mu.\frac{1.}{R'_{11}}).\cos\phi_j$
Q_{18}	$-K.(1.-\mu)\frac{e_2}{2.R'_{12}.h_1}$
Q_{19}	$+D.\frac{1.}{h_1.h_2}((2.-\mu)\frac{1.}{2.h_1}.\sin\phi_j + (1.-\mu)\frac{1.}{2.R_1}.\cos\phi_j)$
Q_{20}	$-D.\frac{1.}{h_1^2.h_2}.(2.-\mu).\sin\phi_j - 2.Q_{22}$
Q_{21}	$+D.\frac{1.}{h_1.h_2}.((2.-\mu)\frac{1.}{2.h_1}.\sin\phi_j - (1.-\mu).\frac{1.}{4.R_1}.\cos\phi_j)$
Q_{22}	$+D.\frac{1.}{2.h_1^3}.\sin\phi_j$
Q_{23}	$-K.(\frac{1.}{R'_{22}}+\mu.\frac{1.}{R'_{11}}).\sin\phi_j$
Q_{24}	$+K.(1.-\mu).\frac{e_3}{2.R'_{12}h_1}$
Q_{25}	$-D.\frac{1.}{h_1.h_2}.((2.-\mu)\frac{1.}{2.h_1}.\cos\phi_j - (1.-\mu)\frac{1.}{4.R_1}.\sin\phi_j)$
Q_{26}	$+D.(2.-\mu)\frac{1.}{h_1^2.h_2}.\cos\phi_j - 2.Q_{28}$
Q_{27}	$-D.\frac{1.}{h_1.h_2}.((2.-\mu)\frac{1.}{2.h_1}.\cos\phi_j - (1.-\mu)\frac{1.}{4.R_1}.\sin\phi_j)$
Q_{28}	$-D.\frac{1.}{2.h_1^3}.\cos\phi_j - 2.D.(\frac{1.}{h_2^2}+\mu.\frac{1.}{h_1^2})$
Q_{29}	$+K.(\frac{1.}{R'_{22}}+\mu.\frac{1.}{R'_{11}}).(e_2.\cos\phi_j - e_3.\sin\phi_j)$
Q_{30}	$+D.\mu.\frac{1.}{h_1^2}$
Q_{31}	$-D.\frac{1.}{2.h_1^2.h_2}.(e_2.\sin\phi_j + e_3.\cos\phi_j)$
Q_{32}	$-2.(Q_{31}+Q_{34})+D.\frac{1.}{h_2^2}$
Q_{33}	$+2.(Q_{31}+Q_{34})+D.\frac{1.}{h_2^2}$
Q_{34}	$D.\frac{1.}{2.h_2^3}.(e_2.\sin\phi_j + e_3.\cos\phi_j)$

TABLE 5.2 Coefficients O_k, P_k and Q_k required for the difference analogue of the edge member loading expressions. (section 5.2)

$$w^1_{bj} = w^1_{sj} + e_2 \cdot \left(\frac{\partial w_2}{\partial z_1}\right)_{bj} + e_3 \cdot \left(\frac{\partial w_3}{\partial z_1}\right)_{bj} \cdot \frac{R_3}{R_{11}} , \qquad (5.13)$$

$$w^2_{bj} = w^2_{sj} - e_3 \cdot \left(\frac{\partial w_3}{\partial z_2}\right)_{bj} , \qquad (5.14)$$

$$w^3_{bj} = w^3_{sj} + e_2 \cdot \left(\frac{\partial w_3}{\partial z_2}\right)_{bj} , \qquad (5.15)$$

$$\left(\frac{\partial w_3}{\partial z_2}\right)_{bj} = \left(\frac{\partial w_3}{\partial z_2}\right)_{sj} . \qquad (5.16)$$

Here e_2 and e_3 refer to the eccentricities of the shell-edge member intersection with respect to the edge member centroidal axis and are considered positive if this intersection lies at positions of increasing z_2 and z_3 with respect to the edge member centroidal axis. Because displacements w^k_{bj} and w^k_{sj} both refer to the spatial coordinate set z_k, rotation transformations are not required. In the following, because both the displacements w^k_{bj} and w^k_{sj} are not generally defined, the eccentricities e^i_2 and e^i_3 assume the special sense of referring to the eccentricities of the grid line $(3,j)$ with respect to (b,j). These values are shown in section 8.3 to depend upon the particular orientation of the grid (i,j), with respect to the edge member.

5.4 THE RULED SURFACE HYPERBOLIC PARABOLOID

Assumptions of section 4.3 once again apply, with the following additional restrictions to edge beam geometry:

1. The edge member centroidal axis is straight and everywhere parallel to the shell surface at the edge, which implies that

$$\frac{1}{R_3} = 0., \quad \text{and} \quad e_3 = \text{constant}.$$

2. That the vertical centroidal plane of the edge beam is everywhere parallel to the plane defined by the (z_1, z_3) axes. Therefore

$$\frac{1}{R_1} = 0., \quad \text{and} \quad e_2 = \text{constant}.$$

3. Cross-sectional area of the beam is constant.

Equation (5.1) to (5.4) then reduce to

$$\left[+Q_1 \quad +Q_0 \quad +Q_1\right] W^1_{bj} + H^1_j = 0., \quad (5.17)$$

$$\left[+P_2 \quad +P_1 \quad +P_0 \quad +P_1 \quad +P_2\right] W^2_{bj} + H^2_j - \left(\frac{dK_3}{dz_1}\right)_j = 0., \quad (5.18)$$

$$\left[+Q_8 \quad +Q_7 \quad +Q_6 \quad +Q_7 \quad +Q_8\right] W^3_{bj} + H^3_j + \left(\frac{dK_2}{dz_1}\right)_j = 0., \quad (5.19)$$

$$\begin{matrix} -Q_{10} & -Q_9 & -Q_{10} \\ \left[\quad\quad\quad\quad\quad\quad\right] & & \\ +Q_{10} & +Q_9 & +Q_{10} \end{matrix} W^3_{bj} + K^1_j = 0., \quad (5.20)$$

with corresponding internal forces and moments given by

$$N_j^1 = \left[-Q_4 \quad \oplus \quad +Q_4 \right] W_{bj}^1 , \qquad (5.21)$$

$$M_j^1 = \begin{bmatrix} +Q_{12} & & -Q_{12} \\ & \oplus & \\ -Q_{12} & & +Q_{12} \end{bmatrix} W_{bj}^3 , \qquad (5.22)$$

$$M_j^2 = \left[+Q_{14} \quad +Q_{13} \quad +Q_{14} \right] W_{bj}^3 , \qquad (5.23)$$

$$M_j^3 = \left[+P_8 \quad +P_7 \quad +P_8 \right] W_{bj}^2 . \qquad (5.24)$$

The discretised loading components (5.9) to (5.12) become

$$H_j^1 = \begin{bmatrix} -Q_6 \\ \oplus \\ +Q_6 \end{bmatrix} W_{sj}^1 + \left[-P_9 \quad \oplus \quad +P_9 \right] W_{sj}^2 + \left[Q_{15} \right] W_{sj}^3 , \qquad (5.25)$$

$$H_j^2 - \left(\frac{dK_3}{dz_1}\right)_j =$$

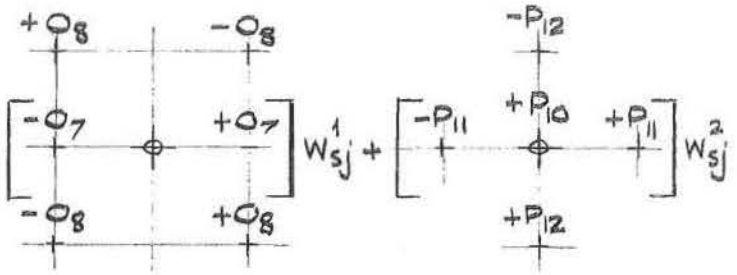

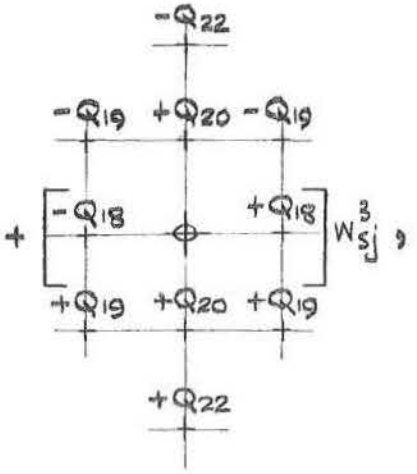

(5.26)

$$H_j^3 + \left(\frac{dK_2}{dz_1}\right)_j = G_{bj}^3 +$$

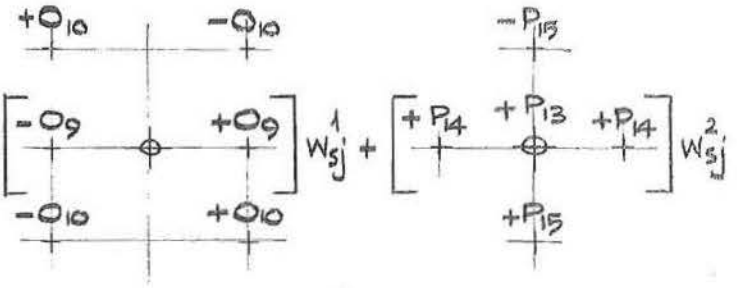

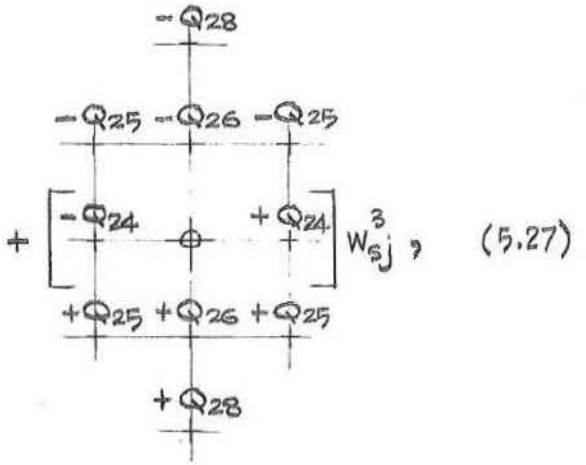

(5.27)

$$K_j^1 = \left[-Q_{11} \quad +Q_{11} \right] W_{sj}^1 + \left[-P_{16} \quad +P_{16} \right] W_{sj}^2 +$$

$$+ \left[\begin{array}{ccc} & -Q_{34} & \\ -Q_{31} & +Q_{33} & -Q_{31} \\ +Q_{30} & +Q_{29} & +Q_{30} \\ +Q_{31} & +Q_{32} & +Q_{31} \\ & +Q_{34} & \end{array} \right] W_{sj}^3 \,, \qquad (5.28)$$

where it is assumed G_{bj}^k , (k = 1,2) are zero.

The coefficients required in (5.17) to (5.28) may be obtained from tables 5.1 and 5.2, but for convenience they are listed in their reduced form in table 5.3. The torsional stiffness I_1 is obtained using the technique of St. Venant reported in reference [54], and is given as

$$I_1 = \frac{\gamma . b_b . t_b^{\,3}}{2(1+\mu)} \,, \qquad (5.29)$$

where γ is a coefficient dependent upon the ratio $\frac{b_b}{t_b}$.

It can be shown that the solution of equations (4.19) to (4.21), with associated boundary conditions (5.17) to (5.20) and (5.25) to (5.28), is dependent upon the dimensionless

geometric parameters λ_k, (k = 1,6), defined as:

$$\left.\begin{aligned} \lambda_1 &= \frac{f}{a}, \\ \lambda_2 &= \frac{t_s}{a}, \end{aligned}\right\} \quad \text{Shell geometry}$$

$$\left.\begin{aligned} \lambda_3 &= \frac{t_b}{t_s}, \\ \lambda_4 &= \frac{b_b}{a}, \end{aligned}\right\} \quad \text{Beam geometry}$$

$$\left.\begin{aligned} \lambda_5 &= \frac{e_3}{t_b}, \\ \lambda_6 &= \frac{e_2}{b_b}, \end{aligned}\right\} \quad \text{Shell-beam intersection geometry}$$

In subsequent chapters these parameters are used to define the unique shell-edge beam geometry.

O_0	$-2.O_1$	P_{11}	$+E_s \frac{m^2}{2.(1.+\mu)} \frac{t_s.e_2}{a^2}$
O_1	$+E_b.m^2.\frac{t_b.b_b}{a^2}$	P_{12}	$+E_s \frac{m}{2.(1.-\mu^2)} \frac{t_s}{a}.\cos\phi_j$
O_4	$+E_b.\frac{m}{2.}.\frac{t_b.b_b}{a}$	P_{13}	$-2.P_{14}$
O_6	$+E_s \frac{m}{4.(1.+\mu)}.\frac{t_s}{a}$	P_{14}	$-E_s.\frac{m^2}{2.(1.+\mu)}.\frac{t_s.e_3}{a^2}$
O_7	$+E_s \frac{\mu.m}{2.(1.-\mu^2)}.\frac{t_s}{a}.\cos\phi_j$	P_{15}	$+E_s \frac{m}{2.(1.-\mu^2)}.\frac{t_s}{a}.\sin\phi_j$
O_8	$+E_s \frac{m^2}{8.(1.+\mu)}.\frac{t_s.e_2}{a^2}$	P_{16}	$-E_s.\frac{m}{2.(1.-\mu^2)}.\frac{t_s}{a}.($
O_9	$+E_s.\frac{\mu.m}{2.(1.-\mu^2)}.\frac{t_s}{a}.\sin\phi_j$		$+e_2.\cos\phi_j - e_3.\sin\phi_j)$
O_{10}	$-E_s.\frac{m^2}{8.(1.+\mu)}.\frac{t_s.e_3}{a^2}$	Q_6	$+6.Q_8$
O_{11}	$-E_s.\frac{\mu.m}{2.(1.-\mu^2)}.\frac{t_s}{a}.($	Q_7	$-4.Q_8$
	$+e_2.\cos\phi_j - e_3.\sin\phi_j)$	Q_8	$-E_b.\frac{m^4}{12.}.\frac{b_b t_b^3}{a^4}$
P_0	$+6.P_2$	Q_9	$-2.Q_{10}$
P_1	$-4.P_2$	Q_{10}	$+E_b.\frac{m^3}{2.(1.+\mu)}.\frac{\gamma t_b.b_b^3}{a^3}$
P_2	$-E_b.\frac{m^4}{12.}.\frac{t_b.b_b^3}{a^4}$	Q_{12}	$+E_b.\frac{m^2}{4.(1.+\mu)}.\frac{\gamma t_b.b_b^3}{a^2}$
P_7	$-2.P_8$	Q_{13}	$-2.Q_{14}$
P_8	$+E_b.\frac{m^2}{12.}.\frac{t_b.b_b^3}{a^2}$	Q_{14}	$-E_b.\frac{m^2}{12.}.\frac{b_b.t_b^3}{a^2}$
P_9	$+E_s \frac{m}{4.(1.+\mu)}.\frac{t_s}{a}$	Q_{15}	$-E_s \frac{1.}{(1.+\mu)}.\frac{f.t_s}{a^2}$
P_{10}	$-2.P_{11}$	Q_{18}	$-E_s \frac{m}{2.(1.+\mu)}.\frac{f.t_s.e_2}{a^3}$

cont.

TABLE 5.3 Coefficients O_k, P_k and Q_k required for the difference analogue of the ruled surface hyperbolic paraboloid boundary equations (section 5.4).

Q_{19}	$E_s \frac{(2.-\mu).m^3}{24.(1.-\mu^2)} \cdot \frac{t_s^3}{a^3} . \sin\phi_j$	Q_{29}	$2.\frac{(1.+\mu)}{\mu} . Q_{30}$
Q_{20}	$2.(Q_{19}+Q_{22})$	Q_{30}	$E_s \frac{m^2}{12.(1.-\mu^2)} \cdot \frac{t_s^3}{a^2}$
Q_{22}	$E_s \cdot \frac{m^3}{24.(1.-\mu^2)} \cdot \frac{t_s^3}{a^3} . \sin\phi_j$	Q_{31}	$E_s \cdot \frac{m^3}{24.(1.-\mu^2)} \cdot \frac{t_s^3}{a^3} .($ $+ e_2 . \sin\phi_j + e_3 . \cos\phi_j)$
Q_{24}	$E_s \frac{m}{2.(1.+\mu)} \cdot \frac{f.t_s.e_3}{a^3}$		
Q_{25}	$E_s \cdot \frac{(2.-\mu).m^3}{24.(1.-\mu^2)} \cdot \frac{t_s^3}{a^3} . \cos\phi_j$	Q_{32}	$4.Q_{31} + \frac{1.}{\mu} . Q_{30}$
Q_{26}	$2.(Q_{25}+Q_{28})$	Q_{33}	$4.Q_{31} + \frac{1.}{\mu} . Q_{30}$
Q_{28}	$E_s \cdot \frac{m^3}{24.(1.-\mu^2)} \cdot \frac{t_s^3}{a^3} . \cos\phi_j$	Q_{34}	Q_{31}

TABLE 5.3 (continued) Coefficients O_k, P_k and Q_k required for the difference analogue of the ruled surface hyperbolic paraboloid boundary equations (section 5.4)

PART II

NUMERICAL INVESTIGATIONS

CHAPTER SIX

SOLUTION OF DIFFERENCE EQUATIONS

This section considers a number of possible methods by which the difference equations set up in chapters 4 and 5 may be solved. It is shown that direct solution methods, even those employing the banded properties so common in lower order finite difference analogues with physically restrictive boundary conditions, are prohibitive for the cases of shallow shells with realistic edge constraints. Iteration methods are therefore considered, and a method designed to meet the special limitations imposed by available computing machinery. Section 6.3 summarises typical programmed problems, while complete listings of a number of illustrative programmes are given in appendex A.

6.1 DIFFERENCE EQUATIONS AS MATRIX EQUATIONS

Application of the shell difference equations of chapter 4, at each of the nodal points (i,j) within the region of differential dependence, results in a set of simultaneous linear algebraic equations. It is seen that within the vicinity of the boundary, the equations of section 4.3 require the definition of a number of pivotals exterior to the domain of differential dependence. These conditions are provided by applying each of the boundary conditions of section 5.4, in

such a way that for a given grid line z_1 = constant (it being assumed as previously that the boundary lies at z_2 = constant), there exists one equation for the definition of each and every one of the pivotals required by the internal analogues. Ordering these equations so that the coefficient of w_{ij}^k in its respective difference equation becomes the leading diagonal element a_{rr} of the matrix $\mathbf{A}$, it is possible to write the above operations as

$$\mathbf{A}.\mathbf{w} = \mathbf{p}, \qquad (6.1)$$

where $\mathbf{w}$ and $\mathbf{p}$ are respectively vectors of displacement components w_{ij}^k and loading components p_{ij}^3. It should be noted that the difference grid subscript ij has little or no significance in the ordering of $\mathbf{A}$, and it has been assumed that the problem is sufficiently well posed so that for each boundary pivotal there exists one associated boundary condition. The resulting system of N simultaneous algebraic equations for the determination of N pivotal variables may generally be considered in three distinct ways.

The first method may be used when the boundary pivots are determined explicitly, such as the case of the plane Dirichlet problem [25], and consists of assigning fixed numerical values to the boundary pivotals which are then used to modify the load vector $\mathbf{p}$. In the present context the method is extremely limited. The special case of reducing the

biharmonic problem of transversely loaded flat plates with simple supports to the equivalent solution of two explicit simultaneous Poisson equations, is one of the few applications in the bending theory of shells and plates. This restriction to lower order equations eliminates this method for the objectives of section 1.2, and is therefore not considered further.

Although similar in many respects to the first method, the second method is considerably more general in its application. Provided the boundary conditions can be expressed as relatively simple explicit combinations of internally defined pivotals, the matrix $\mathbb{A}$ can be reduced by row permutations so that only internally defined values of w_{ij}^{k} are required in vector w. In this context, "internally" and "externally" are used to denote pivotals which are respectively within and external to the domain of differential dependence. This is seen to correspond to the method of modifying the internal difference molecules, using the associated boundary conditions in such a way that no externally defined pivotals are required. This method has been used to advantage where boundary conditions are relatively simple combinations of low order derivatives of the dependent variables[43,51], but in cases of complex boundary constraint such as those developed in chapters 3 and 5, the method becomes either extremely tedious or prohibitive.

In contrast to the generally accepted techniques outlined above, the third method uses matrix $\mathbf{A}$ in its unreduced form. Although this results in a matrix of higher order, and also the possibility of deterioration in matrix conditioning (this latter speculation has yet to be demonstrated), the overall savings in both computer storage and economy with which programmes embodying large variation of boundary types may be written make this method, at least in the present research, superior to those outlined in the above.

Details of the method, as well as the ordering of matrix $\mathbf{A}$ are further considered in section 6.3.

6.2 SOLUTION OF MATRIX EQUATIONS

Because of the special circumstances of these investigations, this aspect of the present work assumed importance out of proportion to all other factors. An extensive review of the methods available and the literature pertaining to the solution of equation (6.1), where $\mathbf{A}$ results from the discretisation of some partial differential equation, may be found in reference [24]

The method, to be applicable to the class of problem considered in this thesis, must be simple, easily adaptable to include wide varieties of boundary type and capable of solution of matrices of the order of $N = 1000$. Clearly then, direct methods, even those utilizing the sparseness of the difference matrix, were prohibitive. Indirect methods were therefore

suggested, and although a number of techniques have previously been used with success, storage requirements indicate the use of first order linear methods, and in particular the method of successive over-relaxation [59, 28].

6.2.1 The Method of Successive Over-Relaxation

This method, which may be considered as a machine orientated extension of the relaxation method developed by Southwell [52], was first introduced by Young [59] for the solution of the plane Dirichlet's problem, and independently by Frankel [28], who for the same problem termed it the "extrapolated Liebmann" method. Restrictive conditions upon the matrix coefficients, which are sufficient, but not necessary for the method to be assured of convergence, have been given in reference [59] and in summarised form in [55]. While no theoretical justification for convergence exists for cases where these conditions are either not satisfied or are considerably weakened, the results of numerical experiments indicate that convergence is possible where such relaxations upon the matrix conditioning are made [61].

If matrix A is written in the form

$$A = -L + I - U \quad , \tag{6.2}$$

where $-U$ and $-L$ represent the normalised upper and lower triangular matrices and I the unity matrix, it is possible to represent the method of successive over-relaxation [42] by the equation

$$W^{(k+1)} = \left[I - \beta . L\right]^{-1} \left[\beta . U + (1-\beta) . I\right] . W^{(k)} + \left[I - \beta . L\right]^{-1} . \beta . q . \quad (6.3)$$

In this case q is given by

$$q_r = \frac{1}{a_{rr}} . P_r \, , \quad (6.4)$$

while β represents the over-relaxation factor. Equation (6.3) is in a form suitable for the estimation of the optimum over-relaxation factor β_o, and is discussed further in section 6.2.2 for the stationary single step point over-relaxation method (see [42] for terminology). Equation 6.3 may be reduced to

$$W_r^{(k+1)} = W_r^{(k)} - \frac{\beta}{a_{rr}} \left[\sum_{s=1}^{r-1} a_{rs} . W_s^{(k+1)} + \sum_{s=r}^{n} a_{rs} . W_s^{(k)} - P_r \right] , \quad (6.5)$$

which is the form to be used in the remainder of this present work. Reference [42] summarises and compares a number of iterative methods in current usage, and while other methods in special circumstances may be more efficient (Engeli, for example [22], has estimated that accelerated symmetric over-relaxation applied to biharmonic problems converges at twice the rate of the equivalent stationary process), the present method is retained for its simplicity and versatility.

6.2.2 Determination of the Optimum Acceleration Factor

In order that the successive over-relaxation method be effectively applied, it is necessary to estimate as closely as possible the optimum value for the acceleration factor β_o .

For certain cases, such as for Dirichlet's problem upon rectangular regions, explicit expressions for the optimum acceleration factor β_o in terms of grid spacing, are available [61]. For the more general problem however, no such simple closed analytic expressions exist, and the determination of β_o requires the value of β which minimizes the spectral radius of the iteration matrix H, where H is given by

$$H = \left[I - \beta.L\right]^{-1}.\left[\beta.U + (1-\beta).I\right]. \qquad (6.6)$$

This is, in general, a non-trivial task, often requiring as much, if not more work than the determination of the solution of (6.1). An alternate method is therefore desirable.

6.2.2(a) Numerical Experiments with Flat Plates

Initially, it was hoped that after a study of the nature of β (using numerical procedures) for the case of the biharmonic problem of transversely loaded flat plates, these results could be extended to the related problem of the ruled surface hyperbolic paraboloid. Accordingly, curves were plotted, showing the influence of boundary conditions, grid size, grid rectangularity and boundary shape upon the value of β_o, but these were later found to have little or no resemblance to the equivalent conditions where applied to even very shallow ruled surface hyperbolic paraboloid shells. The influence of geometric parameters λ_1 and λ_2 were found to be greater than those considered above.

One interesting fact however emerged from this study. For the solution of Poisson's equation an over estimate of β_o rather than an under estimate is likely to be beneficial to the rates of convergence[61,25]. This is shown in figure 6.1, where it is seen that although oscillations occur in modulus of the displacement vector $\delta^{(k)}$, where $\delta^{(k)}$ is given by

$$\delta^{(k)} = w^{(k)} - w^{(k-1)}, \qquad (6.7)$$

they are seen to be very heavily damped. These results were obtained during the solution of a square, simply supported flat plate using simultaneous Poisson's equations (see reference[54]) and a grid size of $\frac{1}{10}$th the span.

In contrast with this behaviour an over estimate of β_o for the related biharmonic problem, see figure 6.2, results in unstable oscillations, increasing in amplitude with the number of iterations and having a period of 1 iteration cycle. This phenomenon suggests a possible lower bound approach to the estimation of β_o and is developed in a form suitable for the present research in section 6.2.2(b).

6.2.2(b) Method of Approximating Optimum Acceleration Factors

Carre[12] outlines a method whereby successive over-relaxation yields estimates of the optimum acceleration factor β_o, which are improved continuously as the solution proceeds. The method is applicable to symmetric positive definite matrices

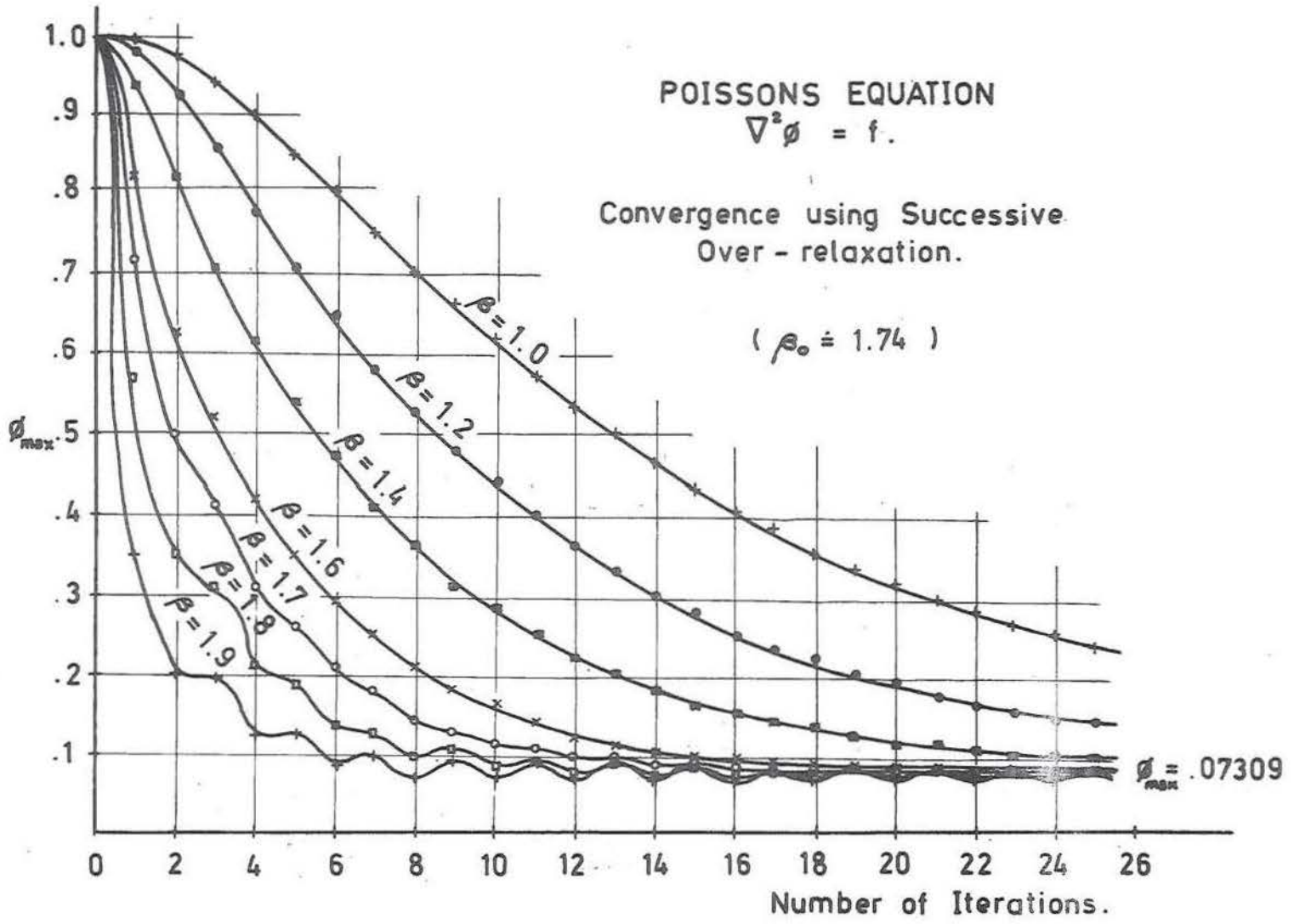

Fig. 6.1 Effect of varying over - relaxation factor β.

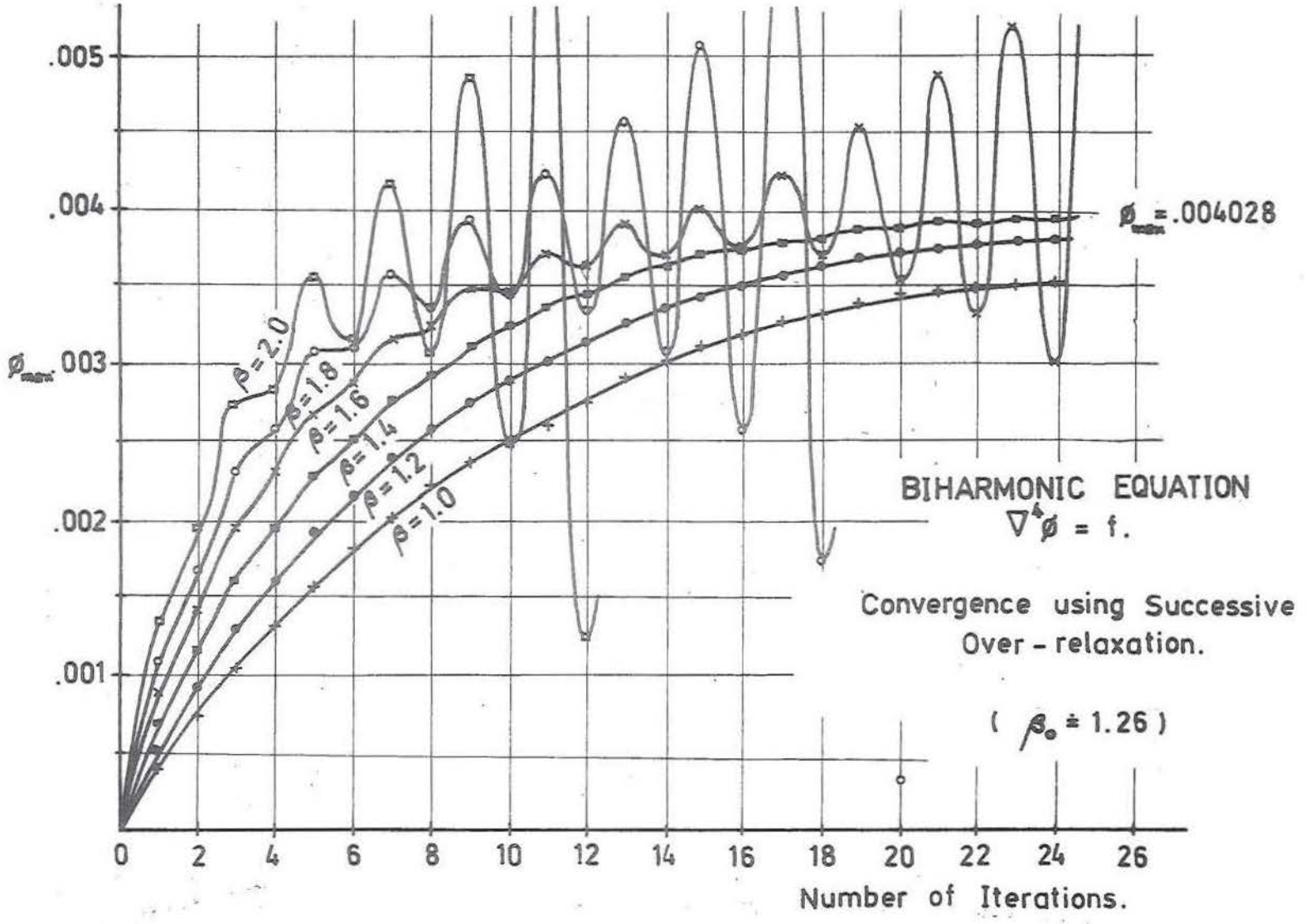

Fig. 6.2 Effect of varying over - relaxation factor β.

posessing Young's "Property A"[60], and therefore severely restricts its application in the present investigation. If however we use the property of the biharmonic over-relaxation indicated in section 6.2.2(a), it is possible to devise a method whereby successive estimates to the optimum acceleration factor β_o are once again improved as the solution proceeds.

For this purpose we define the velocity vector $\nu^{(k)}$ by

$$\nu^{(k)} = \delta^{(k)} - \delta^{(k-1)}, \qquad (6.8)$$

and if $\eta^{(k)}$ is used to denote some modulus of this vector $\nu^{(k)}$, such as the numerically largest element or the sum of the elements, then it is possible by observing whether $\eta^{(k)}$ alternates in sign, to detect whether β lies in the range $\beta_o < \beta < 2.0$. Figure 6.3 shows in detail the behaviour of the numerically largest element for the biharmonic analogue, with $\beta = 1.4$ (an over estimate of the optimum acceleration factor), from the 5th to the 15th iteration. It is seen that the small discontinuities in this modulus of $w^{(k)}$, quickly cause alternations in sign of the same modulus of the velocity vector $\nu^{(k)}$. It would be possible to define a higher order derivative with respect to iterations in order that these oscillations be detected at an earlier stage, but this would require additional computation and is therefore not considered.

This behaviour is used in the following to approximate the position of the optimum acceleration factor.

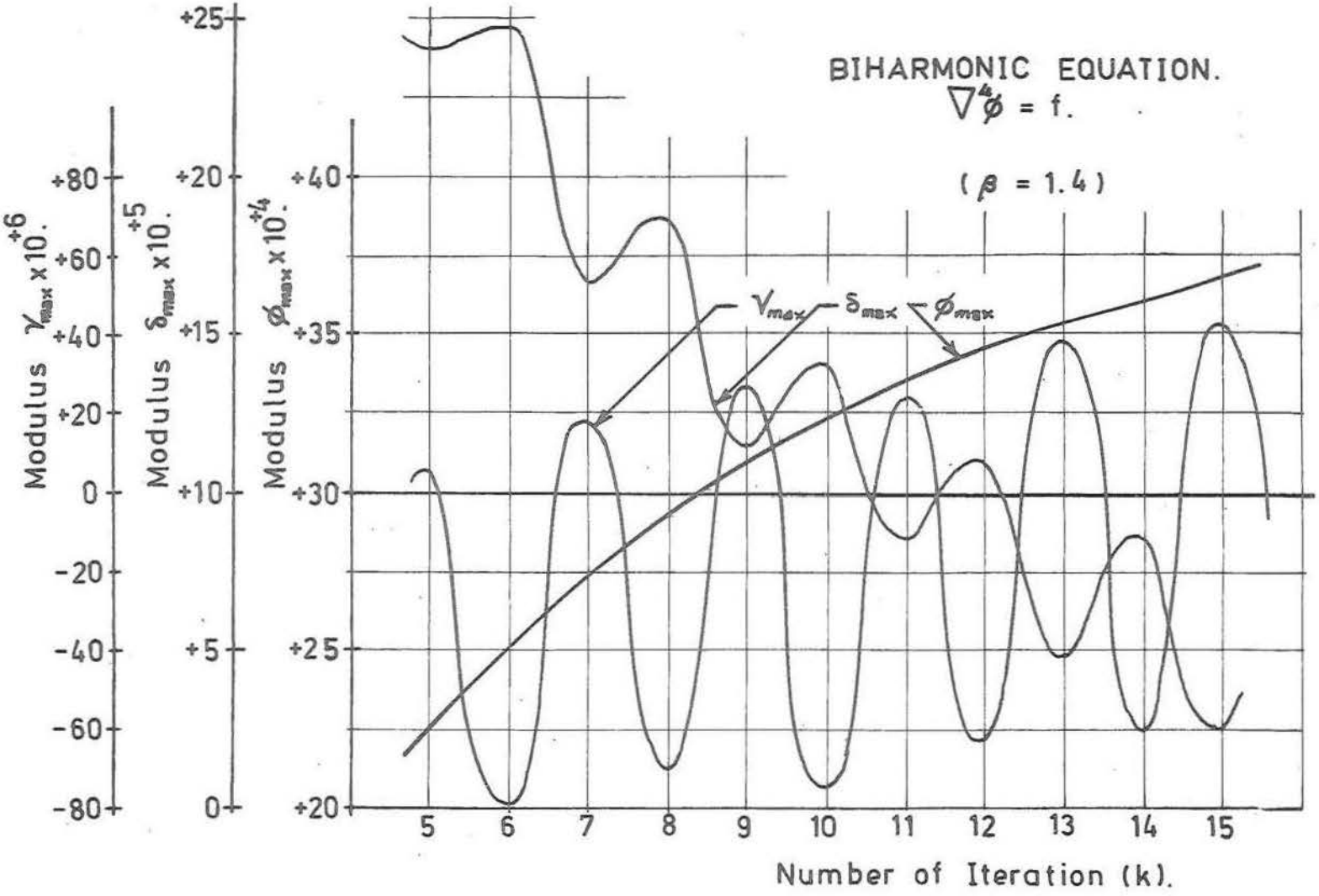

Fig. 6.3 Magnified oscillations resulting from an over estimate of β_o.

An initial estimate of β_o is made in the region $1.0 \leq \beta < \beta_o$. For this purpose, unless some previously found approximation for a particular problem is used, the value of unity is normally preferred. After some 5 to 10 iterations, the velocity modulus $\eta^{(k)}$ is determined for successive iterations, and if found to be a smooth function the value of β is incremented by 0.1. This process is repeated until the first value of β produces alternations in sign of successive values of $\eta^{(k)}$, at which time the previous best estimate of β is taken. At this stage it is usually necessary to stabilise the process, by iterating at this value of β for considerably more than 10 iterations, after which a similar procedure is followed, except that β is incremented in steps of 0.01. It is normally possible to determine in a short time, a reasonably accurate estimate of the optimum acceleration factor, which, if thought desirable, could be continuously improved as the solution proceeds. Normally, however, the process is terminated after an under estimate to 2 decimal places is determined.

6.3 DESCRIPTION OF COMPUTER PROGRAMMES

During the course of this work a large number of computer programmes were written. They all follow a similar procedure of solution, and although details are changed to suit the particular requirements of the problem, the flow diagram is generally constant. In section 6.3.1 the layout of the

difference grid as used in these programmes in relation to the z_k , (k = 1,2) axes is given, and the ordering of solution indicated by the flow diagrams of section 6.3.2. Details of boundary computation are discussed further in chapter 8, with appendix A listing in full a number of typically programmed problems written (using PDQ Fortran) for an IBM 1620 Model 1 computer.

The load term of equation (4.21) may be written as

$$p^3_{ij} \cdot \frac{h^4}{D} = k_{p^3_{ij}} \cdot \frac{qL^4}{D} \cdot \frac{1}{m^4} \quad , \tag{6.9}$$

where L is the shell span, q the load magnitude per unit area and $k_{p_{ij}3}$ a dimensionless coefficient describing the normal load distribution. If the dependent variables of equations (4.19) to (4.21) are replaced by

$$w^k_{ij} = k_{w^k_{ij}} \cdot \frac{qL^4}{D} \quad , \tag{6.10}$$

then these equations may be normalised to provide the direct computation of the new dependent variables $k_{w^k_{ij}}$. Moreover it is assumed that the p_k , (k = 1,2) load components are zero. The boundary difference system (5.17) to (5.20) and (5.25) to (5.28) may be shown to normalise in a similar manner. Results from all computer programmes are given in terms of the dimensionless displacement components $k_{w^k_{ij}}$ and the dimensionless stress and moment resultant coefficients ($k_{n^{kl}_{ij}}$, $k_{m^{kl}_{ij}}$), (k,l = 1,2) which are related to the absolute stress and moment resultants as follows:

$$n_{ij}^{kl} = k_n{}_{ij}^{kl} \cdot qL \,, \tag{6.11}$$

$$m_{ij}^{kl} = k_m{}_{ij}^{kl} \cdot qL^2 \,. \tag{6.12}$$

Presentation of results for all examples of normal loading are given in terms of these dimensionless coefficients, although the order of magnitude is defined to suit the requirement of the problem.

6.3.1 Difference Grid Orientation

The conventional difference equations of sections 4.3.1 and 5.4, for shell and edge conditions of a ruled surface hyperbolic paraboloid, were derived under the assumptions

$$h_1 = h_2 = h \,,$$

$$\frac{a}{b} = 1 \,.$$

Further, for numerical convenience, it is assumed that boundary and corner conditions are not only symmetric about the z_1 and z_2 axes, but also about the diagonals adjoining opposite corners (see section 8.2 and figure 6.4). Although this severely restrict the practical application of the programmes, it in no way affects the general objectives outlined in section 1.2. One eighth of the shell area is considered, and for programming convenience this region is chosen so that $-a < z_1 < 0.$ and $-a < z_2 < 0.$. The grid with i and j increasing in the z_2 and z_1 coordinate directions, is orientated such that the projections of the i = 3 and j = 3 grid lines are

colinear with the shell edges at z_2 and z_1 constant. If the grid spacing h is

$$h = \frac{a}{m} ,$$

then the restriction upon m is $m \leq 16$. For practical reasons, $m = 2$ is the lower bound, so that any integral value of m in the range $2 \leq m \leq 16$ is acceptable. Although this restriction upon m is not imposed by storage limitations, the excessive time required for the solution of equation (6.1) with $m > 16$ is prohibitive.

The diagrid used for the modified finite difference technique is placed at + 0.5h out of phase with the grid described above. Because of the similarity of the methods, this is not considered further.

6.3.2 Layout of Computer Programmes

In section 3.6 the distinction between displacement and traction edge conditions is indicated, while in section 8.2 the implications resulting from this distinction for the case of finite difference representation are demonstrated. The following considers each of these extreme cases, it being assumed that intermediate boundary conditions, such as simple supports and certain edge beam representations, may be developed as mixed cases of these. Figure 6.5 shows the general flow chart of all programmes.

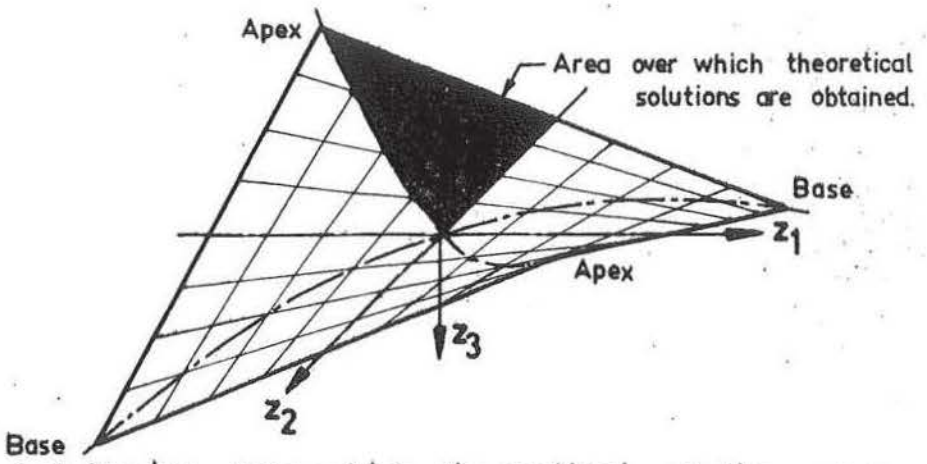

(a) Region over which theoretical solutions are obtained. (see detail below).

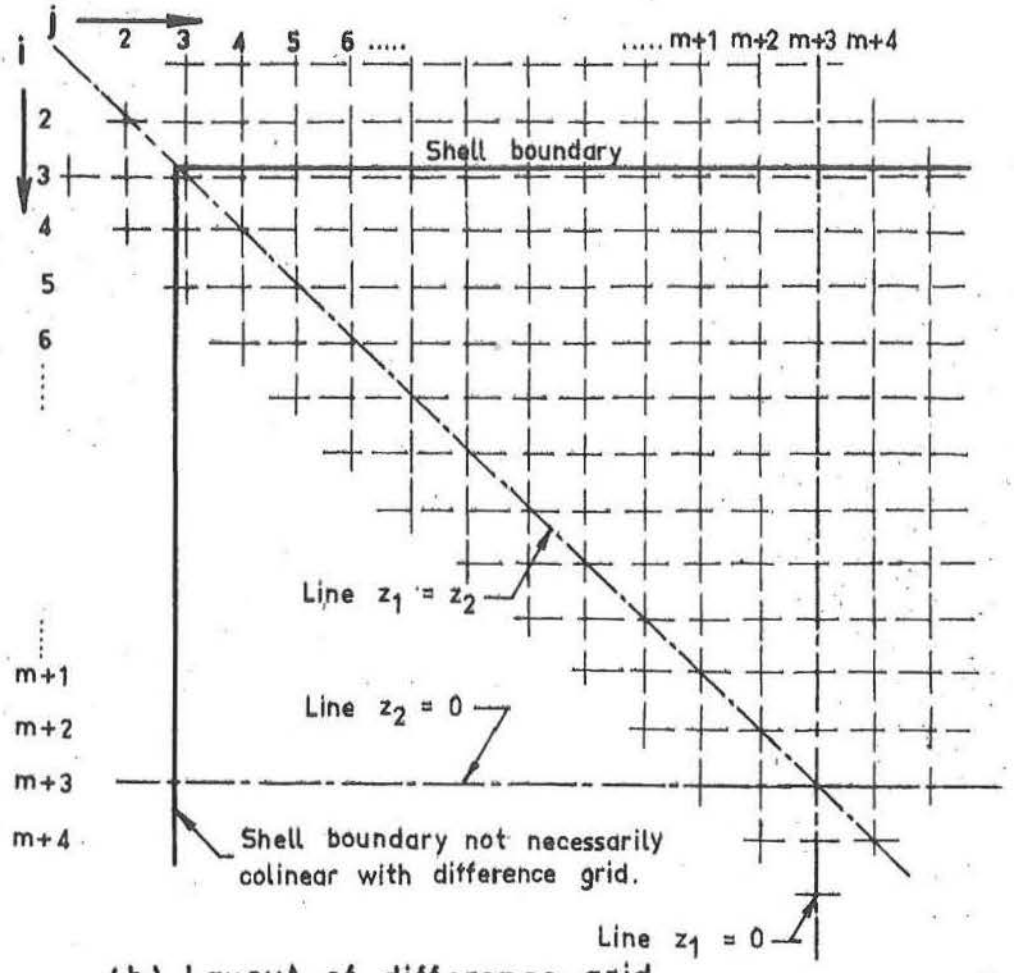

(b) Layout of difference grid.

Fig. 6.4 Layout of difference grid with respect to (z_1, z_2) axes.

Computer storage of 4,000 words (a floating point number of 8 significant decimal digits requires storage of 1 word) was such that the above computation had to be broken into a number of separate chapters, with card output being used to connect each of these programmes. The broken lines and numbers in figure 6.5 indicate the extent of each of these chapters, while those operations not included in programmes were manual decisions.

All programmes were written to handle shells of uniform material properties, and shell geometry. Edge beams were considered as uniform in both depth and breadth and although provision for variation of E between edge beam and shell has been provided, no numerical experiments to this end have been carried out.

6.3.2(a) Displacement Boundary

In this particular case dependent variables w_{ij}^{k} are given explicitly at the boundary. Therefore it is only necessary to apply the differential analogues at points lying within this boundary. Figure 6.6(a) shows in detail the iteration block lying between (a) and (b) in figure 6.5, for the case of the displacement boundary.

6.3.2(b) Traction Boundary

In this case, because the differential equation is applicable at the boundary, the boundary conditions necessarily

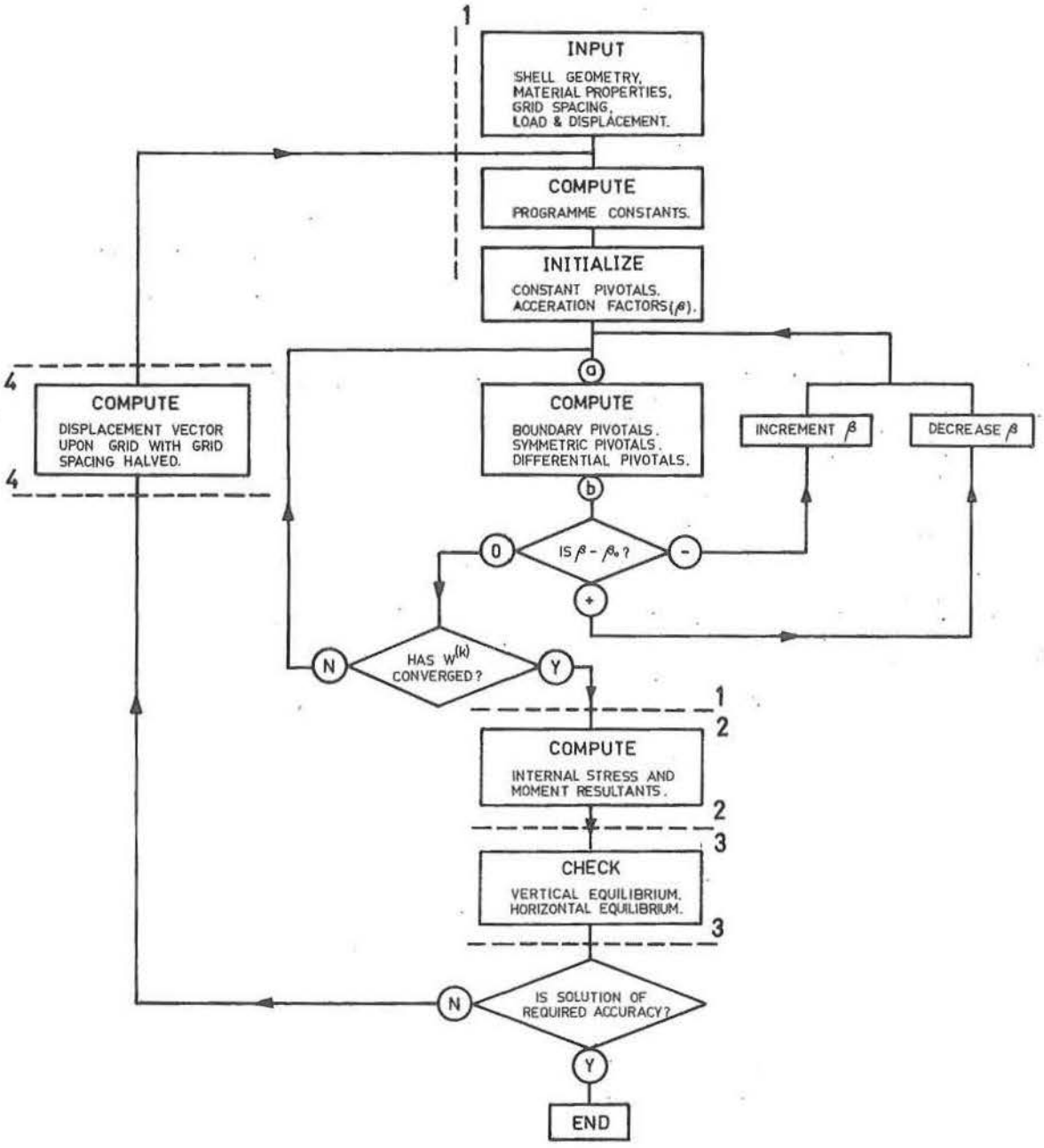

Fig. 6.5 Flow diagram of all computer programmes. Numbers and ---- indicate extent of individual programmes.

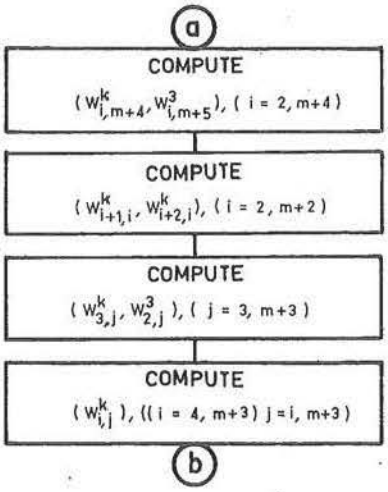

(a) Displacement boundary representation.

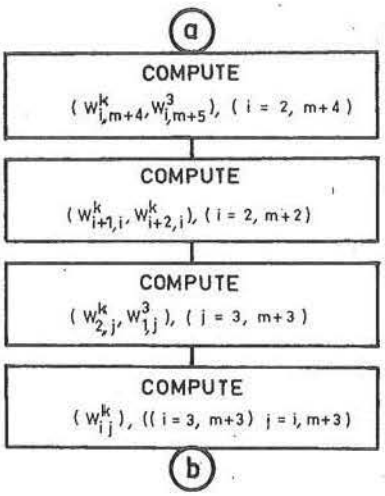

(b) Traction boundary representation.

Fig. 6.6 Details for flow diagram of figure 6.5 between (a) & (b).

must define (w^k_{2j}, w^3_{1j}), $(j = 3, m+3)$. The iteration block (a) to (b) in figure 6.5 for this case, is shown in figure 6.6(b).

6.4 DISCUSSION

Iterative methods possess the valuable property of allowing approximate solutions (those obtained on a coarse grid for example) to act as input for a more refined solution. This has the effect of greatly reducing the labour, for obtaining solutions to a predetermined accuracy, on a given grid size, and has been utilised to the full in the course of this work. A more important advantage in the use of iterative methods, is that once a solution has been obtained for a given class of shell, this solution may be used as input to obtain similar solutions for shells with shell and edge parameters slightly perturbed. This is valuable in the preparation of design tables, or as an analysis design tool. For this latter objective the programmes described could very easily be extended to include non-symmetric shells with greater varieties of corner and boundary support conditions, as well as non-uniform material properties and shell geometry. As the present investigation was not to develop design programmes, these refinements have not been carried out.

Although the majority of computations were carried out on an IBM 1620 computer, parameter studies reported in chapters 8 and 9, and final convergences for $m = 16$ grids in chapter 7, were obtained using a CDC 3600 machine. Table 6.1 shows for a

typical problem, the order of work required to obtain solutions of accuracy such that some modulus of the displacement vector $\delta^{(k)}$ is less than .005% of the same modulus of the vector $w^{(k-1)}$. The numbers of iterations are estimated assuming that initial input for any one grid size comprise the interpolated values obtained from the next coarse grid, and also that an estimate to 2 decimal figures of the optimum acceleration factor has been obtained. The details of this table would depend both upon the shell geometry and boundary and corner support conditions, so that these figures can only be considered as giving orders of magnitude.

The order of total time required for obtaining solutions is seen to be large and although a number of solutions have been obtained with $m = 16$, grid sizes of $m = 8$ are probably the practical upper limit where an IBM 1620 computer is employed. If on the other hand one employed a more up to date computer such as the CDC 3600, the respective times are shown to be reduced by a factor of 1400. For machines of these capabilities it is estimated that a grid of $m = 32$ would be practical.

m	Number of Unknown w_{ij}^k				No. of Iter.	Time per Iter.(sec)		Total Time (hr.)	
	w_{ij}^1	w_{ij}^2	w_{ij}^3	w_{ij}^k		IBM 1620	CDC 3600	IBM 1620	CDC 3600
4	36	36	48	120	100	10	.007	.25	
8	79	79	102	260	400	40	.029	4.5	.003
16	221	221	258	700	1000	160	.115	45.0	.028
32				2150	4000	840	.600	950.0	.750

TABLE 6.1 Details of Work Estimates for Typically Programmed Problems.

CHAPTER SEVEN

ACCURACY OF DIFFERENCE SOLUTIONS

Considering the large number of authors who have reported finite difference solutions of the thin shallow shell equations in their various special forms, it is surprising that few have attempted to assess the "reliability" or "numerical accuracy" with which these solutions have been obtained. Noor and Veletsos [43] consider in detail particular cases of second order translational shells with opposite edges simply supported, while Utku [56] demonstrates that with the restrictions upon grid size imposed by storage limitations for his computer programmes, the convergence for the two dimensional problem is inadequate.

If it is assumed that the shallow shell equations provide a sufficiently accurate mathematical model for the bending of ruled surface hyperbolic paraboloids, and if the closed analytic solution of these equations at a particular position (ij) is denoted by $w_{k_{ij}}$, deviations from this value may arise from the following:

1. Truncation errors due to discretisation of the differential equations.

2. Truncation errors due to discretisation of the boundary equations (assuming once again that the boundary differential

system is a sufficiently accurate mathematical model).

3. Round-off errors due to limitations of numerical solution procedures.

Employing the iterative method described in Chapter 6, round-off errors, although not eliminated, are systemised to such an extent that at any stage of solution it is possible to estimate the order of accuracy achieved from successive iterates of approximations to w_{ij}^k, where w_{ij}^k once again denotes the exact solution of the discretised representation. Care must be taken however that the iterative process is not terminated too early. On the other hand, in certain badly conditioned cases of the matrix $\mathbf{A}$, and where a direct solution method is employed, round-off may cause marked deviations from the true discretised solution w_{ij}^k. The remainder of this chapter is concerned with the estimation and possibilities of reducing the discretisation errors 1 and 2.

Section 7.1 outlines a number of possible techniques for the reduction of discretisation errors, and, where suitable, in section 7.3 these techniques are used in an attempt to accelerate convergence of w^k to w_k. Convergences using the conventional finite difference representation for each of the clamped, simple, free and beam boundary conditions, are presented in section 7.2.

7.1 METHODS FOR THE REDUCTION OF DISCRETISATION ERRORS

The discretised form of the thin shallow shell equations (4.9) to (4.11) with stress resultants (4.12) to (4.17), and the thin shallow edge member equations (5.1) to (5.4), were derived using difference expressions with truncation errors consisting predominantly of terms of the order h^2 . In this section a number of suggested techniques for reducing this overall discretisation error are reviewed and discussed with particular reference to the present investigation.

7.1.1 Difference Grid Refinement

Just as the convergence and rates of convergence for the successive over-relaxation iteration method are theoretically justified for very restrictive classes of matrix $\mathbb{A}$, so the convergence and rates of convergence of w^k to w_k as the grid size $h \rightarrow 0$. have been shown for similarly very restrictive differential forms and associated boundary conditions. Bounds for solutions may only be obtained numerically by computing w^k on successively finer difference grids. When used as a method of reducing truncation error however, this technique tends to be rather brutal. The order of $\mathbb{A}$ is increased by a factor of 4 on reducing the grid size by a factor of 2, which corresponds to an increase in work required to obtain a solution of approximately a factor of 16 . Although the actual time taken may be considerably reduced using the technique of section 6.4, in general, unless convergence is extremely pronounced, this

method is inefficient in obtaining w_k . In such cases extrapolation may be used to advantage, although extreme care must be exercised. For this process, estimates on grid sizes h and 0.5h are used to extrapolate to the case of zero grid size, using a formula such as

$$w_k \doteq \frac{4}{3} \cdot w^k_{h/2} - \frac{1}{3} \cdot w^k_h \,, \qquad (7.1)$$

or higher order extrapolation where more than two estimates to w_k have been determined. Shortcomings of this method are demonstrated in section 7.3.2(c).

A second method by which difference grids may be refined, is that of the graded grid. With this method, the difference grid is refined by varying amounts over the region of differential dependence, so that in regions of high gradients of dependent variables the difference grid is considerably refined compared to regions where the gradients of dependent variables are small. Such is the case of the shell boundary zone. Although the method avoids the large increases of the order of matrix A , as for the uniform grid refinement above, it has the disadvantages that adaption to computing machines is difficult, and it requires the development of a number of specialised difference molecules in the coarse to fine grid transition. These increased programming difficulties, involving large increases in storage requirements, alone make this method unsuitable for the present research.

7.1.2 Higher Order Difference Analogues

To enable the discretisation errors to be reduced it is necessary to introduce a greater number of pivotals into the computation molecules, so that further terms in the Taylor series expansions may be eliminated. Such is the case of the 9 point Laplacian operator where the predominant error term, although proportional to h^2, has a constant of proportionality less than the corresponding 5 point formula. This technique has been employed to advantage for Dirichlet's problem, but for the analogous biharmonic problem the use of higher order computational molecules results in the necessity for the definition of a greater number of boundary pivotals. These additional boundary pivots invariably require the use of some approximate technique, such as extrapolation or the use of one boundary condition to define more than one pivotal, thereby severely reducing the overall accuracy of the discretisation. Further, the use of higher order molecules increases the number of non zero elements of matrix $\mathbb{A}$, and therefore the computational labour required per iteration. It is also found to increase the spectral radius of the iteration matrix $\mathbb{H}$ and therefore severely decrease the rate of convergence with successive iterations. For these reasons the method is not considered further.

The shallow ruled surface hyperbolic paraboloid shell equations are of such a form that, by using the grid layout of section 4.3.2, all odd differentials are given in discrete form

with grid of half that used for the equivalent conventional technique. The method, known as the "modified" technique was first used by Chuang and Veletsos [16] in the solution of cylindrica shells, and later extended by Noor and Veletsos [43] to the case of the second order translational shells. While reductions in truncation errors are obvious from the marked increase of convergence of w^k to w_k, the method involves the same computational labour per iteration. Special problems arising from the use of iterative solution methods, as well as the difficulties of boundary representation, in general, somewhat offset these advantages for the ruled surface hyperbolic paraboloi

A further method whereby truncation errors may be reduced is suggested in the present problem by the critical nature of the boundary conditions. Because small changes in boundary condition result in drastic changes in shell behaviour (this is shown in chapter 8), it is expected that by decreasing the truncation error of these boundary conditions it should be possible to greatly reduce the overall discretisation error, and thus considerably accelerate the convergence of w^k to the analytic solution w_k. This technique has been employed to advantage by Abramowitz and Cahill [1] where the normal modes of vibration of a square clamped plate with boundary truncation errors of the order of h^n, $(n = 1,6)$ are determined. It is found that the use of more accurate boundary analogues yield more significant improvement in accuracy than does decrease in mesh width, and that

the condition $n = 4$ provides the optimum value for this improvement. Computational effort for boundary pivotals is considerably greater than that for the conventional representation. When this increased work is expressed as a percentage of the total work per iteration it becomes negligible, so that for small increases in computational labour it is possible to achieve marked increases in numerical accuracy. Once again however, it is found that the use of higher order boundary analogues result in a successive over-relaxation iteration matrix H, having spectral radius considerably greater than the corresponding conventional representation.

Clearly then, before any of these suggested methods are used it is important to assess the total work to achieve a given accuracy. Although the use of high order difference equations may improve the accuracy at a given mesh size, the total computational work required may be considerably greater.

7.1.3 Deferred Correction

If the truncation errors are expressible in difference form, and provided these differences indicate sufficiently well-behaved solutions, it is possible to substitute any of the above difference solutions into a difference approximation of the discretisation error to determine a numerical estimate of the truncation errors for each of the computation molecules. If e is used to represent the vector of these truncation errors, then

equation (6.1) is resolved with e replacing P, for the dependent variable δw_o. This is then added to the original solution w_o of (6.1), to provide an improved estimate of w. w in this context is used to denote the vector of discretised analytic values of $w_{k_{ij}}$, as distinct from the solution of (6.1). In matrix notation this process is represented by

$$w_o = A^{-1}.P \,,$$

$$e = B.w_o \,, \qquad (7.2)$$

$$\delta w_o = -A^{-1}.e \,,$$

$$w_1 = w_o + \delta w_o \,, \qquad (7.3)$$

where B represents the matrix of discretised truncation error operators. If necessary the process may be further refined to yield an estimate of w_2.

Using direct solution techniques this method is seen to be extremely powerful, in that for the estimate of δw_o using equation (7.3) the value of A^{-1} has previously been determined. The success of the method therefore depends upon the ease with which the matrix B may be derived. Biharmonic problems, for example, may be shown to have predominant truncation errors involving sixth derivatives, and therefore computation molecules spanning at least 7 pivotal positions. Hence, difficulties are likely to be met in determining the elements of B at or near the boundary, a problem which may be overcome

in part at least, by the use of non-symmetric analogues at these positions.

Where an indirect solution method is used, such as the successive over-relaxation iteration technique, equation (7.3) involves the solution of a second matrix equation of the same order as that of (6.1). In this case however, it is not necessary to continue the iteration to the same order of accuracy as the first solution, for the reason that a 1% error in the estimate of δw_o is likely to affect the estimate of w_1 by less than 0.01%, which is comparable to that obtained in the determination of w_o. Even using iteration then, the method is a practical proposition, provided the matrix B can be determined without the expense of excessive computational labour. Computational labour in this context includes not only actual machine time required for the solution of (7.2), but also the total throughput time of formulating, programming and checking such a problem. This difficulty is clearly demonstrated when the simplest of correction terms for the truncation errors of the shallow shell and associated boundary condition equations are derived. Because of limitations in computer storage, the method is not considered further.

7.2 CONVERGENCE STUDIES FOR THE RULED SURFACE HYPERBOLIC PARABOLOID

Preliminary numerical studies upon flat plates indicated the marked influence of boundary conditions upon the rates of

convergence with successive grid refinement. The convergence as the mesh width is decreased, for each of the clamped, simple, free and beam edged ruled surface hyperbolic paraboloids, is determined using the conventional finite difference shell and boundary representations described in sections 8.2 to 8.3.

In figures 7.1 to 7.4, the notation used is:

—·—·— grid with m = 2,

—··—··— grid with m = 4,

— — — grid with m = 8,

——— grid with m = 16.

All figures are plotted using internal stress and displacement dimensionless coefficients described in section 6.3, while q is used to denote the intensity of normal loading per unit area.

7.2.1 Clamped Boundary

Figure 7.1 shows the results on typical cross-sections of a clamped edge ruled surface hyperbolic paraboloid, with boundary conditions described in section 8.2.1 and dimensionless ratios of

$$\lambda_1 = 0.20, \qquad \lambda_2 = 0.0165, \qquad \nu = 0.00. \tag{7.4}$$

With the rapid convergence of k_{w_3} (a 0.5% change occurs in the maximum ordinate from m = 8 to m = 16), it is not

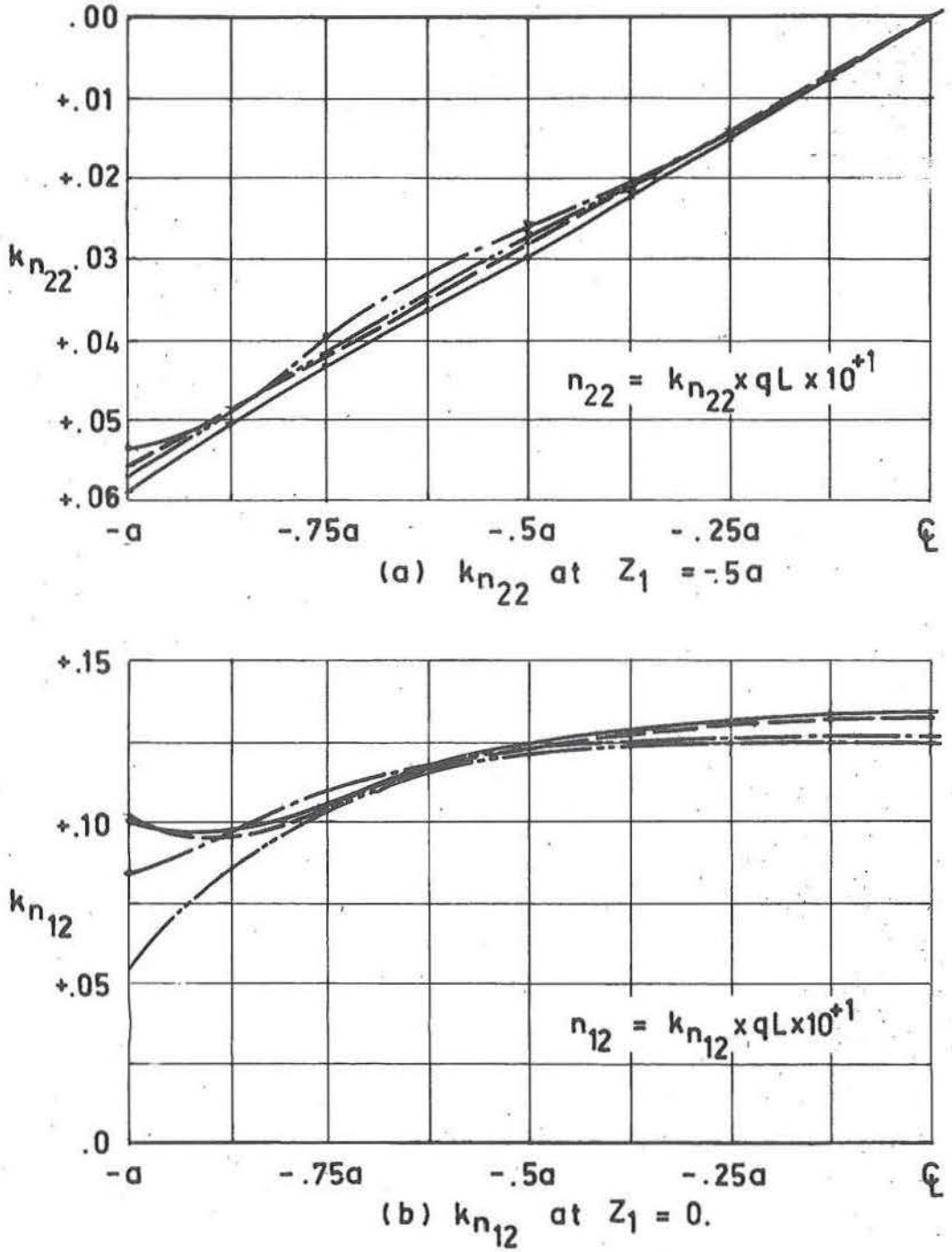

Fig. 7.1 Ruled surface hyperbolic paraboloid with all edges clamped. Convergence using conventional finite differences, with boundary analogue $O(h^2)$.

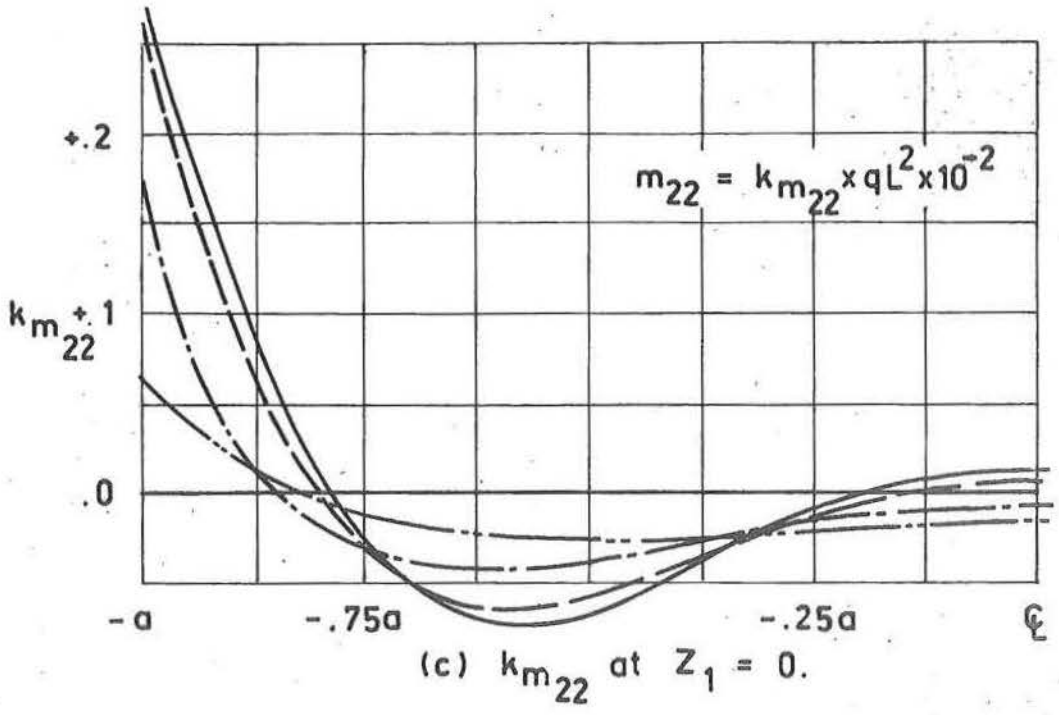

(c) $k_{m_{22}}$ at $Z_1 = 0.$

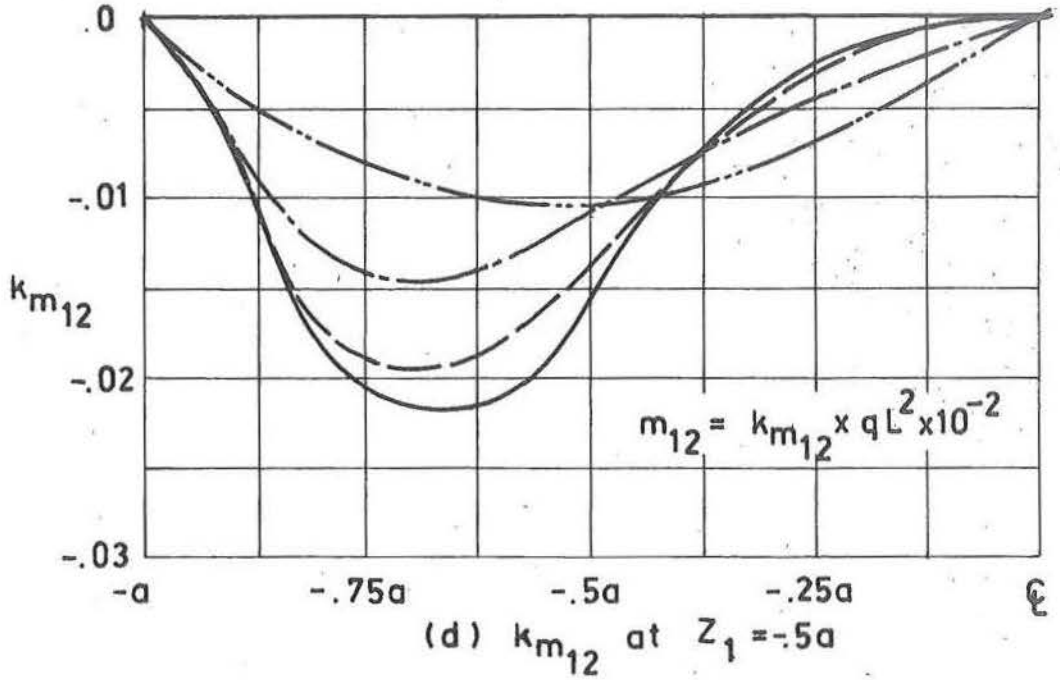

(d) $k_{m_{12}}$ at $Z_1 = -.5a$

Fig. 7.1 (continued) Ruled surface hyperbolic paraboloid with all edges clamped. Convergence of moments using conventional finite difference method.

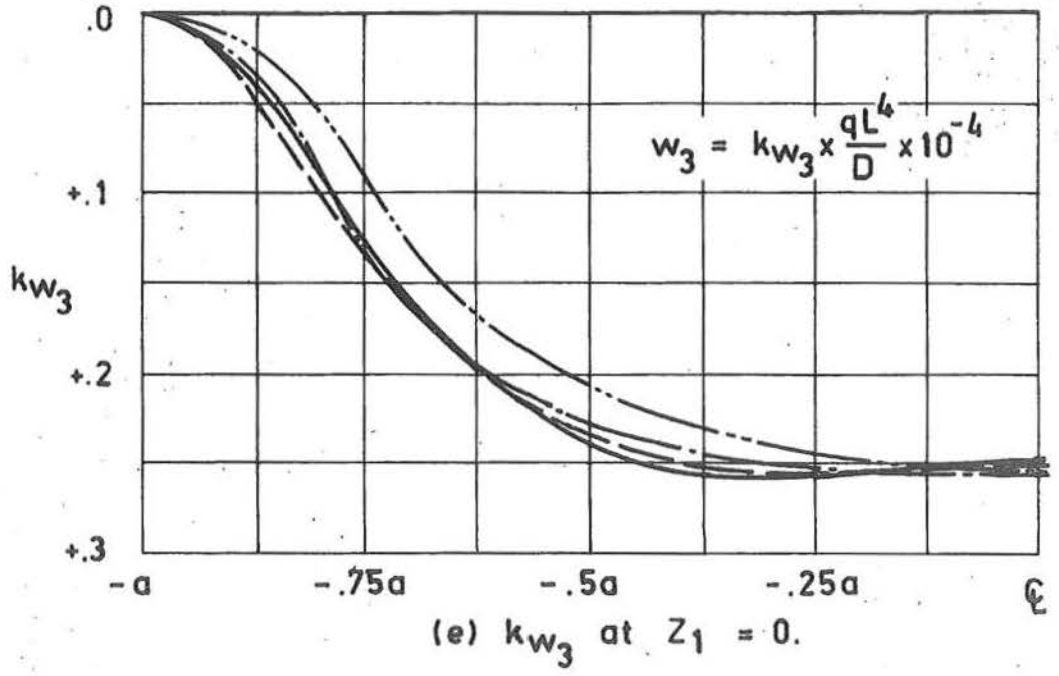

(e) k_{w_3} at $Z_1 = 0.$

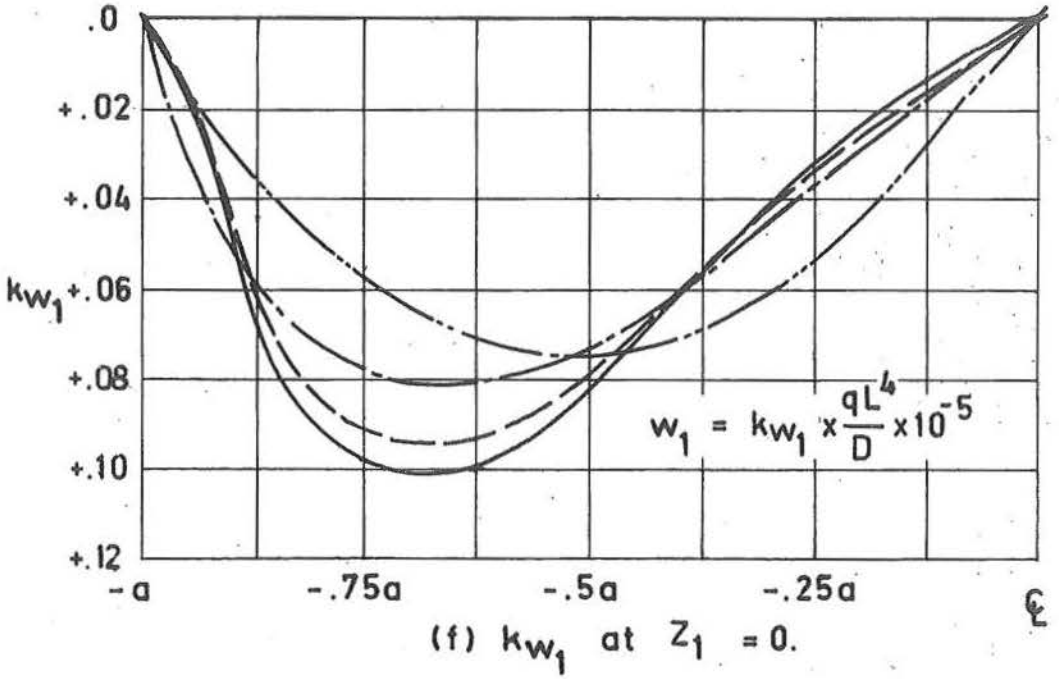

(f) k_{w_1} at $Z_1 = 0.$

Fig. 7.1 (continued) Ruled surface Hyperbolic Paraboloid with all edges clamped. Convergence of displacements using Conventional Finite Difference Method.

surprising that moment resultants $k_{m_{22}}$ and $k_{m_{12}}$ show that convergence for practical purposes is achieved - a 2.5% change for the same grid refinement as above occurring in $k_{m_{22}}$ at the position (o,-a). Displacement coefficients k_{w_1} converge at a somewhat slower rate than the corresponding k_{w_3} (at (0,-75a), the maximum ordinate of k_{w_1}, a change of 7% occurs for a grid refinement from $m = 8$ to $m = 16$), so that the rapid convergence of both $k_{n_{12}}$ and $k_{n_{22}}$, is surprising. This is especially so when it is considered that the truncation error in obtaining first derivatives using conventional analogues, is greater than that for obtaining second derivatives. In fact grid sizes of $m = 2$ and $m = 4$ are reasonable in obtaining estimates of in-plane stress resultants, but may severely underestimate both moment resultants and deflections.

7.2.2 Simple Boundary

Using a shell of the same geometric dimensionless ratios as used in section 7.2.1, figure 7.2 shows convergence for the related simply supported boundary at the same shell cross-sections. Convergence for displacements are an improvement upon those of the clamped boundary. The maximum horizontal displacement, for example, is changed by 4.5% from grid $m = 8$ to $m = 16$ as compared with 7.0% for the equivalent clamped boundary. If it is considered that the difference in convergence rates can be explained by differences in total discretisation errors, and that the total discretisation error is a combination

of the individual discretisation errors of differential and boundary analogues, this result is surprising.

For both the simple and clamped shell the discretisation of those pivotal positions within the region of differential dependence are constant. Differences in convergence rates must therefore be dependent upon the relative discretisation errors of the boundary representations, which in turn are functions of the individual truncation errors. For the clamped boundary, each of the Dirichlet type conditions

$$w_{3j}^{k} = 0., \quad (j = 3, m+4)$$

are given with zero truncation error, so that the total boundary discretisation error is contained in the approximation to w_{2j}^{3}, ($j = 3, m+3$) given by

$$w_{2j}^{3} = w_{4j}^{3} + \frac{h^2}{6.}\left(\frac{\partial^3 w_3}{\partial z_1^3}\right)_{3j}, \quad (j = 4, m+3) \quad (7.5)$$

On the other hand, the total discretisation error for the simple support is given by some combination of the truncation errors for each of w_{2j}^{k}, ($k = 2, 3$), given by

$$w_{2j}^{2} = w_{4j}^{2} + \frac{h^2}{6.}\left(\frac{\partial^3 w_3}{\partial z_1^3}\right)_{3j}, \quad (j = 4, m+3) \quad (7.6)$$

$$w_{2j}^{3} = -w_{4j}^{3} + \frac{h^2}{12.}\left(\frac{\partial^4 w_3}{\partial z_1^3}\right)_{3j}, \quad (j = 4, m+3) \quad (7.7)$$

and although each of these truncation errors is a little less than that of (7.5), it is expected that their total would be

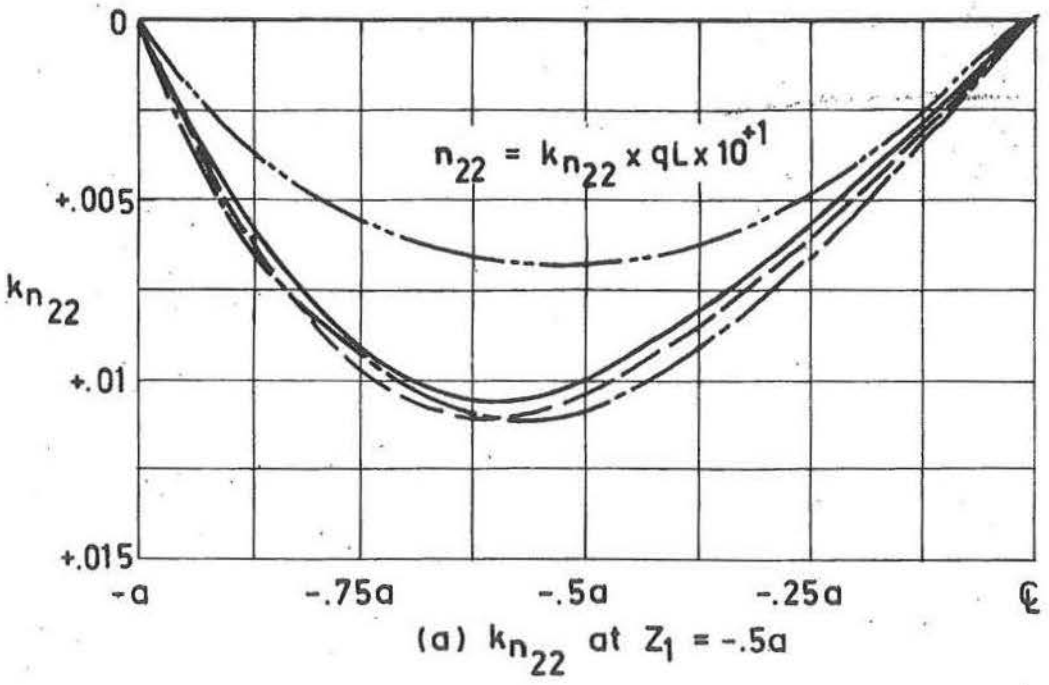

(a) $k_{n_{22}}$ at $Z_1 = -.5a$

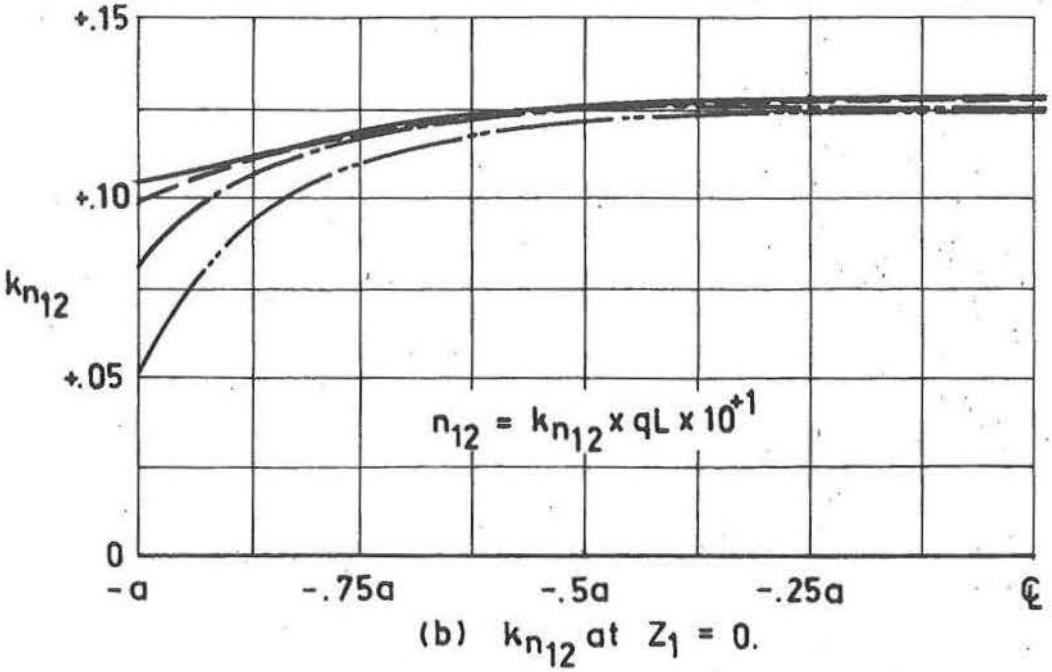

(b) $k_{n_{12}}$ at $Z_1 = 0.$

Fig. 7.2 Ruled surface hyperbolic paraboloid with all edges simply supported. Convergence using conventional finite differences, with boundary analogue $O(h^2)$.

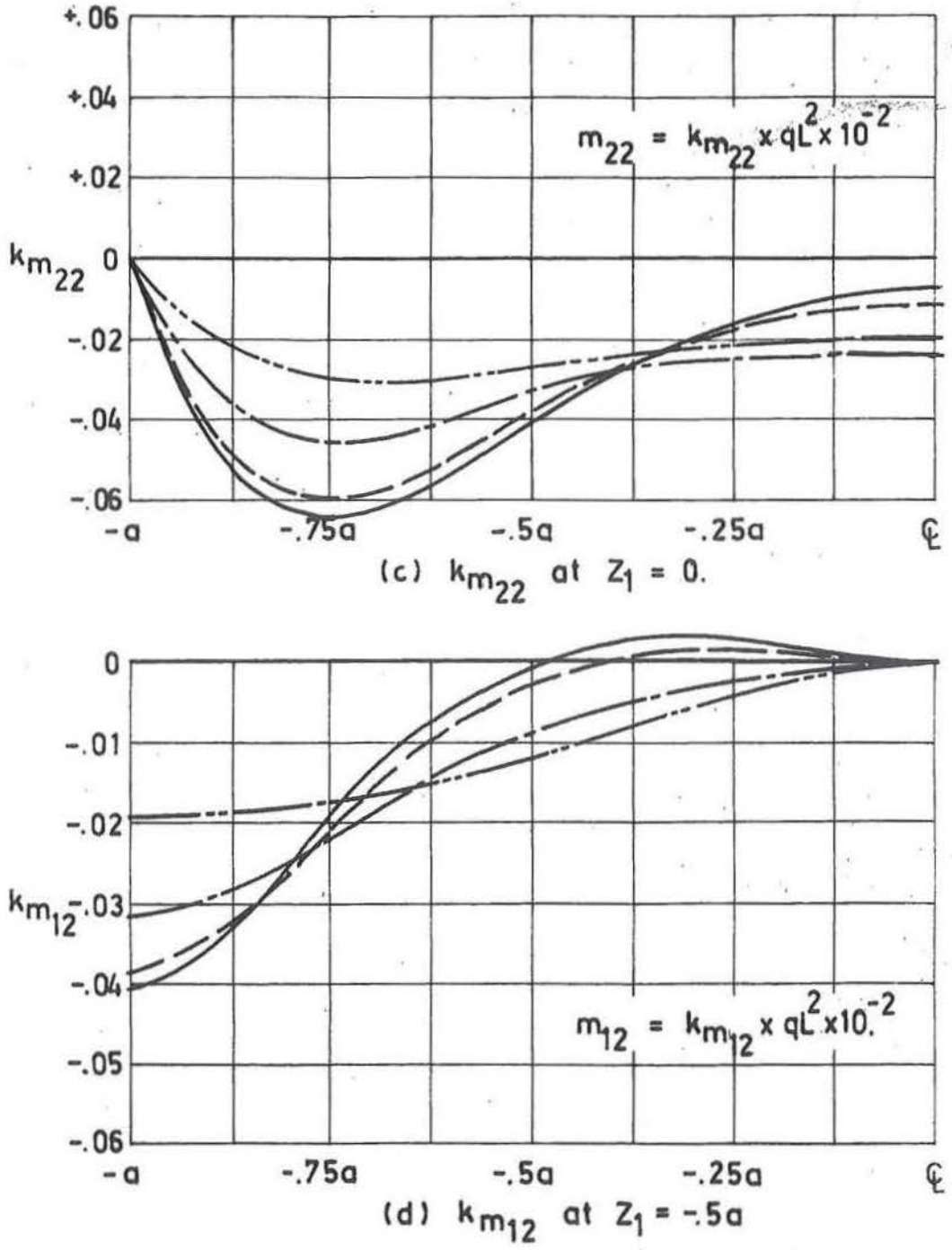

Fig. 7.2 (continued) Ruled surface hyperbolic paraboloid with all edges simply supported. Convergence of moments using conventional finite difference method.

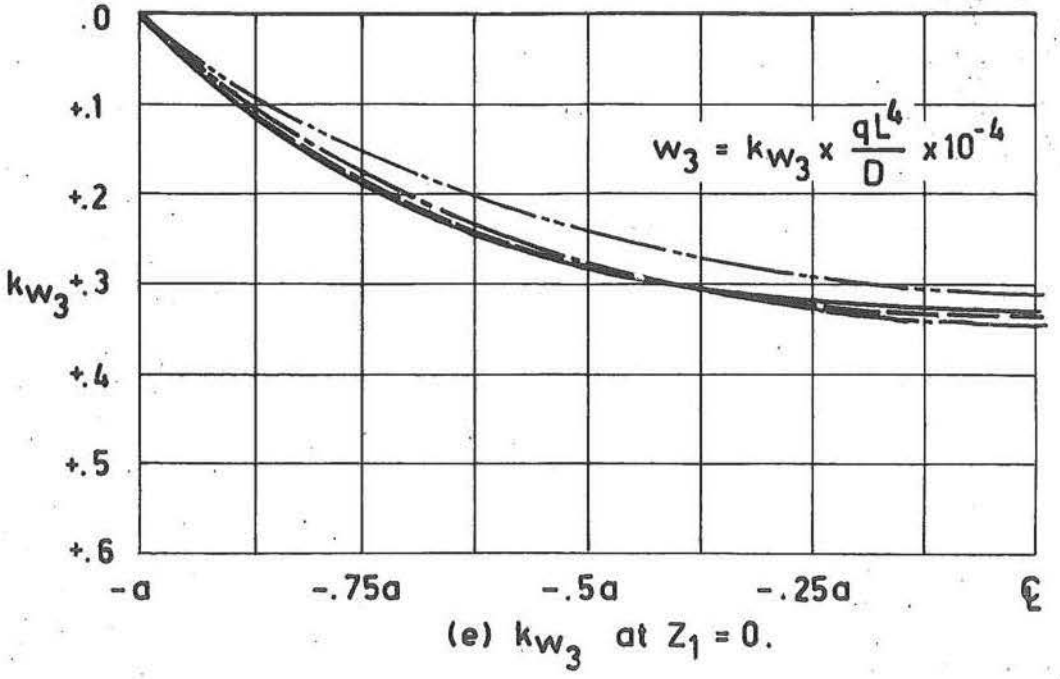

(e) k_{w_3} at $Z_1 = 0$.

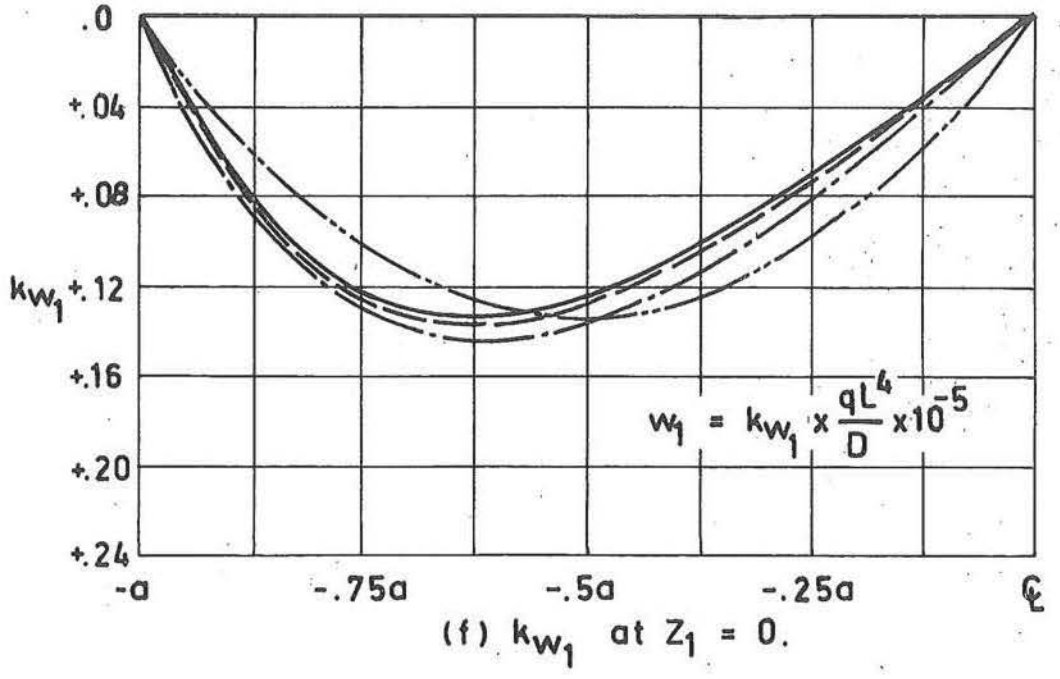

(f) k_{w_1} at $Z_1 = 0$.

Fig. 7.2 (continued) Ruled surface hyperbolic paraboloid with all edges simply supported. Convergence of displacements using conventional finite differences.

greater. Further, for the simple support it is necessary to apply the differential analogue (4.20) at each of the positions $(3,j)$, $(j = 3,m+3)$ in order that w^2_{3j} be defined. This in turn requires the definition of w^1_{2j}, (see section 8.2.2) using

$$w^1_{2j} = -w^1_{4j} + \frac{4.f}{a.m}\left(w^3_{4j}\right) + \frac{h^2}{12.}\left(\frac{\partial^4 w_1}{\partial z_2^4}\right)_{3j} + \frac{2.f}{a.m}\left(\frac{h^2}{6.}\left(\frac{\partial^3 w_3}{\partial z_2^3}\right)_{3j}\right), \quad (7.8)$$

so that in addition to the truncation errors of (7.6) and (7.7) there are those involved in the definition of w^2_{3j} and w^1_{2j}. In spite of this, the convergence indications are that the total discretisation error for the clamped boundary is greater than that for the simple boundary.

7.2.3 Free Boundary

With a shell of the same geometric dimensionless ratios as given in section 7.2.1, the convergence of the free edge ruled surface hyperbolic paraboloid is shown in figure 7.3. Corner conditions are those given in section 8.2.3. Of all the cases considered, this is seen to display convergence most clearly. Whereas for the clamped and simple support the difference between $m = 4$ and $m = 8$ grids are often of the same order as the difference between $m = 8$ and $m = 16$ grids, in the freely supported shell the latter is very much less than the former. Unfortunately however, this does not imply that the absolute convergence is superior (the maximum horizontal displacement k_{w_1} changes by 6% from $m = 8$ to $m = 16$), but means that the difference between the $m = 4$ and $m = 8$ grids as a

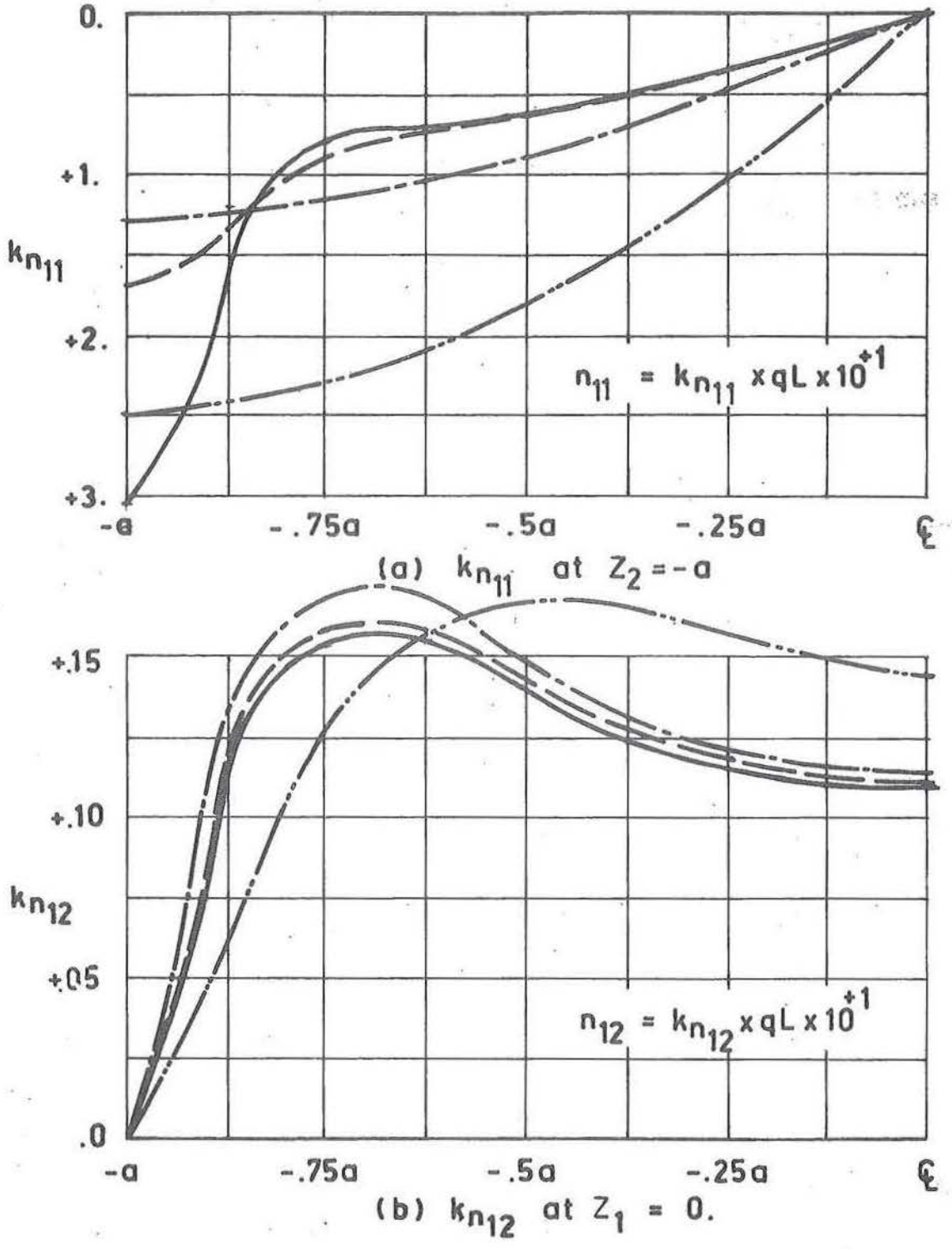

Fig. 7.3 Ruled surface hyperbolic paraboloid with all edges free and corners clamped. Convergence using conventional finite difference method.

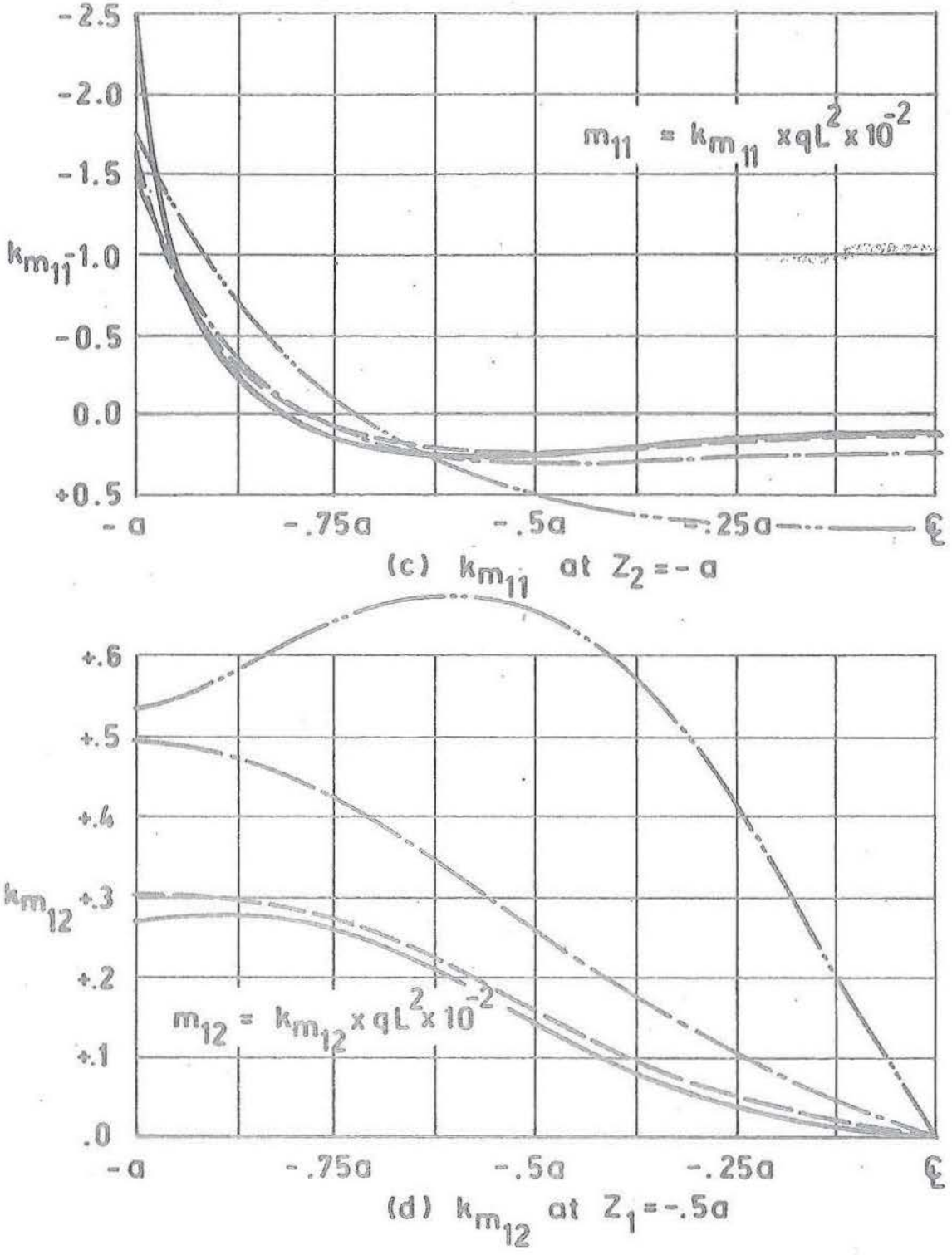

Fig. 7.3 (continued) Ruled surface hyperbolic paraboloid with all edges free and corners clamped. Convergence using conventional finite difference method.

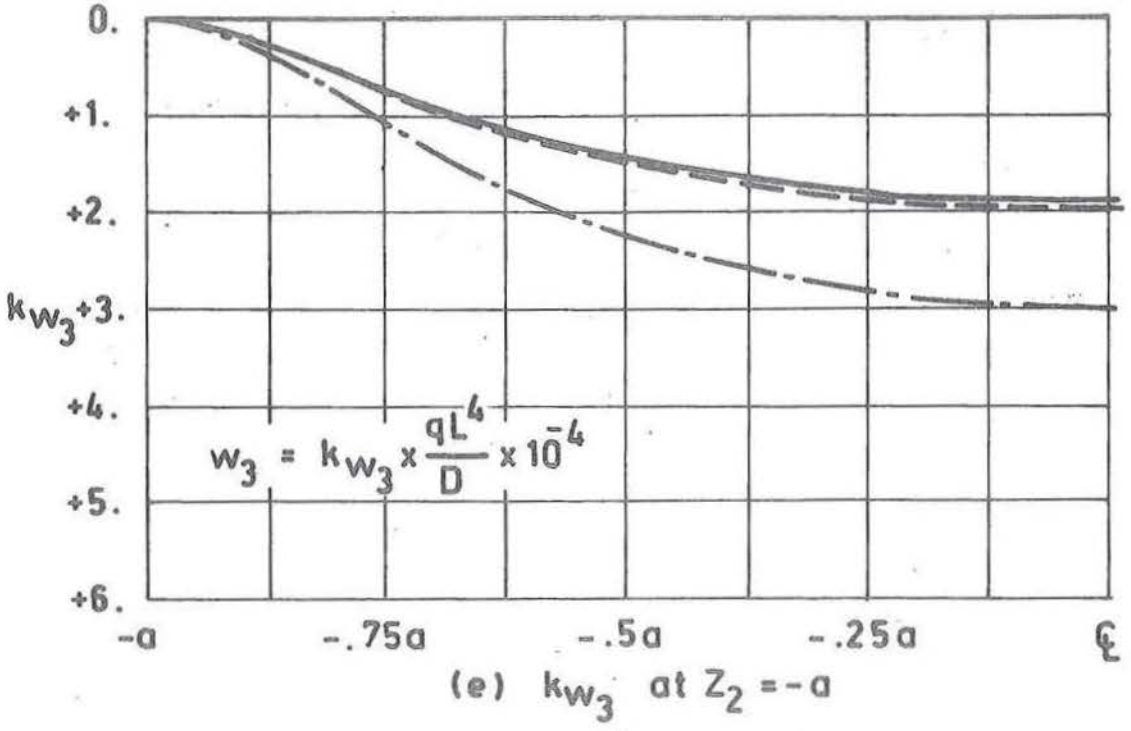

(e) k_{w_3} at $Z_2 = -a$

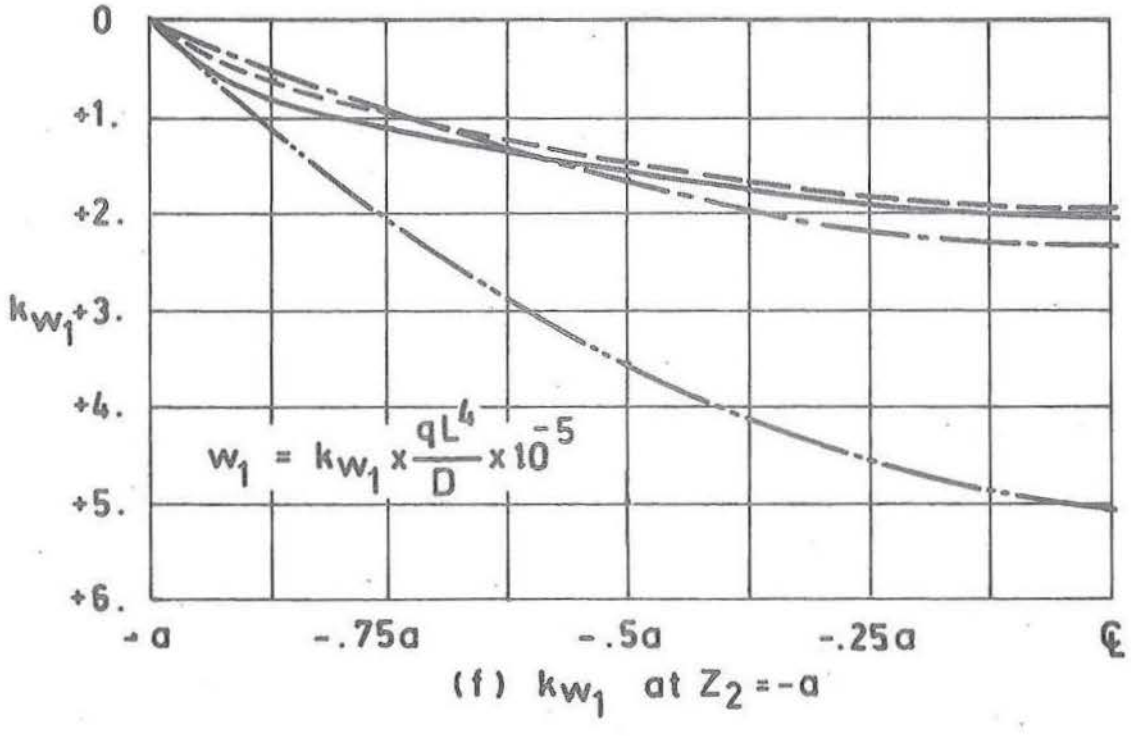

(f) k_{w_1} at $Z_2 = -a$

Fig. 7.3 (continued) Ruled surface hyperbolic paraboloid with all edges free and corners clamped. Convergence using conventional finite difference method.

percentage of the absolute value of the dependent variable for the free edge, is considerably greater than the corresponding difference for the simple and clamped supports. Hence the reliability of coarse grids for the present boundary is less than that for the simple or clamped condition.

7.2.4 Edge Beam Boundary

The convergence studies of this section employ the particular edge member boundary analogue described in section 8.3.2(c). For a shell of the same geometric dimensionless ratios as given in section 7.2.1, and shell-edge member interaction dimensionless ratios of

$$\lambda_3 = 4.5 ,$$
$$\lambda_4 = .05 ,$$
$$\lambda_5 = .00 ,$$
$$\lambda_6 = .00 ,$$

with $E_b = E_s$, the convergence is shown in figure 7.4. For this case $m = 2$ resulted in a system of equations unstable in the iteration sense, so that no solutions are given.

Convergence of displacements are seen to be inadequate for this case - maximum values of k_{w_1} and k_{w_3} changing by 25% and 14% with grid refinement from $m = 8$ to $m = 16$. It is surprising therefore to find that corresponding stress resultants $k_{n_{12}}$ and moment resultants $k_{m_{11}}$ show rapid convergence. When the physical restrictions of this boundary

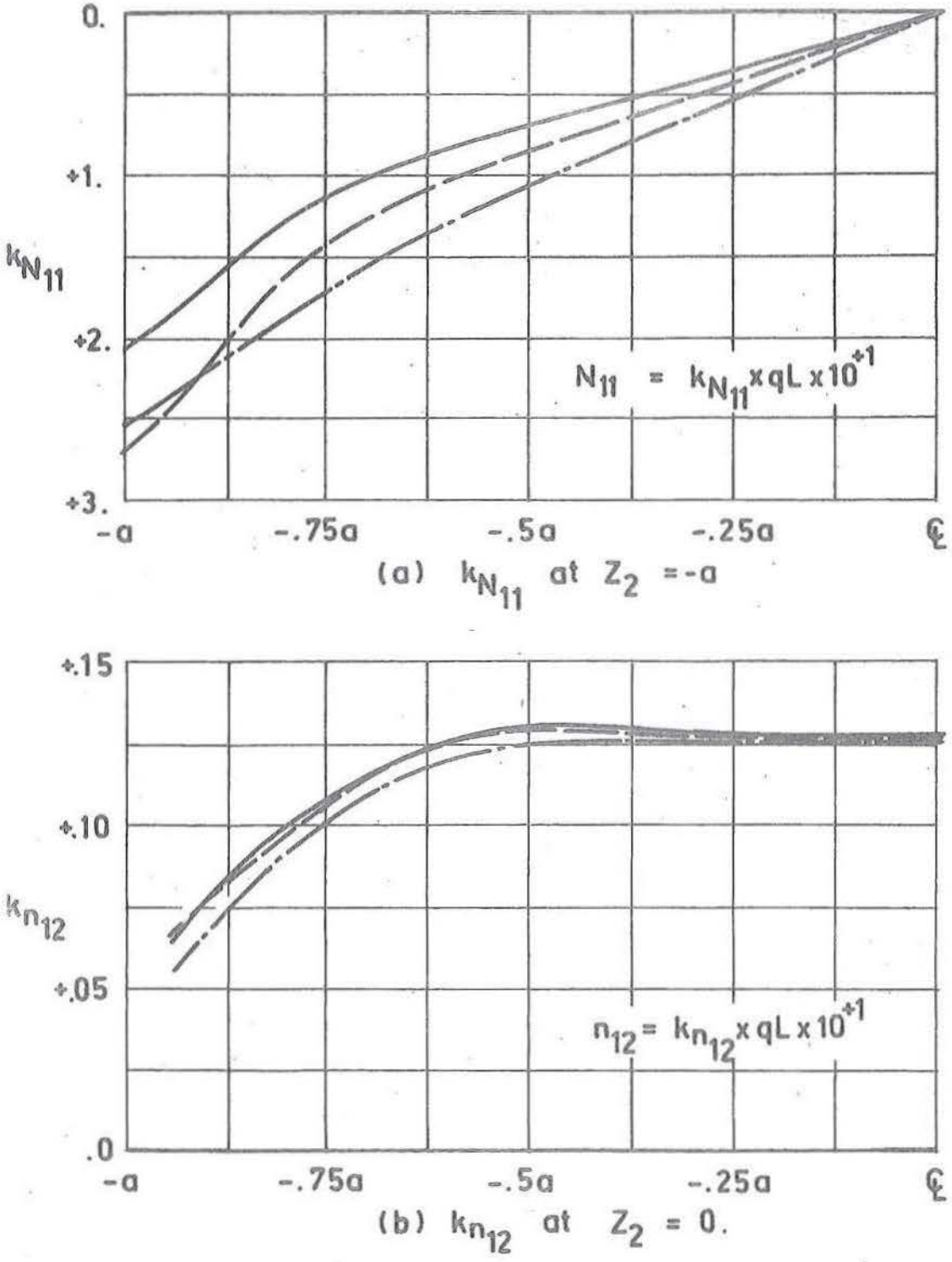

Fig. 7.4 Ruled surface hyperbolic paraboloid with edge beams clamped at corners. Convergence using conventional finite difference method.

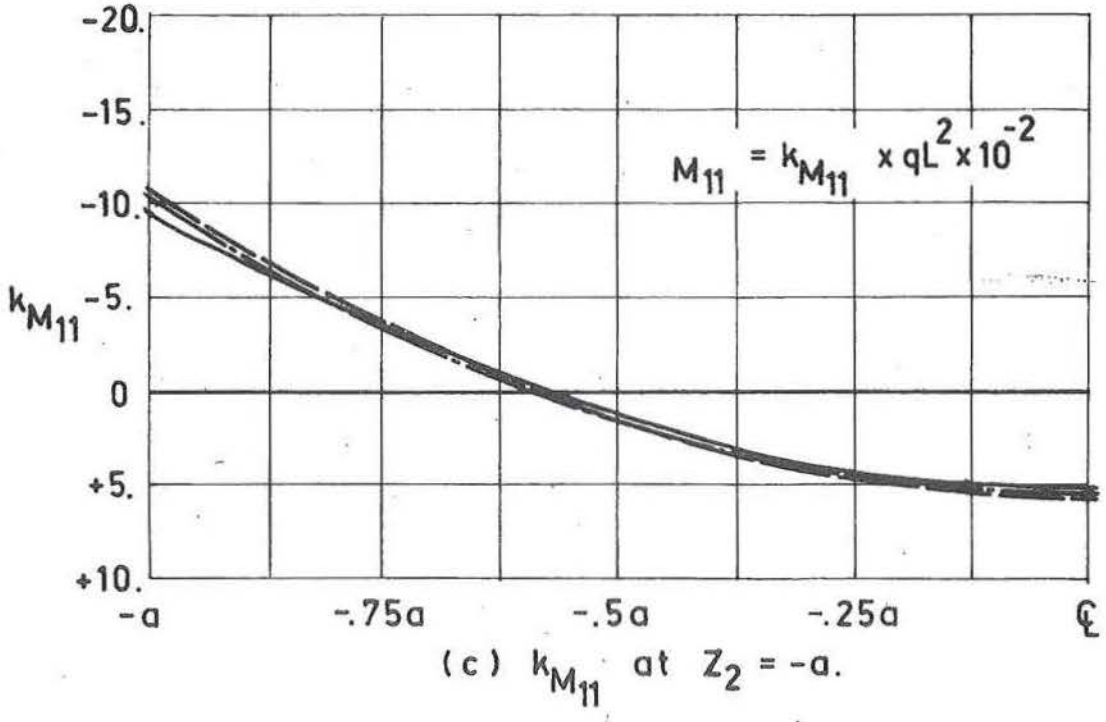

(c) $k_{M_{11}}$ at $Z_2 = -a.$

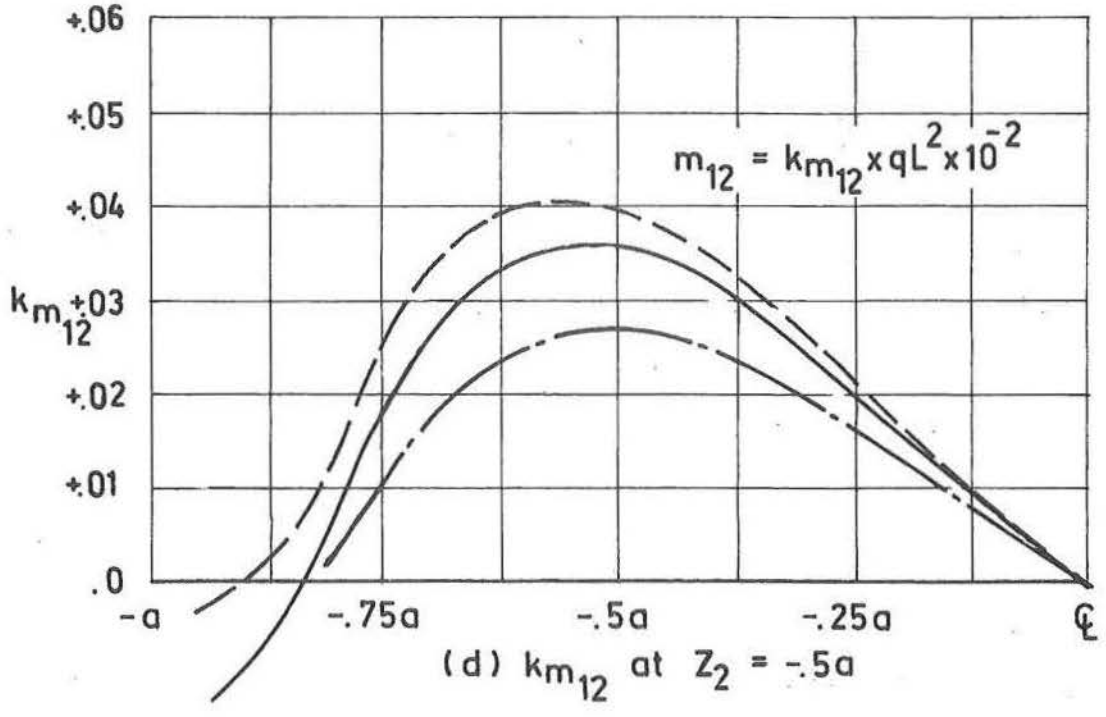

(d) $k_{m_{12}}$ at $Z_2 = -.5a$

Fig. 7.4 (continued) Ruled surface hyperbolic paraboloid with edge beams clamped at corners. Convergence using convential finite difference method.

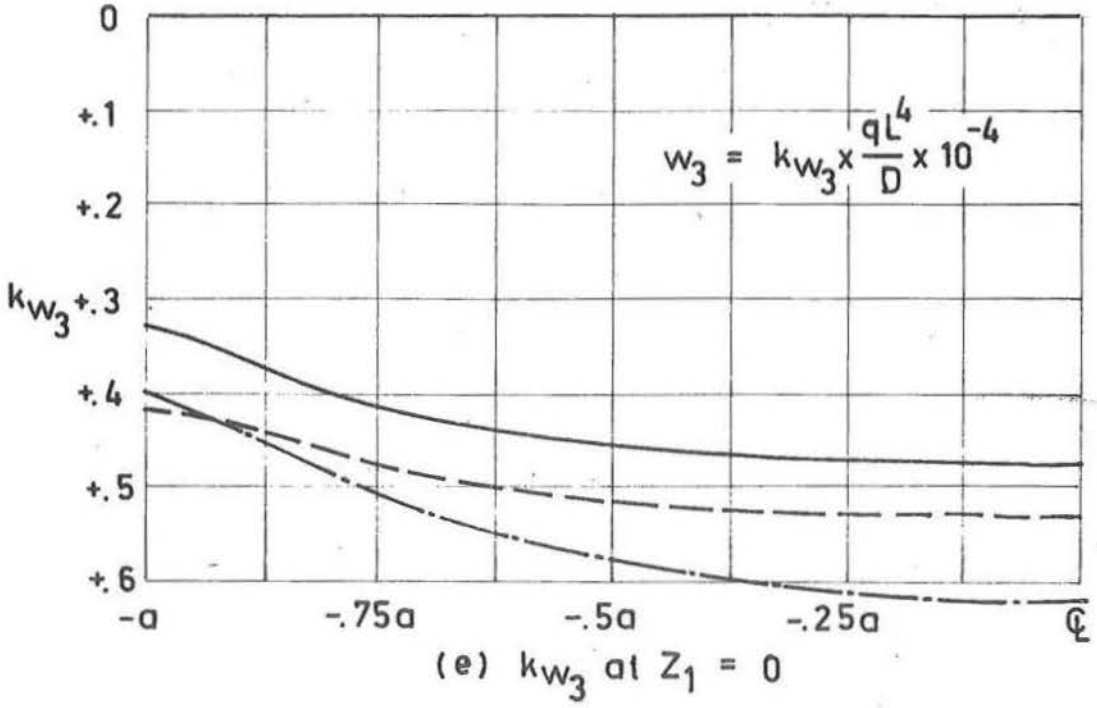

(e) k_{w_3} at $Z_1 = 0$

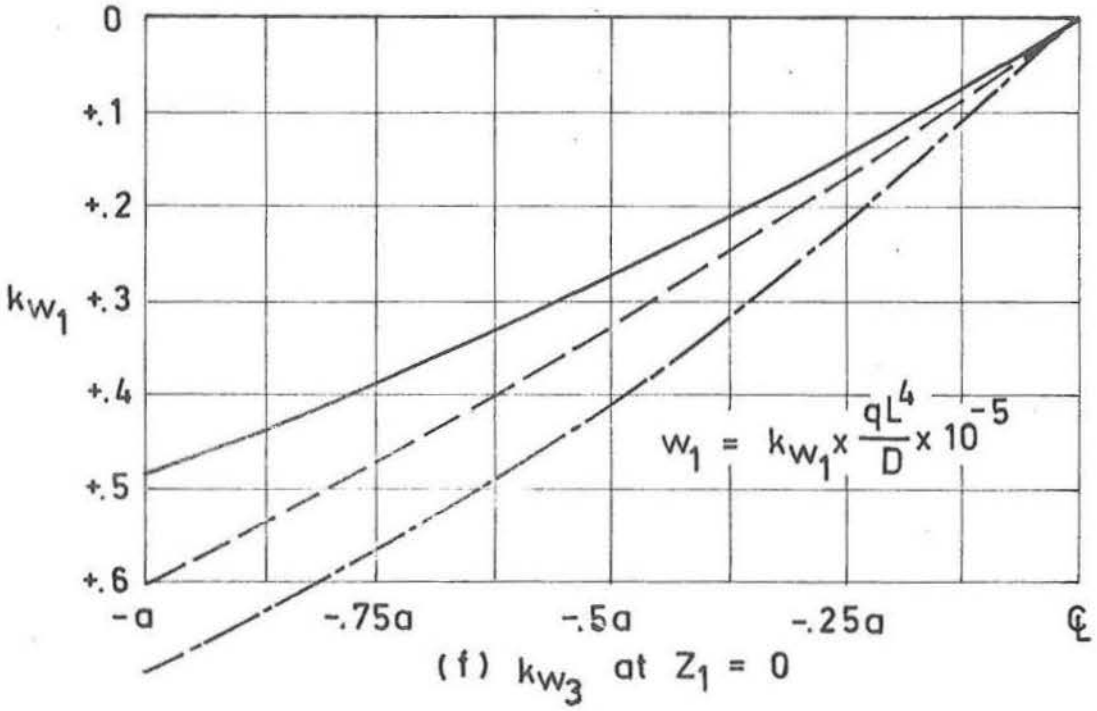

(f) k_{w_3} at $Z_1 = 0$

Fig. 7.4 (continued) Ruled surface hyperbolic paraboloid with edge beams clamped at corners. Convergence using conventional finite difference method.

analogue, such as the equating of shell internal actions at a position $(4,j)$ which varies in position with respect to the fixed boundary $(3,j)$, are considered with the numbers of complex terms discretised, the poor convergence of k_{w_k} is to be expected.

In presentation of the above, cross-sections containing the maximum ordinates of each quantity have been chosen, so it is likely that minimum convergence rates have been presented. Convergence of complete cross-sections are shown in preference to the convergence of particular points, for reasons which are obvious, when for example the convergence of $k_{m_{11}}$ at $(-0.625a,-a$ for the free edged shell shown in figure 7.3(c) is considered. For each of the boundary types studied, it has been found that geometric and material properties have small influences upon the nature of convergence which implies that the above examples are capable of wider generality within the class of boundary representation.

7.3 NUMERICAL EXPERIMENTS IN THE REDUCTION OF TRUNCATION ERRORS

A number of the methods for the reduction of truncation errors suggested in section 7.1 are applied to the examples considered in section 7.2. As an introduction however, the method of higher order boundary representation is applied to both the bending of clamped single span beams and single panel

flat plate.

7.3.1 Numerical Experiments on Beam and Plates

In order that estimates for the effects of boundary truncation error be determined, a preliminary study was made upon a number of single span beams and flat plates. Typical of the results were those pertaining to the encastré single span beam and single panel flat plate. In this section these results are summarised.

If $\left(\frac{\partial w_3}{\partial z_2}\right)_{3j}$ again denotes the normal derivatives of vertical deflection at the boundary z_2 constant, the following difference equations for the determination of w^3_{2j} (where i = 3 is once again considered colinear with the boundary) may be written [1].

$$
\begin{aligned}
w^3_{2j} &= +w^3_{3j} - \frac{1}{2}.h.\left(\frac{\partial^2 w_3}{\partial z_2^2}\right)_{3j},\\
w^3_{2j} &= +w^3_{4j} - \frac{1}{2}.h^2.\left(\frac{\partial^3 w_3}{\partial z_2^3}\right)_{3j},\\
2.w^3_{2j} &= -3.w^3_{3j} + 6.w^3_{4j} - w^3_{5j} - \frac{1}{2}.h^3.\left(\frac{\partial^4 w_3}{\partial z_2^4}\right)_{3j},\\
6.w^3_{2j} &= -20.w^3_{3j} + 36.w^3_{4j} - 12.w^3_{5j} + 2.w^3_{6j} - 2.h^4.\left(\frac{\partial^5 w_3}{\partial z_2^5}\right)_{3j},\\
24.w^3_{2j} &= -130.w^3_{3j} + 240.w^3_{4j} - 120.w^3_{5j} + 40.w^3_{6j} - 6.w^3_{7j} + 4.h^5.\left(\frac{\partial^6 w_3}{\partial z_2^6}\right)_{3j},\\
120.w^3_{2j} &= -924.w^3_{3j} + 1800.w^3_{4j} - 1200.w^3_{5j} + 600.w^3_{6j} - 180.w^3_{7j} + 24.w^3_{8j} - \frac{120}{7}h^6\left(\frac{\partial^7 w_3}{\partial z_2^7}\right)_{3j},
\end{aligned}
\qquad (7.9)
$$

Results for the clamped beam under uniform normal load q per unit length have been determined on successively finer grids

(with $m = 1,2,4,8$) for each of the boundary analogue expressions in (7.9). In figure 7.5 these results are summarised by plotting the convergence of central beam deflections and moments. To the scale used, the $n = 5$ and 6 solution lines coincide with that of $n = 4$, so that these are not shown. The remarkable increase in accuracy with decrease in discretisation error is at once obvious. For example, by using the analogue with $n = 4$, a mesh with $m = 2$ yields estimates of k_{w_3} to the same order of accuracy as a grid with $m = 8$ where the conventional analogue with $n = 2$ is employed. Similar conclusions may be derived for the convergence of moments, although the increased accuracy with increasing n is less pronounced.

Corresponding to the above study, the encastré flat plate with uniform load q has also been considered with boundary analogue increasing in the order of n, ($n = 1,6$). Results for central plate deflections and moment are shown in figure 7.6, where trends similar to those for the beam are illustrated. For the flat plate however, the increased accuracy is slightly less marked than for the beam, this no doubt being due to the increased significance of the differential analogue which tends to reduce the overall effect of errors in the boundary analogue.

It has also been found that as the truncation error of the boundary analogue is reduced (that is as n increases), the spectral radius of the iteration matrix H for both beams

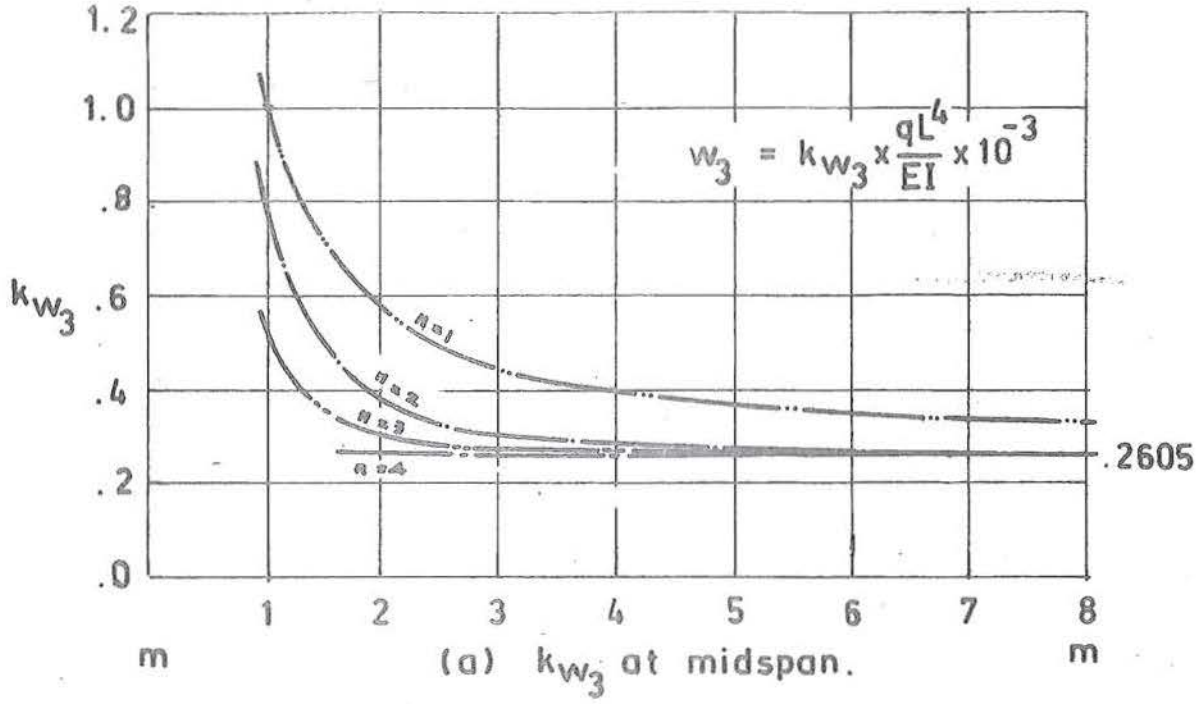

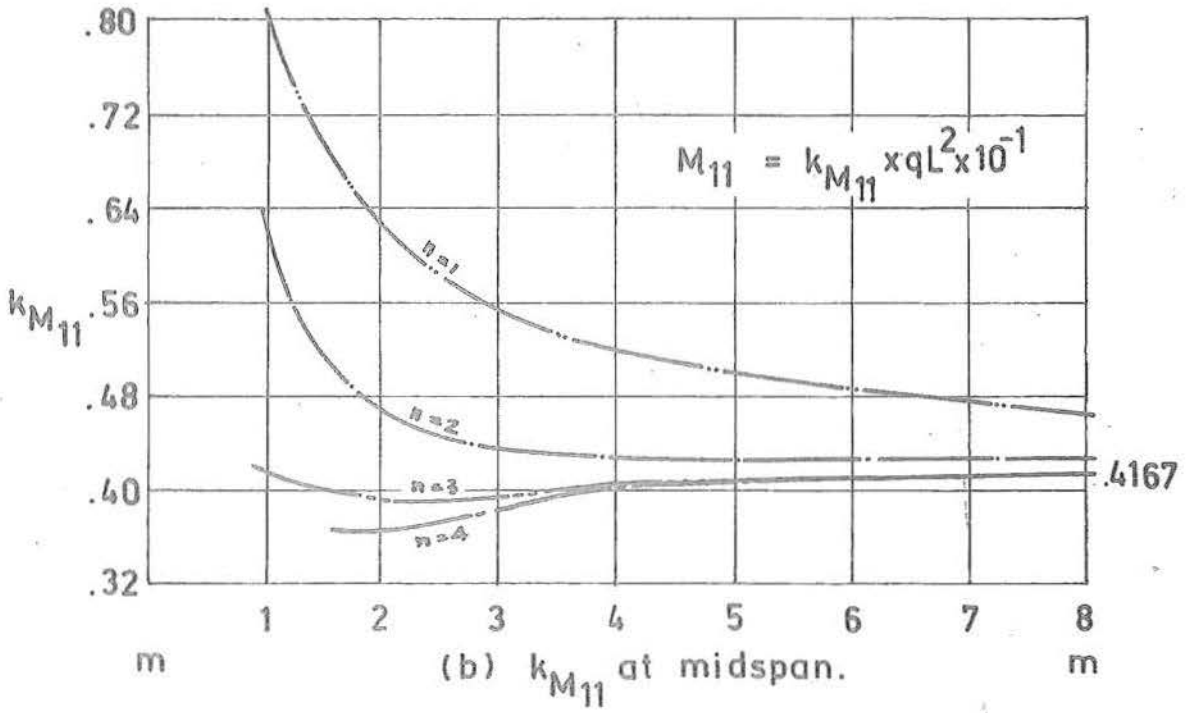

Fig. 7.5 Beam with ends clamped. Convergence as a function of boundary analogue truncation error. Truncation error $O(h^n)$.

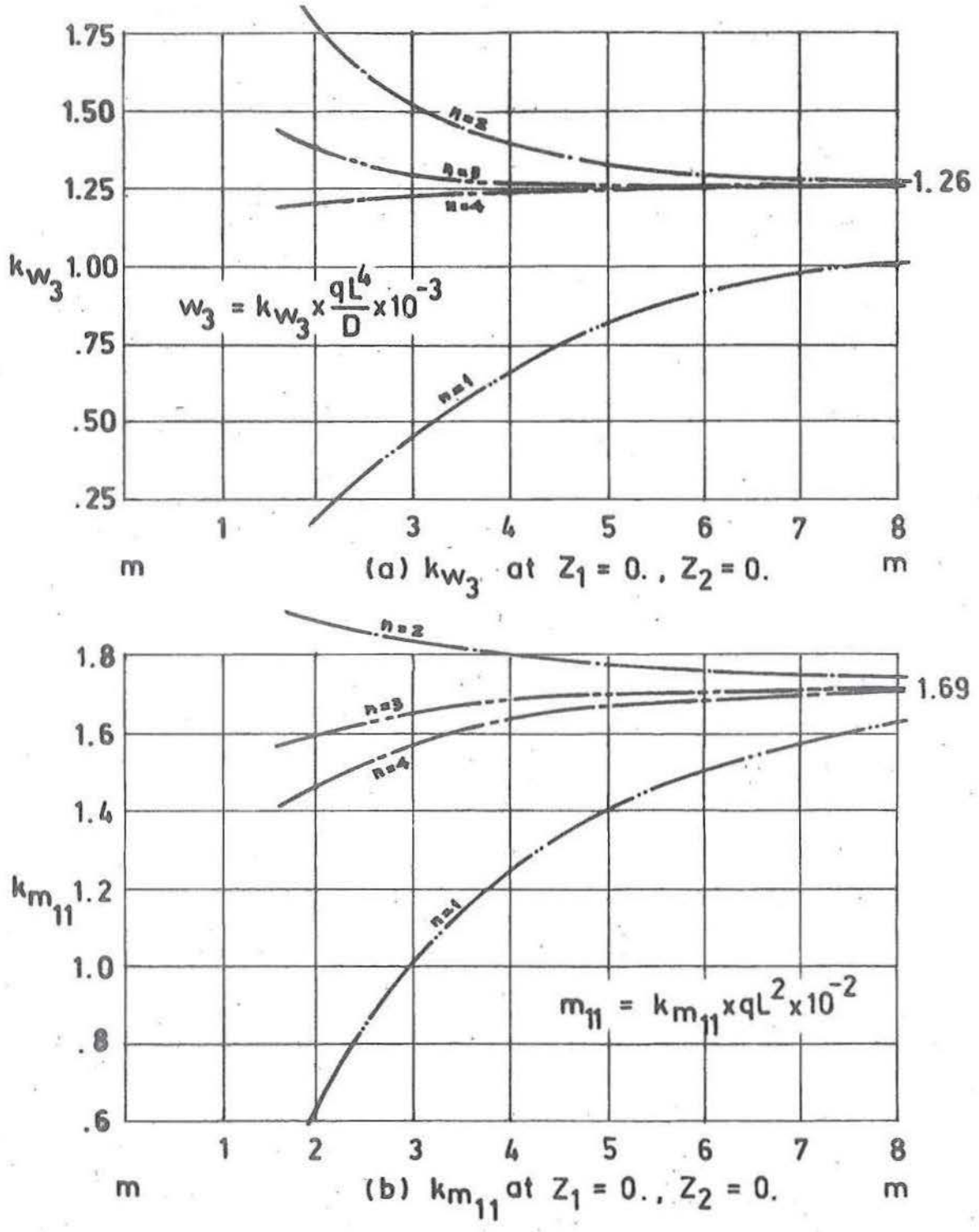

Fig. 7.6 Rectangular plate with all edges clamped. Convergence as a function of boundary analogue truncation error. Truncation error $O(h^n)$.

and plates increases considerably. This results in a greater computational effort to obtain converged solutions on the same grid size than for the conventional technique. Where an efficiency criteria of these methods is defined as the minimal total computing effort to obtain a given numerical accuracy, then it is not sufficient, where iteration is used, to compare the efficiency from the final resulting accuracy of w^k. Hence, although $n = 4$ provides the optimum analogue for the final accuracy of solutions, a value of $n = 3$ is found to be overall more efficient where the method of successive over-relaxation is used.

Before attempting to extend this technique to the ruled surface hyperbolic paraboloid, one further fact emerging from this study is noted. In figure 7.6 it is observed that for both k_{w_3} and $k_{m_{11}}$ the analogue with $n = 2$ provides an upper bound approach to the solution w^k, while the analogue $n = 4$ is a lower bound solution. This suggests a possible technique for determination of error bounds for discretised solutions rather than employing the time expensive techniques of section 7.2. For example, the mid-span normal deflections k_{w_3} of the flat plate are given by 0.001267 and 0.001223 for the analogues $n = 4$ and $n = 2$ respectively, indicating that the exact solution lies between these limits. The most accurate solution found in the present study is 0.001255, compared with 0.00126 reported by Timoshenko [54] of the work of Boobnov [9].

Unfortunately the upper and lower bound approach to the solution w^k was not found to occur at all other points over the vector space, and hence this behaviour may be used to determine the bounds for particular individual points but not the complete vector W .

7.3.2 Numerical Experiments on Ruled Surface Hyperbolic Paraboloids

In this section the methods of section 7.3.1 are extended to include the case of the ruled surface hyperbolic paraboloid with simple and clamped boundary supports. The modified finite difference method is also applied to the same shells.

7.3.2(a) Higher Order Boundary Analogues

Conventional finite difference solutions with $m = 8$ and $m = 16$ are plotted in figures 7.7 and 7.8, and the corresponding solution with $m = 8$ using the higher order boundary analogue. The notation used is:

——— Conventional techniques with $m = 16$.

– – – " " " $m = 8$.

—·—·— Higher order boundary analogue with $m = 8$.

Equation 7.9(d) is used to provide expressions w^3_{2j} for the clamped shell, and similar expressions w^2_{2j} for the simply supported shell. For the latter shell the condition of

$$\frac{\partial^2 w_3}{\partial z_2^2} = 0 , \qquad \text{at } z_2 = -a$$

provides the expression

$$20.\, w^3_{2j} = 35.\, w^3_{3j} - 6.\, w^3_{4j} - 14.\, w^3_{5j} + 6.\, w^3_{6j} + w^3_{7j} + \frac{161.}{180.} h^4 \left(\frac{\partial^6 w_3}{\partial z_\Sigma^6}\right)_{3j} \quad (710)$$

for the determination of w^3_{2j} .

Figure 7.7(c) to (f) shows that the higher order boundary analogues provide superior estimates of both displacements and moments in the vicinity of the boundary. At a distance of 0.5a from the boundary however, the conventional analogue appears to be superior. The in-plane stress resultants are given by approximately the same order of accuracy, although it is likely that had the solution w^k upon $m = 16$ for the conventional analogue converged exactly to the solution w_k , the higher order boundary method may provide superior estimates of $k_{n_{22}}$. Higher order boundary analogues for the simple support from figure 7.8, have an even smaller effect on shell behaviour than for the case of clamped supports. Had solutions from $m = 4$ been plotted, the same trends would have been observed.

It is concluded that because the simple support has an overall boundary truncation error less than that of the clamped support (this was demonstrated in section 7.2.2), the influence of decreased boundary truncation error effects the simple support to a lesser extent than the clamped support. Also, the influences of higher order boundary analogues for ruled

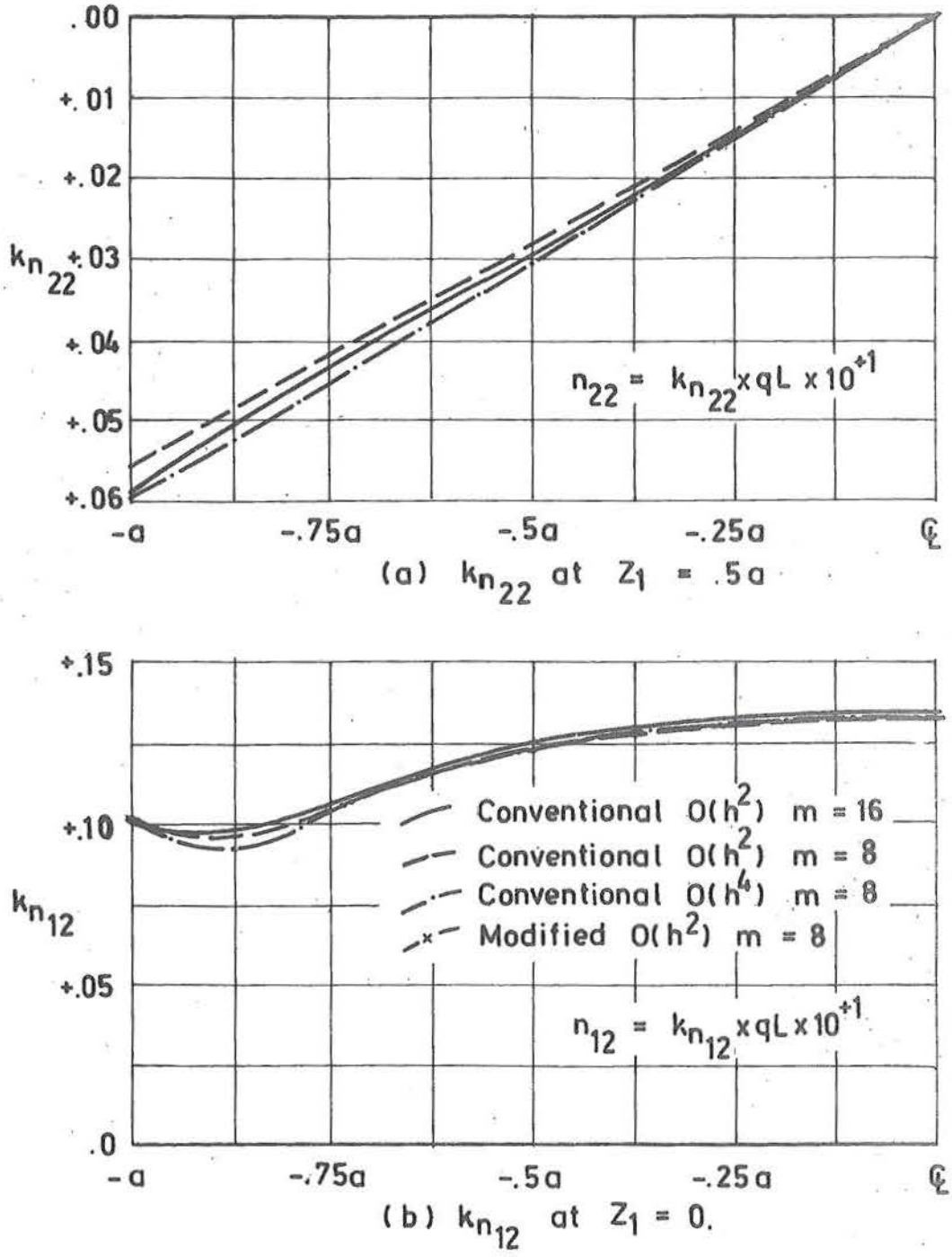

Fig. 7.7 Ruled surface hyperbolic paraboloid with all edges clamped. Comparison of conventional technique with boundary analoque $O(h^2)$ and $O(h^4)$, and modified technique. Grid with m = 8.

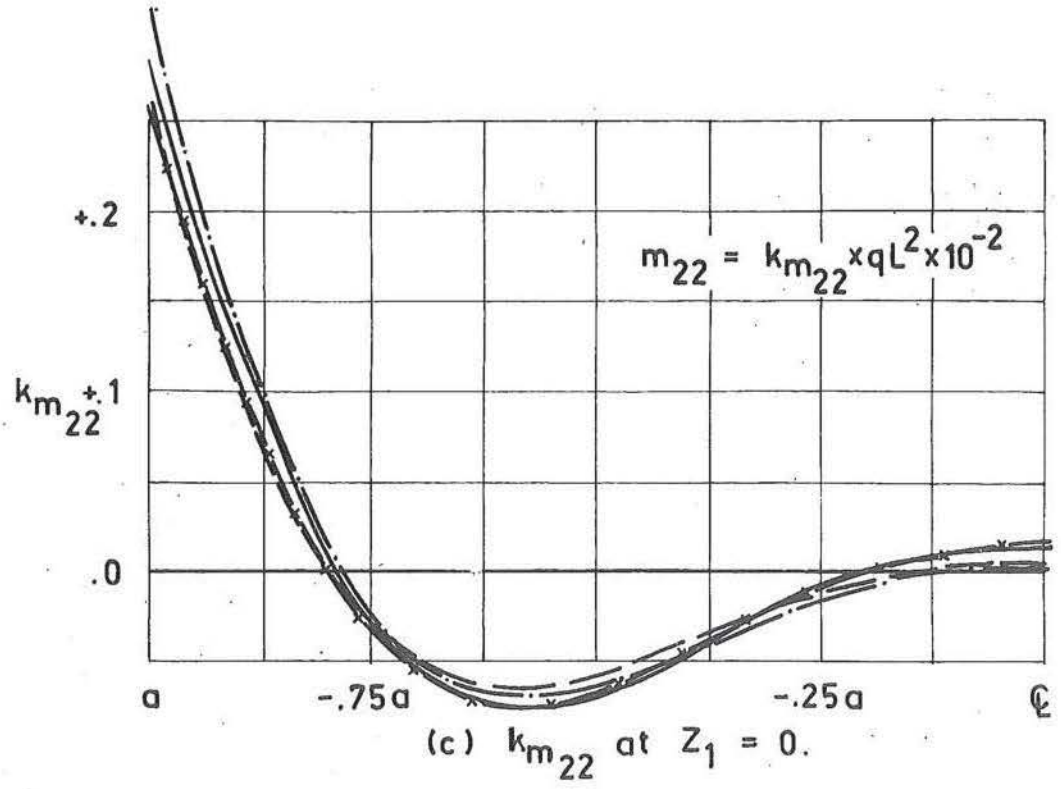

(c) $k_{m_{22}}$ at $Z_1 = 0.$

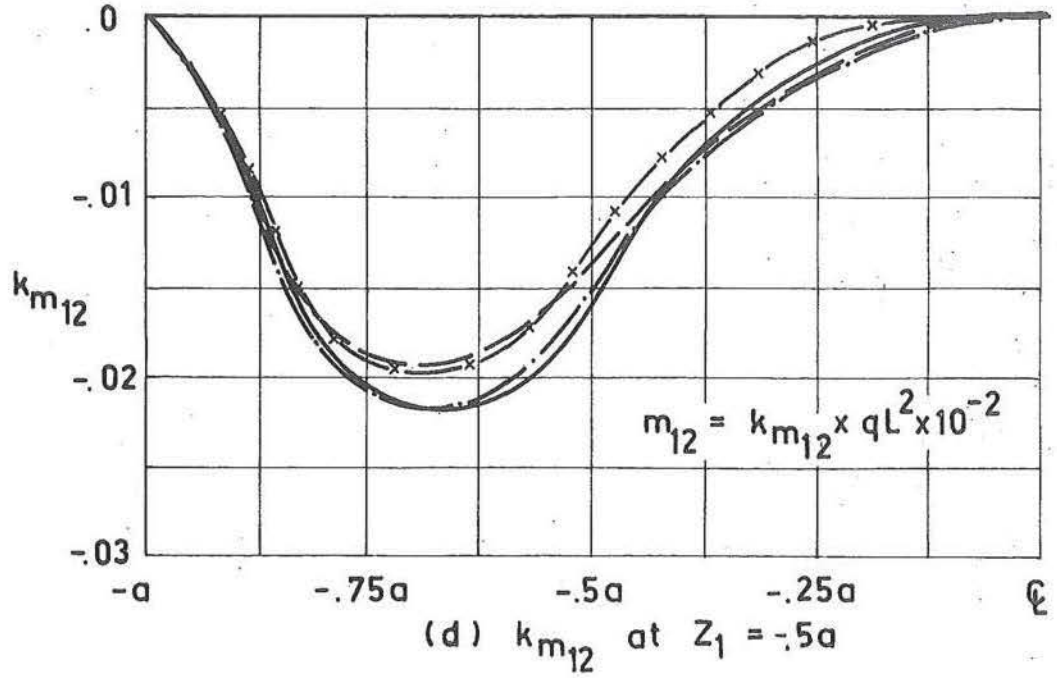

(d) $k_{m_{12}}$ at $Z_1 = -.5a$

Fig. 7.7 (continued) Ruled surface hyperbolic paraboloid with all edges clamped. Comparison of conventional technique with boundary analoque $O(h^2)$ and $O(h^4)$, and modified technique. Grid with m = 8.

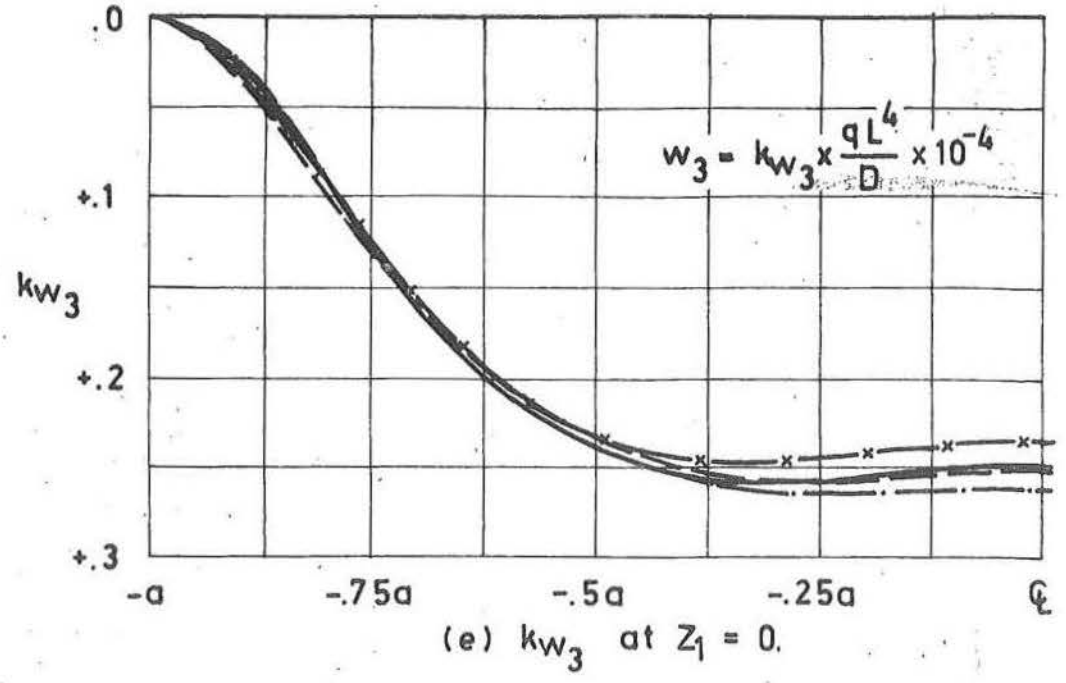

(e) k_{w_3} at $Z_1 = 0.$

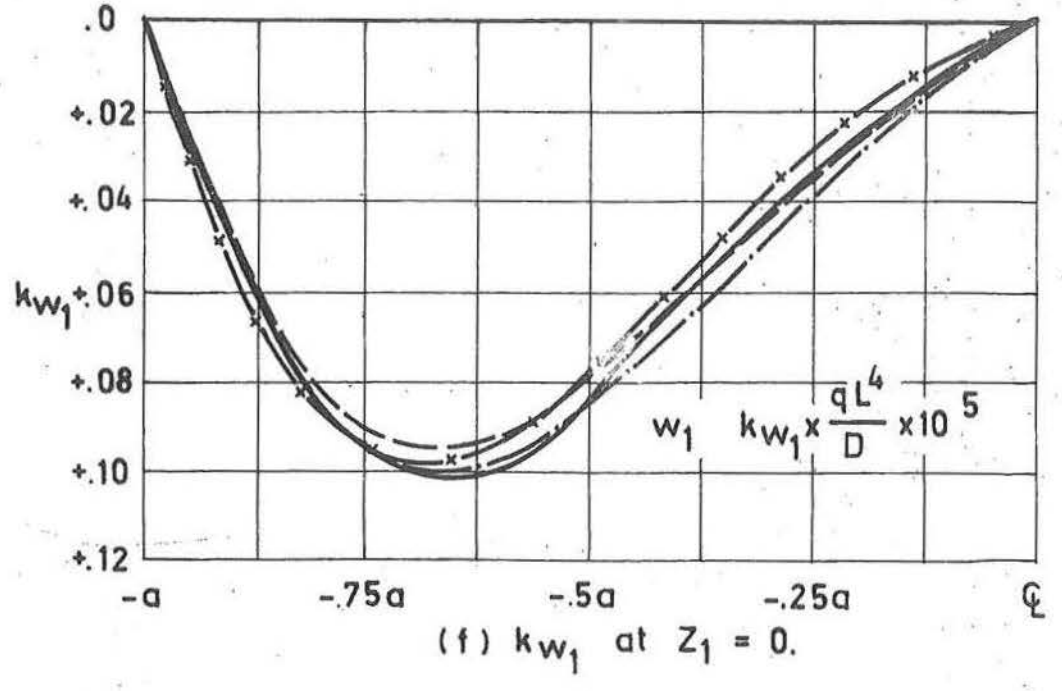

(f) k_{w_1} at $Z_1 = 0.$

Fig. 7.7 (continued) Ruled surface hyperbolic paraboloid with all edges clamped. Comparison of conventional technique with boundary analogue $O(h^2)$ and $O(h^4)$, and modified technique. Grid with m = 8.

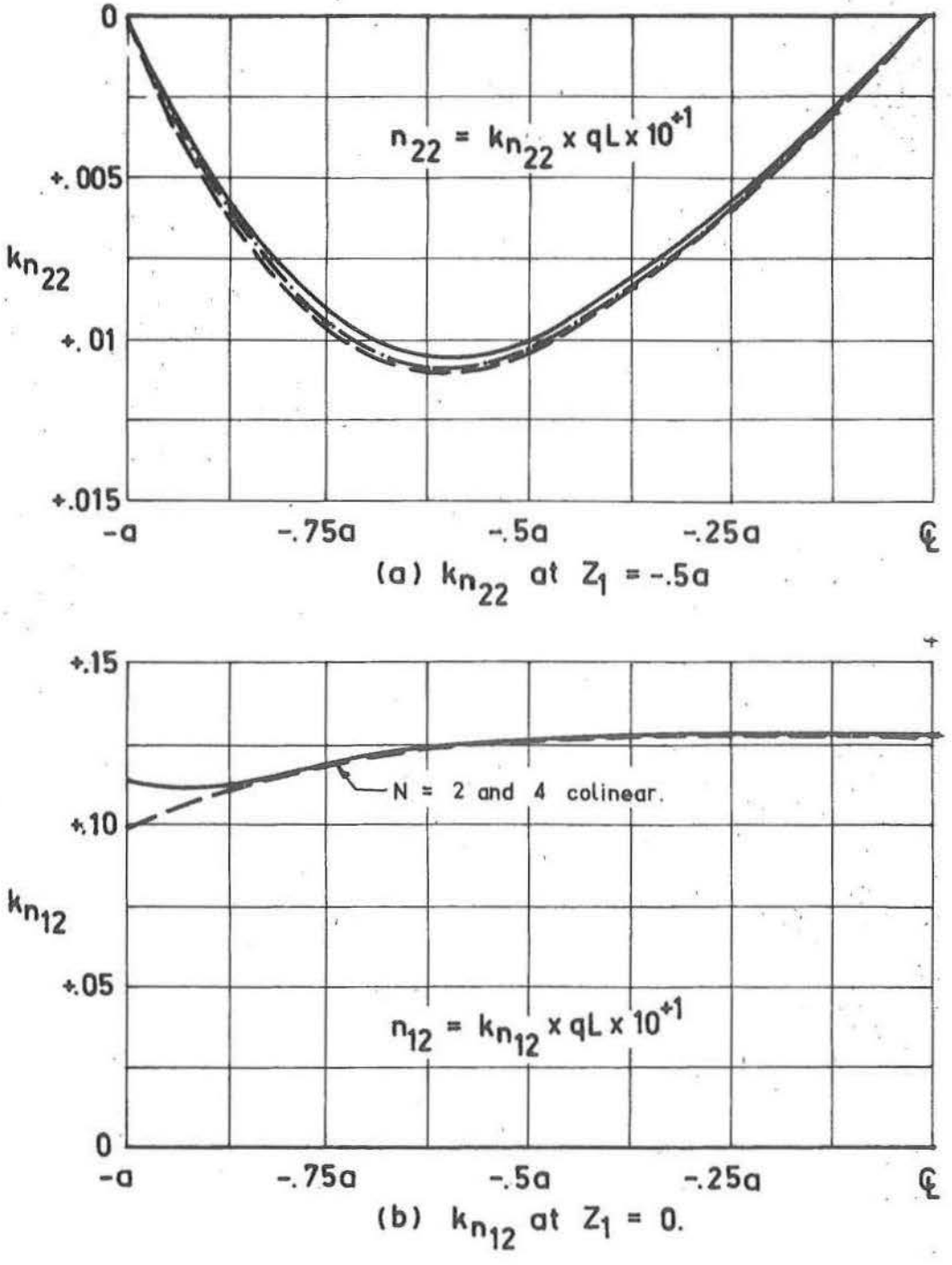

Fig. 7.8 Ruled surface hyperbolic paraboloid with all edges simply supported. Comparison of conventional technique with boundary analoque $O(h^2)$ and $O(h^4)$, and modified technique. Grid with m = 8.

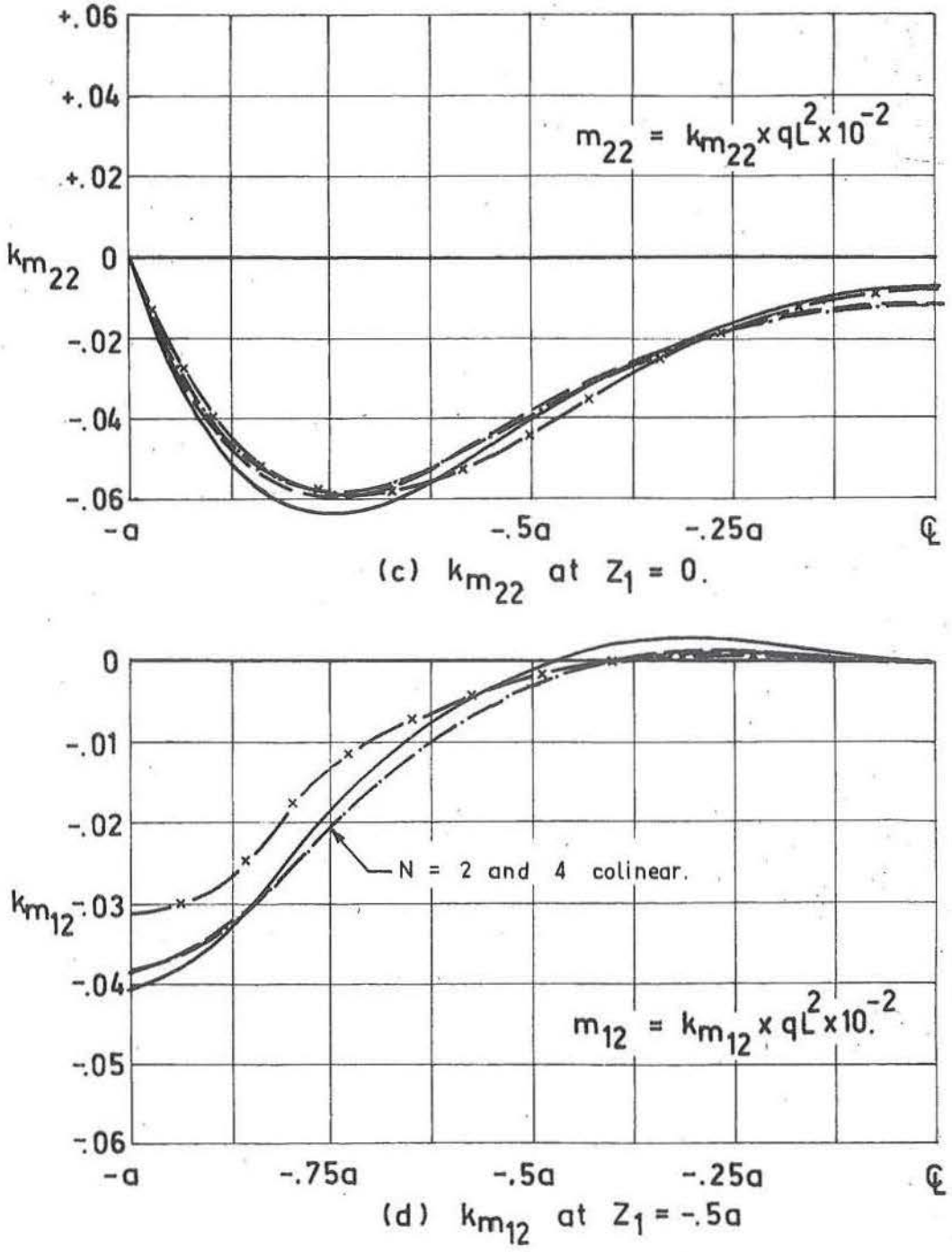

Fig. 7.8 (continued) Ruled surface hyperbolic paraboloid with all edges simply supported. Comparison of conventional technique with boundary analogue $O(h^2)$ and $O(h^4)$, and modified technique. Grid with $m = 8$.

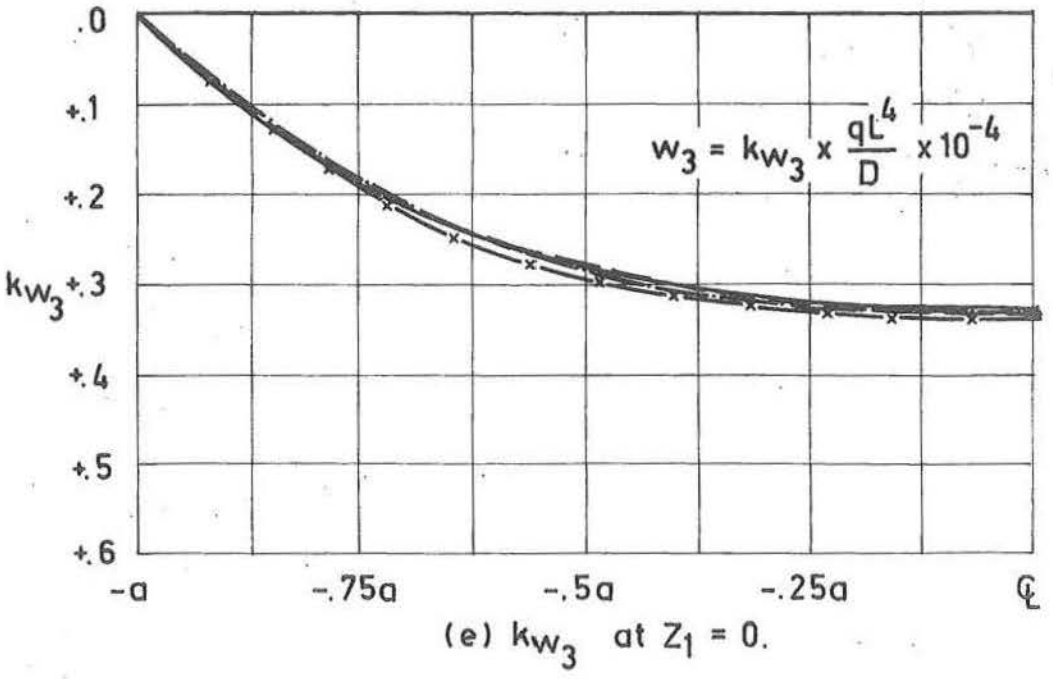

(e) k_{w_3} at $Z_1 = 0$.

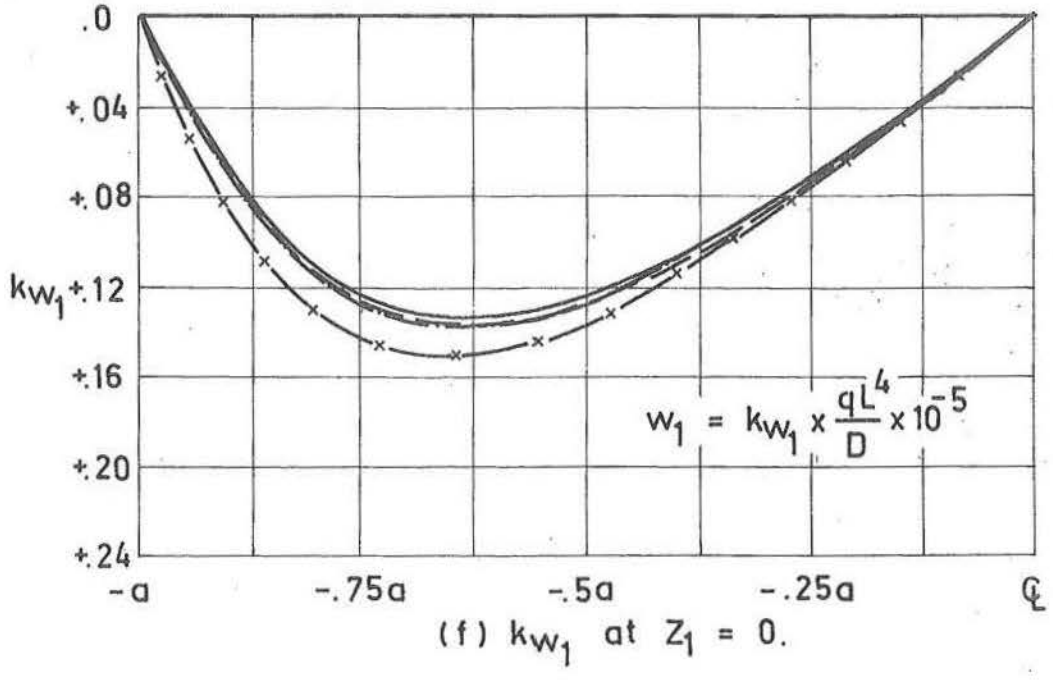

(f) k_{w_1} at $Z_1 = 0$.

Fig. 7.8 (continued) Ruled surface hyperbolic paraboloid with all edges simply supported. Comparison of conventional technique with boundary analogue $O(h^2)$ and $O(h^4)$, and modified technique. Grid with $m = 8$.

surface hyperbolic paraboloid shells, are very much less than for the corresponding beams or plates.

7.3.1(b) Modified Finite Difference Method

For a grid with $m = 8$ the solutions of clamped and simply supported ruled surface hyperbolic paraboloid shells using the modified finite difference technique, are shown in figures 7.7 and 7.8 with notation —x— .

Generally, and especially in the regions of boundary influence, this method is less accurate than the corresponding conventional finite difference technique. In view of the phenomonal increase in convergence rates reported[43] for the related second order translational problem, this behaviour is disappointing and must be attributed to the severe increase in boundary truncation errors. In contrast with the translational shell, the advantages of the higher order differential analogues for the ruled surface hyperbolic paraboloid are seen to be offset by the decrease in accuracy with which a number of the boundary conditions may be represented.

7.3.2(c) Extrapolation Methods

To demonstrate both the potentials and dangers of the extrapolation method, the following two examples of point extrapolation are considered.

The first example considers the value of $k_{n_{12}}$ for the free edge shell (given in figure 7.3(b), at the position

$(0, -.5a)$, as being a sufficiently smooth function of m, at least for $m \geq 2$, for application of the method of extrapolation. With $k_{n_{12}}$ at this point on grids of $m = 4$ and $m = 8$ given by 1.465 and 1.434, the application of (7.1) yields

$$k_{n_{12}} = 1.408$$

as representing the extrapolated value upon the zero grid. This compares favourably with the value of 1.410 given for the $m = 16$ grid.

As a second example, the displacement k_{w_1} of the free edge shell (shown in figure 7.3(f)) is chosen as typical of a badly behaved function of m. This case, for $m = 4$ and 8 at the point $(0, -a)$, yields 2.319 and 1.947 as successive estimates to k_{w_1}. Application of (7.1) yields in this case

$$k_{w_1} = 1.823$$

as an estimate of k_{w_1} on zero grid size. This is seen to be an inferior estimate of the value 2.067 given by $m = 16$ to that given on the $m = 8$ grid.

Generalising then, it can be seen that the method of grid extrapolation is normally not a practical technique for the reduction of truncation errors. Although it may provide a better estimate for certain well posed points, it is never certain, especially where a two point extrapolation is employed, that the extrapolated value is a superior estimate to those

already obtained.

7.4 CONCLUSIONS

Although analytic solutions are not available, the convergence of solutions for all boundary conditions considered in section 7.2 using the conventional finite difference technique, with the exception of the edge beam which is further considered in chapter 8, are within acceptable limits for practical purposes. For these purposes, use of mesh sizes with $m = 8$ is adequate, and although in general $m = 4$ provides acceptable estimates of in-plane stresses, the values given for displacements and moments may be in significant error.

Techniques for the reduction of truncation errors described in section 7.1 and applied in section 7.3 to the case of the ruled surface hyperbolic paraboloid are shown, where iterative solution methods are used, to be inferior in overall computational efficiency to the conventional method. Although in certain cases the method of higher order boundary representation may provide greater overall accuracy, and therefore efficiency where a direct solution procedure is used, the increase in spectral radius of the iteration matrix H generally results in greater computational effort for the same accuracy where an indirect technique is employed. In certain circumstances these methods may be beneficial in providing either an independent check upon the solutions using conventional methods, or for providing bounds of solutions.

CHAPTER EIGHT

THE INFLUENCE OF BOUNDARY SUPPORTS

The critical nature of support structures upon the overall behaviour of the ruled surface hyperbolic paraboloid has long been recognised and although the majority of studies verifying this have been of an empirical nature (see section 10.1), the theoretical solutions presented also indicate that this assertion is correct. In this chapter an outline of the theoretical results obtained in past research using the method of finite differences is given for those studies pertaining to the ruled surface hyperbolic paraboloid. Although this review is by no means exhaustive it is felt that it covers the major contributions to this particular field.

Section 8.2 considers the special cases of the clamped, simple and freely supported boundaries. By presenting these results in detail, the critical nature of the boundaries is shown. Also, the differences in problem formulation (indicated in sections 3.6 and 6.3) between the degenerate cases of clamped and free edge supports are illustrated. The influence of corner support conditions is demonstrated by three examples in which the localised influence of both corner moment constraints, the effect of supports over a finite area and the critical behaviour of diagonal thrust members, is shown.

Each of these corner conditions is applied to the free edge shell. In chapter 12 the same trends are shown to apply to the beam supported shell.

A number of suggested boundary analogues for the ruled surface hyperbolic paraboloid with edge beam supports are considered in sections 8.3 and 8.4. The advantages and disadvantages of each of these are discussed with special attention taken to ensure that the analogues, with suitable choice of beam dimensions, are consistent with the degenerate cases of clamped and free edge support. For the particular boundary representation chosen, the relative influences of the four support modes - vertical flexure, horizontal flexure, torsion and extension of the edge beam are considered. In addition, the influence of a number of second order boundary effects are studied in section 8.4. A simplified boundary analogue, presented in section 8.6, embodies all those factors which are likely to affect the final solutions by an order equal to the expected numerical accuracy (see section 7.2).

For the purpose of discussion in this chapter, the term "membrane" applies to the stress system resulting from the solution of the classical membrane theory (see example [5,46]), while "bending" refers to the stresses and displacements caused by the introduction of bending effects. The "membrane" stress, referred to the z_k coordinates, is pure in-plane shear which at $\frac{\pi}{4}$ to the z_1 and z_2 axes is principal direct stress.

"Bending" consists of all the flexural stresses plus any differences in in-plane stresses between the membrane solutions and the bending solutions.

8.1 THEORETICAL REVIEW

Extensive reviews of the theoretical solutions pertaining to the ruled surface hyperbolic paraboloid are presented in references [13, 51].

This section therefore considers only the work directly concerned with the finite difference solutions of the bending theory for this class of shell.

Gupta [29] considered the case of the ruled surface hyperbolic paraboloid with edges clamped both flexurally and extensionally. As well as not employing to the full the conditions of symmetry, the solution contains a number of minor errors first observed by Sled [50]. Also considering a flexurally clamped ruled surface hyperbolic paraboloid, but with the conditions of simple support for the extension action, Soare [51] obtained solutions for a number of symmetrically positioned uniform loads. This boundary condition, like that of the simple support considered in section 7.2.2, is of little more than academic interest, although it does have a number of advantages in representing the limit case as the ratio λ_3 increases (this is demonstrated in section 8.3.2(c)).

Dayaratnam and Gerstle[18], in a combined bending-buckling study of the ruled surface hyperbolic paraboloid were the first, it appears, to consider the interaction of a shell-edge beam boundary. The edge beam was considered as possessing finite stiffness in both the vertical flexural and torsional modes, while the extensional or membrane conditions were those of the simple support. Although this model is an attempt to include the effects of the edge beam, it omits the predominant mode for the ruled surface hyperbolic paraboloid edge beam interaction - that is the extensional stiffness. In addition, shell internal actions are computed at the beam centroidal axis, a condition which is clearly physically incorrect, while in order to overcome a difficulty arising from this formulation it is assumed that the analogue of $\frac{\partial^3 w_3}{\partial z_2^3}$ at the boundary is zero. Since this term provides a major contribution to the effective boundary shear ($q_{22} + \frac{\partial m_{12}}{\partial z_1}$), the edge beam vertical flexural equation is incorrectly formulated.

In a second paper, Gupta[30] considerably improves this boundary edge beam representation by considering an edge beam of finite vertical and extensional stiffness. These conditions (at least for the edge beam reported) are shown in section 8.6 to be the predominant modes, and once again the remaining conditions are those of the corresponding simple support. The boundary analogue used is that of the traction boundary with grid orientation II (of section 8.3.3(b)), and for this reason

it is likely to yield solutions for edge beams of small dimensions which are superior to solutions for the method described in 8.3.2(a).

It is noted that for each of the above described investigations, solutions were sought using the stress function and normal displacement formulation for the thin shallow shell equations. Although this may result in a slight improvement of numerical accuracy over the results using the three displacement components, the use of a grid with $m = 4$, from the results of chapter 7, introduces significant truncation errors for the determination of bending behaviour.

Probably the first application of the finite difference method to the analysis of a ruled surface hyperbolic paraboloid shell to assist a design problem, was reported by Chronowicz [15]. Employing a modified model of that of Gupta [30] he was able to conclude that the free edged shell, due to the resulting large displacements, was not an architecturally feasible model. Results are not presented and although it is indicated that accuracy is checked by summation of vertical forces, no details are given.

8.2 DEGENERATE BOUNDARY CONDITIONS

To facilitate comparitive studies, each of the clamped, simple and free edged boundary results for a typical shell are given in detail. Further, the difference in boundary representation between the clamped and freely supported shell demonstrates

the difference in finite difference formulation of the displacement and traction edge types. The shells chosen are those presented in the convergence studies of section 7.2 with dimensionless ratios

$$\begin{aligned} \lambda_1 &= 0.20, \\ \lambda_2 &= 0.0165, \\ \mu &= 0.000 \end{aligned} \tag{8.1}$$

and difference grids with $m = 16$.

For convenience, and because it is often illustrative to compare surface stresses due to bending and membrane action, the factors to convert $(k_{m_{kk}}, k_{n_{kk}})$, $(k = 1,2)$ to corresponding surface stresses $(\sigma_{m_{kk}}, \sigma_{n_{kk}})$, $(k = 1,2)$ are given by

$$\begin{aligned} \sigma^{t}_{m_{kk}} &= (-1)^{k}.864.0.k_{m_{kk}}.q, \\ \sigma^{b}_{m_{kk}} &= (-1)^{k+1}.864.0.k_{m_{kk}}.q, \\ \sigma_{n_{kk}} &= +1200.k_{n_{kk}}.q, \end{aligned} \tag{8.2}$$

where the t and b superscripts refer to the top and bottom shell surfaces.

It can be shown that the surface stress is only dependent upon the applied loading where dimensional similitude of (8.1) is assured. For the sake of convenience q is considered as unity in the following discussion.

The difference grid orientation of section 6.3.1 is used, and because solutions have been obtained over $\frac{1}{8}$ the shell area, the conditions of symmetry and or antisymmetry about the z_2 axis and the diagonal given by $z_1 = z_2$ are reviewed. About the line z_2, the conditions

$$\frac{\partial w_1}{\partial z_1} = \frac{\partial^2 w_2}{\partial z_1^2} = \frac{\partial w_3}{\partial z_1} = 0. \qquad (8.3)$$

are given exactly by the difference expressions

$$\begin{aligned} w^1_{i\,m+4} &= +w^1_{i\,m+2}\,, \\ w^2_{i\,m+4} &= -w^2_{i\,m+2}\,, \\ w^3_{i\,m+4} &= +w^3_{i\,m+2}\,, \\ w^3_{i\,m+5} &= +w^3_{i\,m+1}\,. \end{aligned} \qquad (1 \leq i \leq m+5) \quad (8.4)$$

About the diagonal $z_2 = z_1$ conditions of mirror symmetry apply, in that

$$\begin{aligned} w^1_{i+r\,i} &= +w^2_{i\,i+r}\,, \\ w^2_{i+r\,i} &= +w^1_{i\,i+r}\,, \quad (r = 1,2),\ (1 \leq i \leq m+3) \quad (8.5) \\ w^3_{i+r\,i} &= +w^3_{i\,i+r}\,. \end{aligned}$$

These conditions are derived using the principle of superposition.

8.2.1 Clamped Supports

The general boundary equations for the hyperbolic paraboloid,

given in section 3.5 and 3.6, where it is assumed that

$$\frac{K}{E_b A} = \frac{K}{E_b I_3} = \frac{D}{E_b I_3} = \frac{K}{E_b I_2} = \frac{D}{E_b I_2} = \frac{K}{E_b I_1} = \frac{D}{E_b I_1} = 0., \quad (8.6)$$

and further that

$$\frac{G_1}{E_b A} = \frac{G_2}{E_b I_3} = \frac{G_3}{E_b I_2} = 0., \quad (8.6)$$

become

$$\frac{\partial^2 w_1}{\partial z_1^2} = \frac{\partial^4 w_2}{\partial z_1^4} = 0., \quad \text{at } z_2 = -a \quad (8.7)$$

$$\frac{\partial^3 w_3}{\partial z_1^2 \partial z_2} = \frac{\partial^4 w_3}{\partial z_1^4} = 0.$$

Assuming conditions of clamped corners

$$w_1 = w_2 = w_3 = 0., \quad \text{at } z_1 = z_2 = -a \quad (8.8)$$

$$\frac{\partial w_1}{\partial z_2} = \frac{\partial w_2}{\partial z_1} = \frac{\partial w_3}{\partial z_1} = \frac{\partial w_3}{\partial z_2} = 0.,$$

the equations (8.7) upon integration reduce to

$$w_1 = w_2 = w_3 = \frac{\partial w_3}{\partial z_2} = 0., \text{ at } z_2 = -a \quad (8.9)$$

which in finite difference form are given by

$$w_{3j}^1 = w_{3j}^2 = w_{3j}^3 = 0., \quad \text{at } j = 3, m+3 \quad (8.10)$$

$$w_{2j}^3 = w_{4j}^3 .$$

It can similarly be shown that the discretised form of the general equations (5.17) to (5.28) also reduce to these

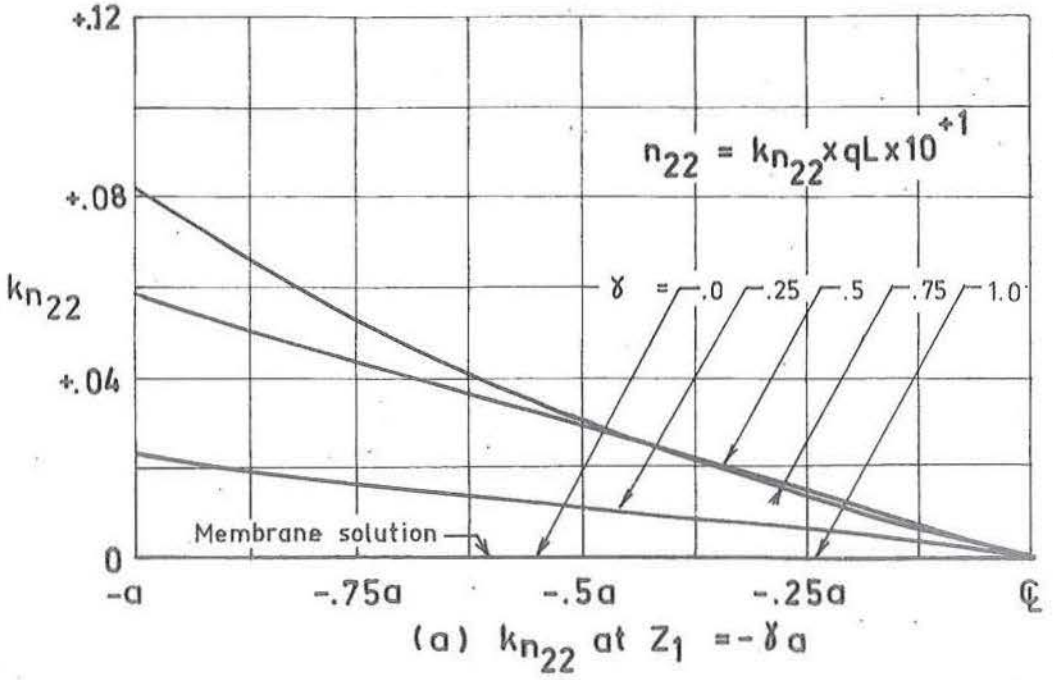

(a) kn_{22} at $Z_1 = -\gamma a$

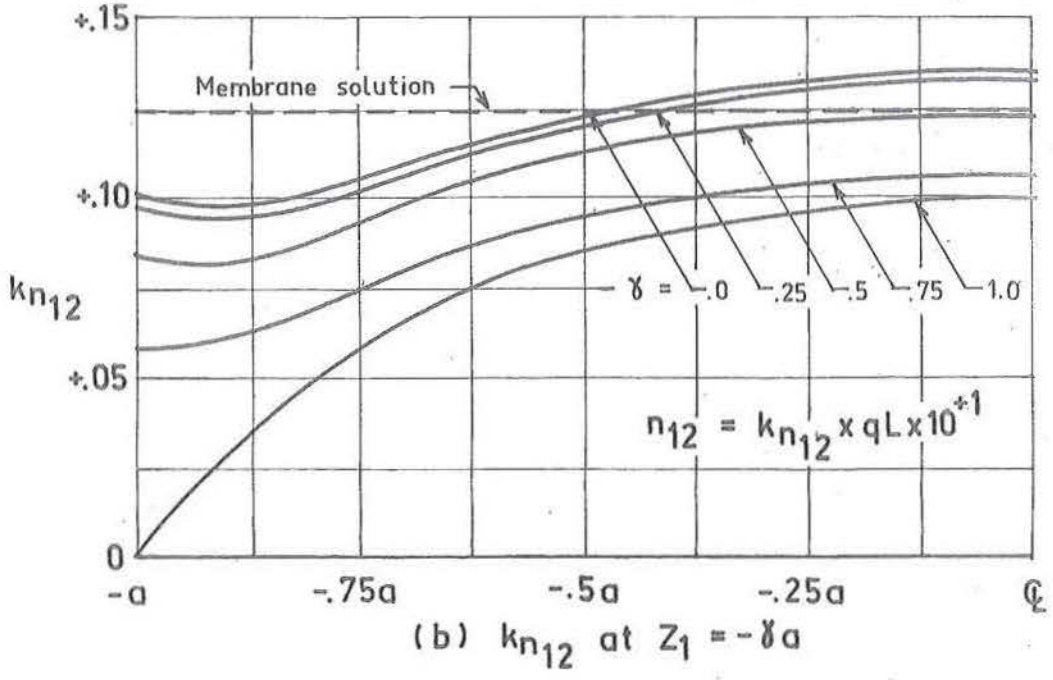

(b) kn_{12} at $Z_1 = -\gamma a$

Fig. 8.1 Ruled surface hyperbolic paraboloid with all edges clamped. Distribution of stress resultants at cross sections $Z_1 = -\gamma a$.

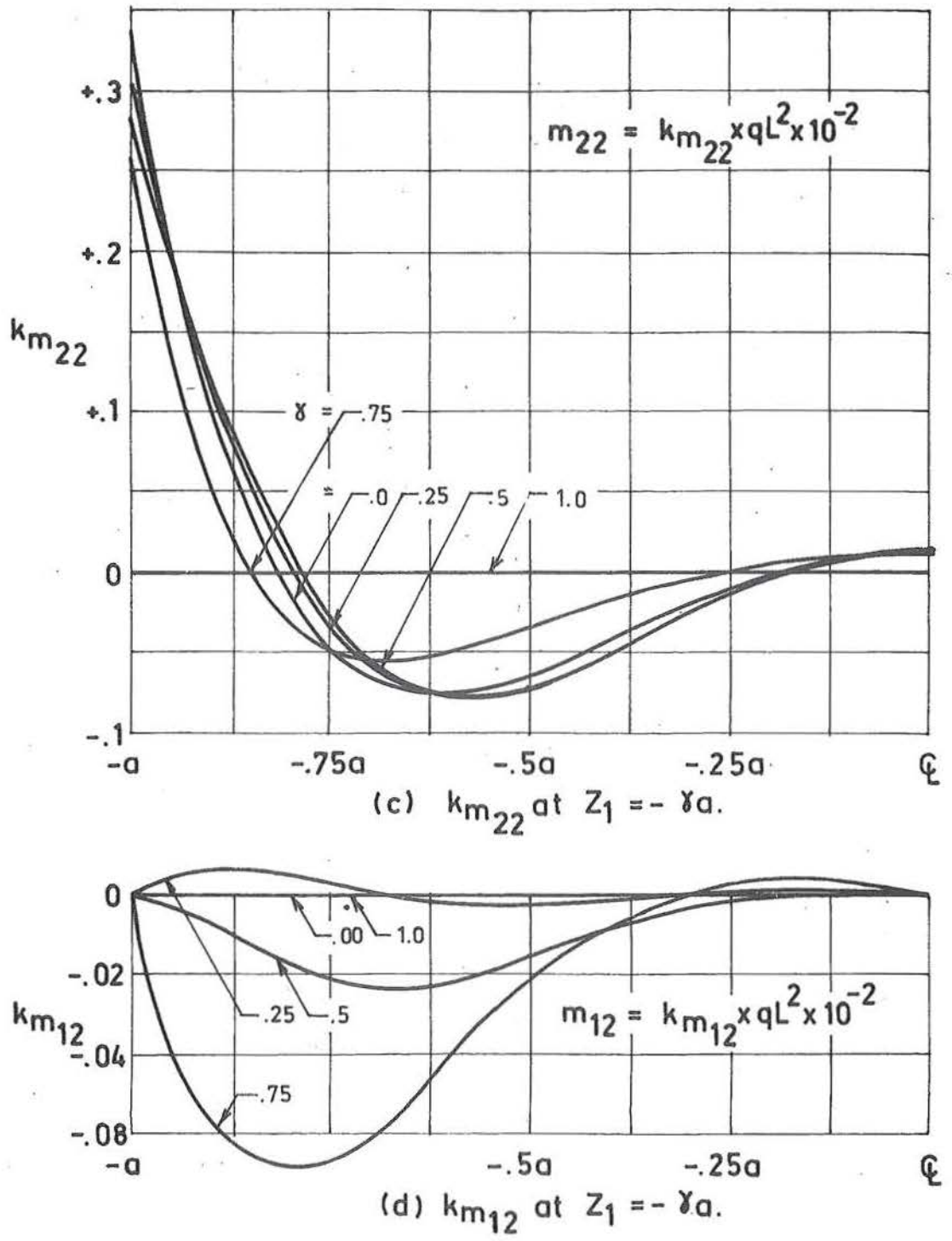

Fig. 8.1 (continued) Ruled surface hyperbolic paraboloid with all edges clamped. Distribution of moment resultants. at cross sections $Z_1 = -\gamma a$.

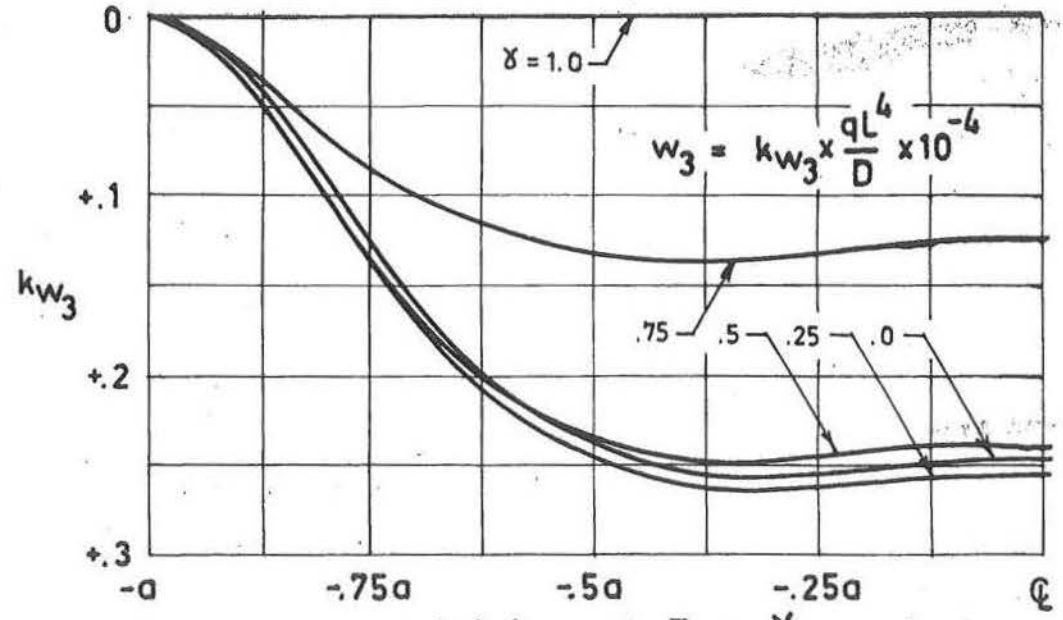

(e) k_{w_3} at $Z_1 = -\gamma a$.

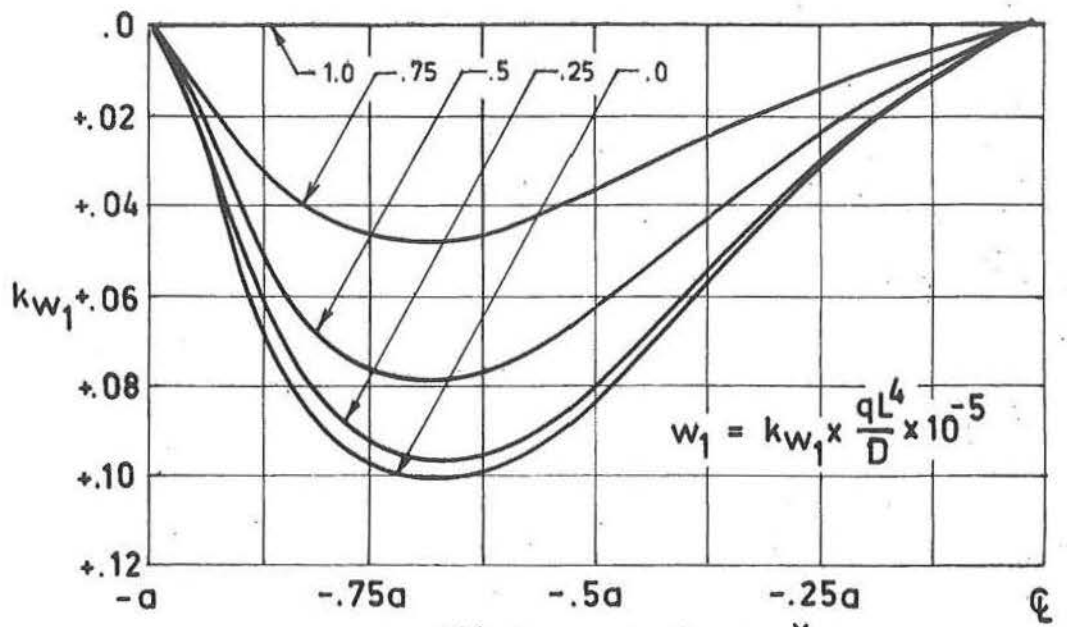

(f) k_{w_1} at $Z_1 = -\gamma a$.

Fig 8.1 (continued) Ruled surface hyperbolic paraboloid with all edges clamped. Distribution of displacements at cross sections $Z_1 = -\gamma a$.

conditions with the assumptions of (8.6) to (8.8).

Figure 8.1 shows the distribution of direct stress resultants, stress couples and displacements at five cross-sections over one quarter the shell surface. The considerable divergence of $k_{n_{12}}$ from that of the membrane state in the region $|z_1, z_2| > 0.5a$, shown in figure 8.1(b), is accompanied by correspondingly high bending stresses, and therefore displacement gradients. The principal stress of 150 psi for the membrane state is shown by using equations (8.2), to be of the order of 50% less than the top surface stresses at $z_2 = -a$ as predicted using bending theory. At the shell centre, $|z_1, z_2| < 0.5a$, however, in-plane shear stress $k_{n_{12}}$ is within $\pm$ 10% of that of the membrane solution, with the result that the bending solution plays a less significant role. For example at $(-.5a, -.5a)$ (the extreme position of bending in this arbitrarily defined shell centre), the membrane stress is 40% greater than the bottom surface bending stress, while at (0,0) it is of the order of 900% greater.

This demonstrates that even at positions considerably out of the so called boundary zone (see for example Reissner[46]) the bending stresses although considerably reduced are of the order of those resulting from membrane theory. In section 8.2.4 therefore, a further criteria for the boundary zone is discussed.

8.2.2 Simple Support

Once again making the assumptions of equations (8.6), except that for this particular case the second and seventh of these conditions are replaced with

$$\frac{E_b I}{K} = \frac{E_b I_1}{D} = 0. \qquad (8.11)$$

respectively, the general equations of section 3.5 may be reduced to the form

$$\frac{\partial^2 w_1}{\partial z_1^2} = n_{22} = m_{22} = \frac{\partial^4 w_3}{\partial z_1^4} = 0. \qquad (8.12)$$

When these conditions are combined with the clamped corner conditions of (8.8) they reduce to

$$\begin{aligned} w_1 &= w_3 = 0., \\ \frac{\partial w_2}{\partial z_2} &= 0., \qquad \text{at } z_2 = -a \\ \frac{\partial^2 w_3}{\partial z_2^2} &= 0., \end{aligned} \qquad (8.13)$$

which, in finite difference form, become

$$\begin{aligned} w_{3j}^1 &= w_{3j}^3 = 0., \\ w_{2j}^2 &= w_{4j}^2, \qquad j = 4, m+3 \\ w_{2j}^3 &= -w_{4j}^3. \end{aligned} \qquad (8.14)$$

The pivotals w_{3j}^2 are defined by the application of the z_2 equilibrium equation (2.26) and not by the boundary conditions as in the case of conditions (8.10) of section 8.2.1. For this purpose it is necessary to either eliminate the $\frac{\partial^2 w_1}{\partial z_1 \partial z_2}$

term from equation (2.26), or define the pivotals w^1_{2j}. Since no simple expression for $\frac{\partial w_1}{\partial z_2}$ at the boundary as a function of z_1 exists, the first alternative is not considered further; instead the z_1 equilibrium equation (2.25) is applied at grid positions $(3,j)$, $(j = 3,m+3)$ in order that w^1_{2j} be defined. Because

$$\frac{\partial w_1}{\partial z_1} = \frac{\partial w_2}{\partial z_2} = 0, \qquad \text{at} \quad z_2 = -a$$

equation (2.25) reduces to

$$\frac{\partial^2 w_1}{\partial z_2^2} + \frac{2f}{a^2} \cdot \frac{\partial w_3}{\partial z_2} = 0, \qquad (8.15)$$

which provides the finite difference expression

$$w^1_{2j} = -w^1_{4j} - \frac{2.f}{a.m} \cdot w^3_{4j} \qquad (8.16)$$

for the definition of w^1_{2j}. Equation (4.20) may therefore, with the conditions (8.14) and (8.16), be applied at the boundary $(3,j)$, $(j = 3,m+3)$, where it is noted that the term $\frac{\partial w_3}{\partial z_1}$ is eliminated.

The impractical nature of this particular boundary condition may be observed by the often conflicting requirements of conditions (8.11) and the conditions of (8.6) which are applicable. In certain cases, the edge diaphram for example, these conditions are closely approximated and have been justified in a number of experimental studies [38,10]. Additional to this, it is shown in sections 8.3.2(c) that this boundary condition provides a better approximation to the

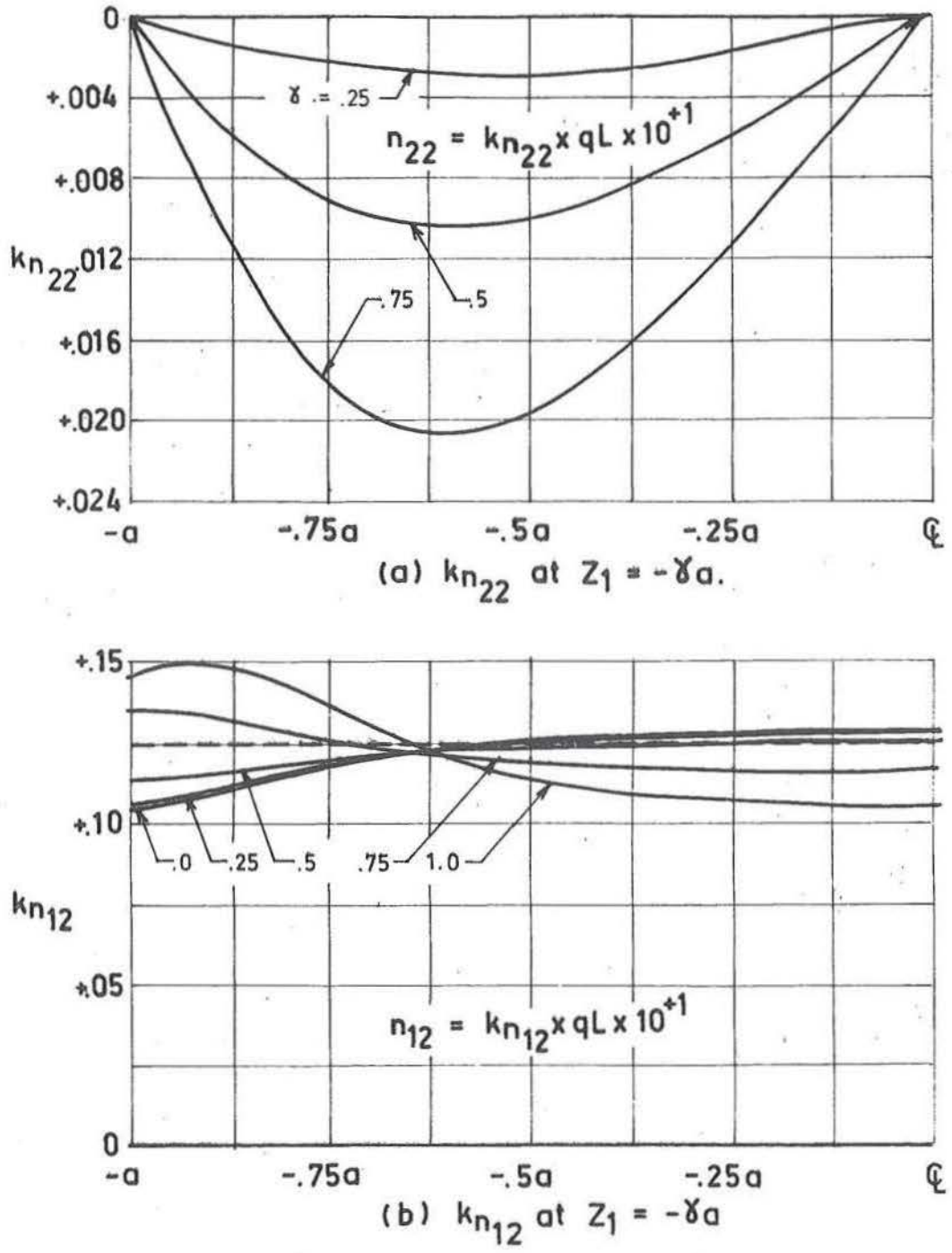

Fig. 8.2 Ruled surface hyperbolic paraboloid with all edges simply supported. Distribution of stress resultants at cross sections $Z_1 = -\gamma a$.

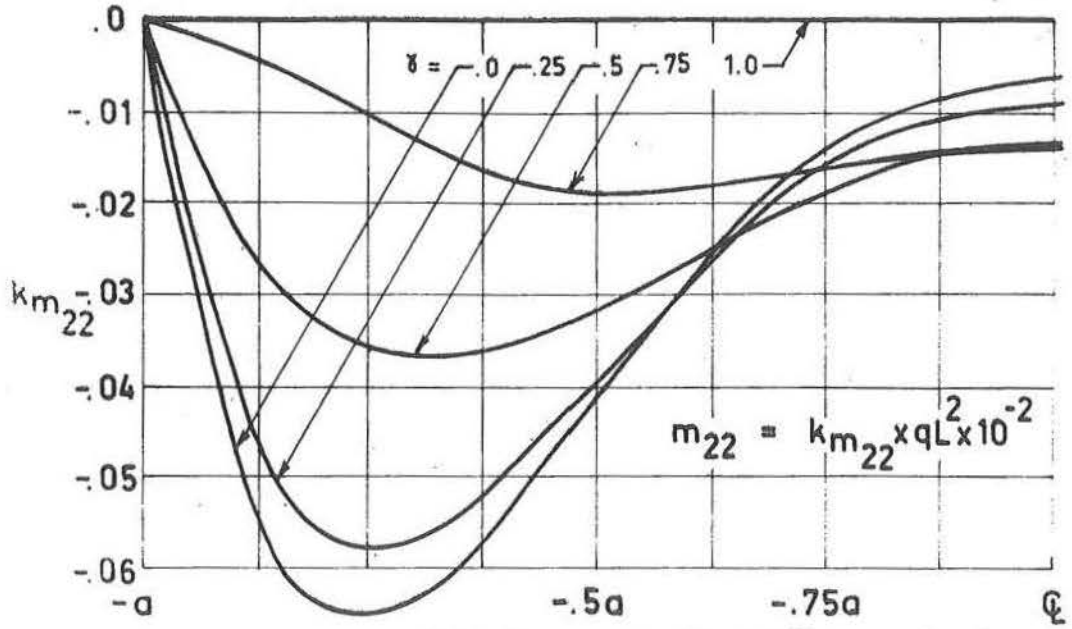

(c) $k_{m_{22}}$ at $Z_1 = -\gamma a$.

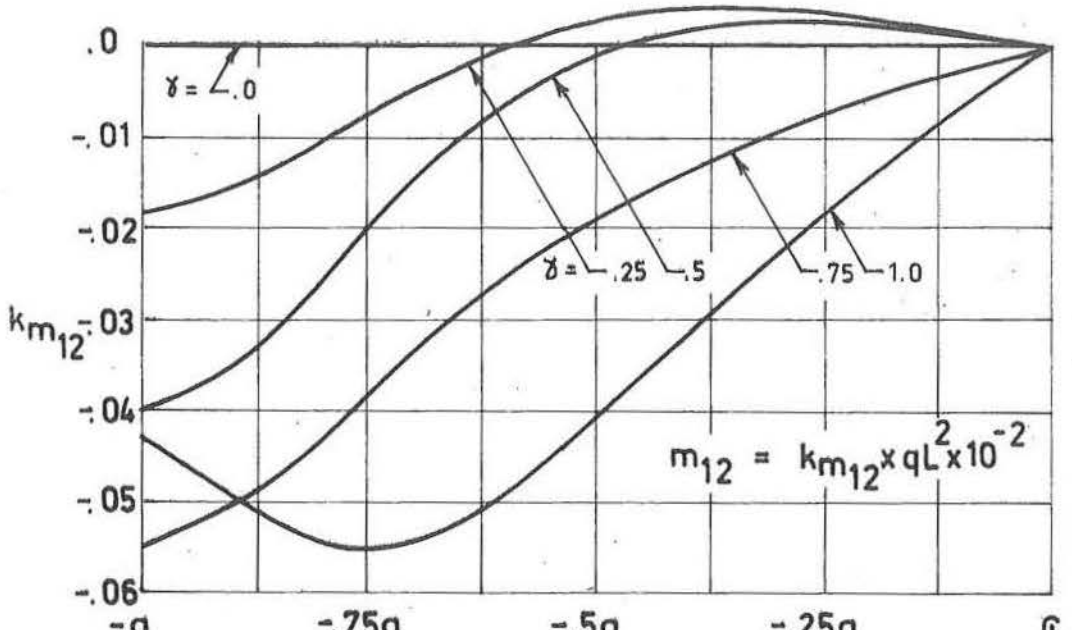

(d) $k_{m_{12}}$ at $Z_1 = -\gamma a$.

Fig. 8.2 (continued) Ruled surface hyperbolic paraboloid with all edges simply supported. Distribution of moment resultants at cross sections $Z_1 = -\gamma a$.

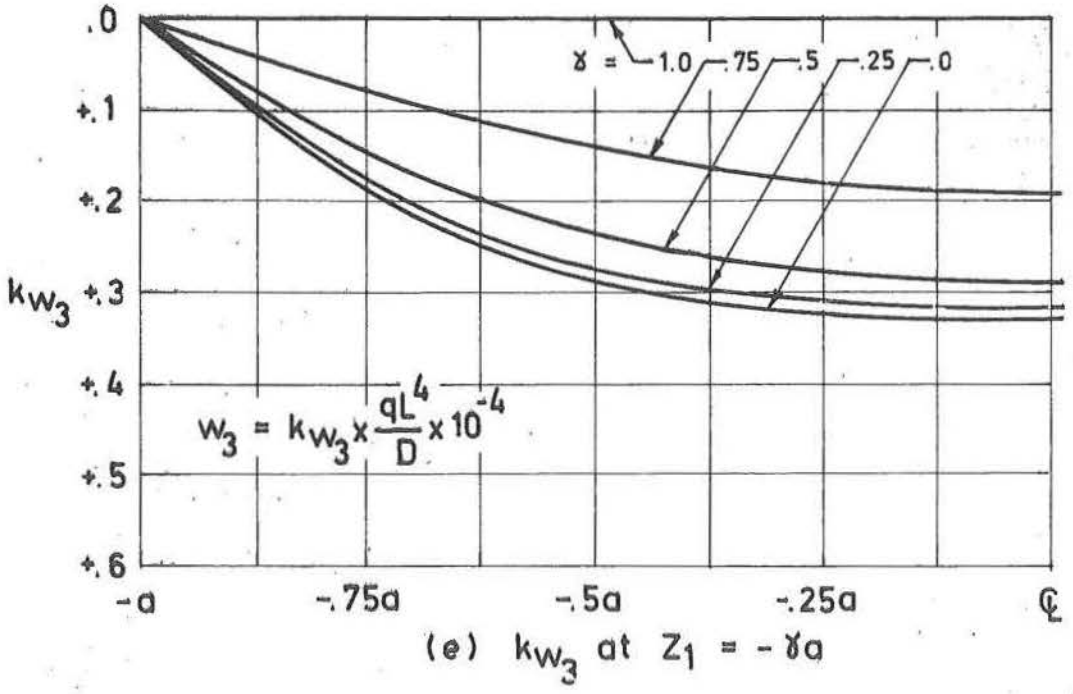

(e) k_{w_3} at $Z_1 = -\gamma a$

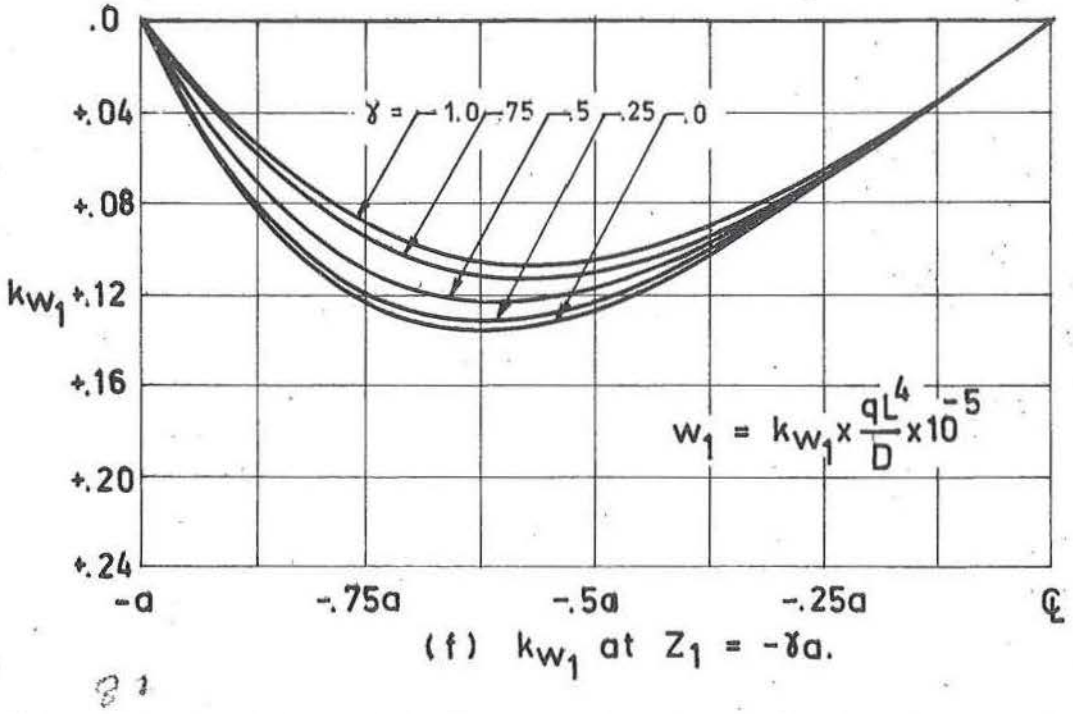

(f) k_{w_1} at $Z_1 = -\gamma a$.

Fig. 8.2 (continued) Ruled surface hyperbolic paraboloid with all edges simply supported. Distribution of displacements at cross sections $Z_1 = -\gamma a$.

behaviour of the shell-edge beam interaction, especially where the ratio $\lambda/4$ is small, than the clamped shell of section 8.2.1.

In figure 8.2 the results of this boundary type are plotted at the same cross sections as for the clamped edge shell. It is seen that the very much smaller deviations of $k_{n_{12}}$ from the corresponding membrane state ($\pm$ 25% over the complete shell), result in decreased bending stress resultants (25% those of the clamped shell) and stress couples (20% those of the clamped shell), although the maximum negative stress couple $k_{m_{22}}$ is of the same order as that of the clamped shell.

8.2.3 Free Edge

With the assumption that the equations (8.6) are equal to infinity, or what reduces to the same condition $t_b = b_b = 0$, the equations of sections 3.5 and 3.6 reduce to

$$n_{12} = n_{22} = m_{22} = q_{22} + \frac{\partial m_{12}}{\partial z_1} = 0., \quad \text{at } z_2 = -a \tag{8.17}$$

which, in terms of displacement components, result in

$$\begin{aligned} \frac{\partial w_1}{\partial z_2} + \frac{\partial w_2}{\partial z_1} + \frac{2.f}{a^2} \cdot w_3 &= 0., \\ \frac{\partial w_2}{\partial z_2} + \nu \cdot \frac{\partial w_1}{\partial z_1} &= 0., \\ \frac{\partial^2 w_3}{\partial z_2^2} + \nu \cdot \frac{\partial^2 w_3}{\partial z_1^2} &= 0., \\ \frac{\partial^3 w_3}{\partial z_2^3} + (2.-\nu) \cdot \frac{\partial^3 w_3}{\partial z_2 \partial z_1^2} &= 0., \end{aligned} \qquad \text{at } z_2 = -a \tag{8.18}$$

Because the boundary grid line i = 3 lies within the region of differential dependence, the conditions (8.18) are used to define pivotals which are required by the difference equations (4.19) to (4.21) and exterior to this region. Accordingly (w^k_{2j}, w^3_{1j}), (j = 4, m+3) are defined

$$
\begin{aligned}
w^1_{2j} &= w^1_{4j} - \left(w^2_{3j+1} - w^2_{3j-1} \right) - \frac{4.f}{a.m} \cdot w^3_{3j} \,, \\
w^2_{2j} &= w^2_{4j} - \mu \cdot \left(w^1_{3j+1} - w^1_{3j-1} \right) \,, \\
w^3_{2j} &= -w^3_{4j} - \mu \cdot \left(w^3_{3j+1} + w^3_{3j-1} \right) + 2.(1+\mu) \cdot w^3_{3j} \,, \\
w^3_{1j} &= w^3_{5j} + (2.-\mu) \cdot \left(w^3_{4j+1} + w^3_{4j-1} - w^3_{2j+1} - w^3_{2j-1} \right) - 2.(3-\mu)\left(w^3_{4j} - w^3_{2j} \right).
\end{aligned}
\qquad (8.19)
$$

The additional pivotals required at the corner (-a, -a) are provided from equations (8.8), with the additional pivotal being defined by using a second order extrapolation formula. These result in

$$
\begin{aligned}
w^1_{33} = w^2_{33} = w^3_{33} &= 0. \,, \\
w^1_{23} &= w^1_{43} \,, \\
w^2_{23} &= -w^2_{43} \,, \\
w^3_{23} &= w^3_{43} \,.
\end{aligned}
\qquad (8.20)
$$

Results are presented in figure 8.3 at the same cross-sections as those of the clamped and simply supported shells. If the corner singularities are neglected (this would be the case of a practical structure which would have some form of

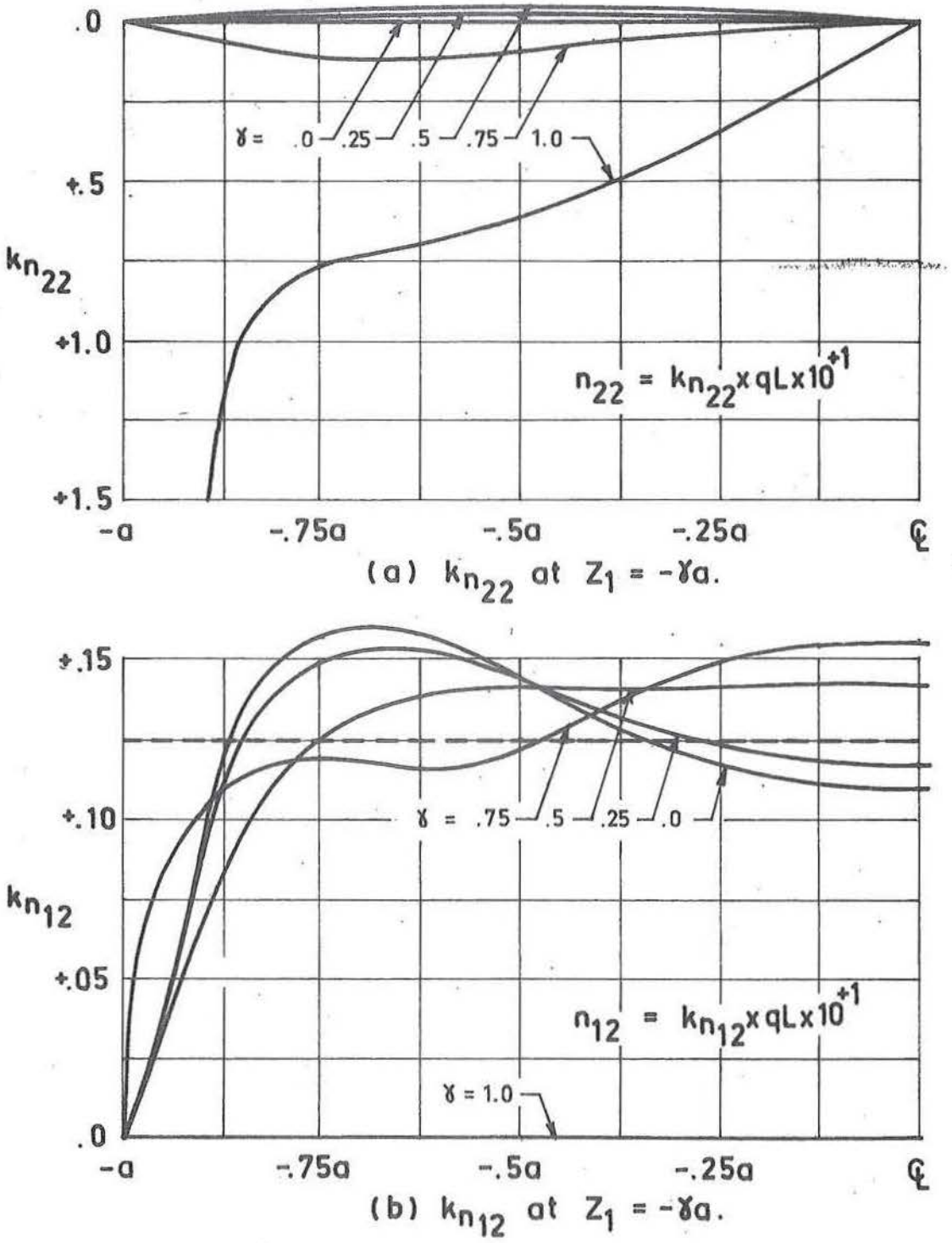

Fig. 8.3 Ruled surface hyperbolic paraboloid with all edges free and corners clamped. Distribution of stress resultants at $Z_1 = -\gamma a$.

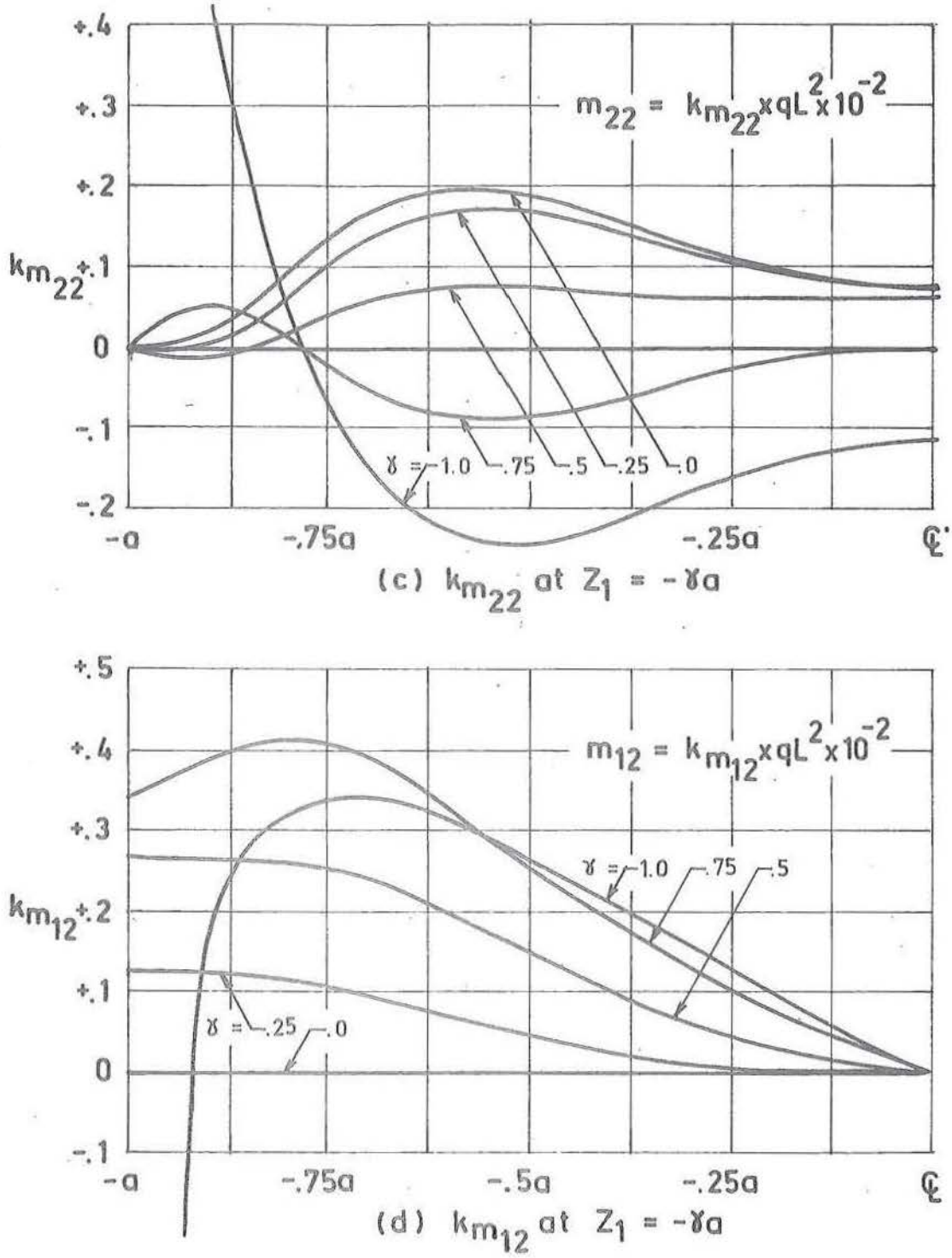

Fig. 8.3 (continued) Ruled surface hyperbolic paraboloid with all edges free and corners clamped. Distribution of moment resultants at $Z_1 = -\gamma a$.

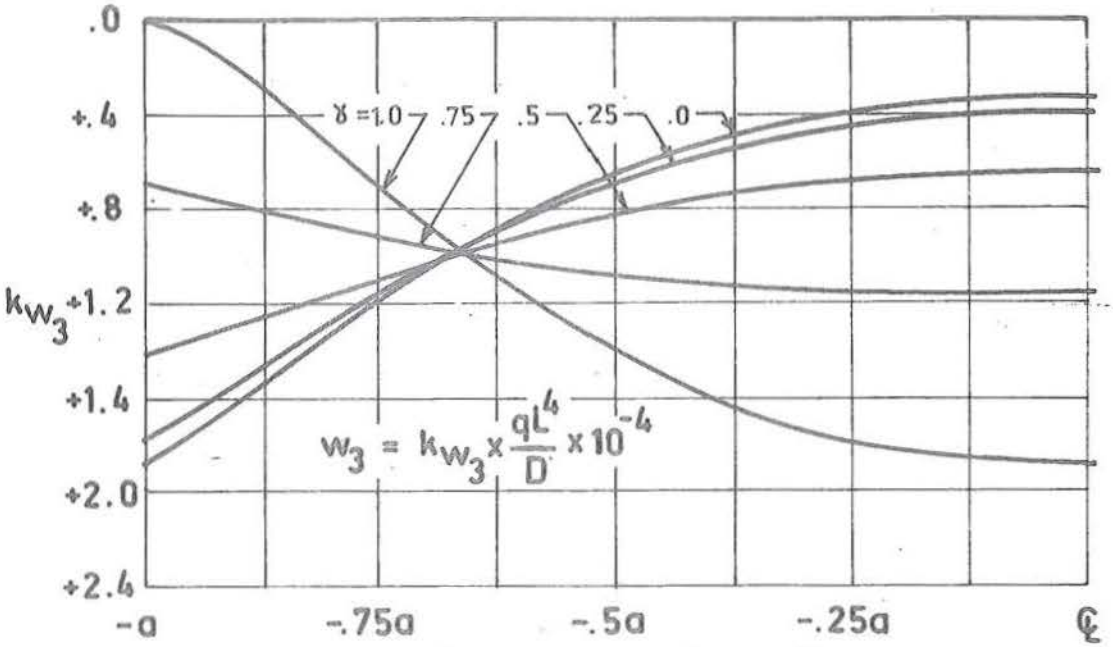

(e) k_{w_3} at $Z_1 = -\gamma a$.

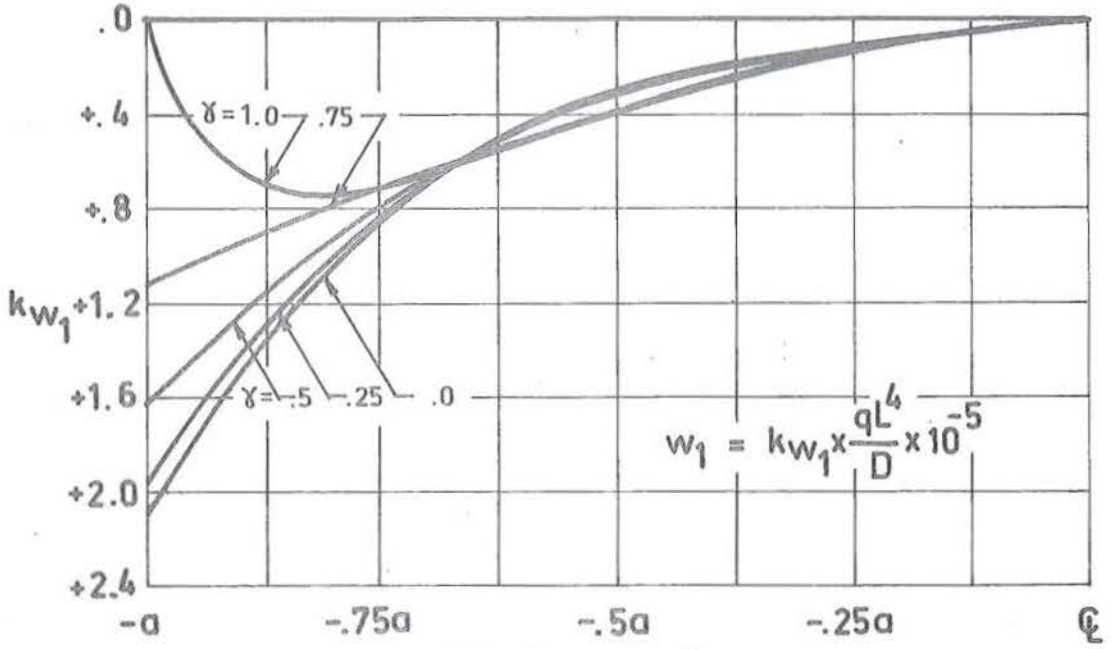

(f) k_{w_1} at $Z_1 = -\gamma a$.

Fig. 8.3 (continued) Ruled surface hyperbolic paraboloid with all edges free and corners clamped. Distribution of displacements at $Z_1 = -\gamma a$.

distributed support), it is seen that the maximum tensile bending stress at the bottom surface is 650% greater than the corresponding membrane stress, while the maximum top surface tensile stress is considerably greater than this figure. Even at the shell centre $|z_1,z_2| \leq 0.5a$, the bending stresses are of the order of 60% greater than those of the membrane state. Deflections are of the order of 700% higher than those occurring in either the simple or clamped shell.

Considering this behaviour, as well as the complete breakdown of shear transfer at the boundary, it is surprising to find that in-plane shear stresses quickly assume values of the order of those predicted by the membrane theory. Within the region $|z_1,z_2| \leq .75a$, the shear $k_{n_{12}}$ is within $\pm$30% the value given for the membrane theory, and in chapter 10 the percentage of vertical and horizontal load carried by this shear force is shown to quickly assume predominance over the bending effects. As a result of the adverse effects of bending shear, in the region $|z_1,z_2| \leq 0.75a$, the in-plane shear stress $k_{n_{12}}$ carries a greater amount of load than is applied externally.

8.2.4 Discussion

The most significant result emerging from this study is seen to be the independence of in-plane shear stresses, especially in the region $|z_1,z_2| \leq 0.75a$, from the effects of

boundary support conditions. Also, that these in-plane shears are sufficiently well predicted using the membrane analysis.

In the past it has become popular to think of the ruled surface hyperbolic paraboloid as being an essentially membrane predominant shell with an edge strip, of the order of 0.25a in width, which is subject to the influence of bending[46]. If this edge zone is defined as being the area where the in-plane shear stress is perturbed significantly from that predicted by the membrane analysis, this assertion of the edge zone could be regarded as correct. On the other hand, if the existence of an edge zone is defined as the region in which surface stresses resulting from bending action are of greater order than those of the principal stresses due to membrane analysis, then this edge zone should be considered over the entire shell. If a rational design method is to be employed, this latter approach must be the conclusion from this study.

8.3 THE EDGE BEAM

In section 8.2.1 the pure displacement boundary conditions of the clamped support are shown to represent the limiting case of the general equations of sections 3.5 and 3.6 if it is considered that the edge beam displacement is determined by the loading resulting from internal shell actions. The free or pure traction boundary conditions of section 8.2.3 in contrast to this, are shown as the limiting case of these equations if

the shell internal actions at the boundary are thought of as being determined by the action of the edge beam. Considered in a more heuristic manner, the first represents the edge beam loaded by the shell, while the second the shell loaded by the edge beam; this corresponds to whether the equations (3.25) to (3.28) are viewed from left to right, or from right to left.

Employing an "exact" method of solution, such as that used by Jenkins for the cylindrical shell [36] or the extension by Powell to the translational shell [45], this distinction is seen to be trivial. Where the method of finite difference is used, it is seen to determine at which points in the region of the boundary are defined by the shell equilibrium equations (4.19) to (4.21), and which are determined using the boundary equations (5.17) to (5.28).

Following sections consider a number of possible analogues for the representation of the edge beam shell interaction. For ease of presentation and because a number of terms of equation (3.21) to (3.35) may be omitted without adversely affecting the generality of the discussion, the following forms are considered:

$$
\begin{aligned}
&E_b A \left(\frac{\partial^2 w_1}{\partial z_1^2}\right)_b + K\cdot\left(\frac{1-\nu}{2}\right)\cdot\left(\frac{\partial w_1}{\partial z_2} + \frac{\partial w_2}{\partial z_1} + \frac{2\cdot f}{a^2}\cdot w_3\right)_s = 0.,\\
&E_b I_3 \left(\frac{\partial^4 w_2}{\partial z_1^4}\right)_b - K\cdot\left(\frac{\partial w_2}{\partial z_2} + \nu\cdot\frac{\partial w_1}{\partial z_1}\right)_s = 0.,\\
&E_b I_2 \left(\frac{\partial^4 w_3}{\partial z_1^4}\right)_b + D\cdot\left(\frac{\partial^3 w_3}{\partial z_2^3} + (2-\nu)\cdot\frac{\partial^3 w_3}{\partial z_2 \partial z_1^2}\right)_s - G_3 = 0.,\\
&E_b I_1 \left(\frac{\partial^3 w_3}{\partial z_1^2 \partial z_2}\right)_b + D\cdot\left(\frac{\partial^2 w_3}{\partial z_2^2} + \nu\cdot\frac{\partial^2 w_3}{\partial z_1^2}\right)_s = 0..
\end{aligned}
\qquad (8.21)
$$

With the similar neglect of all terms containing e_2, e_3 and $\sin\phi$ (which are considered as second order), as well as the omission of $\cos\phi$, the difference equations of section 5.4 reduce to:

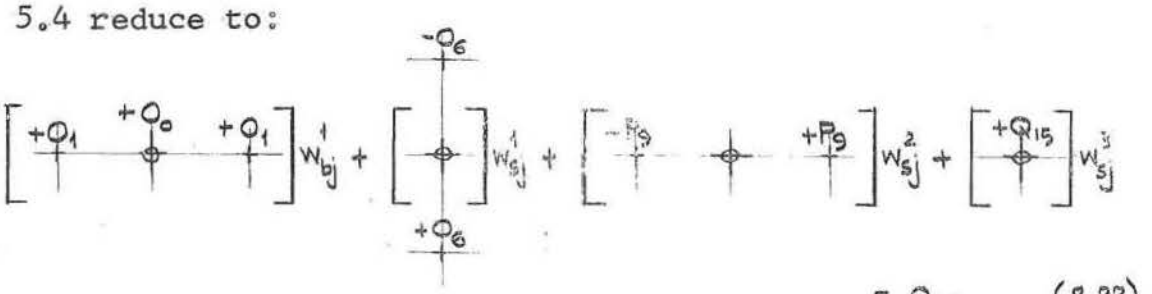

$$= 0., \qquad (8.22)$$

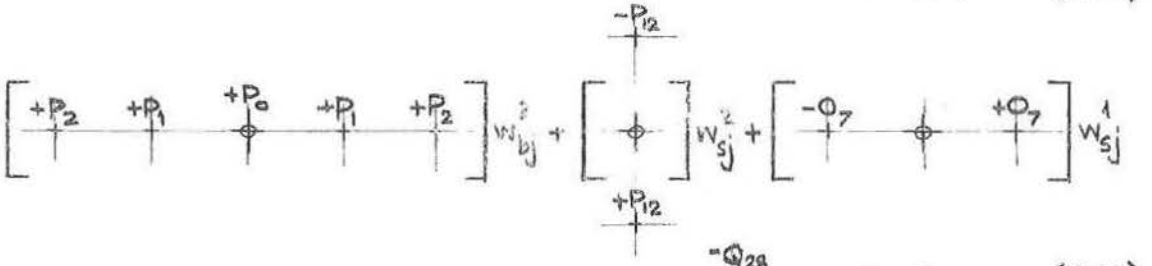

$$= 0., \qquad (8.23)$$

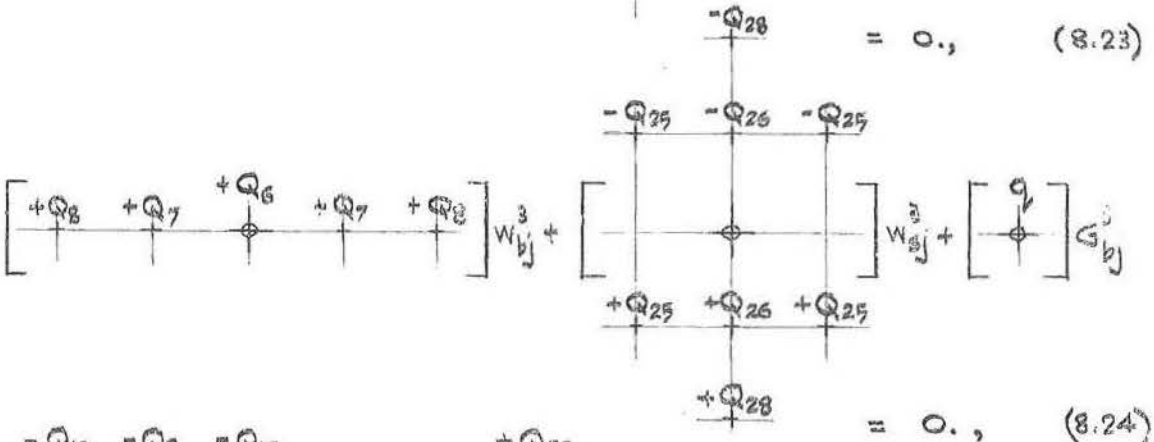

$$= 0., \qquad (8.24)$$

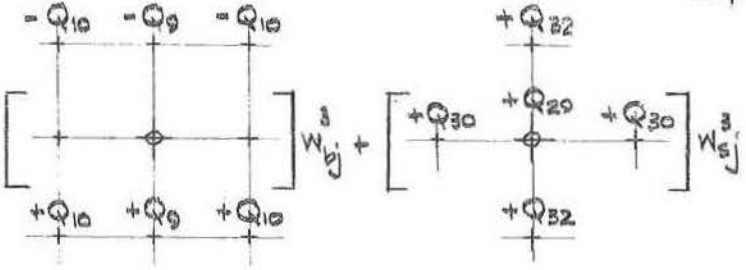

$$= 0., \qquad (8.25)$$

where the required coefficients O_k, P_k and Q_k are listed in table 8.1.

O_0	$-2.O_1$	Q_8	$-E_b.\frac{m^4}{12.}.\frac{b_b.t_b^3}{a^4}$
O_1	$+E_b.m^2.\frac{t_b.b_b}{a^2}$	Q_9	$-2.Q_{10}$
O_6	$+E_s\frac{m}{4.(1.+\mu)}.\frac{t_s}{a}$	Q_{10}	$+E_b.\frac{m^3}{4.(1.+\mu)}.\frac{t_b.b_b^3}{a^3}$
O_7	$+E_s\frac{\mu.m}{2.(1.-\mu^2)}.\frac{t_s}{a}$	Q_{15}	$+E_s\frac{1.}{(1.+\mu)}.\frac{f.t_s}{a^2}$
P_0	$+6.P_2$	Q_{25}	$-E_s\frac{m^3.(2.-\mu)}{24.(1.-\mu^2)}.\frac{t_s^3}{a^3}$
P_1	$-4.P_2$	Q_{26}	$-2.(Q_{25}+Q_{28})$
P_2	$-E_b.\frac{m^4}{12.}.\frac{t_b.b_b^3}{a^4}$	Q_{28}	$-E_s\frac{m^3}{24.(1.-\mu^2)}.\frac{t_s^3}{a^3}$
P_9	$+E_s.\frac{m}{4.(1.+\mu)}.\frac{t_s}{a}$	Q_{29}	$-2.\frac{(1.+\mu)}{\mu}.Q_{30}$
P_{12}	$+E_s.\frac{m}{2.(1.-\mu^2)}.\frac{t_s}{a}$	Q_{30}	$+\frac{1.}{\mu}.Q_{30}$
Q_6	$+6.Q_8$	Q_{32}	$+E_s.\frac{\mu.m^2}{12.(1.-\mu^2)}.\frac{t_s^3}{a^2}$
Q_7	$-4.Q_8$		

TABLE 8.1 Coefficients O_k, P_k and Q_k required for the simplified ruled surface hyperbolic paraboloid edge beam difference analogue, as used in section 8.3.

8.3.1 Difference Grid Orientation

Before a meaningful working model can be established, it is necessary to orientate the difference grid (i,j) in such a way that the $i = b$ and the $i = s$ row subscripts, as used in the above equations and in chapter 5, may be referred to one or more of the (i,j) grid lines. For the definition of beam actions it would be convenient for a difference grid line to be colinear with the edge beam centroidal axis, while for the shell actions a difference grid line colinear with the shell-edge beam intersection would be convenient. Unless the beam is of such dimensions that $0.5\, b_b = h$ both these requirements cannot be met, and some approximations are necessary in order that one set of actions and displacements be defined.

Figure 8.4 diagramatically shows the above two grid orientations, which are termed grid orientation I and II. It is assumed that the shell difference equations (4.19) to (4.21) are applied without modification at all nodal positions defined at or within the beam-shell intersection. For this reason conditions must be provided from the boundary equations (5.17) to (5.28), for the determination of two grid lines exterior to this first row of differential dependence.

8.3.2 Displacement Edge Beam

In sections 8.2.1 and 8.2.2 it can be observed that shear and direct and flexural stresses normal to the boundary are

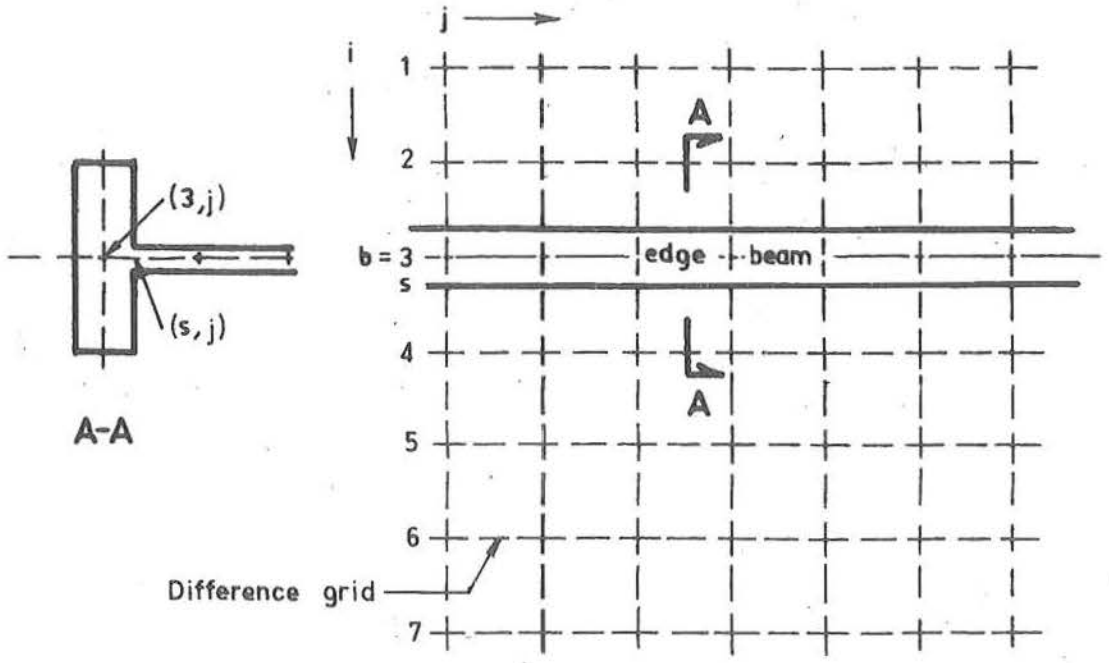

(a) Grid orientation I.

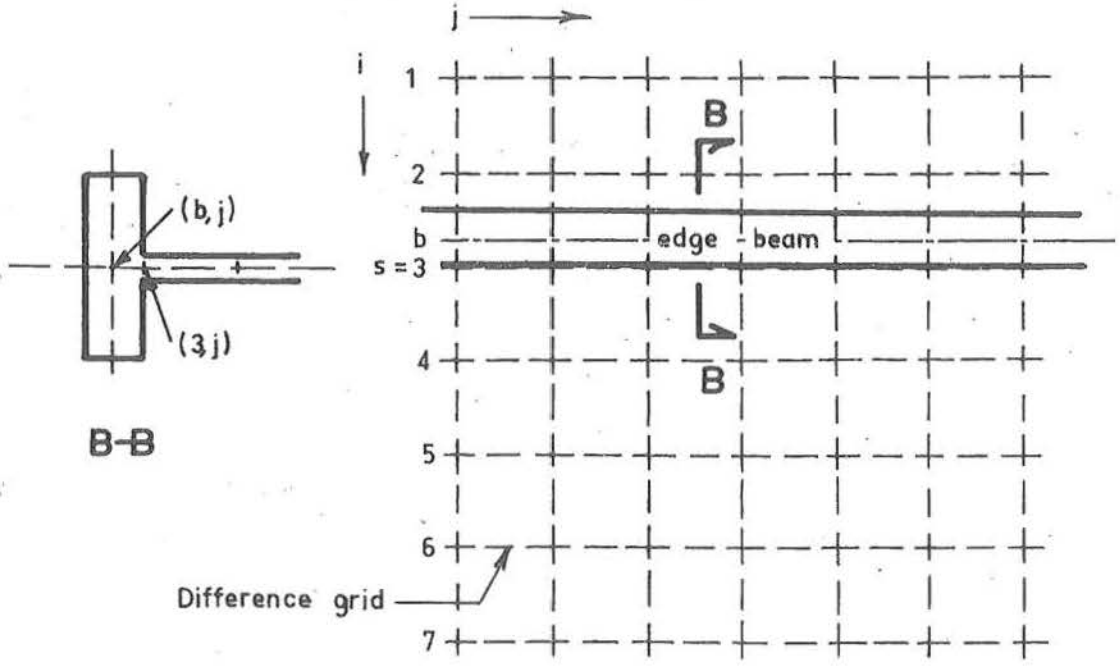

(b) Grid orientation II.

Fig. 8.4 Difference grid orientation with respect to the edge beam centroidal axis.

generally high at edges with zero displacements. Similarly, shells with large edge members, and thus small edge displacements, are accompanied by high shear and normal stresses at the beam-shell intersection. If the values of these relatively large quantities were determined in terms of difference in the small quantities, considerable round-off would occur. Hence, for boundaries of this type, the edge displacements are determined from the internal stress resultants - or the small quantities in terms of the large. For this reason equations (8.21) are considered as providing conditions for the determination of $(w^k_{bj}\ ,\ w^3_{b-ij})$, $(\ j = 4,m+3\ )$.

8.3.2(a) Grid Orientation I

The beam centroidal axis, subscripted b , is considered colinear with the grid line $i = 3$ as shown in figure 8.4(a), while the shell - beam intersection in general is not colinear with any of the defined grid lines. Approximation to the shell stress and moment resultants at the beam - shell intersection must therefore be made.

Employing the conventional analogues for the determination of H^k and K^k as given in section 5.4, it is necessary to approximate the position of the shell - beam intersection. An example of this method is the definition of the shell actions H^k and K^k at the grid line $i = 4$, which requires only those external pivots defined by the boundary conditions. A well

posed numerical problem, corresponding to the conventional techniques of section 7.2, is therefore achieved for beams of large dimensions where the limiting case can be seen to be the clamped support.

An alternative method to that indicated above, corresponds to the methods of higher order boundary representation outlined in section 7.3. For this, analogues for the values of $(w^k_{sj}\ ,\ (\frac{\partial^r w_k}{\partial z_2^r})_{sj})$, $(\ r = 1,2,3)$, at the position (s,j), $(j = 4,m+3)$ may be developed in terms of non-symmetric combinations of w^k_{rj} at the pivotal positions (r,j), $(r = 2,3,4...)$, $(j = 4,m+3)$, with truncation errors of any desired magnitude. In the same way that the methods of higher order boundary representation previously produced matrices with high spectral radii, this present method was found to require a greater amount of computational labour for the same accuracy. Where direct solution methods are employed however, this technique is seen to greatly improve the physical representation and therefore the likely numerical accuracy.

8.3.2(b) Grid Orientation II

Because in this case w^k_{3j}, $(\ j = 4,m+3\ )$ are defined by the shell difference equations, the edge beam displacements and rotations obtained from (8.21) must be used to define the displacements w^k_{2j} , $(\ j = 4,m+3\ )$ and w^3_{1j} , $(\ j = 4,m+3\ )$. Some forms of extrapolation formulae will necessarily be required,

so that the method in addition to being subject to considerable discretisation errors will also inadequately represent the degenerate displacement boundary.

8.3.2(c) Numerical Studies

Employing the displacement edge condition of 8.3.2(a), and approximating the internal shell stresses and moments at the boundary by those given at grid positions $(4,j)$, $(j = 4,m+3)$, numerical results were obtained for a number of shell and edge beam geometries. The programme used for this study has been briefly outlined in section 6.3, while a complex listing is given in appendix A .

Figure 8.5 (a)-(f) shows a selection of results from such a study. For comparative reasons the shell geometry is chosen as that given by (8.1), while the beam dimensions used provide the following geometric coefficients:

$$\lambda_3 = 1.5,\ 3.0,\ 4.5,\ 6.0,$$
$$\lambda_4 = 0.05,$$
$$\lambda_5 = 0.00,$$
$$\lambda_6 = 0.00.$$

Grids with m = 8 were used for all cases, and although this results in considerable discretisation errors, see section 7.2, all studies are subject to similar errors so that comparisons are justified.

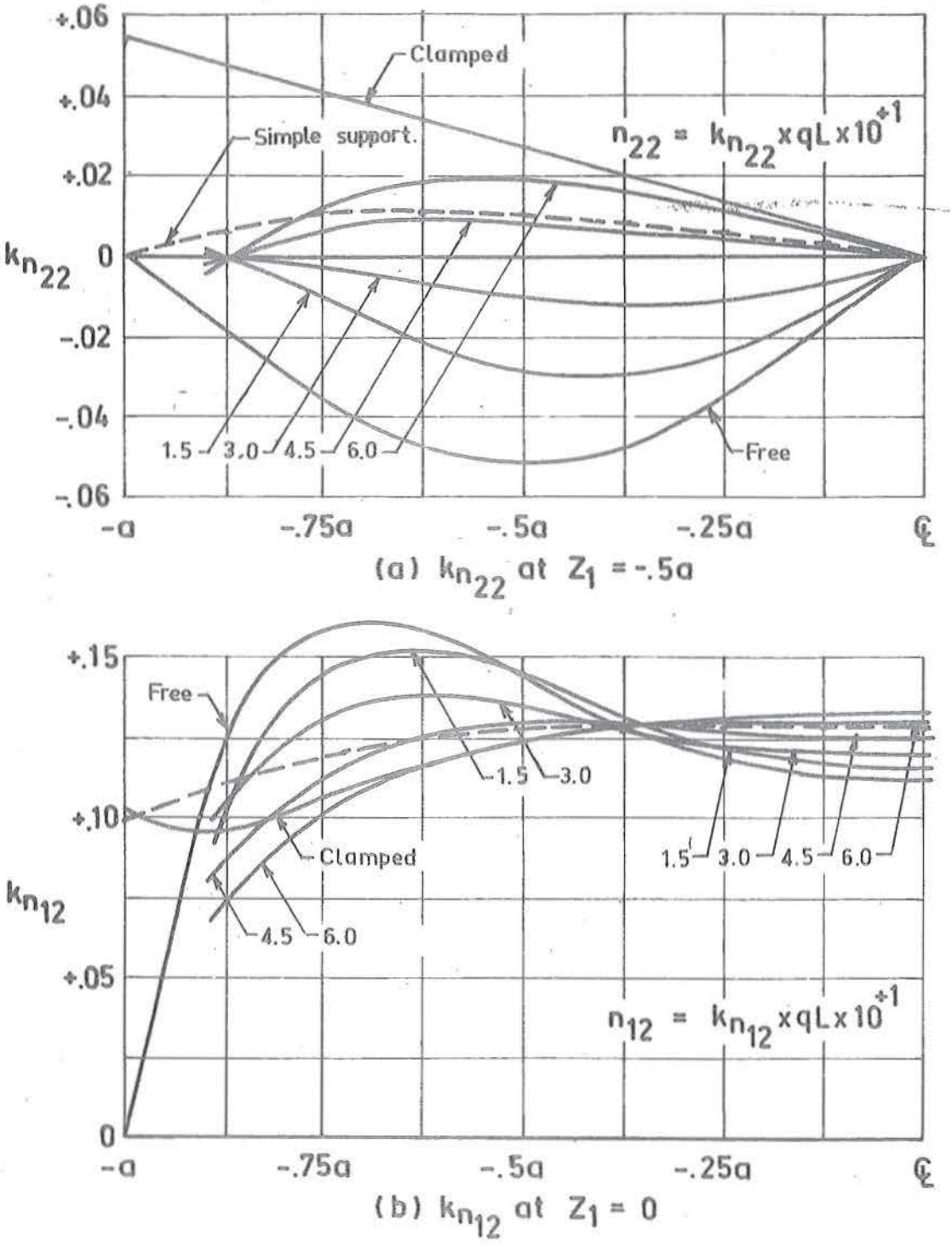

Fig. 8.5 Ruled surface hyperbolic paraboloid with edge beams clamped at corners. Influence of λ_3, where $\lambda_1 = .2$, $\lambda_2 = .0165$, $\lambda_4 = .05$, $\nu = .0$ and $m = 8$. Free and clamped edge results also shown.

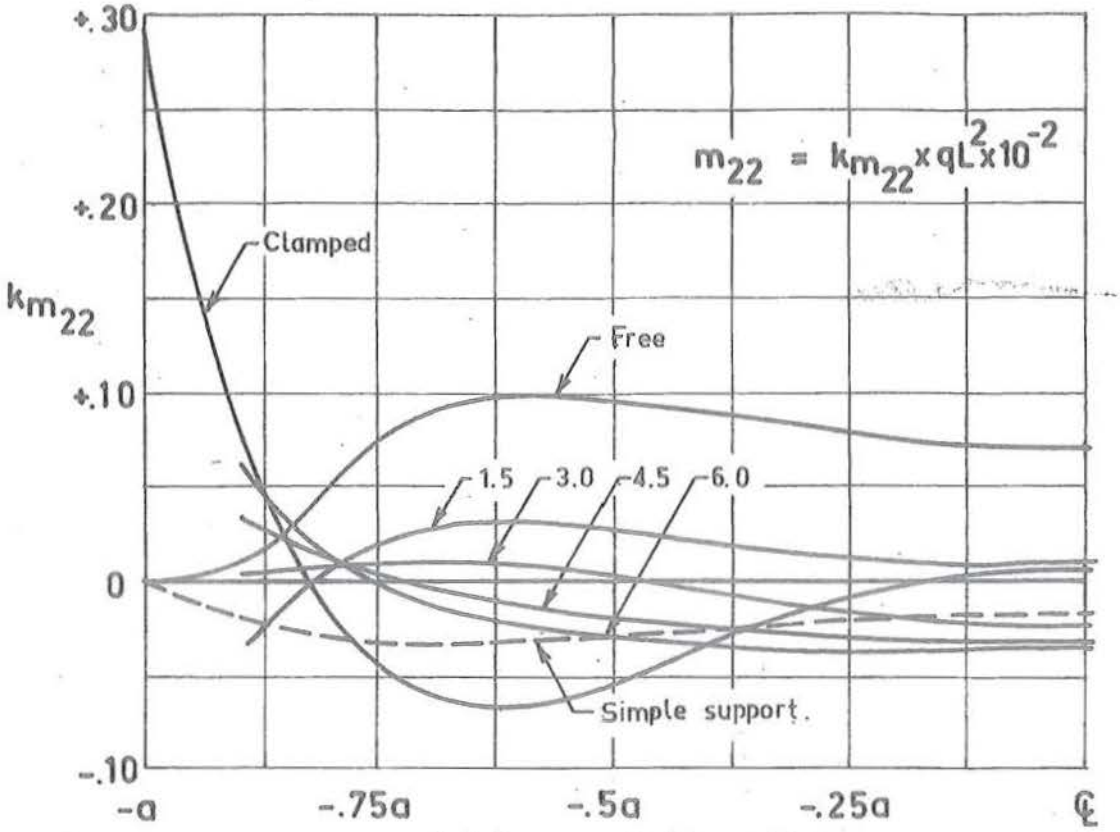

(c) km_{22} at $Z_1 = -.5a$

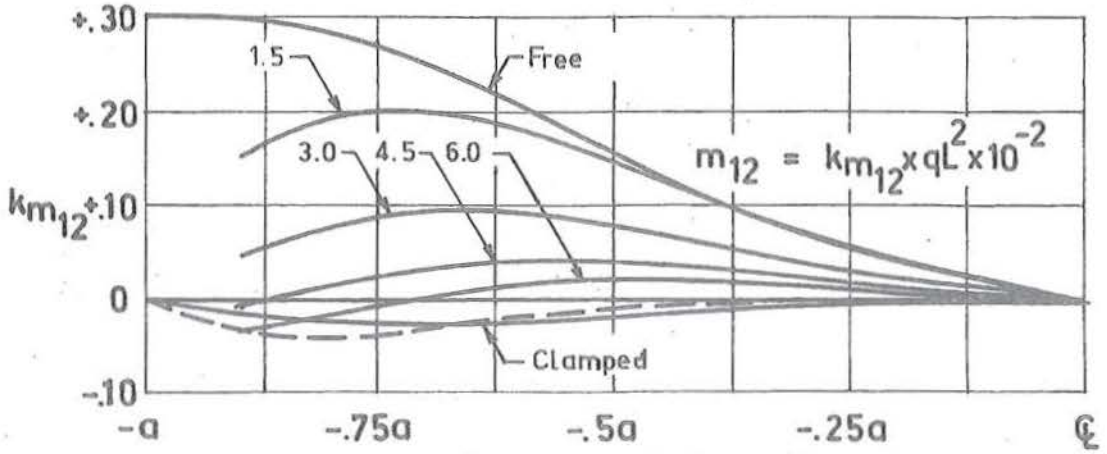

(d) km_{12} at $Z_1 = -.5a$

Fig. 8.5 (continued) Ruled surface hyperbolic paraboloid with beam edges clamped at corners. Influence of λ_3. Free and clamped edge results also shown.

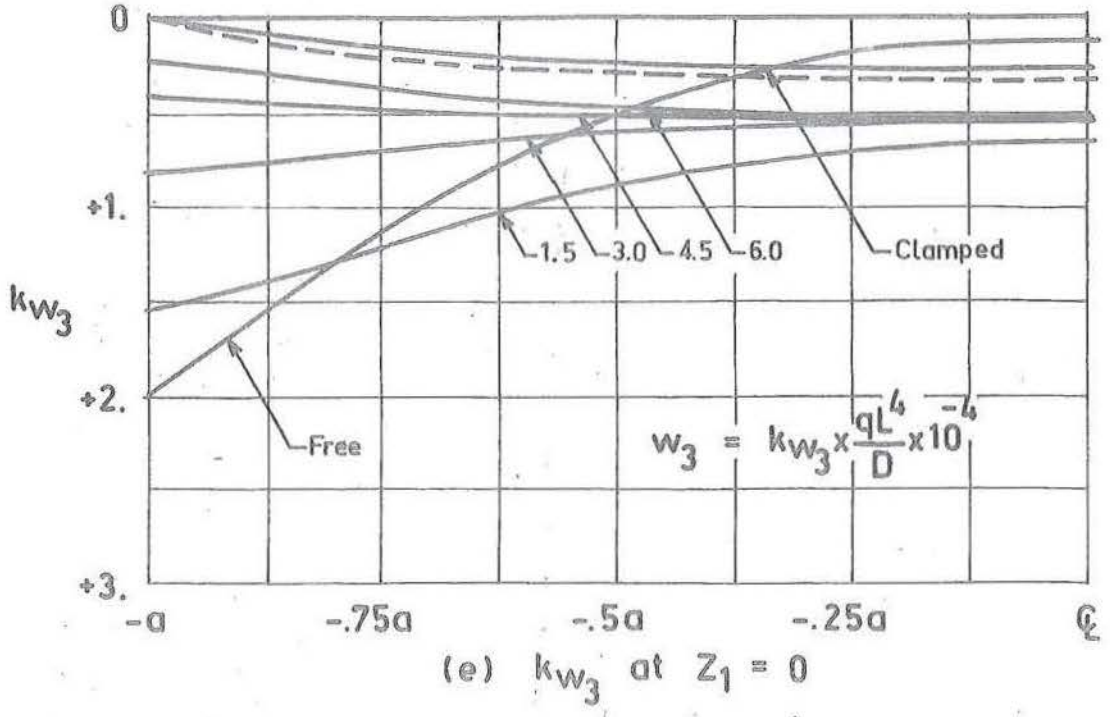

(e) k_{w_3} at $Z_1 = 0$

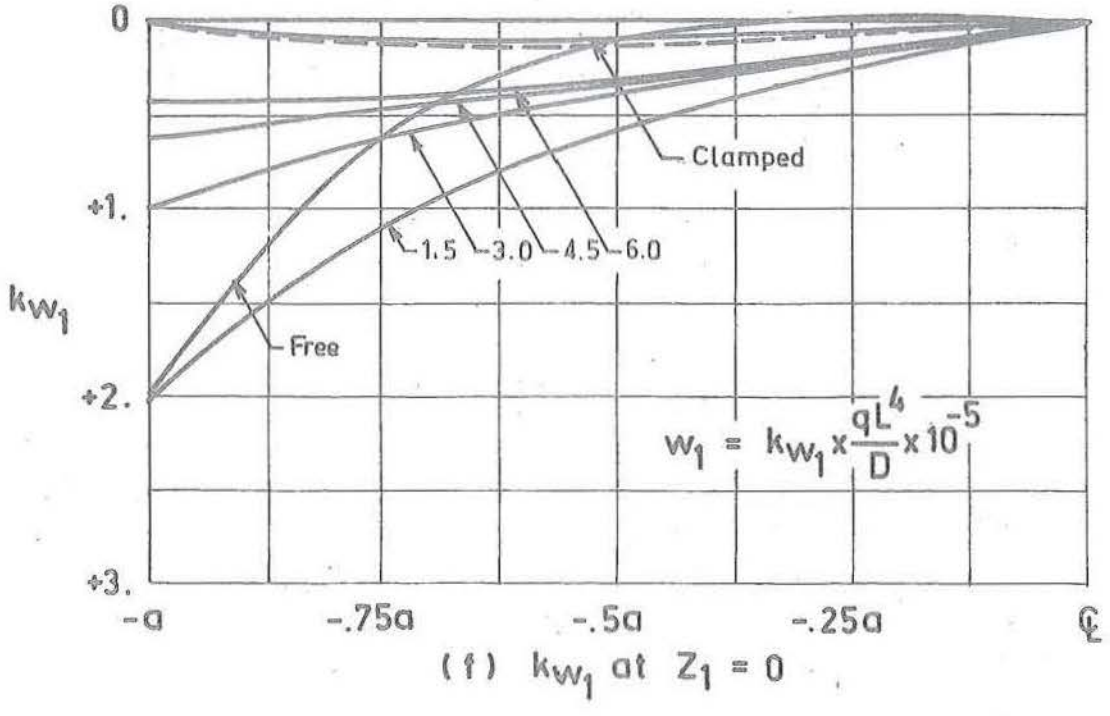

(f) k_{w_1} at $Z_1 = 0$

Fig. 8.5 (continued) Ruled surface hyperbolic paraboloid with edge beams clamped at corners. Influence of λ_3. Free and clamped edge results also shown.

For ease of reference results obtained for the simple, clamped, and free edged shell are also given with grids of $m = 8$. The gradual transition from the displacement boundary to the traction boundary is observed as the beam thickness is decreased relative to the shell thickness. It is also seen that for the particular ratio of beam breadth to shell breadth λ_4 , the in-plane stresses at the boundary are approximated in the degenerate case by the simple support condition. This condition is that considered by Soare[51]. The transition is even more evident from the displacement profiles given in figure 8.5(e) and (f), from which it can be concluded that the displacement edge beam results are realistic estimates of shell-beam interaction for λ_3 in the range 1.5 to 6.0, with the accuracy increasing as λ_3 increases. For $\lambda_3 > 6.0$ this analogue has been shown to converge to that of the model of Soare, while increasing the breadth has the effect of producing the clamped support.

The very good estimates for beams of small dimensions, which intuitively are thought to be of the traction type, is surprising. As the iteration method became unstable in the iterative sense for $\lambda_3 < 1.5$, it appears there is a high correlation between physical and numerical instability.

Because the behaviour of the shell with $\lambda_3 = 4.5$ lies midway between the displacement and traction boundaries, these results are presented in detail in figure 8.6(a)-(f), for a

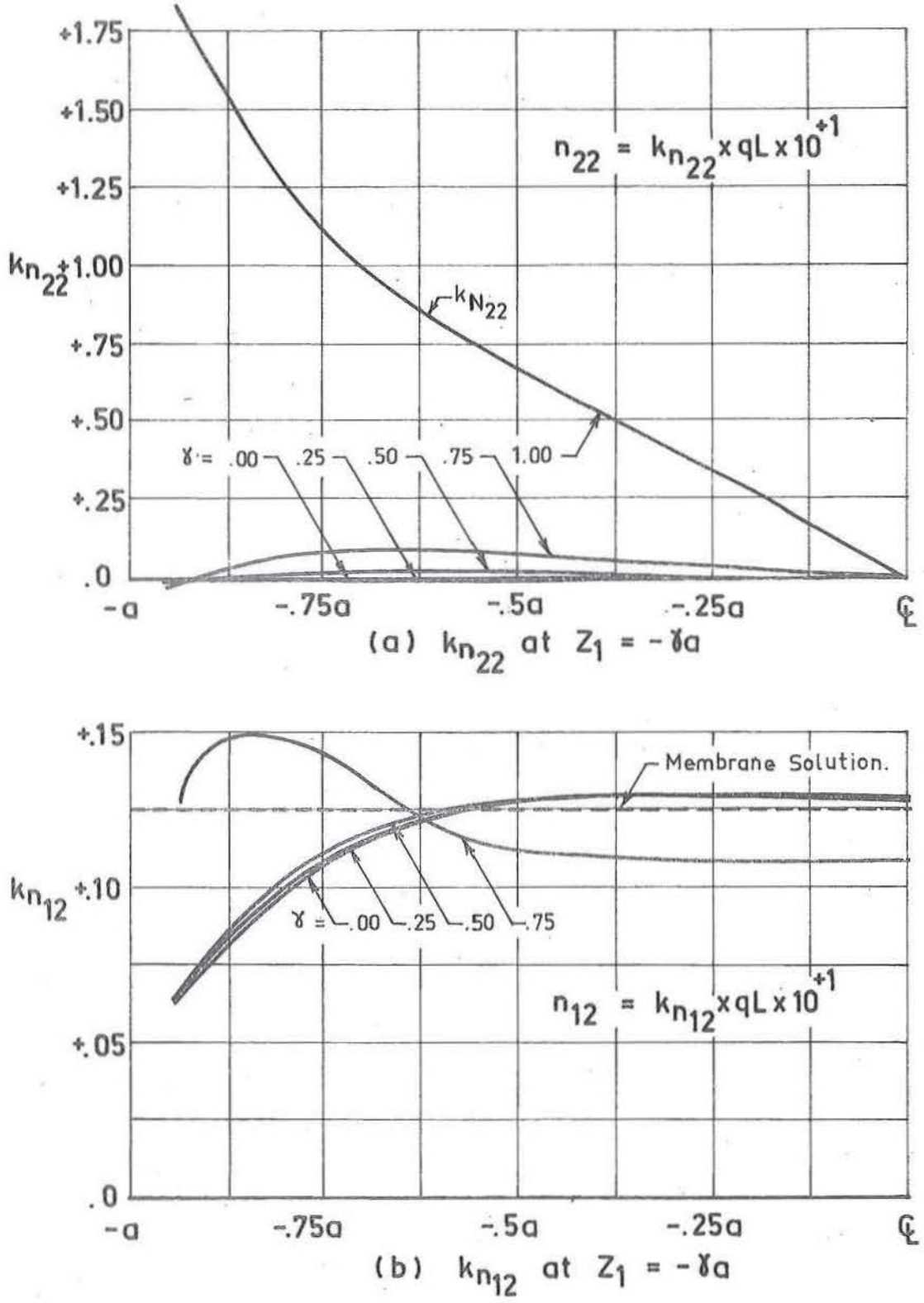

Fig. 8.6 Ruled surface hyperbolic paraboloid with edge beams clamped at corners. Distribution of stress resultants at cross sections $Z_1 = -\gamma a$.

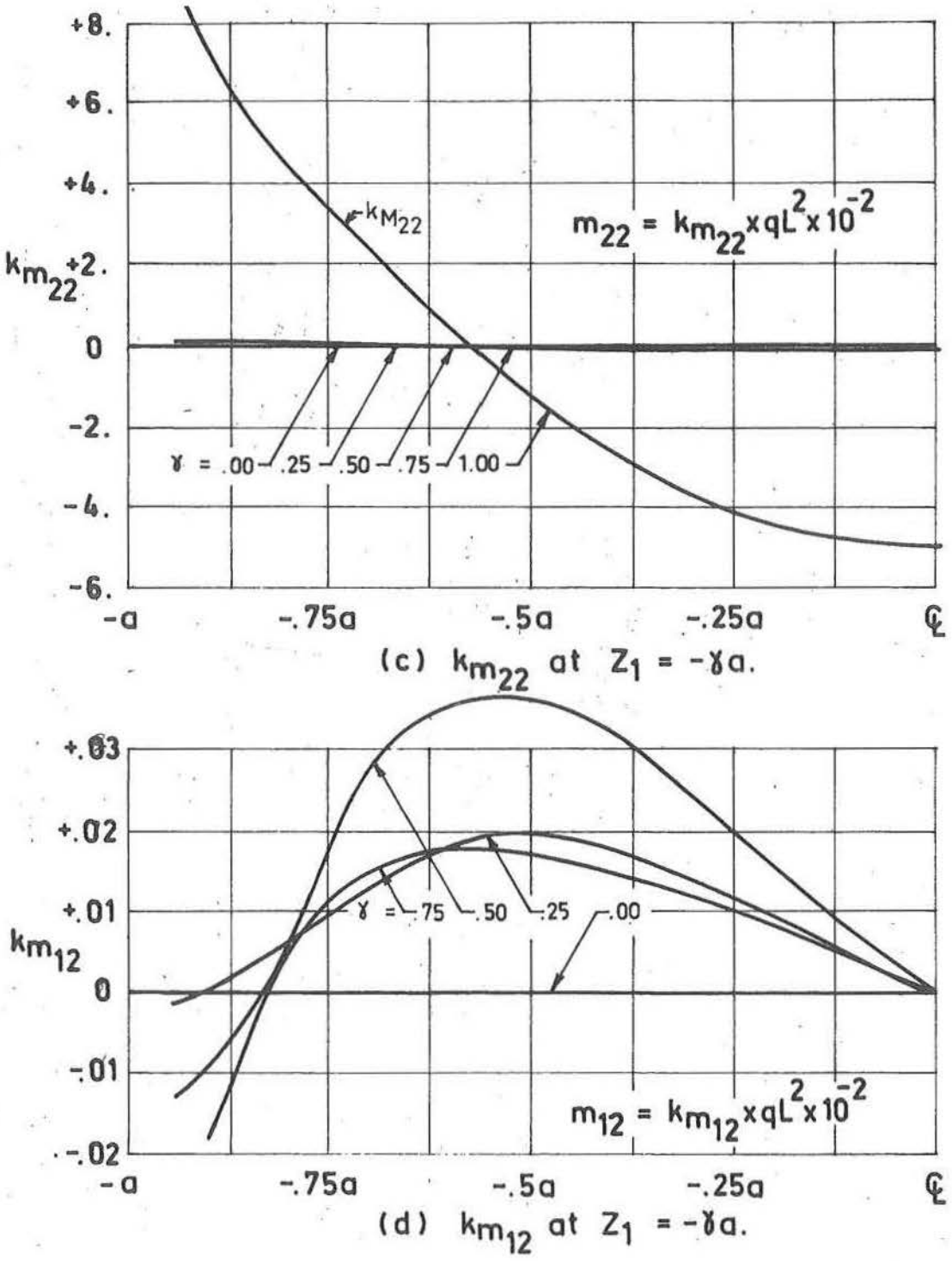

Fig. 8.6 (continued) Ruled surface hyperbolic paraboloid with beam edges clamped at corners. Distribution of moment resultants along $Z_1 = -\gamma a$.

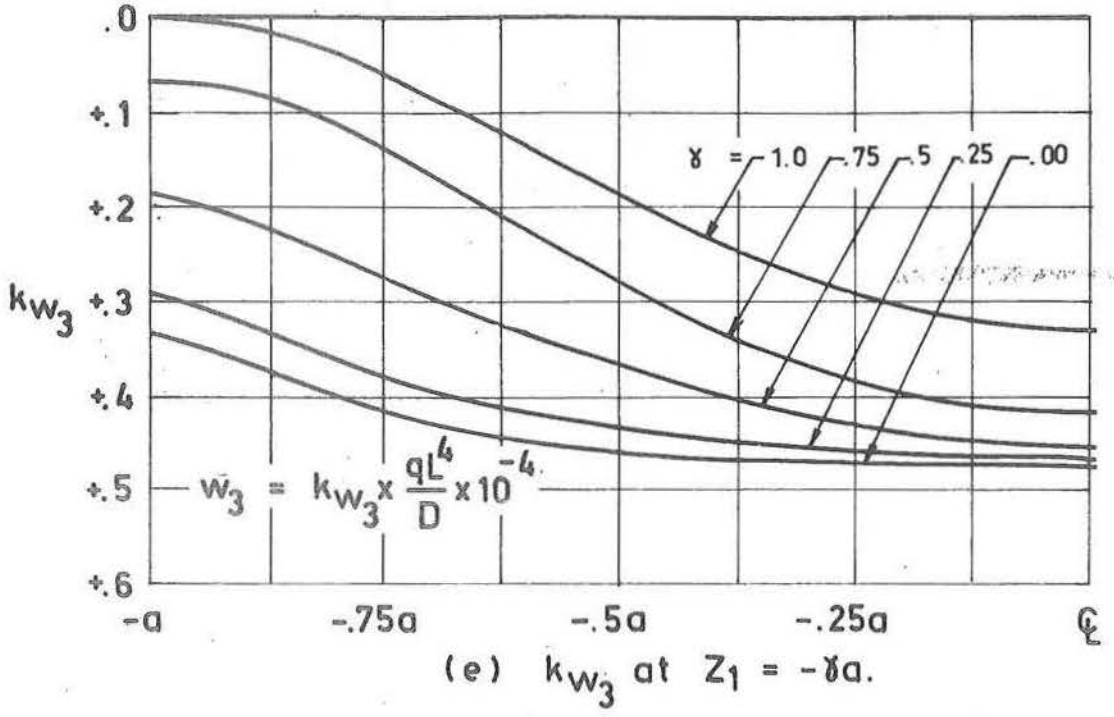

(e) k_{w_3} at $Z_1 = -\gamma a$.

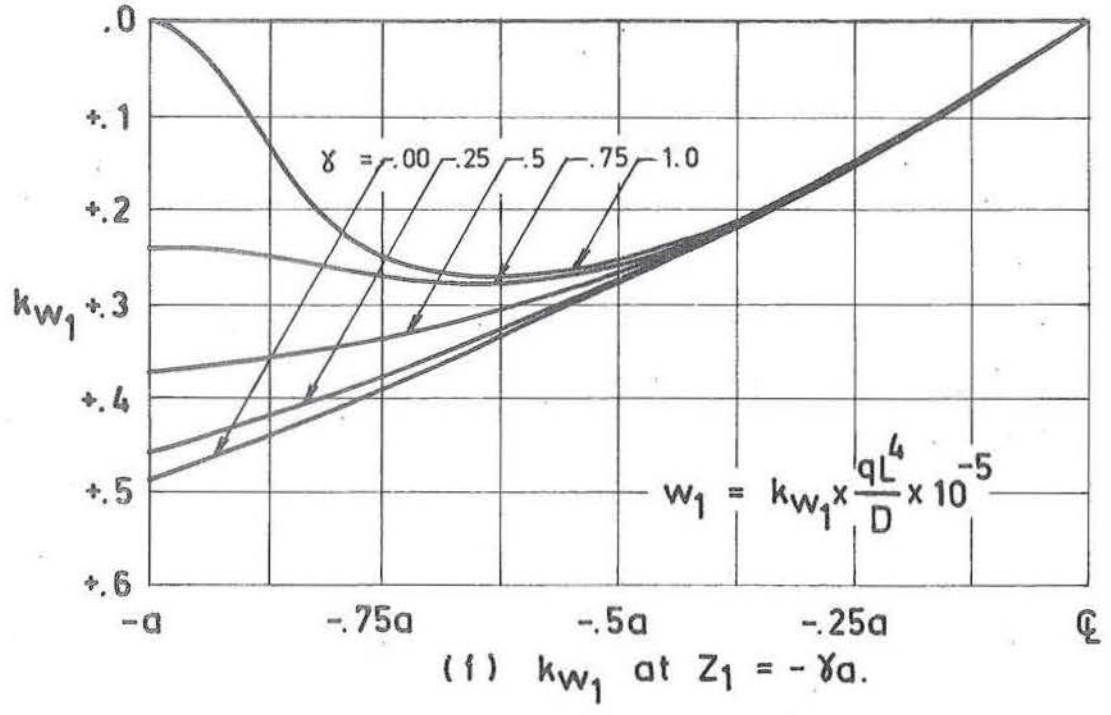

(f) k_{w_1} at $Z_1 = -\gamma a$.

Fig. 8.6 (continued) Ruled surface hyperbolic paraboloid with edge beams clamped at corners. Distribution of displacements along $Z_1 = -\gamma a$.

grid with m = 16 . In-plane shear in the region $|z_1, z_2| \leq .75a$ is within $\pm$ 15% of that predicted by membrane theory, with the actual distribution closely approximating that of the equivalent simple support given in figure 8.2(b). As in the free edged shell, where the breakdown of membrane shear results in high direct stresses in the edge zone, so the edge zone of the beam edged shell is typified by high direct stress load. This similarity of behaviour is seen on comparing figure 8.2(a) with 8.6(a), but whereas in the free edged shell the high boundary direct stress resultants are accompanied by high surface stresses for the beam edged shell these stresses are considerably smaller. In both cases the boundary zone of high direct stresses is very narrow, the shell direct stresses rapidly reducing to the same order as those of the equivalent clamped or simply supported shells.

Trends similar to those for in-plane stresses are noted for the distribution of bending moments. The twisting moments $k_{m_{12}}$ are of similar magnitude to those of the simple support, but the moment resultants $k_{m_{11}}$ at the edge $z_1 = -a$ are of the order of twenty times those of the free edged shell. This redistribution of shell moments to the edge beam results in flexural stresses in the body of the shell of the same order as those of the simple support, while the surface stresses in the edge beam are of the same order as those at the edge of the free shell. It should be remembered that the

stresses are inversely proportional to the square of the thickness. Vertical displacements are of the same order and of similar profile to those of the simply supported shell, while the horizontal displacements are of similar profile but 25% in magnitude to those of the free edge shell.

8.3.3 Traction Edge Beam

Edges with zero shears and stresses normal to the boundary, from section 8.2.3 are seen to be accompanied by large displacements. Once again, with reasoning similar to that of section 8.3.1 it would seem desirable that these stresses be determined in terms of the difference in large displacements. Equation (8.21) in this case provide conditions for the determination of n_{12}, n_{22}, m_{22} and $q_{22} + \frac{\partial m_{12}}{\partial z_1}$ at the positions (s,j), $(j = 4,m+3)$.

8.3.3(a) Grid Orientation I

As in section 8.3.2(a) some approximation must be made to the stresses and moments at the position (s,j), but unlike the displacement boundary the definition of stress in this case is likely to be critical. It is also noted that neither of the techniques for the approximation of stress and moment resultants outlined above, will converge to the degenerate free edge on suitable choice of beam dimensions. Physically, this orientation produces a badly posed problem.

8.3.3(b) Grid Orientation II

The definition of stress and moment resultants at the position $(3,j)$ in this case provides direct expressions for the determination of (w^k_{2j}, w^3_{1j}), $(j = 3,m+3)$, while in general some approximation is required for the computation of edge beam actions and displacements. As in section 8.3.2(a), where the approximation of shell edge actions is likely to be of less consequence than the approximation of critical edge displacements, so in the present system the approximation of edge displacements is likely to be of less significance than the approximation of the critical shell edge actions. A well posed problem,which can be seen to reduce to the degenerate free edge shell on suitable choice of beam-shell parameters, is therefore achieved.

8.3.3(c) Numerical Studies

The traction edge beam representation described in section 8.3.3(b) with edge beam displacements computed using the expressions (5.13) to (5.16) was used for a parameter study similar to that described in section 8.3.2(c) for the displacement edge beam. The solutions obtained were found to be approximately consistent with the degenerate free edged shell for all values of λ_4 where $\lambda_3 = 1.0$, while for $\lambda_4 = 0.00$ the solution was identical to this limit case.

Employing $\lambda_4 = 0.05$, to be consistent with section 8.3.2(c), solutions were sought for values of $\lambda_3 = 1.00$, 1.25, 1.500. With $\lambda_3 = 1.00$ the iterative method became unstable and required the use of time expensive under-relaxation to obtain solutions, while for $\lambda_3 > 1.0$ the solution techniques became completely unstable with severe under-relaxation having no influence. Results are for this reason not presented.

8.3.4 Discussion

Convergence of the above displacement and traction boundaries to their respective degenerate cases, are shown to depend upon grid orientations at the boundary. For the determination of beam displacements the grid orientation I was shown to be superior while for the determination of edge stress and moment resultants the grid orientation II provided a more efficient model. Grid I is therefore considered consistent with the displacement conditions, and grid II consistent with the traction conditions.

Using the method of iteration and employing consistent grid orientations, the bounds of applicability for each of the displacement and traction boundary types were determined in sections 8.3.2(c) and 8.3.3(c). For edge beams with thickness of the order of the thickness of the shell (that is, no edge beam) the traction representation is superior, but becomes numerically unstable for values of the ratio $\lambda_3 > 1.0$. The displacement representation provides a more realistic model

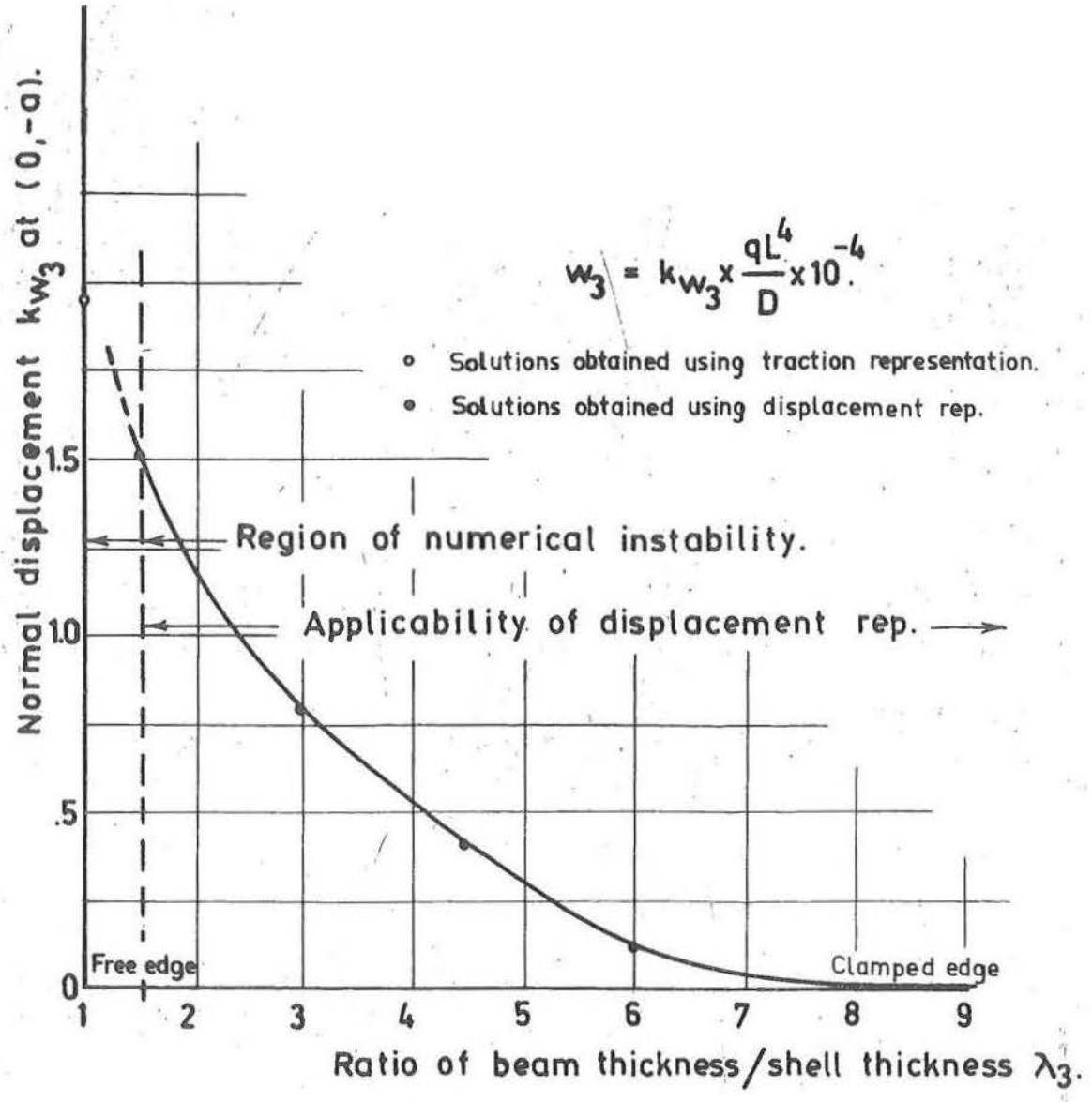

Fig. 8.7 Ruled surface hyperbolic paraboloid with beam edges and corners clamped. Applicability of the traction and displacement edge beam formulations, where $\lambda_1 = 0.2$, $\lambda_2 = 0.0165$, $\lambda_4 = 0.05$, $\nu = 0.00$ and $m = 8$.

where $\lambda_3 > 1.5$, although it appears from the results of Gupta [30] and Chronowicz [15] that the range of applicability for the traction condition may be extended with the use of direct methods. Thus, for practical situations, where λ_3 from stiffness considerations is usually of the order of 2.5 or greater, the use of the displacement analogue is preferable. This is especially the case where iterative solution methods are employed.

Figure 8.7 summarises the results obtained from both the traction and displacement edge beam representations using consistent grid orientations. Computed values of k_{w_3} at the position $(0,\bar{a})$, are shown as black dots for the displacement boundary results, and open dots for the results from the traction boundary type. It can be seen that edge beams in the region $1.0 < \lambda_3 < 1.5$ are likely to present problems where an iterative solution technique is employed. Further numerical studies are required to determine whether similar trends occur for shells and edge beams of varying geometry.

8.4 SECOND ORDER EDGE BEAM EFFECTS

The results presented in section 8.3 refer to solutions obtained using the simplified forms (8.22) to (8.25) of the general boundary difference equations given in section 5.4. In this section, an attempt is made to assess whether or not

the omission of these second order terms and the boundary displacement transformations are consistent with the expected numerical accuracy of section 7.2. As a prerequisite to this study, it was thought desirable that for a particular case of edge beam geometry, the relative influences of each of the boundary support modes should be determined. In this way it is possible to isolate which of the numerous second order terms in expressions for (H_k, k_k), $(k = 1,2,3)$ are liable to play a significant part in the overall behaviour. For example it can be seen in figure 8.5(a) that the stress resultant $k_{n_{22}}$ is essentially given by zero for all values of λ_3. It is therefore reasonable to assume that because this mode has little influence upon the overall behaviour, that its second orders will be of even less significance. Further, this study will provide additional information as to which support modes are justifiably neglected for an approximate analysis.

8.4.1 The Influence of Support Mode

The behaviour of the shell described in section 8.3.2(c), with $\lambda_3 = 4.5$, is investigated in order that the relative influences of each support mode be ascertained. As a starting point, the corresponding simply supported shell of section 8.2.2 with $m = 4$ is used, and successively each of the four support conditions relaxed or constrained as appropriate to produce the full beam-shell interaction. The numbering system

used in figure 8.8 refers to the following conditions:

(1) Edge with simply supported boundary conditions, as given in section 8.2.2, except that the condition

$$w^3_{3j} = 0$$

is replaced with the edge beam vertical flexure difference expression (8.24).

(2) As in (1), except that the condition

$$w^1_{3j} = 0,$$

is replaced with the edge beam extensional difference expression (8.22).

(3) As in (2), except that the condition

$$w^3_{2j} = - w^3_{4j}$$

is replaced with the edge beam torsional difference expression (8.25).

(4) In this case all the simple support conditions of section 8.2.2 are replaced with the corresponding edge beam conditions of (8.22) to (8.25).

Once again the use of grid size m = 4 produces significant truncation errors, but because these are likely to affect each problem to a similar degree, the results are sufficient for comparative purposes.

Figure 8.8(a) to (f) summarises the results of this study. It can be seen that the vertical flexural and exten-

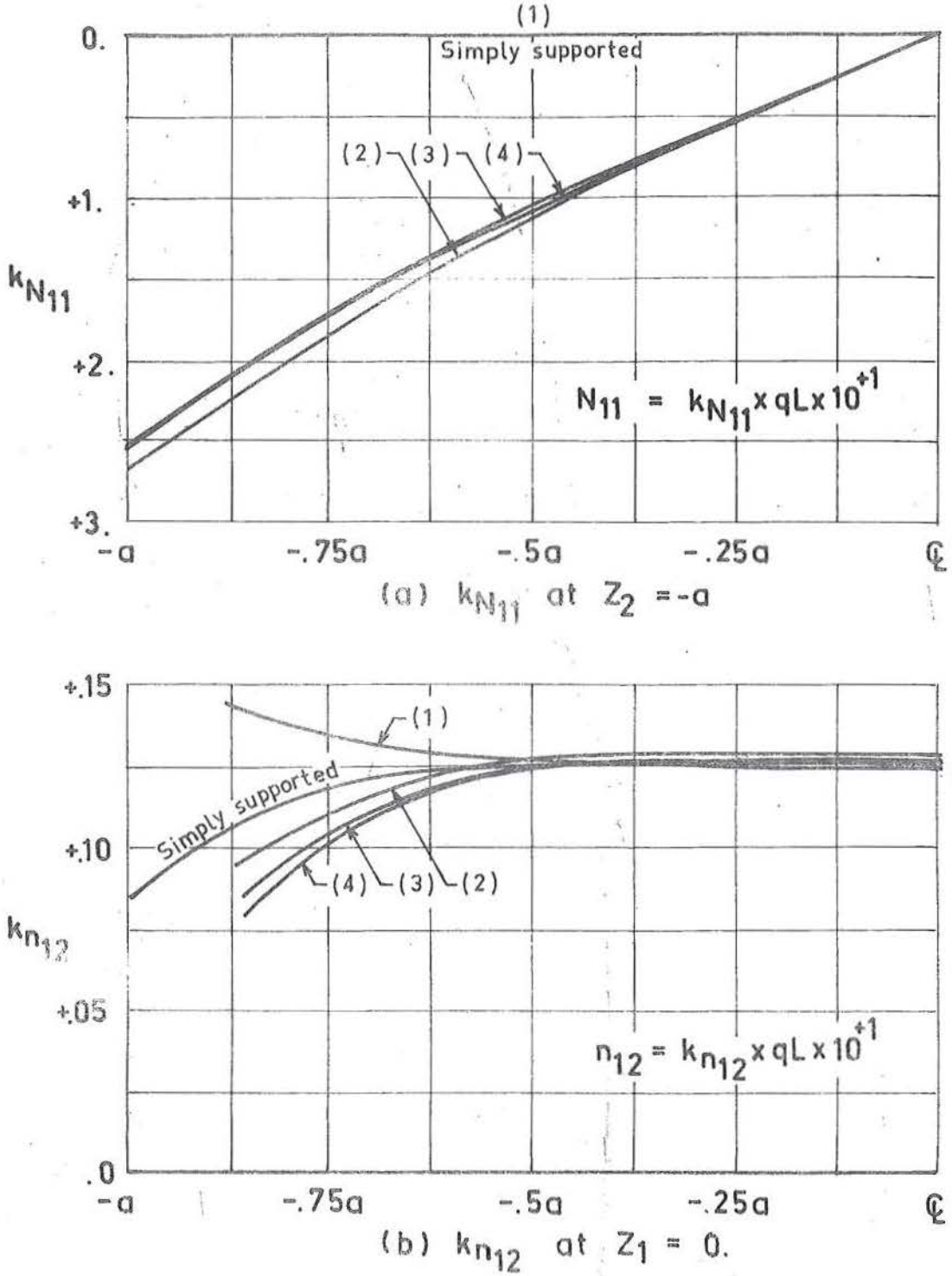

Fig. 8.8 Ruled surface hyperbolic paraboloid. Simply supported, and successive influence of finite (1) vertical, (2) extensional, (3) torsional and (4) lateral edge beam stiffness, where $\lambda_1 = .2$, $\lambda_2 = .0165$, $\lambda_3 = 4.5$, $\lambda_4 = .05$, $\mu = .00$ and $m = 8$.

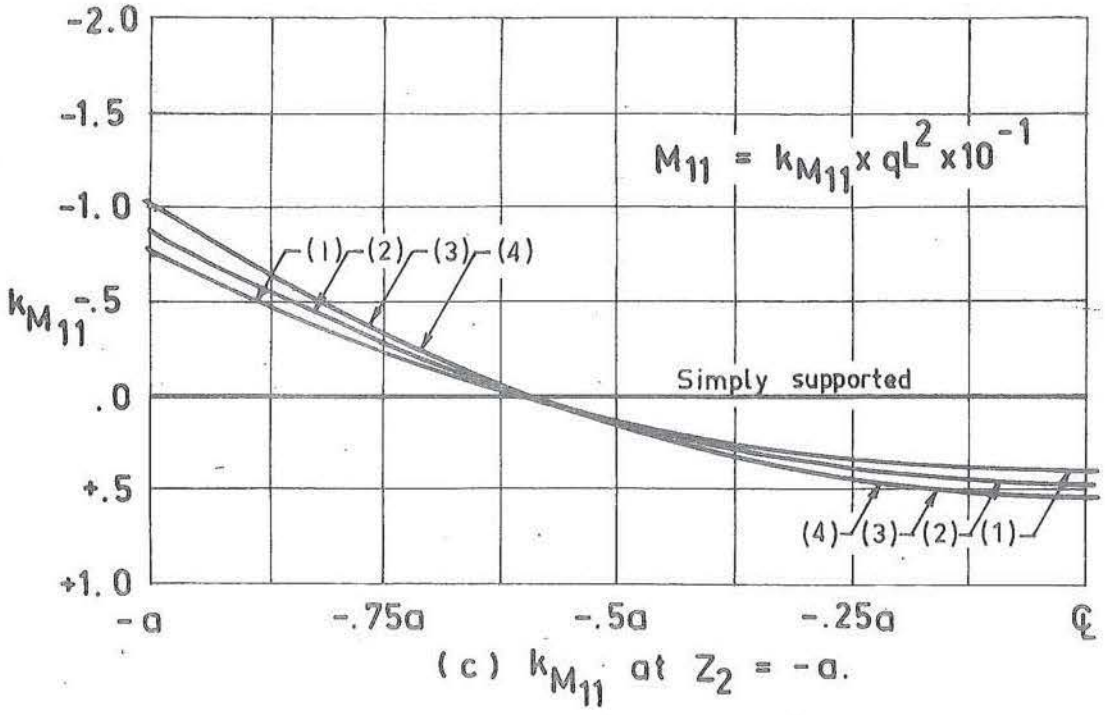

(c) $k_{M_{11}}$ at $Z_2 = -a$.

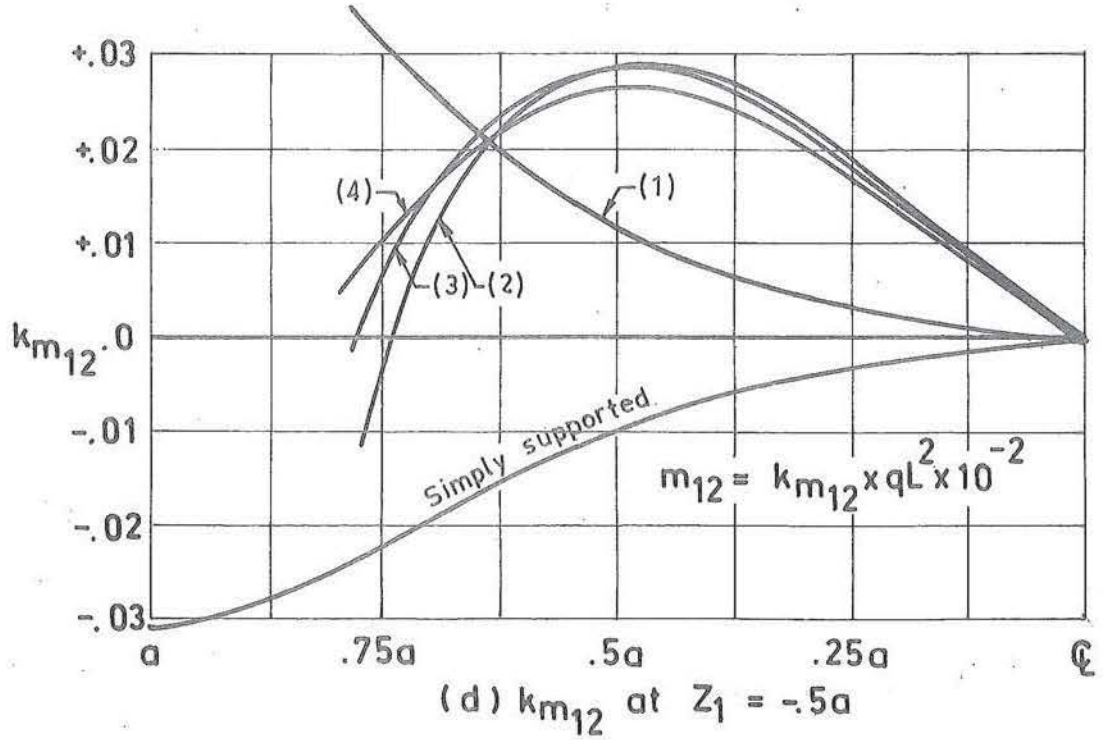

(d) $k_{m_{12}}$ at $Z_1 = -.5a$

Fig. 8.8 (continued) Ruled surface hyperbolic paraboloid. Simply supported, and successive influence of finite (1) vertical, (2) extensional, (3) torsional and (4) lateral edge beam stiffness, where $\lambda_1 = .2$, $\lambda_2 = .0165$, $\lambda_3 = 4.5$, $\lambda_4 = .05$, $\mu = .00$ and $m = 8$.

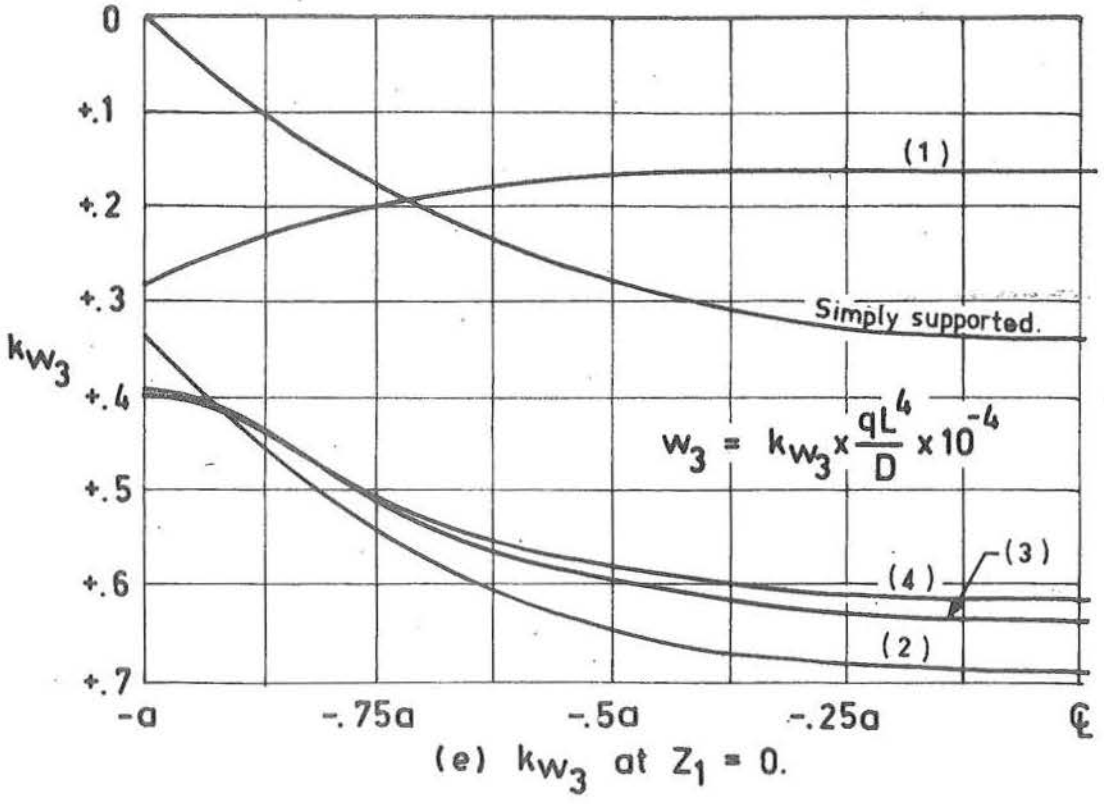

(e) k_{w_3} at $Z_1 = 0$.

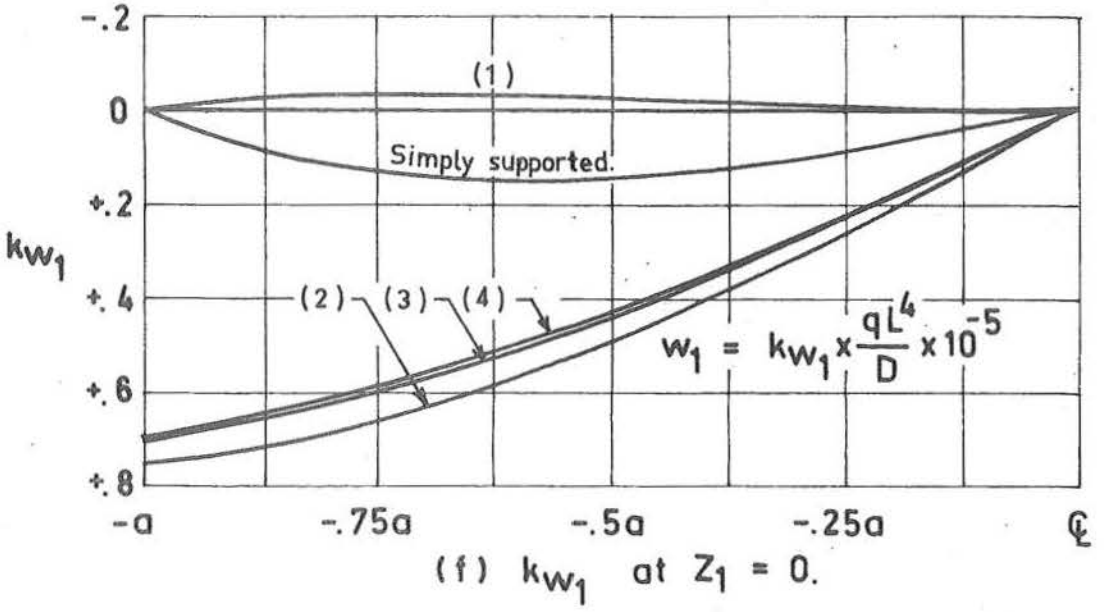

(f) k_{w_1} at $Z_1 = 0$.

Fig. 8.8 (continued) Ruled surface hyperbolic paraboloid. Simply supported, and successive influence of finite (1) vertical, (2) extensional, (3) torsional and (4) lateral edge beam stiffness, where $\lambda_1 = .2$, $\lambda_2 = .0165$, $\lambda_3 = 4.5$, $\lambda_4 = .05$, $\mu = .00$ and $m = 4$.

sional behaviour of the edge beam are the more important modes. Torsion and lateral bending are seen to have an overall influence of little more than 12%, which could have been reduced considerably by use of the clamped flexural mode instead of simple support. For this reason in section 8.4.3 only the second order terms contained in the expressions for $H_3 + \frac{dk_2}{dz_1}$ and H_1 are considered.

8.4.2 The Influence of Displacement Transformation at the Boundary

The results of section 8.3.2 are derived assuming that the grid line $i = 3$ is colinear with the edge beam centroidal axis, which physically implies that the shell passes through the edge beam centroidal axis as shown in figure 8.9.

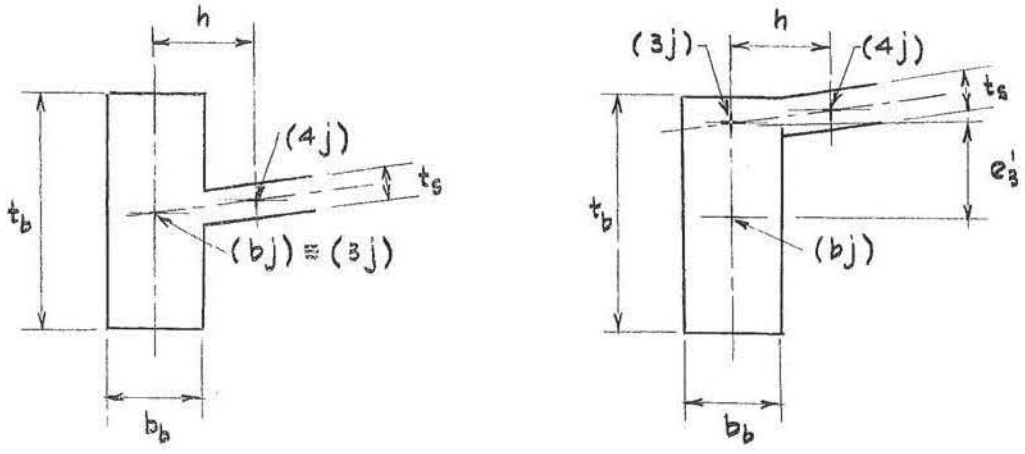

(a) Section 8.3.2 (c)
$e_3^1 = e_3 = 0$,
$e_2^1 = 0$.

(b) Section 8.4.2
$e_3^1 = e_3$,
$e_2^1 = 0$.

Fig. 8.9 Shell-Beam Intersection for Grid Orientation I.

For architectural reasons however, it is normal to have either the top or the bottom of the edge member flush with the corresponding shell surface, so that the shell beam intersection will be eccentric to the beam centroidal axis. In section 5.3 the transformation relating displacements at this junction and the beam centroidal axis were given. For the case of grid orientation I however, expressions are required relating the displacements w^k_{bj} , (j = 3,m+3) and w^k_{3j} , (j = 3,m+3) , which are given by

$$w^1_{bj} = w^1_{3j} + e'_3 \cdot \frac{\partial w_3}{\partial z_1} , \qquad (8.26)$$

$$w^2_{bj} = w^2_{3j} - e'_3 \cdot \frac{\partial w_3}{\partial z_2} , \qquad (8.27)$$

$$w^3_{bj} = w^3_{3j} , \qquad (8.28)$$

$$\left(\frac{\partial w_3}{\partial z_2}\right)_{bj} = \left(\frac{\partial w_3}{\partial z_2}\right)_{3j} , \qquad (8.29)$$

where e'_3 represents the vertical distances between grid lines $i = 3$ and the beam centroidal axis. For present application

$$e'_3 \doteq e_3 .$$

In this case, the displacements w^k_{bj} , (k = 1,2) in equations (8.22) and (8.23) are replaced by the expressions

$$w^1_{bj} = w^1_{3j} + \frac{m.e_3}{2.a} (w^3_{3j+1} - w^3_{3j-1}) , \qquad (8.30)$$

$$w^2_{bj} = w^2_{3j} - \frac{m.e_3}{2.a} (w^3_{4j} - w^3_{2j}) . \qquad (8.31)$$

In order that the influence of these edge transformations be determined, the results from the model of section 8.3.2(c), with zero edge-shell eccentricity, $\lambda_3 = 4.5$ and $m = 8$, are used to provide approximations to the displacement distribution of a new model with all parameters the same as those of section 8.3.2(c), except that the maximum possible eccentricity of $\lambda_5 = -0.39$ is applied. It is assumed that the edge member centroidal displacement remains constant for these models, thus the transformations (8.30) and (8.31) are used to determine the orders of change likely to occur in w^k_{3j}, $(k = 1,2,3)$. Table 8.2 shows the new estimates of w^k_{bj} (the previous w^k_{3j}), which are combined with estimates of the rotations $\frac{\partial w_3}{\partial z_k}$, $(k = 1,2)$ at positions $(3,j)$ using the expressions

$$ {}_k w^1_{3j} = {}_k w^1_{bj} - .12\left({}_k w^3_{3j+1} - {}_k w^3_{3j-1} \right), \qquad (8.32) $$

$$ {}_k w^2_{3j} = {}_k w^2_{bj} + .12\left({}_k w^3_{4j} - {}_k w^3_{2j} \right), \qquad (8.33) $$

to provide approximations to the new magnitude of w^k_{3j}, $(k = 1,2)$. Also shown are the changes expressed as percentage of the original w^k_{3j}, $(k = 1,2)$.

It is seen from this example that the influence upon w^1_{3j} (the predominant support mode for the ruled surface hyperbolic paraboloid) is likely to be great, and although this qualitative study can only be regarded as illustrative,

j	3	4	5	6	7	8	9	10	11
$k_{w_{bj}}1$	.000	.177	.304	.399	.473	.530	.571	.596	.604
$k_{w_{bj}}2$	.000	.260	.361	.358	.320	.259	.182	.094	.000
$k_{w_{bj}}3$	.000	.239	.797	1.530	2.309	3.025	3.596	3.961	4.087
A	.000	-.094	-.153	-.178	-.176	-.152	-.111	-.058	.000
$k_{w_{3j}}1$	.000	.083	.151	.221	.297	.378	.460	.538	.604
%	0	-53	-51	-45	-37	-29	-20	-10	0
B	.000	.014	.023	.027	.028	.028	.028	.027	.027
$k_{w_{3j}}2$	.000	.274	.384	.389	.348	.287	.210	.121	.027
%	0	5	9	8	9	11	15	29	0

$$A = -0.12 \times (k_{w_{3j+1}}3 - k_{w_{3j-1}}3),$$

$$B = +0.12 \times (k_{w_{4j}}3 - k_{w_{2j}}3).$$

$$w^k_{bj} = k_{w_{bj}}k \times \frac{qL^4}{D} \times 10^{-5},$$

$$w^k_{3j} = k_{w_{3j}}k \times \frac{qL^4}{D} \times 10^{-5}.$$

TABLE 8.2 Influence of edge transformations, described in section 8.4.2. Percentages express the change in displacement as a fraction of the original edge displacements.

it does indicate that the overall shell-beam behaviour is significantly affected.

In order to check the influence of the boundary transformations, the programme used for the investigation of section 8.3.2(c) was modified to include possible eccentricities of the grid line $(3,j)$ with respect to (b,j). A slight error in this programme modification should be mentioned, although it is felt to have little influence upon the results obtained. Because the shell beam is no longer of the form which assures symmetry and or antisymmetry about the (z_1,z_2) axes, it is incorrect to assume these in the solution. This fact is seen to produce an anomoly in the symmetry boundary conditions about the z_2 axis in the programme. If it is assumed, as in equations (8.4), that the displacements

$$w^1_{i\,m+4} = w^1_{i\,m+2} ,$$

are symmetric, then because $\frac{\partial w_3}{\partial z_1}$ is an antisymmetric function about the z_2 axis

$$w^1_{b\,m+4} \neq w^1_{b\,m+2} .$$

However, because $\frac{\partial w_3}{\partial z_1}$ is zero at the beam midspan this is a very small error at small distances from the z_2 axis.

Figure 8.10(a)-(f) shows the influences of λ_5 (the ratio of vertical eccentricity to beam thickness) upon the overall shell behaviour. It is seen that the in-plane displacements are appreciably affected, w_1 at $(0,-a)$ changing

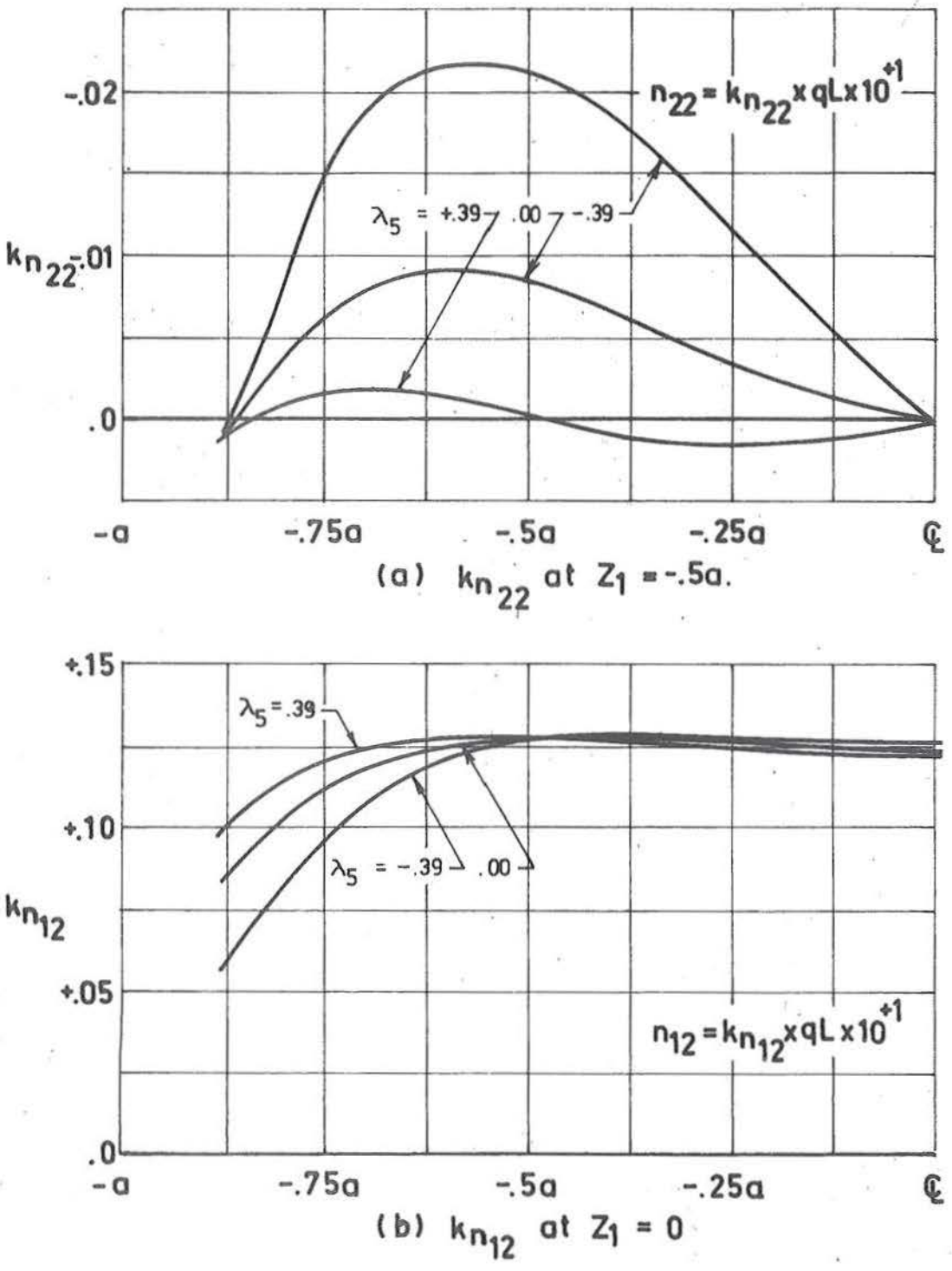

Fig. 8.10 Ruled surface hyperbolic paraboloid with beam edges clamped at corners. Influence of λ_5, where $\lambda_1 = .2$, $\lambda_2 = .0165$, $\lambda_3 = 4.5$, $\lambda_4 = .05$, $\lambda_6 = .00$, $\mu = .00$ and $m = 8$.

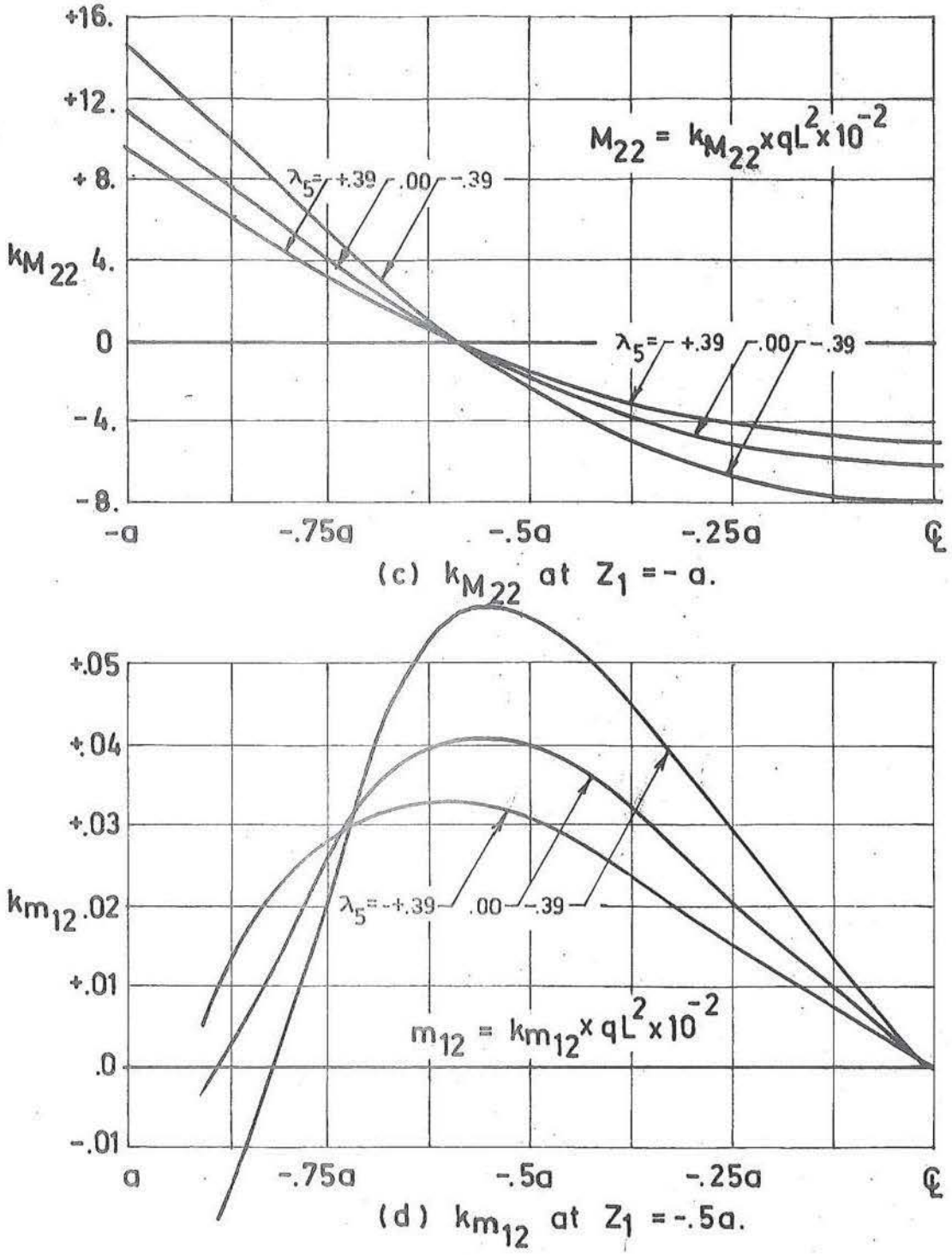

Fig. 8.10 (continued) Ruled surface hyperbolic paraboloid with beam edges clamped at corners. Influence of λ_5, where $\lambda_1 = .2$, $\lambda_2 = .0165$, $\lambda_3 = 4.5$, λ_4 .05, $\lambda_6' = .00$, = .00 and $m = 8$.

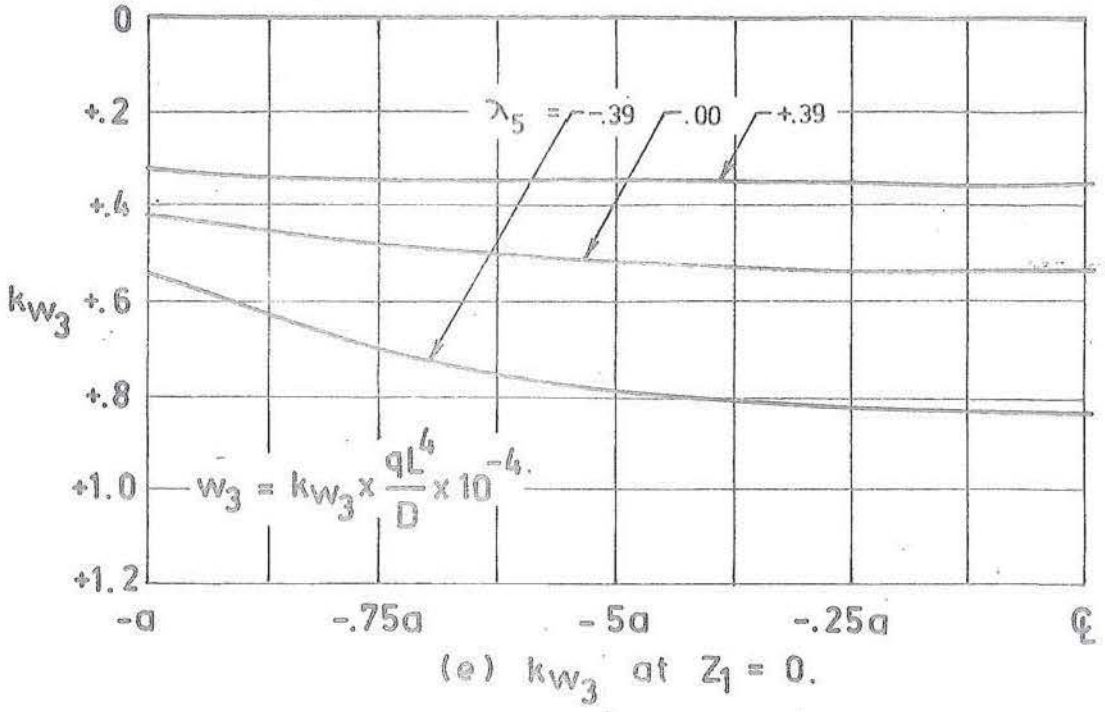

(e) k_{w_3} at $Z_1 = 0$.

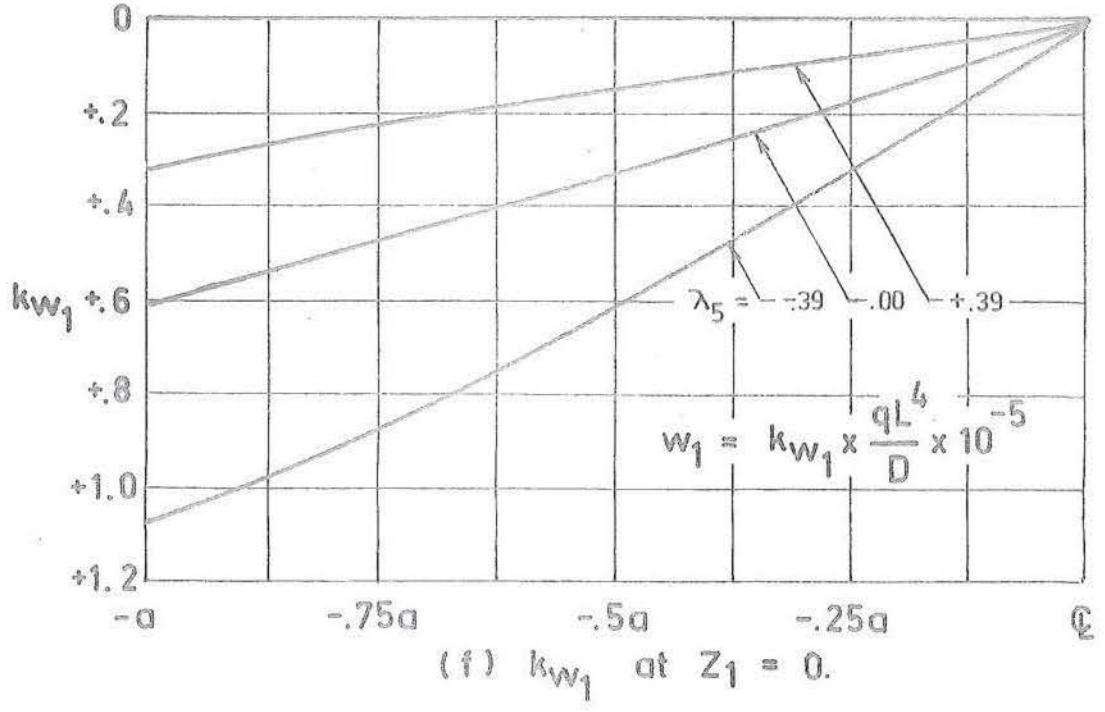

(f) k_{w_1} at $Z_1 = 0$.

Fig. 8.10 (continued) Ruled surface hyperbolic paraboloid with beam edges clamped at corners. Influence of λ_5, where $\lambda_1 = .2$, $\lambda_2 = .0165$, $\lambda_3 = 4.5$, $\lambda_4 = .05$, $\lambda_6' = .00$, $\mu = .00$, and $m = 8$.

by 50% for a change in λ_5 from 0.0 to 0.39. Correspondingly, in-plane stresses are also increased considerably in the vicinity of the edge beam. These results cannot be interpreted as providing the correct influence of λ_5, but they do indicate in a more quantitative manner than those of table 8.2 the likely overall effects of this eccentricity.

8.4.3 The Influence of Second Order Load Terms

In section 8.4.1, the dominance of the extensional and vertical flexural modes indicated that if second orders were to affect the behaviour of the shell-beam interaction, it would be the second orders in the approximations to the loading H_1 and $H_3 + \frac{\partial k_2}{\partial z_1}$ of these particular modes. To determine the magnitude of the various second order terms, the solution of section 8.3.2(c) with $\lambda_3 = 4.5$ was used with $m = 16$. Table 8.3 shows the magnitude of the stress resultants involved in the expression

$$H_3 + \frac{dk_2}{dz_1} = \left(q_{22} + \frac{dm_{21}}{dz_1}\right).\cos\phi + n_{22}.\sin\phi + \frac{\partial n_{12}}{\partial z_1}.e_3$$

at the grid locations $(4, j)$, $(j = 4, m+3)$ with only odd pivotals being shown. Difference approximations to $\frac{\partial m_{21}}{\partial z_1}$ and $\frac{\partial n_{21}}{\partial z_1}$ are obtained using the expressions

$$\left(\frac{\partial m_{21}}{\partial z_1}\right)_{4j} \doteq m.\left(k_{m^{21}_{4j+1}} - k_{m^{21}_{4j-1}}\right).qL,$$

$$\left(\frac{\partial n_{21}}{\partial z_1}\right)_{4j} \doteq \frac{m}{2.a}\left(k_{n^{21}_{4j+1}} - k_{n^{21}_{4j-1}}\right).qL,$$

where it is noted that all loading is given in terms of qL (or load per unit length) to be consistent with q_{22}.

It can be seen from the last four rows of table 8.3, that the total load applied from second order terms is very much greater than that applied by the first order terms. However, it does not follow that these second orders will have a proportionally significant influence upon the overall shell behaviour. The majority of the loading from second orders is applied at or near the abutment corners, and will therefore have a smaller effect than the smaller loading applied at the beam centre. Because the loading from second orders is of greater magnitude than that resulting from first orders, a programme was written to determine numerically the quantitative influence for a particular example. For this purpose, the edge beam programme containing edge displacement transformations described in section 8.4.2 was modified to include the $e_3 \cdot \frac{\partial n_{21}}{\partial z_1}$ terms, and results were determined for the example of $\lambda_5 = -.39$ and $m = 8$. It was found that the inclusion of this second order term had very little effect upon the overall shell behaviour. Displacements k_{w_3} and k_{w_1} were changed by less than 0.1% and 0.5%, and no measurable difference was noted in stress and moment resultants. Results are therefore not presented, and because the total load contribution from the $n_{22} \cdot \sin\phi$ terms was less than that from the $e_3 \cdot \frac{\partial n_{21}}{\partial z_1}$ terms (see table 8.3), they are not considered.

j	5	7	9	11	13	15	17	19
$\sin \phi_j$	.172	.148	.124	.100	.072	.048	.024	.000
$\cos \phi_j$	.984	.987	.992	.995	.997	1.000	1.000	1.000
$k_{q_{22}}$	-.015	-.006	.011	.020	.023	.023	.022	.022
$k_{m_{12}}$	-.007	-.024	-.022	-.012	-.005	-.001	-.000	.000
$\frac{\partial k_{m_{12}}}{\partial z_1}$	-.003	-.001	.001	.001	.000	.000	.000	.000
$k_{n_{21}}$	2.317	1.274	.797	.680	.660	.674	.697	.655
$\frac{\partial k_{n_{12}}}{\partial z_1}$	-.134	-.334	-.096	-.022	.000	.010	.003	.000
$k_{n_{22}}$	1.343	-.064	-.030	-.001	-.000	.000	.000	.000
A	-.018	-.007	.012	.021	.023	.023	.022	.022
B	.231	-.010	-.004	.000	.000	.000	.000	.000
%	1005	44	17	0	0	0	0	0
C	.079	.197	.057	.013	.000	-.006	-.002	.000
%	344	866	248	57	0	26	9	0

$$A = \left(k_{q_{22}} + \frac{\partial k_{m_{12}}}{\partial z_1}\right) \cdot \cos \phi \,, \qquad B = k_{n_{22}} \cdot \sin \phi \,, \qquad C = -e_3 \cdot \frac{\partial k_{n_{12}}}{\partial z_1} \,.$$

TABLE 8.3 Influence of second order terms upon edge member loading. Percentages computed as a fraction of the maximum contribution from A .

8.4.4 Discussion

Because the results presented are by necessity for a particular case, caution should be exercised in drawing conclusions. It is indicated that edge beam extension and vertical flexure are the important edge support modes for the particular geometry chosen, and this result is capable of generalisation to other shell-edge systems for the ruled surface hyperbolic paraboloid, but not to other shell classes.

For structures with the shell-edge beam intersection eccentric to the beam centroidal axis, boundary displacement transformations were found to have a significant influence upon overall shell behaviour, while the influence of second order terms was found to be negligible. It is likely that these latter observations will be equally relevant to other shell forms and edge member configurations.

8.5 CORNER CONDITIONS

All examples of this chapter have hitherto considered the clamped corner as given by condition (8.8). This section considers numerically the influence upon overall shell behaviour of perturbations in the corner support modes. The free edge shell of section 8.2.3 is considered in particular, although the same trends have been found in the beam supported shell.

8.5.1 Influence of Constraint Nodes:

It is demonstrated in section 10.1 that the normal shear stresses, even in the region of the corner singularity, carry a small proportion of the applied vertical and resulting horizontal loadings. From section 8.2.3 however, it can be seen that this bending action is accompanied by very high moment resultants at the corners and therefore correspondingly high surface stresses. The removal of bending moments will thus alter in a very small way the overall supporting action of the shell, while the adverse high bending stresses at the corners are eliminated. Flexural corner conditions

$$w_3 = \frac{\partial^2 w_3}{\partial z_1^2} = \frac{\partial^2 w_3}{\partial z_2^2} = 0. \qquad (8.34)$$

are applied and reduce to difference expressions

$$\begin{aligned} w^3_{33} &= 0 \,, \\ w^3_{23} &= -\, w^3_{43} \,, \\ w^3_{32} &= -\, w^3_{34} \,. \end{aligned} \qquad (8.35)$$

The results of this change in corner conditions are shown by (2) in figure 8.11(a)-(f). The high negative corner bending moments are seen to be eliminated, while positive moments, in-plane stress resultants and displacements at small distances from the corners, are unaffected by the corner relaxation.

Referring once again to the results of section 10.1, it is evident from the high proportion of vertical and horizontal

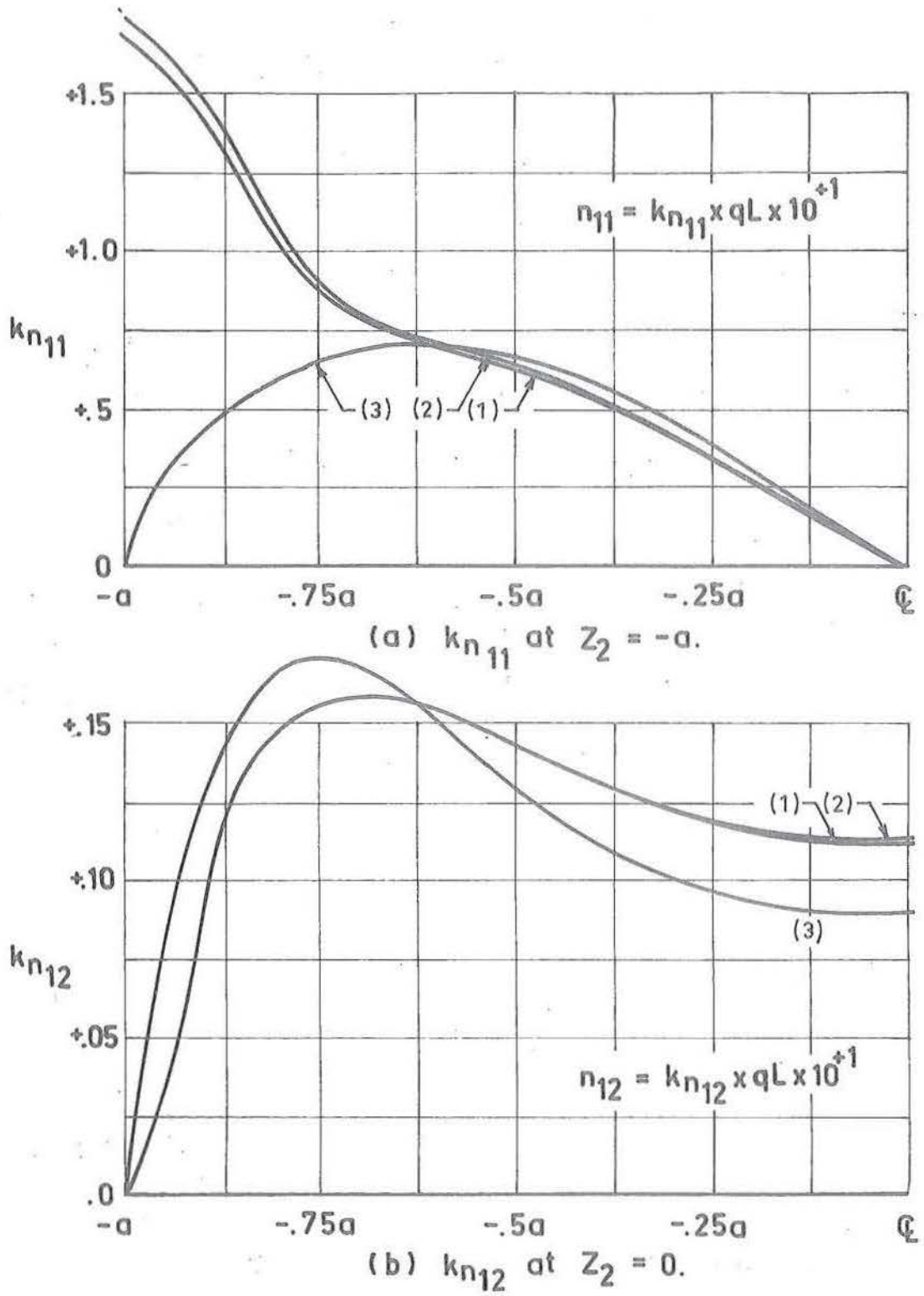

Fig. 8.11 Ruled surface hyperbolic paraboloid with edges free and corners (1) clamped, (2) clamped extensionally simply supported flexurally, and (3) free extensionally clamped flexurally.

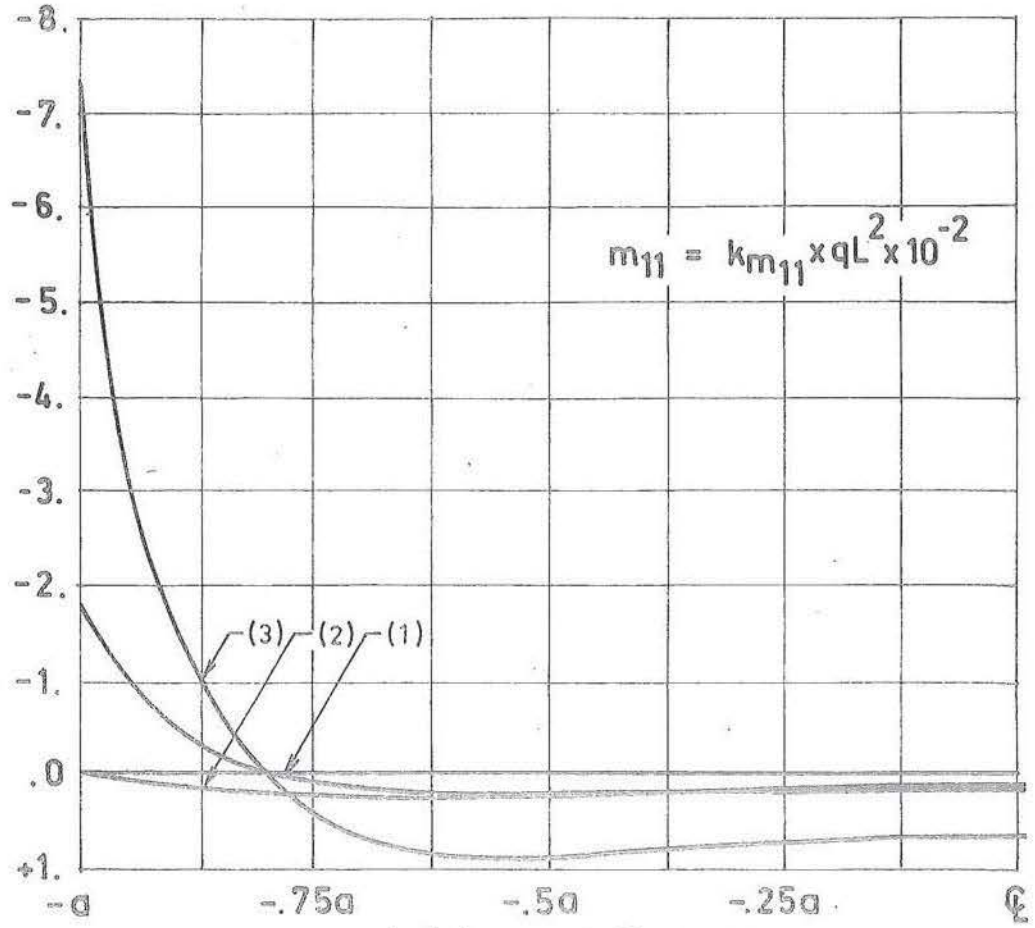

(c) $k_{m_{11}}$ at $Z_2 = -a$.

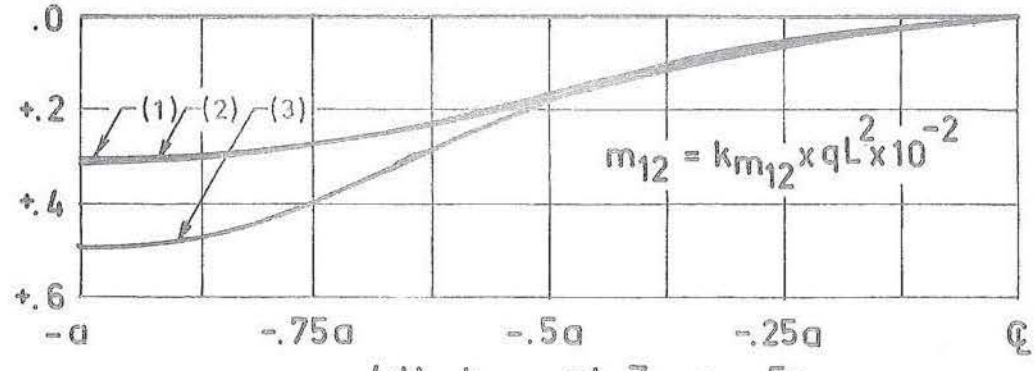

(d) $k_{m_{12}}$ at $Z_2 = -.5a$.

Fig. 8.11 (continued) Ruled surface hyperbolic paraboloid with edges free and corners: (1) clamped, (2) clamped extensionally simply supported flexurally, and (3) free extensionally clamped flexurally

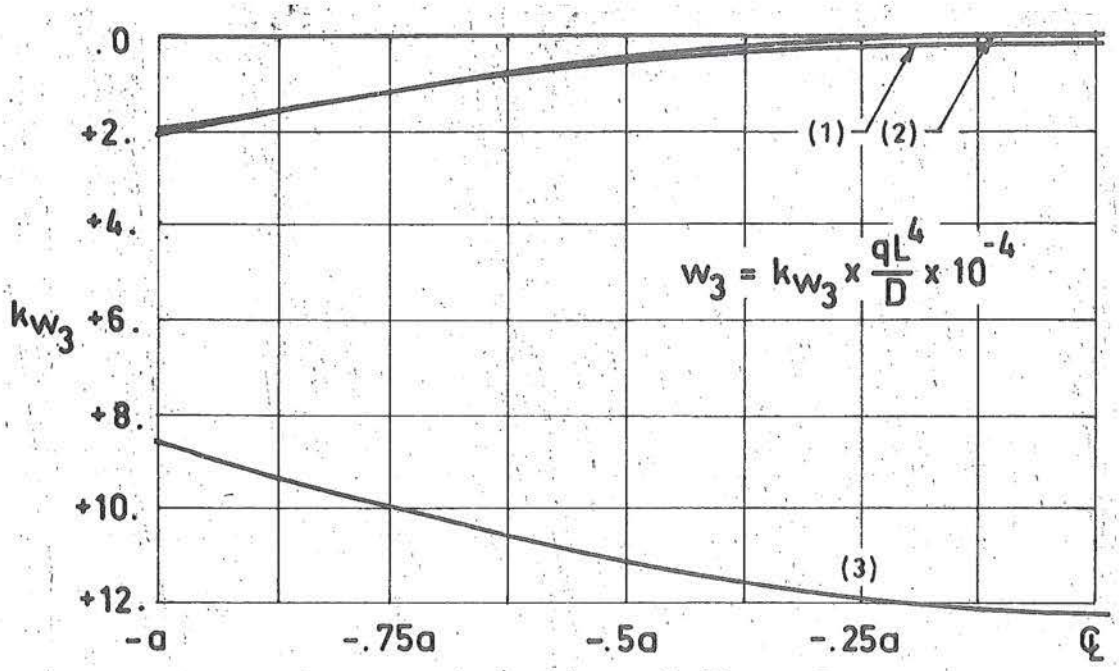

(e) k_{w_3} at $Z_1 = 0$.

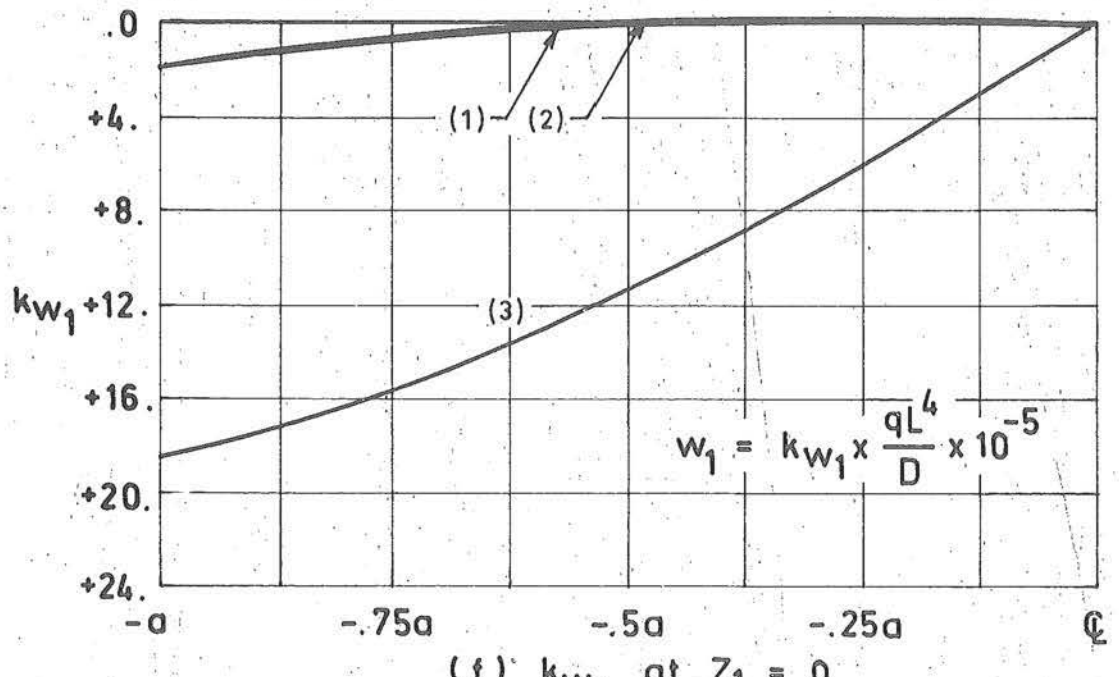

(f) k_{w_1} at $Z_1 = 0$

Fig. 8.11 (continued) Ruled surface hyperbolic paraboloid with edges free and corners (1) clamped, (2) clamped extensionally simply supported flexurally, and (3) free extensionally clamped flexurally.

loading resisted by direct stresses that the membrane shear force is rapidly converted into direct stresses at the boundary. Relaxing this particular support mode may therefore be expected to result in drastic changes in shell behaviour. For this the conditions

$$n_{12} = n_{21} = n_{11} = n_{22} = 0. \text{ at } |z_1 z_2| = a \tag{8.36}$$

are combined with the conditions of flexurally clamped corner given by (8.8). Equilibrium equations (2.25) and (2.26) must now be employed to define the pivotals w^k_{33} , (k = 1,2) , which combined with the free boundary conditions of section 8.2.3 may be shown to result in the conditions

$$\begin{aligned} \frac{\partial^2 w_1}{\partial z_1^2} &= \frac{\partial^2 w_1}{\partial z_2^2} = 0 , \\ \frac{\partial^2 w_2}{\partial z_2^2} &= \frac{\partial^2 w_2}{\partial z_1^2} = 0 , \end{aligned} \tag{8.37}$$

for the determination of w^k_{33} , (k = 1,2) . Using the conditions of symmetry and the corner condition

$$\frac{\partial w_1}{\partial z_1} = \frac{\partial w_2}{\partial z_2} = 0 , \tag{8.38}$$

which result from (8.36), it can be shown that (8.37) and (8.38) result in the following difference expressions

$$w^1_{23} = w^2_{23} = w^1_{33} = w^2_{33} = w^1_{34} = w^2_{34} = 0.. \tag{8.39}$$

Therefore it is only necessary to apply the differential equations at the pivotal positions $(3,j)$, $(j = 4,m+3)$, the value of w^k_{43}, $(k = 1,2)$ being used to determine w^k_{33}, $(k = 1,2)$.

In Figure 8.11(a) - (f) the results for this corner condition are indicated by (3). It can be seen that the elimination of the predominant load carrying medium at the corners results in all vertical load being carried by normal shear stress, with a corresponding increase in the orders of magnitude of both moment resultants and displacements.

For comparative purposes, the results for the shell with all corners clamped flexurally and extensionally are indicated as (1).

8.5.2 Influence of Area of Support

It was indicated in section 8.2.3 that in order to reduce the corner singularities, practical structures would employ some form of corner conditions which supported the shell over a finite area. Such is the case of the model described in subsequent sections. Theoretical programmes for the free and displacement edge beam, described in sections 8.2.3 and 8.3.2(c), have been modified to include this effect. With a grid with $m = 16$, it can be seen from figure 8.12 that the shell is effectively clamped along the grid lines $(i,6)$, $(i = 3,6)$ and $(6,j)$, $(j = 3,6)$.

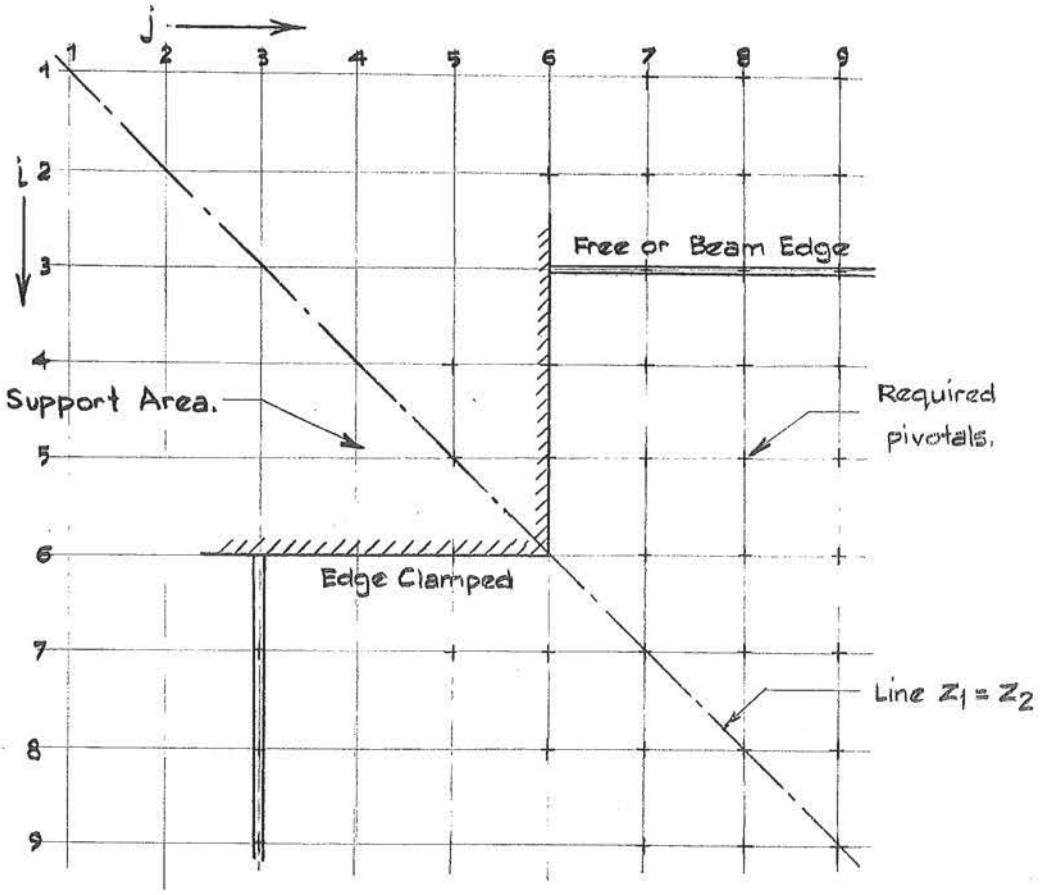

Fig. 8.12 Detail of clamped corner support over a finite area, for the example of section 8.5.2.

while for (3,j), (j = 7,19) the conditions of the free or beam edge apply. Using the clamped edge conditions of section 8.2.1, the required unknowns at the corner are given by

$$\begin{aligned} w^{k}_{i6} &= 0, \ (k = 1,2,3), \ (i = 2,6) \\ w^{3}_{i5} &= w^{3}_{i7}, \ (i = 3,5) . \end{aligned} \tag{8.40}$$

The influences of this finite corner support for the free edge shell are shown in figure 8.13(a) to (f). The direct

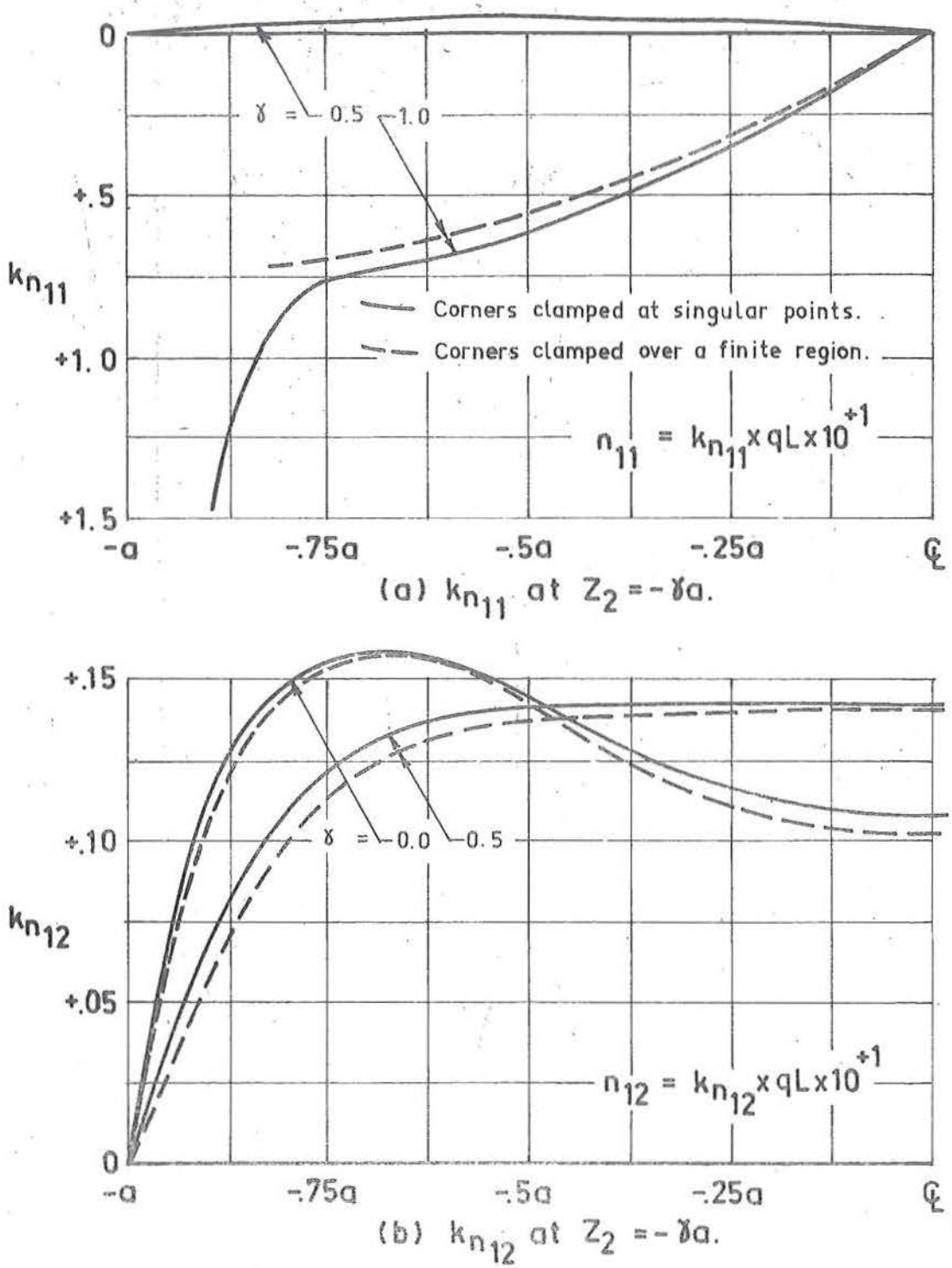

Fig. 8.13 Ruled surface hyperbolic paraboloid with edges free and corners clamped. Influence of corners clamped over a finite region, where $\lambda_1 = 0.20$, $\lambda_2 = 0.0165$, $\mu = 0.00$ and $m = 8$.

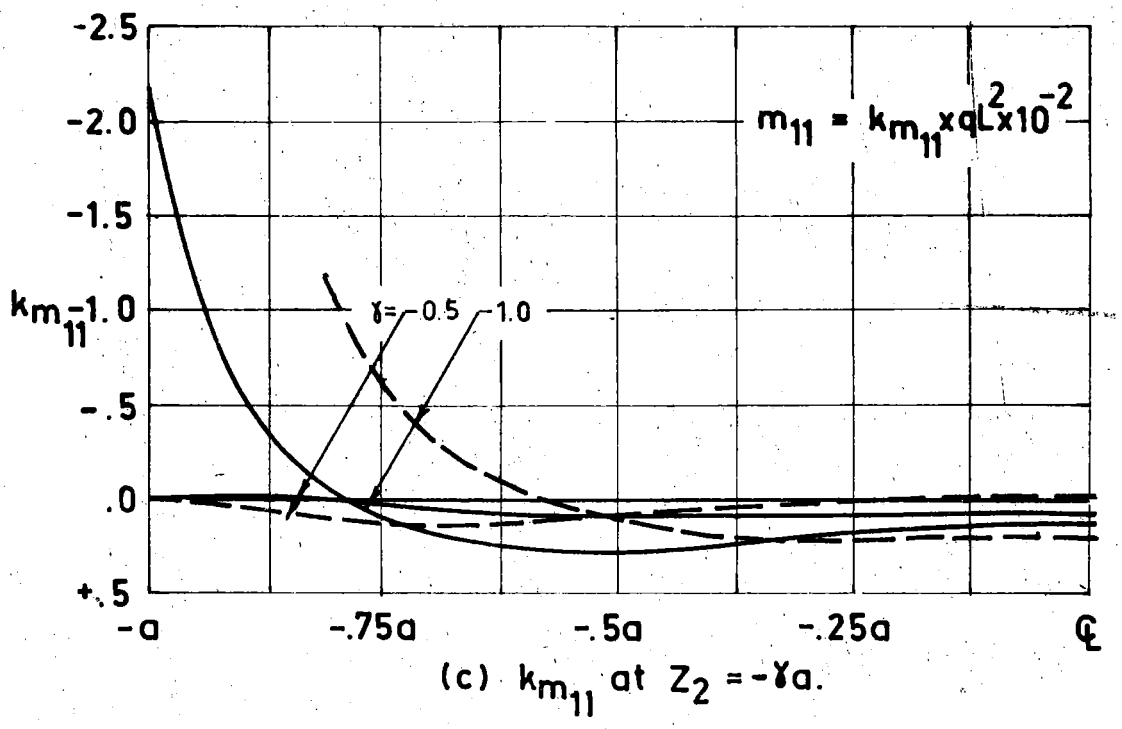

(c) $k_{m_{11}}$ at $Z_2 = -\gamma a$.

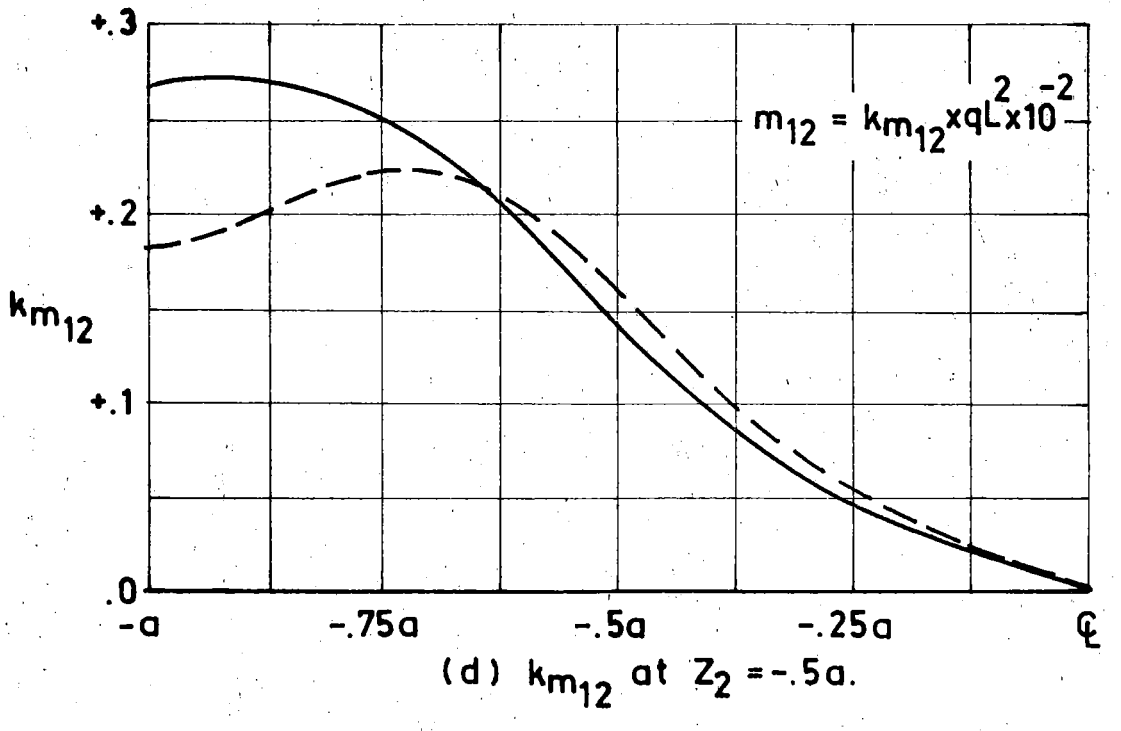

(d) $k_{m_{12}}$ at $Z_2 = -.5a$.

Fig. 8.13 (continued) Ruled surface hyperbolic paraboloid with edges free and corners clamped. Influence of corners clamped over a finite region.

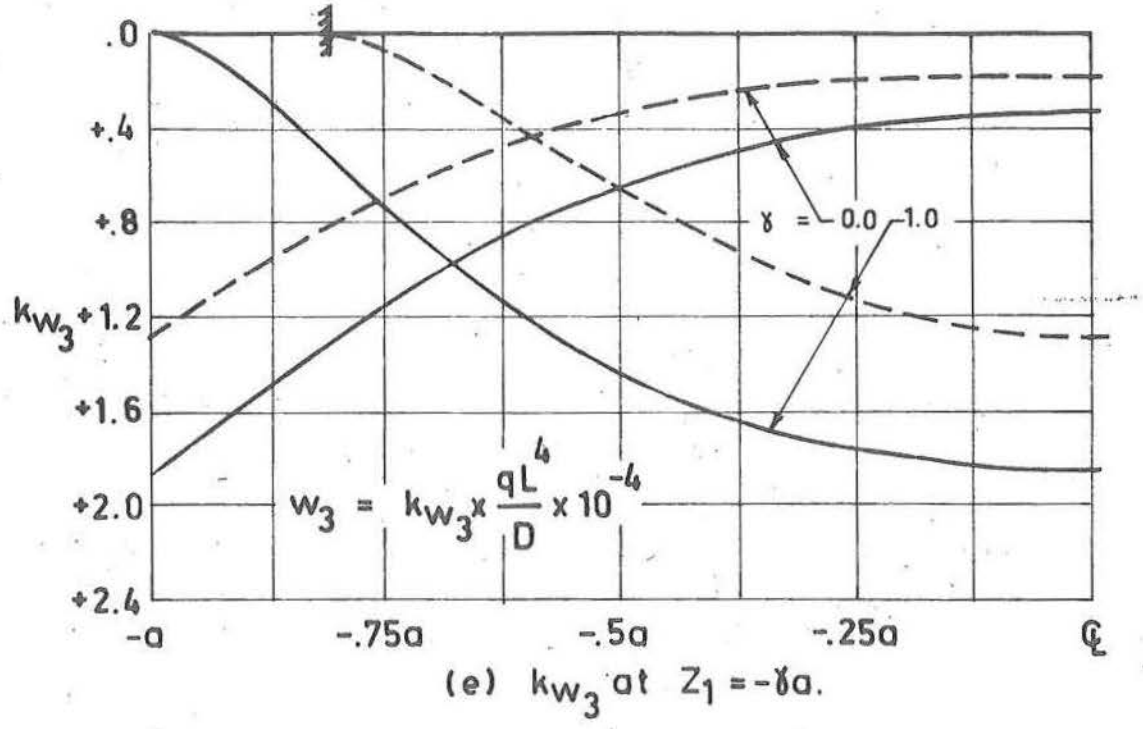

(e) k_{w_3} at $Z_1 = -\gamma a$.

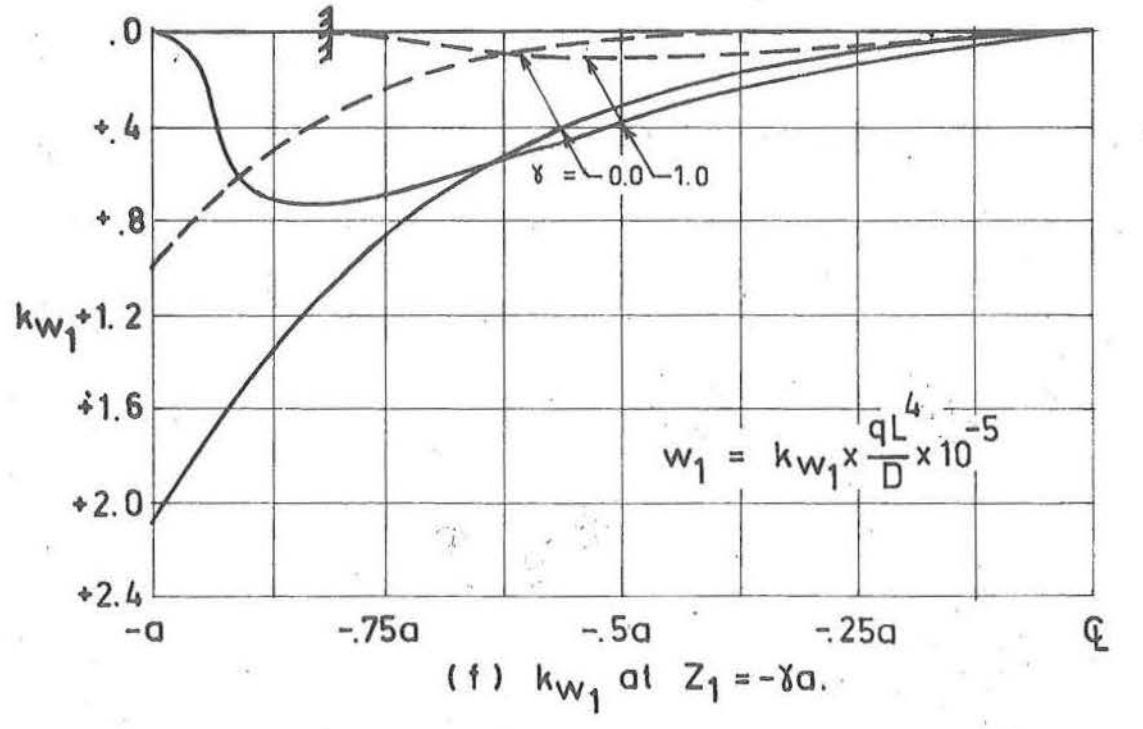

(f) k_{w_1} at $Z_1 = -\gamma a$.

Fig. 8.13 (continued) Ruled surface hyperbolic paraboloid with edges free and corners clamped. Influence of corners clamped over a finite region.

stress along the edge is virtually unchanged, except that the singular point at the corner is removed. Edge moment resultants, although of similar profile, are displaced due to the effective shortening of this edge strip. Vertical displacements are as expected - reduced.

8.5.3 Discussion

The critical influence of the extensional stiffness of the edge strip, whether this be a beam or the edge zone for the free edged shell, has been shown in section 8.4.1. It is therefore not surprising that changes in boundary conditions for this extensional beam behaviour cause marked changes in overall shell behaviour. This emphasises the need in practical design for a theoretical model which makes allowance for any horizontal flexibility of either the tie bars or corner abutments. Conversely, if these corner displacements cannot be controlled, an indication of the expected lateral stiffness is required.

In the same way that torsional effects of edge beams have little influence upon the overall shell behaviour, the influence of moment rigidity at the shell corner also has little significance. However, the use of corner supports with zero moment resistance (for example the use of a pin) has been shown to considerably reduce the maximum surface stresses due to bending moments, while at the same time only affecting to a small degree the other shell actions. To further decrease corner stresses,

the use of corners supported over a relatively large area is to be recommended.

8.6 CONCLUSIONS

The agreement of in-plane shears with those predicted by membrane analysis is shown for all boundary and corner support conditions considered. It is also shown that for each of these support conditions, the stresses due to bending, even at the shell centre, are at least of the same order as the principal stresses due to membrane action. In the edge zone $|z_1, z_2| > .75a$ the membrane principal stresses are of insignificant magnitude in comparison with those resulting from bending action. Considering the diversity of solutions obtained for the extreme cases of boundary and corner support conditions, the need for an analysis embodying all critical modes of these conditions is apparent.

For edge beams of practical dimensions, the extensional and vertical flexural support modes should be considered, while for systems where the shell-edge member intersection is significantly eccentric to the edge beam centroidal axis, the influence of boundary transformations must be included. Second order terms, in the estimation of edge member vertical loading, are of little significance, and may be justifiably neglected in approximate solution techniques. The importance of diagonal corner support control cannot be over emphasised, and must be

included in any design analysis. Just as there is little to be gained by carrying out a bending analysis if the correct boundary conditions are not provided, there is little point in providing the correct boundary conditions if the corner support conditions are not satisfactorily represented.

CHAPTER NINE

COMPARATIVE STUDIES OF SHELL BEHAVIOUR

In order to determine the influence of shell geometry and material properties, the following chapter considers a number of numerical examples for shells, with variations in the parameters:

1. The rise to span ratio λ_1.
2. The thickness to span ratio λ_2.
3. Poissons Ratio μ .

The clamped, simple and free boundaries described in sections 8.2.1 to 8.2.3 are studied, and as a typical example of the edge beam of section 8.3.2(c), the particular case of $\lambda_4 = 4.5$ is considered. Conclusions are of a qualitative nature, because only uniform normal loading q over the complete shell and edge beam is investigated, and a limited number of solutions are presented. When the impractical nature of the corner constraints are realised, little is to be gained from a more extensive study. Programmes described in sections 8.2.1 to 8.2.3 and 8.3.2(c) are used to obtain all solutions on grids with $m = 8$.

It should be noted that the solution of equations (2.25) to (2.27) for each of the degenerate boundary conditions can be

shown to depend upon one geometric parameter only - that of $\frac{t_b}{f}$ [43,51] . As the absolute values of displacements, and therefore stress and moment resultants, depend upon the dimensionless ratios λ_1 and λ_2 , to determine the effect of these parameters, a number of correction factors must be applied. The ratios λ_1 and λ_2 are used as they relate directly those variables used in design. To ensure that all solutions are unique, care is taken that the ratio λ_{1/λ_2} is always different.

9.1 THE INFLUENCE OF λ_1

Figures 9.1 to 9.4 show summarised results for the clamped, simple, free and beam edged supported structures, and in all cases λ_1 is incremented from 0.1 to 1.0 in steps of 0.1.

It is noted that changes in shell behaviour are extremely rapid for shells in the range $0. < \lambda_1 < 0.3$, and for $\lambda_1 > 0.3$ the displacements and stress and moment resultants quickly converge to limits at which the values of stress and displacements are very much less than for shells of moderate slope. The application of the "shallow" forms of the shell equations at values of $\lambda_1 > 0.3$ is questionable, and further work is required to determine at what values of λ_1 , the influence of non-shallow terms is likely to affect shell behaviour to a greater extent than the expected numerical accuracy. Considerations similar to those of section 8.4 could be applied to

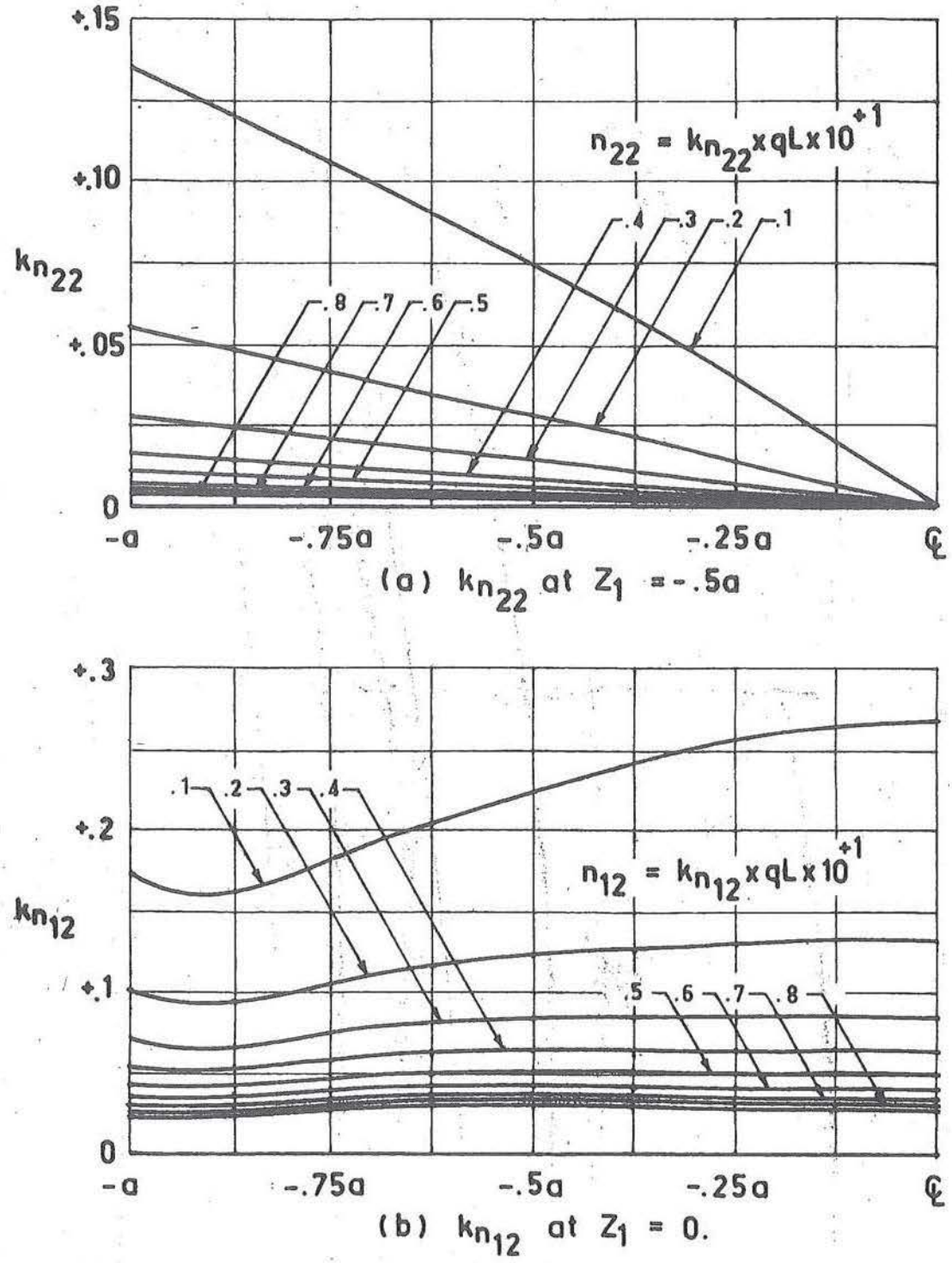

Fig. 9.1 Ruled surface hyperbolic paraboloid with all edges clamped. Influence of λ_1, where $\lambda_2 = .0165$, $\mu = .00$ and $m = 8$.

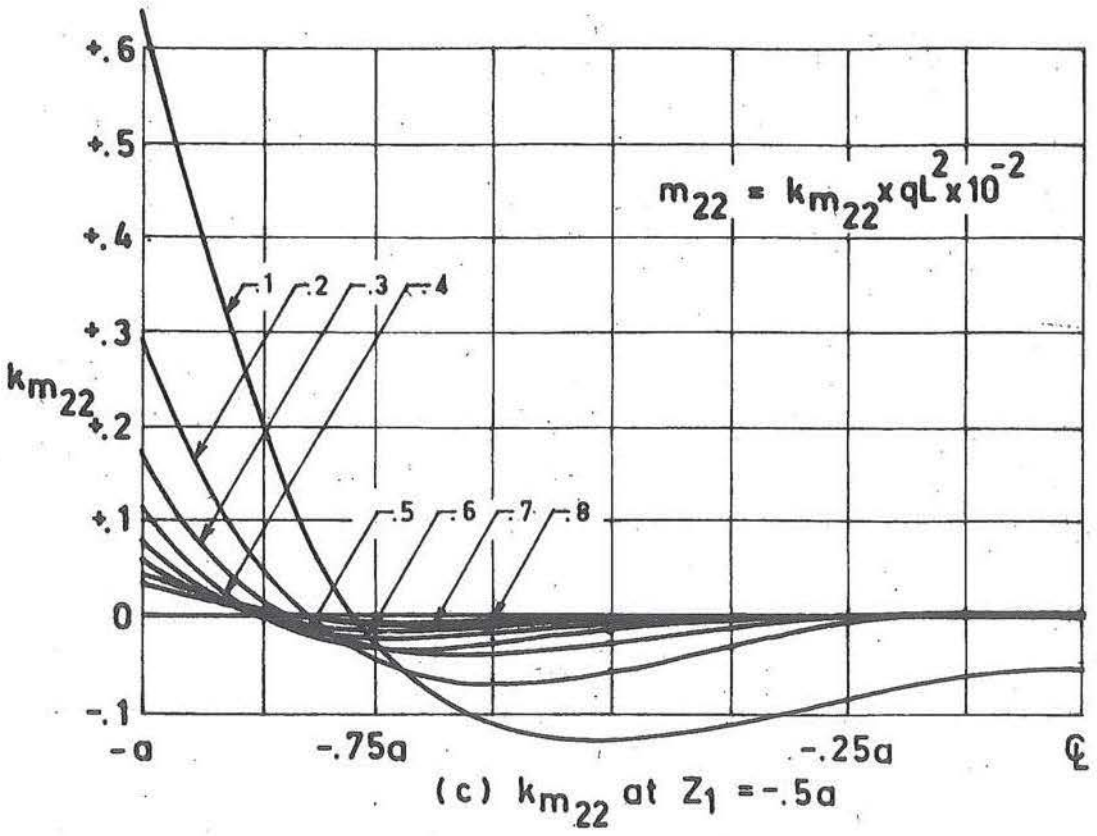

(c) km_{22} at $Z_1 = -.5a$

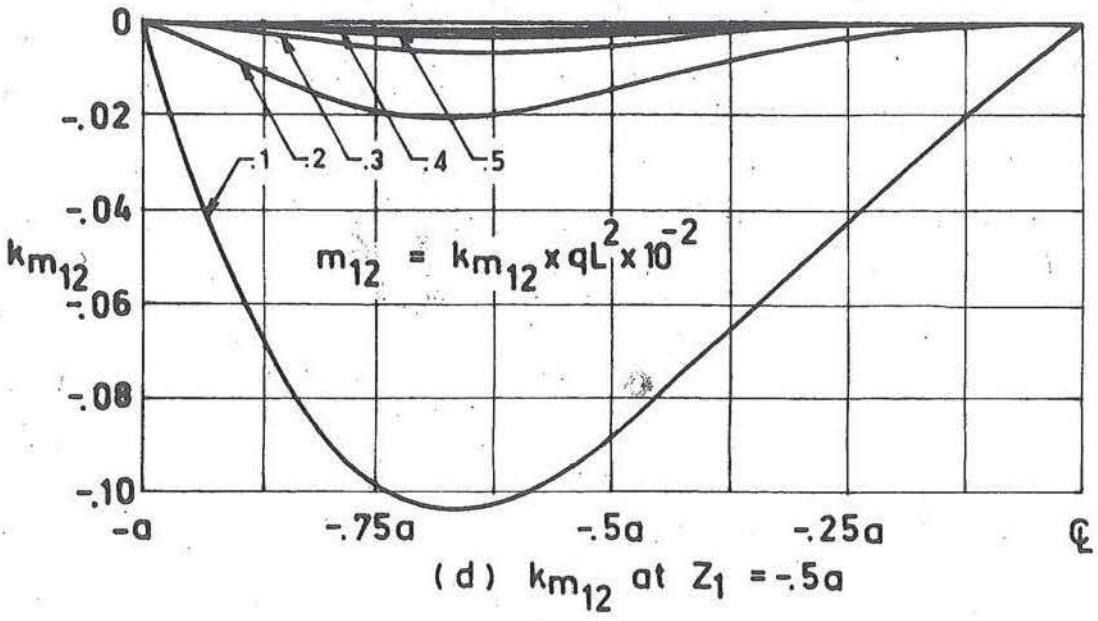

(d) km_{12} at $Z_1 = -.5a$

Fig. 9.1 (continued) Ruled surface hyperbolic paraboloid with all edges clamped. Influence of λ_1, where $\lambda_2 = .0165$, $\mu = .00$ and $m = 8$.

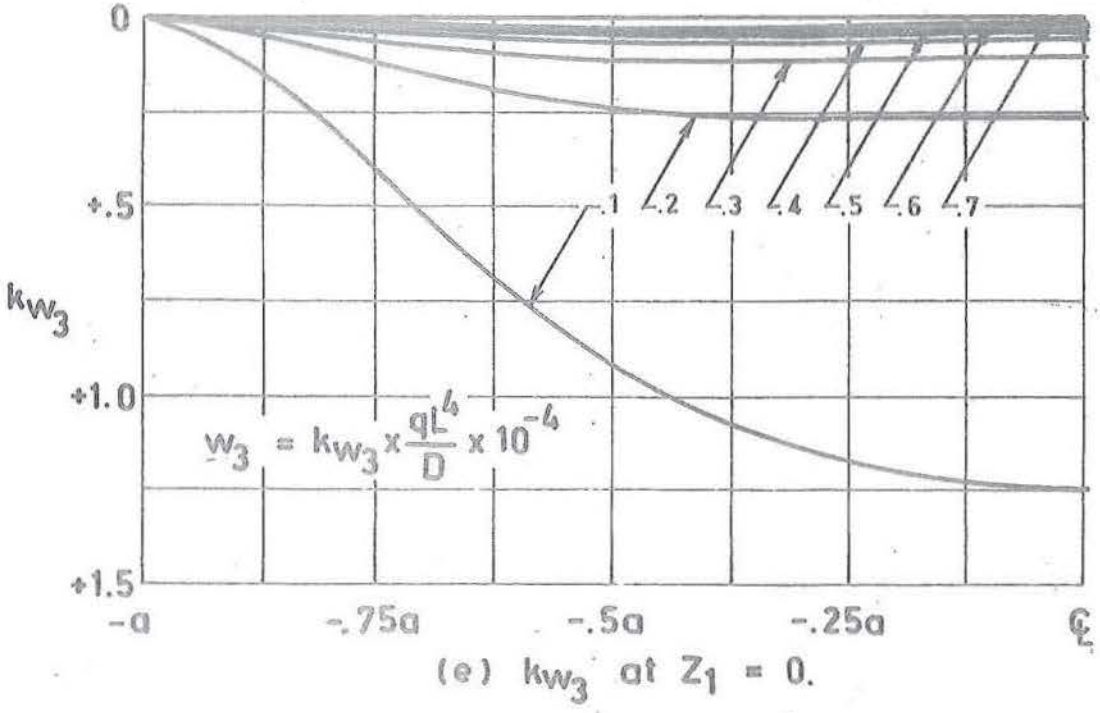

(e) k_{w_3} at $Z_1 = 0$.

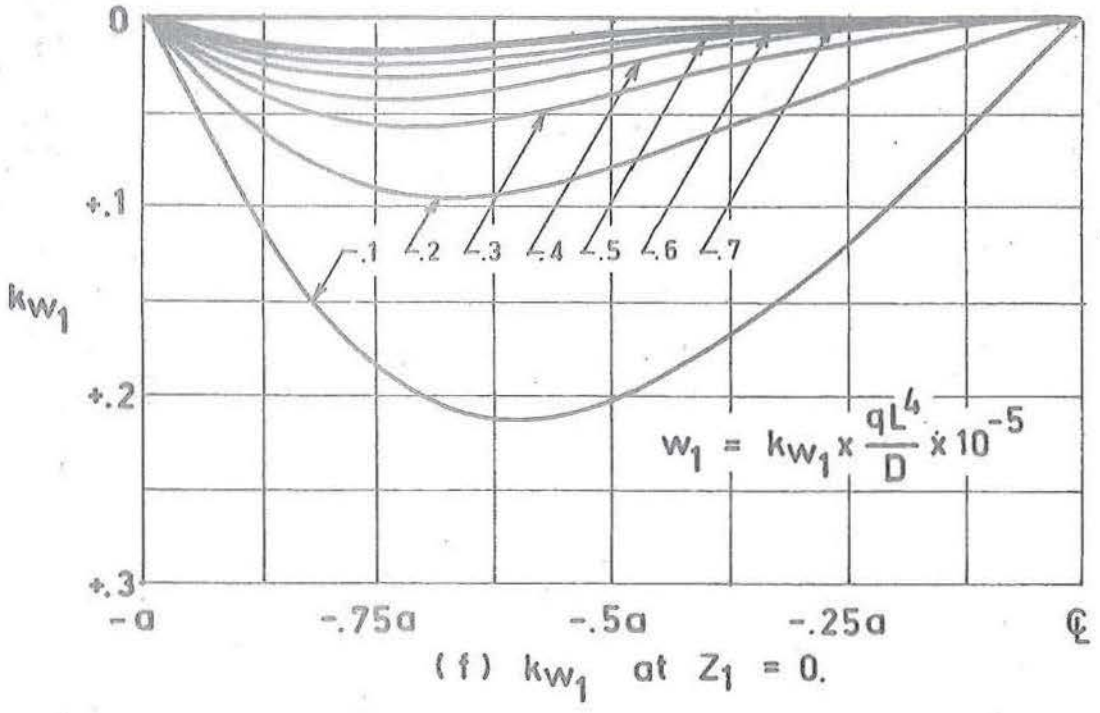

(f) k_{w_1} at $Z_1 = 0$.

Fig. 9.1 (continued) Ruled surface hyperbolic paraboloid with all edges clamped. Influence of λ_1, where $\lambda_2 = .0165$, $\mu = .00$, and $m = 8$.

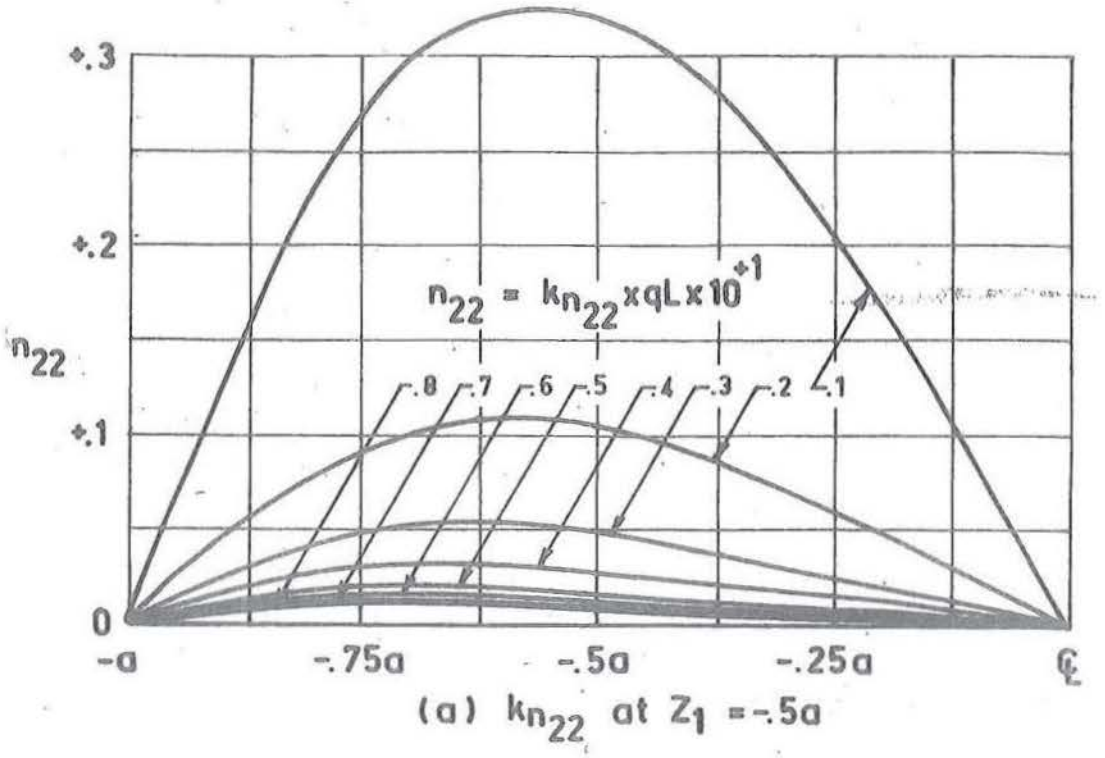

(a) $k_{n_{22}}$ at $Z_1 = -.5a$

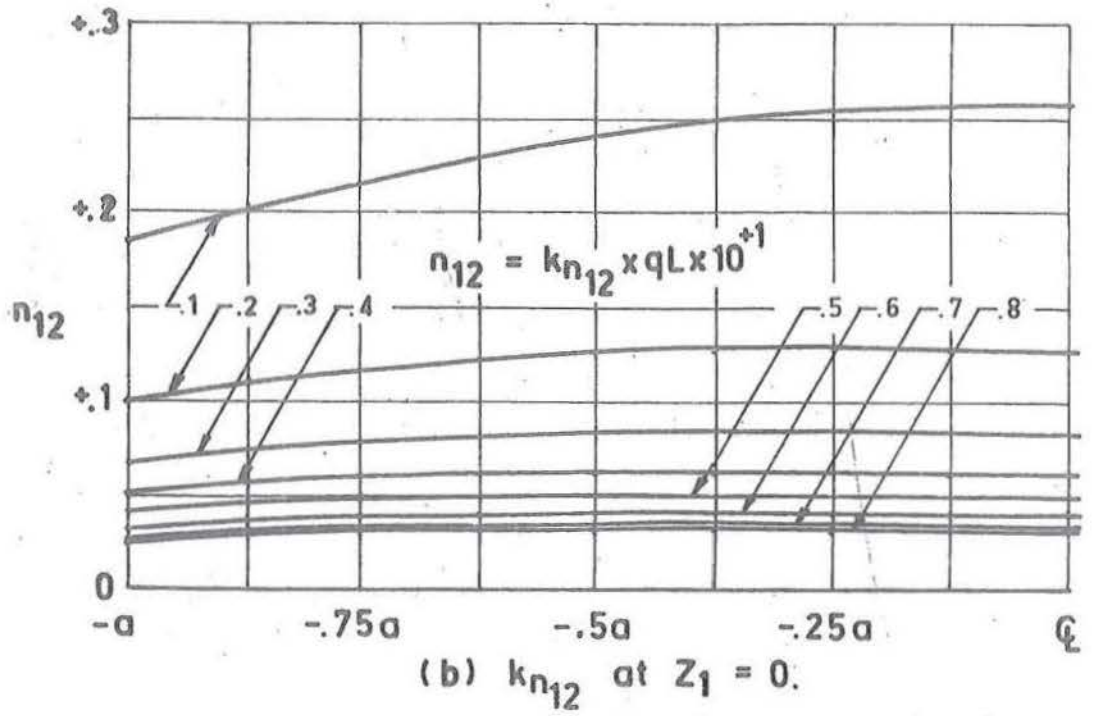

(b) $k_{n_{12}}$ at $Z_1 = 0.$

ig. 9.2 Ruled surface hyperbolic paraboloid with all edges simply supported. Influence of λ_1, where $\lambda_2 = .0165$, $\mu = .00$, and $m = 8$.

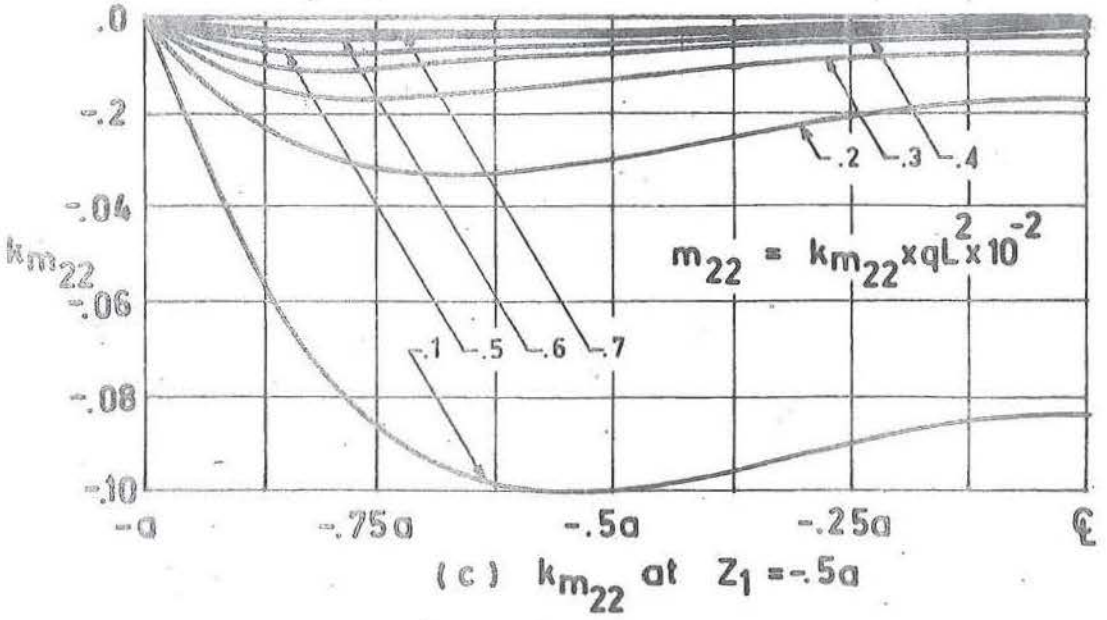

(c) km_{22} at $Z_1 = -.5a$

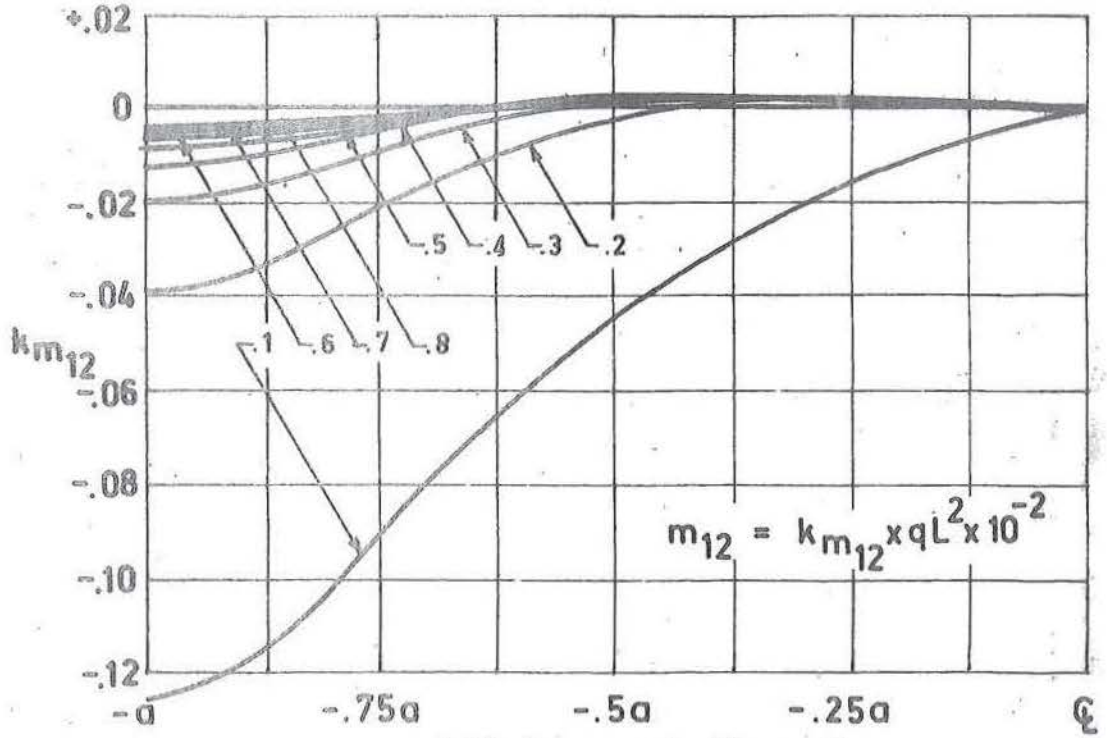

(d) km_{12} at $Z_1 = -.5a$

Fig. 9.2 (continued) Ruled surface hyperbolic paraboloid with all edges simply supported. Influence of λ_1, where $\lambda_2 = .0165$, $\mu = .00$, and $m = 8$.

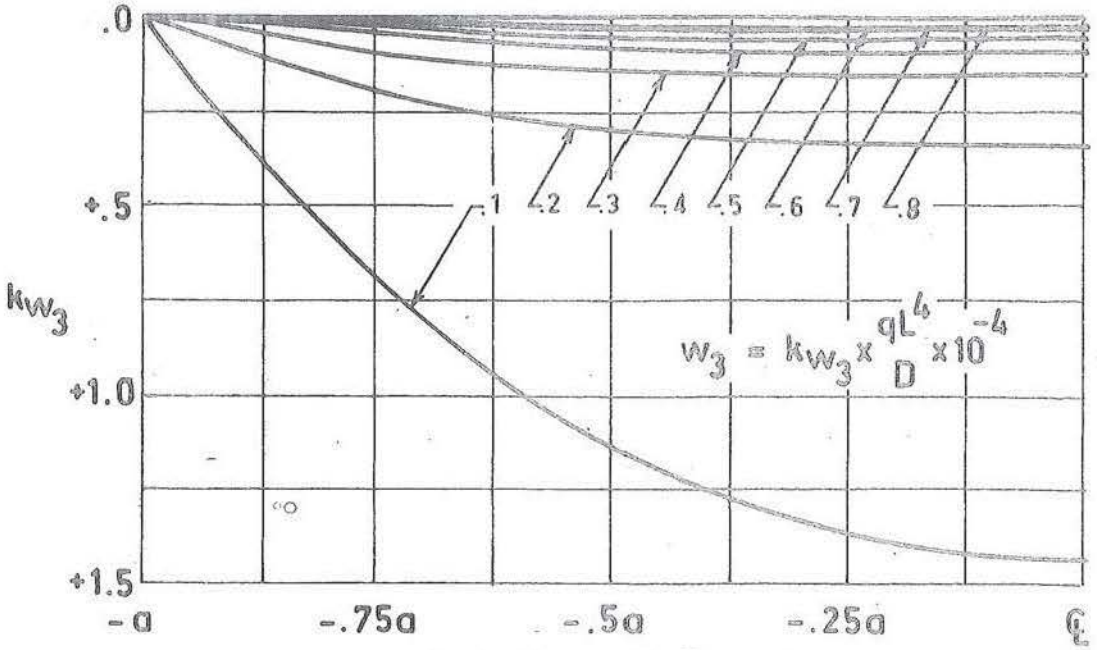

(e) k_{w_3} at $Z_1 = 0$.

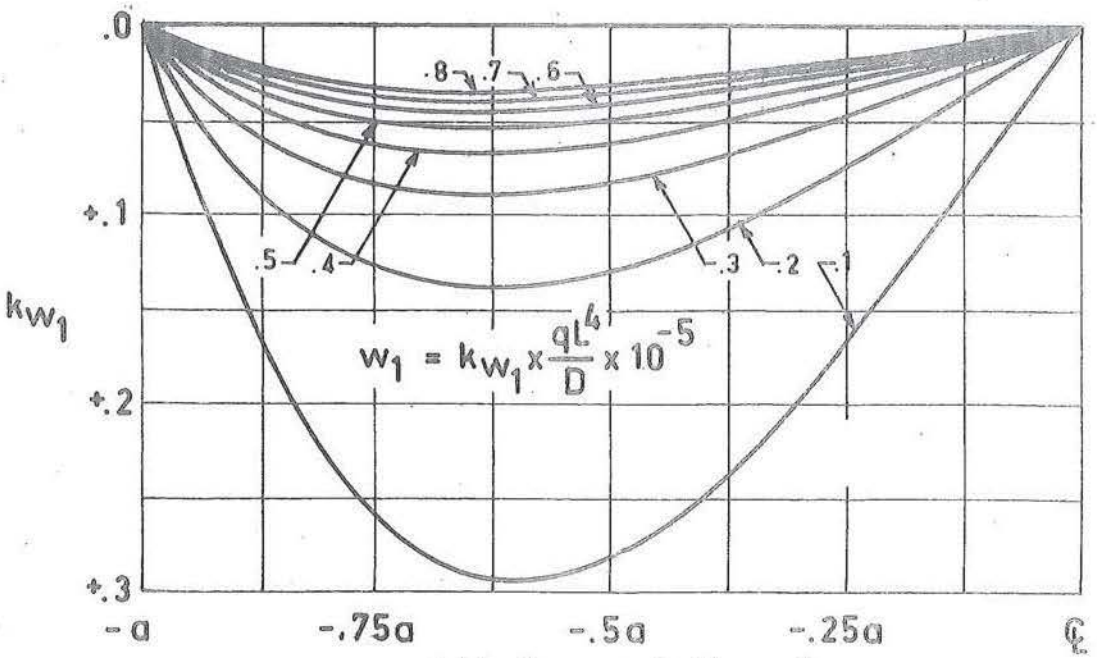

(f) k_{w_1} at $Z_1 = 0$.

Fig. 9.2 (continued) Ruled surface hyperbolic paraboloid with all edges simply supported. Influence of λ_1, where $\lambda_2 = .0165$, $\mu = .00$ and $m = 8$.

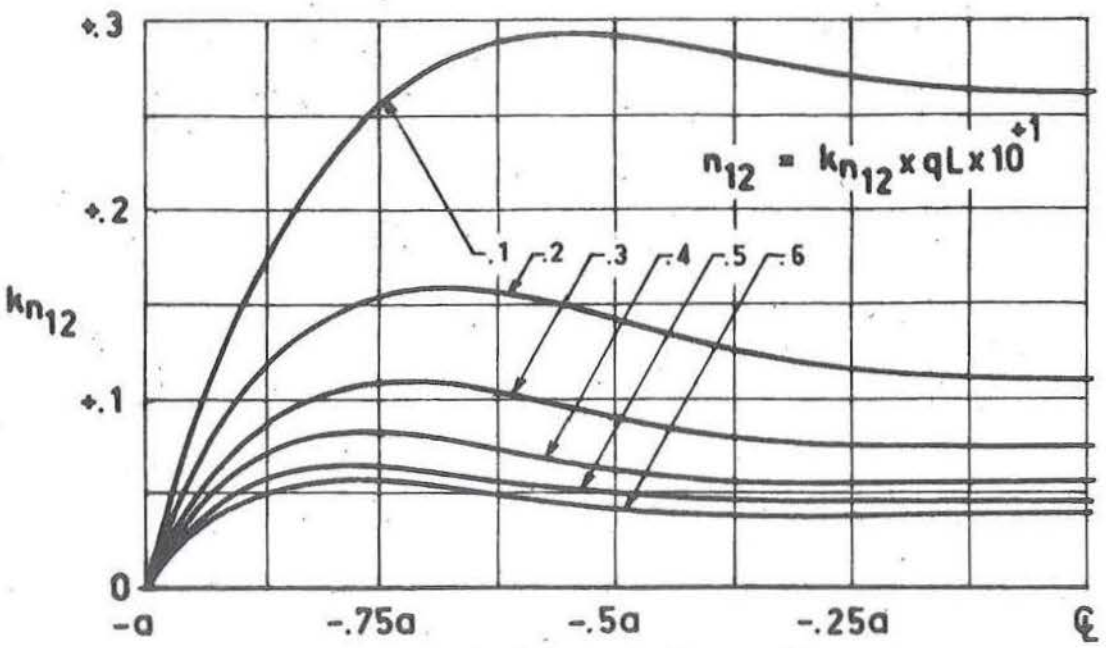

(a) kn_{12} at $Z_1 = -.5a$

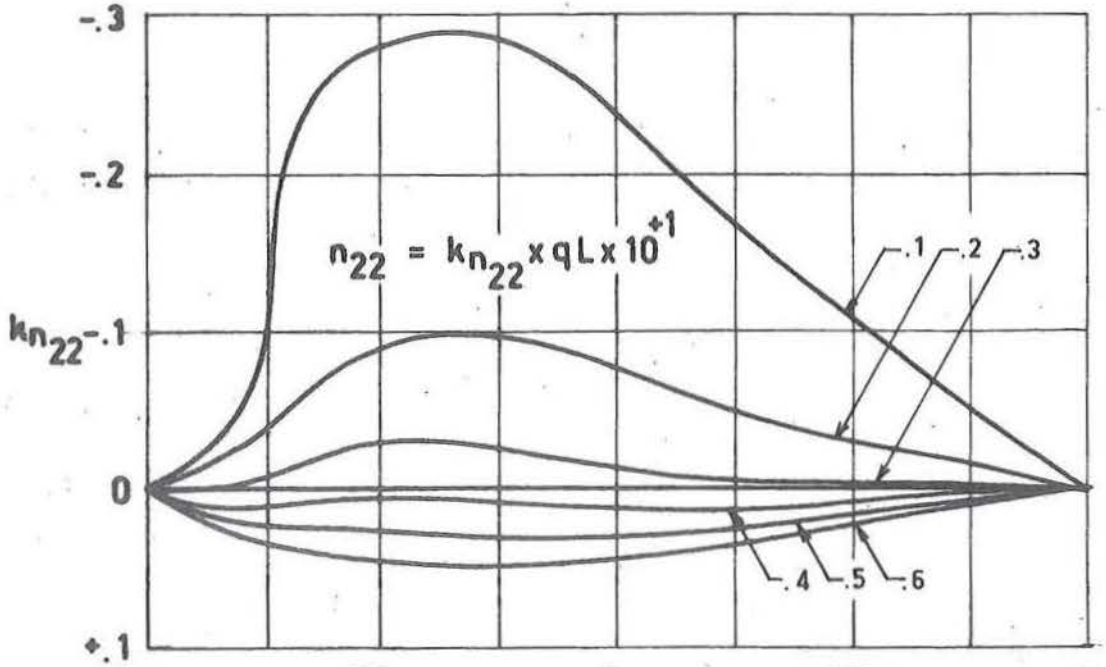

(b) kn_{22} at $Z_1 = -.75a$

Fig. 9.3 Ruled surface hyperbolic paraboloid with edges free and corners clamped. Influence of λ_1, where $\lambda_2 = .0165$ $\mu = .00$ and $m = 8$.

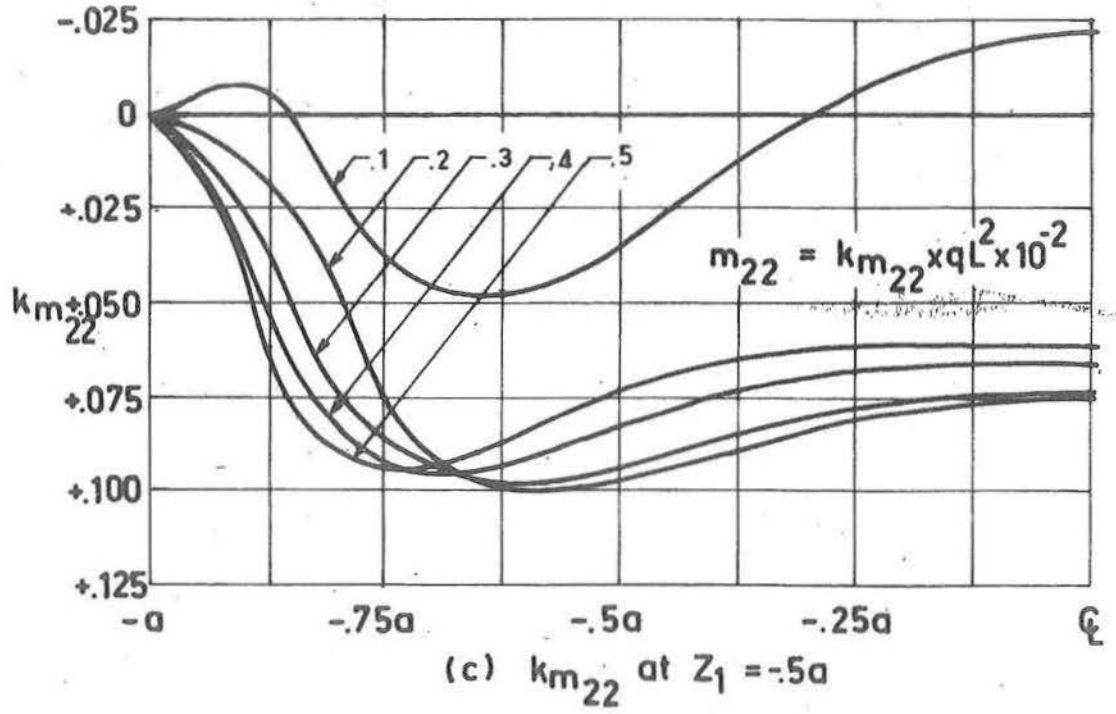

(c) km_{22} at $Z_1 = -.5a$

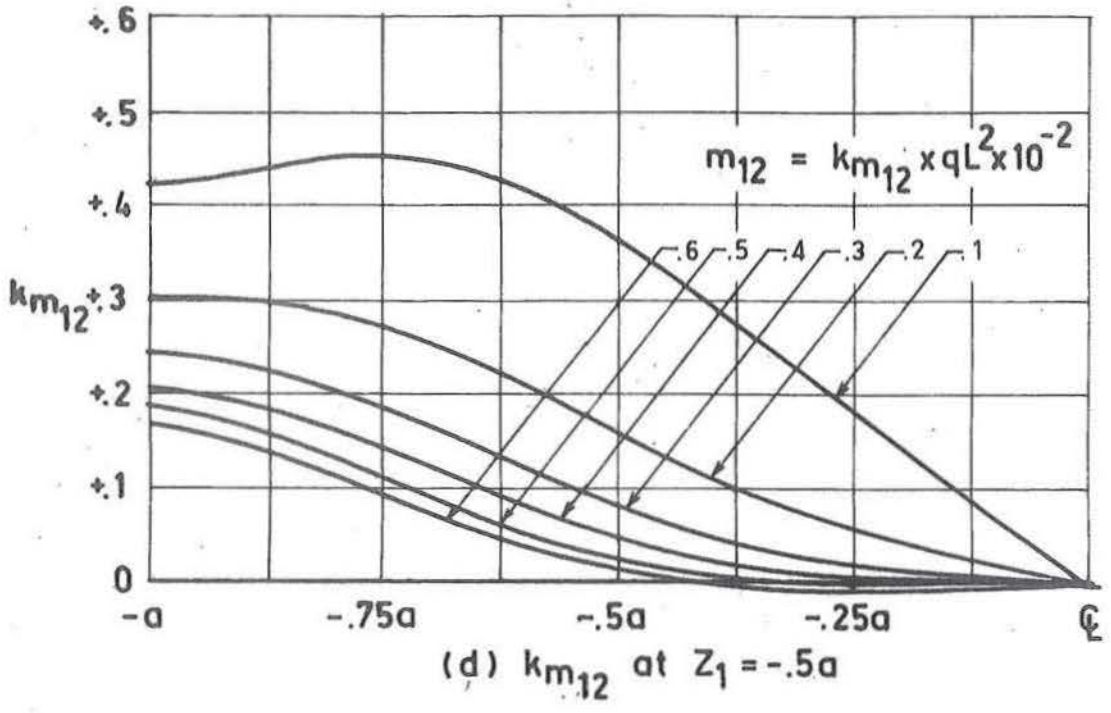

(d) km_{12} at $Z_1 = -.5a$

Fig. 9.3 (continued) Ruled surface hyperbolic paraboloid with edges free and corners clamped. Influence of λ_1, where $\lambda_2 = .0165$, $\mu = .00$ and $m = 8$.

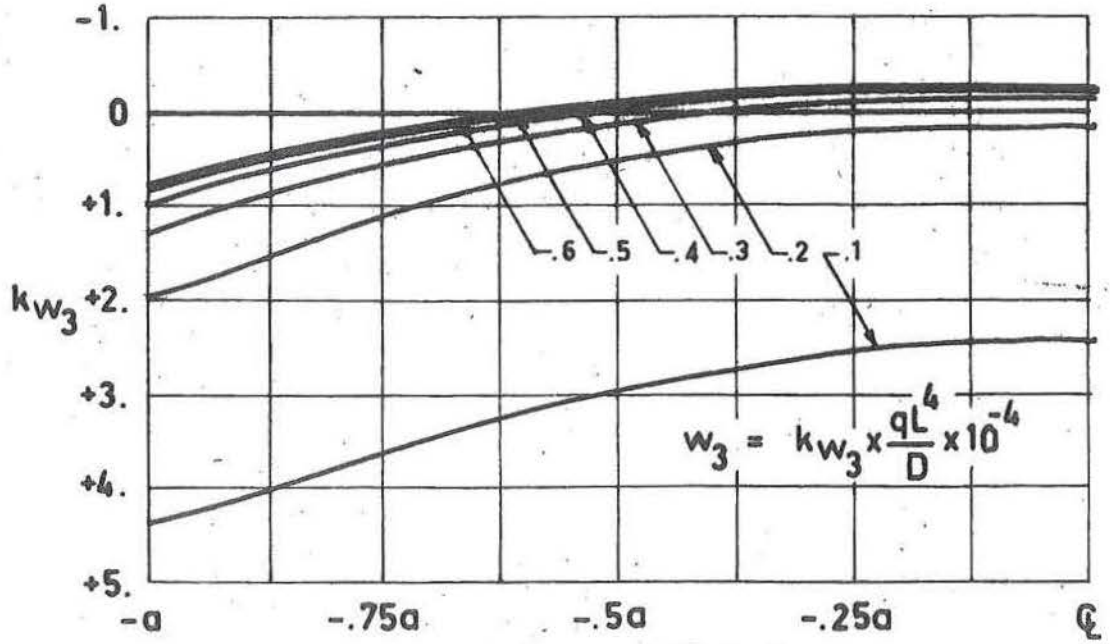

(e) k_{w_3} at $Z_1 = 0$.

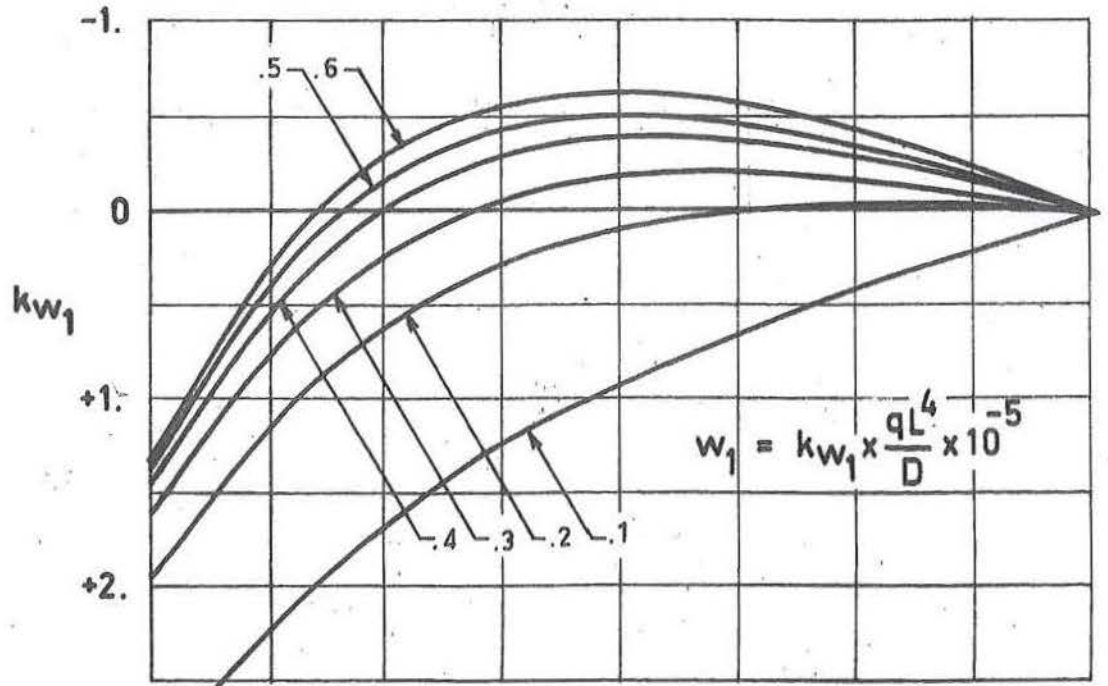

(f) k_{w_1} at $Z_1 = 0$.

Fig. 9.3 (continued) Ruled surface hyperbolic paraboloid with edges free and corners clamped. Influence of λ_1.

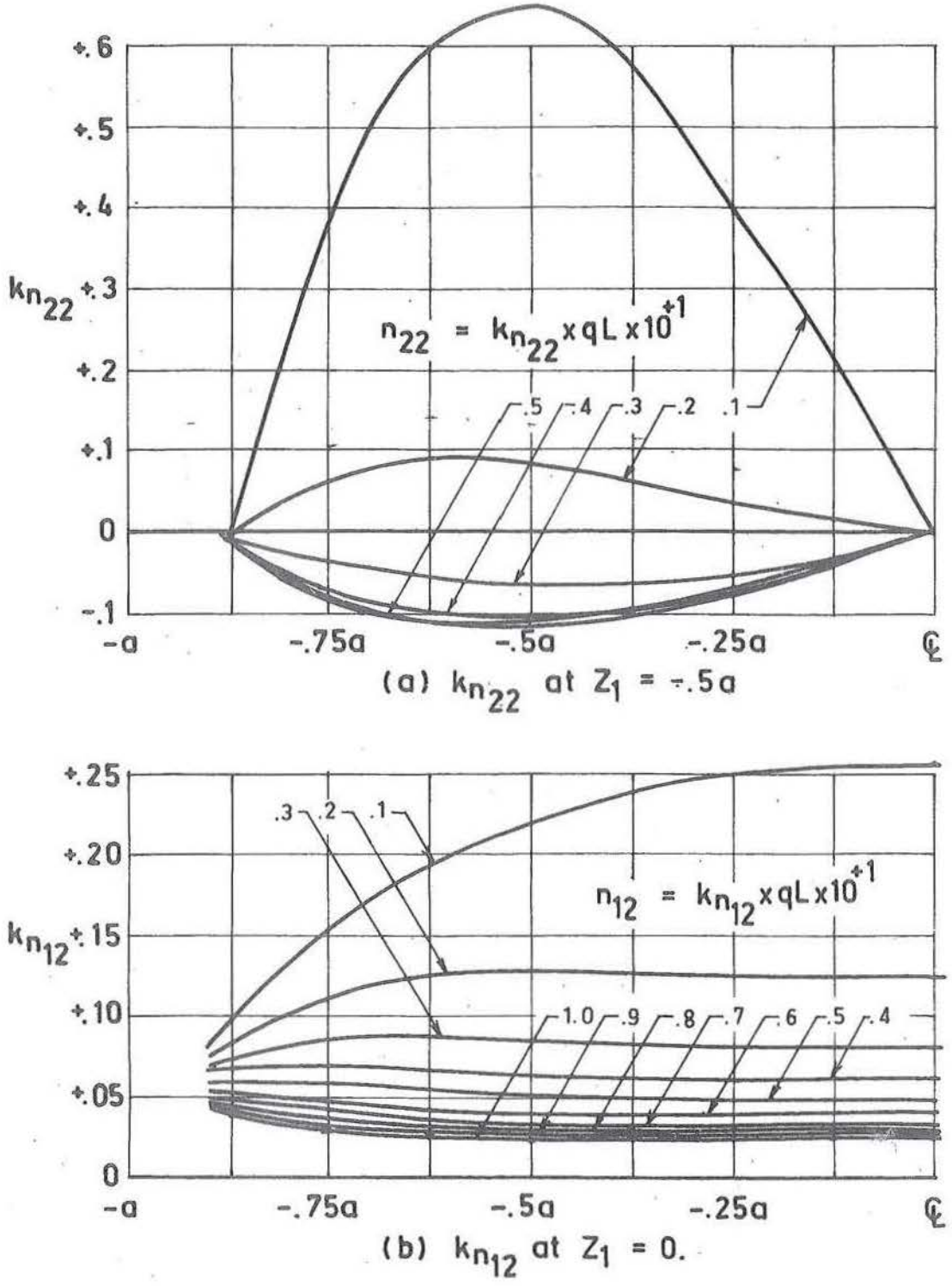

Fig. 9.4 Ruled surface hyperbolic paraboloid with edge beams clamped at corners. Influence of λ_1, where $\lambda_2 = .0165$, $\lambda_3 = 4.5$, $\lambda_4 = .05$, $\mu = .00$ and $m = 8$.

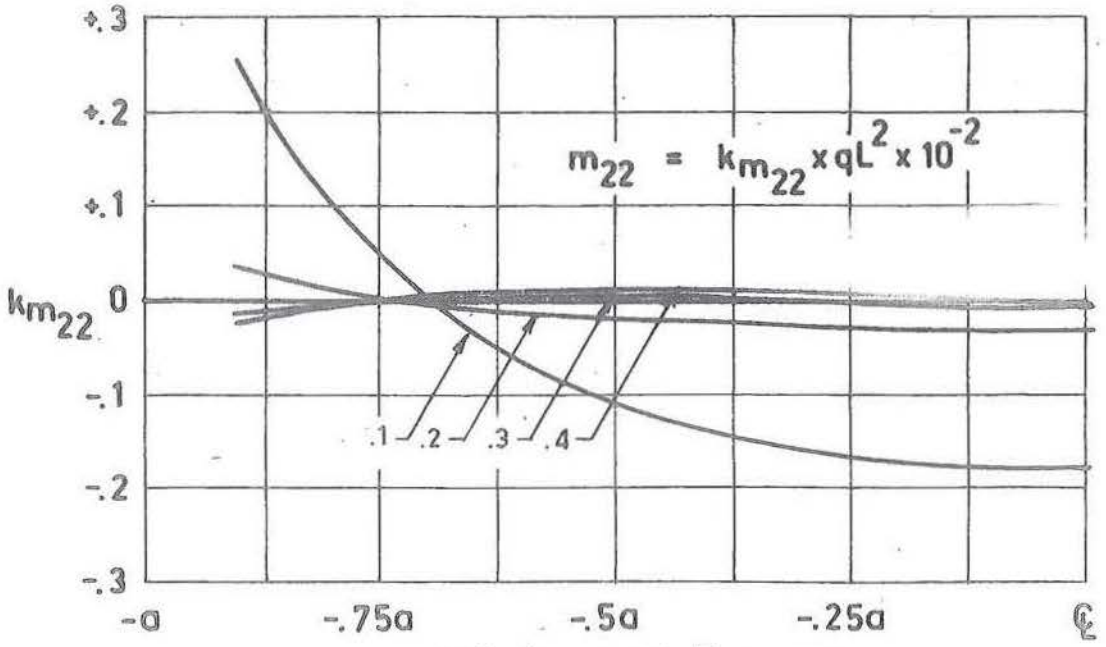

(c) $k_{m_{22}}$ at $Z_1 = -.5a$

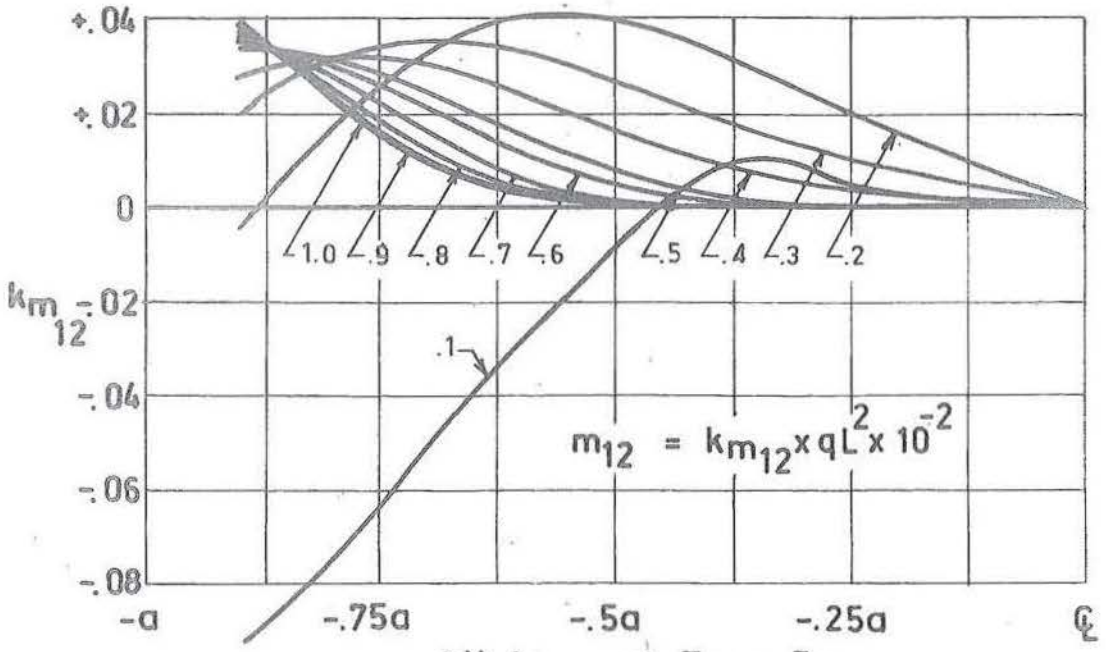

(d) $k_{m_{12}}$ at $Z_1 = -.5a$

Fig. 9.4 (continued) Ruled surface hyperbolic paraboloid with edge beams clamped at corners. Influence of λ_1.

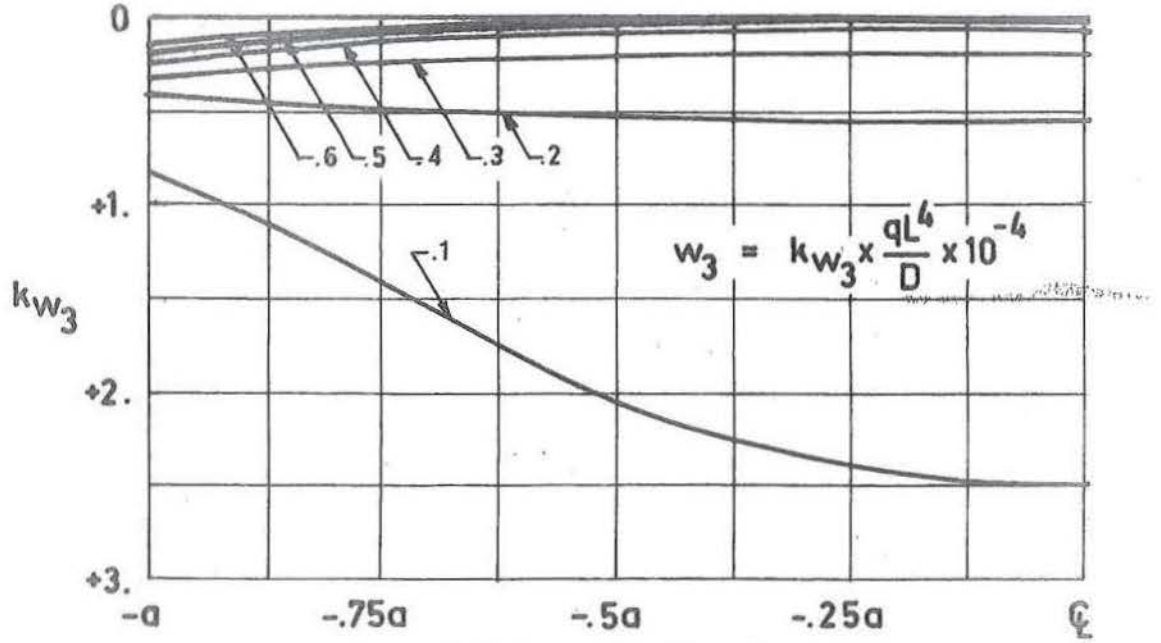

(e) k_{w_3} at $Z_1 = 0.$

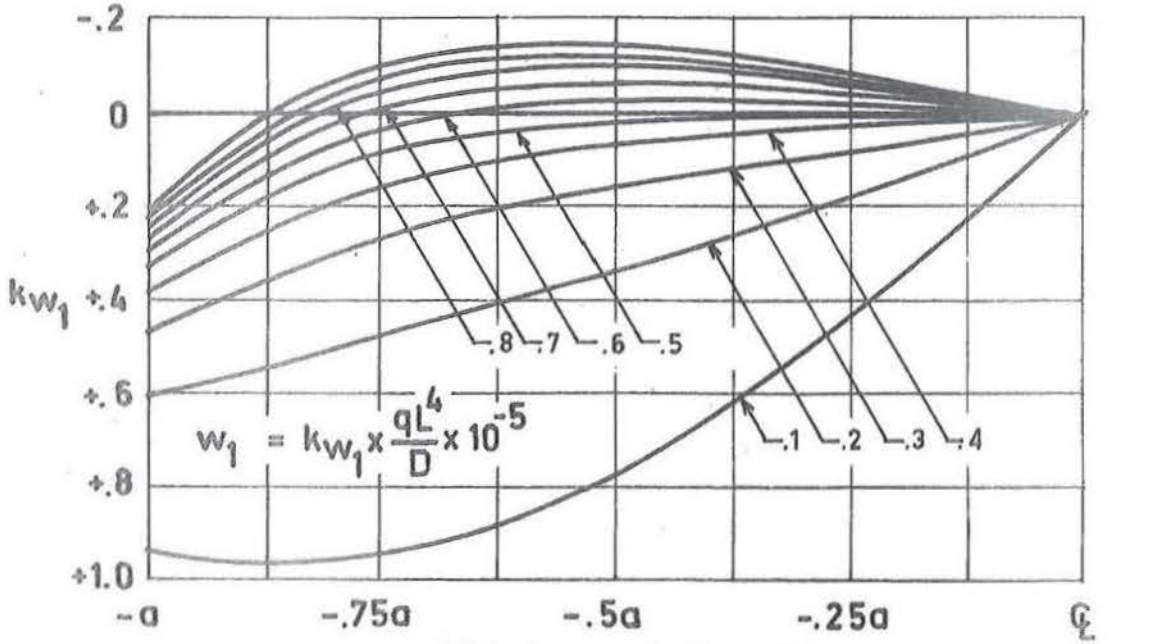

(f) k_{w_1} at $Z_1 = 0.$

Fig. 9.4 (continued) Ruled surface hyperbolic paraboloid with edge beams and corners clamped. Influence of λ_1.

determine what errors, in the estimation of curvatures and stress resultants in terms of displacement components, are likely to occur for $\lambda_1 > 0.3$, and programmes written to include a number of these effects. Because large changes in shell geometry at these values of λ_1 cause small changes in overall shell behaviour, it is likely that the influence of small non-shallow correction terms will be second order.

For a given boundary type, the general shape of the stress, moment and displacement profiles are essentially constant for all values of λ_1, with only the magnitude changing. This is especially so in the well behaved displacement or clamped boundary, where these magnitudes are seen to change in approximately the same ratio as the in-plane shear stress $k_{n_{12}}$. Because the value of the in-plane shear stress may be closely approximated (at the shell centre) by the membrane solutions, it is not unreasonable to assume that, given one bending solution, it is possible to predict the approximate value of the solution for any other value of λ_1. This behaviour can be observed by comparing the ratios of maximum stress and moment resultants of the clamped shell with those of membrane shear for successive values of λ_1.

9.2 INFLUENCE OF λ_2

Only the results of the pure traction or free edged boundary are given, as similar trends were observed

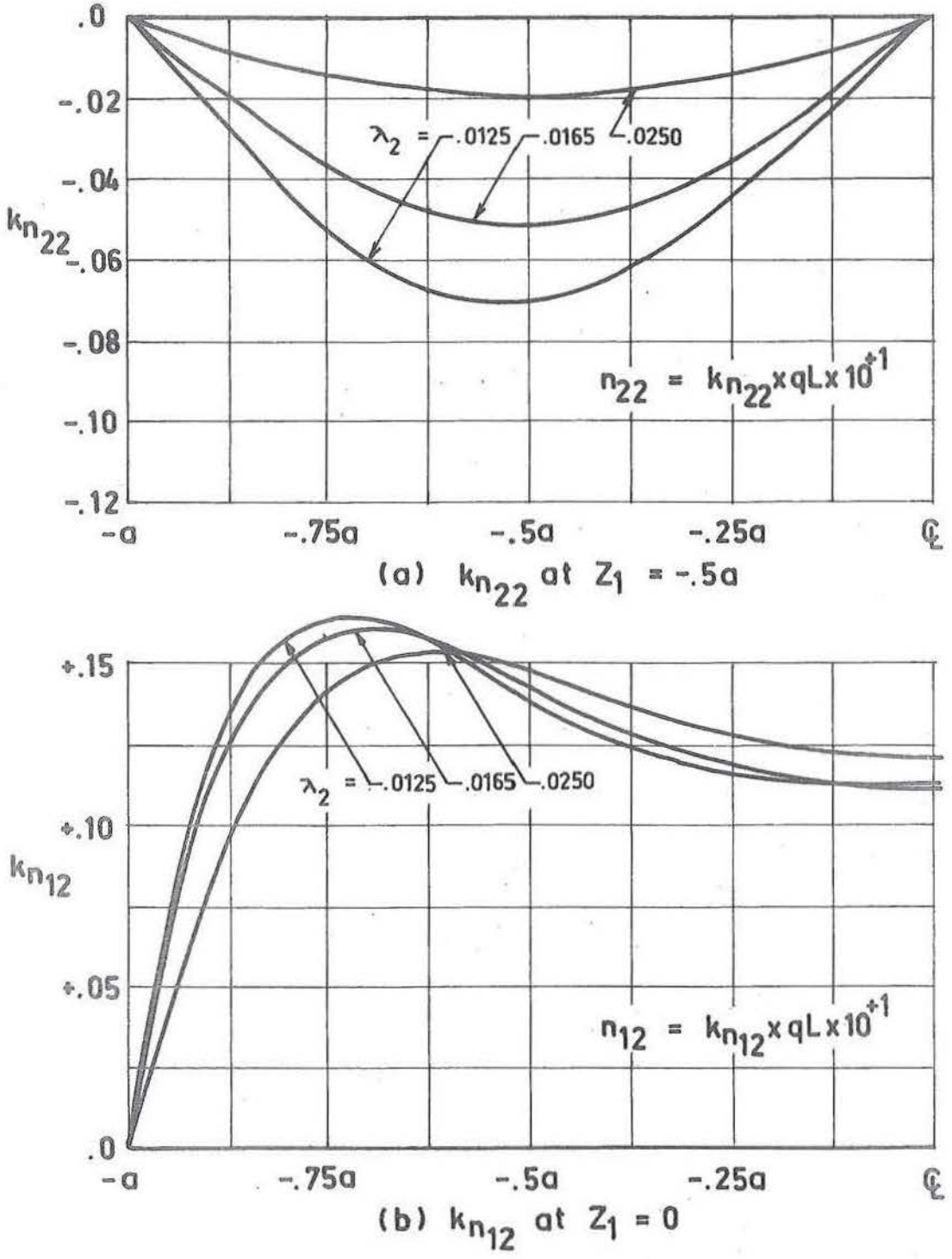

Fig. 9.5 Ruled surface hyperbolic paraboloid with edges free and corners clamped. Influence of λ_2, where $\lambda_1 = .2$, $\nu = .00$ and $m = 8$.

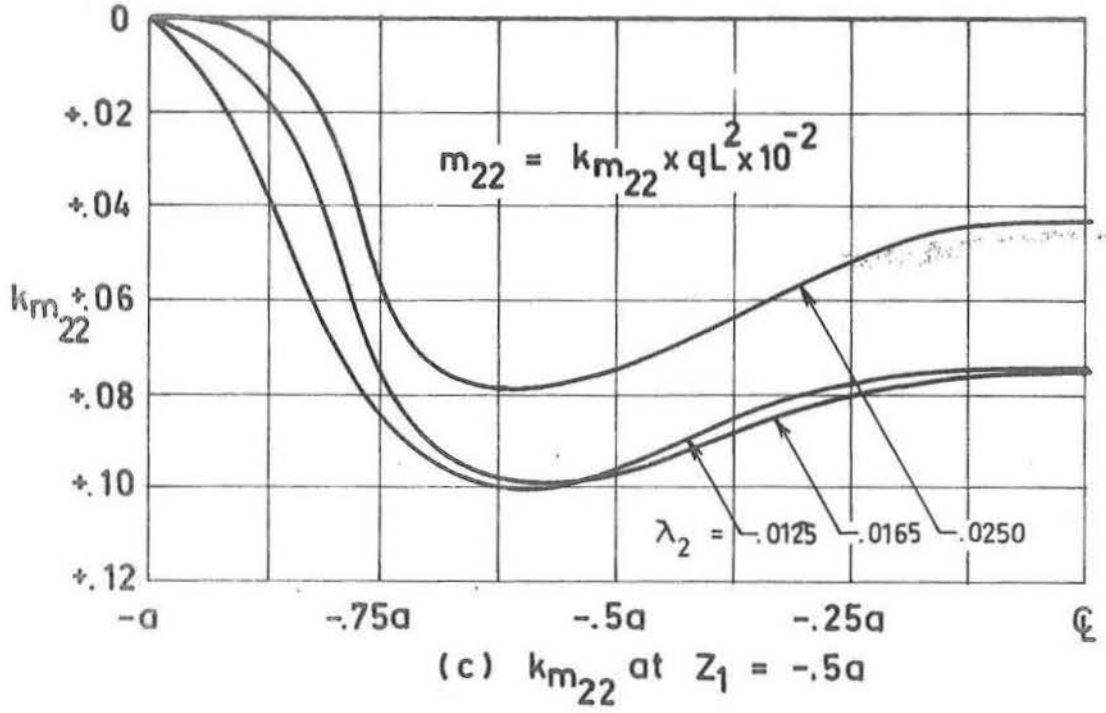

(c) km_{22} at $Z_1 = -.5a$

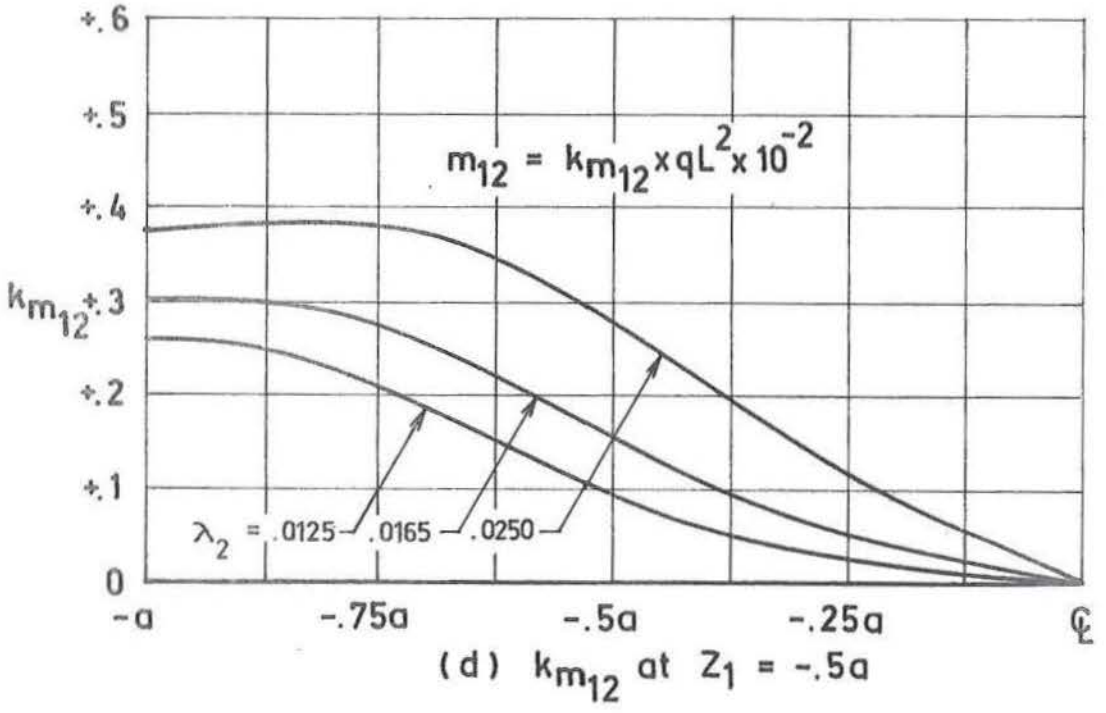

(d) km_{12} at $Z_1 = -.5a$

Fig. 9.5 (continued) Ruled surface hyperbolic paraboloid with edges free and corners clamped. Influence of λ_2, where $\lambda_1 = .2$, $\mu = .00$ and $m = 8$.

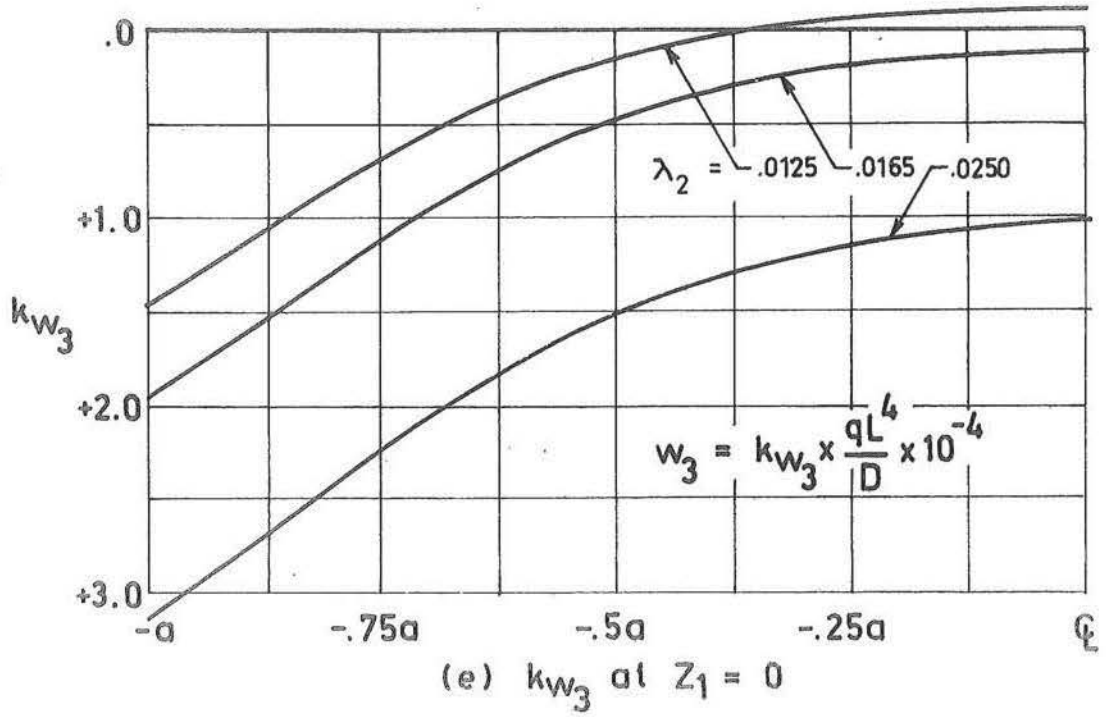

(e) k_{w_3} at $Z_1 = 0$

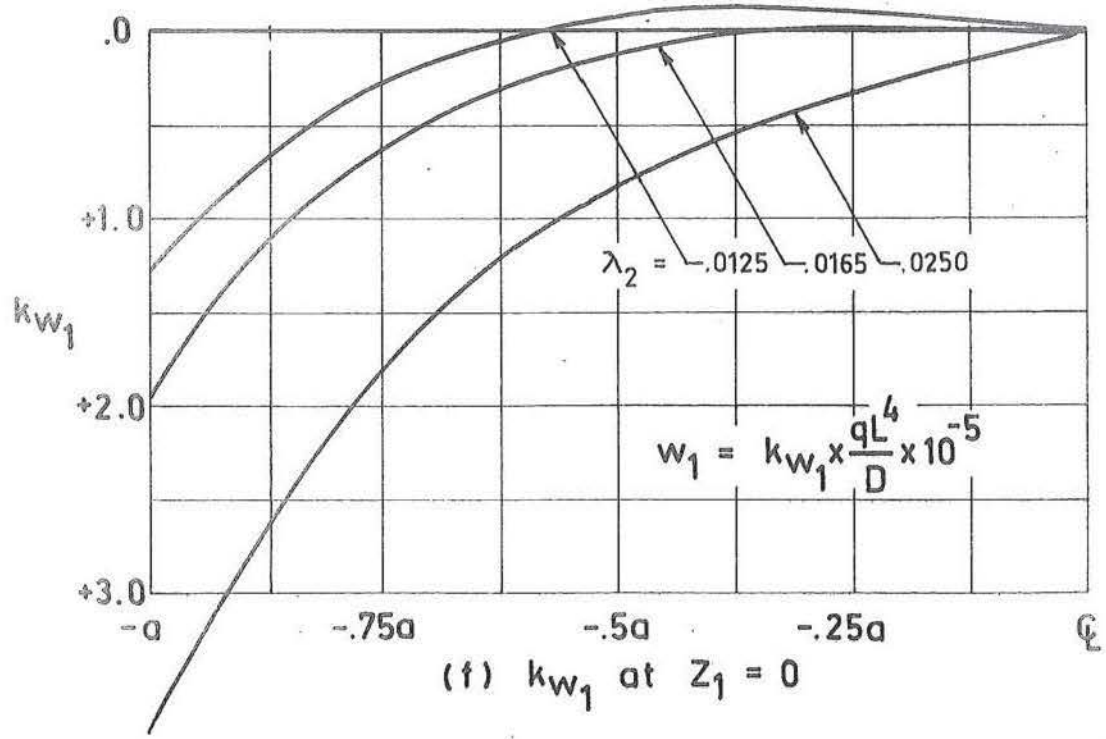

(f) k_{w_1} at $Z_1 = 0$

Fig. 9.5 (continued) Ruled surface hyperbolic paraboloid with edges free and corners clamped. Influence of λ_2, where $\lambda_1 = .2$, $\mu = .00$ and $m = 8$.

in the results from other boundary types. Figure 9.5(a) to (f) shows the results for λ_2 = 0.0125, 0.0165, 0.0250. In-plane stress resultants are observed to considerably decrease as the ratio λ_2 increases, while the bending moments are seen to increase. It is clear that the plate bending action predominates over membrane action as the thickness relative to the span increases. Remembering that surface stresses are inversely proportional to shell thickness for direct stresses and shell thickness squared for bending stresses, it is noted that direct surface stresses are considerably decreased for increase in λ_2, while moment surface stresses may at some positions increase. This implies that if surface stresses due to direct stresses are critical, an increase in overall shell thickness is likely to be beneficial, while if bending is critical this in general will not be the case.

Displacement coefficients are given in terms of plate stiffnesses, which vary from shell to shell. To obtain direct comparisons of absolute displacements the values given in figures (e) and (f) for the ratios λ_2 = 0.0125 and 0.0250 should be multiplied by 2.300 and 0.288 respectively. All results then refer to the plate stiffness of the shell with λ_2 = 0.0165. Although k_{w_k}, (k = 1,2,3) increases the absolute values of w_k, (k = 1,2,3) in general decrease. The decrease being more pronounced in the in-plane displacements w_k, (k = 1,2).

9.3 INFLUENCE OF ν

The free edged results for ν = 0.00, 0.15, 0.30 are presented as typifying the trends found for shells of all boundary types. These results are shown in figure 9.6(a) to (f).

In-plane stress resultants are reduced as ν increases, while bending moment resultants are considerably increased. Although this observation is of little significance in design (it being difficult to vary ν in order to produce a required result) it does indicate the importance of including the effects of ν in a design analysis. For example, neglect of ν for the present shell is seen to underestimate bending surface stresses at (-.875a, -.875a) by 100%, while at (0, -.875a) these are underestimated by 24% for a shell with ν = 0.30.

Displacement coefficients are presented and if the absolute displacements are required the value given in figure 9.6(e) and (f) for the Poisson's ratio ν = 0.15 and 0.30 should be multiplied by 0.978 and 0.910 respectively. Even so, neglect of ν is seen to underestimate by 25% the vertical displacements at (0, - a).

9.4 CONCLUSIONS

The extreme deviations of shell behaviour from that of the flat plate, and therefore the increase in load carrying

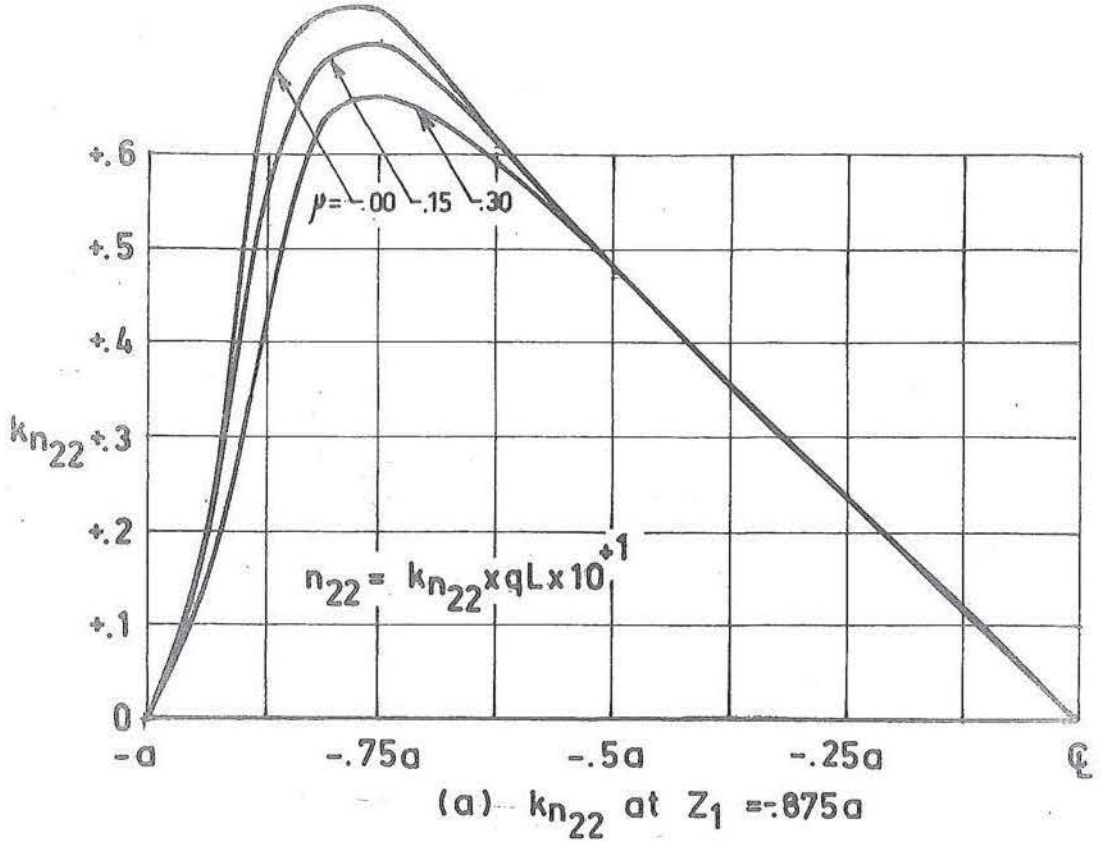

(a) $k_{n_{22}}$ at Z_1 = .875a

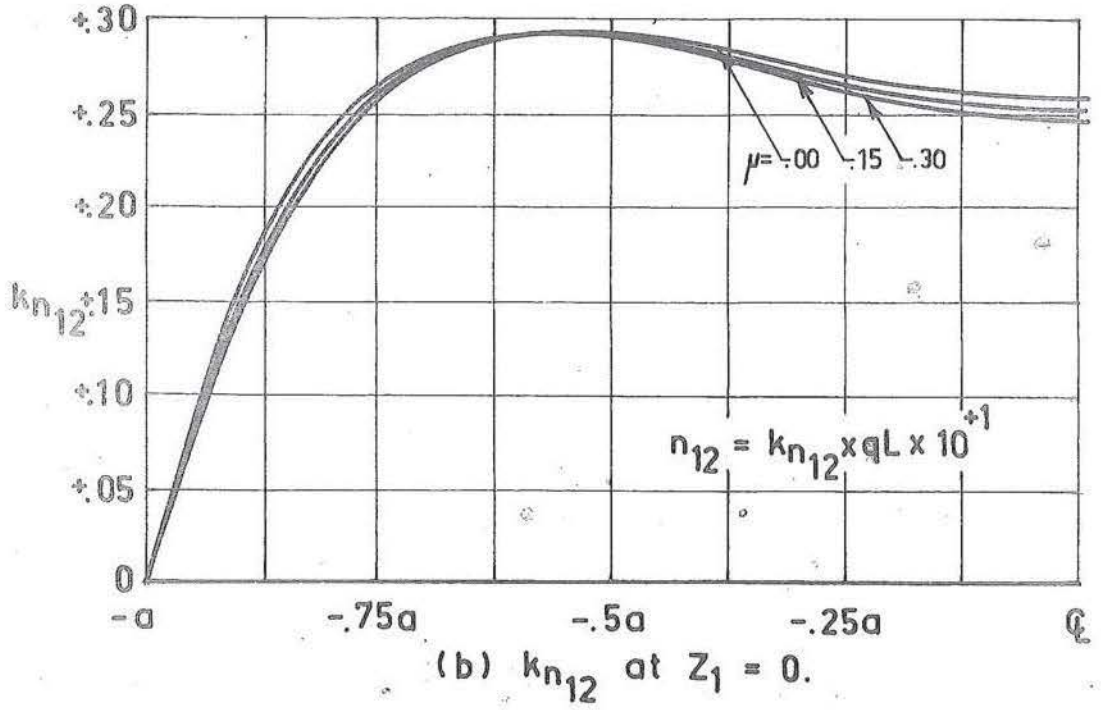

(b) $k_{n_{12}}$ at Z_1 = 0.

Fig. 9.6 Ruled surface hyperbolic paraboloid with all edges free and corners clamped. Influence of μ, where λ_1 = .1, λ_2 = .0165 and m = 8.

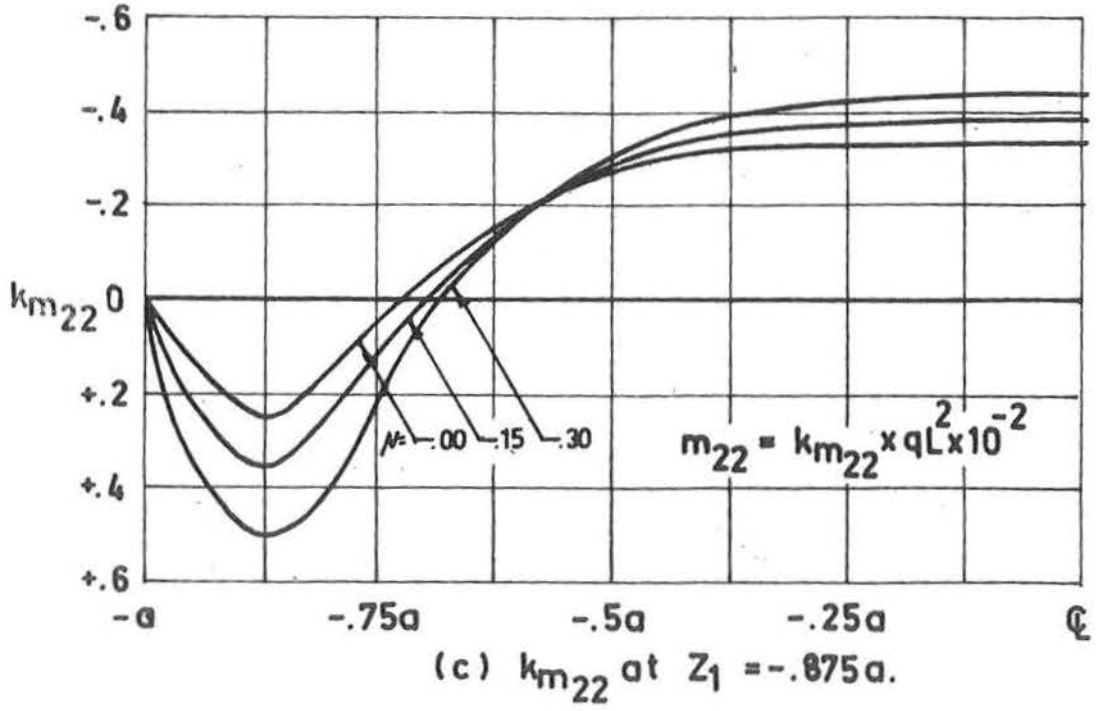

(c) km_{22} at $Z_1 = -.875a$.

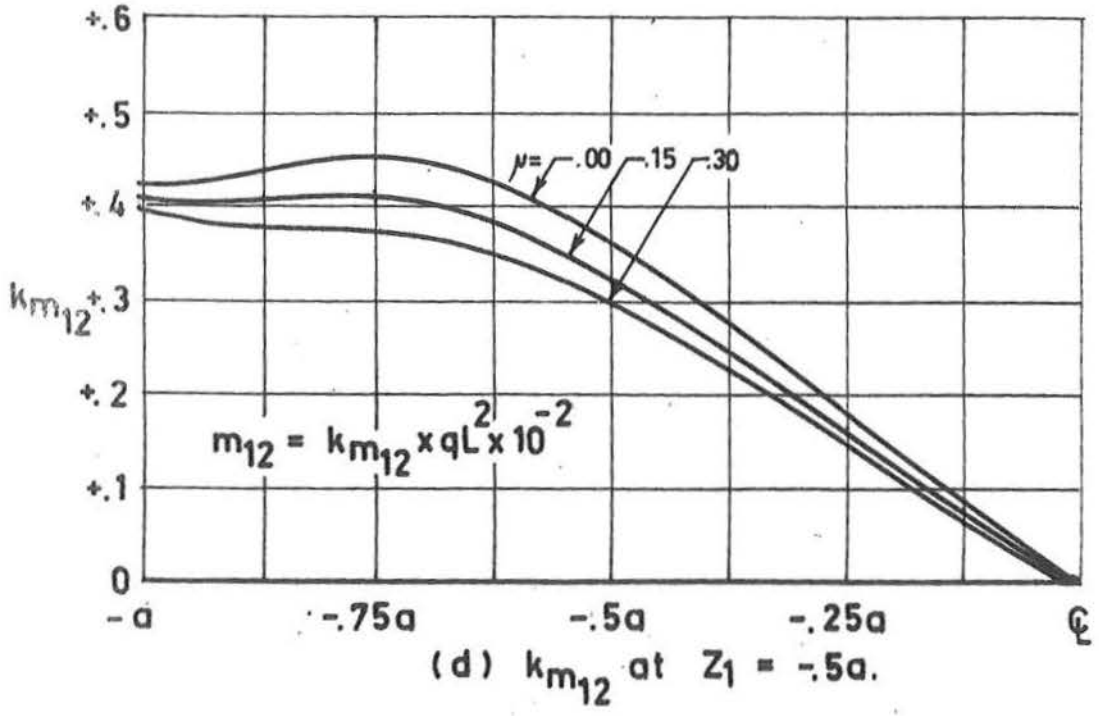

(d) km_{12} at $Z_1 = -.5a$.

Fig. 9.6 (continued) Ruled surface hyperbolic paraboloid with all edges free and corners clamped. Influence of μ, where $\lambda_1 = .1$, $\lambda_2 = .0165$ and $m = 8$.

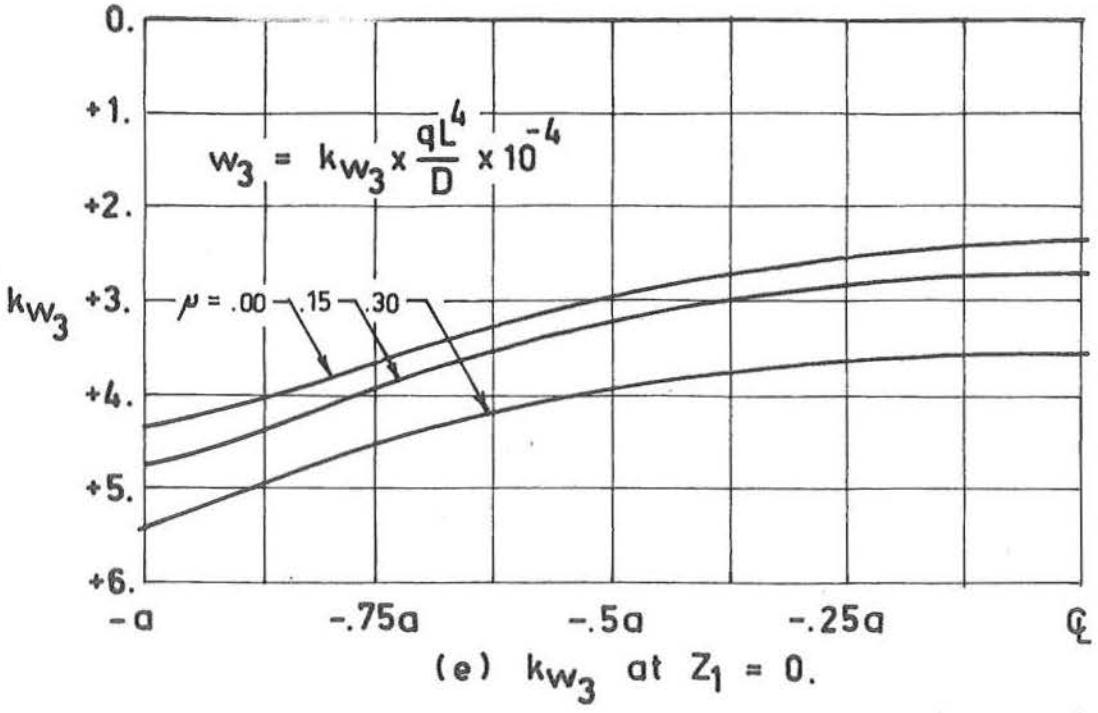

(e) k_{w_3} at $Z_1 = 0.$

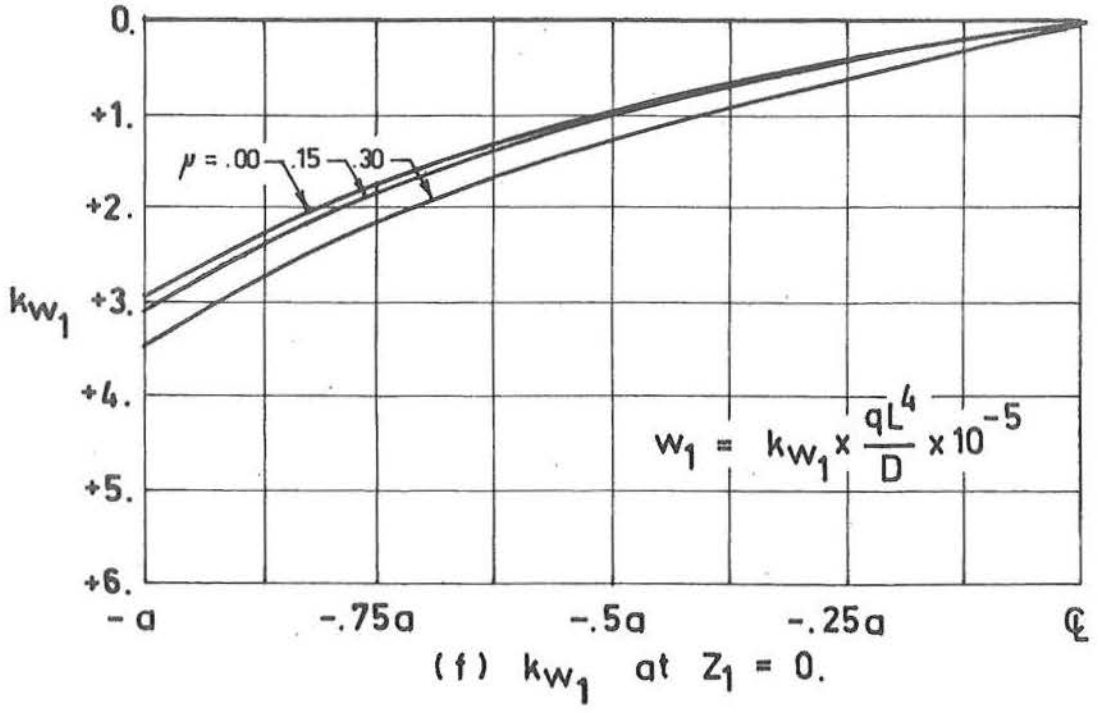

(f) k_{w_1} at $Z_1 = 0.$

Fig. 9.6 (continued) Ruled surface hyperbolic paraboloid with all edges free and corners clamped. Influence of μ, where $\lambda_1 = .1$, $\lambda_2 = .0165$ and $m = 8$.

efficiency, is apparent. This increase in efficiency is likely to be somewhat offset in shells of high λ_1 by the increasing constructional difficulties and therefore rising cost.

Neglecting the extreme influence of shape factors for $\lambda_1 < 0.1$ it is seen on comparing the results of this chapter with those of chapter 8, that the overall influences of boundary and corner support conditions are likely to be of greater significance than those resulting from geometry and material property changes. It is also noted that changes in Poisson's ratio do not seriously affect the stress and moment resultants but do have a marked influence upon displacements.

CHAPTER TEN

EQUILIBRIUM CHECKS AND COMPARISONS

The solution method developed in chapter 6 was applied in chapters 7 to 9 to a large variety of shell problems with varied geometric and support conditions. Although convergence for these solutions is shown in chapter 7, there has hitherto been no indication as to whether the solutions are correct. It should be noted that convergence alone is sufficient to verify the uniqueness of solutions only, and does not provide information upon whether the solutions obtained are those of the initial differential system.

This chapter, for the same examples considered in sections 7.2 and 8.2 to 8.3, checks to ensure that equilibrium in the z_k coordinate directions is satisfied. As a further check, the clamped and simple support programmes were used to solve the same shell problems considered by Chetty and Tottenham[13].

10.1 EQUILIBRIUM CHECKS

In this section, both vertical and horizontal equilibrium checks are developed in a form suitable for application to each of the boundary cases considered in sections 8.2 and 8.3. In addition to verifying the solutions obtained, the results are seen to provide valuable information concerning the relative load carrying contributions of each of the internal stress

resultants.

10.1.1 Method for Equilibrium Checks

The shell shown in figure 4.1, is cut so that a square is removed with $(z_1, z_2) = (\pm \gamma a, \pm \gamma a)$ as corners. Figure 10.1 shows the membrane and bending stress resultants acting upon one quarter of this symmetric region.

From the conditions of symmetry, outlined in section 8.2,

$$\begin{aligned} k_{n_{11}} &= k_{q_{11}} = 0, \quad \text{at } z_1 = 0 \\ k_{n_{22}} &= k_{q_{22}} = 0, \quad \text{at } z_2 = 0. \end{aligned} \tag{10.1}$$

If the value of i (the grid row notation) at the position $z_2 = -\gamma a$ is denoted by r, the value of j (the grid column notation) at $z_1 = -\gamma a$ is also given by r, then provided γa is an integral value of h (the grid spacing), r is given by

$$r = (1 - \gamma)\ m + 1. \tag{10.2}$$

The summation of vertical components of stress resultants around the perimeter of the region shown in figure 10.1 is denoted by V_{1_r}, and the individual components of V_{1_r} resulting from $(k_{n_{kk}}, k_{n_{kl}}, k_{q_{kk}})$, $(k,l = 1,2, k \neq l)$ by V_{2_r}, V_{3_r} and V_{4_r} respectively. Hence,

$$V_{1_r} = V_{2_r} + V_{3_r} + V_{4_r}. \tag{10.3}$$

The applied vertical loading over this same square is given by V_{0_r}, where

$$V_{0_r} = \frac{\gamma^2}{4} \cdot qL^2 . \qquad (10.4)$$

In a similar manner H_{1_r} represents the summation of all horizontal stress resultants along the lines $z_1 = -\gamma a$ and $z_2 = -\gamma a$, in the z_1 coordinate direction, with H_{2_r}, H_{3_r} and H_{4_r} denoting the individual components arising from each of $(k_{n_{kk}}, k_{n_{kl}}, k_{q_{kk}})$, $(k, l = 1,2,\ k \neq 1)$ respectively. Hence

$$H_{1_r} = H_{2_r} + H_{3_r} + H_{4_r} \qquad (10.5)$$

with H_{0_r} representing the summation of $k_{n_{21}}$ along the line $z_2 = 0$ in the z_1 coordinate direction.

If ϕ and θ represent the slope of the shell surface about the z_1 and z_2 coordinates, and are considered clockwise positive along these axes, then the values of (V_{k_r}, H_{k_r}), $(k = 2,3,4)$ are given by

$$V_{2_r} = -qL \cdot \int_0^{-\gamma a} k_{n_{22}} \cdot \sin\phi \cdot dz_1 + qL \cdot \int_0^{-\gamma a} k_{n_{11}} \cdot \sin\theta \cdot dz_2, \qquad (10.6)$$

$$V_{3_r} = +qL \cdot \int_0^{-\gamma a} k_{n_{12}} \cdot \sin\theta(\gamma a) \cdot dz_1 - qL \cdot \int_0^{-\gamma a} k_{n_{21}} \cdot \sin\phi(\gamma a) \cdot dz_2, \qquad (10.7)$$

$$V_{4_r} = -qL \cdot \int_0^{-\gamma a} k_{q_{22}} \cdot \cos\phi \cdot \cos\theta(\gamma a) \cdot dz_1 +$$

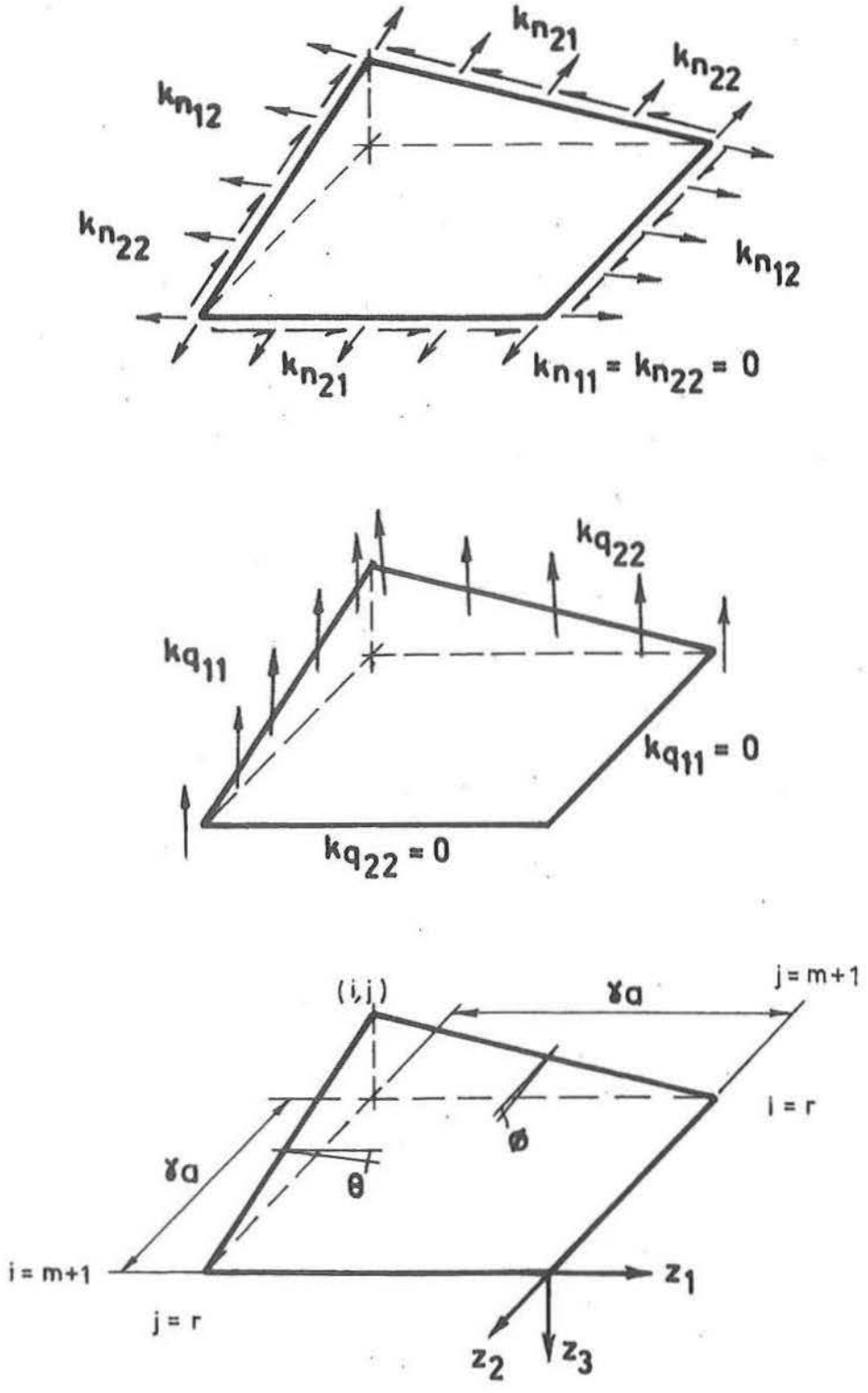

Fig. 10.1 Region of shell considered for equilibrium checks.

$$-qL.\int_{o}^{-\gamma a} kq_{11}.\cos\theta.\cos\phi(\gamma a).dz_2, \quad (10.8)$$

$$H_{2r} = -qL.\int_{o}^{-\gamma a} kn_{11}.\cos\theta.dz_2, \quad (10.9)$$

$$H_{3r} = -qL.\int_{o}^{-\gamma a} kn_{12}.\cos\theta(\gamma a).dz_1, \quad (10.10)$$

$$H_{4r} = -qL.\int_{o}^{-\gamma a} kq_{11}.\cos\phi(\gamma a).\sin\theta.dz_2 +$$

$$+ qL.\int_{o}^{-\gamma a} kq_{22}.\cos\phi.\sin\theta(\gamma a).dz_2, \quad (10.11)$$

where $\phi(\gamma a)$ and $\theta(\gamma a)$ are the values of ϕ and θ at the position $(-\gamma a, -\gamma a)$. The value of H_{O_r}, using the conditions of (10.1), is given by

$$H_{O_r} = + qL.\int_{o}^{-\gamma a} k_{n_{12}}.dz_1. \quad (10.12)$$

Using the symmetry properties of this region, conditions (10.6) to (10.11) may be written

$$V_{2r} = -2.qL.\int_{o}^{-\gamma a} kn_{22}.\sin\phi.dz_1, \quad (10.13)$$

$$V_{3r} = -2.qL.\int_{o}^{-\gamma a} kn_{12}.\sin\phi(\gamma a).dz_1, \quad (10.14)$$

$$V_{4_r} = -2 \cdot qL \cdot \int_0^{-\gamma a} kq_{zz} \cdot \cos\phi \cdot \cos\phi(\gamma a) \cdot dz_1 , \qquad (10.15)$$

$$H_{2_r} = -qL \cdot \int_0^{-\gamma a} k\eta_{zz} \cdot \cos\phi \cdot dz_1 , \qquad (10.16)$$

$$H_{3_r} = -qL \cdot \int_0^{-\gamma a} k\eta_{12} \cdot \cos\phi(\gamma a) \cdot dz_1 , \qquad (10.17)$$

$$H_{4_r} = +qL \cdot \int_0^{-\gamma a} kq_{zz} \cdot (\cos\phi(\gamma a) \cdot \sin\phi + \cos\phi \cdot \sin\phi(\gamma a)) \cdot dz_1 . \qquad (10.18)$$

Equations (10.13) to (10.18) are in terms of quantities defined in the region considered in preceding chapters, so that no additional information is necessary.

Using the first order numerical integration

$$\int_0^h f(z_1) \cdot dz_1 \doteq \frac{f(0) + f(h)}{4} \cdot \frac{L}{m} , \qquad (10.19)$$

the equations (10.13) to (10.18) above reduce to

$$V_{2_r} = k_{V_{2_r}} \cdot qL^2 , \qquad (10.20)$$

$$V_{3_r} = k_{V_{3_r}} \cdot qL^2 , \qquad (10.21)$$

$$V_{4_r} = k_{V_{4_r}} \cdot qL^2 , \qquad (10.22)$$

$$H_{2_r} = k_{H_{2_r}} \cdot qL^2, \tag{10.23}$$

$$H_{3_r} = k_{H_{3_r}} \cdot qL^2, \tag{10.24}$$

$$H_{4_r} = k_{H_{4_r}} \cdot qL^2, \tag{10.25}$$

where the dimensionless coefficients $(k_{V_{k_r}}, k_{H_{k_r}})$, $(k = 2,3,4)$ are given by

$$k_{V_{2_r}} \doteq -\frac{1}{2m} \cdot \left(\sum_{j=r}^{m} \left(k_{n^{22}_{rj}} \cdot \sin\phi_j + k_{n^{22}_{rj+1}} \cdot \sin\phi_{j+1} \right) \right), \tag{10.26}$$

$$k_{V_{3_r}} \doteq -\frac{1}{2m} \cdot \left(\sum_{j=r}^{m} \left(k_{n^{12}_{rj}} + k_{n^{12}_{rj+1}} \right) \right) \cdot \sin\phi_r, \tag{10.27}$$

$$k_{V_{4_r}} \doteq -\frac{1}{2m} \cdot \left(\sum_{j=r}^{m} \left(k_{q^{22}_{rj}} \cdot \sin\phi_j + k_{q^{22}_{rj+1}} \cdot \sin\phi_{j+1} \right) \right) \cdot \cos\phi_r, \tag{10.28}$$

$$k_{H_{2_r}} \doteq -\frac{1}{4m} \cdot \left(\sum_{j=r}^{m} \left(k_{n^{22}_{rj}} \cdot \cos\phi_j + k_{n^{22}_{rj+1}} \cdot \cos\phi_{j+1} \right) \right), \tag{10.29}$$

$$k_{H_{3_r}} \doteq -\frac{1}{4m} \cdot \left(\sum_{j=r}^{m} \left(k_{n^{12}_{rj}} + k_{n^{12}_{rj+1}} \right) \right) \cdot \cos\phi_r, \tag{10.30}$$

$$k_{H_{4_r}} \doteq +\frac{1}{4m} \cdot \left(\sum_{j=r}^{m} \left(k_{q^{22}_{rj}} \cdot \left(\cos\phi_r \cdot \cos\phi_j + \cos\phi_j \cdot \cos\phi_r \right) + k_{q^{22}_{rj+1}} \cdot \left(\cos\phi_r \cdot \sin\phi_{j+1} + \cos\phi_{j+1} \cdot \sin\phi_r \right) \right) \right). \tag{10.31}$$

The applied loading V_{0_r} and H_{0_r} are given in a similar manner by:

$$V_{0_r} = k_{V_{0_r}} \cdot qL^2, \tag{10.32}$$

$$H_{0_r} = k_{H_{0_r}} \cdot qL^2, \tag{10.33}$$

with the dimensionless coefficients $k_{V_{0_r}}$ and $k_{H_{0_r}}$ given as

$$k_{V_{0_r}} \doteq + 0.25 \times \gamma^2, \tag{10.34}$$

$$k_{H_{0_r}} \doteq + \frac{1.}{4.m} \left(\sum_{j=r}^{m} \left(k_{n^{12}_{m+1j}} + k_{n^{12}_{m+1j+1}} \right) \right). \tag{10.35}$$

The programme to carry out these equilibrium checks is listed in Appendix A.

10.1.2 Clamped Support

Employing the shell of section 7.2.1 with $m = 16$, table 10.1 shows the results of numerical integrations (10.20) to (10.31) for $r = 1$ to 16. For all values of r the summation of vertical and horizontal internal stresses agree to within 2% of the applied vertical and horizontal loading at $z_2 = 0$. The poor results for both k_{V_1} and k_{H_1} at the boundary are due to the necessity of employing approximate non symmetric analogues for the determination of internal stress resultants at these positions. The agreement is seen to improve considerably as γ decreases, so that for $\gamma \leq .75$

($r \geq 5$) the agreement is to less than 1% and for $\chi < .5$ ($r > 9$) the agreement is within 0.5%.

It can also be observed from table 10.1 that the percentages of vertical and horizontal loading carried by in-plane shear stress of $k_{V_{3_r}}$ and $k_{H_{3_r}}$, given by $k = 3$ in the formulae

$$\text{percentage of } k_{V_{k_r}} = \frac{k_{V_{k_r}}}{k_{V_{1_r}}} \times 100\%, \; k = 2,3,4 \quad (10.36)$$

$$\text{and percentage of } k_{H_{k_r}} = \frac{k_{H_{k_r}}}{k_{H_{i_r}}} \times 100\%, \; k = 2,3,4 \quad (10.37)$$

quickly become predominant over the total contribution from $k_{n_{22}}$ and $k_{q_{22}}$. This once again indicates that the assertions of section 8.2 concerning the existence of a boundary zone are correct if this boundary zone is defined as that region in which in-plane shear stress supports a major portion of the applied loading. See also section 8.2.4.

10.1.3 Simple Support

Table 10.2 shows listings of $(k_{V_{k_r}}, k_{H_{k_r}})$, $((k = 0,4), r = 1,16)$ for the simply supported shell described in sections 7.2.2 and 8.2.2. Agreement between applied vertical and horizontal loading, and the resulting internal action, is of the same order as that for the clamped shell of section 10.1.2. In the present shell the predominance of the in-plane shear

r	$^{k}H_{2r}$	%	$^{k}H_{3r}$	%	$^{k}H_{4r}$	%	$^{k}H_{1r}$	$^{k}H_{0r}$
1	.0016	-.3	-.2393	52.9	-.2148	47.4	-.4525	.2500
2	-.0029	1.3	-.2079	96.4	-.0047	2.2	-.2156	.2197
3	-.0055	2.9	-.1794	95.1	-.0035	1.8	-.1885	.1914
4	-.0061	3.7	-.1547	94.8	-.0022	1.3	-.1631	.1650
5	-.0055	4.0	-.1326	95.2	-.0010	.7	-.1393	.1406
6	-.0044	3.7	-.1127	96.0	-.0001	.1	-.1173	.1181
7	-.0031	3.2	-.0944	97.2	.0004	-.5	-.0971	.0976
8	-.0020	2.5	-.0775	98.4	.0008	-1.0	-.0787	.0791
9	-.0011	1.9	-.0620	99.6	.0009	-1.5	-.0622	.0625
10	-.0006	1.2	-.0480	100.6	.0009	-1.9	-.0476	.0478
11	-.0002	.8	-.0355	101.4	.0007	-2.2	-.0350	.0351
12	-.0001	.4	-.0248	102.0	.0005	-2.4	-.0243	.0244
13	-.0000	.2	-.0159	102.3	.0004	-2.5	-.0155	.0156
14	-.0000	.0	-.0089	102.5	.0002	-2.6	-.0087	.0087
15	-.0000	.0	-.0039	102.6	.0001	-2.7	-.0038	.0039
16	-.0000	.0	-.0010	102.7	.0000	-2.7	-.0009	.0009

r	$^{k}V_{2r}$	%	$^{k}V_{3r}$	%	$^{k}V_{4r}$	%	$^{k}V_{1r}$	$^{k}V_{0r}$
1	.0043	-.7	-.5984	106.0	.0297	-5.2	-.5643	.6092
2	-.0117	2.0	-.5545	98.0	.0005	-.1	-.5656	.5757
3	-.0218	4.0	-.5127	95.9	.0004	-.0	-.5342	.5414
4	-.0256	5.1	-.4760	94.9	.0002	-.0	-.5014	.5063
5	-.0250	5.3	-.4423	94.6	.0001	-.0	-.4672	.4704
6	-.0215	5.0	-.4099	95.0	.0000	-.0	-.4315	.4335
7	-.0168	4.2	-.3777	95.7	-.0000	.0	-.3946	.3958
8	-.0120	3.3	-.3447	96.6	-.0000	.0	-.3568	.3575
9	-.0078	2.4	-.3102	97.5	-.0000	.0	-.3182	.3186
10	-.0046	1.6	-.2743	98.3	-.0000	.0	-.2790	.2793
11	-.0024	1.0	-.2370	98.9	-.0000	.0	-.2395	.2397
12	-.0011	.5	-.1986	99.4	-.0000	.0	-.1998	.1999
13	-.0004	.2	-.1594	99.7	-.0000	.0	-.1599	.1599
14	-.0001	.1	-.1198	99.8	-.0000	.0	-.1200	.1200
15	-.0000	.0	-.0799	99.9	-.0000	.0	-.0800	.0800
16	-.0000	.0	-.0400	99.9	-.0000	.0	-.0400	.0400

TABLE 10.1 Ruled surface hyperbolic paraboloid with edges clamped. Vertical and horizontal equilibrium checks for shell with $\lambda_1 = 0.20$, $\lambda_2 = 0.0165$, $\nu = 0.00$ and $m = 16$.

r	$^{k}H_{2r}$	%	$^{k}H_{3r}$	%	$^{k}H_{4r}$	%	$^{k}H_{1r}$	$^{k}H_{0r}$
1	-.0549	28.2	-.1460	75.0	.0064	-3.3	-.1945	.2500
2	-.0473	22.4	-.1306	61.8	-.0332	15.7	-.2113	.2197
3	-.0386	20.7	-.1246	66.8	-.0232	12.4	-.1865	.1914
4	-.0302	18.6	-.1169	72.0	-.0152	9.3	-.1624	.1650
5	-.0227	16.2	-.1075	77.1	-.0091	6.5	-.1394	.1406
6	-.0163	13.8	-.0967	82.1	-.0047	4.0	-.1177	.1181
7	-.0112	11.5	-.0847	86.7	-.0017	1.7	-.0976	.0976
8	-.0073	9.3	-.0721	90.9	.0002	-.2	-.0793	.0791
9	-.0046	7.3	-.0593	94.6	.0012	-2.0	-.0627	.0625
10	-.0026	5.5	-.0470	97.9	.0016	-3.5	-.0480	.0478
11	-.0014	4.1	-.0355	100.6	.0016	-4.7	-.0353	.0351
12	-.0006	2.8	-.0252	103.0	.0014	-5.8	-.0245	.0244
13	-.0002	1.8	-.0164	104.8	.0010	-6.7	-.0156	.0156
14	-.0000	1.0	-.0093	106.3	.0006	-7.3	-.0088	.0087
15	-.0000	.4	-.0042	107.3	.0003	-7.8	-.0039	.0039
16	-.0000	.1	-.0010	107.9	.0000	-8.0	-.0009	.0009

r	$^{k}V_{2r}$	%	$^{k}V_{3r}$	%	$^{k}V_{4r}$	%	$^{k}V_{1r}$	$^{k}V_{0r}$
1	-.2236	37.9	-.3652	61.9	-.0010	.1	-.5898	.5951
2	-.1972	37.0	-.3483	65.3	.0127	-2.3	-.5328	.5644
3	-.1674	32.6	-.3561	69.8	.0139	-2.7	-.5095	.5340
4	-.1380	28.4	-.3598	74.1	.0124	-2.5	-.4854	.5027
5	-.1104	24.0	-.3585	78.0	.0099	-2.1	-.4591	.4702
6	-.0858	19.9	-.3516	81.7	.0071	-1.6	-.4303	.4366
7	-.0646	16.2	-.3389	84.9	.0047	-1.1	-.3988	.4016
8	-.0470	12.9	-.3205	87.8	.0028	-.7	-.3647	.3654
9	-.0330	10.0	-.2969	90.4	.0015	-.4	-.3284	.3279
10	-.0220	7.6	-.2689	92.6	.0006	-.2	-.2903	.2893
11	-.0139	5.5	-.2370	94.5	.0002	-.0	-.2507	.2497
12	-.0080	3.8	-.2020	96.1	.0000	-.0	-.2100	.2092
13	-.0041	2.4	-.1644	97.5	-.0000	.0	-.1686	.1681
14	-.0017	1.3	-.1249	98.5	-.0000	.0	-.1267	.1265
15	-.0005	.6	-.0840	99.3	-.0000	.0	-.0846	.0845
16	-.0000	.1	-.0422	99.8	-.0000	.0	-.0423	.0423

TABLE 10.2 Ruled surface hyperbolic paraboloid with edges simply supported. Vertical and horizontal equilibrium checks for shell with $\lambda_1 = 0.20$, $\lambda_2 = 0.0165$, $\nu = 0.00$ and $m = 16$.

r	k_{H2_r}	%	k_{H3_r}	%	k_{H4_r}	%	k_{H1_r}	k_{H0_r}
1	-.1951	74.0	-.0000	.0	-.0682	25.8	-.2633	.2500
2	-.0585	27.1	-.1644	76.2	.0072	-3.3	-.2156	.2197
3	-.0364	19.1	-.1668	87.5	.0128	-6.7	-.1905	.1914
4	-.0159	9.7	-.1624	99.2	.0146	-8.9	-.1637	.1650
5	-.0004	.3	-.1521	109.5	.0137	-9.8	-.1389	.1406
6	.0081	-6.9	-.1353	116.4	.0109	-9.4	-.1163	.1181
7	.0109	-11.4	-.1143	119.3	.0075	-7.8	-.0958	.0976
8	.0103	-13.3	-.0920	118.7	.0042	-5.4	-.0775	.0791
9	.0080	-13.0	-.0708	115.7	.0016	-2.6	-.0612	.0625
10	.0053	-11.4	-.0521	111.1	-.0001	.3	-.0469	.0478
11	.0031	-9.2	-.0365	106.0	-.0011	3.1	-.0345	.0351
12	.0016	-6.7	-.0242	100.9	-.0013	5.7	-.0240	.0244
13	.0006	-4.4	-.0148	96.5	-.0012	7.8	-.0153	.0156
14	.0002	-2.6	-.0080	93.0	-.0008	9.5	-.0086	.0087
15	.0000	-1.2	-.0034	90.4	-.0004	10.7	-.0038	.0039
16	.0000	-.4	-.0008	88.9	-.0001	11.4	-.0009	.0009

r	k_{V2_r}	%	k_{V3_r}	%	k_{V4_r}	%	k_{V1_r}	k_{V0_r}
1	-.4879	102.8	-.0000	.0	.0133	-2.8	-.4745	.6220
2	-.1575	26.3	-.4384	73.4	-.0008	.1	-.5968	.6111
3	-.1004	17.3	-.4767	82.3	-.0014	.2	-.5786	.5821
4	-.0356	6.6	-.4999	93.0	-.0016	.3	-.5372	.5416
5	.0197	-4.0	-.5073	103.7	-.0015	.3	-.4890	.4949
6	.0547	-12.4	-.4923	112.2	-.0011	.2	-.4387	.4454
7	.0694	-17.8	-.4575	117.6	-.0007	.1	-.3888	.3958
8	.0687	-20.1	-.4092	120.0	-.0003	.1	-.3409	.3475
9	.0587	-19.8	-.3543	119.8	-.0001	.0	-.2957	.3014
10	.0447	-17.6	-.2979	117.6	-.0000	.0	-.2532	.2577
11	.0306	-14.3	-.2439	114.3	.0000	-.0	-.2132	.2165
12	.0186	-10.6	-.1940	110.6	.0000	-.0	-.1752	.1773
13	.0098	-7.1	-.1486	107.1	.0000	-.0	-.1387	.1399
14	.0042	-4.0	-.1075	104.1	.0000	-.0	-.1033	.1038
15	.0012	-1.8	-.0698	101.8	.0000	-.0	-.0685	.0687
16	.0001	-.4	-.0343	100.4	.0000	-.0	-.0341	.0342

TABLE 10.3 Ruled surface hyperbolic paraboloid with free edges damped at corners. Vertical and horizontal equilibrium checks for shell with $\lambda_1 = 0.20$, $\lambda_2 = 0.0165$, $\nu = .00$ and $m = 16$.

r	k_{H2_r}	%	k_{H3_r}	%	k_{H4_r}	%	k_{H1_r}	k_{H0_r}
2	-.0355	16.4	-.1689	78.3	-.0110	5.1	-.2155	.2197
3	-.0232	12.2	-.1602	84.4	-.0063	3.3	-.1898	.1914
4	-.0183	11.1	-.1433	87.0	-.0030	1.8	-.1647	.1650
5	-.0131	9.3	-.1272	90.1	-.0006	.4	-.1410	.1406
6	-.0082	6.9	-.1114	93.6	.0007	-.6	-.1189	.1181
7	-.0045	4.5	-.0955	96.8	.0014	-1.4	-.0985	.0976
8	-.0020	2.4	-.0795	99.3	.0015	-1.8	-.0800	.0791
9	-.0005	.9	-.0640	101.1	.0012	-2.0	-.0633	.0625
10	.0000	-.1	-.0495	102.0	.0009	-1.9	-.0486	.0478
11	.0002	-.6	-.0365	102.2	.0005	-1.5	-.0357	.0351
12	.0002	-.8	-.0253	102.0	.0002	-1.1	-.0248	.0244
13	.0001	-.7	-.0161	101.4	.0001	-.6	-.0159	.0156
14	.0000	-.5	-.0090	100.7	.0000	-.2	-.0089	.0087
15	.0000	-.2	-.0039	100.1	-.0000	.1	-.0039	.0039
16	.0000	-.0	-.0009	99.6	-.0000	.4	-.0009	.0009

r	k_{V2_r}	%	k_{V3_r}	%	k_{V4_r}	%	k_{V1_r}	k_{V0_r}
2	-.0940	17.3	-.4504	82.9	.0013	-.2	-.5432	.5572
3	-.0701	13.3	-.4579	86.8	.0007	-.1	-.5274	.5340
4	-.0615	12.2	-.4410	87.8	.0003	-.0	-.5022	.5057
5	-.0478	10.1	-.4240	89.8	.0001	-.0	-.4717	.4735
6	-.0321	7.3	-.4051	92.6	-.0000	.0	-.4373	.4383
7	-.0181	4.5	-.3820	95.4	-.0001	.0	-.4003	.4008
8	-.0077	2.1	-.3536	97.8	-.0001	.0	-.3614	.3619
9	-.0011	.3	-.3203	99.6	-.0000	.0	-.3216	.3219
10	.0021	-.7	-.2833	100.7	-.0000	.0	-.2812	.2815
11	.0031	-1.3	-.2438	101.3	-.0000	.0	-.2406	.2409
12	.0027	-1.3	-.2029	101.3	-.0000	.0	-.2001	.2003
13	.0018	-1.1	-.1616	101.1	-.0000	.0	-.1598	.1599
14	.0009	-.7	-.1205	100.7	-.0000	.0	-.1196	.1197
15	.0002	-.3	-.0799	100.3	.0000	-.0	-.0796	.0796
16	.0000	-.0	-.0398	100.0	.0000	-.0	-.0397	.0397

TABLE 10.4 Ruled surface hyperbolic paraboloid with beam edges clamped at corners. Vertical and horizontal equilibrium checks for shell with $\lambda_1 = 0.20$, $\lambda_2 = 0.0165$, $\lambda_3 = 4.50$, $\lambda_4 = 0.05$, $\nu = 0.00$, and $m = 16$.

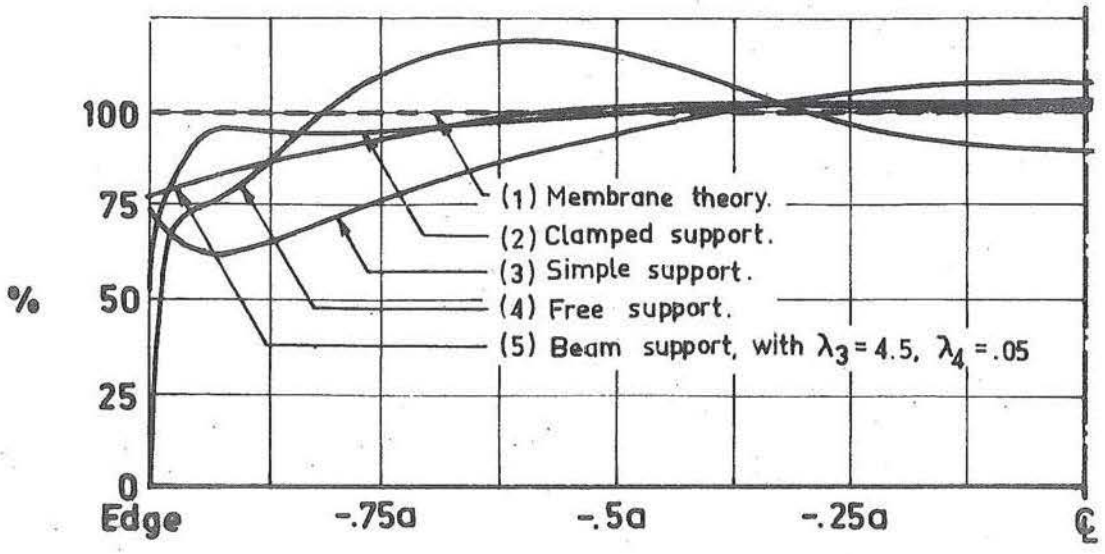

(a) Percentage of total vertical load carried by membrane shear as a function of boundary condition and position on the shell. (sect.10.1)

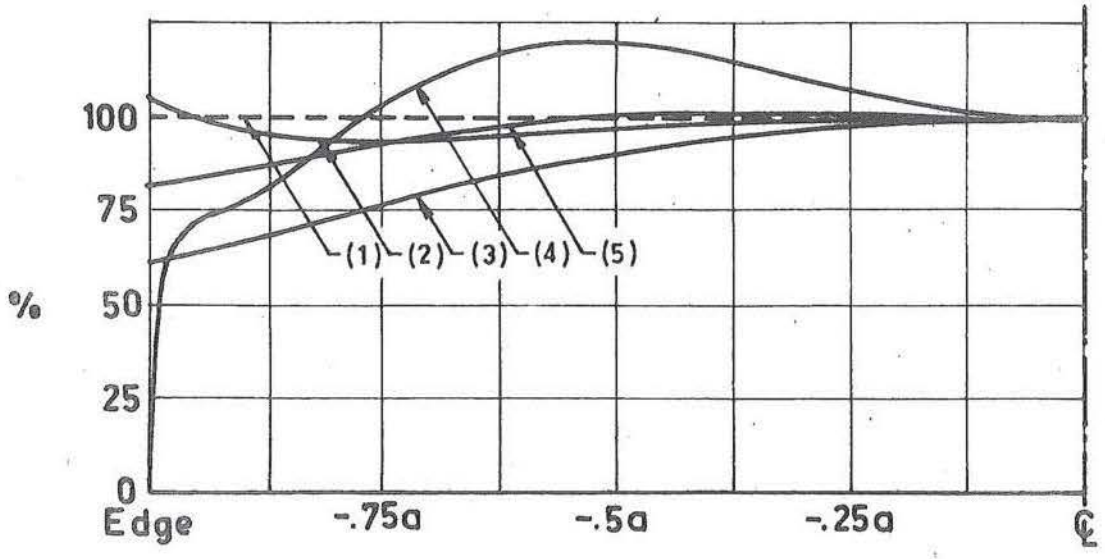

(b) Percentage of total horizontal load carried by membrane shear as a function of boundary condition and position on the shell. (sect .10.1)

Fig.10.2 Ruled surface hyperbolic paraboloid with $\lambda_1 = .2$, $\lambda_2 = .0165$, $\mu = .00$, m = 16 and corners clamped.

stress in carrying applied loading is less pronounced than for the clamped shell. At $\gamma = .5$ $(r = 9)$ this percentage is approximately 90%, as compared to the 98% of the clamped shell. This behaviour is demonstrated more clearly in the figures 10.2(a) and (b).

10.1.4 Free Edge

The results for the free edged shell of sections 7.2.3 and 8.2.3 are listed in table 10.3. It is observed that the correlation between applied and internal reactive forces is (with the exception of $\gamma = 1.0$ $(r = 1)$) less than 2%. In contrast with the clamped and simply supported shells the agreement in the present case is approximately constant throughout the shell area. The correlation of reactive forces and applied loading at the boundary to 5% is remarkable when it is considered that all applied loading is carried by singular bending action at the corner support.

Figure 10.2 clearly shows the adverse effects of bending for the beamless ruled surface hyperbolic paraboloid. In addition to the low stiffness, and localised stress peaks (shown in chapter 8), the in-plane shear $k_{n_{12}}$ supports a load greater than that actually applied.

10.1.5 Beam Edge

The example of sections 7.2.4 and 8.3.2(c) is chosen as being typical of this class of intermediate displacement-

traction boundary type shell. As before, agreement of vertical forces is to within 2% over the range $0. < \gamma < .9375$, and tends to be considerably less than this figure. Except for the cross-sections $r = 2$ and 3 the correlation between internal horizontal forces in the z_1 coordinate direction at the grid position $z_2 = 0$ and those for $r = 2$ to m is to within 0.5%. As expected the behaviour of this shell is seen from figure 10.2 to lie between the simply supported and free edged shell.

10.1.6 Conclusions

The close agreement of both applied vertical and horizontal forces to the summations of internal reactive stresses is shown. It is further demonstrated that in-plane shears quickly become predominant in carrying both vertical and horizontal components of internal stresses. This is especially the case for shells with boundary conditions of the traction type where the load carring characteristics quickly assume those of the membrane shell.

One further observation resulting from this study, although this could have been predicted from the results of chapter eight, is the independence of the total horizontal load component $k_{H_{0_1}}$ to the effects of boundary support support condition. Figure 10.3 indicates that for shells only supported at the corners the diagonal tie force T_1 may be predicted from

$$T_1 = \sqrt{2} \cdot H_{o_r} \cdot \qquad (10.38$$

In addition it can be seen from table 10.5, where the values of $k_{H_{0_1}}$ have been collected and compared to the membrane solution, that these horizontal forces are approximated by those of the membrane solution. It should be noted that the value of $k_{H_{0_1}}$ listed for the beam edged shell neglects the influence of shear between $r = 1$ and 2, so that the results given are likely to be 6% low.

	$k_{H_{0_1}}$	k_{T_1}
Clamped Edged Shell	.6092	.860
Simple Edged Shell	.5951	.841
Free Edged Shell	.6220	.880
Beam Edged Shell	.5572	.789
Membrane Solution	.6250	.885

TABLE 10.5 Dependence of $k_{H_{0_1}}$ and k_{T_1} upon the effects of boundary support conditions.

These results, combined with the critical behaviour of the corner support ties, as demonstrated in section 8.5, provide a powerful á priori design tool. T_1 may be estimated from

$$T_1 = k_{T_1} \cdot qL^2,$$

where

$$k_{T_1} = \frac{1}{4\sqrt{2}} \cdot \frac{a}{f},$$

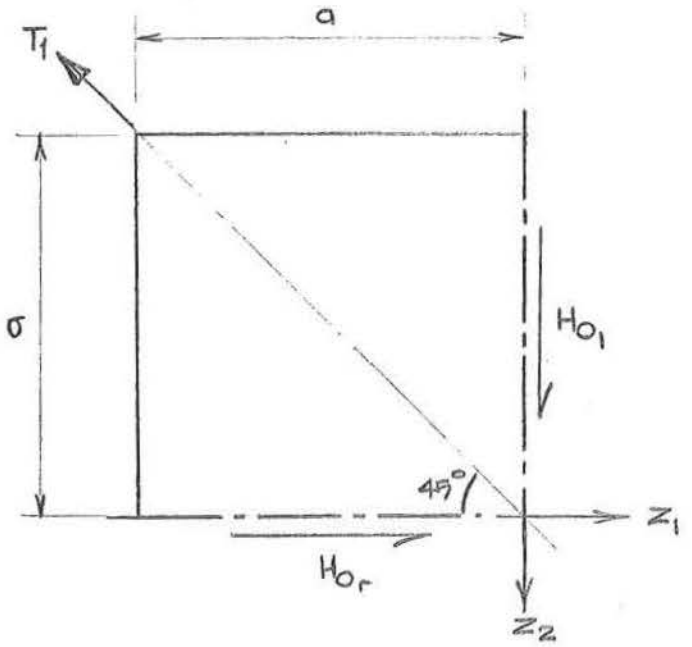

Fig.10.3 Estimation of T_1 from H_{O_1}.

so that for a given shell parameter λ_1 it should be possible to quickly estimate the practicability of various spans L .

10.2 COMPARISONS WITH EXISTING SOLUTIONS

In sections 7.2 and 7.3 solutions using three independent difference formulations, namely the conventional, higher order and modified methods, were obtained. Although physically independent, these solutions could conceivably contain a number of common errors through some consistent programming fault. This possibility is eliminated when the results of section 10.1 are considered. However, it was thought desirable

that the programmes should be checked against the solutions for shells reported in the literature. For this purpose the solutions obtained by Chetty and Tottenham [13] for the clamped and simply supported shell are considered.

10.2.1 The Clamped Shell

The clamped shell considered by Chetty and Tottenham was of dimensionless ratios

$$\lambda_1 = 0.202,$$
$$\lambda_2 = 0.0387,$$
$$\nu = 0.39.$$

Figure 10.4 shows the close agreement between the solution using the conventional finite differences technique of section 7.2.1 with $m = 8$, and that of Chetty and Tottenham for Bongard's simplified equations. It is seen that $k_{n_{12}}$, $k_{m_{22}}$ and k_{w_3} are in agreement to within 1.6%, 10% and 2.1% respectively. These figures are comparable with the differences between the solutions of figure 7.1 with $m = 8$ and $m = 16$, and in the same direction, so that if $m = 16$ had been used for the present study it is likely that the agreement could have been improved.

10.2.2 The Simply Supported Shell

The solutions for the particular shell

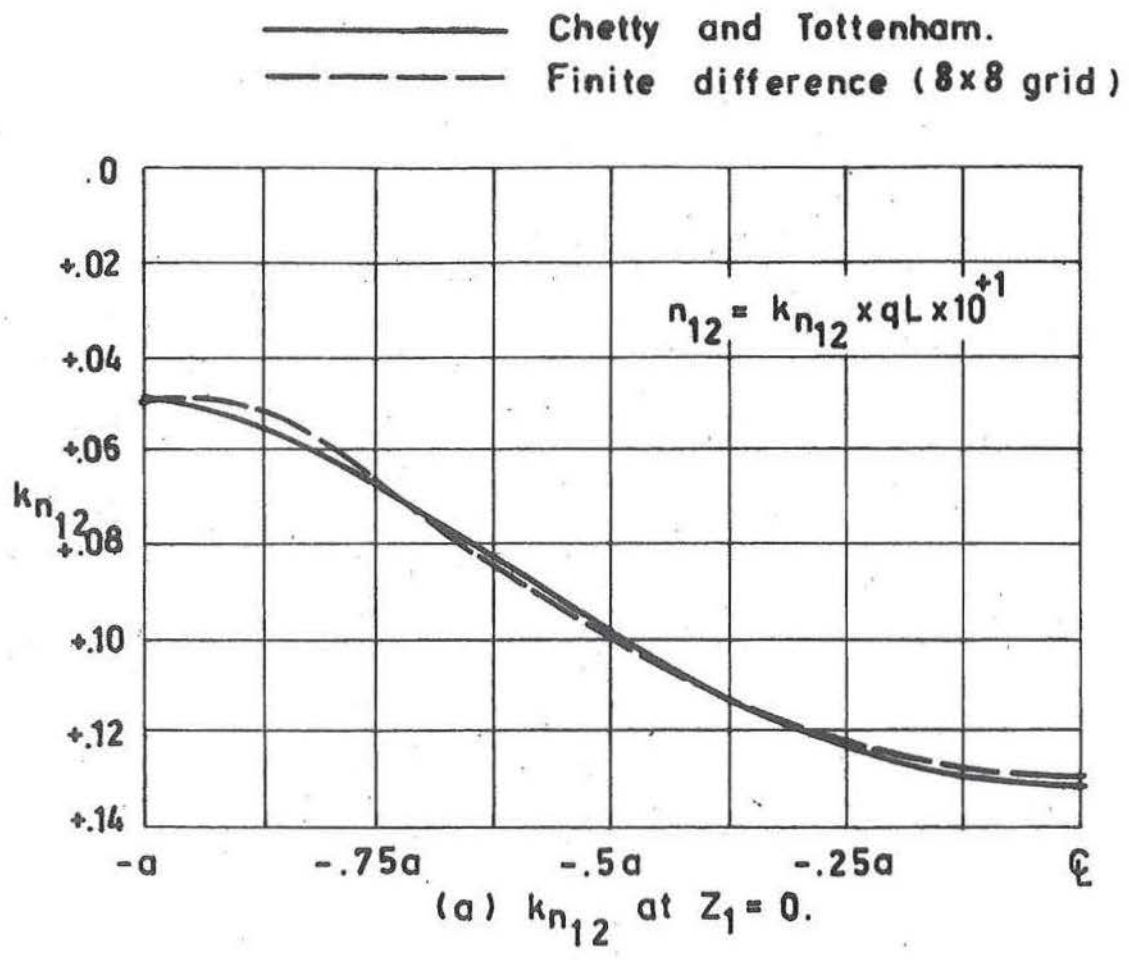

Fig. 10.4 Ruled surface hyperbolic paraboloid with all edges clamped. Comparison with the solution of Chetty and Tottenham.[13]

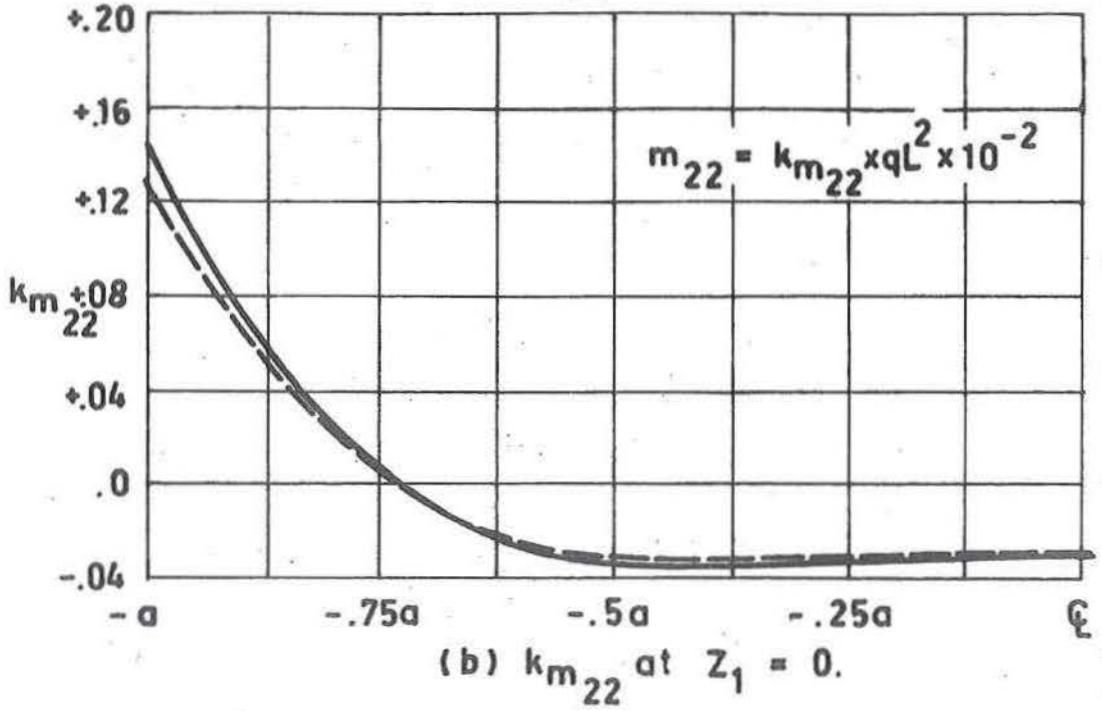

(b) $k_{m_{22}}$ at $Z_1 = 0.$

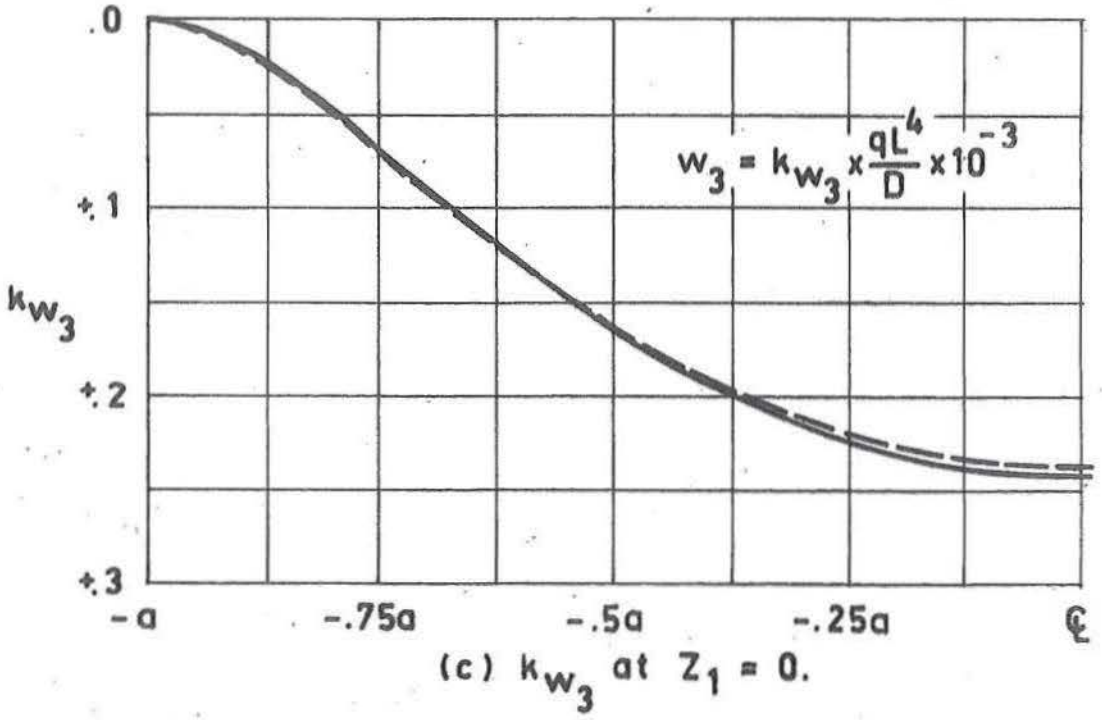

(c) k_{w_3} at $Z_1 = 0.$

Fig. 10.4 (continued) Ruled surface hyperbolic paraboloid with all edges clamped. Comparison with the solution of Chetty and Tottenham.

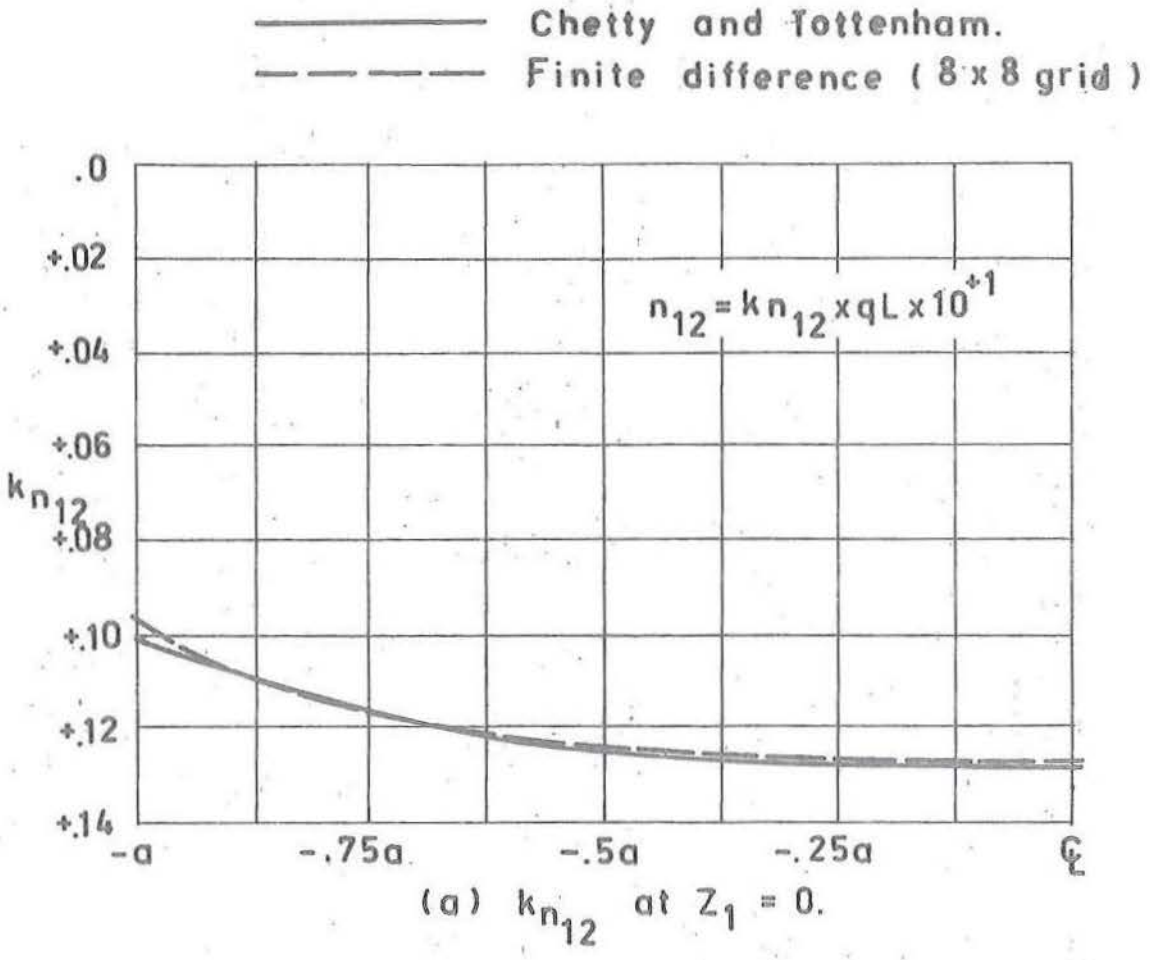

Fig. 10.5 Ruled surface hyperbolic paraboloid with all edges simply supported. Comparison with the solution of Chetty and Tottenham.[13]

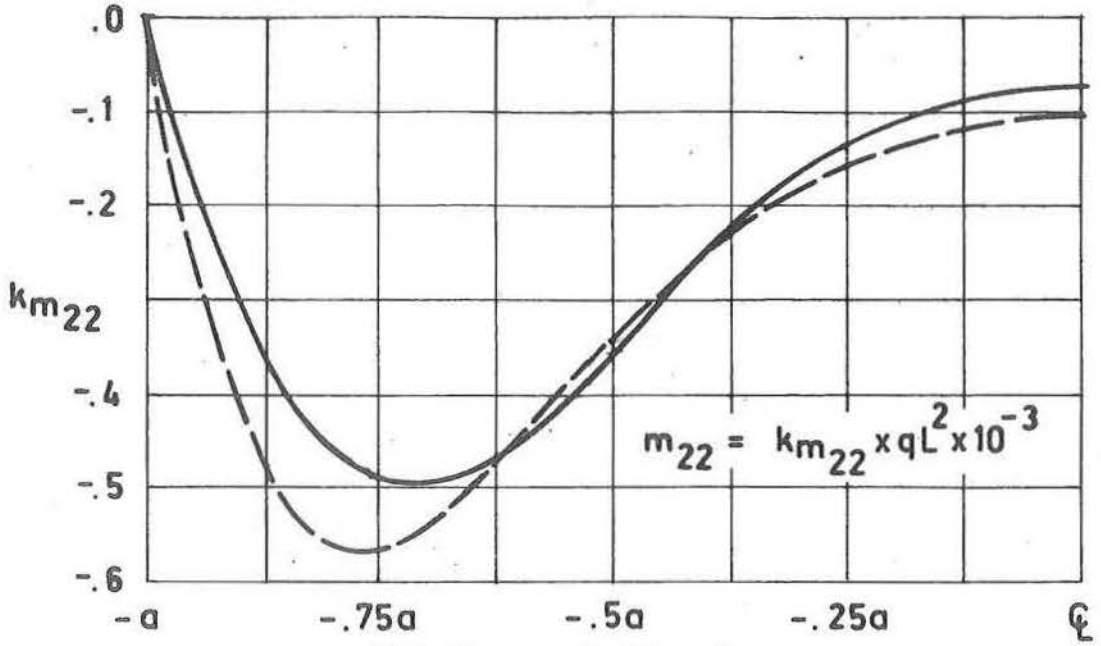

(b) $k_{m_{22}}$ at $Z_1 = 0.$

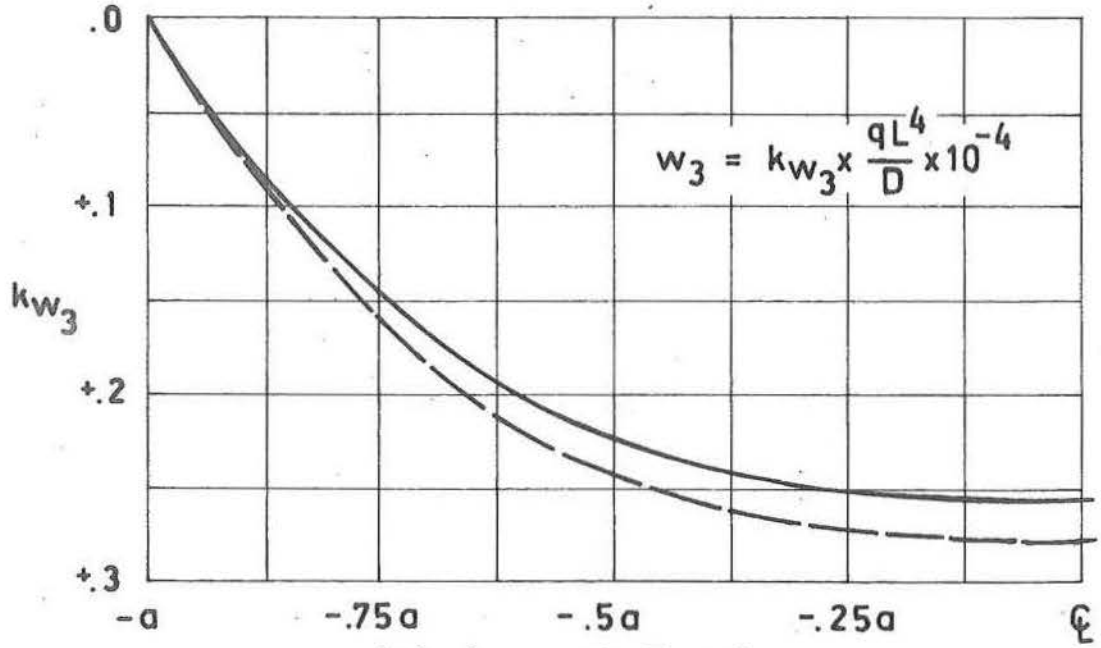

(c) k_{w_3} at $Z_1 = 0.$

Fig. 10.5 (continued) Ruled surface hyperbolic paraboloid with all edges simply supported. Comparison with the solution of Chetty and Tottenham.

$$\lambda_1 = 0.200,$$
$$\lambda_2 = 0.0139,$$
$$\nu = 0.160,$$

given in reference [13] are shown in figure 10.5. Correlation, which is within 1.2%, 16.4% and 8.4% for $k_{n_{12}}$, $k_{m_{22}}$ and k_{w_3} is slightly worse than for the equivalent clamped shell. One possible explanation for these discrepancies, is that the results of reference [13] are presented in graphical form with scales of 4.0 inch, 0.5 inch and 2.0 inch representing the maximum ordinates of $k_{n_{12}}$, $k_{m_{22}}$ and k_{w_3}. The values of $k_{m_{22}}$ and k_{w_3} can therefore be expected to contain significant round-off errors. Again, the agreement verifies the present solution technique.

PART III

MODEL INVESTIGATIONS

CHAPTER ELEVEN

DESIGN OF MODEL

The numerical results obtained for the simple and clamped boundary shells are shown in section 10.2 to be consistent with the results of other authors using independent techniques of solutions. This, combined with statics checks, serves as sufficient verification of these rather impractical boundary types. On the other hand, the boundary conditions most closely resembling those of the practical situation, namely the free edge and beam edge supports, have not been experimentally verified in a satisfactory manner.

Previous to 1961, a number of design orientated model tests were carried out on both single and grouped ruled surface hyperbolic paraboloids (see for example[39, 23, 48]). All tests indicated that membrane stress analysis was in significant error, especially in regions of boundary influence. Further, although the nature of the edge members greatly influenced the overall shell behaviour, the in-plane shear stresses were in reasonable agreement with those resulting from membrane solutions. In order that the extent of this boundary influence be determined, Ahuja[3] constructed a reinforced concrete, single panel, ruled surface hyperbolic paraboloid, with provision to attach

edge members of variable stiffnesses. Although time prevented him from obtaining his objective, he was successful in showing the critical nature of the corner conditions. Batchelor[7], using the same model as Ahuja, completed this joint project separating the influences of both variable edge members and corner tie stiffnesses. Corner displacements, although measured, were not controlled. This, in addition to uncertainties due to the effects of discrete point loads and edge member-corner-shell interaction, make any quantitative comparison difficult. Because of the unreliable nature of the strain readings, all conclusions were based purely upon deflection records. Jones[37], using a mortar model, attempted to control corner displacements by providing an adjustable tie rod at the base diagonal. Control of the apex was once again neglected, as were the rotations at the base corners. Although this work seemingly confirmed the assertions of Batchelor[7] that corner rotations may play a significant part in shell behaviour - it was not suitable for comparative studies.

Dayaratnam and Gerstle[18] attempted a comparative study between an elastic model and the results of a theoretical solution. Displacements only were recorded on a 1/16" thick ruled surface hyperbolic paraboloid, with sand bags simulating uniform loading. When the shell dimensions, loading method, lack of control of corner displacements and limited instrumentation are considered, as well as the limitations of the

theoretical analysis (see section 8.3), the close agreement is surprising. This agreement may partially be explained by the relatively large edge members. In fact they approach the condition of the simple support, which has the effect of making the shell less sensitive to the effects of corner constraint and small geometric imperfections.

By employing a laminated timber, ruled surface hyperbolic paraboloid model, and recording both strains and deflections, Gupta [30] was able to achieve very close agreements with the results of a theoretical study in the results presented. The lack of relevant information concerning corner control and measurement, the uncertainties in the use of chains as uniform loading and in the behaviour of laminated timber and the absence of detailed experimental results make comparisons with the present theoretical work difficult.

The need for a model test programme satisfying all the assumptions made in elastic shell analysis is apparent. It was proposed to construct an elastic model such that boundary conditions, initially free, could be varied without adversely affecting the edge member-corner-shell interaction to the case of edge beam supports. Corner displacements, including rotations, should not only be instrumented, but also adjustable so that a number of possible corner conditions could be investigated. Also, because of trouble experienced by past investigators working with air pressure loading on other

classes of shell, it was decided that corner vertical reactions as well as diagonal thrusts should be measured. The shell behaviour would be determined from both strain and deflection measurement.

11.1 OBJECT OF MODEL TEST

The general object of the present model investigation was to verify the numerical procedures used in the solution of a discrete analogue of the thin shallow shell theory. It was also hoped that the results would provide further information which may assist in the design of future numerical and experimental programmes for this class of shell. In particular it was hoped to determine;

1. the influence of boundary constraints on overall shell behaviour when subject to uniform loading;

2. effect of varying corner support conditions with special emphasis on the influence of diagonal displacement control;

and, where practicable, to compare the results with those obtained in chapter 8.

11.2 MODEL GEOMETRY

Theoretical solutions, obtained from computer analysis, were used to determine the rise to span ratio λ_1 and thickness to span ratio λ_2, for which the maximum flexural strains would

be of the same order as those resulting from membrane action. This analysis neglected corner singularities, which, because of practical requirements would be removed in the model tests. Suitable ratios were found to be $\lambda_1 = 0.20$ and $\lambda_2 = 0.020$.

The limited lateral dimensions of the moulding oven determined the span of the shell at $L = 30$ inch, resulting in shell rise $f = 3$ inch, thickness $t_s = 0.24$ and corresponding dimensionless ratios of

$$\lambda_1 = 0.20,$$
$$\lambda_2 = 0.016.$$

With these dimensions a uniform loading of 0.25 psi would produce measurable strains and deflections in both the free and beam edged models. Additional advantages in using a relatively thick shell were, that the shell behaviour was less sensitive to small changes in shell thickness, and that the stiffening effects due to attachment of strain gauges and deflection targets were reduced.

Three edge conditions encompassing each of the three boundary types considered in section 8.3.4 were envisaged. They were the free edge corresponding to the pure traction boundary, the beam of small dimensions falling into the traction-displacement boundary transition, and the edge beam of large dimensions which may be considered as of the pure

displacement type. Time limitations made it possible to investigate only the first and an intermediate case between the last two. To comply with these requirements the beam thickness t_b was chosen at 1.125 inch and the beam breadth b_b at 0.75 inch, resulting in

$$\lambda_3 = 4.5,$$
$$\lambda_4 = 0.05,$$

for the second series of model tests. This edge beam was found to be typical of those existing structures reported in the literature[6,19]. The edge beam was orientated as in figure 12.2, and shaped in such a way that the thickness measured at the vertical centroidal axis was always constant at 1.125 inch.

11.3 CORNER SUPPORT CONDITIONS

Three combinations of corner support conditions were envisaged on both the free and edge beam supported shells. These were:

1. Both apex and base clamped flexurally and clamped extensionally (extensionally is used to signify the membrane action).

2. Base and apex clamped flexurally, base clamped extensionally and the apex free extensionally.

3. Both apex and base clamped flexurally and free extensionally.

It was also hoped, that a sufficient number of further tests employing diagonal displacement loading could be carried out to enable any combination of two tests to be added, using superposition to provide an independent check on any of the other cases. For example, by adding numerically suitable multiples of the results of the uniform normal load test with both apex and base clamped to the results from the test with diagonal displacement loading across the base diagonal, it should be possible to reproduce the case of the shell with uniform normal loading with apex clamped and base clamped flexurally, but free extensionally. Other possibilities are shown in section 14.3.

The impractical nature of the corner conditions chosen, as well as the sensitivity of shell behaviour upon these corner conditions, are demonstrated by the immense difficulty, even under laboratory conditions, of consistent simulation. Details of the corner supports and the method of attachment of edge beams are considered further in chapter 12.

11.4 MODEL MATERIAL

In view of the general objectives of the present model study, the requirements on model material were particularly high. Homogeneity, ease of forming and a consistent and predictable relationship between stress and strain were

essential. Hergenroder and Rusch [32] outlined the serious disadvantages of both concrete and plaster, while the elastic properties and homogeneity of laminated timber are extremely uncertain. The high modulus of elasticity and the difficulty of forming non-developable shapes make the use of aluminium or ferrous alloys impractical, while although glass-reinforced polyester or epoxy resins have suitably low modulus or elasticity the problems associated with orthotopy and thickness control detract from their use [44]. Litle [40] has discussed fully the relative merits of a number of commercially-obtainable plastics, and because a heat-drape forming technique was proposed, use of thermoplastics, and in particular an acrylic, was particularly attractive. Vinyls were unsuitable because they have the serious disadvantage that jointing both vinyl to vinyl and vinyl to epoxy, is extremely difficult. A compromise, which included ease of forming and jointing, suitable elastic properties and availability, indicated the use of poly (methyl methacrylate) obtainable locally under the trade name of "Perspex".

Problems associated with elastic properties and creep varying with temperature were minimised by carrying out all tests in a room controlled in both temperature (to $\pm$ 0.25° C) and humidity. Although detailed information on the properties of perspex is given in the ICI Publication "Perspex" [33] tests were carried out to determine the value of Young's modulus,

Poisson's ratio and further information of the characteristics of creep. These tests are given in detail in appendix B, the results of which are summarised in table 11.1.

PROPERTY	AS LISTED IN REFERENCE [33]	AS DETERMINED APPENDIX B
Flexural Modulus ($lb./in.^2$)		
1 minute value	$0.420 \pm 0.015 \times 10^{-6}$	$0.520 \pm 0.005 \times 10^{-6}$
15 minute value	$0.415 \pm 0.015 \times 10^{-6}$	$0.494 \pm 0.005 \times 10^{-6}$
60 minute value	$0.408 \pm 0.015 \times 10^{-6}$	$0.482 \pm 0.005 \times 10^{-6}$
Poisson's Ratio	0.35	0.320 ± 0.005
Ultimate Stress ($lb./in.^2$)		
Flexural	$20,000 \pm 1,000$	
Tensile	$12,000 \pm 500$	
Coefficient of Thermal Expansion $20^{\circ}C$		
Linear	7.3×10^{-5}	
Volume	2.2×10^{-4}	

TABLE 11.1 Properties of "Perspex"

CHAPTER TWELVE

CONSTRUCTION OF SHELL MODEL AND SUPPORT FRAME

An outline of the construction of the shell model is followed by a brief description of the method used for loading the shell. Consideration is finally given to the corner support arrangements, and the form of the model supporting rig.

12.1 MODEL CONSTRUCTION

12.1.1 Manufacture of Mould

A mild steel frame of $1\frac{1}{2}$" x $1\frac{1}{2}$" x $\frac{1}{8}$" angle produced the necessary mould rigidity and resistance to heat distortion as well as supplying the straight edge generators for screening the mould surface. The mould frame is shown in plate 12.1. The mould surface was formed by a 1" layer of plaster of paris covering a layer of wood lathes. As well as being a convenient mould material, plaster of paris has the porous properties which are necessary for heat contact with perspex. Acetic acid was used as a set inhibitor for the plaster of paris.

After initial forming, the mould surface was preshunk by heating through 150° C for a period of four hours. The surface was then reshaped, and a precise level and staff calibrated in $\frac{1}{100}$" were used to check the mould geometry. It was found that maximum deviations of spot heights from the

required shape were $\pm$ 0.05".

12.1.2 Moulding Shell

As expected, it was found that thickness variations over the original perspex sheet were large (0.240 $\pm$ 0.010 inch), but because heat and strain distortions on forming were found to be greater than these, no attempt was made at correction. The original perspex sheet was cut four inches oversize to allow for distortion, placed upon the mould in an oven with facility to programme temperature against time for an indefinite period and temperature range of 20° to 250° C, and formed using the normalising cycle as specified by ICI[34]. The complete heat cycle, including holding temperature constant at the normalising temperature of 140° C for a three hour period, the plastic solid transition of 105-110° C for a period of four hours (longer than that specified), and cooling to room temperature at the rate of 4° C per hour, took a total time of thirty hours. Although programming facilities were used to reproduce temperature gradients, the more critical constant temperatures were controlled manually to $\pm$ 0.5° C. Figure 12.1 shows the normalising cycle used in the present work.

To prevent surface damage and excessive practical difficulty a gravity-heat-drape forming method was used, and although the model did not conform exactly to the mould,

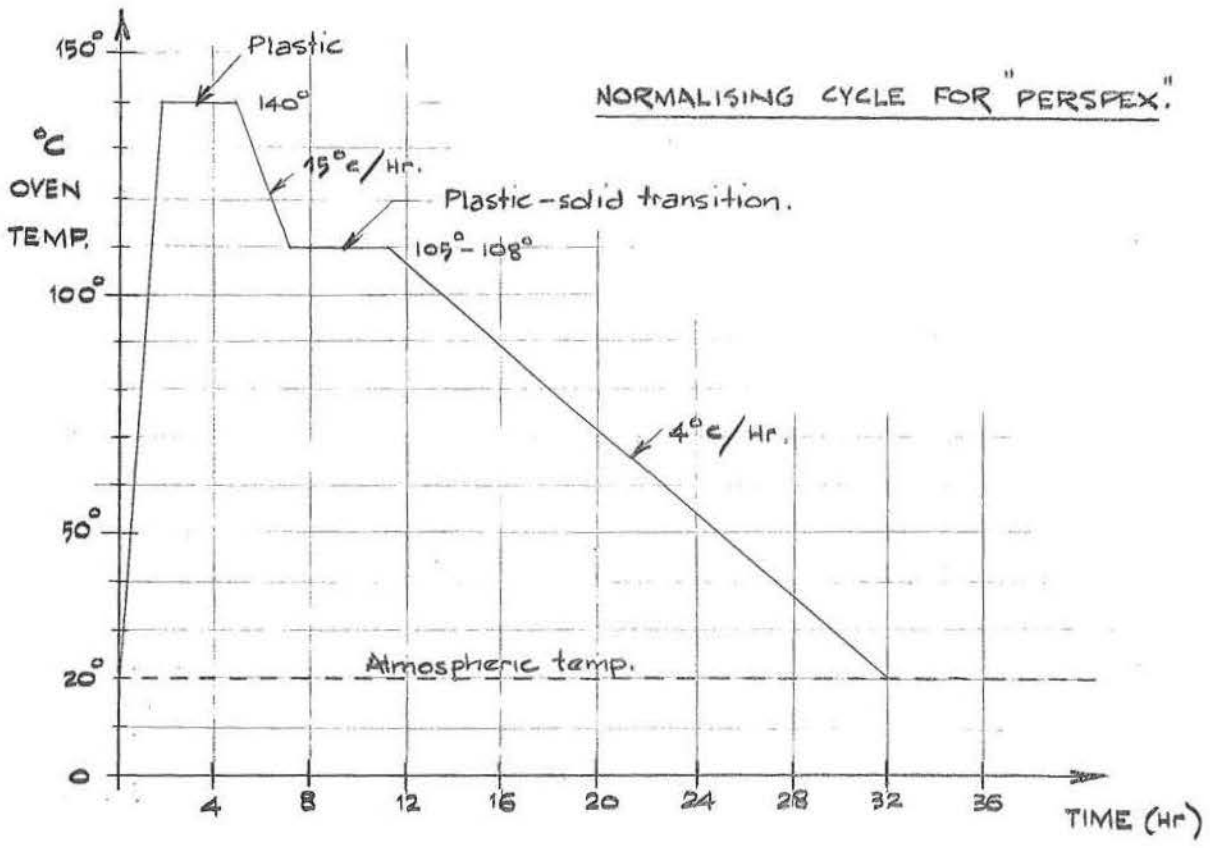

Figure 12.1 Normalising Cycle Used for Moulding Shell Model.

deviations were found to be nowhere greater than 0.05 inch. This could not be improved on subsequent heat treatment. Machined test beam samples were placed upon a sheet of plate glass with absorbent paper between the sample and plate glass to prevent surface damage at high temperatures. The test beams were subject to the same heat treatment as the shell model.

12.1.3 Corner Blocks

A rotary grinder was used to trim the shell edge so that it was 30 inch square in plan. In order that the shell be adequately supported at the corners, (other reasons are given

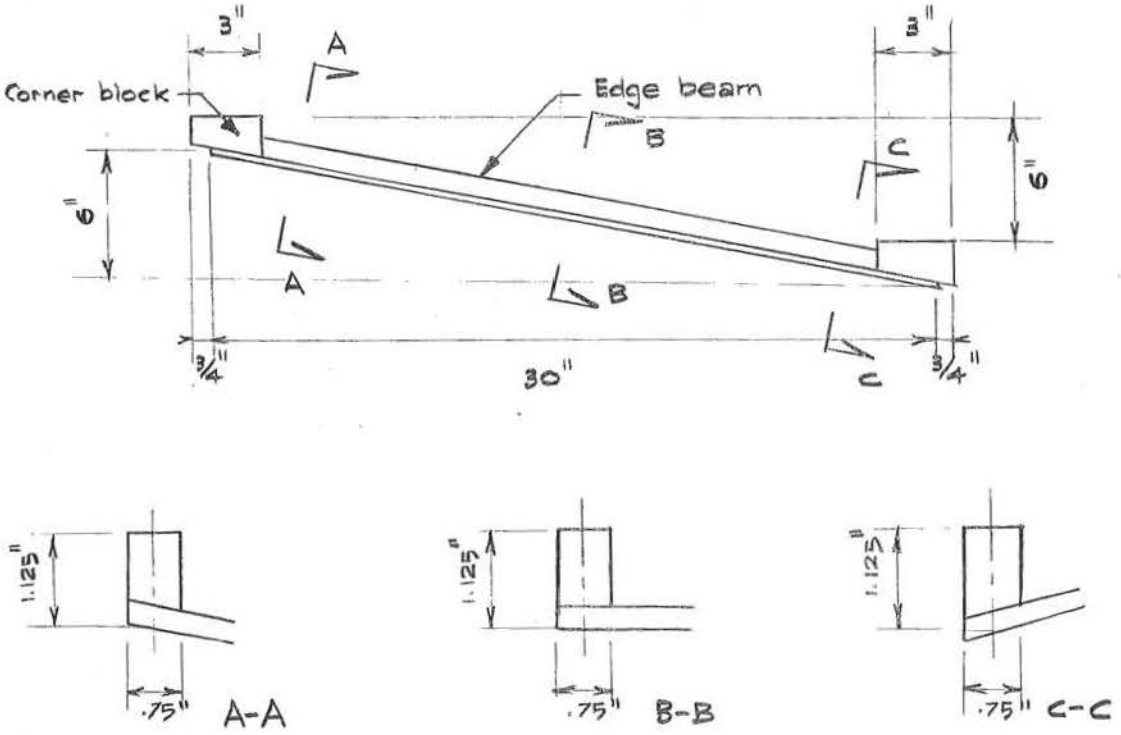

Fig.12.2 Details of Corner Blocks and Edge Beam Orientation.

in section 8.5), it was necessary to provide corner blocks which could be attached monolithically to the shell. Blocks of perspex 3" x 3" were shaped to follow the shell surface at the corners, while the top surfaces were machined to the horizontal. These are shown in figure 12.2.

Clamps were employed to position the corner blocks, and "Tensole 7" was used to fill the resulting gap. After hardening for four days the completed shell was annealled [34] to relieve residual stresses due both to cementing and machining.

12.1.4 Edge Beams

After the testing of the free edged shell was completed, the support superstructure and the strain gauges along the top edges of the shell were removed, and the edge strip cleaned and roughened in preparation for edge beam attachment. The edge beams were shaped from a ¾" thick perspex sheet to follow the twist of the shell edge, and also to maintain a constant thickness when measured at the vertical beam centroidal axis. This orientation of edge beams is shown in figure 12.2.

Once again clamps were employed to position edge beams and "Tensole 7" was used to fill the small gaps between edge beam, shell and corner blocks. Adhesive tape was used for masking the shell, and cellophane sheets for protecting strain gauges on the upper surface. The rig was designed so that it was not necessary to remove the shell from the loading box at any stage, and the complete operation, including application of strain gauges, took less than eight days. It was not possible to re-anneal the model.

12.2 LOADING DEVICE

For the present investigation the requirements for the loading system were:

1. It should apply uniform radial loads only.

2. The upper face, for reasons to be seen later, in connection with deflection measurements, and preferably the lower face, should be readily accessible.

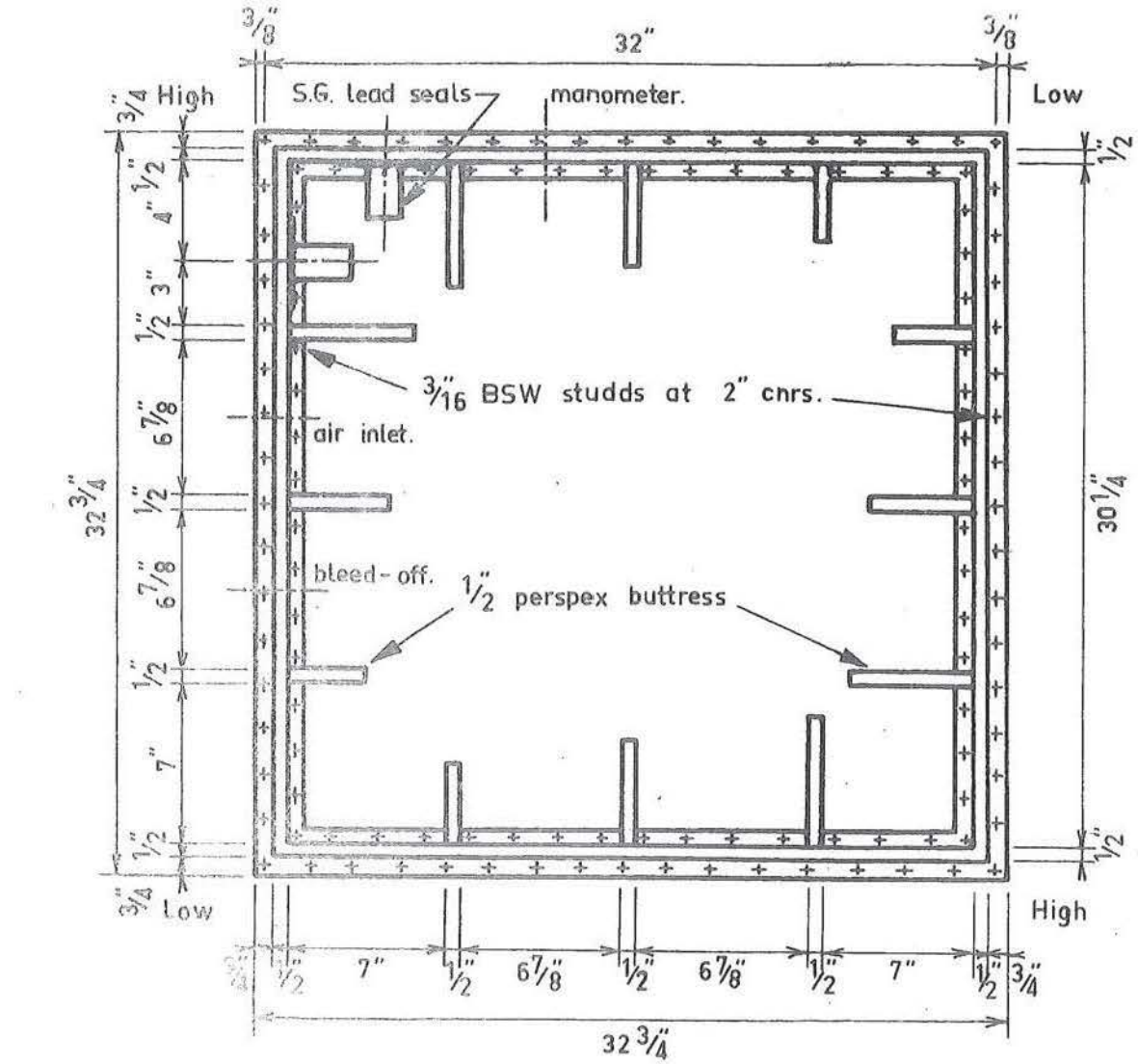

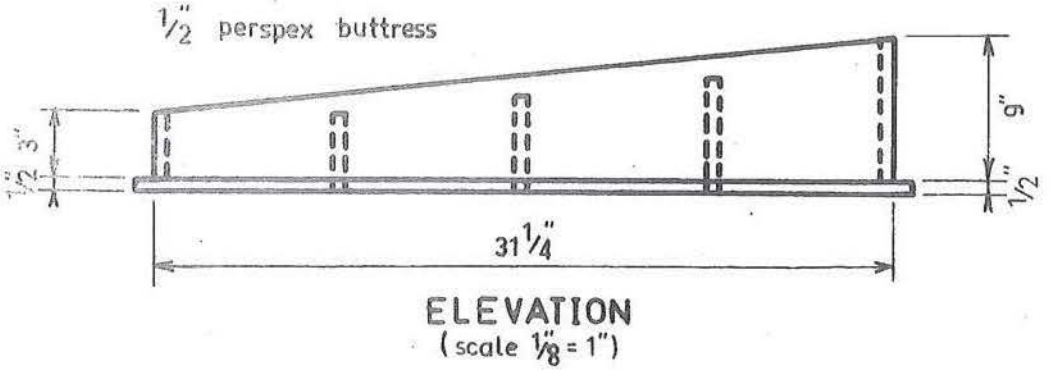

Fig. 12.3 Detail of air load box. (see plate 12.2).

3. It should not interfere in any way with the edge freedom of the shell, and be capable of allowing an unimpaired edge movement of at least 0.25 inch.

4. The load should be capable of accurate control for long periods and applied in a simple manner.

5. It should not in any way alter the properties of the shell.

A system in which the shell formed the top of a box which could be loaded with compressed air was chosen rather than a system applying a number of discrete loads (Powell [44]) or an air bag system (Dick [19]).

The system used consisted of a perspex air box, shown in figure 12.3, bolted to a mild steel base. The air bubble between the shell and the air box was adjusted to $\frac{1}{8}$" width before each test. Details of the edge sealing of the shell to the air box, as well as the device for adjusting the air bubble size are shown in figure 12.4.

Because the top surface was required free of obstruction, the loading had to be from below, which meant that unless a suction was used, the supporting structures had to be from above. This alternative of air pressure, with the shell supported from above, was finally chosen for practical reasons as it was extremely difficult to provide controlled corner supports as well as sealing for air pressures in the case of suction loading. The large number of strain gauge leads required

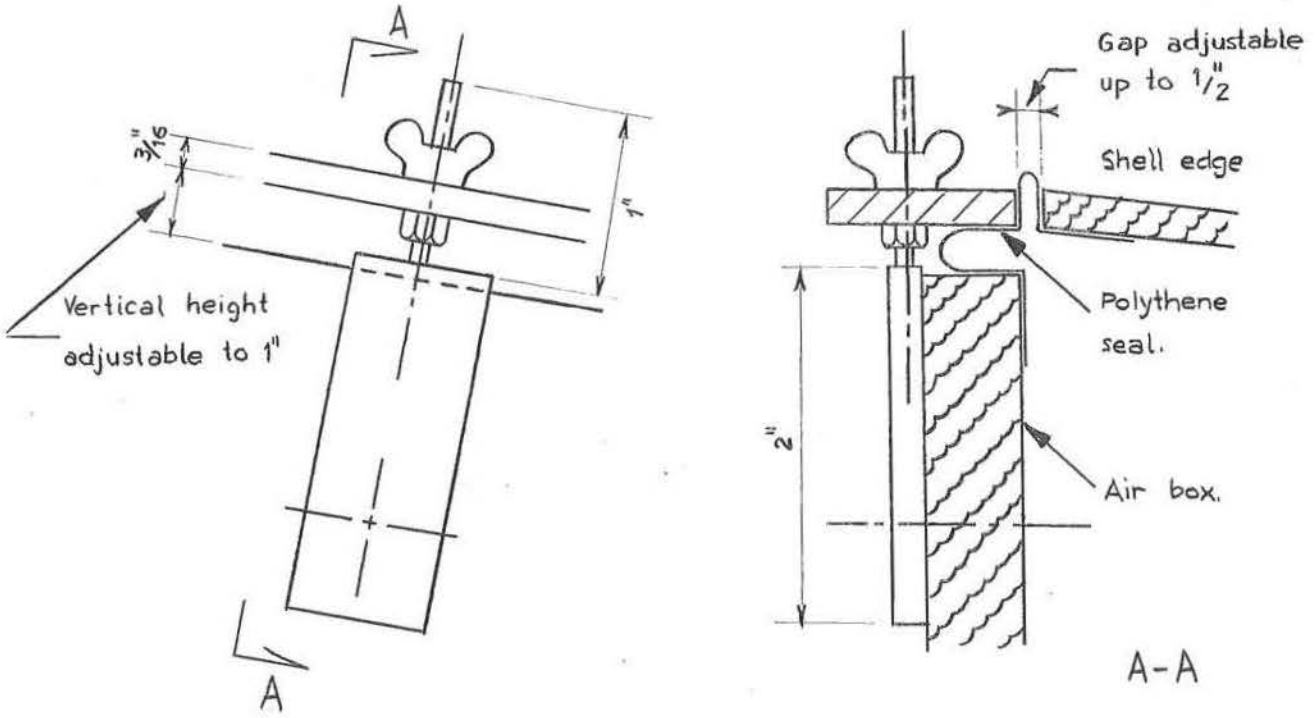

Fig. 12.4 Details of shell edge seal.

on the bottom surface were passed through two cylinders, and sealed for air pressure using wax.

A series of three reducing valves were used to reduce in suitable steps the line air pressure of 100 psi to the working pressure of 0 to 0.5 psi , while stability of pressure over a long period of time was achieved by means of a bleed-off valve. Pressure measurement using a simple manometer was accomplished to an accuracy of 0.05 inch of water (corresponding to less than 1% at normal working pressure of 0.25 psi). The bleed-off also served the purpose of preventing accidental application of over pressure.

The complete load applying system and measuring device was light, portable and could easily be adapted to any other shell form. While all the above requirements are satisfied, it has the additional advantage over past techniques that the ease of construction avoids expensive air bags and piston-cylinder arrangements, as well as eliminating undesirable effects due to discrete point loading.

12.3 THE TEST FRAME

The basic requirements of the test rig were to equilibrate the corner shell reactions without excessive deformations of the frame occurring, and to provide a seal for the base of the air box. The main frame, constructed from 6" x 3½" RSJ section, was in the form of a cornerwise diagonal cross, with two foot 6" x 3½" RSJ vertical uprights butt welded at each of the corners. A sheet of $\frac{3"}{16}$ plate was spot welded to the top surface of the frame, with $\frac{7"}{32}$ holes drilled to carry the $\frac{3"}{16}$ studs from the air box.

Short cantilevers from the corner vertical uprights, also of 6" x 3½" RSJ section, were used to transfer corner shell reactions to the test frame, and by use of 8-⅜" diameter bolts could be adjusted vertically to accommodate any corner arrangement. Extensions to the uprights, required for the base corners were bolted on and could be removed to enable the test frame to be moved through doors. The completed rig, although not

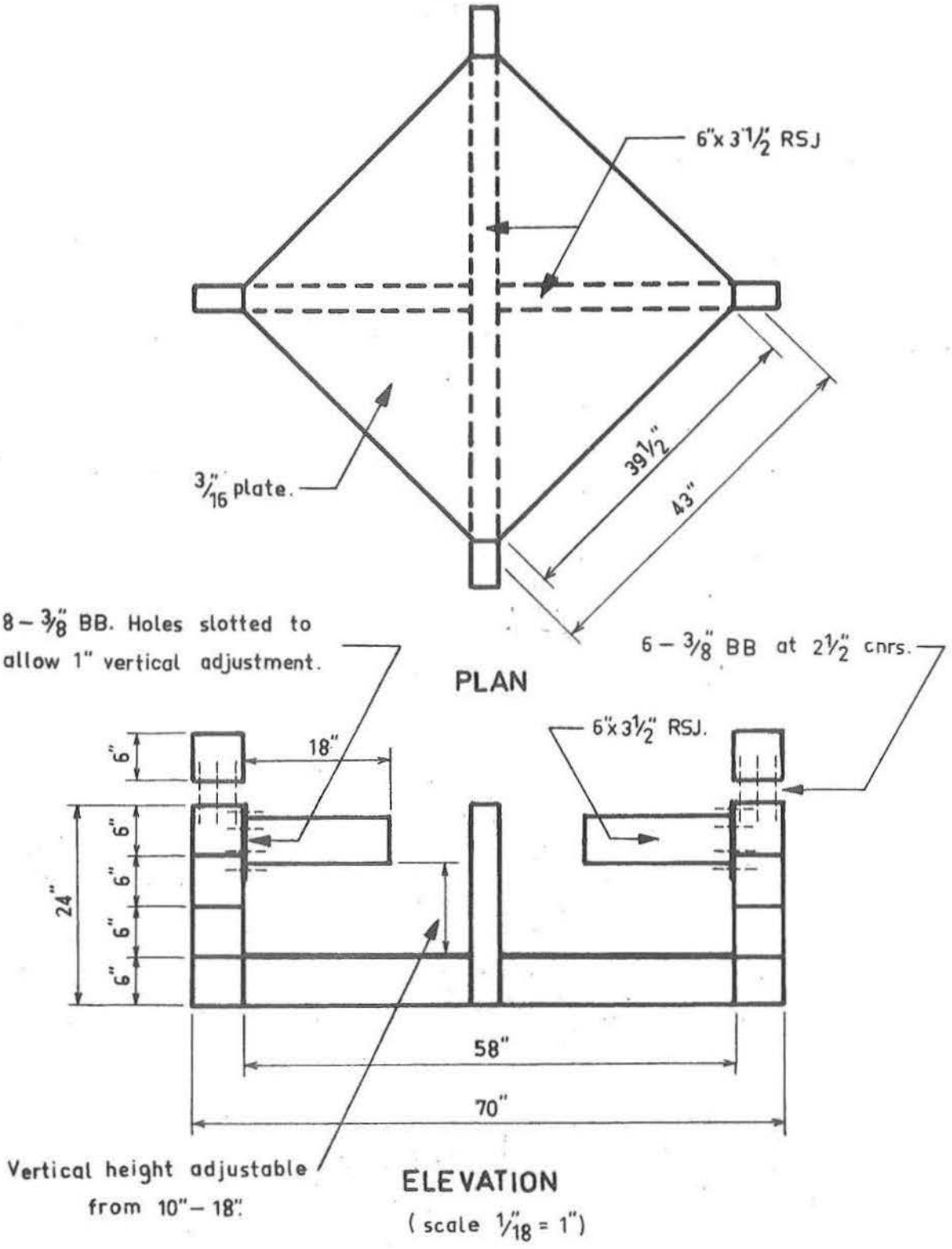

Fig. 12.5 Model support frame. (see plate 12.3).

light, was both portable and adaptable to a large variety of shell shapes. Figure 12.5 and plate 12.3 show the general layout of the test frame.

12.4 THE SUPPORTS

Both corner vertical reactions and base diagonal thrust were to be measured. In conflict with this requirement of finite vertical rigidity, the support mechanisms should be capable of providing complete vertical and rotational rigidity, while at the same time offering no resistance to movement in the horizontal plane. The resulting system of three load cells between two rigid plates, as shown in figure 12.6, is a compromise between these considerations, and has been designed to provide flexural moment rigidity as well as lateral moment stability.

Before the load cells could become operative, the complete weight of the shell, strain gauge wires, corner supports and load cells must be carried by an initial air pressure. Since this weight amounts to approximately 100 lb. it would be necessary to apply a pressure of 0.1 psi at which shell strains become excessive, and increase the chance of error. Also from creep considerations it was necessary to completely stabilise the shell at zero setting, which required leaving the model at 0.1 psi for a period of twenty four hours. An alternative solution was therefore desirable.

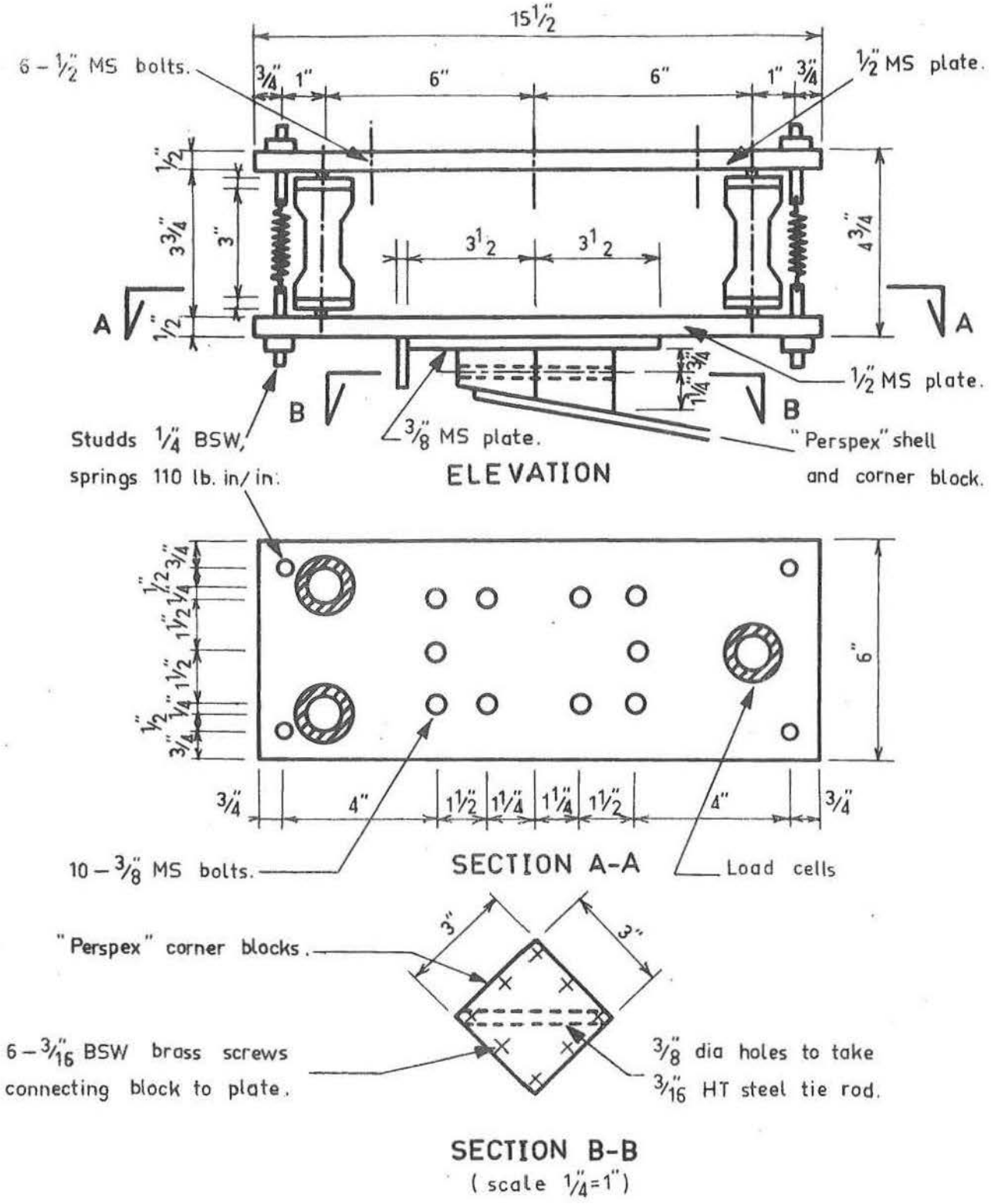

Fig. 12.6 Detail of corner support set up for clamped condition. (see plate 13.1).

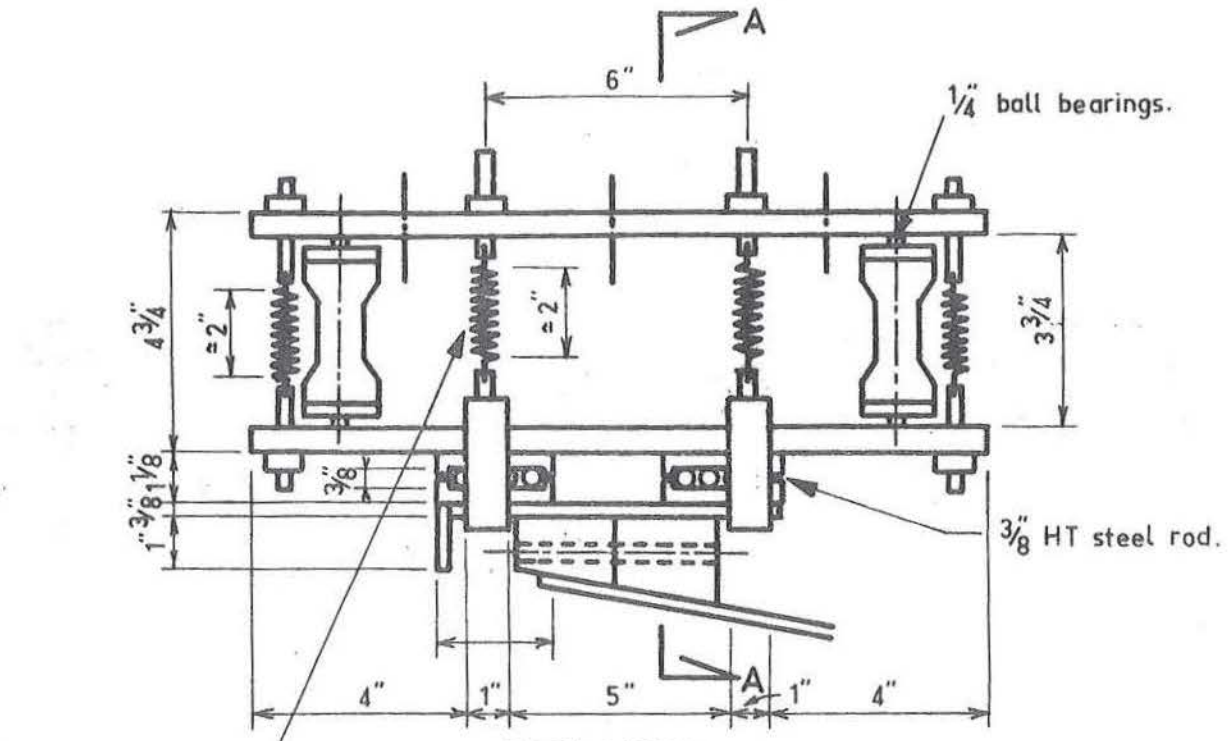

ELEVATION

Studds ¼" BSW,
springs 110 lb. in/in.

Corner studds and
springs not shown.

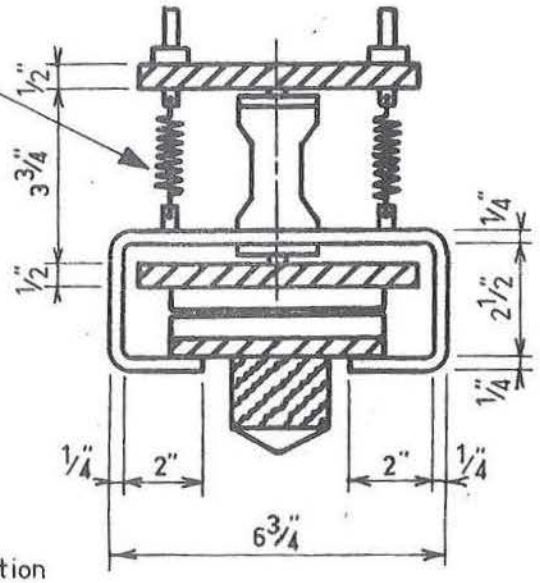

To be read in conjunction
with figure 12.6

SECTION A-A
(Scale ¼" = 1")

Fig. 12.7 Detail of corner support set up for roller condition. (see plates 12.4 & 13.1).

This was afforded by using a form of corner prestressing. Four stiff springs were tensioned so that each load cell had an initial prestress of some 20 lb. With this arrangement, not only was the complete weight of corner supports and shell carried, but also the corner system was capable of providing moment resistance. A further set of springs were required at each corner for simulation of flexurally clamped, but extensionally free corner conditions. Details of both clamped and roller supports are shown in figures 12.6 and 12.7 and plates 12.4 and 13.1 show these as used during testing.

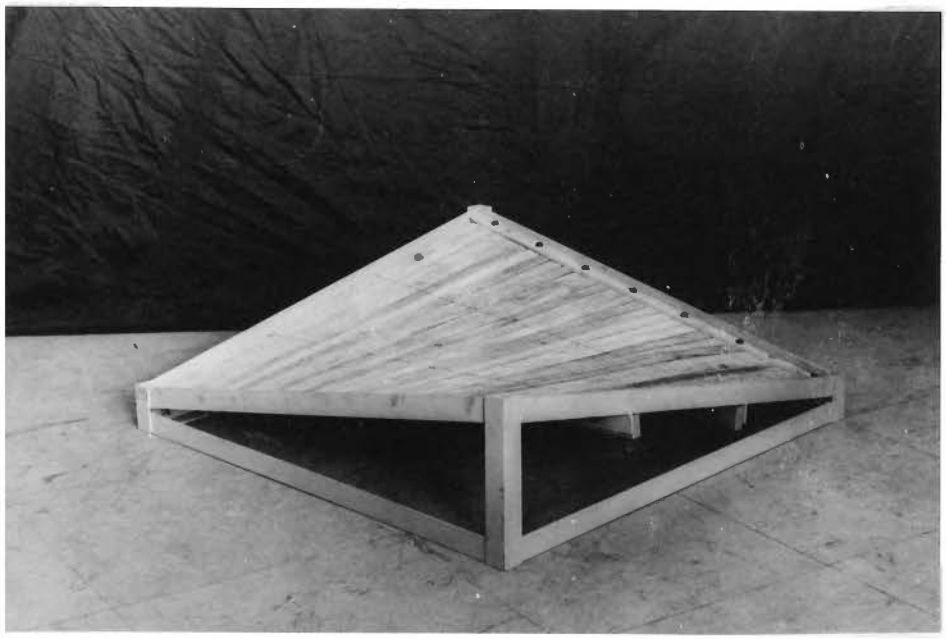

PLATE 12.1 The Mould Frame.

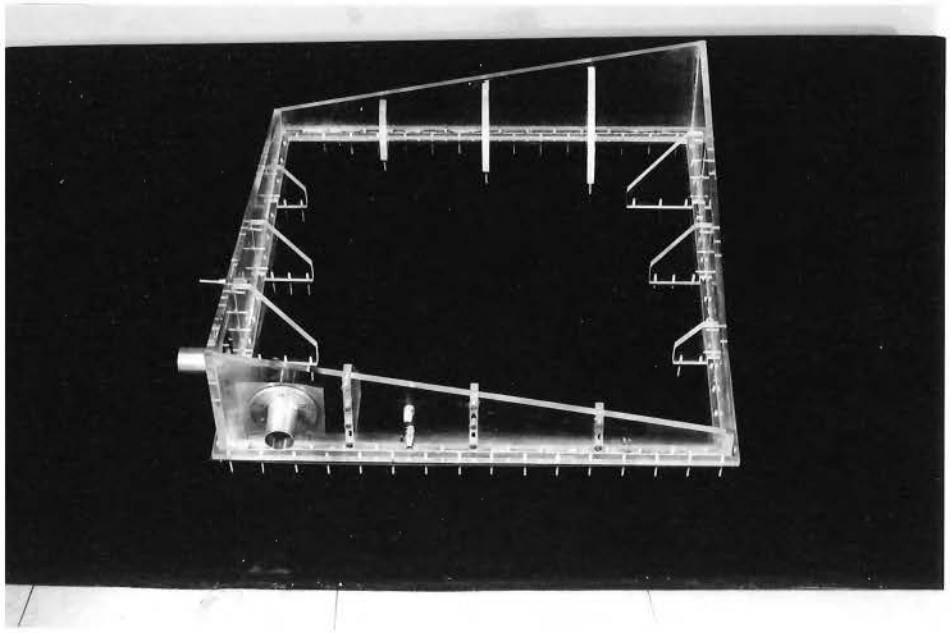

PLATE 12.2 Air Loading Box

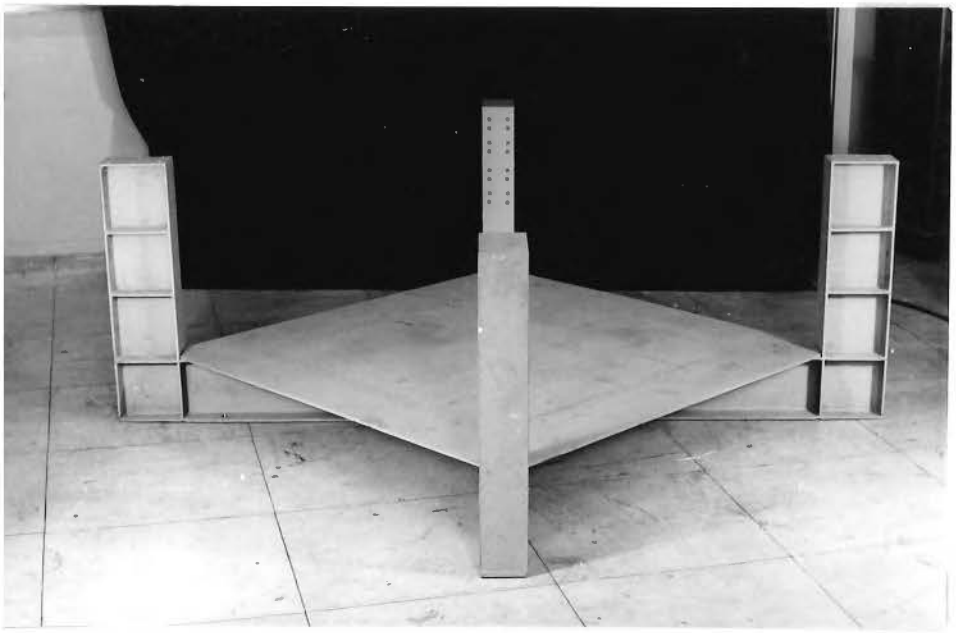

PLATE 12.3 The Test Frame

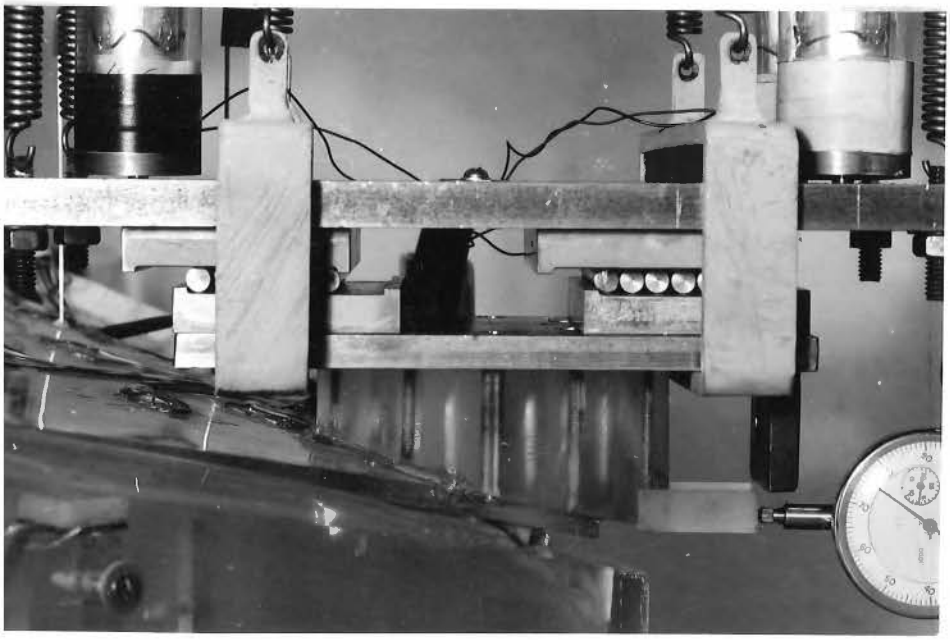

PLATE 12.4 Detail of Apex Corner Roller Support.

CHAPTER THIRTEEN

INSTRUMENTATION AND TEST PROCEDURES

In this chapter, details of the instrumentation and procedures employed for the testing and processing of experimental results are outlined for the model described in the previous chapters.

13.1 INSTRUMENTATION

13.1.1 Strain Measurement

As one of the more important purposes of the present experimental investigation was to determine the influences of boundary and corner conditions, the distribution of electric resistance strain gauges was designed according to this need. Figure 13.1 shows the distribution of rosette gauges in a regular grid pattern, with basic module (except for the edge gauges) of $\frac{1}{8}$ a. This module was chosen so that direct comparisons could be made with theoretical solutions.

Along the shell edge in-plane shear stresses were thought to be negligible, this, and because a limited number of triple rosette gauges were available, determined the use of 90^{o} rosette gauges. By strain gauging the shell over $\frac{1}{4}$ the area, valuable symmetry checks were obtained for the case of symmetric loading and boundary conditions. Additional overall symmetry

checks were achieved by strain gauging the opposite quadrant of the shell in three pertinent locations. In all, a total of 172 gauges were applied to the shell surfaces, providing information at 33 locations.

The active gauges were connected by means of standard length lead wires through two switch boxes to a Budd P-350 portable strain indicator. All gauges were temperature compensated for perspex, had $\frac{1}{8}$" gauge lengths, and were manufactured by the Budd Company. Aluminium compensated gauges mounted on aluminium were used to provide the stable dummy for all gauges. Budd GA1 cement and accelerator were used for cementing strain gauges, while a nitrile rubber solution was used to provide mechanical protection and waterproofing. The resistance and resistance correction properties of the standard lead wires and switch boxes as well as the advantages in the use of Budd gauges may be found in reference [10], while the specifications of gauges used, recommended procedures for application and properties of accessories are outlined in reference [11].

13.1.2 Deflection Measurement

Deflection measurements during preliminary testing using $^{1}/_{1000}$ inch "Mercer" dial gauges were found to be extremely unreliable. This was attributed to the extremely flexible behaviour of certain forms of "perspex" model ruled surface hyperbolic paraboloids. The excessive lateral deformations

caused the dial pointers to be not only more sensitive to small localised surface imperfections, but also increased the possibilities of stem sticking. For this, and other reasons, it was decided that an indirect method of deflection measurement should be used. A number of techniques were considered but the method employing the use of a precise level appeared to be the most suitable.

An automatic Cooke, Troughton and Simms precise level was mounted upon a travelling microscope manufactured by J. Swift and Co. By adjusting the line of sight to coincide with the top of a deflection target, both before and after loading, it was possible to record the true vertical deflection of as many points as were required. Deflection targets were constructed from $^{1}/_{16}$ inch brass rod attached to the shell using Phillip's strain gauge waterproofing compound. The tops of the targets were filed square and coated with blackboard paint so that readings with the white background were made considerably easier. A pencil beam spotlight, with brightness control, was mounted upon the precise level in order that it could be focussed upon the target being sighted at any one time. The advantages of this system, as well as further constructional and operating details, are fully discussed by Bryant [10]. The confined space of the room used for testing made it possible to sight only limited areas of the shell surface. It was this restriction, and that caused by the positions of strain gauges,

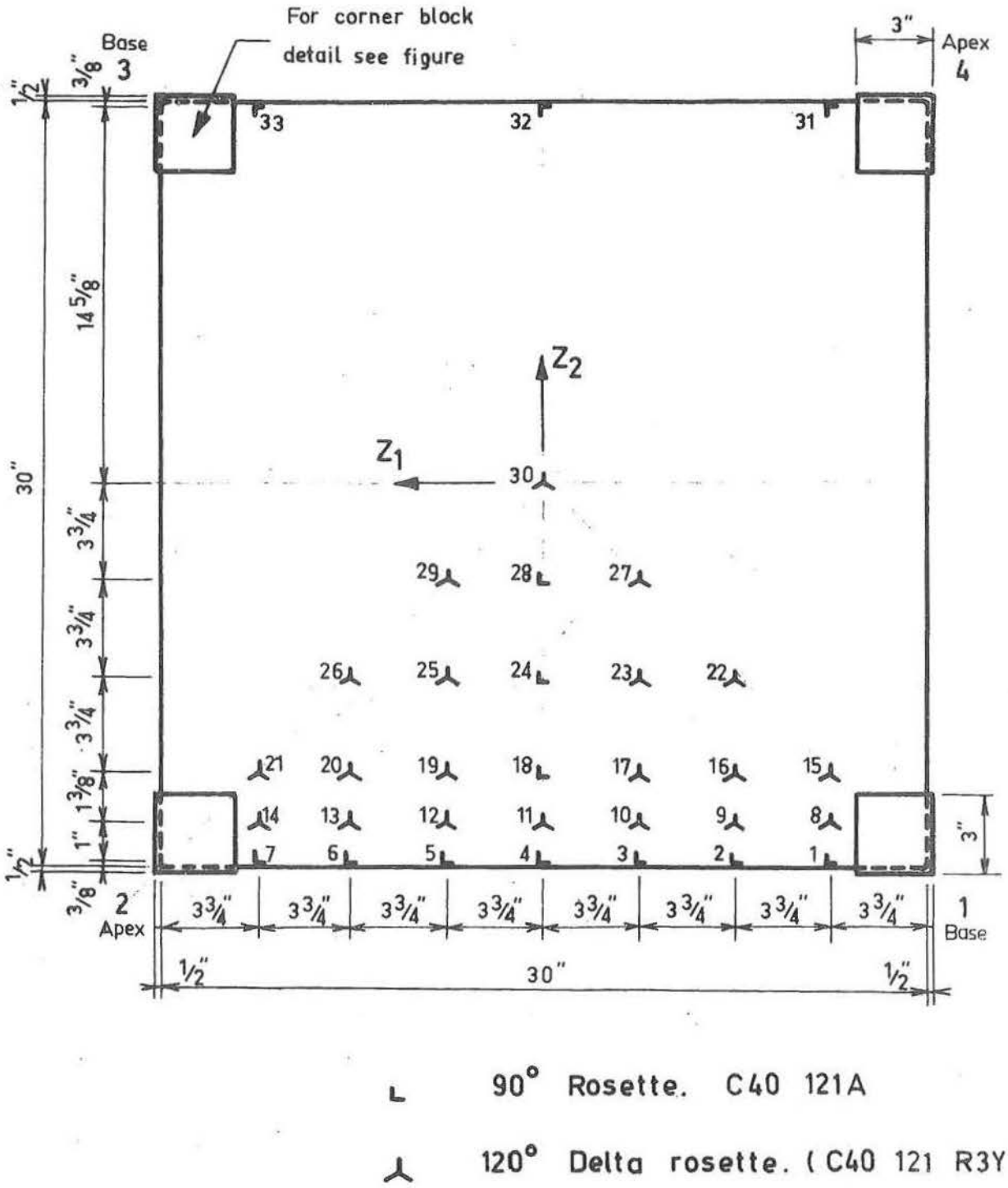

Fig. 13.1 Electric resistance strain gauge distributipn on the shell model. Dimensions are in plan projections of actual surface measurements.

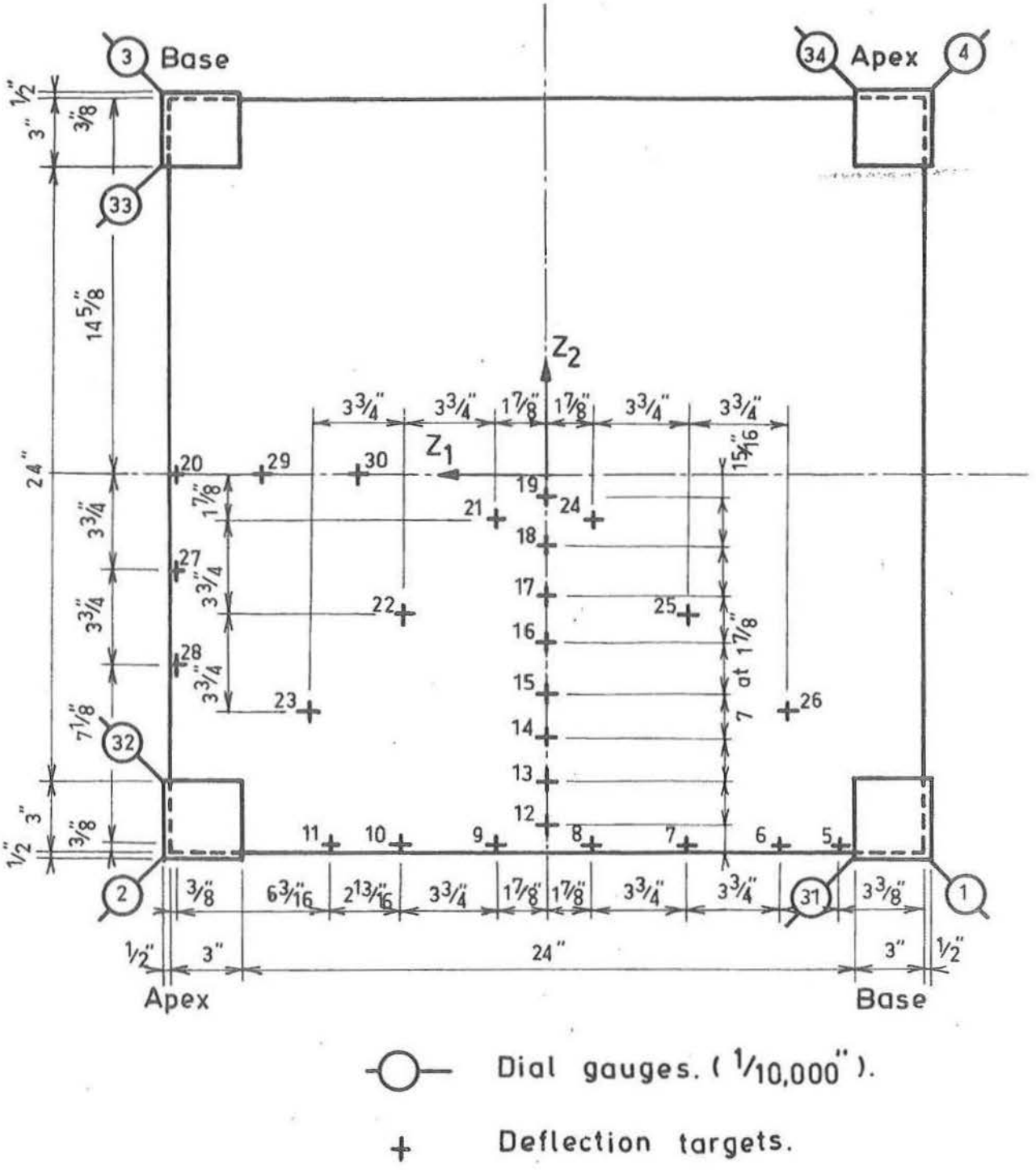

Fig. 13.2 Distribution of deflection targets and dial gauges on the shell model. Dimensions are in plan projections of actual surface measurements.

which determined the distribution of deflection targets.

13.1.3 Load Cells

As indicated in section 12.3 the requirements for the load cells were:

1. To measure accurately the total reactive forces at each corner.

2. Provide rigidity required for the assumption of vertical and rotational fixity.

3. Be capable of transferring no horizontal shear force to test rig.

The resulting load cell solution was designed to have characteristics of 1.25μstrain per pound load. The prestressing springs at corners had characteristics of 1000 μ strain per pound and were therefore of negligible stiffness in comparison with the load cells. A 1½" diameter rod of high strength aluminium alloy was used because of its superior machining properties, and turned to have a gauged wall thickness of 25/1000" at a diameter of one inch.

Four Budd aluminium compensated strain gauges, wired with two pairs of two series connected gauges in parallel were used as active gauges on each load cell to eliminate the effects of bending. As a further precaution against bending, and also to provide the required horizontal mechanism, mild steel caps were seated with $\frac{3}{16}$" diameter ball bearings into

both the top and bottom support plates. In all, thirteen such load cells were constructed, the first acting as a trial and subsequently being used as the stable dummy indicated in section 13.1.1.

13.1.4 Tie Bars

As shown in section B-B of figure 12.6 the base perspex corner blocks were drilled diagonally with $\frac{3}{8}$ inch diameter holes at a line $\frac{3}{4}$ inch above the shell corner. Through this a $\frac{5}{16}$ inch diameter steel rod was passed, and at one end a fixed head was attached and seated through a ball race to an extension of the corner block top plate. At the other end a similarly seated adjustable screw nut arrangement was provided. Forces in the tie rod could be measured by four steel compensated strain gauges connected in a manner similar to the load cells of section 13.1.3 to eliminate bending strains.

At the apex similar short ties were used to transfer diagonal forces back to the test frame. These ties were not strain gauged.

13.1.5 Corner Displacement Measurement

Each corner of the shell was provided with two 1/10,000 inch Mercer dial gauges, one measuring diagonal displacement and the other the displacement perpendicular to the diagonal. With these readings, it was possible to determine whether the

shell corners were displaced symmetrically with respect to the centre of the shell. The major use of the corner displacement gauges was in conjunction with the control of corner displacements. For this control the tie rod was adjusted so that the corner displacements were zero or of a specified magnitude.

13.2 TEST PROCEDURE

After the application of strain gauges, the shell was sealed into the load box and attached to the test rig which had previously been assembled in a room with the temperature stable at $20^{o} \pm .25^{o}$ C and constant humidity. Before the supports, tie rods, dial gauges, deflection targets and other ancillary equipment were added, tests were carried out to ensure that all strain gauges were working satisfactorily. In most cases faulty gauges could be corrected or replaced, but gauges 7 and 59 were in positions which would have necessitated a greal deal of further work to repair. Preliminary tests were also carried out to ensure that air currents induced by opening doors, the refrigeration plant, and flow of compressed air through the air box had no significant adverse effects on strain gauge readings.

13.2.1 Attaching Corner Supports

The cantilever support base, as well as the load cell top plate, were first attached approximately in the correct

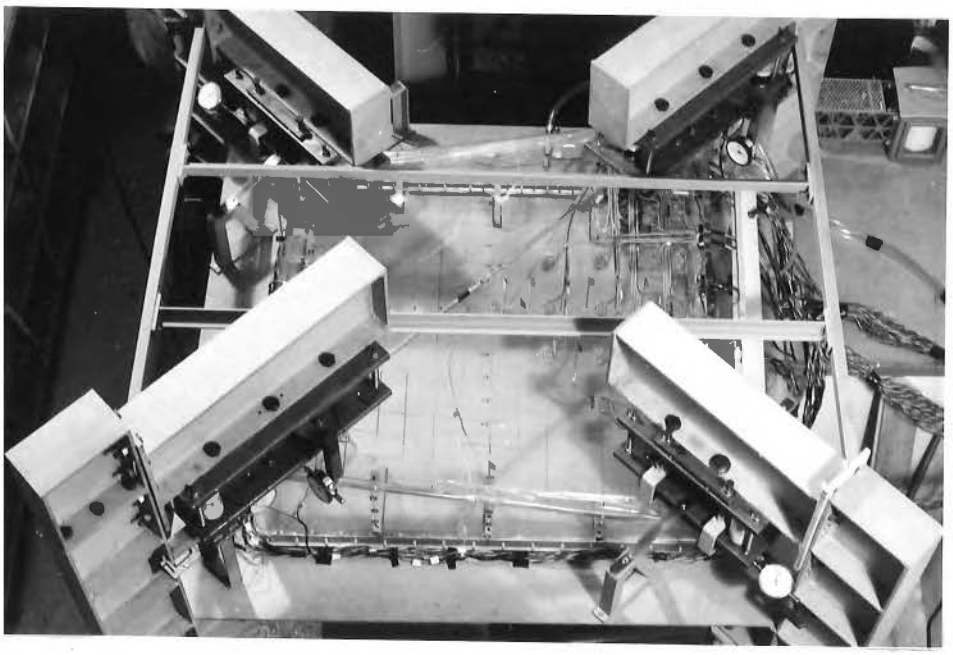

PLATE 13.1 Complete Apex Roller Support.

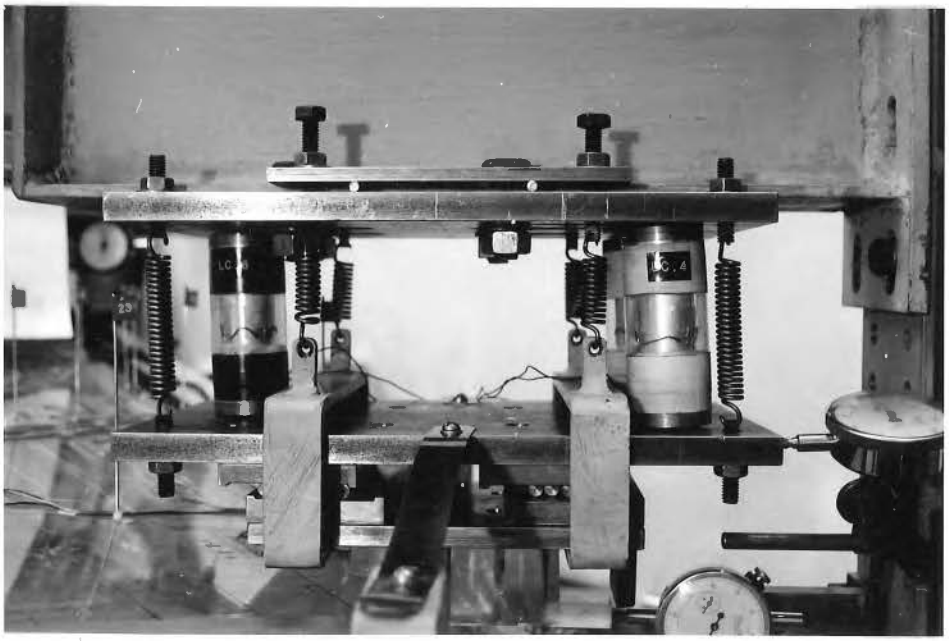

PLATE 13.2 Model Assembled for Testing.

position and the bottom plate was then suspended from this by means of the four corner prestressing springs. Load cells were then positioned, and the springs pretensioned so that each load cell had approximately fifty pound initial compressive force. Depending upon whether a clamped or roller support was required, the support was lowered on to the shell corner blocks and rigidly attached by 8-$\frac{3}{8}$ inch diameter bolts (see figure 12.6), or further pretensioned by four additional springs through two roller arrangements. The prestressing system for the latter support condition was similar to that used for prestressing the load cells (section 12.3), and it is shown in detail in figure 12.7, and as set up for testing in plate 13.1. After the shell weight had been taken, the residual compressive load in the load cells was approximately twenty pounds. Diagonal displacement adjustments, if these were necessary, were made at the same time.

Because of the flexible nature of the shell model and the relatively bulky nature of the support structures, high strains were often incurred within the shell during the attachment of corner supports. As these strains were followed by significant creep strains over the next few hours, the rig was left after assembly for not less than 24 hours in order that all strains be stabilised during testing. With this stable datum it was necessary to devise a load cycle in order that, if creep could not be eliminated, it could at least be

systematically allowed for.

13.2.2 Test Load Cycle

Elms[20] has suggested two possible techniques for the systematic elimination of creep using linear visco-elastic systems. The first consists of a short period (10 seconds) cyclic load technique, where one gauge only is recorded after a constant time interval on each load cycle. In the second, the load is applied for a sufficiently long period of time for further creep strain to be negligible, and therefore all readings can be taken at a consistent effective Young's modulus. Because it was necessary to adjust diagonal displacements after each load increment, this adjustment taking approximately five minutes, the first alternative, especially where a large number of gauges are being employed, would be extremely tedious and time consuming. While the second load cycle would be preferable, it also involves a considerable time for each load cycle.

A compromise was therefore used in which a 15 minute period was allowed to elapse before readings were taken after each change in load. During this period, corner adjustments were made and the majority of creep strain took place. The additional creep between 15 minutes and 60 minutes (the time for taking all readings) although small could be systematically allowed for using the effective modulus of elasticity technique developed in appendix B.

Diagonal displacement loading was applied by adjusting opposite corners in a number of small equal steps, in such a way that each corner was displaced symmetrically with respect to the shell centre. The loading cycle was the same as that used for air pressure loading.

13.2.3 Recording of Results

After loading and at the end of the 15 minutes stabilization period, strain gauge readings were taken with consistent ordering at intervals of 15 seconds. Although warm up drifts were appreciable they were found to be independent of strain magnitude, and could be eliminated by reading all gauges at a 15 second interval after switching (See appendix B). Load cell and tie rod strain readings were taken at the start and end of the load cycle.

The influence of creep upon deflection readings after 15 minutes, when the reading accuracy is remembered, was considered negligible. Thus, although deflection targets were read using a similar time sequence and ordering as strain readings, no creep corrections were made to the final results. These deflection readings were taken simultaneously with strain readings.

Strains were read to the nearest microstrain, while deflection readings could be determined to the nearest 1/1000 inch. The total time required for a complete set of strain

readings was 45 minutes, and therefore 60 minutes for each load cycle. The load was then removed, and a similar procedure carried out for the no load cycle. In all, 8 load cycles could be completed in the course of a normal working day.

13.3 PROCESSING OF RESULTS

All pressure, deflection and strain readings were recorded on computer data sheets, and punched directly on to cards. A series of three computer programmes reduced and processed this data.

13.3.1 Programme 1

Used to list in full the experimental results with means and standard deviations. Reading or recording errors were immediately obvious from inspection.

All readings obtained in pressure tests were reduced to an equivalent 6 inch of water pressure, while corner displacement tests were reduced to a total diagonal displacement of 0.05 inch. This reduction enabled direct comparison to be made between tests with varying pressure or diagonal displacement.

13.3.2 Programme 2

Surface strains $(\epsilon^{t}_{kk}, \epsilon^{b}_{kk})$, $(k = 1,2)$ for double rosette positions and $(\epsilon^{t}_{k2}, \epsilon^{b}_{k1})$, $(k, 1 = 1,2)$ for triple rosette

positions were computed [10] in the z_k, $(k = 1,2)$ coordinate directions. Once again all readings were reduced to the equivalent six inch water pressure or 0.05 inch diagonal displacement.

13.3.3 Programme 3

The value of the fifteen minute effective Young's modulus and Poisson's ratio (obtained in appendix B) were read and used to convert the surface strains $(\epsilon^t_{kl}, \epsilon^b_{kl})$, $(k,l = 1,2)$ to surface stresses $(\sigma^t_{kk}, \sigma^b_{kk})$, $(k = 1,2)$ for double rosettes gauge positions, and $(\sigma^t_{kl}, \sigma^b_{kl})$, $(k = 1,2)$ for triple rosette positions. Stress resultants (n_{kk}, m_{kk}), $(k = 1,2)$ at each of the double rosette locations and (n_{kl}, m_{kl}), $(k,l = 1,2)$ at triple rosette locations were then computed and listed in terms of lb. and inch units, and dimensionless coefficients $(k_{n_{kl}}, k_{m_{kl}})$, $(k,l = 1,2)$ for the cases of air pressure loading. This latter conversion was carried out in order that direct comparisons be made with theoretical solutions of part II. Deflections w_3 were also listed in terms of inch units and coefficients k_{w_3} where applicable. Summarised listings of stress resultants $(k_{n_{kl}}, k_{m_{kl}})$ $(k,l = 1,2)$ for uniform normal load tests (Series A) are given in chapter 14. The stress and moment resultants for the diagonal displacement tests (Series B) were converted to an equivalent 0.05 inch diagonal displacement and listed as (n_{kl}, m_{kl}), $(k,l = 1,2)$ in lb. units. These are also listed in chapter 14.

Load cells and tie rod strain readings were converted using the experimentally obtained calibration factors to give the corresponding forces, and finally total corner reactions were listed. Listings of surface strains for all model tests are given in appendix C.

CHAPTER FOURTEEN

MODEL TEST RESULTS

Summarised results for all model tests are presented. Both the free and beam edged shells, described in section 11.2, are considered under the action of uniformly distributed loading for each of the corner support combinations outlined in section 11.3. In section 14.3 these results are then combined with the results from a number of tests employing controlled diagonal displacement loading, so that a number of independent checks upon model behaviour are made. In section 14.4 the results of one example of each of the free and beam edge model tests are compared with those obtained theoretically from modified forms of the programmes used in chapters 7 to 9. To determine the likely origins of differences between these solutions, section 14.5 employs the results of chapter 9 and certain model test results to estimate the possible effects of a number of shell parameters upon these differences.

For the presentation of experimental results, the z_k axes are orientated as shown in figure 13.1. The experimental shell is consistent with the theoretical shell shown in figure 4.1, except that the base and apex corners are interchanged. This small modification is seen to affect only the in-plane direct stresses.

CORNER CONDITION	TEST NUMBER	
	FREE EDGE	BEAM EDGE
Apex and base clamped flexurally and extensionally	1	4
Apex and base clamped flexurally, Apex free and base clamped extensionally	2	5
Apex and base clamped flexurally and free extensionally	3	6

TABLE 14.1 Numbering system used for naming model tests.

The notation used in naming the model tests is given by a test number, as described in table 14.1, followed by either an "A" to denote uniform surface loading or "B" to denote controlled diagonal displacement loading. Corner displacements are considered positive if the diagonal is shortened, and negative if the diagonal is lengthened.

14.1 RESULTS FOR LOADING 'TYPE A'

In order to be consistent with the results presented in chapters 6 to 10, the results in the following sections are given in terms of the dimensionless coefficients described in chapter 6. For all tests strain gauges 8 and 59 were not operative, so the results at gauge positions 2 and 13 are in general, incorrect. For convenience tables C.1 to C.11 list the

results for models 1A through to 6A in terms of surface strains for a unit normal load.

14.1.1 Free Edged Shell

14.1.1(a) Model Test 1A

The results presented in table 14.2 and 14.5 for this test are the averages of 4 independent test runs which are described further in section 14.5.

The 15% and 60% differences in $k_{n_{11}}$ and $k_{m_{11}}$ between gauge positions 1 and 7 indicate that symmetry about the Z_k, ($k = 1, 2$) axes was not completely achieved (percentages are computed as the difference expressed as a percentage of the larger value). This same conclusion is reached on comparing any other axi-symmetry gauges, or from the corner vertical reactions. A number of possible reasons for this symmetry breakdown, as well as the results of tests designed to eliminate these effects, are further considered in section 14.5. Symmetry about the diagonals is seen to be considerably better with 2.3% and 18.4% differences occurring in the values of $k_{n_{11}}$ and $k_{m_{11}}$ between the gauge positions 1 and 33 respectively. When the high gradient of $k_{m_{11}}$ at the gauge positions 1 and 33 is considered, this seemingly high lack of agreement is not unreasonable. Figure 14.1 shows displacements k_{w_3} and stress and moment resultants at pertinent shell cross-sections.

14.1.1(b) Model Test 2A

Displacements are presented in table 14.5 with table 14.3 listing stress and moment resultants and corner reactive forces.

As in test 1A, gauges 31 to 33 indicate that symmetry about the diagonals was achieved, although moment resultants $k_{m_{11}}$ were considerably lower than at gauge positions 1, 4 and 7. For reasons similar to those given for test 1A, this large absolute difference only affects the actual stress profiles in a small way. From the approximate symmetry in moment resultants $k_{m_{11}}$ about the z_2 axis it can be assumed that the assumption of flexural clamping at the apex was justified. On the other hand, the significant positive stress resultants $k_{n_{11}}$ at gauge positions 7, 14 and 31 indicate that some diagonal thrust was resisted by the corner roller support mechanisms.

It can be observed from a comparison of tables 14.2 and 14.3, or from figure 14.1, that stress and moment resultants for models 1A and 2A are of approximately the same order of magnitude over most of the shell surface. For shell 2A the high positive direct stresses of shell 1A are eliminated at the apex corners. The maximum positive direct stress $k_{n_{11}}$ was for model 2A, 37% that recorded for the maximum of test 1A.

Stress resultants $k_{q_{kk}}$, $(k = 1,2)$ are shown in chapter 10 to be of little significance in carrying applied loading in the free edged shell. It is therefore to be expected that the

high shear and direct stress resultants at the base corners should be accompanied by a redistribution of reactive force to these corners. This is seen to be the case for test 2A, where the apex reactive force is 12% of the base reaction.

14.1.1(c) Model Test 3A

For this model the stress and moment resultants are listed in table 14.4 with the displacements at positions 1 to 30 given in table 14.5.

From a comparison of moment resultants $k_{m_{11}}$ at gauge positions 1, 4, and 7 with those at 33, 32 and 31, it can be concluded that bending action is symmetric about the z_k, $(k=1,2)$ axes and the diagonals. This can be further verified by considering any other pairs of theoretically symmetric gauges such as 14 and 8, or the displacements at target positions 7 and 10, 8 and 9, 23 and 26.

The behaviour of stress resultants $k_{n_{kl}}$, $(k,l = 1,2)$, although symmetric about the diagonals, shows that symmetry about the z_k, $(k = 1,2)$ axes was not achieved. From appendix C it can be seen that the surface stresses result predominantly from plate action. The rather random nature of $k_{n_{11}}$ and $k_{n_{12}}$ is therefore expected, although $k_{n_{12}}$ does show a certain amount of systemmatic behaviour.

The drastic effects upon the stress distribution when the predominant load carrying modes are eliminated are shown by

either comparing tables 14.2 and 14.3 with 14.4, or from figure 14.1. Maximum moment for test 3A is some 700% greater than the maximum moments for model tests 1A or 2A, while the maximum displacement is of the order of 2500% greater. Virtually all load is carried by plate action so that normal displacements and moments are of the same order as the corresponding flat plate. The impractical nature of this support condition is best illustrated by considering a typical concrete shell of span L = 50 feet loaded by self weight. The maximum central deflection is 18 inch, and the bending stresses at the shell centre are $\pm$ 1300 psi.

14.1.2 Beam Edged Shell

14.1.2(a) Model Test 4A

The stress and moment resultants presented in table 14.6 and the displacements shown in table 14.9 are the averages of three independent test runs. Corner reactions and tie forces were obtained in run 1 only (see appendix C).

The poor agreement between $k_{n_{11}}$ and $k_{m_{11}}$ at positions 1 and 7 again indicates that symmetry about the z_k, ($k = 1,2$) axes was not completely achieved. The general agreement of $k_{n_{11}}$ and $k_{m_{11}}$ between gauge positions 1, 4 and 7 and 33, 32 and 31 indicates that symmetry about the shell diagonals was achieved. Displacement k_{w_3} and stress and moment resultants are presented at pertinent shell cross-sections in figure 14.2.

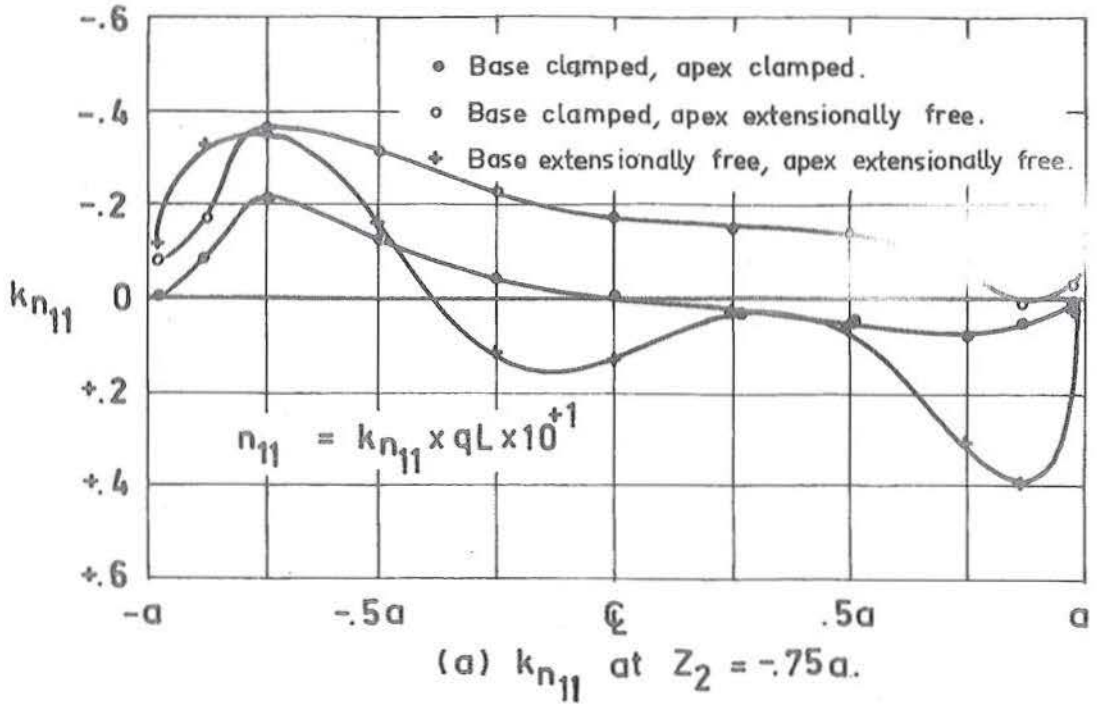

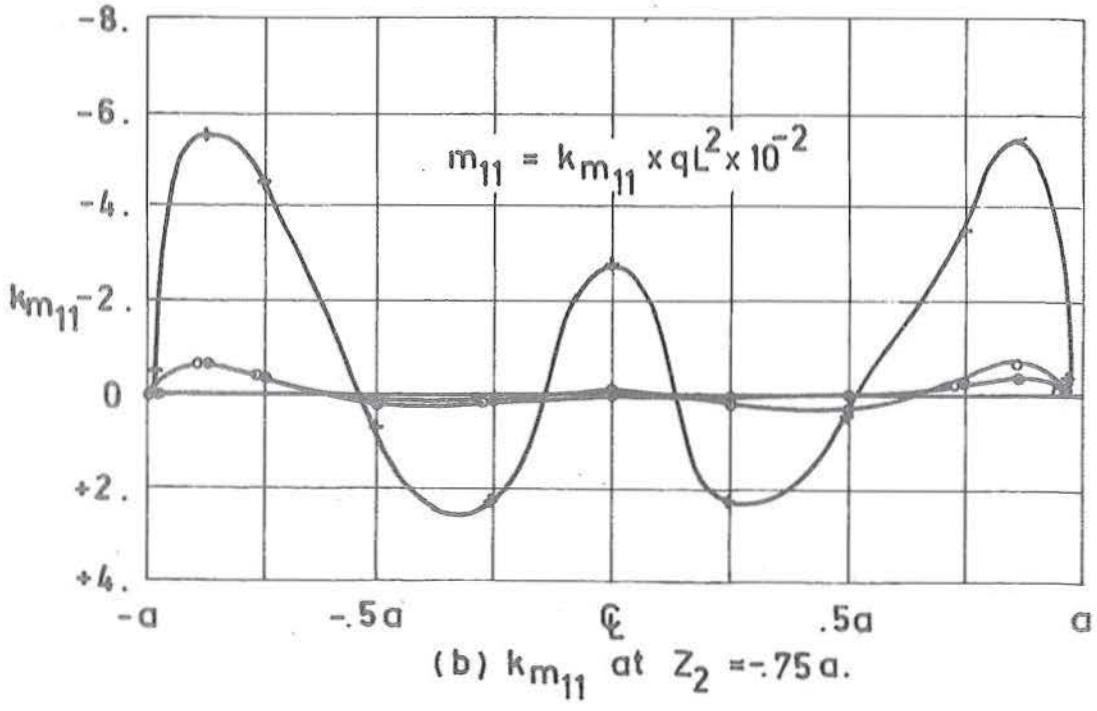

Fig. 14.1 Ruled surface hyperbolic paraboloid with free edges. Influence of corner constraint on experimental behaviour.

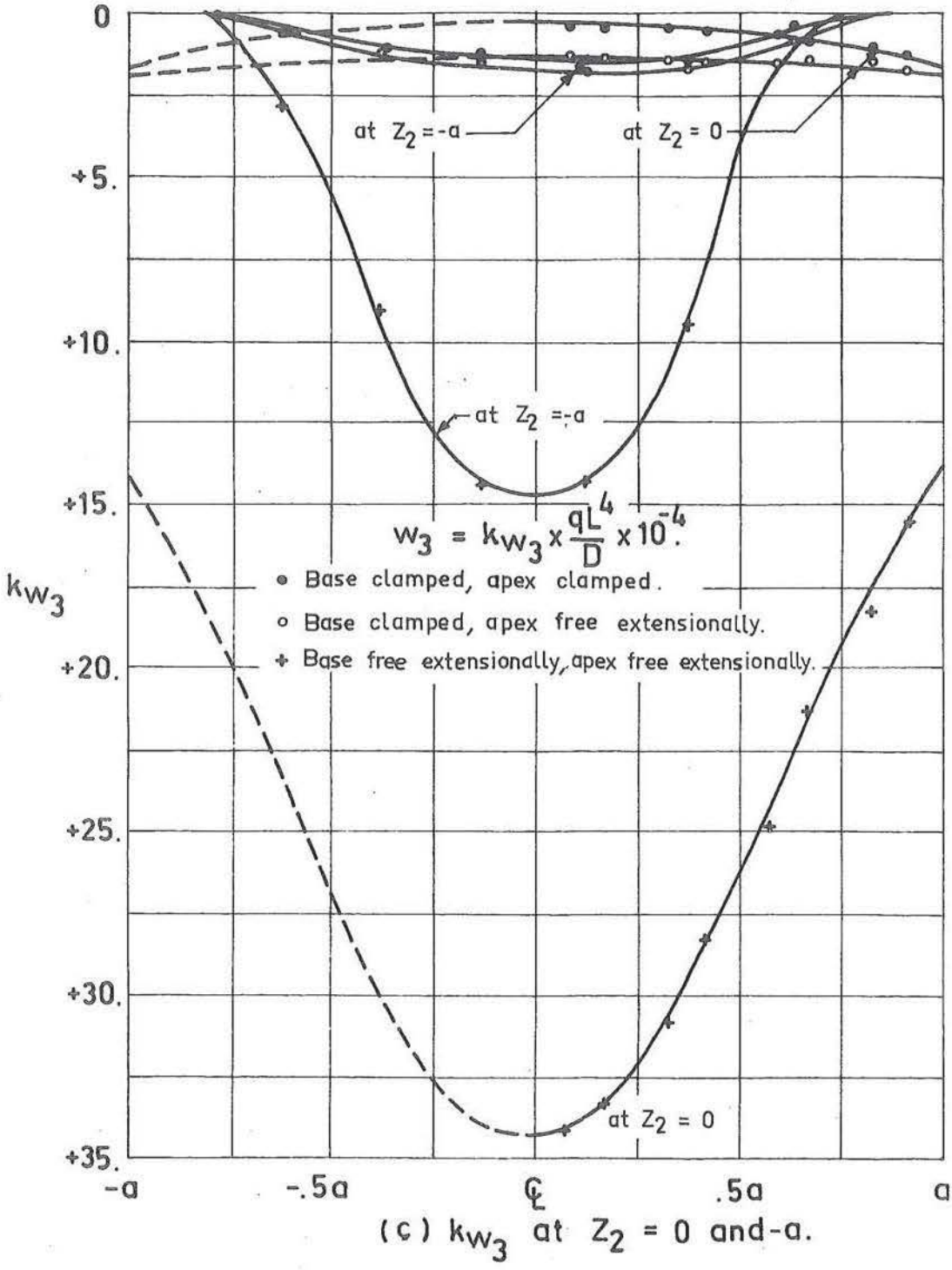

Fig. 14.1 (continued) Ruled surface hyperbolic paraboloid with free edges. Influence of corner constraint on experimental behaviour.

RULED SURFACE HYPERBOLIC PARABOLOID.

(MODEL TEST 1 A.)

FREE EDGES, WITH APEX AND BASE CORNERS CLAMPED FLEXURALLY AND EXTENSIONALLY.

GAUGE POS	DIRECT STRESSES (LB/IN)			BENDING STRESSES (LB.IN/IN)		
	$k_{n_{11}}$	$k_{n_{22}}$	$k_{n_{12}}$	$k_{m_{11}}$	$k_{m_{22}}$	$k_{m_{12}}$
1	-5.999	.770		-.0108	-.0010	
2	-1.270	1.908		-.0029	-.0019	
3	-4.037	.331		.0009	0.0000	
4	-1.575	.103		.0013	0.0000	
5	1.283	-.062		.0021	0.0000	
6	4.064	-.326		.0021	0.0000	
7	5.087	-.502		-.0043	-.0002	
8	-6.155	-1.211	.737	-.0059	-.0061	.0004
9	-3.526	.514	.522	.0021	-.0005	-.0012
10	-2.195	.226	.910	.0008	-.0005	-.0006
11	-.720	.113	1.124	.0006	-.0006	-.0001
12	.822	.044	1.211	.0013	-.0003	.0005
13	2.122	-.153	.969	.0011	-.0006	.0015
14	3.344	.582	.801	-.0039	-.0038	.0006
15	-1.972	-2.149	1.562	-.0030	-.0037	-.0032
16	-1.169	.601	1.197	.0009	-.0011	-.0015
17	-.459	.240	.523	.0004	-.0009	-.0017
18	.009	.178		0.0000	.0014	
19	.233	.085	1.577	.0004	-.0014	.0005
20	.520	-.273	1.344	.0001	-.0012	.0016
21	.822	.928	1.047	-.0028	-.0025	.0019
22	.575	.538	1.454	-.0008	-.0002	-.0011
23	.518	.455	1.429	-.0004	-.0013	-.0003
24	.199	.195		.0002	.0014	
25	-.225	-.018	1.354	-.0007	-.0017	.0003
26	-.390	-.555	1.326	-.0010	-.0012	.0010
27	.256	.315	1.235	-.0006	-.0003	0.0000
28	.060	.147		.0004	.0005	
29	-.115	-.055	1.087	-.0007	-.0006	.0001
30	-.054	-.013	1.032	-.0001	0.0000	.0001
31	4.182	-.327		-.0046	0.0000	
32	-1.287	-.022		.0010	.0001	
33	-5.863	.302		-.0090	-.0009	

CORNER REACTIONS (LBS)

1	2	3	4	TOTAL
66.5	32.0	63.8	32.9	195.3 (196.0)

TIE FORCE (LBS)

167.0

TABLE 14.2 Stress and moment resultants for model test 1A.

RULED SURFACE HYPERBOLIC PARABOLOID.

(MODEL TEST 2 A.)

FREE EDGES, WITH BASE CORNERS CLAMPED FLEXURALLY AND EXTENSIONALLY, APEX CORNERS CLAMPED FLEXURALLY AND FREE EXTENSIONALLY.

GAUGE POS	DIRECT STRESSES (LB/IN)			BENDING STRESSES (LB.IN/IN)		
	$k_{n_{11}}$	$k_{n_{22}}$	$k_{n_{12}}$	$k_{m_{11}}$	$k_{m_{22}}$	$k_{m_{12}}$
1	-7.727	.923		-.0108	-.0009	
2	-1.895	2.059		-.0039	-.0020	
3	-5.176	.509		.0005	-.0001	
4	-3.316	.381		.0017	-.0001	
5	-.655	.109		.0028	0.0000	
6	1.876	-.090		.0032	0.0000	
7	1.796	-.416		-.0074	-.0007	
8	-8.639	-1.658	1.676	-.0063	-.0067	.0011
9	-5.121	.583	.509	.0013	-.0009	-.0007
10	-3.790	.327	.673	.0007	-.0005	-.0004
11	-2.590	.312	.936	.0011	-.0006	-.0001
12	-1.098	.199	1.152	.0021	-.0003	.0007
13	0.000	-.601	.746	.0028	0.0000	.0016
14	.272	.144	-.272	-.0063	-.0076	-.0013
15	-3.718	-3.535	2.696	-.0039	-.0047	-.0029
16	-3.189	.199	1.275	0.0000	-.0017	-.0011
17	-2.313	.272	.399	.0004	-.0009	-.0015
18	-1.764	.330		-.0007	.0010	
19	-1.610	.183	1.446	.0013	-.0007	.0006
20	-1.518	-.530	.969	.0025	0.0000	.0020
21	-.823	-.786	-.146	-.0032	-.0030	.0025
22	-.549	-.347	1.446	-.0011	-.0001	-.0010
23	-.746	.218	1.275	0.0000	-.0005	-.0003
24	-.798	.363		-.0008	.0001	
25	-1.138	-.146	1.249	.0006	.0004	0.0000
26	-1.084	-1.249	1.066	.0012	.0019	.0008
27	.238	.183	1.175	0.0000	.0006	-.0 2
28	.147	.424		-.0008	-.0011	
29	.184	0.000	1.130	.0005	.0014	-.0005
30	.239	.276	1.092	.0013	.0012	-.0006
31	1.281	.035		-.0074	0.0000	
32	-3.101	.166		.0007	-.0001	
33	-8.787	.275		-.0060	-.0004	

CORNER REACTIONS (LBS)

1	2	3	4	TOTAL
91.5	12.6	79.0	9.0	192.4 (196.0)

TIE FORCE (LBS)

268.0

TABLE 14.3 Stress and moment esultants for model test 2A.

RULED SURFACE HYPERBOLIC PARABOLOID.

(MODEL TEST 3 A.)

FREE EDGES, WITH BASE AND APEX CORNERS CLAMPED FLEXURALLY AND FREE EXTENSIONALLY.

GAUGE POS	DIRECT STRESSES (LB/IN)			BENDING STRESSES (LB.IN/IN)		
	$k_{n_{11}}$	$k_{n_{22}}$	$k_{n_{12}}$	$k_{m_{11}}$	$k_{m_{22}}$	$k_{m_{12}}$
1	-6.593	-1.153		-.0763	-.0044	
2	1.019	-2.296		-.0033	-.0033	
3	9.970	-1.330		.0228	-.0015	
4	8.987	-1.001		.0297	-.0013	
5	5.230	-.436		.0205	-.0013	
6	3.426	.126		-.0047	-.0016	
7	3.339	.144		-.0505	-.0035	
8	-10.098	3.316	1.238	-.0566	-.0556	.0267
9	4.666	-1.293	2.515	.0044	-.0071	.0030
10	3.827	-.910	.199	.0231	-.0008	.0005
11	3.216	-.219	-1.452	.0272	-.0007	.0024
12	1.061	-.164	-1.647	.0206	-.0018	.0023
13	.309	3.609	-.746	-.0001	-.0046	-.0030
14	1.129	-3.973	-.546	-.0494	-.0560	-.0281
15	3.627	6.052	-.381	-.0447	-.0399	.0006
16	1.603	-1.403	.601	.0066	-.0076	-.0005
17	-1.166	-1.676	.673	.0225	.0010	-.0007
18	-1.323	-.569		-.0295	-.0019	
19	-.329	.127	-1.629	.0225	0.0000	.0025
20	-.512	-.072	-.767	.0041	-.0078	0.0000
21	-3.075	-.878	-1.481	-.0358	-.0367	-.0021
22	-2.672	-1.115	-1.464	.0072	.0090	-.0030
23	-4.612	-2.989	-.473	.0223	.0129	.0002
24	-5.155	-2.432		-.0327	-.0164	
25	-2.573	.164	-.238	.0272	.0163	.0021
26	-1.029	.035	-.164	.0118	.0109	.0022
27	-1.966	-1.103	-.752	.0234	.0259	-.0002
28	-2.270	-.683		-.0377	-.0323	
29	-.555	-.110	.573	.0330	.0334	.0012
30	1.223	.463	.407	.0353	.0368	-.0008
31	4.959	-.878		-.0536	-.0013	
32	1.292	.073		.0297	-.0012	
33	-6.066	-.569		-.0553	-.0037	

CORNER REACTIONS (LBS)

1	2	3	4	TOTAL
71.1	44.6	20.6	32.9	169.4 (196.0)

TEST FORCE (LBS)

TABLE 14.4 Stress and moment resultants for model test 3A.

RULED SURFACE HYPERBOLIC PARABOLOID.

(MODEL TESTS 1A, 2A, 3A)

NORMAL DISPLACEMENTS COEFFICIENTS k_{w_3}.

TEST	DISPLACEMENT TARGET LOCATION.					
	5	6	7	8	9	10
1A	-.0194	.5317	1.1046	1.3462	1.3872	1.1844
2A	.1067	.5954	1.1844	1.6148	1.7961	1.6051
3A	-.1100	2.7993	9.0841	14.3106	14.2556	9.4983

TEST	DISPLACEMENT TARGET LOCATION.					
	11	12	13	14	15	16
1A	.3019	1.3192	1.0420	.7939	.6137	.4907
2A	.7961	1.7411	1.5145	1.4466	1.5339	1.4304
3A		15.5469	18.3462	21.2750	24.8511	28.2912

TEST	DISPLACEMENT TARGET LOCATION.					
	17	18	19	20	21	22
1A	.4304	.3872	.3430	1.5285	.4196	.4454
2A	1.3786	1.3592	1.2459	1.2135	1.2815	1.3915
3A	30.7734	33.2847	34.1035	17.5145	33.5760	26.0161

TEST	DISPLACEMENT TARGET LOCATION.					
	23	24	25	26	27	28
1A	.4260	.3980	.4595	.5113	1.2848	.7232
2A	1.1488					
3A	10.8996	32.6472	24.0485	10.9126	13.8252	6.4466

TEST	29	30
1A	.8732	.5437
3A	22.2718	28.8058

TABLE 14.5 Normal displacements for model tests 1A, 2A, 3A.

A comparison of either tables 14.2 and 14.6, or figures 14.1 and 14.2, indicates that introduction of an edge beam support considerably stiffens the shell (maximum vertical displacement of model 4A being 39% of 1A). The edge beam also has the effect of reducing moment resultants within the body of the shell (for example $k_{m_{11}}$ at gauge position 8 for the model 4A is 25% that for model 1A). Direct stress resultants are seen to be essentially constant.

14.1.2(b) Model Test 5A

Displacements are given in table 14.9 and stress and moment resultants in table 14.7. For this test vertical reactions and tie rod forces were not measured, and a modification to the corner conditions indicated by (2) in section 11.3 was used. The base was not clamped extensionally, but was provided with rollers while the apex was effectively clamped. In figure 14.2 this solution is transformed in order that the results be consistent with those given for model 2A in figure 14.1.

The large differences in $k_{n_{11}}$ and $k_{m_{11}}$ between gauge positions 1, 4 and 7 and gauge positions 33, 32 and 31, indicate the extreme lack of symmetry in model behaviour. The provision of the roller support to the beam edge shell has a similar effect as the same provision on the free edged shell. Direct tensile stresses are considerably reduced, while at the same time the

shell stiffness is affected to a small degree. Figures 14.1 and 14.2 also demonstrate that all comments concerning the influence of edge beams made in section 14.1.2(a) apply equally to the present shell model. The order of bending stresses in model 5A is considerably reduced compared to that of 2A, while the efficient in-plane stresses are only slightly affected.

14.1.2(c) Model Test 6A

As in model test 3A, the increase in both moment resultants and displacements for test 6A over those of 4A or 5A, is apparent from tables 14.8 and 14.9 and figure 14.2. In the present test the large increases in moments are confined to the edge beams, while the shell moment resultants $k_{m_{11}}$ are affected to a smaller degree. It is therefore concluded that although the addition of an edge beam considerably improves the behaviour of this particular corner support condition, the adverse effects of these supports still cause this particular system to be an impractical solution. For the practical example considered in section 14.1.1(c) the maximum deflection is 5 inches, and the bending stresses at the shell centre are $\pm$ 300 psi.

14.1.3 Conclusions

The influence of uniform normal loading is shown for shells with varying edge and corner support conditions. The conclusions for the influence of corner conditions are in

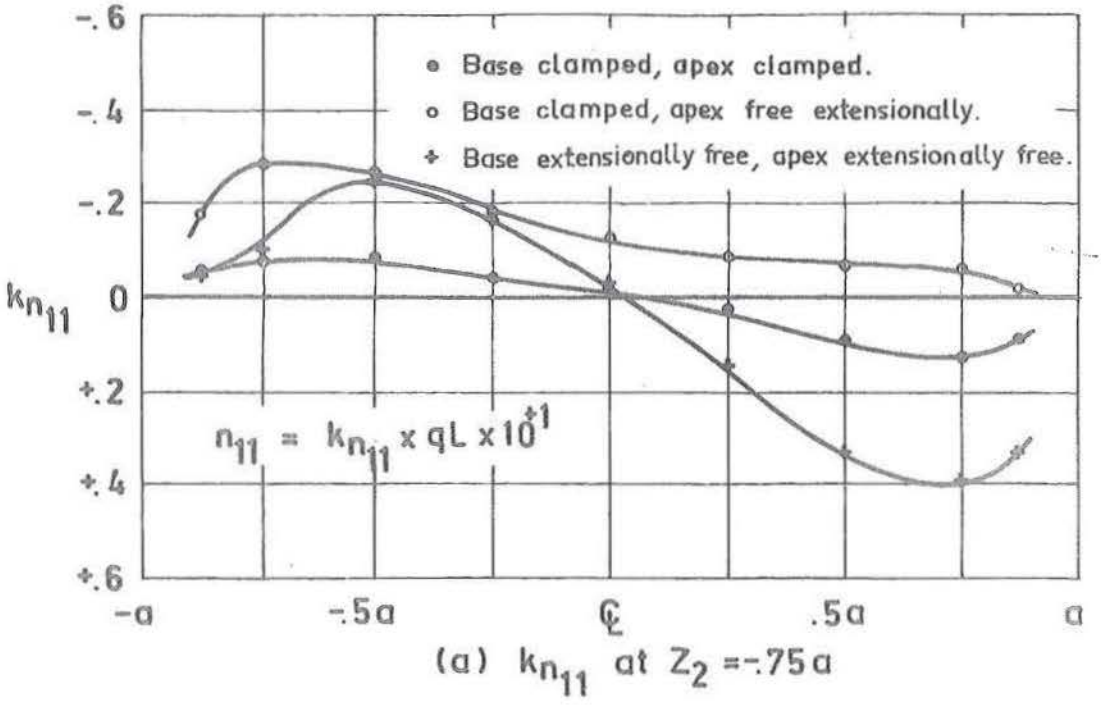

(a) $k_{n_{11}}$ at $Z_2 = -.75a$

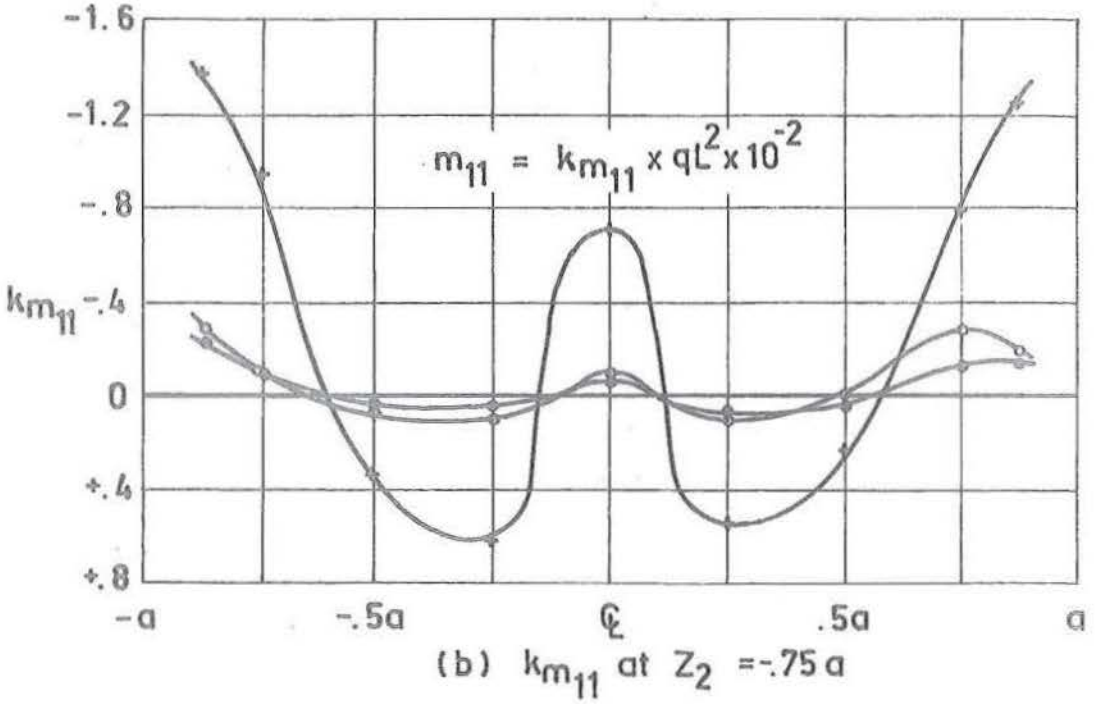

(b) $k_{m_{11}}$ at $Z_2 = -.75a$

Fig. 4.2 Ruled surface hyperbolic paraboloid with beam edges. Influence of corner constraint on experimental behaviour.

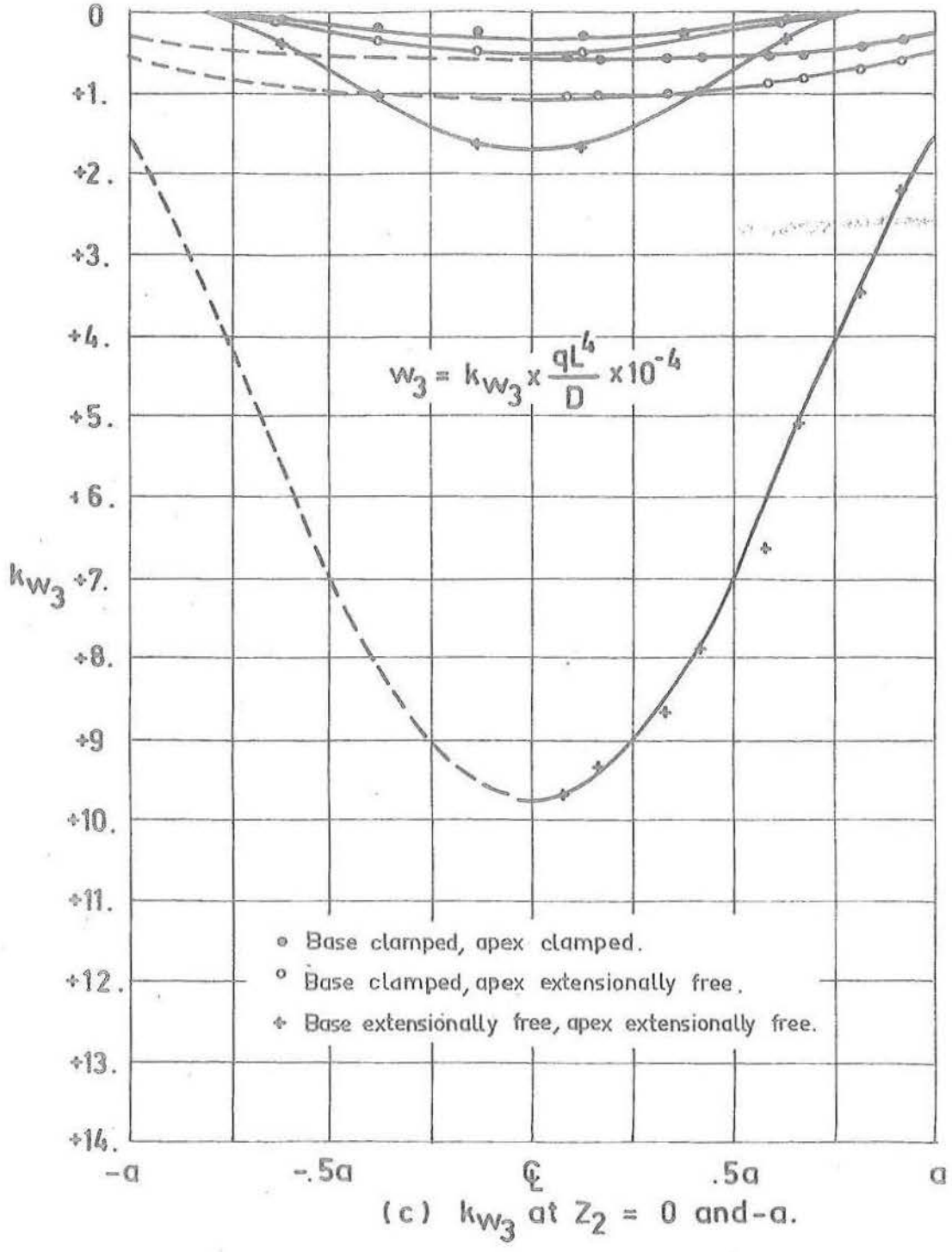

Fig. 4.2 (continued) Ruled surface hyperbolic paraboloid with beam edges. Influence of corner constraint on experimental behaviour.

RULED SURFACE HYPERBOLIC PARABOLOID.

(MODEL TEST 4 A.)

BEAM EDGES, WITH APEX AND BASE CORNERS CLAMPED FLEXURALLY AND EXTENSIONAL Y.

GAUGE POS	DIRECT STRESSES (LB/IN)			BENDING STRESSES (LB.IN/IN)		
	$k_{n_{11}}$	$k_{n_{22}}$	$k_{n_{12}}$	$k_{m_{11}}$	$k_{m_{22}}$	$k_{m_{12}}$
1	-9.992	.062		-.0600	.0013	
2	-3.141	1.194		-.0236	-.0085	
3	-1.119	.144		.0192	-.0052	
4	2.226	-.082		.0348	-.0028	
5	4.657	-.042		.0348	-.0028	
6	5.544	.128		.0170	-.0008	
7	5.171	-.192		-.0354	.0024	
8	-1.354	-.479	1.408	-.0015	-.0020	.0009
9	-1.104	.053	1.037	-.0001	-.0007	.0002
10	-.837	.053	.953	.0002	0.0000	0.0000
11	-.819	.081	1.184	.003	.0002	0.0000
12	.212	-.170	.664	.0005	.0004	0.0000
13	1.311	.193	.478	.0002	-.0001	-.0002
14	2.836	.904	1.014	-.0006	-.013	.0005
15	-.746	-.782	1.500	-.0009	-.0009	.0002
16	-.441	-.019	.872	-.0004	.0003	0.0000
17	-.412	.018	.126	.0005	.0007	-.0014
18	-.073	-.078		-.0006	-.0009	
19	.285	-.248	.999	.0007	.0009	0.0000
20	1.194	.140	.926	-.0005	.0003	0.0000
21	1.304	1.359	1.304	-.0011	-.0006	0.0000
22	-.163	-.115	1.225	.0006	.0007	-.0002
23	.061	.266	1.342	.0003	.0007	-.0001
24	.150	-.090		-.0003	-.0006	
25	.188	-.067	1.291	.0001	.0002	0.0000
26	.195	.062	1.242	.0003	.0002	.0002
27	.061	-.061	1.365	.0002	.0002	-.0001
28	.024	-.074		.0002	0.000	
29	.006	-.208	1.321	0.0000	.0001	.0001
30	-.098	-.208	1.259	0.0000	0.000	0.0000
31	5.777	.436		-.0768	.0095	
32	1.199	-.566		.0275	-.0062	
33	-1.416	.144		-.0715	.0022	

CORNER REACTIONS (LBS)

1	2	3	4	TOTAL
53.5	40.2	52.1	39.5	186.2 (196.0)

TIE FORCE (LBS)

166.1

TABLE 14.6 Stress and moment resultants for model test 4A.

RULED SURFACE HYPERBOLIC PARABOLOID.

(MODEL TEST 5 A.)

BEAM EDGES, WITH BASE CORNERS CLAMPED FLEXURALLY AND EXTENSIONALLY, APEX CORNERS CLAMPED FLEXURALLY AND FREE EXTENSIONALLY.

GAUGE POS	DIRECT STRESSES (LB/IN)			BENDING STRESSES (LB.IN/IN)		
	$k_{n_{11}}$	$k_{n_{22}}$	$k_{n_{12}}$	$k_{m_{11}}$	$k_{m_{22}}$	$k_{m_{12}}$
1	-3.158	0.000		-.0759	-.0015	
2	.667	.243		.0018	.0051	
3	5.603	.061		.0440	.0075	
4	8.701	-.250		.0653	.0039	
5	10.447	-.255		.0547	.0031	
6	10.916	-.518		.0179	-.0016	
7	11.459	-.707		-.0557	-.0043	
8	1.293	.126	.583	-.0017	-.0028	.0013
9	.509	-.016	.838	0.0000	-.0009	.0002
10	.381	-.072	.910	.0005	-.0002	0.0000
11	.789	-.072	.826	.0009	.0003	-.0002
12	1.629	-.273	.621	.0009	.0006	-.0003
13	3.061	.564	.710	.0003	-.0003	-.0005
14	5.504	1.730	2.169	-.0010	-.0016	-.0001
15	.618	.327	.381	-.0010	-.0007	.003
16	.655	.090	.801	.0008	.0005	0.0000
17	.855	-.126	.181	.0011	.0011	-.0013
18	1.212	-.312		-.0013	-.0012	
19	1.738	-.329	1.098	.0012	.0010	-.0002
20	2.672	.366	1.446	-.0001	-.0002	-.0002
21	2.746	2.836	2.489	-.0027	-.0017	.0002
22	.566	.530	1.061	.0013	.0014	-.0002
23	.801	.181	1.256	.0012	.0011	-.0002
24	1.015	-.181		-.0013	-.0010	
25	1.010	-.090	1.323	.0005	.0001	.0001
26	.899	.698	1.487	-.0005	-.0006	.0004
27	.367	.090	1.378	.0008	.0002	0.0000
28	.295	-.036		-.0003	-.0001	
29	.239	.036	1.278	.0002	0.0000	.0004
30	-.129	-.166	1.315	-.0002	.0002	.0003
31	15.935	-.261		-.1027	.0132	
32	-1.633	-3.530		.0046	-.0280	
33	-2.595	.215		-.1081	-.0014	

CORNER REACTIONS (LBS)

1	2	3	4	TOTAL
NOT MEASURED.				

TIE FORCE (LBS)

NOT MEASURED.

TABLE 14.7 Stress and moment resultants for model test 5A.

RULED SURFACE HYPERBOLIC PARABOLOID.

(MODEL TEST 6 A.)

BEAM EDGES, WITH BASE AND APEX CORNERS CLAMPED FLEXURALLY AND FREE EXTENSIONALLY.

GAUGE POS	DIRECT STRESSES (LB/IN)			BENDING STRESSES (LB.IN/IN)		
	$k_{n_{11}}$	$k_{n_{22}}$	$k_{n_{12}}$	$k_{m_{11}}$	$k_{m_{22}}$	$k_{m_{12}}$
1	-2.229	-1.238		-.2451	.0177	
2	-.181	-.486		-.0048	-.0156	
3	11.518	3.672		.1473	-.0413	
4	8.449	2.458		.2391	-.0287	
5	2.050	4.166		.2023	-.0235	
6	-8.707	3.769		.0350	-.0081	
7	19.121	1.995		-.2726	.0298	
8	2.169	-.601	1.986	-.0082	-.0138	.0084
9	-.966	-.636	-.016	-.0021	-.0088	.0050
10	-3.189	-.272	-1.147	.0011	-.0063	.0015
11	-3.621	-.053	-1.470	.0023	-.0048	-.0006
12	-2.361	-.255	-1.701	.0020	-.0041	-.0023
13	.966	-1.493	-1.056	-.0002	-.0023	-.0043
14	5.723	3.316	2.076	-.0065	-.0124	-.0064
15	-1.056	-1.384	.892	-.0094	-.0081	.0048
16	-2.441	-1.347	-.546	.0034	.0005	.0037
17	-1.639	-.290	-.655	.0061	.0041	.0011
18	-.219	-.238		-.0071	-.0043	
19	1.409	-.199	-.639	.0053	.0029	-.0021
20	3.276	1.189	.530	.0021	-.0010	-.0034
21	3.990	3.678	2.579	-.0078	-.0069	-.0026
22	-.749	-1.427	.127	.0091	.0089	.0010
23	.418	-.509	.346	.0098	.0101	.0004
24	1.506	-.307		-.0095	-.0093	
25	2.664	.256	.569	.0078	.0070	-.002
26	2.481	2.113	.770	.0044	.0037	-.0011
27	.109	-2.389	1.359	-.0095	.0061	.0002
28	.443	-.350		-.0092	-.0087	
29	.647	.129	1.073	.0088	.0086	.0007
30	-.889	-.592	1.612	.0083	.0084	.006
31	33.710	2.013		0.000	.0957	
32	15.498	-5.166		.0608	-.0965	
33	3.172	-2.307		-.2864	.0140	

CORNER REACTIONS (LBS)

1	2	3	4	TOTAL
NOT MEASURED.				

TIE FORCE (LBS)

NOT MEASURED.

TABLE 14.8 Stress and moment resultants for model test 6A.

RULED SURFACE HYPERBOLIC PARABOLOID.

(MODEL TESTS 4A, 5A, 6A)

NORMAL DISPLACEMENT COEFFICIENTS k_{w_3}.

TEST	DISPLACEMENT TARGET LOCATION.					
	5	6	7	8	9	10
4A		.0755	.1607	.2308	.2826	.1607
5A		.1326	.3300	.4789	.4822	
6A		.3851	1.0291	1.5889	1.6860	

TEST	DISPLACEMENT TARGET LOCATION.					
	11	12	13	14	15	16
4A	.0527	.3289	.4012	.4724	.4939	.5404
5A	.1035	.5922	.6990	.8122	.8899	.9870
6A	.3042	2.2071	3.4854	5.0679	6.6796	7.8576

TEST	DISPLACEMENT TARGET LOCATION.					
	17	18	19	20	21	22
4A	.5383	.5188	.5350	.2815	.4713	.4811
5A	.9999	1.0226	1.0323	.4854	1.0032	.7313
6A	8.6666	9.3171	9.6245	1.7411	9.3430	6.7896

TEST	DISPLACEMENT TARGET LOCATION.					
	23	24	25	26	27	28
4A	.3031	.6278	.5857	.2912	.2202	.1380
5A	.3171			.6148	.3915	.2459
6A	2.6440	10.0194		2.9449	1.4045	.7572

TEST	29	30
4A	.3936	.4660
5A	.7669	.9449
6A	4.8317	7.6343

TABLE 14.9 Normal displacements for model tests 4A, 5A, 6A.

agreement with those given for the theoretical study of section 8.5, while the influence of the edge beams are also seen to verify the results of sections 8.2 and 8.3. In addition the provision of roller supports at the apex with the diagonal tie at the base, greatly improves the stress distribution within the shell without adversely affecting the overall shell stiffness. The importance of providing diagonal ties, whose strain magnitude is controlled in order that corner displacements be minimised, cannot be over emphasised. It is also seen that the effect of base diagonal displacement greatly influences the distribution of in-plane shear stresses, and that membrane solutions become meaningless where corner supports are unable to transfer in-plane stresses.

14.2 RESULTS FOR LOADING 'TYPE B'

In this section displacement and stress and moment resultants are presented in lb. in. units for total diagonal displacement loadings of 0.05 inch. Gauges 8 and 59 were not functioning, so that as previously all reduced readings at gauge positions 2 and 13 are in error. Complete listings of average surface strains for each test are given in tables C.12 to C.14 of appendix C.

14.2.1 Free Edged Shell

14.2.1(a) Model Test 2B

A total diagonal displacement (diagonal displacement is

considered as the sum of the corner displacements across the diagonal) of 0.01 inch was applied across the base diagonal by means of tie rod adjustment. As an inward base diagonal displacement results in an outward movement of the apex diagonal, and because the apex ties were capable of restraining inward movement only, it was necessary to provide the apex ties with an initial tensile prestressing force which was greater than the expected compressive force. In this way diagonal displacement at the apex could be controlled by means of the existing tensile tie bars.

Stress and moment resultants are given in table 14.10 and deflections are listed in table 14.13. The tables show that the considerable diagonal force, associated with the diagonal displacement of 0.05 inch, is transferred by column action along a relatively thin edge strip to the apex supports where the compressive force is resisted by the "apex ties". Stress and moment resultants, as well as normal displacements are seen to be small within the body of the shell. The results of this test clarify further the reasons for the small differences in shell behaviour between model test 1A and 2A. In section 14.3 this is shown by combining these results with the results of model test 2A to provide a check upon the behaviour of model test 1A.

14.2.1(b) Model Test 3B

A total diagonal displacement of 0.04 inch was applied across the base diagonal, while the apex corners were free to move horizontally. The results are presented in tables 14.11 and 14.13.

Diagonal symmetry is seen to be superior to that of model test 2B, although 19% and 36% differences occur in n_{11} and m_{11} between gauge positions 1 and 33. Bending symmetry about the z_k, $(k = 1,2)$ axes is seen by comparison of m_{11} at 1 and 7 where only a 4% difference occurs.

A comparison of tables 14.10 and 14.11 or the displacements of models 2B and 3B in table 14.13 shows that the diagonal stiffness of the present model is considerably less than that of model 2B, and that the stress and moment resultants within the body of the shell are very much greater. The large displacements and stresses incurred with small diagonal thrusts indicate that the removal of small diagonal tie forces from model 2A will result in a marked change in model behaviour. These results are combined in section 14.3 with those of test 3A in an attempt to simulate the behaviour of model test 2A.

14.2.2 Beam Edged Shell

For the beam edged shell, it was not possible to provide sufficient tensile prestressing force in the apex ties to enable full control of the corners when the shell was subject

to a base diagonal displacement. An equivalent test to 2B was not possible.

14.2.2(a) Model Test 6B

To enable a direct combination of model test 6B and 6A, to simulate model test 5A (reported in section 14.3), the diagonal displacement for this test was applied at the apex diagonals with the base corners supported upon rollers. The results are presented in tables 14.12 and 14.13.

Comparison of n_{11} at gauge positions 1, 4 and 7 with those at 33, 32 and 31 again indicates that symmetry about the diagonals was not completely achieved.

The significant compressive direct stresses in the region of the base corners are difficult to explain. The large stress and moment resultants and the high displacements, as in test 3B, indicate the important contribution of diagonal displacements where the other diagonal corners are extensionally free. As similar trends were found on combining 6A and 6B, to those found for combination of 3A and 3B, a superposition check upon model 5A was not carried out.

14.3 CHECKS UPON MODEL BEHAVIOUR

In the absence of a completely strain gauged cross-section, equilibrium checks were not possible, although overall equilibrium was indicated by the agreement to within $\pm$ 4%

RULED SURFACE HPERBOLIC PARABOLOID.

(MODEL TEST 2 B.)

FREE EDGES, WITH BASE CORNERS CLAMPED FLEXURALLY AND EXTENSIONALLY, APEX CORNERS CLAMPED FLEXURALLY AND FREE EXTENSIONAL Y.

BASE DIAGONAL DISPLACEMENT OF +.05 INCH.

GAUGE POS	DIRECT STRESSES (LB/IN)			BENDING STRESSES (LB.IN/IN)		
	n_{11}	n_{22}	n_{12}	m_{11}	m_{22}	m_{12}
1	-74.	-325.	23.	0.		
2	-69.	12.	7.	40.		
3	-144.	12.	13.	13.		
4	-237.	-30.	3.	12.		
5	-285.	-1.	15.	22.		
6	-182.	-331.	24.	26.		
7	-338.	-309.	-8.	30.		
8	-93.	-329.	35.	-109.	79.	124.
9	-146.	-125.	-1.	-2.	55.	-8.
10	-204.	-74.	2.	15.	7.	-14.
11	-258.	-85.	7.	14.	-45.	-47.
12	-280.	-126.	18.	25.	-39.	-20.
13	-150.	-319.	60.	-90.	-23.	-30.
14	-286.	-399.	-97.	-7.	-122.	-44.
15	-52.	-214.	-52.	-153.	108.	121.
16	-189.	-146.	-40.	-58.	54.	-9.
17	-230.	-117.	-11.	-4.	10.	-42.
18	-101.	-248.	9.	21.		
19	-243.	-112.	49.	-4.	-49.	-25.
20	-103.	-252.	112.	-109.	-49.	-42.
21	-61.	-357.	-12.	-290.	-86.	-168.
22	-138.	-115.	-63.	-125.	22.	-38.
23	-176.	-89.	3.	-70.	-2.	-41.
24	-65.	-167.	-25.	27.		
25	-103.	-71.	79.	-60.	-60.	6.
26	22.	-142.	103.	-175.	-69.	7.
27	-35.	-15.	-42.	-41.	-13.	-13.
28	-13.	-22.	-15.	33.		
29	4.	22.	44.	-8.	-40.	48.
30	21.	28.	-2.	40.	-19.	42.
31	-141.	-175.	17.	13.		
32	-257.	-89.	-4.	47.		
33	-128.	-380.	14.	3.		

CORNER REACTIONS (LBS)

1	2	3	4	TOTAL
-60.5	+62.4	-82.3	+54.0	-26.4 (00.0)

TIE FORCE (LBS)

314.9

TABLE 14.10 Stress and moment resultants for model test 2B.

RULED SURFACE HYPERBOLIC PARABOLOID.

(MODEL TEST 3 B.)

FREE EDGES, WITH BASE AND APEX CORNERS CLAMPED FLEXURAL Y AND FREE EXTENSIONAL Y.

BASE DIAGONAL DISPLACEMENT OF -.05 INCH.

GAUGE POS	DIRECT STRESSES (LB/IN)			BENDING STRESSES (LB.IN/IN)		
	n_{11}	n_{22}	n_{12}	m_{11}	m_{22}	m_{12}
1	353.	15.	-7.	-37.		
2	134.	-20.	-14.	-99.		
3	130.	194.	-10.	-18.		
4	55.	157.	-9.	-13.		
5	-31.	77.	-2.	-4.		
6	-120.	17.	4.	1.		
7	168.	-207.	27.	-4.		
8	369.	105.	186.	-95.	-71.	-21.
9	118.	188.	4.	-96.	1.	-29.
10	85.	119.	3.	-21.	-10.	-27.
11	47.	94.	5.	-22.	-23.	-28.
12	-146.	74.	1.	-12.	-47.	-16.
13	-60.	60.	15.	18.	-55.	14.
14	125.	-140.	155.	-163.	36.	-21.
15	184.	20.	195.	-1.	-13.	-135.
16	85.	89.	32.	-43.	-10.	-60.
17	54.	79.	13.	-28.	21.	-43.
18	64.	52.	-31.	13.		
19	16.	72.	10.	-20.	-54.	-25.
20	-11.	94.	16.	13.	-69.	16.
21	88.	-44.	110.	-41.	-49.	57.
22	38.	-8.	12.	7.	-18.	-61.
23	21.	20.	6.	-18.	-27.	-43.
24	89.	5.	-13.	-7.		
25	18.	44.	-5.	13.	-36.	-32.
26	4.	55.	-7.	75.	-47.	-11.
27	-8.	-5.	-19.	9.	-26.	-38.
28	14.	-22.	11.	-34.		
29	-17.	7.	-30.	30.	-19.	-42.
30	-33.	20.	-32.	17.	-17.	-42.
31	119.	-189.	-1.	-1.		
32	69.	99.	-1.	-8.		
33	363.	115.	2.	-17.		

CORNER REACTIONS (LBS)

1	2	3	4	TOTAL
-7.4	+9.5	-7.9	+10.7	+4.8 (0.0)

TIE FORCE (LBS)

38.6

TABLE 14.11 Stress and moment resultants for model test 3B.

RULED SURFACE HYPERBOLIC PARABOLOID.

(MODEL TEST 6 B.)

BEAM EDGES, WITH BASE AND APEX CORNERS CLAMPED FLEXURALLY AND FREE EXTENSIONAL Y.

BASE DIAGONAL DISPLACEMENT OF -.05 INCH.

GAUGE POS	DIRECT STRESSES (LB/IN)			BENDING STRESSES (LB.IN/IN)		
	n_{11}	n_{22}	n_{12}	m_{11}	m_{22}	m_{12}
1	-97.	36.	28.	-4.		
2	8.	-6.	28.	12.		
3	-50.	-89.	-35.	5.		
4	53.	-131.	-34.	4.		
5	137.	-125.	-37.	-5.		
6	138.	31.	-55.	-14.		
7	-15.	382.	10.	-42.		
8	62.	-78.	136.	-100.	-131.	37.
9	34.	-34.	101.	-73.	-76.	72.
10	35.	10.	90.	-76.	-16.	75.
11	41.	55.	86.	-79.	35.	65.
12	40.	74.	97.	-76.	82.	48.
13	25.	36.	96.	11.	136.	-1.
14	90.	-105.	135.	-250.	163.	-110.
15	140.	-75.	134.	-65.	-96.	15.
16	59.	59.	64.	7.	-63.	66.
17	10.	103.	-16.	49.	8.	68.
18	124.	-41.	70.	-53.		
19	-80.	101.	-60.	90.	68.	38.
20	-115.	68.	-56.	29.	100.	-3.
21	46.	-127.	62.	-108.	90.	-28.
22	-4.	107.	6.	126.	-20.	38.
23	-47.	147.	-94.	147.	7.	30.
24	153.	-107.	160.	-137.		
25	-147.	152.	-153.	187.	28.	14.
26	-154.	150.	-155.	145.	44.	10.
27	-89.	155.	-27.	150.	20.	-7.
28	153.	-107.	155.	-119.		
29	-123.	156.	-127.	165.	15.	-6.
30	-81.	134.	-90.	124.	23.	-20.
31	406.	-8.	-50.	33.		
32	24.	35.	78.	-42.		
33	51.	-116.	4.	24.		

CORNER REACTIONS (LBS)

1	2	3	4	TOTAL
NOT MEASURED.				

TIE FORCE (LBS)

NOT MEASURED.

TABLE 14.12 Stress and moment resultants for model test 6B.

RULED SURFACE HYPERBOLIC PARABOLOID.

(MODEL TESTS 2B, 3B, 6B)

NORMAL DISPLACEMENT COMPONENTS k_{w_3}.

	DISPLACEMENT TARGET LOCATION.					
TEST	5	6	7	8	9	10
2B	-29	-112	-333	-720	-583	-266
3B	2	-37	-275	-479	-531	-396
6B		-18	-80	-139	-195	

	DISPLACEMENT TARGET LOCATION.					
TEST	11	12	13	14	15	16
2B	29	-587	-587	-516	-524	-620
3B	-133	-579	-688	-841	-1017	-1143
6B	-38	-290	-582	-940	-1269	-1533

	DISPLACEMENT TARGET LOCATION.					
TEST	17	18	19	20	21	22
2B	-624	-612	-712	-999	-704	-416
3B	-1250	-1335	-1356	-689	-1371	-1140
6B	-1682	-1815	-1839	-262	-1815	-1467

	DISPLACEMENT TARGET LOCATION.					
TEST	23	24	25	26	27	28
2B	-37					
3B	-575					
6B	-869				-234	-155

TEST	29	30
6B	-877	-1418

TABLE 14.13 Normal displacements for model tests 2B, 3B, 6B.

between applied normal loading and measured vertical reactive forces. This section considers an alternate technique using superposition for providing checks on model shell behaviour.

14.3.1 Superposition Checks

14.3.1(a) Check of Model Test 1A

Results of test 2B were added to the results of test 2A so that the corner diagonal displacements δ_1 and δ_3 were eliminated and the combination was equivalent to test 1A. This combination is indicated in Table 14.14 as (2). The transformed results of 2B, denoted (1), were obtained by interchanging the base and apex corners and thereby introduced additional errors.

	Corner Diagonal Displacements (.0001 inch)				Shell Normal Displacements (.0001 inch)						
	1	2	3	4	7	8	9	10	13	16	17
2A	0	50	0	48	366	499	554	496	467	442	385
2B	250	0	250	0	333	720	584	266	587	620	712
(1)	0	250	0	250	266	583	720	333	587	620	712
(2)	0	1	0	-1	314	385	413	431	352	320	245
1A	0	0	0	0	342	416	429	367	312	152	106
%	0		0		7	7	3	15	9	40	32

(1) = Transposed results of test 2B

(2) = 2A + .2 x 2B.

TABLE 14.14 Superposition check upon Test 1A using results from tests 2A and 2B.

Normal displacements at the shell edge are seen to be in agreement to an average of 10%, with the agreement decreasing towards the shell centre (differences between (2) and 1A in the final row of 14.13 are computed as percentages of the maximum normal displacement of model test 1A). Moment and direct stress resultants, as determined from combination of 2B and 2A, can also be shown to follow similar profiles as those of model test 1A.

14.3.1(b) Check of Model Test 2A

In a similar manner to 14.3.1(a) a selection of the results from 3B were multiplied by a constant factor so that when added to the results from model test 3A, the base diagonal displacement was eliminated. The results of this combination are shown as (3) in table 14.15, with model test 2A also shown for comparison.

	Corner Diagonal Displacements (.0001 inch)				Shell Normal Displacements (.0001 inch)						
	1	2	3	4	7	8	9	10	13	16	19
3A	1356	1525	1486	1470	2807	4422	4405	2935	5670	8742	10538
3B	230	176	261	171	275	479	531	396	688	1143	1356
(3)	0	526	6	510	1247	1704	1390	690	1770	2252	2848
(1)	0	250	0	250	266	583	720	333	587	620	712
C_3x 1	0	469	0	469	499	1093	1355	625	1104	1165	1340
(4)	0	57	6	41	748	611	45	65	666	1087	1508
2A	0	49	0	49	366	499	554	496	467	442	385

(3) = 3A+5.67x3B (1) = Transformed results of test 2B.
(4) = B +1.88x(1).

TABLE 14.15 - Superposition check upon test 2A using results from tests 2A and 2B.

It can be seen that (3) , although intermediate between 3A and 2A, fails to predict the apex corner displacements and therefore the displacement distribution within the shell. This can in part be explained by the compressive stresses n_{11} at the positions 7, 14 and 21 in table 14.13, which indicate that the apex corners transmitted considerable diagonal thrust to the test rig thereby reducing the order of corner displacements. These small errors when multiplied by the constant factor of approximately 6 become more than significant so that the lack of agreement is not surprising.

In an effort to correct this apex corner displacement the transposed results of test 2B (indicated by (1) in table 14.14) were used in combination with the results of (3) to provide a model whose apex diagonal displacement is that given in model test 2A. The results of this operation are shown as (4) in table 14.15 where displacements although of the same order as those of 2A at the boundary, are of an order of four times those at the centre. The effects of magnified experimental errors and errors in obtaining differences between large numbers are shown by the difference between displacements at positions 7 and 10.

14.4 COMPARISON OF EXPERIMENTAL AND THEORETICAL RESULTS

The theoretical solutions presented in this section were obtained using the conventional finite difference solution

method with the corner conditions given in section 8.5.2. All solutions were obtained upon difference grids with $m = 16$, and dimensions and elastic properties of the model. Time only permitted the theoretical consideration of the symmetric cases of both the base and apex corners clamped extensionally and flexurally, although in section 8.5.1 the theoretical model of the free edge shell with corners extensionally free and supported at a singular point was considered. This latter shell was shown to exhibit the same trends as model test 3A, but as convergence of the finite difference solution was not achieved, this model was not considered further.

14.4.1 Free Edged Shell

The average model shell thickness, span, rise and Poisson's ratio were

$$\begin{aligned} a &= 15.0 \text{ inch}, \\ t_s &= 0.24 \text{ inch}, \\ f &= 3.00 \text{ inch} \\ \mu &= 0.31, \end{aligned} \tag{14.1}$$

resulting in dimensionless ratios

$$\begin{aligned} \lambda_1 &= 0.20, \\ \lambda_2 &= 0.0160. \end{aligned} \tag{14.2}$$

Employing the corner modification outlined in section 8.5.2, the programme described in section 8.2.3 was used to obtain

the solution for a shell with parameters given by conditions 8.1. These results were used in section 8.5.2 for a comparative study with the same shell supported at a corner singularity. Experimental results at gauge positions lying on a number of cross-sections shown in figure 14.3 are indicated as full black dots, symmetric gauges as open dots and the dotted line represents the curve of best fit. The experimental results are the average for model 1A listed in table 14.2. For the results at constant z_2 cross-sections and where gauges do not span the full width of the shell, such as $k_{n_{12}}$ at $z_2 = -.5a$, the corresponding symmetric values at constant z_1 are presented. In this way the values of $k_{n_{12}}$ (shown in figure 14.3 (d)) at $(-0.5a, -0.75a)$, is that given at gauge position 16. Because at cross-section $z_2 = -0.975a$ (the position of gauges 1 to 7) theoretical solutions were not obtained, the theoretical values presented are the averaged values of those obtained at $z_2 = -1.00a$ and $z_2 = -.9375a$.

The close agreement between theory and experiment can best be seen from the marked similarity in the profiles of $k_{n_{11}}$ and $k_{m_{11}}$ at the cross-sections presented in figure 14.3. Similar trends can be observed from tables 14.16 and 14.17. Although these profiles are of similar shape the experimental values tend to be displaced at consistent percentages in the same direction from the theoretical solution. This systematic error inherent in the shell model and support structures is

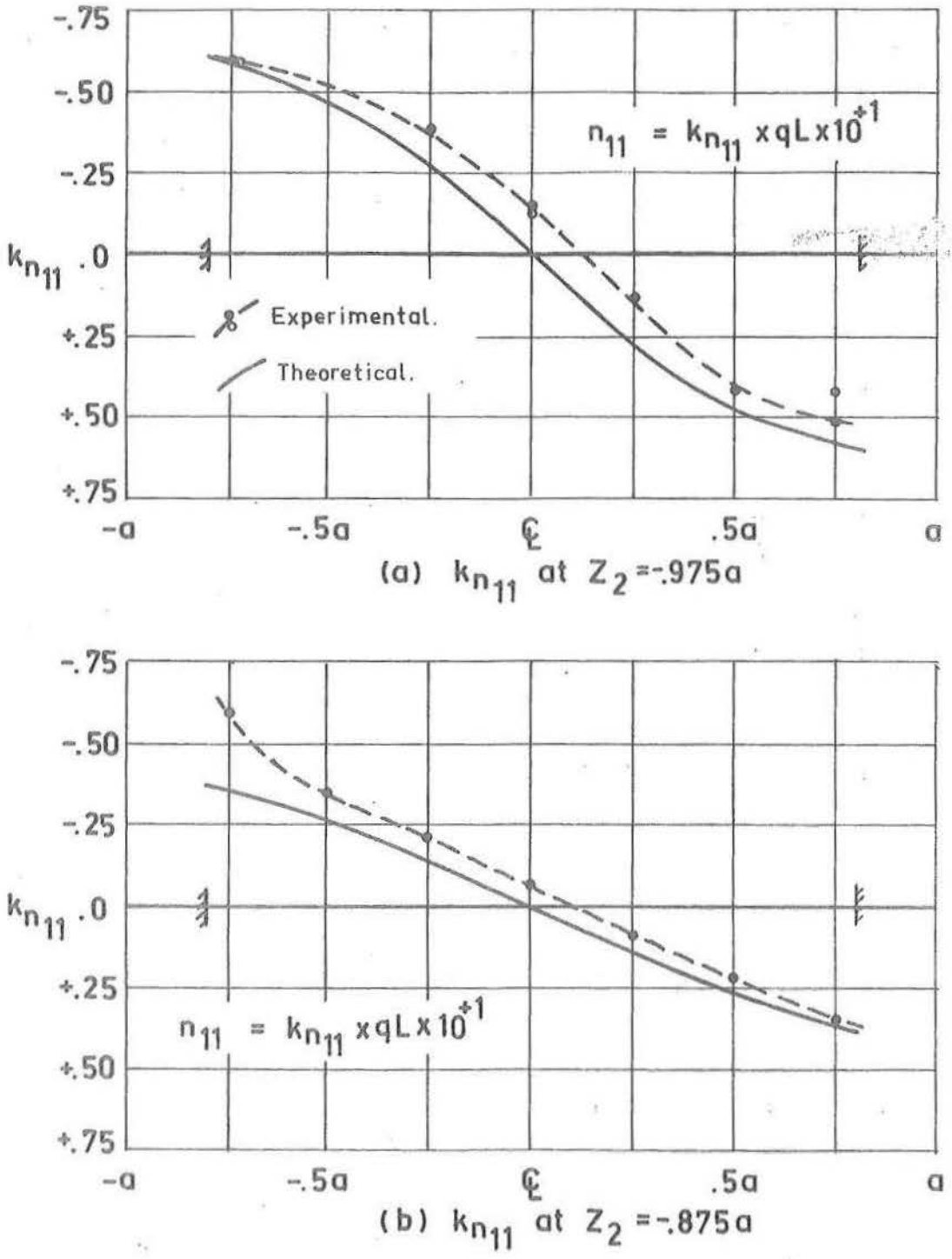

Fig. 14.3 Ruled surface hyperbolic paraboloid with all edges free and corners clamped. Comparison of experimental and theoretical results.

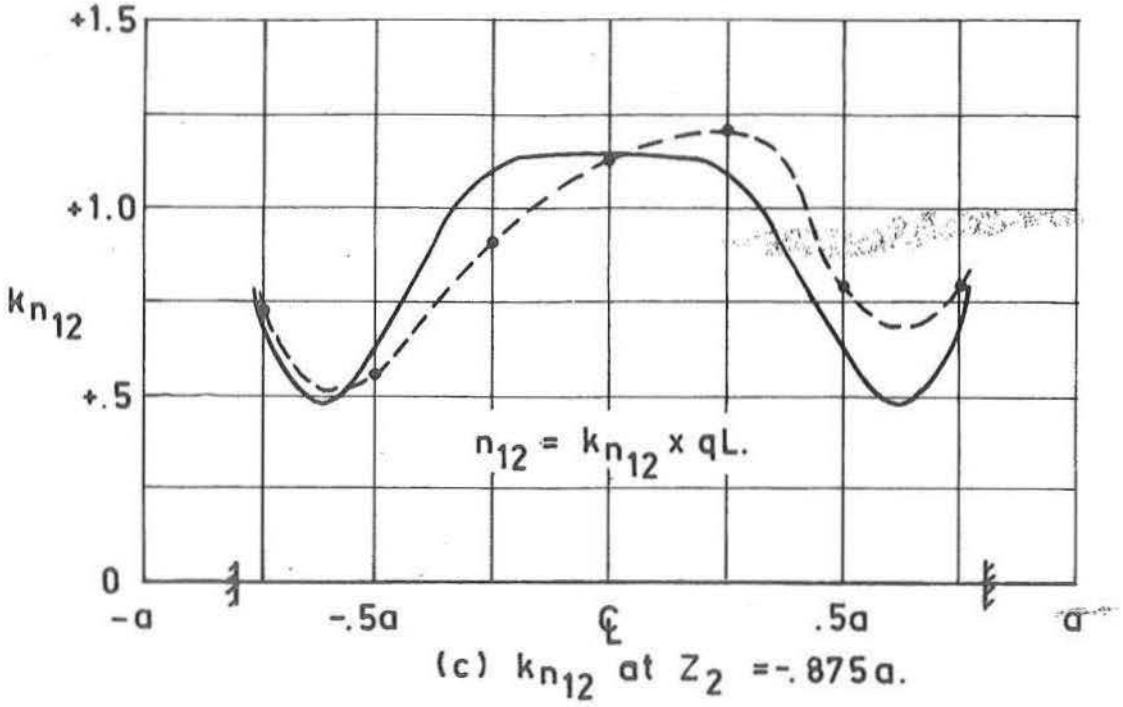

(c) $k_{n_{12}}$ at $Z_2 = -.875a.$

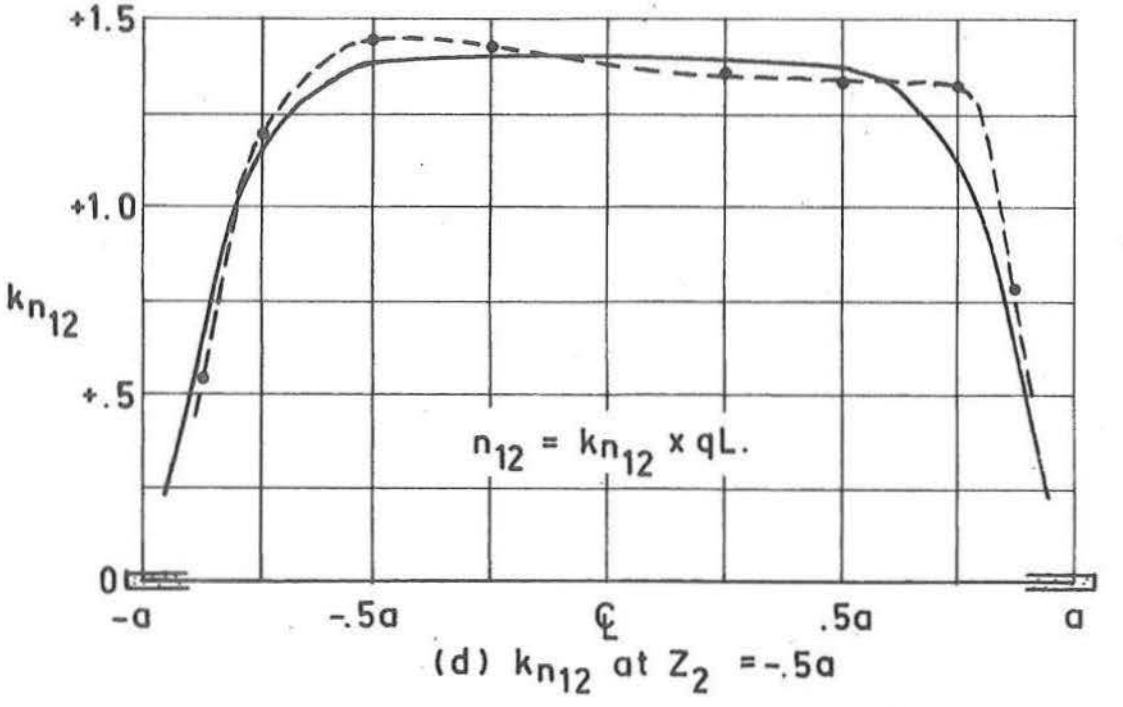

(d) $k_{n_{12}}$ at $Z_2 = -.5a$

Fig. 14.3 (continued) Ruled surface hyperbolic paraboloid with free edges and clamped corners. Comparison of experimental and theoretical results.

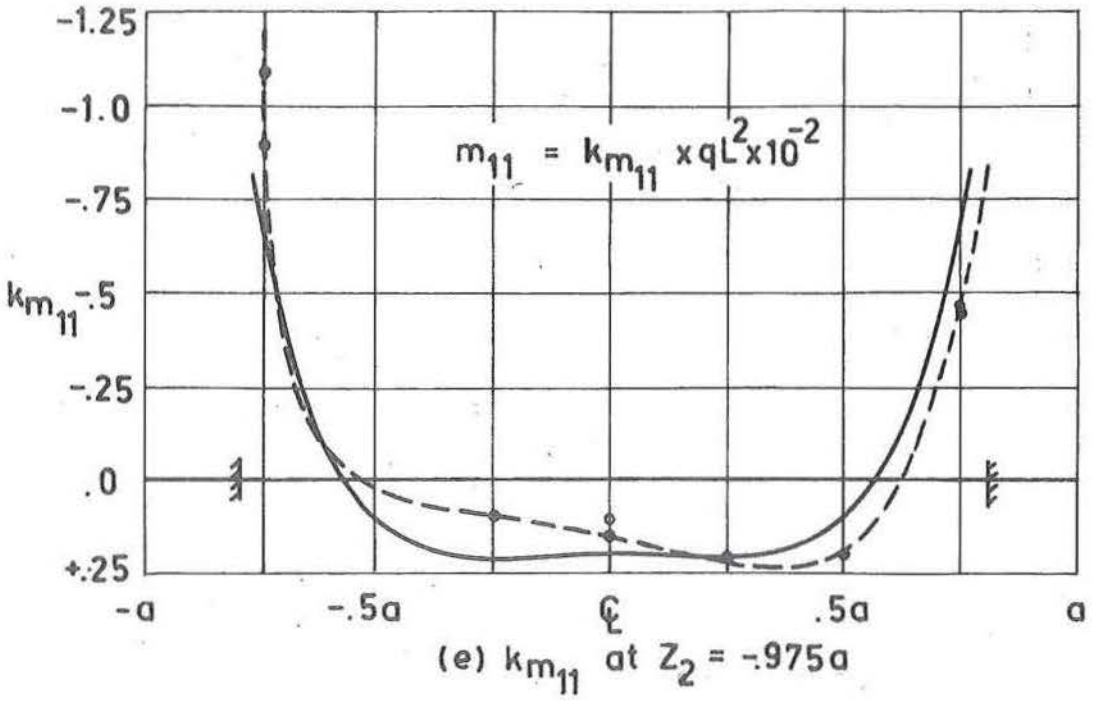

(e) km_{11} at $Z_2 = -.975a$

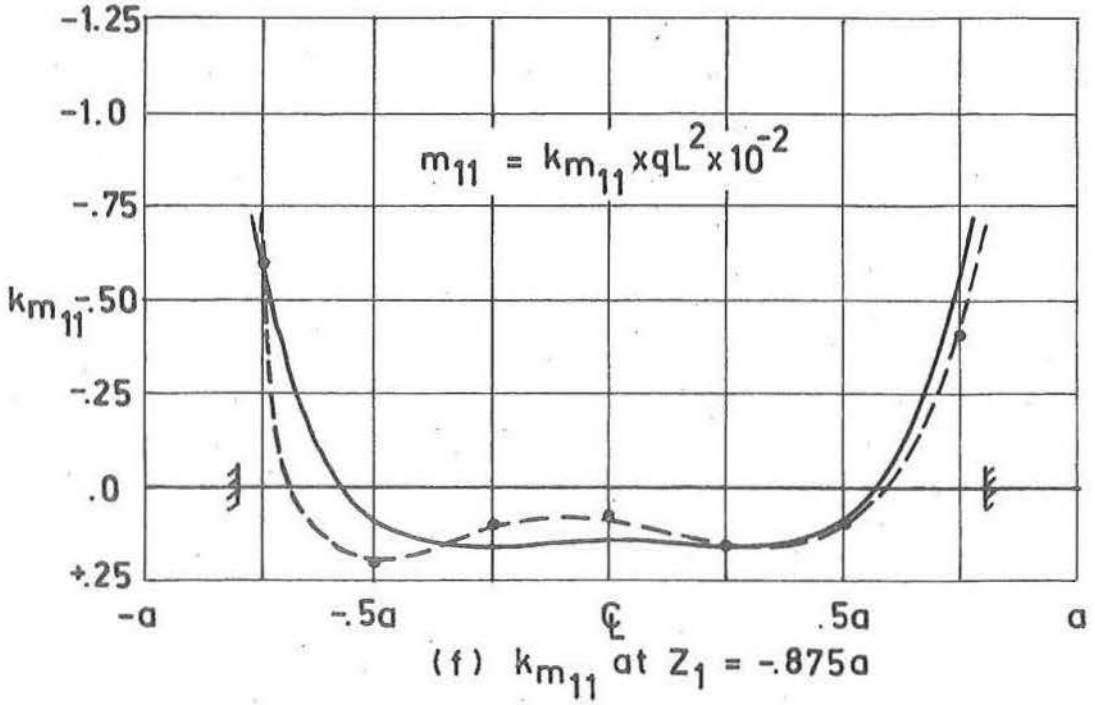

(f) km_{11} at $Z_1 = -.875a$

Fig. 14.3 (continued) Ruled surface hyperbolic paraboloid with all edges free and corners clamped. Comparison of experimental and theoretical results.

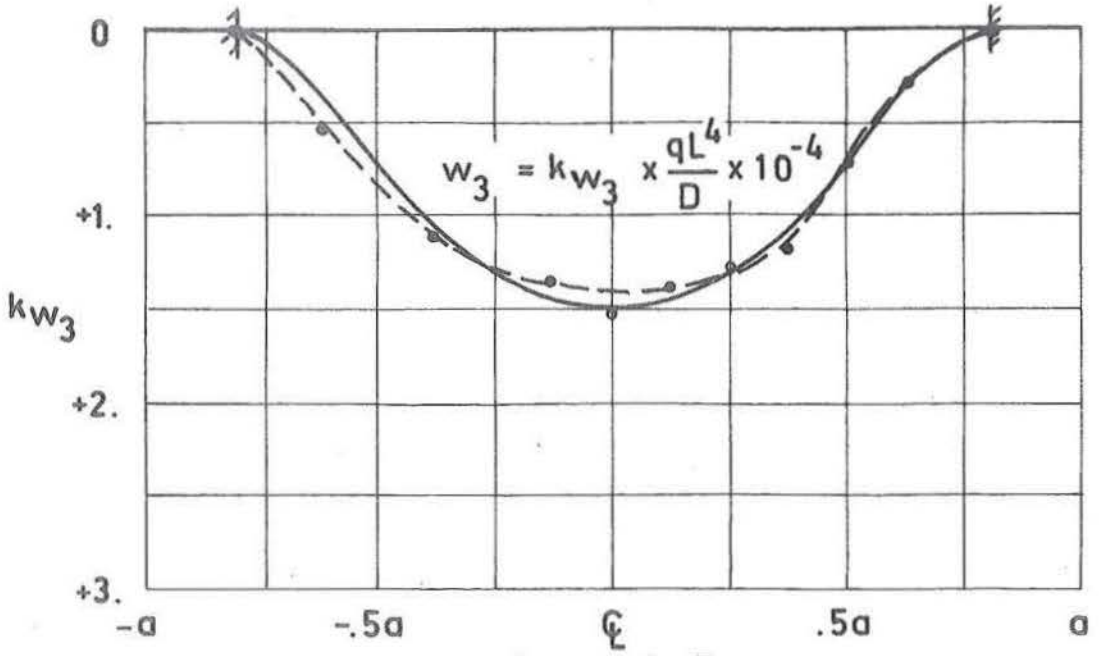

(g) k_{w_3} at $Z_2 = -a$.

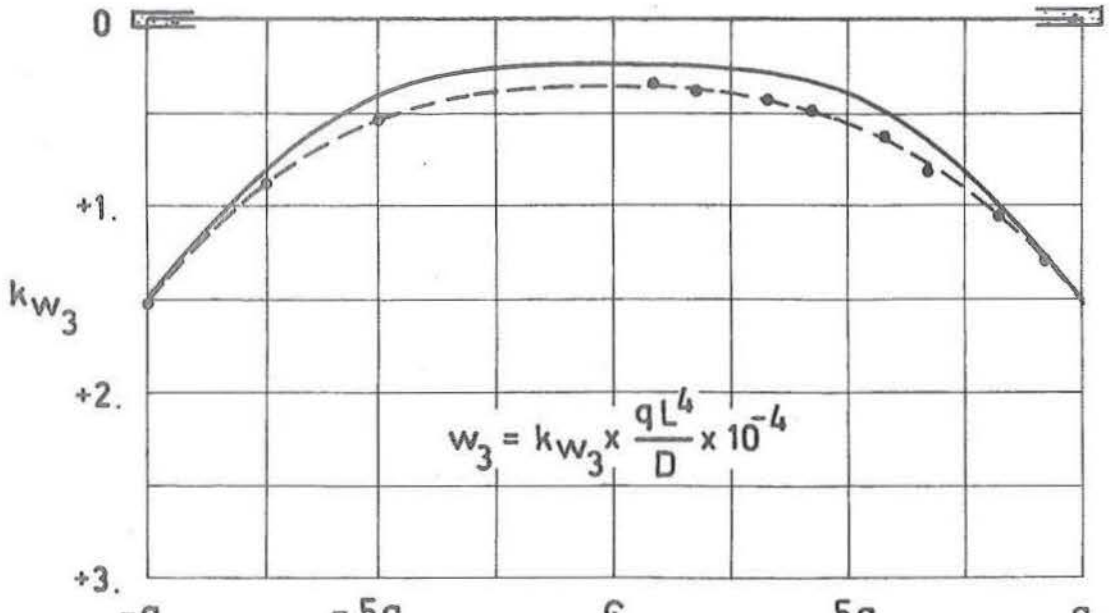

(h) k_{w_3} at $Z_2 = 0$.

Fig. 14.3 (continued) Ruled surface hyperbolic paraboloid with all edges free and corners clamped. Comparison of experimental and theoretical results.

RULED SURFACE HYPERBOLIC PARABOLOID.

(THEORETICAL MODEL 1A.)

FREE EDGES, WITH APEX AND BASE CORNERS
CLAMPED FLEXURALLY AND EXTENSIONALLY.

GAUGE POS	DIRECT STRESSES (LB/IN)			BENDING STRESSES (LB.IN/IN)		
	$k_{n_{11}}$	$k_{n_{22}}$	$k_{n_{12}}$	$k_{m_{11}}$	$k_{m_{22}}$	$k_{m_{12}}$
1	-5.921	-.299	.294	-.0068	-.0009	-.0005
2	-4.744	.014	.167	.0012	.0000	.0018
3	-2.723	.008	.316	.0022	-.0000	-.0009
4	.000	.000	.352	.0019	-.0000	.0000
5	2.723	-.008	.316	.0022	-.0000	.0009
6	4.744	-.014	.167	.0012	-.0000	.0018
7	5.921	.299	.294	-.0068	-.0009	.0005
8	-3.632	-.849	.690	-.0059	-.0028	-.0004
9	-2.634	.126	.642	.0008	-.0005	-.0017
10	-1.398	.066	1.048	.0015	-.0004	-.0009
11	.000	.000	1.158	.0014	-.0006	-.0000
12	1.398	-.066	1.048	.0015	-.0004	.0009
13	2.634	-.126	.642	.0008	-.0005	.0017
14	3.632	.849	.690	-.0059	-.0028	.0004
15	-1.341	-1.341	1.065	-.0033	-.0033	-.0017
16	-.853	.327	1.114	.0001	-.0013	-.0012
17	-.344	.189	1.447	.0006	-.0015	-.0008
18	.000	.000	1.562	.0005	-.0017	-.0000
19	.344	-.189	1.447	.0006	-.0015	.0008
20	.853	-.327	1.114	.0001	-.0013	.0013
21	1.341	1.341	1.065	-.0033	-.0033	.0017
22	.495	.495	1.381	-.0012	.0012	.0012
23	.350	.310	1.400	-.0005	.0018	.0004
24	.000	.000	1.412	-.0002	.0020	-.0000
25	-.350	-.310	1.400	-.0005	.0018	-.0004
26	-.495	-.495	1.381	-.0012	.0012	-.0012
27	.216	.216	1.170	-.0006	.0006	.0001
28	.000	.000	1.095	-.0000	.0005	-.0000
29	-.216	-.216	1.170	-.0006	.0006	-.0001
30	.000	.000	.989	.0002	-.0002	-.0000
31	5.921	.299	.294	-.0068	.0009	-.0005
32	.000	.000	.352	.0019	.0000	.0000
33	-5.921	-.299	.294	-.0068	.0009	.0005

TABLE 14.16 Theoretical results for model 1A.

RULED SURFACE HYPERBOLIC PARABOLOID.

(MODEL TEST 1 A.)

FREE EDGES, WITH BASE AND APEX CORNERS
CLAMPED FLEXURALLY AND FREE EXTENSIONALLY.

GAUGE POS	DIRECT STRESSES (LB/IN)			BENDING STRESSES (LB.IN/IN)		
	$k_{n_{11}}$	$k_{n_{22}}$	$k_{n_{12}}$	$k_{m_{11}}$	$k_{m_{22}}$	$k_{m_{12}}$
1	-5.999	.770		-.0108	-.0010	
2	-1.270	1.908		-.0029	-.0019	
3	-4.037	.331		.0009	0.0000	
4	-1.575	.103		.0013	0.0000	
5	1.283	-.062		.0021	0.0000	
6	4.064	-.326		.0021	0.0000	
7	5.087	-.502		-.0043	-.0002	
8	-6.155	-1.211	.737	-.0059	-.0061	.0004
9	-3.526	.514	.522	.0021	-.0005	-.0012
10	-2.195	.226	.910	.0008	-.0005	-.0006
11	-.720	.113	1.124	.0006	-.0006	-.0001
12	.822	.044	1.211	.0013	-.0003	.0005
13	2.122	-.153	.969	.0011	-.0006	.0015
14	3.344	.582	.801	-.0039	-.0038	.0006
15	-1.972	-2.149	1.562	-.0030	-.0037	-.0032
16	-1.169	.601	1.197	.0009	-.0011	-.0015
17	-.459	.240	.523	.0004	-.0009	-.0017
18	.009	.178		0.0000	.0014	
19	.233	.085	1.577	.0004	-.0014	.0005
20	.520	-.273	1.344	.0001	-.0012	.0016
21	.822	.928	1.047	-.0028	-.0025	.0019
22	.575	.538	1.454	-.0008	-.0002	-.0011
23	.518	.455	1.429	-.0004	-.0013	-.0003
24	.199	.195		.0002	.0014	
25	-.225	-.018	1.354	-.0007	-.0017	.0003
26	-.390	-.555	1.326	-.0010	-.0012	.0010
27	.256	.315	1.235	-.0006	-.0003	0.0000
28	.060	.147		.0004	.0005	
29	-.115	-.055	1.087	-.0007	-.0006	.0001
30	-.054	-.013	1.032	-.0001	0.0000	.0001
31	4.182	-.327		-.0046	0.0000	
32	-1.287	-.022		.0010	.0001	
33	-5.863	.302		-.0090	-.0009	

TABLE 14.17 Experimental results for model test 1A.

discussed further in section 14.5. In-plane shear stresses $k_{n_{12}}$ are in close agreement at the shell centre and even at the edges where the gradients of $k_{n_{12}}$ with respect to z_2 are high, the shear profile is well predicted by the finite difference solution. Actual average deviations were found to be 9%, 8% and 18% for the stress and moment resultants $k_{n_{11}}$, $k_{n_{12}}$ and $k_{m_{11}}$ respectively (percentages have been computed as the difference at each gauge position as a fraction of the maximum ordinate).

Normal displacements, especially those along the shell boundary, are in close agreement. An average deviation of 6% was found, although the correlations at the shell edge were superior to those at the shell centre.

14.4.2 Beam Edged Shell

The shell dimensions given in (14.1) when combined with the average beam dimensions

$$\begin{aligned} t_b &= 1.12 \text{ inch}, \\ b_b &= 0.75 \text{ inch}, \end{aligned} \tag{14.3}$$

result in the beam dimensionless parameters

$$\begin{aligned} \lambda_3 &= 4.67, \\ \lambda_4 &= 0.05. \end{aligned} \tag{14.4}$$

The programme described in section 8.3.2(c) was used with the corner modifications of section 8.5.2, so that the beam shell

orientation parameters used in the theoretical solution were:

$$\begin{aligned} \lambda_5 &= 0.00, \\ \lambda_6 &= 0.00. \end{aligned} \tag{14.5}$$

The programme described in section 8.3.2(c), with $m = 16$, and corner conditions of section 8.5.2 was used to determine the solution with parameters given by (14.1) to (14.5). Theoretical solutions are again shown as full lines in figure 14.4, with experimental values plotted with full and open dots connected by a dotted line.

The correlation between experiment and theory follows the same patterns as the free edged shell, except that the breakdown in symmetry at the edge beam is more pronounced in the present model. Similar behaviour can be observed in gauges 33, 32 and 31. Failure to simulate the theoretical corner support in the model is again the predominant reason for this systematic error.

In-plane shear stress $k_{n_{12}}$ is again in close agreement at the shell centre but suffers asymmetry consistent with that of the edge beam near the shell boundary. Gradients of $k_{n_{12}}$ with respect to z_2 at the positions $z_2 = -.875a$ are high, so that large absolute differences in $k_{n_{12}}$ have a small effect on actual shear distribution normal to this boundary.

Theoretical normal displacements k_{w_3} are observed in figures 14.4(g) and (h) to be well predicted at the boundary,

but consistently low at the shell centre. In the theoretical model λ_5 was taken as zero, while in the experimental model the shell-beam intersection was at an eccentricity of

$$e_3 = -.44 \text{ inch} \qquad (14.6)$$

to the edge beam centroidal axis. When combined with the dimensions of (14.3) this yields

$$\lambda_5 = -.39 \qquad (14.7)$$

as the edge beam-shell intersection vertical eccentricity parameter. In section 8.4.2 the influence of this eccentricity was determined for a model of very similar geometry, support conditions and material properties to that of the theoretical model considered in this section. It can be seen from figure 8.10 that $\lambda_5 = -.39$ increases the central shell displacement by 56%, while the displacement at the edge beam is increased by 29%. Application of this same boundary transformation to the present theoretical model can be expected to have a similar effect upon displacement (it being assumed that the convergence on successive grid refinements is similar for both models), so that the theoretical central deflection would be increased to $k_{w_3} = 0.650$. This overestimates the experimental deflection at target 19 by some 21%, but when the convergence rates (with successive grid refinements) of section 7.2 shown in figure 7.4 are considered, this difference in displacements could be explained by the discretisation error. Time did not permit

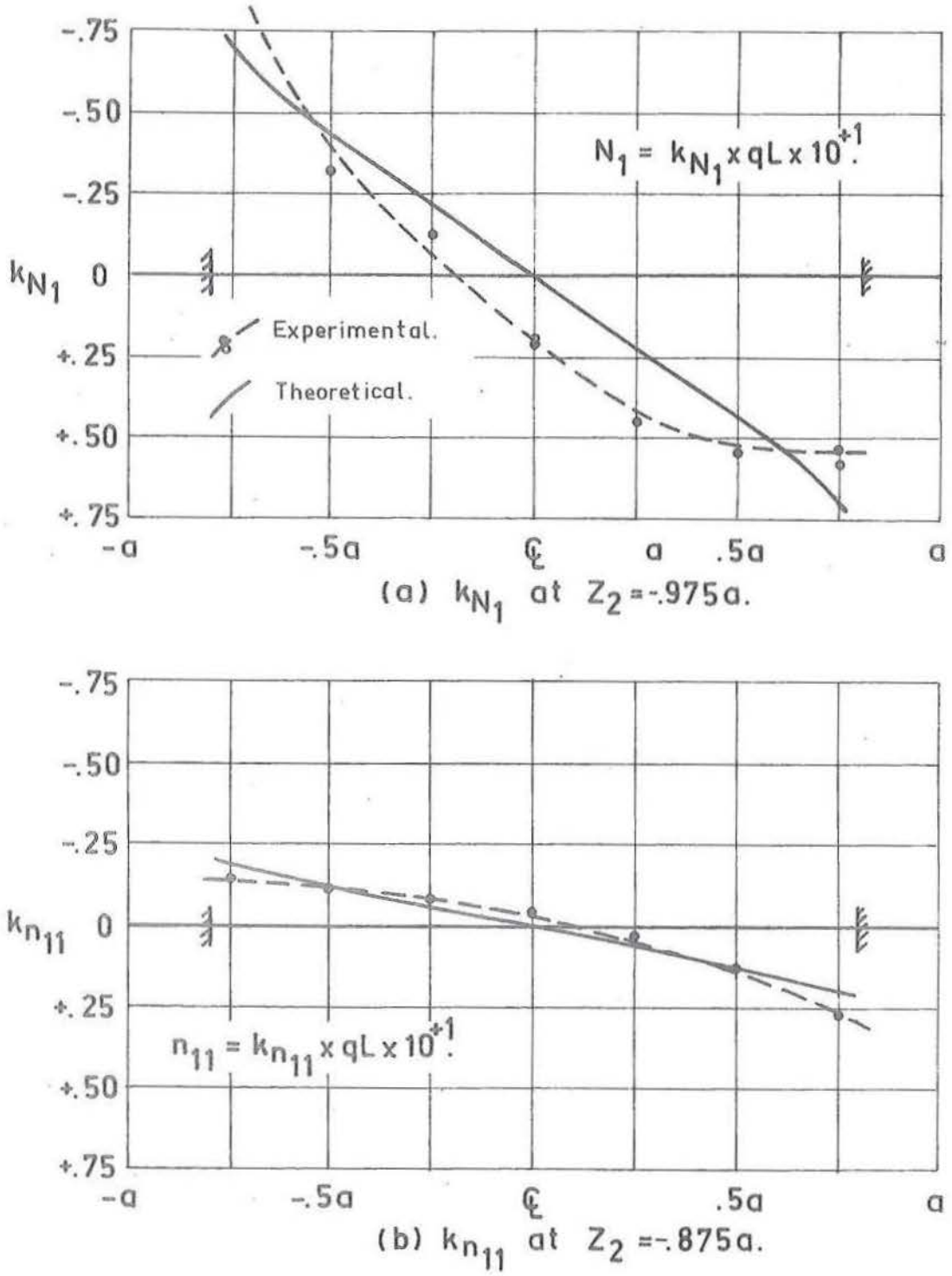

Fig. 14.4 Ruled surface hyperbolic paraboloid with all beam edges clamped at corners. Comparison of experimental and theoretical results.

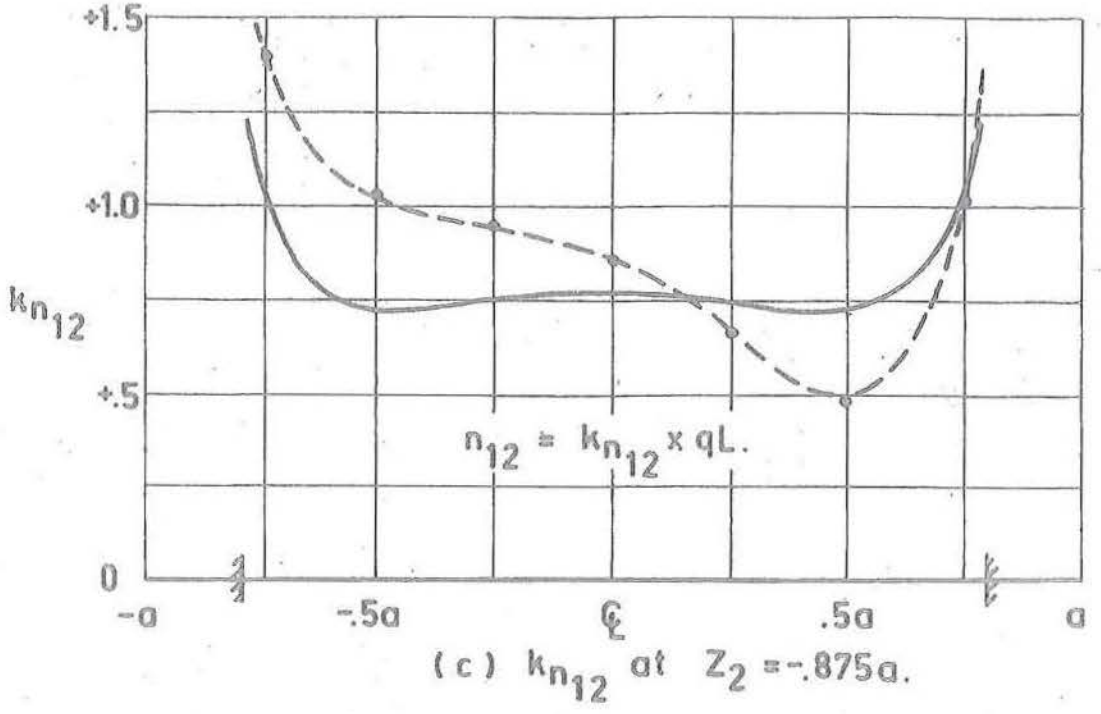

(c) $k_{n_{12}}$ at $Z_2 = -.875a.$

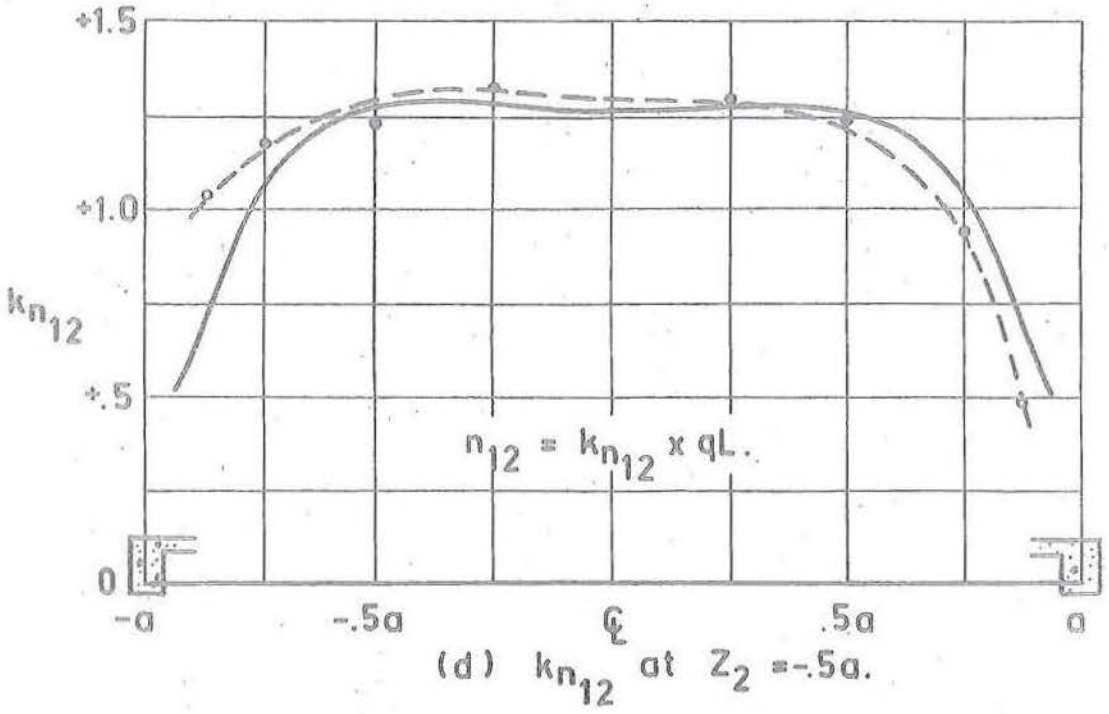

(d) $k_{n_{12}}$ at $Z_2 = -.5a.$

Fig. 14.4 (continued) Ruled surface hyperbolic paraboloid with beam edges and clamped corners. Comparison of experimental and theoretical results.

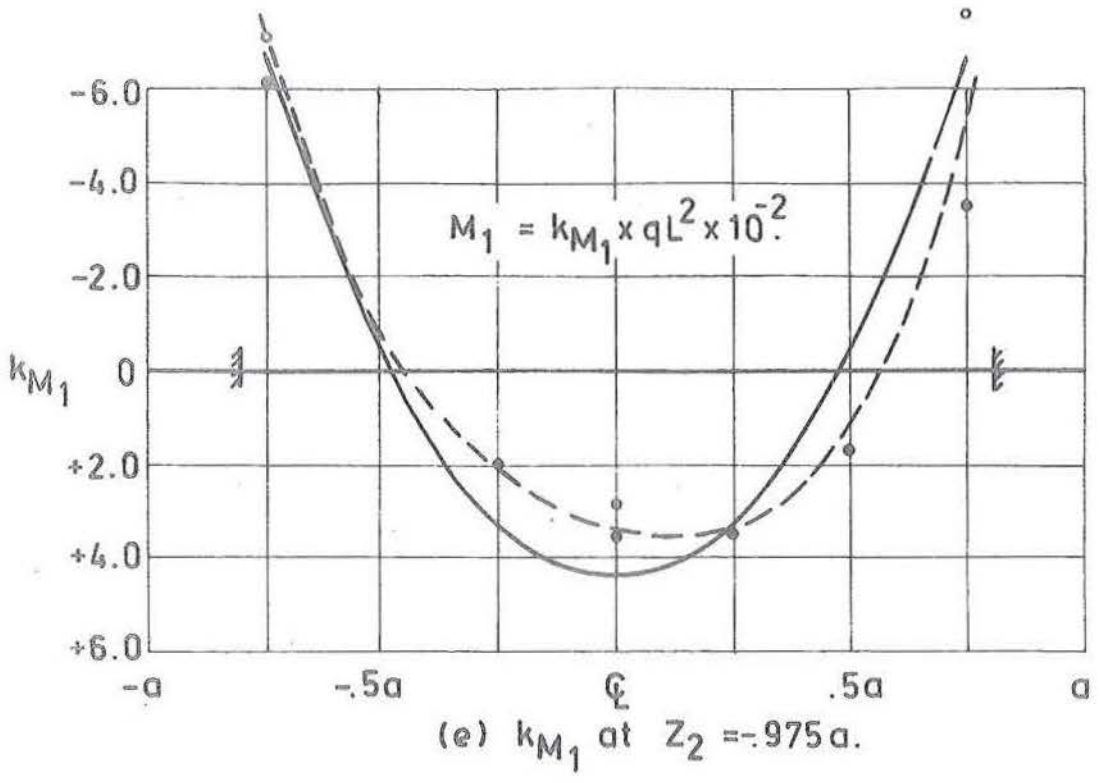

(e) k_{M_1} at $Z_2 = -.975a$.

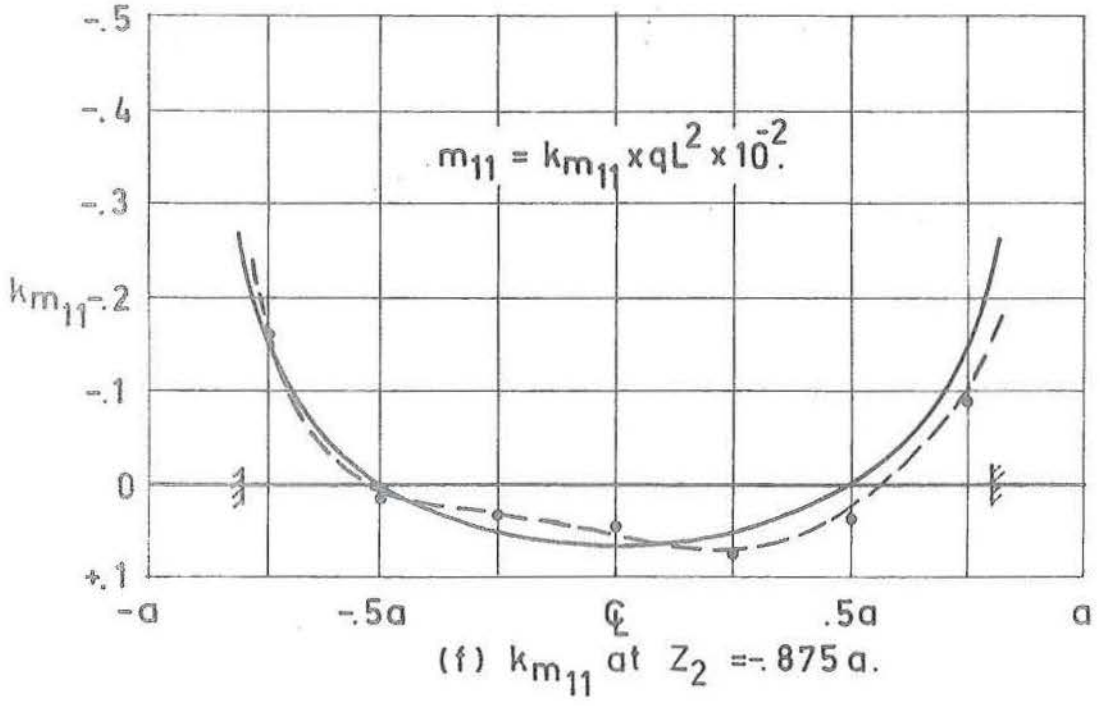

(f) $k_{m_{11}}$ at $Z_2 = -.875a$.

Fig. 14.4 (continued) Ruled surface hyperbolic paraboloid with beam edges and clamped corners. Comparison of experimental and theoretical results.

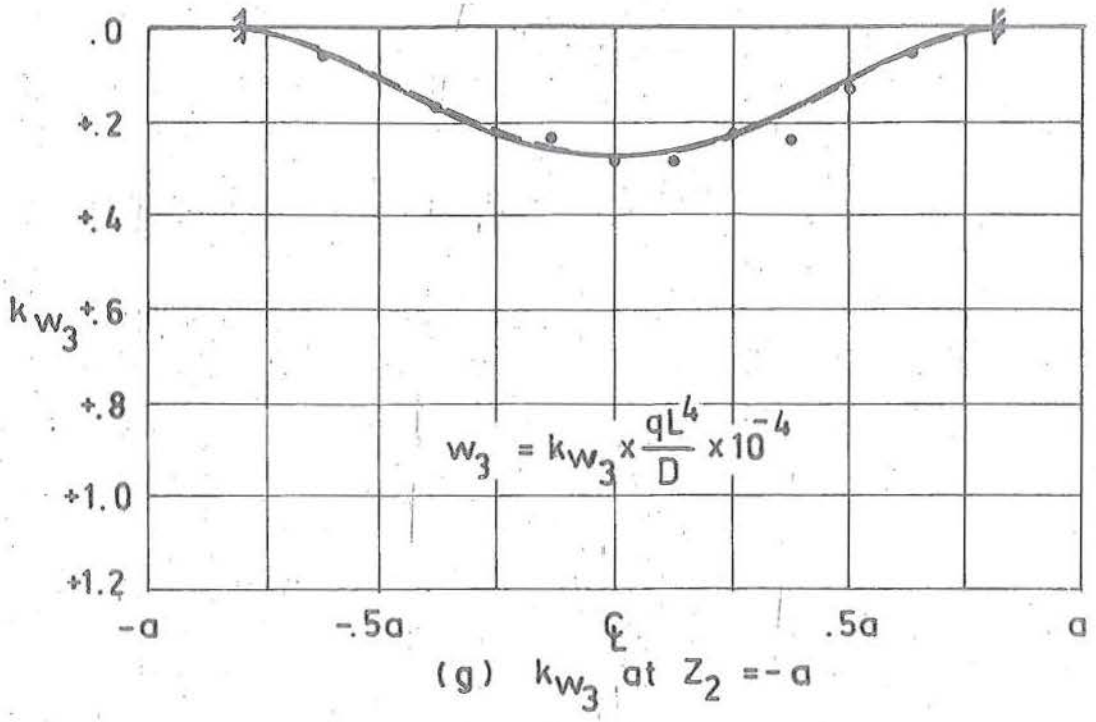

(g) k_{w_3} at $Z_2 = -a$

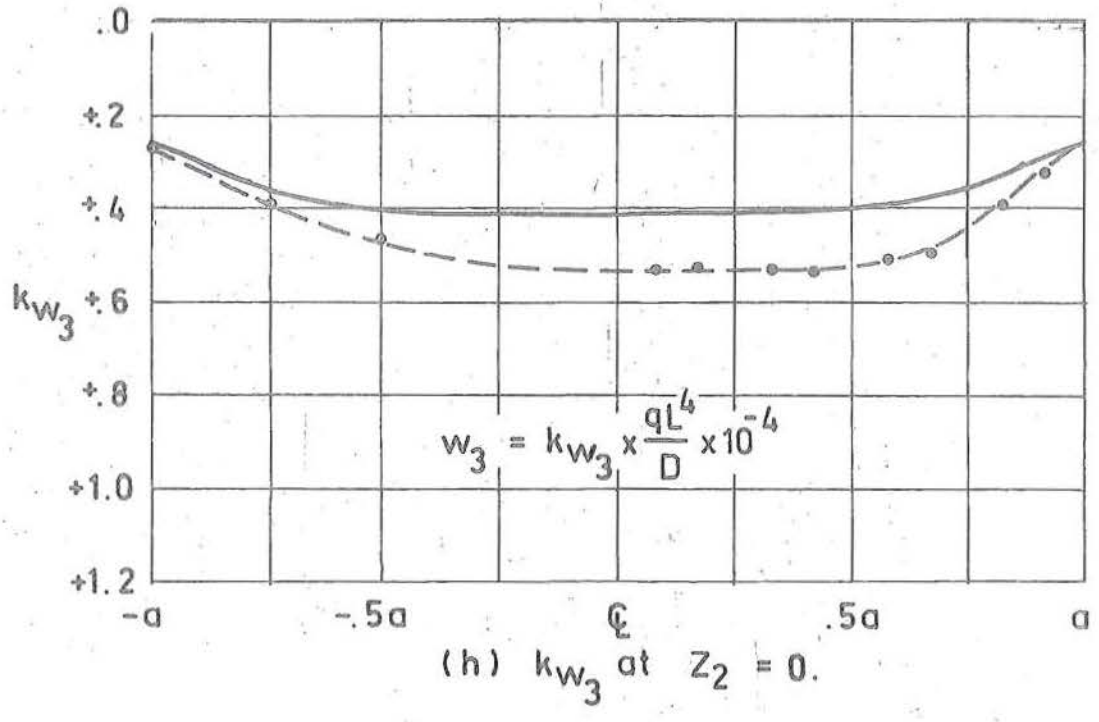

(h) k_{w_3} at $Z_2 = 0$.

Fig. 14.4 (continued) Ruled surface hyperbolic paraboloid with beam edges clamped at corners. Comparison of experimental and theoretical results.

RULED SURFACE HYPERBOLIC PARABOLOID.

(THEORETICAL MODEL 4A.)

BEAM EDGES, WITH APEX AND BASE CORNERS CLAMPED FLEXURALLY AND EXTENSIONALLY.

GAUGE POS	DIRECT STRESSES (LB/IN)			BENDING STRESSES (LB.IN/IN)		
	$k_{n_{11}}$	$k_{n_{22}}$	$k_{n_{12}}$	$k_{m_{11}}$	$k_{m_{22}}$	$k_{m_{12}}$
1	-7.041			-.0673		
2	-4.365			-.0061		
3	-2.324			.0315		
4	.000			.0436		
5	2.324			.0315		
6	4.365			-.0061		
7	7.041			-.0673		
8	-1.884	-.714	1.053	-.0015	-.0009	-.0005
9	-1.231	-.010	.717	.0001	-.0001	.0001
10	-.560	.023	.753	.0005	.0002	-.0000
11	.000	.000	.759	.0007	.0003	-.0000
12	.560	-.023	.753	.0005	.0002	-.0000
13	1.231	.010	.717	.0001	-.0001	-.0001
14	1.884	.714	1.053	-.0015	-.0009	-.0005
15	-1.156	-1.156	1.462	-.0012	-.0012	.0000
16	-.921	-.083	1.060	.0002	.0001	-.0001
17	-.418	+.055	1.025	.0006	.0006	-.0001
18	.000	.000	1.029	.0007	.0007	-.0000
19	.418	-.055	1.025	.0006	.0006	.0001
20	.921	.083	1.060	.0002	.0001	.0001
21	1.156	1.156	1.462	-.0012	-.0012	-.0000
22	-.158	-.158	1.284	.0002	.0002	-.0003
23	-.086	.057	1.281	.0003	.0002	-.0002
24	.000	.000	1.271	.0004	.0003	-.0000
25	.086	-.057	1.281	.0003	.0002	.0002
26	.158	.158	1.284	.0002	.0002	.0003
27	.035	.035	1.292	.0001	.0001	-.0001
28	.000	.000	1.274	.0002	.0001	-.0000
29	-.035	-.035	1.292	.0001	.0001	.0001
30	.000	.000	1.249	.0001	.0001	-.0000
31	+7.041			-.0673		
32	.000			.0436		
33	-7.041			-.0673		

TABLE 14.18 Theoretical results for model 4A.

RULED SURFACE HYPERBOLIC PARABOLOID.

(MODEL TEST 4 A.)

BEAM EDGES, WITH APEX AND BASE CORNERS CLAMPED FLEXURALLY AND EXTENSIONALLY.

GAUGE POS	DIRECT STRESSES (LB/IN)			BENDING STRESSES (LB.IN/IN)		
	$k_{n_{11}}$	$k_{n_{22}}$	$k_{n_{12}}$	$k_{m_{11}}$	$k_{m_{22}}$	$k_{m_{12}}$
1	-9.992	.062		-.0600	.0013	
2	-3.141	1.194		-.0236	-.0085	
3	-1.119	.144		.0192	-.0052	
4	2.226	-.082		.0348	-.0028	
5	4.657	-.042		.0348	-.0028	
6	5.544	.128		.0170	-.0008	
7	5.171	-.192		-.0354	.0024	
8	-1.354	-.479	1.408	-.0015	-.0020	.0009
9	-1.104	.053	1.037	-.0001	-.0007	.0002
10	-.837	.053	.953	.0002	0.0000	0.0000
11	-.819	.081	1.184	.0003	.0002	0.0000
12	.212	-.170	.664	.0005	.0004	0.0000
13	1.311	.193	.478	.0002	-.0001	-.0002
14	2.836	.904	1.014	-.0006	-.0013	.0005
15	-.746	-.782	1.500	-.0009	-.0009	.0002
16	-.441	-.019	.872	-.0004	.0003	0.0000
17	-.412	.018	.126	.0005	.0007	-.0014
18	-.073	-.078		-.0006	-.0009	
19	.285	-.248	.999	.0007	.0009	0.0000
20	1.194	.140	.926	-.0005	.0003	0.0000
21	1.304	1.359	1.304	-.0011	-.0006	0.0000
22	-.163	-.115	1.225	.0006	.0007	-.0002
23	.061	.266	1.342	.0003	.0007	-.0001
24	.150	-.090		-.0003	-.0006	
25	.188	-.067	1.291	.0001	.0002	0.0000
26	.195	.062	1.242	.0003	.0002	.0002
27	.061	-.061	1.365	.0002	.0002	-.0001
28	.024	-.074		.0002	0.0000	
29	.006	-.208	1.321	0.0000	.0001	.0001
30	-.098	-.208	1.259	0.0000	0.0000	0.0000
31	5.777	.436		-.0768	.0095	
32	1.199	-.566		.0275	-.0062	
33	-11.416	.144		-.0715	.0022	

TABLE 14.19 Experimental results for model test 4A.

the checking of this speculation, but it is felt certain that this displacement behaviour would have been predicted to an even greater degree of accuracy had the effect of λ_5 been considered in the theoretical model.

As the influence of λ_5 upon stress and moment resultant distribution was found to be very small, the conclusions concerning the distribution of these quantities will remain unchanged.

Full, averaged experimental and theoretical results are presented in tables 14.18 and 14.19. It is surprising to find the agreement between theory and experiment for small values of $(k_{n_{kl}}, k_{m_{kl}})$, $(k,l = 1,2)$.

14.4.3 Conclusions

It is concluded from the generally close correlation of both stress and moment resultants and normal displacements for the theoretical and experimental models, that the use of finite difference techniques for the free and beam edged hyperbolic paraboloid shells is justified. For the estimation of shell stiffness, the importance of employing the correct corner arrangement has been shown, while for the edge beam shell terms containing λ_5 should be included. These refinements where necessary should also be made for the estimation of maximum stress and moment resultants, although within the shell the more approximate methods may provide sufficient accuracy.

The extreme difficulty of simulating the theoretical boundary conditions, even under controlled laboratory conditions, also suggest that for the design of prototype structures care should be taken to include the effects of corner displacements and rotations as these must invariably exist. Although corner rotations have an effect in the vicinity of the corner supports, the influence of diagonal corner support displacements is experienced throughout the shell.

14.5 ACCURACY OF MODEL TESTS

This discussion is of a qualitative rather than a quantitative nature, although in section 14.5.3 an attempt is made to assess the likely effects of discrepancies between the theoretical and the experimental models incurred in construction, setting up and testing. Because the experimental test programme was designed to verify the theoretical solutions of part II, it is considered that geometry and support condition differences are errors in the experimental model.

14.5.1 Reading Accuracy

Those errors which arise from reading, recording or processing mistakes are included along with those resulting from roundoff of all load, strain and deflection readings. Obvious reading, recording or processing mistakes could normally be eliminated (using the output from programme I of section 13.3), so that only mistakes in the less significant decimal places

were included in the results. Reading accuracies of $\pm$.05 inch of water, $\pm$1 μstrain and $\pm$0.001 inch for pressure, strain and deflections respectively, gave readings with average standard deviations of $\pm$3 μstrain and $\pm$0.0015 inch, which for normal strain and deflection magnitudes resulted in average percentage deviations of $\pm$3% and $\pm$5% for strains and deflections. These figures are dependent not only upon the model being tested, but also upon the gauge and load magnitude, and therefore provide an indication only.

Small mistakes and reading roundoff errors were minimised by carrying out repeated tests and load cycles upon the same model set up. For this reason their influence in causing possible deviations between experiment and theory is not considered further. In fact the scatter between individual tests was found to be small, and very much less than the effects of imperfections inherent in the model as set up.

14.5.2 Imperfections of Experimental Model

14.5.2(a) Errors Dependent Upon Corner Support Conditions

The results of sections 14.1 to 14.3 demonstrated the critical influence of corner conditions upon shell behaviour, and the lack of agreement between the corner conditions assumed in the theoretical solutions and those achieved in the experimental model. Assumptions of flexural rigidity at the corners for all model tests were justified, although small differences

in rotational rigidity between apex and base corners were possible, and could explain the assymmetry of $k_{m_{11}}$ in figures 14.3 and 14.4. Initially differences in rotational rigidity were attributed to the differences in stiffness between base and apex corner supports. The possible influence of tie rods providing an effective restraining moment at the base corners and moments in the opposite sense at the apex corners, was also considered. To determine the influence of these effects four tests, with corner load cells successively replaced with short lengths of 6" x 3" channel section securely precompressed using high tensile steel bolts, were carried out for model test 1A and three similar tests for model test 4A. The results of these tests are given in tables C.1 to C.4 and C.7 to C.9. It was evident that the influence of differing corner rigidities was small, with little resulting improvement in flexural symmetry.

The influence of errors in support moment rigidity can be expected from the results of section 8.5 to be of second order importance in comparison with errors in diagonal displacements. It is indicated from the assymmetry of $k_{n_{11}}$ in figures 4.3 and 4.4. that the extensionally clamped corner was not completely simulated, although great care was taken in control of corner diagonal displacements. While dial gauges 1 to 4 (figure 13.2) were controlled and measured to $\pm$0.0001 inch, the readings of dial gauges 31 to 34 showed that both rotation about the z_3 axis and the translation of the shell as a whole along the z_1

and z_2 axes took place. Including these lateral translations of the shell, which could be measured but not controlled, the resulting accuracy of diagonal control could be considered as $\pm$ .0005 inch at the loads used. Because these errors were found to be consistent for a given test they are not included in the reading errors of section 14.5.1.

14.5.2(b) Errors Dependent Upon Geometric Properties

The influence of errors in estimation of shell thickness, span and rise are considered. Local effects of errors in thickness cause consistent percentage errors to be introduced in the conversion from surface stresses to stress and moment resultants. Because the thickness at a particular position can generally be measured to a high degree of accuracy, it is unlikely that these effects will be significant. Overall effects from the lack of thickness control may introduce significant differences in shell behaviour. In the present test the thickness control was to within $\pm$ .01 inch. In section 14.5.3 this is combined with the $\pm$ .05 inch and $\pm$ .10 inch accuracy in determination of the span and the maximum expected deviation of shell from the assumed geometry (see section 12.1), to provide an estimate of the quantitative influence of geometric properties.

14.5.2(c) Errors Dependent Upon Elastic Properties

Errors in the estimation of E_s, assuming E_s constant throughout the shell, influences the absolute shell displacements

but have no effect upon the values of k_{w_3} or stress and moment resultants. The effect of errors in μ have an influence on both k_{w_3} and stress and moment resultants, although the actual influence is likely to be small. Section 14.5.3 therefore, does not consider the effect of either E_s or μ .

14.5.3 Estimation of Possible Errors

Each of the major sources of error, considered in section 14.5.2, is represented by the independent variables ξ_k .

For the effect of corner extensional stiffness, $\delta\xi_1$ is given by $\pm .0005$, while $\frac{\partial w_3}{\partial \xi_1}$ at the representative positions $(0,0)$ and $(0,-a)$ is given by

$$\begin{aligned} \frac{\partial w_3}{\partial \xi_1} &= 5.7 \text{ inch/inch, at } (0,0) \\ \frac{\partial w_3}{\partial \xi_1} &= 5.2 \text{ inch/inch, at } (0,-a) \end{aligned} \qquad (14.8)$$

For the computations of the above gradients, the experimental results for model test 2B and its transformation shown as (1) in table 14.14 are added causing the base corners to move outwards a distance equal to the inward displacements of the apex corners. A linear relationship between diagonal displacements and the resulting normal deflections is assumed.

Estimates of the overall influence of errors in span, vertical rise z_3 and lack of thickness control are combined to provide likely deviations in λ_1 and λ_2 . It is assumed

that the 0.10 inch possible deviation of the shell model from the desired shape occurs in the estimation of the total shell rise (2f), yielding λ_1 in the range

$$\lambda_1 = \frac{(6.00 \pm 0.10)}{(30.00 \pm 0.05)} = 0.200 \pm .003,$$

so that $\delta\xi_2$ is given by

$$\delta\xi_2 = \delta\lambda_1 = \pm .003. \qquad (14.9)$$

The behaviour of the shell , with average of 0.01 inch possible variation in the shell thickness of 0.24 inch, is assumed to lie within the limits of shells with average thickness as of 0.23 inch and 0.25 inch. Although this approach fails to predict asymmetry of behaviour due to severe thinning at the apex and thickening at the base, it should provide some indication as to the possible effects of thickness variation. The dimensionless ratio λ_2 should lie within the limits

$$\lambda_2 = \frac{(0.24 \pm 0.01)}{(15.00 \pm .025)} = 0.0160 \pm .0007,$$

with $\delta\xi_3$ therefore given as

$$\delta\xi_3 = \delta\lambda_2 = \pm .0007. \qquad (14.10)$$

The gradients $\frac{\partial w_3}{\partial \xi_k}$, $(k = 2,3)$ are provided from the theoretical parameter studies of sections 9.1 and 9.2. Values of w_3 for $\lambda_1 = .1, .2, .3, .4$ are used in the difference expression

$$\frac{\partial w_3}{\partial \xi_2} \doteq \frac{1.}{6.\Delta\xi_2}\cdot\left(-2.(w_3)_{.1} - 3.(w_3)_{.2} + 6.(w_3)_{.3} - (w_3)_{.4}\right), \qquad (14.11)$$

where $(w_3)_1$ represents the value in inches of the displacements w_3 for $\lambda_1 = .1$, to provide

$$\begin{aligned} \frac{\partial w_3}{\partial \xi_2} &= 3040.0 \text{ inch}, \quad \text{at } (0, 0) \\ \frac{\partial w_3}{\partial \xi_2} &= 4070.0 \text{ inch}, \quad \text{at } (0, -a) \end{aligned} \tag{14.12}$$

as the gradients of $\frac{\partial w_3}{\partial \xi_2}$ at $(0,0)$ and $(0,-a)$ respectively. In a similar manner the gradients $\frac{\partial w_3}{\partial \xi_3}$ are determined using the values of w_3 for $\lambda_2 = 0.0125, 0.0165, 0.0250$ and the expression

$$\frac{\partial w_3}{\partial \xi_3} \doteq \frac{1.}{(\Delta\xi_3)_1(\Delta\xi_3)_2((\Delta\xi_3)_1 + (\Delta\xi_3)_2)} \cdot \left((\Delta\xi_3)_1^2 \cdot (w_3)_{.0250} - \right.$$
$$\left. - ((\Delta\xi_3)_1^2 - (\Delta\xi_3)_2^2) \cdot (w_3)_{.0165} - (\Delta\xi_3)_2^2 \cdot (w_3)_{.0125}\right), \tag{14.13}$$

where $(\Delta\xi_3)_1$ and $(\Delta\xi_3)_2$ are given by

$$\begin{aligned} (\Delta\xi_3)_1 &= 0.0040, \\ (\Delta\xi_3)_2 &= 0.0085, \end{aligned} \tag{14.14}$$

resulting in

$$\begin{aligned} \frac{\partial w_3}{\partial \xi_3} &= 4.96 \text{ inch}, \text{ at } (0, 0) \\ \frac{\partial w_3}{\partial \xi_3} &= 6.82 \text{ inch}, \text{ at } (0, -a) \end{aligned} \tag{14.15}$$

The results of these approximations are shown in table 14.20 where all figures are in units of 0.0001 inch, and percentages shown are the possible errors expressed as a ratio of the maximum value of w_3.

Pos. (z_1, z_2)	w_3	$\frac{\partial w_3}{\partial \xi_1}$	A	%	$\frac{\partial w_3}{\partial \xi_2}$	B	%	$\frac{\partial w_3}{\partial \xi_3}$	C	%
$(0, 0)$	106.	5.7	29.	7.	3040.	$\pm$9.	2.	49600.	$\pm$35.	8.
$(0, -a)$	420.	5.7	26.	6.	4070.	$\pm$12.	3.	68150.	$\pm$48.	11.

A Influence of errors in corner diagonal displacements, $\left[\delta\xi_1 \cdot \frac{\partial w_3}{\partial \xi_1}\right]$.

B Influence of errors in λ_1, $\left[\delta\xi_2 \cdot \frac{\partial w_3}{\partial \xi_2}\right]$.

C Influence of errors in λ_2, $\left[\delta\xi_3 \cdot \frac{\partial w_3}{\partial \xi_3}\right]$.

TABLE 14.20 Estimation of important error in w_3, at the positions $(0,0)$ and $(0,-a)$. Percentages computed as the ratio of possible errors, to the maximum displacement w_3 at $(0,-a)$.

14.5.4 Conclusions

The approximate error analysis above shows that at the loads employed for testing, differences between w_3 for the theoretical and experimental models could be of the same order as those experienced in the model test results. Although these figures are likely to be overestimates of the possible deviations, they do indicate the relative importance of the three parameters considered. Large errors in the geometry are likely to have a smaller effect than the overall influence of small errors in either diagonal displacements control or shell thickness.

Similar trends can be shown for stress and moment resultants, although the effects of errors are considerably less. It is also possible that the asymmetry in behaviour of all shell models could be attributed, not to the lack of corner support control, but to the thickness distribution caused by forming the shell model. It was found that the shell in the region of the apex was considerably thinner than at the base, so that a redistribution of stress and moment resultants would be expected. Whether or not this could explain the asymmetry could only be determined from further numerical studies, although the changes introduced by overall thickness variations indicate that this could possibly be the case.

CHAPTER FIFTEEN

DISCUSSION AND CONCLUSIONS

The ease with which a large variety of boundary and corner conditions were considered clearly demonstrates the practicability and, more important, the adaptability of the finite difference solution technique. Although all results were obtained for the ruled surface hyperbolic paraboloid it is felt that the conclusions are capable of wider generalisation. For this reason the more important observations and conclusions derived for the hyperbolic paraboloid are summarised and assumed to apply in a slightly modified form to shells of other geometric shapes.

15.1 METHOD OF SOLUTION

The difference coefficient matrix was retained in its unreduced form, in preference to reduced forms, for reasons of simplicity of formulation. Although this results in a difference coefficient matrix (chapter 6) of higher order, the increased time required for solution is a small disadvantage in comparison with the problems associated with storage if this technique is not used.

When the successive over-relaxation iteration method was employed it was found that computer storage of 4,000 words

offered no difficulties for the solution of difference grids with as many as one or two thousand pivotal positions. Time was found to be the limiting factor, especially where computers of limited arithmetic speed were employed, but it could be considerably reduced by using an approximation to the optimum acceleration factor. The method developed for generating an approximation to the optimum acceleration factor considerably decreased the total solution time.

As well as savings in storage, the present method has an additional advantage that small changes in shell geometry and boundary condition can be made with a minimum of programming effort. Previous solutions may be used as initial input for new problems to considerably reduce the total time required for solution. The most serious disadvantage of the method, as compared with the direct methods, is that differing load distributions require completely independent solutions. For research purposes, the preparation of design tables, or the optimisation of design for a given loading, the method is greatly superior and from adaptability considerations alone is recommended.

15.2 ACCURACY OF FINITE DIFFERENCE SOLUTIONS

For the conventional finite difference technique, convergence as the difference grid is refined was shown to be adequate for all boundary types considered, with the possible

exception of the edge beam. For design purposes, convergence is probably adequate for difference grids with $m = 8$. Solutions obtained for coarse grids ($m < 16$), although providing adequate estimation of in-plane stress resultants, may be in serious error for the estimation of shell stiffness or bending stress resultants.

Of the suggested methods for the improvement of numerical accuracy for a given grid size, the methods of higher order boundary representation and modified finite difference technique were particularly attractive because of their apparent small increases in computational labour. It was found that the conditioning of the iteration matrix using these methods, resulted in a generally greater computational effort for the same numerical accuracy. Unless a direct solution method is employed, these techniques for the reduction of discretisation error offer little advantage over the conventional technique in over-all computational efficiency. The use of these higher order methods results in small increases in numerical accuracy. When the results presented by Noor and Veletsos are considered, it appears that this is one result which is not capable of generalisation.

15.3 INFLUENCE OF BOUNDARY SUPPORT CONDITION

The extreme differences in shell behaviour between the clamped and free edge shells indicate that the influence of the

boundary edge beam should be considered. For all the considered boundary conditions with corners held in position, the in-plane shear stress distribution was found to be in close agreement with that predicted from the membrane theory. From this result it has become popular to regard the load carrying characteristics of this class of shell as essentially membrane, an assertion that is further justified by the predominance of the in-plane shear stresses in carrying both vertical and horizontal loading (chapter 10). Surface stresses arising from bending action were found to be very much greater than those of the membrane state at the boundary, and at least of the same order at the shell centre. For this reason the boundary zone should be considered to cover the complete area of the shell.

As a first approximation to the shell-edge member interaction, the edge beam may be considered as providing no resistance to in-plane direct stresses normal to the boundary and infinite torsional rigidity, while the vertical bending and longitudinal extension of this edge member should be considered. For cases in which the edge member centroidal axis is eccentric to the shell-beam intersection, the influence of boundary displacement transformations should be included. The influence of "second order" terms in the edge-shell equilibrium compatibility relationship was found to be negligible

The requirements of providing edge members sufficiently stiff to limit both the shell flexibility and maximum surface

stress, indicate that for practical structures the displacement boundary formulation is superior. This formulation becomes necessary for reasons of numerical instability where iterative solution methods are used. It is also suggested that a relationship exists between badly posed physical problems and numerical instability.

Both the theoretical studies of chapter 8 and the experimental investigation of chapter 14 demonstrate the critical influence of the corner diagonal displacement. The removal of the diagonal load carrying member completely breaks down the load carrying capacity of in-plane shear stress and therefore increases the flexibility and bending stresses within the shell. The behaviour of the free edged shell with no diagonal corner restraint, closely approaches that of the related flat plate - a condition which is to be avoided. The overall influence of corner rotational rigidity was shown to be of secondary importance, affecting only those regions of the shell in the vicinity of the corner supports.

15.4 INFLUENCE OF SHELL GEOMETRY

The results of chapter 10 demonstrate, that as the shell rise to span ratio λ_1 increases, so the stress and moment resultants decrease, with the decrease being extremely marked for $\lambda_1 < 0.3$. Outside this range, large increases in λ_1 result in small decreases in shell flexibility or surface

stresses, so that shells in the range $0.3 < \lambda_1 < 0.5$ appear to represent the most efficient structures.

Examples show that an increase in the shell thickness to span ratio λ_2, has little influence upon reducing moment surface stresses, and considerably reduces the in-plane direct surface stress. The stiffening effect of increasing λ_2 increases the contribution of bending stresses in the load carrying characteristics, thereby reducing the direct surface stresses. In cases where bending stress is critical, increase in λ_1 is likely to be of greater benefit than increasing λ_2, although localised increases in shell thickness may be beneficial.

15.5 CHECKS UPON SOLUTIONS

For all the shells considered the uniqueness and existence of solutions was shown from the convergence in chapter 7. One example of each considered boundary types was checked to ensure that the conditions of equilibrium were satisfied in order to show that these solutions are correct. Correlation between applied vertical and horizontal loading, with the summation of vertical and horizontal internal stress components was found at all cross-sections to be within 2%.

As further verification of these solutions, one example of each of the simple and clamped shells is compared with the

solutions reported in reference [13]. In both cases, the close agreement indicates that the use of difference grids with $m = 8$ are sufficient for practical purposes, and for the estimation of in-plane stresses grid with $m = 4$ would be adequate

Results for the free and beam edged shells compare favourably (chapter 14) to the results of model studies. Displacements were found to be well predicted (10%), and stress and moment resultants were within acceptable limits (15%). It is likely that had the model behaved in a more symmetric manner, the agreement could have been considerably improved.

In addition to the correlation of particular model studies with the theoretical solutions, it can be seen that the overall behaviour characteristics of the model are in agreement with those derived in the theoretical studies. Additional information concerning the influences of corner support conditions not obvious from the initial theoretical investigations was obtained from the experimental investigation. The danger of drawing inferences from either experimental or theoretical results alone is indicated, and the complementary role of theory and experiment in design is recommended.

Although the single panel ruled surface hyperbolic paraboloid may in certain circumstances be an efficient load supporting system, great care is required to ensure that the necessary boundary conditions are provided. Where these conditions are not provided, the resulting shell may become

extremely inefficient.

15.6 RECOMMENDATIONS FOR FURTHER RESEARCH

Employing the methods outlined in this thesis, the following topics are suggested for further consideration.

(a) Boundary Edge Members: Employing the method of successive over-relaxation, it was found that the displacement boundary edge member representation in the range $\lambda_3 \geq 1.5$ was superior to that using the traction type boundary conditions. Where direct solution methods, such as matrix inversion, are used it is suggested that the range of applicability of the traction boundary representation may be considerably extended. Further numerical work to compare solutions obtained using the traction and displacement boundary representations in the region $\lambda_3 \leq 6.0$ could then be carried out, and a method devised to determine the expected reliability of each method. It would also be instructive to investigate possible methods of increasing both the physical and numerical accuracy of the edge member shell interaction difference analogues.

(b) Extension to Other Shell Forms: Extension to include the effects of shell geometry and material properties which are functions of the position in space. With the programmes developed, the exact analysis of a shell model with non-uniform thickness and small geometric imperfections could be investigated. Also the consideration of other classical

shell forms such as the elliptic, cylindrical and hyperbolic shells of translation could be studied under the influence of varying boundary and corner conditions.

(c) Consideration of Non-Linear Behaviour: With the programme extensions indicated in (b) it would be possible to superimpose the absolute shell displacements for a given loading upon the original shell profile and determine the modified shell geometry. With this modified shell geometry a new solution could be obtained, and a similar process repeated. The load displacement relationship could be determined for shells with a number of typical boundary types to determine which forms are susceptible to the effects of geometric changes due to large displacements and at what magnitude of loading.

(d) Influence of Non-Shallow Terms: For shells of large λ_1 the influence of a number of the terms neglected in the shallow shell assumptions could be investigated. These terms, if found to have an influence upon the resulting solutions, could then be included in a study of the range in which their neglect is likely to have an effect less than the expected numerical accuracy.

(e) Comparison of Solution Methods: A comparison of the present solutions with similar solutions obtained using one of the physical analogue methods would be valuable in providing information as to the relative overall efficiency of any of these methods. In particular there has been a great deal of

speculation as to the merits of the finite difference and the finite element solution techniques.

(f) Extension to Other Structural Forms: The success of extension of the present techniques to structural forms such as shear walls, arch dams, hanging roofs, flat slabs and elastic buckling to mention a few, will depend upon the rate at which the over-relaxation method converges. If convergence properties are found to be acceptable, there is no reason why the method should not provide valuable information upon the behaviour of complex forms of any of these structures.

B I B L I O G R A P H Y

1. ABRAMOWITZ, M. and CAHILL, W.F. - "On the Vibrations of a Square Clamped Plate". J. Assoc. Comp.Mach., No.2, 1955, pp.162-168.

2. ABU-SITTA, S.H. - "The Stresses in Doubly-Curved Shell Roofs of Positive Gaussian Curvature". Ph.D. Thesis, Dept. of Civil and Municipal Engineering, University College, University of London, March 1964.

   - "Finite Difference Solutions of the Bending Theory of the Elliptic Paraboloid". Bull. of the Int. Assoc. for Shell Structures, No.20, Dec.1964.

3. AHUJA, B.B. - "Stress Distribution in Shells of Negative Gaussian Curvature". Ph.D. Thesis, Imperial College of Science and Technology, London, October 1961.

   - "An Investigation of the Strain Distribution in Reinforced Concrete Shallow, Thin Shells of Negative Gaussian Curvature". Proc. Symp. on Shell Research, Delft, 1961.

4. APELAND, K. and POPOV, E.P. - "Analysis of Bending Stresses in Translational Shells". Proc. of the Colloquium on Simplified Calculation Methods of Shell Structures, Brussels, Sept. 1961.

5. AIMOND, F. - "Treatise on Statics of Parabolic Hyperboloidal Shells Not Stiff in Bending". Intern'l Assoc. for Bridge and Structural Engineering, Publications, Vol. 4, 1936, pp.1-112.

6. ARUP, O. and JENKINS, R.S. - "The Design of Reinforced Concrete Factory at Brynmawr" - Proc. I.C.E. 1952/3.

7. BATCHELOR, B. de V. - "Stress Distribution in some Shells of Negative Gaussian Curvature with Particular Reference to Edge Effects". Ph.D., Imperial College of Science and Technology, London, October 1963.

8. BONGARD, W. - "Zur Theorie and Berechnung von Schalentragwerken in Form Gleichseitiger Hyperbolischer Paraboloide". Bautechnik-Archiv. Vol.15 (1956).

9. BOOBNOV, I.G. - "Theory of Structures of Ships", Vol.2, St. Petersburg, 1914.

10. BRYANT, A.H. - "A Theoretical and Experimental Investigation of Prestressed Cylindrical Shell Roofs". Ph.D. Thesis, University of Canterbury, Christchurch, New Zealand, 1966.

11. "BUDD Strain Gages and Accessories, Catalogue and Price List - BG 2400". Instrument Division, The Budd Co., Phoenixville, U.S.A.

12. CARRÉ, B.A. - "The Determination of the Optimum Accelerating Factor for Successive Over-Relaxation". Computer Journal 4, pp.73-78, 1961.

13. CHETTY, S.M.K., TOTTENHAM, H. - "An Investigation into the Bending Analysis of Hyperbolic Paraboloid Shells". Indian Concrete Journal, July 1964, pp.248-258.

14. CHILVER, A.H. - An Introduction to the Basic Behaviour of Shells and Plates from "Introduction to Structural Problems in Nuclear Reactor Engineering". Pergamon Press, London, 1962.

15. CHRONOWICZ, A. - "Reinforced Concrete Roof to Swimming Pool". Civil Eng. and Public Works Review, March 1963.

16. CHUANG, K.P. - "Analysis of Cylindrical Shell Roofs by use of Energy Principles and Finite Differences". Ph.D. Thesis, Univ. of Illinois, Urbana, Ill. U.S.A. 1962.

17. DALLEY, J.W. and RILEY, W.F. - "Experimental Stress Analysis" McGraw Hill Book Co., N.Y., U.S.A. 1965.

18. DAYARATNAM, P. - "Buckling and Bending Analysis of Hyperbolic Paraboloid Shells". Ph.D. Thesis, University of Colorado, 1962.

DAYARATNAM, P. and GERSTLE, K.H. - "Model Study of a Hyperbolic Paraboloid Shell Supported on Four Elastic Edge Beams". The Indian Concrete Journal. April 1963, vol.37, pp.131-135.

19. DICK, G.T.S. - "Folded Plate Structures - An Experimental Investigation". M.E. Thesis, University of Canterbury, Christchurch, New Zealand, 1965.

20. ELMS, D.G. - "Experimental Methods in Structural Engineering" Department of Extension Studies and Department of Civil Engineering, University of Canterbury, 1966.

21. ELMS, D.G. and BILLINGTON, D.P. - "A Critique of Thin Shell Theories". Department of Civil Engineering Research Report No. 63-1, Princeton University, Princeton, New Jersey, February 1963.

22. ENGELI, M., GINSBURG, T.H., RUTISHAUSER, H. and STIEFEL, E. - "Refined Iterative Methods for Computation of the Solution and the Eigenvalues of Self-Adjoint Boundary-Value Problems". Basle: Birkhauser, 1959.

23. FLINT, A.R. - "Some Model Tests in Shell Structures as an Aid to Design". Proc. Symposium of Shell Research, Delft, 1961.

24. FORSYTHE, G.E. - "Solving Linear Algebraic Equations Can Be Interesting". Bull. Amer. Math. Soc., Vol.59, pp.299-329.

25. FORSYTHE, G.E. and WASOW, W.R. - "Finite-Difference Methods For Partial Differential Equations". John Wiley & Sons., N.Y., 1960.

26. FOX, L. - Editor of "Numerical Solution of Ordinary and Partial Differential Equations". Pergamon Press, London, 1962.

27. FOX, L. - "Mixed Boundary Conditions in the Relaxation Treatment of Biharmonic Problems", Proc. Roy.Soc. A-Vol.189, 1947.

28. FRANKEL, S. - "Convergence Rate of Iterative Treatments of Partial Differential Equations". Mathematical Tables and Other Aids to Computation, Vol.4 (1950), pp.65-75.

29. GUPTA, N.C. DAS. - "Using Finite Difference Equations to Find the Stresses in Hypar Shells". Civil Eng. and Public Works Review, February 1961, pp. 199-201.

30. GUPTA, N.C. DAS. - "Edge Disturbances in a Hyperbolic Paraboloid". Civil Eng. and Public Works Review, February 1963.

31. HENDRY, A.W. - "Elements of Experimental Stress Analysis". Pergamon Press, 1964.

32. HERGENRÖDER, A., and RÜSCH, H. - "Recent Findings in the Testing of Models". Proc. Symposium of Shell Research, Delft, 1961.

33. ICI Properties, Perspex Acrylic Materials.

34. ICI Machining Perspex Acrylic Materials.

35. ICI Cementing Perspex Acrylic Materials.

36. JENKINS, R.S. - "Theory and Design of Cylindrical Shell Structures". Ove Arup and Partners, London, 1947.

37. JONES, L.L. - "Tests on a One-Tenth Scale Model of a Hyperbolic Paraboloid Shell Roof". Magazine of Concrete Research, March 1961.

38. KELLEY, D.R. - "The Influence of Edge Beam and End Diaphragm Stiffness on the Stress Distribution in a Cylindrical Shell Roof". Ph.D. Thesis, Queen Mary College, University of London, 1963.

39. LEICESTER, R. and MASSEY, P.C. - "Model Analysis of a Concrete Shell Roof". Arch. Science Rev., Nov. 1960.

40. LITLE, W.A. - "Reliability of Shell Buckling Predictions". Research Monograph No.25, The M.I.T. Press, Cambridge, Massachusetts.

41. LOVE, A.E.H. - "A Treatise on the Mathematical Theory of Elasticity". Cambridge University Press, 1934.

42. MARTIN, D.W. and TEE, G.J. - "Iterative Methods for Linear Equations with Symmetric Positive Definite Matrices". Computer J. Vol.4., 1961.

43. NOOR, A.K. and VELETSOS, A.S. - "A Study of Doubly Curved Shallow Shells". Report prepared as Doctoral Dissertation, University of Illinois, Urbana, Illinois, November 1963.

44. POWELL, G.H. - "A Study of Reinforced Concrete Shell Roofs Employing Observations on Model Structures". Ph.D. thesis, University of Canterbury, Christchurch, New Zealand, 1964.

45. POWELL, G.H. - "Interaction of Edge Beams with Doubly Curved Shells". Proc.Amer. Soc. of Civil Engineers, ST.3, June 1966.

46. REISSNER, E. - "On Some Aspects of the Theory of Thin Elastic Shells". Bost. Soc. of Civil Engineers, 1955, pp. 100-133.

47. ROCHA, M. - "Model Studies of Structures in Portugal". Lab. Nac. de Eng. Civ., Lisbon, Pub. No. 84 (English trans. available as NRC TT-970, Nat. Res. Council of Can. Div. of Bldg. Res., 1961).

48. ROWE, R.E. - "Tests on Four Types of Hyperbolic Shells". Proc. Symp. of Shell Research, Delft, 1961.

49. SHAW, F.S. - "An Introduction to Relaxation Methods". N.Y. Dover Publications, 1953.

50. SLED, J.J. - Letter to the Editor, Civil Engineering and Public Works Review, pp. 1409, Nov. 1962.

51. SOARE, M. - "A Numerical Approach to the Bending Theory of Hypar Shells". Part 1 Indian Concrete Journal, Feb.1966. Part 2 Indian Concrete Journal, March 1966.

52. SOUTHWELL, R.V. - "Relaxation Methods in Theoretical Physics' Oxford Univ. Press, 1946.

53. STANTON, R.G. - "Numerical Methods for Science and Engineering". Englewood Cliffs, N.J., Prentice-Hall, 1961.

54. TIMOSHENKO, S. and WOINOWSKY - KRIEGER, S. - "Theory of Plates and Shells". Second Edition, McGraw Hill Book Co., 1959.

TIMOSHENKO, S. - "Strength of Materials". D. Van Nostrand Co., N.Y., 1955.

55. TODD, J. - Editor of "A Survey of Numerical Analysis". McGraw Hill Book Co., N.Y., 1962.

56. UTKU, S. - "Utilization of Digital Computers in the Stress Analysis of Shells". Doctor of Science, M.I.T., Cambridge, Massachusetts, May 1960.

57. VLASOV, V.Z. - "The Basic Differential Equations in the General Theory of Elastic Shells". (Prikladnaia Matematika i Mekhanika, vol.8, 1944) also National Advisory Committee for Aeronautics (U.S.A.) Tech. Memo, No. 1241.

58. WANG, C.T. - "Applied Elasticity". McGraw Hill Book Co. 1953.

59. YOUNG, D. - "Iterative Methods for Solving Partial Difference Equations of Elliptic Type". Doctoral Thesis, Harvard University, 1950.

60. YOUNG, D. - "Iterative Methods for Solving Partial Difference Equations of Elliptic Type". Trans. Amer. Math. Soc., Vol.76, 1954.

61. YOUNG, D. - "ORDVAC solutions of the Dirichlet Problem". J. Assoc. Comput. Mach., Vol.2, 1955.

A P P E N D I X A

COMPUTER PROGRAMMES

As examples of the more important boundary conditions considered, the conventional finite difference programmes with boundary analogues containing truncation errors of the order of h^2 are listed. Descriptions of the theory involved in these programmes are given in the sections indicated in Table A.1.

PROGRAMME	SECTION DESCRIBED
1	8.2.1 and 8.2.2
2	8.3.2(c)
3	8.2.3
4	8.3.3(c)
5	10.1

TABLE A.1 Sections in thesis describing theory of computer programmes listed.

The input-output notation used in programmes 1 to 5, and the equivalent symbols used in the thesis are presented in table A.2. The symbol NBA used in programme 1 defines either the simple support (NBA = 1) or the clamped support (NBA = 2).

FORTRAN Symbol	THESIS Notation	FORTRAN Symbol	THESIS Notation	FORTRAN Symbol	THESIS Notation
A	a	BETA	β	VSUMT	$k_{V_{2_r}}$
H	f	NI	(k)	PVSUMT	%
TS	t_s	N1	$k_{n_{ij}}^{11}$	VSUMS	$k_{V_{3_r}}$
TB	t_b	N2	$k_{n_{ij}}^{22}$	PVSUMS	%
BB	b_b	N3	$k_{n_{ij}}^{12}$	VSUMQ	$k_{V_{4_r}}$
E2	e_2	M1	$k_{m_{ij}}^{11}$	PVSUMQ	%
E3	e_3	M2	$k_{m_{ij}}^{22}$	VSUM	$k_{V_{1_r}}$
CT	δ	M3	$k_{m_{ij}}^{12}$	SVE(I)	$k_{V_{0_r}}$
CMU	μ	M4	$k_{m_{ij}}^{21}$	HSUMT	$k_{H_{2_r}}$
M	m	Q1	$k_{q_{ij}}^{11}$	PHSUMT	%
Q(I,J)	$k_{p_{ij}}^{3}$	Q2	$k_{q_{ij}}^{22}$	HSUMS	$k_{H_{3_r}}$
G(J)	$k_{G_j}^{3}$	ES	E_s	PHSUMS	%
u(I,J)	$k_{w_{ij}}^{1}$	EB	E_b	HSUMQ	$k_{H_{4_r}}$
v(I,J)	$k_{w_{ij}}^{2}$	T(I,J)	$k_{n_{ij}}^{22}$	PHSUMQ	%
w(I,J)	$k_{w_{ij}}^{3}$	S(I,J)	$k_{n_{ij}}^{12}$	HSUM	$k_{H_{1_r}}$
U1	$k_{w_{ij}}^{1}$	Q(I,J)	$k_{q_{ij}}^{22}$	SHE(I)	$k_{H_{0_r}}$
U2	$k_{w_{ij}}^{2}$	I	r		
U3	$k_{w_{ij}}^{3}$				

TABLE A.2 Symbols used in the input and output of programmes 1 to 5.

PROGRAMME 1. Degenerate displacement boundaries, using conventional finite difference technique. Computation of displacement

```
C     HYPERBOLIC PARABOLOID, STRAIGHT GENERATORS. CH. 1 AND 2 A.
C
C     FINITE DIFFERENCE SOLUTION USING DISPLACEMENT VECTOR TECHNIQUE.
C      SQUARE HYPAR SHELL, SYMMETRIC VERTICAL LOAD, WITH....
C         1. SIMPLY SUPPORTED EDGES.
C         2. CLAMPED EDGES.
C
C     SOLUTION OVER 1/8 TH SHELL AREA. TRUNCATION ERROR O(H**2).
C     SOLUTION USING OVER RELAXATION.
C
      DIMENSION U(20,20),V(20,20),W(20,20),Q(17,17)
C     INPUT, SHELL GEOMETRY, LOADING AND INITIAL DISPLACEMENT VECTORS.
    1 READ100,A,H,TS,CMU,M,NBA
  100 FORMAT(3F8.2,12X,F8.2,I4,6X,I4)
      M1=M+1
      M2=M+2
      M3=M+3
      M4=M+4
      YM=M
      C1=1./(2.*YM)**4
      DO31I=1,M1
      DO31J=1,M1
      READ101,Q(I,J)
    3 Q(I,J)=C1*Q(I,J)
      DO51I=1,M4
      DO51J=1,M4
    5 READ102,U(I,J),V(I,J),W(I,J)
  101 FORMAT(E14.8)
  102 FORMAT(3E14.8)
C     INITIALIZATION OF PROGRAM CONSTANTS.
      XM1=(1.-CMU)/2.
      XU2=-2.*(1.+XU1)
      XV1=(1.+CMU)/8.
      XW1=XU1*M/(A*YM)
      ZW1=20.+48.*XU1*(H/YM**2)**2/TS**2
      ZU1=12.*XU1**A/((TS*YM)**2*YM)
      DO61I=1,M4
      IF(NBA-1)27,28,27
   27 V(2,J)=0.
   28 V(J,M2)=0.
      U(M2,J)=0.
      U(2,J)=0.
    6 W(2,J)=0.
      N1=0.
C     INITIALIZATION OF OVER RELAXATION FACTORS.
    7 READ103,BETA1,BETA2,BETA3
  103 FORMAT(3F4.3)
      CND1=BETA1/XU2
      CND2=BETA2/XU2
      CND3=BETA3/ZW1
      C1=-2.*H/(A*YM)
C     COMPUTATION OF BOUNDARY PIVOTALS.
    8 N1=N1+1
      K1=2
C      1. SYMMETRIC PIVOTALS.
      DO91=2,M2
      U(1,M3)=-U(1,M1)
      V(1,M3)=-V(1,M1)
      W(1,M3)=W(1,M1)
      W(1,M4)=W(1,M)
      U(1+1,K1)=V(1,K1+1)
      U(1+2,K1)=V(1,K1+2)
      V(1+1,K1)=U(1,K1+1)
      V(1+2,K1)=U(1,K1+2)
      W(1+1,K1)=W(1,K1+1)
      W(1+2,K1)=W(1,K1+2)
    9 K1=K1+1
      V(M3,M3)=-V(M3,M1)
      U(M3,M3)=U(M3,M1)
      W(M3,M3)=W(M3,M1)
C      2. EDGE PIVOTALS.
      DO12J=3,M2
      IF(NBA-1)11,10,11
   10 W(1,J)=-W(3,J)
      U(1,J)=-U(3,J)+C1*W(3,J)
      V(1,J)=V(3,J)
      GO TO 12
   11 W(1,J)=W(3,J)
   12 K1=3
      W(3,1)=W(1,3)
C     COMPUTATION DIFFERENTIAL PIVOTALS.
      DO141=3,M2
      DO13J=K1,M2
      IF(I-M2)25,23,25
   25 IF(J-M2)22,26,22
   22 ES1=XV1*(U(I-1,J+1)+U(I+1,J-1)-U(I+1,J+1)-U(I-1,J-1))-V(I+1,J)
      ES2=-V(I-1,J)-XU1*(V(I,J+1)+V(I,J-1))-XW1*(W(I,J+1)-W(I,J-1))
      V(I,J)=V(I,J)+CND2*(ES1+ES2-XU2*V(I,J))
   26 ES1=XV1*(V(I+1,J-1)+V(I-1,J+1)-V(I+1,J+1)-V(I-1,J-1))-U(I,J+1)
      ES2=-U(I,J-1)-XU1*(U(I+1,J)+U(I-1,J))-XW1*(W(I+1,J)-W(I-1,J))
      U(I,J)=U(I,J)+CND1*(ES1+ES2-XU2*U(I,J))
   23 ES1=Q(I-1,J-1)-W(I+2,J)-W(I-2,J)-W(I,J+2)-W(I,J-2)-ZW1*W(I,J)
      ES2=8.*(W(I+1,J)+W(I-1,J)+W(I,J+1)+W(I,J-1))
      ES3=2.*(W(I+1,J+1)+W(I+1,J-1)+W(I-1,J+1)+W(I-1,J-1))-ES1-ES2
   13 W(I,J)=W(I,J)-CND3*(ES3+ZU1*(U(I+1,J)-U(I-1,J)+V(I,J+1)-V(I,J-1)))
   14 K1=K1+1
      IF(NBA-1)1,15,24
   15 U(1,2)=V(2,3)
      U(1,M3)=U(1,M1)
      DO16J=3,M1
      ES1=XV1*(U(3,J-1)+U(1,J+1)-U(1,J-1)-U(3,J+1))-XU2*V(2,J)
   16 V(2,J)=V(2,J)+CND2*(ES1-XU1*(V(2,J+1)+V(2,J-1))-V(3,J)-V(1,J))
   24 IF(SENSE SWITCH 1)17,18
   17 PRINT104,N1,U(M,M),V(M,M),W(M2,M2)
  104 FORMAT(2X,I4,3(2X,E10.4))
   18 IF(SENSE SWITCH 2)7,19
   19 IF(SENSE SWITCH 3)20,8
C     DATA OUTPUT.
   20 PUNCH100,A,H,TS,CMU,M,NBA
      DO211=1,M4
      DO21J=1,M4
   21 PUNCH102,U(I,J),V(I,J),W(I,J)
      GO TO 1
      END
```

PROGRAMME 1. (continued) Degenerate displacement boundaries. Interpolation and computation of internal shell actions.

```
C     HYPERBOLIC PARABOLOID, STRAIGHT GENERATORS. CH. 1 AND 2 A.
C
C     INTERPOLATION PROGRAM. GRID INTERVAL HALVED.
C
      DIMENSION U(20,20),V(20,20),W(20,20),Q(20,20),R(20,20)
    1 READ100,A,H,TS,CMU,M
      M4=M+4
      K=2*M
      K4=K+4
      DO21I=1,M4
      DO2J=1,M4
    2 READ101,U(I,J),V(I,J),W(I,J)
      NO=1
    3 DO7I=1,M4
      DO7J=1,M4
      IF(NO-2)4,5,6
    4 R(I,J)=U(I,J)
      GO TO 7
    5 R(I,J)=V(I,J)
      GO TO 7
    6 R(I,J)=W(I,J)
    7 CONTINUE
      DO15I=1,K4
      IA=I/2*2
      IF(IA-I)8,12,8
    8 I2=(I+1)/2+1
      DO11J=1,K4
      JA=J/2*2
      IF(JA-J)9,10,9
    9 J2=(J+1)/2+1
      Q(I,J)=R(I2,J2)
      GO TO 11
   10 Q(I,J)=.5*(R(I2,J2)+R(I2,J2+1))
   11 CONTINUE
      GO TO 15
   12 DO15J=1,K4
      JA=J/2*2
      IF(JA-J)13,14,13
   13 J2=(J+1)/2+1
      Q(I,J)=.5*(R(I2,J2)+R(I2+1,J2))
      GO TO 15
   14 Q(I,J)=.25*(R(I2,J2)+R(I2,J2+1)+R(I2+1,J2)+R(I2+1,J2+1))
   15 CONTINUE
      DO19I=1,K4
      DO19J=1,K4
      IF(NO-2)16,17,18
   16 U(I,J)=Q(I,J)
      GO TO 19
   17 V(I,J)=Q(I,J)
      GO TO 19
   18 W(I,J)=Q(I,J)
   19 CONTINUE
      IF(NO-2)20,20,21
   20 NO=NO+1
      GO TO 3
   21 PUNCH100,A,H,TS,CMU,K
      DO22I=1,K4
      DO22J=1,K4
   22 PUNCH101,U(I,J),V(I,J),W(I,J)
      GO TO 1
  100 FORMAT(3F6.2,12X,F6.2,I4)
  101 FORMAT(3E14.8)
      END


C     HYPERBOLIC PARABOLOID, STRAIGHT GENERATORS. CH. 1 AND 2 A.
C
C     COMPUTATION OF INTERNAL SHELL ACTIONS.
      DIMENSION U(20,20),V(20,20),W(20,20)
    1 READ100,A,H,TS,CMU,M
      N=2*M
      M1=M+1
      M2=M+2
      M3=M+3
      M4=M+4
      XN=N
      B1=(2.*A/TS)**2*XN*6.
      B2=B1*(1.-CMU)/2.
      B3=(2.*A/TS)**2*24.*H/A*(1.-CMU)
      B4=XN**2
      B5=-2.*(1.+CMU)*B4
      B6=(1.-CMU)*XN**2/4.
      B7=XN**3/2.
      DO7I=1,M4
      DO7J=1,M4
    7 READ101,U(I,J),V(I,J),W(I,J)
  100 FORMAT(3F6.2,12X,F6.2,I4)
  101 FORMAT(3E14.8)
      W(1,1)=W(3,3)
      W(1,M3)=W(1,M1)
      PUNCH100,A,H,TS,CMU,M
      PUNCH4
    4 FORMAT(13X,2HU1,10X,2HU2,10X,2HU3,10X,2HN1,10X,2HN2,10X,2HN3/)
      K1=2
      DO61=2,M2
      DO2J=K1,M2
      U1=U(I,J)
      U2=V(I,J)
      U3=W(I,J)
      IF(I-2)8,3,8
    3 D2=B1*(-V(4,J)+4.*V(3,J)-3.*V(2,J))
      D1=D2*CMU
      D3=B2*(-U(4,J)+4.*U(3,J)-3.*U(2,J)+V(2,J+1)-V(2,J-1))+B3*W(2,J)
      GO TO 11
    8 D1=B1*(U(I,J+1)-U(I,J-1)+CMU*(V(I+1,J)-V(I-1,J)))
      D2=B1*(V(I+1,J)-V(I-1,J)+CMU*(U(I,J+1)-U(I,J-1)))
      D3=B2*(U(I+1,J)-U(I-1,J)+V(I,J+1)-V(I,J-1))+B3*W(I,J)
   11 K=I-1
      L=J-1
    2 PUNCH102,K,L,U1,U2,U3,D1,D2,D3
  102 FORMAT(2I3,2X,6E12.6)
    6 K1=K1+1
      PUNCH5
    5 FORMAT(//13X,2HM1,10X,2HM2,10X,2HM3,10X,2HM4,10X,2HQ1,10X,2HQ2/)
      K1=2
      DO18I=2,M2
      DO9J=K1,M2
      C1=-B4*(W(I,J+1)+W(I,J-1)+CMU*(W(I+1,J)+W(I-1,J)))-B5*W(I,J)
      C2=B4*(W(I+1,J)+W(I-1,J)+CMU*(W(I,J+1)+W(I,J-1)))+B5*W(I,J)
      C3=-B6*(W(I+1,J+1)+W(I-1,J-1)-W(I-1,J+1)-W(I+1,J-1))
      C4=-C3
      IF(J-2)15,12,15
   15 ES=-B7*(W(I,J+2)-W(I,J-2)+W(I+1,J+1)+W(I-1,J+1))
      Q1=ES-B7*(-W(I+1,J-1)-W(I-1,J-1)-4.*(W(I,J+1)-W(I,J-1)))
      IF(I-2)13,12,13
   12 ES=3.*B7*(W(3,J)+W(1,J)+W(2,J+1)+W(2,J-1)-2.*W(2,J))
      ES=4.*B7*(W(4,J)+W(2,J)+W(3,J+1)+W(3,J-1)-2.*W(3,J))-ES
      Q2=ES-B7*(W(5,J)+W(3,J)+W(4,J+1)+W(4,J-1)-2.*W(4,J))
      IF(J-2)14,16,14
   16 Q1=Q2
      GO TO 14
   13 ES=-B7*(W(I+2,J)-W(I-2,J)+W(I+1,J+1)+W(I-1,J+1))
      Q2=ES-B7*(-W(I-1,J+1)-W(I-1,J-1)-4.*(W(I+1,J)-W(I-1,J)))
   14 K=I-1
      L=J-1
    9 PUNCH102,K,L,C1,C2,C3,C4,Q1,Q2
   18 K1=K1+1
      GO TO 1
      END
```

PROGRAMME 2. Beam displacement boundary, using conventional finite difference technique. Computation of displacement

```
C     HYPERBOLIC PARABOLOID, STRAIGHT GENERATORS. CH. 7 PT. 1.A 1.
C
C      SQUARE HYPAR SHELL, SYMMETRIC VERTICAL LOADING, WITH....
C       1. EDGE BEAM WITH FINITE LATERAL,
C        TORSIONAL, VERTICAL, AND EXTENSIONAL STIFFNESS.
C         A. CLAMPED BASE.
C         B. CLAMPED APEX.
C
C     SOLUTION OVER 1/8 SHELL AREA, USING OVER RELAXATION
C      OF ORDINARY FINITE DIFFERENCE ANALOGUE OF DISPLACEMENT
C      VECTOR REPRESENTATION OF THIN SHALLOW SHELL EQUATIONS.
C
C     BOUNDARY ANALOGUE O(H**2), AND OF CLASS 1.
C
      DIMENSION U(21,21),V(21,21),W(21,21),Q(17,17)
C     INPUT SHELL GEOMETRY, LOADING, AND INITIAL DISPLACEMENT VECTORS.
    1 READ100,A,H,TS,TB,BB,CMU,M,CT
  100 FORMAT(6F6.2,I4,F6.2)
      M1=M+1
      M2=M+2
      M3=M+3
      M4=M+4
      M5=M+5
      NI=0
      YM=M
      C1=1./(2.*YM)**4
      DO2I=1,M1
      DO2J=1,M1
      READ101,Q(I,J)
    2 Q(I,J)=C1*Q(I,J)
      DO3I=1,M5
      DO3J=1,M5
    3 READ102,U(I,J),V(I,J),W(I,J)
C     INITIALIZATION OF PROGRAM CONSTANTS.
      XU1=(1.-CMU)/2.
      XU2=-2.*(1.+XU1)
      XV1=(1.+CMU)/8.
      XW1=XU1*H/(A*YM)
      ZW1=20.+48.*XU1*(H/(TS*YM**2))**2
      ZU1=12.*XU1*H*A/((TS*YM)**2*YM)
      BW1=2.*(1.+CMU)
      BW2=(2.-CMU)
      BW3=2.*(1.+BW2)
      BW4=A/(2.*YM*BB)
      BW5=(TS/TB)**3/(1.-CMU**2)
      BW6=(TS/BB)**3*4.*A/(CT*TB*YM*(1.-CMU))
      BW7=CMU*BW6+1.
      BW8=2.*((1.+CMU)*BW6+1.)
      BU1=.25*A*TS/(BB*TB*YM*(1.+CMU))
      BU2=4.*H/(YM*A)
      BV1=6.0*TS/TB*(A/(YM*BB))**3/(1.-CMU**2)
      BV2=CMU*BV1
      BV3=1./(6.+BV1)
C     INITIALIZATION OF CONSTANT PIVOTS.
      U(3,3)=0.
      V(3,3)=0.
      W(3,3)=0.
      U(M3,M3)=0.
      V(M3,M3)=0.
C     INITIALIZATION OF OVER RELAXATION FACTORS.
    4 READ103,BETA1,BETA2
  101 FORMAT(E14.8)
  102 FORMAT(3E14.8)
  103 FORMAT(2F4.3)
      CND1=BETA1/XU2
      CND2=BETA1/2.
      CND3=BETA2/ZW1
      CND4=BETA2/6.
    5 NI=NI+1
C     COMPUTATION OF BOUNDARY PIVOTS.
C       A. SYMMETRIC PIVOTS.
      DO61=2,M3
      I1=I+1
      I2=I+2
      U(I,M4)=U(I,M2)
      V(I,M4)=-V(I,M2)
      W(I,M4)=W(I,M2)
      W(I,M5)=W(I,M1)
      U(I1,I)=V(I,I1)
      U(I2,I)=V(I,I2)
      V(I1,I)=U(I,I1)
      V(I2,I)=U(I,I2)
      W(I1,I)=W(I,I1)
    6 W(I2,I)=W(I,I2)
      W(M4,M4)=W(M2,M2)
C       B. EXTERNAL PIVOTS.
    9 W(2,3)=W(3,4)
      DO10J=4,M3
      ES1=V(3,J+2)+V(3,J-2)-4.*(V(3,J+1)+V(3,J-1))
      V(3,J)=BV3*(BV2*(U(4,J+1)-U(4,J-1))+BV1*V(5,J)-ES1)
      ES1=W(2,J+1)+W(2,J-1)-BW6*(W(5,J)+W(3,J))+BW8*W(4,J)
   10 W(2,J)=.5*(ES1-BW7*(W(4,J+1)+W(4,J-1)))
C     COMPUTATION OF INTERNAL PIVOTS.
      K1=4
      DO18I=3,M3
      IF(I-4)12,15,14
   12 DO13J=4,M3
      ES1=U(3,J+1)+U(3,J-1)-2.*U(3,J)+BU1*BU2*W(4,J)
      ES2=ES1+BU1*(U(5,J)-U(3,J)+V(4,J+1)-V(4,J-1))
      U(3,J)=U(3,J)+CND2*ES2
      ES1=W(6,J)-W(2,J)+BW2*(W(5,J+1)+W(5,J-1)-W(3,J+1)-W(3,J-1))
      ES2=4.*(W(3,J+1)+W(3,J-1))+BW5*(Q(1,J-2)+BW4*BW3*(W(5,J)-W(3,J)))
   13 W(3,J)=W(3,J)+CND4*(ES2-W(3,J+2)-W(3,J-2)-6.*W(3,J)-BW5*BW4*ES1)
      GO TO 18
   14 K1=K1+1
   15 DO18J=K1,M3
```

PROGRAMME 2. (continued) Beam displacement boundary. Computation of internal shell and beam actions.

```
      IF(I-M3)16,17,16
   16 ES1=XV1*(V(I+1,J-1)+V(I-1,J+1)-V(I+1,J+1)-V(I-1,J-1))-U(I,J+1)
      ES2=-U(I,J-1)-XU1*(U(I+1,J)+U(I-1,J))-XW1*(W(I+1,J)-W(I-1,J))
      U(I,J)=U(I,J)+CND1*(ES1+ES2-XU2*U(I,J))
      ES1=XV1*(U(I+1,J-1)+U(I-1,J+1)-U(I+1,J+1)-U(I-1,J-1))-V(I+1,J)
      ES2=-V(I-1,J)-XU1*(V(I,J+1)+V(I,J-1))-XW1*(W(I,J+1)-W(I,J-1))
      V(I,J)=V(I,J)+CND1*(ES1+ES2-XU2*V(I,J))
   17 ES1=Q(I-2,J-2)-W(I+2,J)-W(I-2,J)-W(I,J+2)-W(I,J-2)-ZW1*W(I,J)
      ES2=8.(W(I+1,J)+W(I-1,J)+W(I,J+1)+W(I,J-1))+ES1
      ES3=-2.*(W(I+1,J+1)+W(I+1,J-1)+W(I-1,J+1)+W(I-1,J-1))+ES2
      W(I,J)=W(I,J)+CND3*(ES3-ZU1*(U(I+1,J)-U(I-1,J)+V(I,J+1)-V(I,J-1)))
   18 CONTINUE
      IF(SENSE SWITCH 1)19,20
C     OUTPUT SHELL GEOMETRY, AND FINAL DISPLACEMENT VECTORS.
   19 PRINT104,NI,U(M,M3),V(M,M3),W(M3,M3)
   20 IF(SENSE SWITCH 2)4,21
   21 IF(SENSE SWITCH 3)22,5
   22 PUNCH100,A,H,TS,TB,BB,CMU,M,CT
      DO231=1,M5
      DO23J=1,M5
   23 PUNCH102,U(I,J),V(I,J),W(I,J)
  104 FORMAT(14,3E11.5)
      GO TO 1
      END


C     COMPUTATION OF INTERNAL SHELL ACTIONS.
C
      DIMENSION U(21,21),V(21,21),W(21,21)
    1 READ100,A,H,TS,TB,BB,CMU,M,CT
      PUNCH100,A,H,TS,TB,BB,CMU,M,CT
  100 FORMAT(6F6.2,I4,F6.2)
      N=2*M
      M3=M+3
      M5=M+5
      XN=N
      YM=M
      A1=48.*YM*(1.-CMU**2)*TB/TS*(A/TS)**2*BB
      A2=4.*YM**2*(1.-CMU**2)*BB*(TB/TS)**3
      A3=4.*YM**2*(1.-CMU**2)*TB*(BB/TS)**3
      A4=96.*YM**2*(1.-CMU)*CT*TB*(BB/TS)**3
      A5=8.*YM**3*(1.-CMU**2)*BB*(TB/TS)**3
      A6=8.*YM**3*(1.-CMU**2)*TB*(BB/TS)**3
      B1=(2.*A/TS)**2*XN*6.
      B2=B1*(1.-CMU)/2.
      B3=(2.*A/TS)**2*24.*H/A*(1.-CMU)
      B4=XN**2
      B5=-2.*(1.+CMU)*B4
      B6=(1.-CMU)*XN**2/4.
      B7=XN**3/2.
      DO71=1,M5
      DO7J=1,M5
    7 READ14,U(I,J),V(I,J),W(I,J)
   14 FORMAT(3E14.8)
      PUNCH4
    4 FORMAT(13X,2HU1,10X,2HU2,10X,2HU3,10X,2HN1,10X,2HN2,10X,2HN3)
      DO10J=3,M3
      K=1
      L=J-2
      U1=U(3,J)
      U2=V(3,J)
      U3=W(3,J)
      D1=A1*(U(3,J+1)-U(3,J-1))
   10 PUNCH3,K,L,U1,U2,U3,D1
      K1=4
      DO61=4,M3
      DO2J=K1,M3
      U1=U(I,J)
      U2=V(I,J)
      U3=W(I,J)
      D1=B1*(U(I,J+1)-U(I,J-1)+CMU*(V(I+1,J)-V(I-1,J)))
      D2=B1*(V(I+1,J)-V(I-1,J)+CMU*(U(I,J+1)-U(I,J-1)))
      D3=B2*(U(I+1,J)-U(I-1,J)+V(I,J+1)-V(I,J-1))+B3*W(I,J)
      K=I-2
      L=J-2
    2 PUNCH3,K,L,U1,U2,U3,D1,D2,D3
      K1=K1+1
    6 CONTINUE
      PAUSE
      PUNCH5
    5 FORMAT(13X,2HM1,10X,2HM2,10X,2HM3,10X,2HM4,10X,2HQ1,10X,2HQ2)
      DO11,J=3,M3
      K=1
      L=J-2
      C1=A3*(V(3,J+1)+V(3,J-1)-2.*V(3,J))
      C2=-A2*(W(3,J+1)+W(3,J-1)-2.*W(3,J))
      C3=A4*(W(4,J+1)-W(4,J-1)-W(2,J+1)+W(2,J-1))
      Q1=A5*(W(3,J+2)-3.*(W(3,J+1)-W(3,J-1))-W(3,J-2))
      Q2=-A6*(V(3,J+2)-3.*(V(3,J+1)-V(3,J-1))-V(3,J-2))
   11 PUNCH3,K,L,C1,C2,C3,Q1,Q2
      K1=4
      DO181=4,M3
      DO9J=K1,M3
      C1=-B4*(W(I,J+1)+W(I,J-1)+CMU*(W(I+1,J)+W(I-1,J)))-B5*W(I,J)
      C2=B4*(W(I+1,J)+W(I-1,J)+CMU*(W(I,J+1)+W(I,J-1)))+B5*W(I,J)
      C3=-B6*(W(I+1,J+1)+W(I-1,J-1)-W(I-1,J+1)-W(I+1,J-1))
      C4=-C3
      ES=-B7*(W(I,J+2)-W(I,J-2)+W(I+1,J+1)+W(I-1,J+1))
      Q1=ES-B7*(-W(I+1,J-1)-W(I-1,J-1)-4.*(W(I,J+1)-W(I,J-1)))
      ES=-B7*(W(I+2,J)-W(I-2,J)+W(I+1,J+1)+W(I+1,J-1))
      Q2=ES-B7*(-W(I-1,J+1)-W(I-1,J-1)-4.*(W(I+1,J)-W(I-1,J)))
      K=I-2
      L=J-2
    9 PUNCH3,K,L,C1,C2,C3,C4,Q1,Q2
      K1=K1+1
   18 CONTINUE
      GO TO 1
    3 FORMAT(2I4,6E12.6)
      END
```

PROGRAMME 3. Degenerate traction boundary, using conventional finite difference technique. Computation of displacement vector.

```
C
C     HYPERBOLIC PARABOLOID, STRAIGHT GENERATORS. CH. 3 PT. 1.A
C
C      SQUARE HYPAR SHELL, SYMMETRIC VERTICAL LOADING, WITH....
C       1. FREE EDGES.
C        A. CLAMPED BASE.
C        B. CLAMPED APEX.
C
C     SOLUTION OVER 1/8 SHELL AREA, USING OVER RELAXATION
C      OF ORDINARY FINITE DIFFERENCE ANALOGUE OF DISPLACEMENT
C      VECTOR REPRESENTATION OF THIN SHALLOW SHELL EQUATIONS.
C
C     BOUNDARY ANALOGUE O(H**2), AND OF CLASS 1.
C
      DIMENSION U(21,21),V(21,21),W(21,21),Q(17,17)
C     INPUT SHELL GEOMETRY, LOADING, AND INITIAL DISPLACEMENT VECTORS.
    1 READ100,A,H,TS,CMU,M
   24 MC=M/2+3
      M1=M+1
      M2=M+2
      M3=M+3
      M4=M+4
      M5=M+5
      N1=0
      YM=M
      C1=1./(2.*YM)**4
      DO21I=1,M1
      DO2J=1,M1
      READ101,Q(I,J)
    2 Q(I,J)=C1*Q(I,J)
      DO3I=1,M5
      DO3J=1,M5
    3 READ102,U(I,J),V(I,J),W(I,J)
C     INITIALIZATION OF PROGRAM CONSTANTS.
      XU1=(1.-CMU)/2.
      XU2=-2.*(1.+XU1)
      XV1=(1.+CMU)/8.
      XW1=XU1*H/(A*YM)
      ZW1=20.+48.*XU1*(H/(TS*YM**2))**2
      ZU1=12.*XU1*H*A/((TS*YM)**2*YM)
      B1=2.*(1.+CMU)
      B2=2.-CMU
      B3=2.*(1.+B2)
C     INITIALIZATION OF CONSTANT PIVOTS.
      U(3,3)=0.
      V(3,3)=0.
      W(3,3)=0.
      DO26I=1,M5
   26 V(I,M3)=0.
      C1=4.*H/(A*YM)
C     INITIALIZATION OF OVER RELAXATION FACTORS.
    4 READ103,BETA1,BETA2
      CND1=BETA1/XU2
      CND3=BETA2/ZW1
    5 N1=N1+1
C     COMPUTATION OF BOUNDARY PIVOTS.
C      A. SYMMETRIC PIVOTS.
      DO71=2,M3
      I1=I+1
      I2=I+2
      U(I1,1)=V(I,I1)
      U(I2,1)=V(I,I2)
      V(I1,1)=U(I,I1)
      V(I2,1)=U(I,I2)
      W(I1,1)=W(I,I1)
      W(I2,1)=W(I,I2)
      U(I,M4)=U(I,M2)
      V(I,M4)=-V(I,M2)
      W(I,M4)=W(I,M2)
    7 W(I,M5)=W(I,M1)
      U(M4,M4)=-U(M2,M2)
      V(M4,M4)=-V(M2,M2)
      W(M4,M4)=W(M2,M2)
C      B. EXTERNAL PIVOTS.
      U(2,3)=U(4,3)
      V(2,3)=-V(4,3)
      W(2,3)=W(4,3)
      DO10J=4,M3
      U(2,J)=U(4,J)+V(3,J+1)-V(3,J-1)+C1*W(3,J)
      V(2,J)=V(4,J)+CMU*(U(3,J+1)-U(3,J-1))
   10 W(2,J)=-W(4,J)+B1*W(3,J)-CMU*(W(3,J+1)+W(3,J-1))
      DO11J=4,M3
      ES1=B2*(W(4,J+1)+W(4,J-1)-W(2,J+1)-W(2,J-1))+B3*(W(2,J)-W(4,J))
   11 W(1,J)=W(5,J)+ES1
C     COMPUTATION OF INTERNAL PIVOTS.
      DO17I=3,M3
      IF(I-4)12,15,13
   12 K1=4
      GO TO 15
   13 K1=K1+1
   15 DO30J=K1,M2
      ES1=XV1*(U(I+1,J-1)+U(I-1,J+1)-U(I+1,J+1)-U(I-1,J-1))-V(I+1,J)
      ES2=-V(I-1,J)-XU1*(V(I,J+1)+V(I,J-1))-XW1*(W(I,J+1)-W(I,J-1))
   30 V(I,J)=V(I,J)+CND1*(ES1+ES2-XU2*V(I,J))
      DO17J=K1,M3
      ES1=XV1*(V(I+1,J-1)+V(I-1,J+1)-V(I+1,J+1)-V(I-1,J-1))-U(I,J+1)
      ES2=-U(I,J-1)-XU1*(U(I+1,J)+U(I-1,J))-XW1*(W(I+1,J)-W(I-1,J))
      U(I,J)=U(I,J)+CND1*(ES1+ES2-XU2*U(I,J))
      ES1=Q(I-2,J-2)-W(I+2,J)-W(I-2,J)-W(I,J+2)-W(I,J-2)-ZW1*W(I,J)
      ES2=8.*(W(I+1,J)+W(I,J+1)+W(I-1,J)+W(I,J-1))+ES1
      ES3=-2.*(W(I+1,J+1)+W(I-1,J+1)+W(I+1,J-1)+W(I-1,J-1))+ES2
   17 W(I,J)=W(I,J)+CND3*(ES3-ZU1*(U(I+1,J)-U(I-1,J)+V(I,J+1)-V(I,J-1)))
      IF(SENSE SWITCH 1)18,19
C     OUTPUT SHELL GEOMETRY, AND FINAL DISPLACEMENT VECTORS.
   18 PRINT104,N1,U(3,M3),V(MC,MC),W(M3,M3)
   19 IF(SENSE SWITCH 2)4,20
   20 IF(SENSE SWITCH 3)21,5
   21 PUNCH100,A,H,TS,CMU,M
      DO22I=1,M5
      DO22J=1,M5
   22 PUNCH102,U(I,J),V(I,J),W(I,J)
      GO TO 1
  100 FORMAT(3F6.2,12X,F6.2,I4)
  101 FORMAT(E14.8)
  102 FORMAT(3E14.8)
  103 FORMAT(2F4.3)
  104 FORMAT(I4,3(2X,E11.5))
      END
```

PROGRAMME 4. Beam traction boundary, using conventional finite difference technique. Computation of displacement vector.

```
C     HYPERBOLIC PARABOLOID, STRAIGHT GENERATORS. CH. 7 PT. 1. B.
C
C      SQUARE HYPAR SHELL, SYMMETRIC VERTICAL LOADING, WITH...
C       EDGE BEAMS WITH FINITE VERTICAL, EXTENSIONAL,
C       TORSIONAL AND LATERAL STIFFNESS.
C         A. CLAMPED BASE.
C         B. CLAMPED APEX.
C
      DIMENSION U(13,13),V(13,13),W(13,13),Q(13,13)
      DIMENSION S1(13),S2(13),S3(13),S4(13),C(13)
C     INPUT SHELL GEOMETRY, LOADING, AND INITIAL DISPLACEMENT VECTOR.
    1 READ100,A,H,TS,TB,BB,CMU,M,CT,E2,E3
   24 MC=M/2+3
      M1=M+1
      M2=M+2
      M3=M+3
      M4=M+4
      M5=M+5
      N1=0
      YM=M
      C1=1./(2.*YM)**4
      DO21I=1,M1
      DO2J=1,M1
      READ101,Q(I,J)
    2 Q(I,J)=C1*Q(I,J)
      C1=BB/(8.*YM**3*A)
      DO43J=1,M1
      READ101,G(J)
   43 G(J)=C1*G(J)
      DO3I=1,M5
      DO3J=1,M5
    3 READ102,U(I,J),V(I,J),W(I,J)
C     INITIALIZATION OF PROGRAM CONSTANTS.
      XU1=(1.-CMU)/2.
      XU2=-2.*(1.+XU1)
      XV1=(1.+CMU)/8.
      XW1=XU1*H/(A*YM)
      ZW1=20.+48.*XU1*(H/(TS*YM**2))**2
      ZU1=12.*XU1*H*A/((TS*YM)**2*YM)
      B1=2.*(1.+CMU)
      B2=2.-CMU
      B3=2.*(1.+B2)
      BW1=2.*Y1*(1.-CMU**2)*BB/A*(TB/TS)**3
      BU1=4.*YM*TB*BB*(1.+CMU)/(A*TS)
      BW2=.25*CT*Y1*(1.-CMU)*TB/A*(BB/TS)**3
      BW1=.1667*YM**3*(1.-CMU**2)*TB/TS*(BB/A)**3
C     INITIALIZATION OF CONSTANT PIVOTS.
      U(3,3)=0.
      V(3,3)=0.
      W(3,3)=0.
      S1(3)=0.
      S2(3)=0.
      S3(3)=0.
      S4(3)=0.
      DO26I=1,M5
   26 V(I,M3)=0.
      C1=4.*H/(A*YM)
      C2=E2*H/(2.*A)
      C3=E2*H/(2.*A)
C     INITIALIZATION OF OVER RELAXATION FACTORS.
    4 READ108,BETA1,BETA2
      CND1=BETA1/YU2
      CND3=BETA2/YW1
    5 I=N1+1
C     COMPUTATION OF BOUNDARY PIVOTS.
C       A. SYMMETRIC PIVOTS.
      DO12I=2,M3
      I1=I-1
      I2=I-2
      U(I1,1)=V(I,11)
      V(I2,1)=V(I,12)
      W(I1,1)=W(I,11)
      V(12,I)=U(I,12)
      W(11,I)=W(I,11)
      W(12,I)=W(I,12)
      U(I,M4)=U(I,M2)
      V(I,M4)=-V(I,M2)
      W(I,M4)=W(I,M2)
    7 W(I,M5)=W(I,M3)
      U(M4,M4)=-U(M2,M2)
      V(M4,M4)=-V(M2,M2)
      W(M4,M4)=W(M2,M2)
C       B. EXTERNAL PIVOTS.
      U(2,3)=U(4,3)
      V(2,3)=-V(4,3)
      W(2,3)=W(4,3)
      DO44J=4,M5
      S1(J)=C2*(W(4,J)-W(2,J))
      S2(J)=C2*(W(3,J+1)-W(3,J-1))
      S3(J)=C3*(V(3,J+1)-V(3,J-1))
   44 S4(J)=C3*(W(4,J)-W(2,J))
      S1(M4)=S1(M2)
      S2(M4)=-S2(M2)
      S3(M4)=S3(M2)
      S4(M4)=S4(M2)
      S1(M5)=S4(M1)
      S1(2)=S1(4)
      S4(2)=S4(4)
      DO10J=4,M3
      ES1=BU1*(U(3,J+1)+U(3,J-1)+S2(J+1)+S2(J-1)+S3(J+1)+S3(J-1))
      ES1=ES1-2.*BU1*(U(3,J)+S2(J)+S3(J))
      U(2,J)=U(4,J)+V(3,J+1)-V(3,J-1)+C1*W(3,J)+ES1
      ES1=BV1*(V(3,J+2)+V(3,J-2)-4.*(V(3,J+1)+V(3,J-1))+6.*V(3,J))
      ES1=ES1-BV1*(4.*(S1(J+1)+S1(J-1))-S1(J+2)-S1(J-2)-6.*S1(J))
      V(2,J)=V(4,J)+CMU*(U(3,J+1)-U(3,J-1))-ES1
      ES1=BW2*(W(4,J+1)+W(4,J-1)-W(2,J+1)-W(2,J-1))
      ES1=ES1-2.*BW2*(W(4,J)-W(2,J))
   10 W(2,J)=-W(4,J)+B1*W(3,J)-CMU*(W(3,J+1)+W(3,J-1))-ES1
      DO11J=4,M3
      ES1=B2*(W(4,J+1)+W(4,J-1)-W(2,J+1)-W(2,J-1))+B3*(W(2,J)-W(4,J))
      ES1=ES1+BW1*(W(3,J+2)+W(3,J-2)-4.*(W(3,J+1)+W(3,J-1))+6.*W(3,J))
      ES1=ES1-BW1*(S4(J+2)+S4(J-2)-4.*(S4(J+1)+S4(J-1))+6.*S4(J))
   11 W(1,J)=W(5,J)+ES1-G(J)
C     COMPUTATION OF INTERNAL PIVOTS.
      DO17I=3,M3
      IF(I-4)12,15,13
   12 K1=4
      GO TO 15
   13 K1=K1+1
   15 DO30J=K1,M2
      ES1=XV1*(U(I+1,J-1)+U(I-1,J+1)-U(I+1,J+1)-U(I-1,J-1))-V(I+1,J)
      ES2=-V(I-1,J)-XU1*(V(I,J+1)+V(I,J-1))-XW1*(W(I,J+1)-W(I,J-1))
   30 V(I,J)=V(I,J)+CND1*(ES1+ES2-XU2*V(I,J))
      DO17J=K1,M3
      ES1=XV1*(V(I+1,J-1)+V(I-1,J+1)-V(I+1,J+1)-V(I-1,J-1))-U(I,J+1)
      ES2=-U(I,J-1)-XU1*(U(I+1,J)+U(I-1,J))-XW1*(W(I+1,J)-W(I-1,J))
      U(I,J)=U(I,J)+CND1*(ES1+ES2-XU2*U(I,J))
      ES1=Q(I-2,J-2)-W(I+2,J)-W(I-2,J)-W(I,J+2)-W(I,J-2)-ZW1*W(I,J)
      ES2=6.*(W(I+1,J)+W(I,J+1)+W(I-1,J)+W(I,J-1))+ES1
      ES3=-2.*(W(I+1,J+1)+W(I-1,J+1)+W(I+1,J-1)+W(I-1,J-1))+ES2
   17 W(I,J)=W(I,J)+CND3*(ES3-ZU1*(U(I+1,J)-U(I-1,J)+V(I,J+1)-V(I,J-1)))
      IF(SENSE SWITCH 1)18,19
C     OUTPUT SHELL GEOMETRY, AND FINAL DISPLACEMENT VECTORS.
   18 PRINT104,N1,U(3,M3),V(MC,MC),W(M3,M3)
   19 IF(SENSE SWITCH 2)4,20
   20 IF(SENSE SWITCH 3)21,5
   21 PUNCH100,A,H,TS,TB,BB,CMU,M,CT,E2,E3
      DO22I=1,M5
      DO22J=1,M5
   22 PUNCH102,U(I,J),V(I,J),W(I,J)
      GO TO 1
  100 FORMAT(6F6.2,I4,2F6.2)
  101 FORMAT(E14.8)
  102 FORMAT(3E14.8)
  103 FORMAT(2F4.3)
  104 FORMAT(I4,3(2X,E11.5))
      END
```

PROGRAMME 5. Internal equilibrium checks for displacement and traction solutions from programmes 1 to 4.

```
C     PROGRAM TO CHECK VERTICAL AND HORIZONTAL EQUILIBRIUM.
C
      DIMENSION T(17,17),S(17,17),Q(17,17),SHE(17),SVE(17),CN(17),SN(17)
      DIMENSION W(18,18)
C     INPUT OF SHELL GEOMETRY AND INTERNAL STESS RESULTANTS.
    1 READ100,A,H,TS,TB,BB,CMU,M,CT,E2,E3,ES,EB
  100 FORMAT(6F6.2,I4,5F6.2)
      M1=M+1
      M2=M+2
      READ104
  104 FORMAT(1X/)
      DO21=1,M1
      DO2J=1,M1
    2 READ101,W(I,J),T(I,J),S(I,J)
  101 FORMAT(32X,E12.6,12X,2E12.6)
C     CORRECTION TO VERTICAL SHEAR FORCES.
      YM=M
      YM1=M1
      B7=4.*YM**3
      DO431=1,M
      W(I,M2)=W(I,M)
      W(I+1,I)=W(I,I+1)
   43 W(I+2,I)=W(I,I+2)
      READ104
      READ104
      DO31=1,M1
      DO3J=1,M1
    3 READ102,Q(I,J)
  102 FORMAT(68X,E12.6)
      DO441=2,M1
      DO44J=1,M1
   44 Q(I,J)=Q(I,J)+B7*(W(I-1,J+1)-W(I+1,J-1))
C     COMPUTATION OF SHELL SLOPES.
      DO4J=1,M1
      YJ=J
      Y=(YM1-YJ)/YM*H/A
      FUNCT=Y**2+1.
      SN(J)=Y/SQRT(FUNCT)
    4 CN(J)=1./SQRT(FUNCT)
C     COMPUTATION OF RESULTANT SHELL EXTERNAL FORCES.
      C1=1./(4.*YM)
      C2=2.*C1
      SHE(1)=0.
      DO51=1,M
    5 SHE(1)=SHE(1)+C1*(S(I,M1)+S(I+1,M1))
      DO71=1,M
      YI=I
      SVE(I)=.25*((YM1-YI)/YM)**2
      IF(I-1)7,7,6
    6 SHE(I)=SHE(I-1)-C1*(S(I,M1)+S(I-1,M1))
    7 CONTINUE
      SVE(M1)=0.
      SHE(M1)=0.
C     COMPUTATION OF RESULTANT SHELL INTERNAL FORCES.
      PUNCH100,A,H,TS,TB,BB,CMU,M,CT,E2,E3,ES,EB
      IDT1=1
      IDT2=2
      DO91=1,M
      VSUMT=0.
      VSUMS=0.
      VSUMQ=0.
      VSUM=0.
      HSUMT=0.
      HSUMS=0.
      HSUMQ=0.
      HSUM=0.
      DO8J=1,M
      VSUMT=VSUMT-C2*(T(I,J)*SN(J)+T(I,J+1)*SN(J+1))
      VSUMS=VSUMS-C2*(S(I,J)+S(I,J+1))*SN(I)
      VSUMQ=VSUMQ-C2*(Q(I,J)*CN(J)+Q(I,J+1)*CN(J+1))*CN(I)
      HSUMT=HSUMT-C1*(T(I,J)*CN(J)+T(I,J+1)*CN(J+1))
      HSUMS=HSUMS-C1*(S(I,J)+S(I,J+1))*CN(I)
      HSUMQ=HSUMQ+C1*(Q(I,J)+Q(I,J+1))*(SN(J)*CN(I)+CN(J)*SN(I))
      VSUM=VSUMT+VSUMS+VSUMQ
    8 HSUM=HSUMT+HSUMS+HSUMQ
      PVSMT=100.*VSUMT/VSUM
      PVSMS=100.*VSUMS/VSUM
      PVSMQ=100.*VSUMQ/VSUM
      PHSMT=100.*HSUMT/HSUM
      PHSMS=100.*HSUMS/HSUM
      PHSMQ=100.*HSUMQ/HSUM
      PUNCH103,I,VSUMT,PVSMT,VSUMS,PVSMS,VSUMQ,PVSMQ,VSUM,SVE(I),IDT1
    9 PUNCH103,I,HSUMT,PHSMT,HSUMS,PHSMS,HSUMQ,PHSMQ,HSUM,SHE(I),IDT2
  103 FORMAT(I4,4X,F8.4,F6.1,F8.4,F6.1,F8.4,F6.1,4X,F8.4,F8.4,I2)
      GO TO 1
      END
```

A P P E N D I X B

MODEL MATERIAL PROPERTIES

B.1 BENDING TEST ON "PERSPEX"

A carefully machined perspex strip was subjected to the same heat treatment as the shell model. Budd metal film strain gauges were attached so that top and bottom surface strains in the longitudinal and transverse directions were measured in the region of constant moment. The dimensions of the test strip and the loading method are shown in figure B.1.

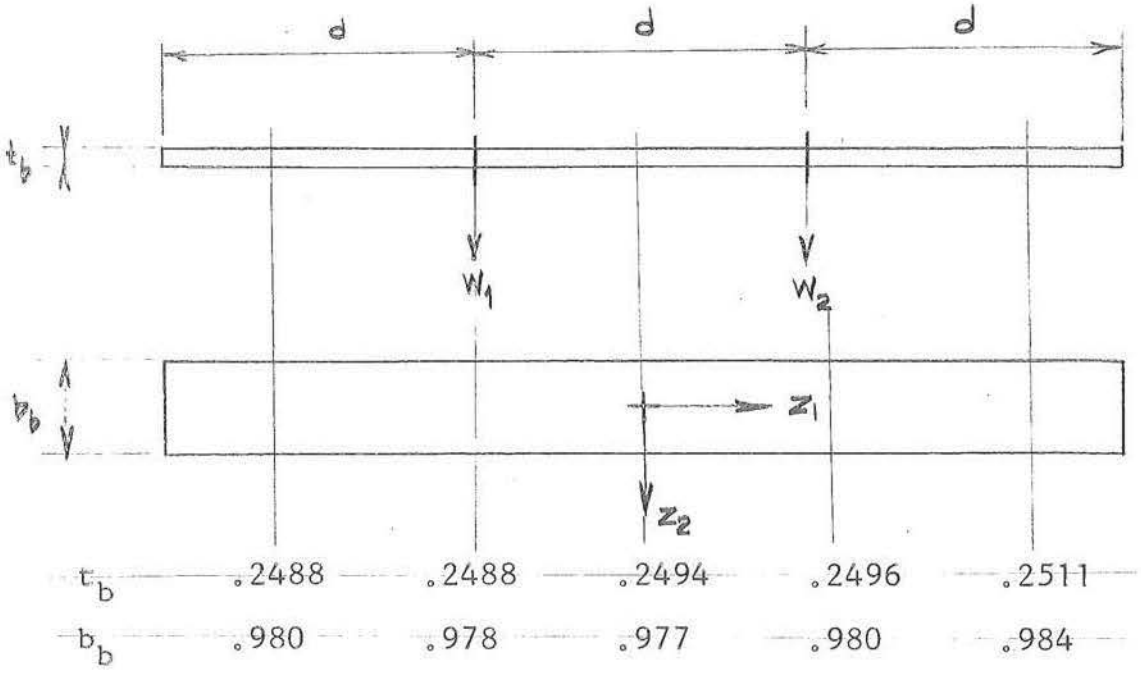

t_b	.2488	.2488	.2494	.2496	.2511
b_b	.980	.978	.977	.980	.984

Average t_b = .2495
Average b_b = .979

FIG. B.1 Dimensions and loading of test beam strip

Loads were applied at the beam third points, and readings of strain and deflection were taken at intervals of 5 minutes for a total time of 60 minutes. The loads were then removed and the process repeated. A number of independent tests were carried out, but as no appreciable differences in behaviour were observed, only the results of one typical test are given.

8.1.1 Strain Measurement

Table B.1 lists numerical averages of top and bottom recorded strains in the longitudinal and transverse directions as a function of time. Also presented are the corresponding values of Poisson's ratio. From a number of similar tests with increasing loads w_1 and w_2, the creep strain at a given instant after loading was found to be a constant proportion of the total strain magnitude. No differences could be determined between the nature of creep on loading and unloading (this is in contrast to the tests performed by Rocha[47] on alkathene).

TIME (min)	0	10	20	30	40	50	60
ϵ_{11} (μ strain)	449.0	476.0	480.0	482.0	485.0	486.0	488.0
ϵ_{22} (μ strain)	135.0	146.5	148.0	148.0	150.0	151.0	151.0
ν	.3006	.3091	.3083	.3071	.3093	.3107	.3094

ϵ_{11} numerical average of ϵ_{11}^t and ϵ_{11}^b,

ϵ_{22} numerical average of ϵ_{22}^t and ϵ_{22}^b.

Average ν = .3078.

TABLE B.1 Results for a typical beam test for the determination of Poisson's ratio .

The average recorded strains listed in table B.1 were corrected for lead wire and switch box resistance, gauge factor and gauge thickness (see reference [10]). With the expression

$$E_s = \frac{6.w.d}{b_b. + b^2} \cdot \frac{2}{\epsilon^*_{11}}, \qquad (B.1)$$

where ϵ^*_{11} is the corrected average surface strain, the variation of Young's modulus is determined as a function of time. For the test presented the relevant data was

$w_1 = 0.600$ lb.,
$w_2 = 0.608$ lb.,
$d = 4$ inch,
$t_b = 0.977$,
$b_b = 0.2495$.

Table B.2 shows the corrected numerical average strains, and corresponding Young's modulii.

TIME (min)	0	10	20	30	40	50	60
ϵ_{11} (μ strain)	449.0	476.0	480.0	482.0	485.0	486.0	488.0
ϵ^*_{11} (μ strain)	455.0	479.0	486.0	488.0	491.0	492.0	494.0
$E_s \times 10^6$ (lb./in.^{2})	.524	.500	.490	.488	.485	.484	.482

TABLE B.2 Young's modulus as determined from strain test.

As an analytic approximation to the variation of $E_s(t)$, a second order polynomial is derived using the values

$$E_s(15) = 0.494 \text{ lb./in.}^2$$
$$E_s(30) = 0.488 \text{ lb./in.}^2$$
$$E_s(60) = 0.482 \text{ lb./in.}^2$$

This quadratic variation is given by

$$E_s(t) = 0.00407.t^2 - 0.517.t + 503.9, \qquad (B.2)$$

and is illustrated in figure B.2.

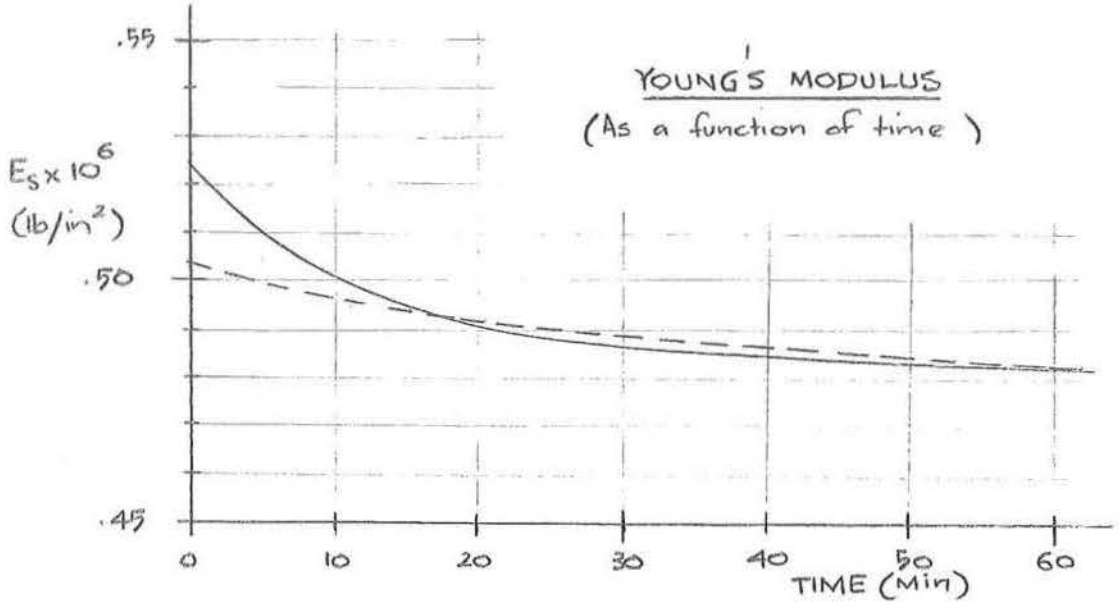

Fig. B.2 Experimental, and quadratic appproximation of $E_s(t)$.

For the purposes of creep correction all experimental strain recordings are reduced to an effective 15 minute strain value using the dimensionless variable $f(t)$, where $f(t)$ is given by

$$f(t) = \frac{E_s(t)}{E_s(15)}, \qquad (B.3)$$

which reduces to

$$f(t) = 0.0000082.t^2 - .00104.t + 0.1013. \qquad (B.4)$$

B.1.2 Deflection Measurement

A micrometer screw measuring directly to $^1/1000$ inch and connected through a contact light circuit was used to determine midspan deflections. It was found that the heat generated by the small arcing on contact was sufficient to markedly alter the properties of the perspex, causing the reliability of these tests to be less than those recording strain. Typical results are shown in table B.3, where $E_s(t)$ is determined using the expression

$$E_s = \frac{w.d.(3.L^2 - 4.d^2)}{2.b_b.t_b^3} . \frac{1}{w_3} , \qquad (B.5)$$

where w_3 is the recorded vertical deflection.

TIME (min)	0	10	20	30	40	50	60
w_3(inch)	.057	.060	.061	.063	.063	.064	.064
$E_s x 10^6$(lb/in.^{2})	.512	.487	.479	.463	.463	.456	.456

TABLE B.3 Young's modulus as determined from deflection test.

B.2 STIFFENING EFFECT OF STRAIN GAUGES

Before the strain gauges were applied deflection tests were carried out on the beam. No appreciable difference in

behaviour to the results of section B.1.2 could be determined. It could therefore be assumed that the stiffening effect of strain gauges on the model could be neglected.

B.3 INFLUENCE OF HEAT TREATMENT UPON ELASTIC PROPERTIES

Similar tests to those described in section B.1 were carried out on a strain gauged test beam which had not undergone heat treatment. Once again no difference in behaviour could be determined.

B.4 WARM-UP DRIFTS

Table B.4 lists the warming drifts (due to switching) for a particular gauge at different absolute strain levels.

TIME (Sec) / STRAIN (μ strain)	0	5	10	15	20	25	30
50		42	47	49	50	50	50
100		93	98	100	100	100	100
200		192	197	199	199	200	200
300		291	296	298	299	300	300

TABLE B.4 Warming drift of a particular strain gauge.

It is seen that within the reading accuracy the warm-up drift is independent of strain magnitude. By recording all strains at a consistent period of time after switching, it is therefore possible to eliminate this effect.

A P P E N D I X C

TABULATED EXPERIMENTAL AVERAGE STRAINS

Average corrected surface strains for all major model tests are presented. The readings have been corrected for switch box and lead wire resistance, gauge factor, shell thickness (reference[10]) and have also been reduced to an effective 15 minute strain.

Individual runs for model tests 1A and 4A were carried out to determine the influence of load cells in corner moment rigidity. Rigid channel sections were used to replace the load cells as indicated in table C.

MODEL TEST	RUN NO.	APEX CORNERS	BASE CORNERS
1A	1	Load cells	Load cells
	2	Rigid blocks	Load cells
	3	Load cells	Load cells
	4	Rigid blocks	Rigid blocks
4A	1	Load cells	Load cells
	2	Load cells	Load cells
	3	Rigid blocks	Rigid blocks

TABLE C - Use of load cells in model tests 1A and 4A.

Results for uniform normal load tests are converted to an effective 0.2175 psi pressure, and diagonal displacement results to an effective 0.05 inch diagonal displacement.

GAUGE POS	STRAIN ϵ_{11} (μSTRAIN)		STRAIN ϵ_{22} (μSTRAIN)		STRAIN ϵ_{12} (μSTRAIN)	
	TOP	BOT	TOP	BOT	TOP	BOT
1	-720.	112.	225.	42.		
2	-198.	0.	86.	205.		
3	-207.	-309.	79.	123.		
4	-49.	-155.	22.	59.		
5	150.	-12.	-50.	0.		
6	308.	164.	-111.	-66.		
7	122.	452.	-75.	-155.		
8	-550.	-143.	-183.	279.	136.	20.
9	-84.	-362.	27.	174.	-103.	244.
10	-81.	-200.	8.	101.	86.	223.
11	-12.	-91.	-21.	64.	153.	192.
12	92.	-18.	-49.	27.	240.	119.
13	162.	72.	-91.	0.	313.	-24.
14	67.	287.	-124.	55.	210.	-4.
15	-176.	14.	-234.	58.	-218.	659.
16	4.	-162.	-14.	136.	1.	393.
17	10.	-76.	-38.	81.	-141.	297.
18	-30.	20.	77.	-64.		
19	37.	-25.	-75.	75.	287.	177.
20	36.	19.	-85.	33.	356.	32.
21	-58.	117.	-32.	87.	360.	-47.
22	-9.	55.	20.	27.	59.	382.
23	23.	28.	-46.	66.	174.	268.
24	1.	21.	60.	-68.		
25	-27.	6.	-71.	60.	228.	167.
26	-48.	3.	-69.	16.	298.	98.
27	-13.	41.	4.	14.	189.	179.
28	15.	-3.	19.	-18.		
29	-23.	24.	-20.	7.	181.	134.
30	-5.	0.	-4.	-4.	171.	127.
31	-38.	468.	0.	-159.		
32	0.	-143.	0.	45.		
33	-738.	49.	206.	45.		

TABLE C.1 Corrected average surface strains for model test 1A, run 1. Uniform normal loading of 0.0725 psi.

GAUGE POS	STRAIN ϵ_{11} (μSTRAIN)		STRAIN ϵ_{22} (μSTRAIN)		STRAIN ϵ_{12} (μSTRAIN)	
	TOP	BOT	TOP	BOT	TOP	BOT
1	-619.	109.	193.	36.		
2	-148.	0.	67.	180.		
3	-166.	-273.	62.	106.		
4	-26.	-131.	11.	48.		
5	182.	-11.	-57.	-3.		
6	348.	146.	-124.	-65.		
7	104.	504.	-74.	-169.		
8	-515.	-156.	-160.	239.	143.	67.
9	-71.	-329.	30.	143.	-65.	207.
10	-69.	-176.	12.	85.	78.	182.
11	-8.	-73.	-10.	47.	150.	180.
12	110.	-17.	-41.	17.	241.	122.
13	190.	47.	-94.	0.	319.	-48.
14	29.	280.	-167.	127.	106.	75.
15	-173.	7.	-191.	2.	-133.	665.
16	-4.	-162.	-9.	118.	-8.	348.
17	5.	-82.	-21.	67.	-131.	256.
18	-33.	4.	63.	-38.		
19	32.	-37.	-54.	62.	298.	162.
20	58.	-18.	-79.	21.	385.	-24.
21	-76.	100.	-45.	107.	342.	-148.
22	4.	32.	5.	10.	87.	327.
23	15.	0.	-11.	61.	141.	232.
24	-11.	-4.	64.	-25.		
25	-52.	-6.	-42.	57.	240.	139.
26	-50.	3.	-50.	-11.	307.	34.
27	-16.	7.	26.	23.	160.	173.
28	7.	-33.	26.	8.		
29	-48.	30.	-8.	2.	178.	122.
30	-25.	14.	7.	7.	181.	140.
31	40.	276.	-22.	-103.		
32	-91.	-8.	46.	-19.		
33	-598.	-45.	158.	63.		

TABLE C.2 Corrected average surface strains for model test 1A, run 2. Uniform normal loading of 0.1450 psi.

GAUGE POS	STRAIN ϵ_{11} (μSTRAIN)		STRAIN ϵ_{22} (μSTRAIN)		STRAIN ϵ_{12} (μSTRAIN)	
	TOP	BOT	TOP	BOT	TOP	BOT
1	-629.	-15.	199.	63.		
2	-245.	-1.	93.	164.		
3	-204.	-272.	76.	105.		
4	-41.	-164.	16.	58.		
5	161.	-32.	-51.	4.		
6	315.	137.	-117.	-65.		
7	114.	472.	-80.	-160.		
8	-469.	-155.	-139.	216.	165.	51.
9	-128.	-291.	36.	150.	-63.	218.
10	-89.	-172.	18.	92.	43.	218.
11	-4.	-83.	-26.	63.	136.	203.
12	120.	-22.	-51.	27.	243.	127.
13	189.	73.	-91.	0.	323.	-25.
14	80.	314.	-134.	80.	235.	38.
15	-142.	9.	-217.	70.	-149.	552.
16	-22.	-113.	-13.	127.	-28.	359.
17	10.	-53.	-29.	78.	-120.	290.
18	-17.	37.	83.	-57.		
19	76.	-20.	-80.	81.	296.	189.
20	70.	33.	-83.	45.	399.	38.
21	-45.	140.	-37.	122.	404.	-41.
22	-11.	79.	42.	29.	66.	357.
23	26.	47.	-38.	75.	179.	265.
24	4.	28.	77.	-59.		
25	-3.	7.	-72.	73.	254.	159.
26	-43.	27.	-70.	25.	342.	91.
27	-18.	48.	4.	21.	190.	190.
28	17.	-3.	26.	-17.		
29	-28.	14.	-23.	25.	181.	144.
30	-10.	3.	7.	-11.	162.	122.
31	58.	492.	-42.	-169.		
32	-38.	-142.	5.	44.		
33	-716.	5.	198.	47.		

TABLE C.3 Corrected average surface strains for model test 1A, run 3. Uniform normal loading of 0.1450 psi.

GAUGE POS	STRAIN ϵ_{11} (μSTRAIN)		STRAIN ϵ_{22} (μSTRAIN)		STRAIN ϵ_{12} (μSTRAIN)	
	TOP	BOT	TOP	BOT	TOP	BOT
1	-590.	-58.	194.	72.		
2	-237.	-1.	93.	143.		
3	-177.	-241.	68.	95.		
4	-12.	-148.	8.	55.		
5	172.	-29.	-57.	2.		
6	316.	129.	-112.	-57.		
7	110.	476.	-66.	-161.		
8	-431.	-160.	-101.	162.	187.	112.
9	-135.	-250.	46.	118.	-50.	213.
10	-82.	-149.	18.	74.	40.	206.
11	13.	-80.	-20.	51.	122.	182.
12	120.	-25.	-47.	23.	228.	111.
13	184.	57.	-87.	0.	303.	-35.
14	56.	296.	-129.	93.	217.	72.
15	-129.	8.	-176.	4.	-60.	509.
16	-48.	-102.	-9.	92.	10.	332.
17	-8.	-54.	-25.	64.	-112.	273.
18	-29.	29.	68.	-54.		
19	65.	-35.	-69.	67.	282.	158.
20	67.	9.	-84.	36.	376.	7.
21	-61.	121.	-22.	118.	388.	-49.
22	-23.	53.	4.	27.	92.	329.
23	6.	29.	-47.	71.	183.	252.
24	2.	26.	74.	-63.		
25	-15.	-8.	-64.	80.	250.	151.
26	-31.	14.	-63.	27.	298.	83.
27	-20.	44.	-7.	22.	191.	180.
28	10.	-6.	40.	-26.		
29	-18.	8.	-21.	27.	183.	136.
30	-3.	-1.	-2.	1.	172.	124.
31	100.	505.	-53.	-177.		
32	10.	-154.	-4.	46.		
33	-710.	126.	203.	17.		

TABLE C.4 Corrected average surface strains for model test 1A, run 4. Uniform normal loading of 0.2175 psi.

GAUGE POS	STRAIN ϵ_{11} (μSTRAIN)		STRAIN ϵ_{22} (μSTRAIN)		STRAIN ϵ_{12} (μSTRAIN)	
	TOP	BOT	TOP	BOT	TOP	BOT
1	-724.	-50.	[illegible]	84.		
2	-281.	-1.	114.	182.		
3	-271.	-324.	103.	134.		
4	-118.	-267.	52.	107.		
5	83.	-160.	-22.	57.		
6	247.	-35.	-84.	8.		
7	-203.	417.	13.	-121.		
8	-631.	-273.	-146.	259.	381.	112.
9	-226.	-364.	62.	179.	-5.	154.
10	-179.	-256.	50.	118.	54.	147.
11	-99.	-206.	19.	105.	127.	149.
12	130.	-159.	-12.	73.	254.	87.
13	132.	-111.	-69.	0.	293.	-75.
14	-156.	181.	-257.	243.	-191.	113.
15	-250.	-43.	-281.	16.	71.	721.
16	-155.	-209.	-12.	145.	56.	322.
17	-101.	-166.	7.	104.	-114.	230.
18	-150.	-58.	105.	-6.		
19	-27.	-160.	-11.	87.	288.	137.
20	34.	-182.	-41.	32.	369.	-89.
21	-129.	64.	-114.	57.	262.	-305.
22	-69.	22.	-2.	-20.	98.	326.
23	-40.	-53.	0.	51.	145.	232.
24	-89.	-16.	52.	19.		
25	-41.	-82.	23.	1.	196.	174.
26	-13.	-65.	17.	-118.	252.	62.
27	6.	16.	33.	-22.	140.	202.
28	-22.	25.	-15.	55.		
29	15.	3.	52.	-56.	106.	226.
30	48.	-30.	45.	-22.	91.	228.
31	-242.	383.	78.	-116.		
32	-141.	-207.	46.	79.		
33	-734.	-246.	223.	109.		

TABLE C.5 Corrected average surface strains for model test 2A. Uniform normal loading of 0.1440 psi.

GAUGE POS	STRAIN ϵ_{11} (μSTRAIN)		STRAIN ϵ_{22} (μSTRAIN)		STRAIN ϵ_{12} (μSTRAIN)	
	TOP	BOT	TOP	BOT	TOP	BOT
1	2082.	-2681.	-566.	650.		
2	193.	0.	-47.	-245.		
3	-409.	1563.	118.	-612.		
4	-757.	1791.	234.	-657.		
5	-586.	1183.	213.	-443.		
6	368.	8.	-43.	-60.		
7	2290.	-1922.	-564.	465.		
8	2165.	-1159.	1618.	-1597.	-2780.	3141.
9	1.	563.	210.	-514.	32.	703.
10	-759.	1216.	221.	-457.	-36.	94.
11	-959.	1321.	316.	-450.	-473.	56.
12	-829.	952.	320.	-375.	-497.	17.
13	-100.	11.	390.	1.	233.	-447.
14	1486.	-1224.	1476.	-1956.	3030.	-3188.
15	1460.	-1266.	1377.	-829.	-133.	23.
16	-269.	495.	303.	-514.	151.	31.
17	-973.	901.	176.	-324.	185.	20.
18	1137.	-1263.	-305.	288.		
19	-963.	921.	307.	-279.	-523.	52.
20	-304.	249.	388.	-378.	-119.	-111.
21	867.	-1177.	1077.	-1069.	28.	-457.
22	-315.	57.	-300.	268.	124.	-550.
23	-979.	570.	-339.	167.	-97.	-46.
24	930.	-1421.	223.	-316.		
25	-1068.	778.	-273.	380.	-273.	202.
26	-408.	294.	-285.	324.	-269.	219.
27	-730.	551.	-801.	746.	-84.	-142.
28	1028.	-1254.	852.	-849.		
29	-954.	899.	-943.	948.	-49.	215.
30	-916.	1035.	-1053.	1061.	157.	-41.
31	2516.	-1937.	-771.	504.		
32	-1170.	1311.	414.	-452.		
33	1924.	-2573.	-484.	628.		

TABLE C.6 Corrected average surface strains for model test 3A. Uniform normal loading of 0.0363 psi.

GAUGE POS	STRAIN ϵ_{11} (μSTRAIN)		STRAIN ϵ_{22} (μSTRAIN)		STRAIN ϵ_{12} (μSTRAIN)	
	TOP	BOT	TOP	BOT	TOP	BOT
1	5.	-321.	1.	105.		
2	0.	-111.	39.	31.		
3	-73.	44.	37.	-27.		
4	-54.	138.	24.	-51.		
5	-14.	175.	10.	-61.		
6	50.	141.	-12.	-44.		
7	189.	3.	-67.	2.		
8	-110.	-24.	-61.	63.	306.	90.
9	-58.	-56.	-6.	52.	184.	131.
10	-24.	-58.	6.	27.	141.	135.
11	-9.	-30.	13.	-6.	132.	135.
12	40.	1.	2.	-32.	106.	108.
13	93.	57.	-21.	0.	55.	106.
14	150.	161.	-49.	53.	119.	231.
15	-55.	1.	-56.	3.	236.	184.
16	-533.	-125.	15.	246.	-716.	169.
17	3.	-34.	31.	-18.	-156.	186.
18	-16.	22.	-36.	26.		
19	49.	3.	10.	-48.	145.	158.
20	65.	120.	0.	-13.	128.	113.
21	17.	91.	53.	88.	245.	191.
22	-7.	-20.	6.	-22.	111.	201.
23	14.	18.	63.	-10.	202.	226.
24	16.	27.	-28.	18.		
25	11.	27.	17.	-11.	213.	189.
26	27.	2.	3.	17.	204.	164.
27	23.	-4.	10.	-11.	191.	233.
28	34.	-11.	-3.	-2.		
29	14.	9.	-18.	-5.	235.	169.
30	-1.	10.	-6.	-15.	201.	180.
31	-52.	184.	40.	-64.		
32	137.	-54.	-52.	30.		
33	-322.	-10.	96.	5.		

TABLE C.7 Corrected average surface strains for model test 4A, run 1. Uniform normal loading of 0.2175 psi.

GAUGE POS	STRAIN ϵ_{11} (μSTRAIN)		STRAIN ϵ_{22} (μSTRAIN)		STRAIN ϵ_{12} (μSTRAIN)	
	TOP	BOT	TOP	BOT	TOP	BOT
1	0.	-328.	-4.	107.		
2	0.	-112.	44.	31.		
3	-74.	45.	40.	-25.		
4	-55.	141.	24.	-52.		
5	-15.	174.	12.	-66.		
6	44.	134.	-8.	-42.		
7	173.	-15.	-64.	10.		
8	-103.	-26.	-77.	70.	327.	83.
9	-62.	-66.	-9.	50.	184.	126.
10	-36.	-63.	17.	16.	147.	152.
11	-1044.	-41.	18.	-8.	-1654.	121.
12	34.	-3.	-1.	-31.	92.	95.
13	90.	65.	-26.	0.	29.	114.
14	136.	158.	-59.	47.	60.	206.
15	-58.	0.	-57.	-3.	253.	192.
16	-28.	-54.	18.	2.	174.	179.
17	-5.	-42.	35.	-22.	-149.	193.
18	-19.	16.	-37.	31.		
19	41.	-1.	15.	-59.	145.	144.
20	69.	42.	3.	-38.	142.	150.
21	9.	95.	27.	61.	190.	172.
22	27.	-32.	43.	-29.	186.	193.
23	-5.	-18.	45.	-20.	153.	233.
24	5.	16.	-35.	11.		
25	19.	2.	-5.	-17.	190.	175.
26	25.	-8.	5.	-12.	221.	138.
27	12.	-5.	0.	-10.	179.	206.
28	5.	-8.	-14.	-4.		
29	-4.	0.	-9.	-17.	200.	175.
30	-14.	6.	-14.	-9.	185.	167.
31	-45.	181.	29.	-65.		
32	139.	-51.	-58.	21.		
33	-309.	-6.	103.	0.		

TABLE C.8 Corrected average surface strains for model test 4A, run 2. Uniform normal loading of 0.2175 psi.

GAUGE POS	STRAIN ϵ_{11} (μSTRAIN)		STRAIN ϵ_{22} (μSTRAIN)		STRAIN ϵ_{12} (μSTRAIN)	
	TOP	BOT	TOP	BOT	TOP	BOT
1	-19.	-323.	-1.	105.		
2	0.	-128.	35.	36.		
3	-78.	21.	39.	-14.		
4	-64.	109.	27.	-43.		
5	-26.	148.	15.	-52.		
6	35.	115.	-6.	-35.		
7	166.	-18.	-61.	10.		
8	-110.	-34.	-71.	57.	328.	121.
9	-70.	-69.	-7.	55.	181.	118.
10	-40.	-69.	10.	30.	142.	135.
11	-15.	-45.	16.	3.	126.	122.
12	24.	-10.	4.	-20.	94.	103.
13	74.	41.	-20.	0.	42.	92.
14	120.	133.	-45.	61.	79.	212.
15	-58.	-1.	-70.	-5.	260.	197.
16	-39.	-56.	7.	9.	176.	173.
17	-16.	-47.	33.	-10.	-145.	183.
18	-27.	7.	-29.	28.		
19	33.	-4.	15.	-46.	145.	148.
20	64.	28.	-2.	-27.	146.	142.
21	5.	80.	34.	59.	177.	172.
22	14.	-27.	13.	-32.	172.	222.
23	4.	-19.	19.	-15.	162.	217.
24	-14.	11.	-29.	18.		
25	10.	4.	0.	-27.	199.	174.
26	18.	-4.	8.	-19.	214.	150.
27	10.	-8.	0.	-16.	177.	215.
28	3.	-7.	-10.	0.		
29	-1.	2.	-2.	-21.	201.	178.
30	-8.	-1.	-11.	-9.	185.	187.
31	-22.	148.	17.	-54.		
32	0.	-46.	-42.	16.		
33	-293.	-32.	102.	7.		

TABLE C.9 Corrected average surface strains for model test 4A, run 3. Uniform normal loading of 0.3263 psi.

GAUGE POS	STRAIN ϵ_{11} (μSTRAIN)		STRAIN ϵ_{22} (μSTRAIN)		STRAIN ϵ_{12} (μSTRAIN)	
	TOP	BOT	TOP	BOT	TOP	BOT
1	151.	-254.	-52.	83.		
2	0.	20.	18.	-16.		
3	-32.	213.	30.	-83.		
4	-32.	313.	16.	-111.		
5	25.	309.	-3.	-108.		
6	131.	216.	-53.	-71.		
7	331.	39.	-124.	-11.		
8	36.	105.	-114.	83.	239.	-74.
9	40.	18.	-51.	32.	155.	95.
10	52.	-8.	-30.	9.	132.	143.
11	79.	14.	-14.	-22.	99.	145.
12	128.	63.	-28.	-59.	56.	131.
13	181.	140.	-40.	0.	41.	172.
14	253.	300.	-52.	56.	306.	329.
15	-4.	62.	-12.	28.	96.	17.
16	64.	8.	8.	-22.	119.	118.
17	82.	19.	13.	-57.	-130.	181.
18	35.	110.	-75.	0.		
19	143.	64.	-19.	-77.	128.	196.
20	140.	145.	-34.	-17.	188.	234.
21	11.	196.	73.	149.	396.	329.
22	63.	-18.	61.	-22.	128.	183.
23	81.	2.	31.	-39.	160.	208.
24	19.	103.	-58.	2.		
25	78.	38.	-24.	-22.	208.	180.
26	26.	51.	3.	44.	265.	174.
27	50.	-12.	0.	-3.	199.	204.
28	3.	31.	-11.	-4.		
29	23.	3.	0.	-3.	237.	137.
30	5.	-13.	0.	-13.	229.	150.
31	47.	326.	0.	-120.		
32	0.	-19.	-110.	17.		
33	-257.	181.	81.	-50.		

TABLE C.10 Corrected average surface strains for model test 5A. Uniform normal loading of 0.2175 psi.

GAUGE POS	STRAIN ϵ_{11} (μSTRAIN)		STRAIN ϵ_{22} (μSTRAIN)		STRAIN ϵ_{12} (μSTRAIN)	
	TOP	BOT	TOP	BOT	TOP	BOT
1	629.	-690.	-257.	238.		
2	0.	-2.	32.	-46.		
3	-251.	590.	230.	-228.		
4	-517.	763.	263.	-269.		
5	-521.	543.	276.	-162.		
6	-249.	-62.	149.	55.		
7	408.	-1029.	-167.	417.		
8	-36.	298.	-548.	406.	1223.	-642.
9	-19.	-68.	-362.	326.	555.	-557.
10	-42.	-304.	-244.	323.	7.	-340.
11	-39.	-361.	-171.	291.	-285.	-146.
12	10.	-266.	-173.	227.	-514.	19.
13	102.	57.	-199.	0.	-635.	325.
14	150.	375.	-355.	525.	-417.	1023.
15	-326.	256.	-279.	161.	667.	-406.
16	27.	-252.	-56.	-10.	336.	-497.
17	120.	-292.	107.	-82.	33.	-227.
18	-251.	234.	-99.	80.		
19	270.	-107.	17.	-88.	-327.	141.
20	264.	61.	-61.	80.	-301.	453.
21	-80.	395.	-56.	327.	87.	665.
22	249.	-282.	193.	-325.	138.	-106.
23	315.	-251.	265.	-336.	100.	8.
24	-196.	375.	-313.	227.		
25	378.	-94.	160.	-222.	54.	115.
26	238.	-38.	173.	-23.	-11.	235.
27	366.	-272.	-1.	-266.	223.	173.
28	-239.	300.	-270.	218.		
29	285.	-218.	237.	-244.	240.	72.
30	196.	-274.	224.	-259.	305.	164.
31	-1213.	420.	510.	-223.		
32	-1.	-433.	-280.	270.		
33	-534.	644.	161.	-256.		

TABLE C.11 Corrected average surface strains for model test 6A. Uniform normal loading of 0.2175 psi.

GAUGE POS	STRAIN ϵ_{11} (μSTRAIN)		STRAIN ϵ_{22} (μSTRAIN)		STRAIN ϵ_{12} (μSTRAIN)	
	TOP	BOT	TOP	BOT	TOP	BOT
1	-165.	-659.	95.	206.		
2	-134.	0.	55.	74.		
3	-302.	17.	119.	19.		
4	-484.	-69.	157.	44.		
5	-591.	-248.	219.	118.		
6	-384.	-688.	164.	265.		
7	-680.	-645.	196.	256.		
8	-212.	-599.	131.	-15.	420.	649.
9	-296.	-252.	89.	74.	286.	-47.
10	-415.	-161.	133.	79.	38.	-235.
11	-528.	-183.	178.	84.	-126.	-234.
12	-579.	-273.	213.	132.	-207.	-107.
13	-342.	-584.	217.	0.	-122.	-161.
14	-519.	-804.	-17.	236.	-649.	-237.
15	-74.	-338.	-73.	-177.	575.	647.
16	-345.	-270.	32.	13.	290.	-49.
17	-460.	-236.	122.	65.	54.	-227.
18	-212.	-513.	84.	199.		
19	-523.	-225.	252.	62.	-263.	-137.
20	-280.	-524.	293.	-38.	-263.	-227.
21	-117.	-541.	14.	-363.	-458.	-868.
22	-241.	-156.	-41.	-177.	119.	-205.
23	-359.	-136.	118.	-87.	-13.	-222.
24	-117.	-356.	-10.	160.		
25	-260.	-107.	226.	-77.	-321.	35.
26	-20.	-179.	195.	-266.	-369.	38.
27	-46.	-6.	-63.	-74.	-74.	-72.
28	-17.	-67.	-23.	82.		
29	-18.	51.	87.	-31.	-215.	257.
30	46.	33.	-19.	64.	-104.	226.
31	-298.	-364.	125.	138.		
32	-519.	-219.	153.	154.		
33	-269.	-773.	110.	246.		

TABLE C.12 Corrected average surface strains for model test 2B. Base diagonal displacement of 0.01 inch.

GAUGE POS	STRAIN ϵ_{11} (μSTRAIN)		STRAIN ϵ_{22} (μSTRAIN)		STRAIN ϵ_{12} (μSTRAIN)	
	TOP	BOT	TOP	BOT	TOP	BOT
1	179.	-376.	-41.	108.		
2	-9.	0.	8.	14.		
3	-86.	124.	26.	-47.		
4	-122.	209.	39.	-76.		
5	-113.	203.	39.	-71.		
6	41.	89.	1.	-40.		
7	475.	-262.	-116.	53.		
8	247.	-153.	209.	-190.	-444.	424.
9	12.	14.	30.	-47.	-52.	160.
10	-93.	114.	25.	-39.	-24.	86.
11	-144.	166.	30.	-49.	-49.	59.
12	-156.	166.	46.	-50.	-45.	38.
13	-53.	76.	61.	0.	98.	-41.
14	294.	-126.	292.	-382.	691.	-539.
15	198.	-146.	184.	-104.	-135.	36.
16	10.	46.	45.	-63.	-39.	62.
17	-100.	110.	11.	-35.	36.	63.
18	164.	-167.	-22.	12.		
19	-164.	169.	13.	-10.	-38.	65.
20	-96.	129.	43.	-32.	44.	75.
21	151.	-139.	221.	-149.	151.	92.
22	-6.	14.	-21.	33.	-3.	-47.
23	-99.	102.	-47.	38.	-24.	-3.
24	165.	-157.	63.	-72.		
25	-165.	169.	-85.	119.	23.	79.
26	-99.	111.	-91.	142.	36.	141.
27	-94.	89.	-112.	123.	55.	-42.
28	172.	-157.	154.	-135.		
29	-131.	165.	-146.	193.	93.	25.
30	-118.	157.	-146.	167.	151.	-37.
31	422.	-241.	-134.	60.		
32	-176.	140.	67.	-49.		
33	104.	-269.	-71.	90.		

TABLE C.13 Corrected average surface strains for model test 3B. Base diagonal displacement of 0.04 inch.

GAUGE POS	STRAIN ϵ_{11} (μSTRAIN)		STRAIN ϵ_{22} (μSTRAIN)		STRAIN ϵ_{12} (μSTRAIN)	
	TOP	BOT	TOP	BOT	TOP	BOT
1	-213.	76.	114.	-31.		
2	0.	-21.	52.	30.		
3	-79.	-184.	-41.	67.		
4	131.	-269.	-104.	92.		
5	314.	-251.	-203.	67.		
6	316.	73.	-199.	-49.		
7	-37.	800.	30.	-325.		
8	40.	-95.	238.	-155.	-700.	198.
9	6.	-23.	183.	-128.	-418.	385.
10	15.	69.	161.	-162.	-87.	402.
11	29.	163.	149.	-196.	187.	350.
12	21.	199.	172.	-202.	435.	255.
13	-8.	66.	179.	0.	724.	-10.
14	72.	-57.	299.	-441.	865.	-584.
15	200.	-111.	184.	-86.	-514.	84.
16	80.	116.	94.	-23.	-338.	352.
17	31.	183.	-39.	23.	45.	364.
18	208.	-50.	65.	-83.		
19	-125.	148.	-72.	120.	361.	205.
20	-198.	120.	-42.	17.	533.	-16.
21	55.	-190.	97.	-139.	480.	-152.
22	-12.	138.	15.	188.	-107.	203.
23	-37.	206.	-161.	206.	39.	162.
24	211.	-132.	228.	-211.		
25	-203.	191.	-218.	284.	151.	76.
26	-214.	173.	-219.	212.	235.	57.
27	-163.	180.	0.	220.	111.	-42.
28	214.	-143.	218.	-174.		
29	-169.	214.	-181.	236.	82.	-36.
30	-108.	194.	-132.	168.	123.	-109.
31	855.	-37.	-358.	72.		
32	0.	98.	143.	-108.		
33	101.	-251.	-23.	122.		

TABLE C.14 Corrected average surface strains for model test 6B. Apex diagonal displacement of 0.04 inch.